Title
Design and Synthesis of Chemical Tools for Imaging Neuronal Activity

Author
Deal, Parker

Publication Date
2018

Peer reviewed|Thesis/dissertation

Design and Synthesis of Chemical Tools for Imaging Neuronal Activity

By

Parker E. Deal

A Dissertation submitted in partial satisfaction of the

requirements for the degree of

Doctor of Philosophy

In

Chemistry

In the

Graduate Division

of the

University of California, Berkeley

Committee in charge:

Professor Evan W. Miller, Chair

Professor Christopher J. Chang

Professor Hillel Adesnik

Fall 2018

Design and Synthesis of Chemical Tools for Imaging Neuronal Activity

By Parker E. Deal

Abstract

Design and Synthesis of Chemical Tools for Imaging Neuronal Activity

By

Parker E. Deal

Doctor of Philosophy in Chemistry
University of California, Berkeley
Professor Evan W. Miller, Chair

The ultimate goal of neuroscience is to correlate the activity of neurons and neuronal networks to higher order behaviors and cognition. This colossal task necessitates a variety of optical tools that can both measure and modulate neuronal activity. This dissertation describes the design, synthesis and characterization of a variety of such tools. In order to interrogate the electrical activity of neuronal circuits directly, we synthesized tetramethylrhodamine-based voltage reporters, or RhoVRs, that possess excitation and emission profiles in the green to orange region of the visible spectrum and use photoinduced electron transfer (PeT) as a trigger for voltage sensing. Two RhoVRs with particularly attractive photophysical properties were developed: RhoVR 1, which possessed the highest voltage sensitivity of any RhoVR (47% $\Delta F/F$ per 100 mV), and RhoVR(Me), a less sensitive (13% $\Delta F/F$ per 100 mV) but far brighter RhoVR (4-fold brighter than RhoVR 1). In order to facilitate the use of RhoVRs in complex tissues such as brain slice or *in vivo*, we developed genetically targetable RhoVRs using the HaloTag system (RhoVR-Halos). RhoVR-Halos maintained the fast kinetics and high sensitivities typical of RhoVRs (up to 34% $\Delta F/F$ per 100 mV) while labeling HaloTag expressing cells with high selectivity in culture, brain slice and *in vivo*. In addition, RhoVRs possess high two-photon cross sections (up to 190 GM), making them excellent candidates for two-photon voltage imaging. While voltage indicators allow for the study of fast voltage dynamics in real time, they necessitate very fast imaging speeds that are not well suited for mapping activity across large neuronal networks. In order to facilitate neuronal activity mapping, we developed a Ca^{2+} integrator MethylAzid-1 (MA-1). MA-1 acts as a coincidence detector for both light and Ca^{2+}, allowing a temporally precise "snapshot" of $[Ca^{2+}]$ to be taken. MA-1 undergoes a 25 nm shift in absorbance upon chelation of Ca^{2+} (K_d = 270 nM) that allows for the selective photolysis of Ca^{2+}-free MA-1 with 400 nm light. The extent of photolysis can be visualized *post hoc* through either "click chemistry" or the fluorogenic reduction of remaining MA-1. In addition to tools which report neuronal activity, we synthesized a new class of photocages based on 6-aminobenzofurans (BFCs) that can be used to selectively release caged compounds, such as neurotransmitters, upon irradiation with UV light. BFCs operate through a photo-induced elimination reaction that generates an extended azaquinone-methide from the excited state. Initial studies revealed BFCs are strong absorbers of UV/Violet light (λ_{max} = 365 nm, ε = 30,000 M^{-1} cm^{-1}) that readily photolyze ($\Phi_{photolysis}$ up to 0.18) to release their caged cargo. Together, this work demonstrates the power of optical tools to study neuronal systems ranging from sub-cellular domains to large networks of neurons and lays the groundwork for their application in complex tissues such as brain slice or *in vivo*.

For My Parents

Table of Contents

Acknowledgements

I would first like to express my gratitude to Professor Evan Miller for his support and guidance over my graduate career. Joining the lab at its inception and watching it grow has been a wonderful experience. I fondly remember the early years working with Evan in the lab and his tutelage helped me grow tremendously as a scientist. Evan is both a source of insightful scientific advice as well as a genuinely good person who cares about his students. While my time at Berkeley wasn't easy, I had an incredible grad school experience and I credit Evan with building the fun, exciting research environment that made it possible. In the end I can't even imagine having worked for anyone else at Berkeley.

The Miller lab as a whole also deserves my thanks for being a great group of scientists and friends. I am especially grateful to my classmates Vincent Grenier, Rishi Kulkarni and Alisha Contractor. Being the four original graduate students in the lab had its challenges, but I was happy to have shared the experience with all of you and I am glad to call you all my friends. I would also like to thank the undergraduates that worked with me, Sarah Al-Abdullatif and Kendall Wong, who helped me with the synthesis of many of the compounds found throughout my dissertation. I would like to thank Gloria Ortiz for all her helpful discussions. She is the most talented synthetic chemist in the lab, helping me with my chemistry problems, and also my best friend. Ali Walker, who was an awesome postdoc in our lab and who taught me almost everything I know about neuroscience and imaging. Finally, Pei Liu, with whom I collaborated with to develop the RhoVR-Halo system. Pei is a very talented scientist and I am going to miss working with her.

I would like to thank my undergraduate advisor, Michael "boss" Haley, who was a wonderful and supportive mentor that put me on the path to graduate school. Despite being Department Head, Professor Haley was always available, even for an undergraduate student like me. I also owe a great deal to my graduate student advisor Aaron Fix, who provided me with the synthetic chemistry skills that helped me succeed at Berkeley.

All my friends in Berkeley. I would have burned out of grad school if it were not for my close group of friends. Some of my best memories were going to Las Vegas after our first year, heading up for weekends at Lake Tahoe and countless camping trips that helped me rejuvenate and made my time at Berkeley so enjoyable. I would also like to thank my soccer teams, Strawspeedies and Soctopus, for giving me a healthy way to relieve some stress!

All my family in the Bay Area, specifically my cousins Matt and Julie, uncle Ivan, aunty Laly, aunty Marilyn and Brooks. It was always nice to get away from the lab for a few hours and eat a home cooked meal or go out and get a nice meal. My sister, who is the most caring and genuine person I know. I am grateful and indebted to her for everything she has done for our family and I am excited for her as she leaves for a new adventure in Europe.

Finally, I would like to thank my parents, whom I dedicate this thesis to and who deserve the most recognition for my accomplishments. From an early age my parents always encouraged me to pursue my interests and gave me a wonderful childhood that made me the person I am today. They provided me with the work ethic which has been the foundation of my success in school and now in research. They always had faith and confidence in me, even when I did not, which helped me through the tougher times of my graduate career. Now that I am finishing up my degree, I am happy knowing that they are proud of me. All in all, I have had a pretty great life so far, so thanks Mom and Dad!

Chapter 1:
Isomerically Pure Tetramethylrhodamine Voltage Reporters (RhoVRs)

Portions of this work were published in the following scientific journal:

Deal, P. E.; Kulkarni, R. U.; Al-Abdullatif, S. H.; Miller, E. W. "Isomerically Pure Tetramethylrhodamine Voltage Reporters" *Journal of the American Chemical Society* **2016**, *138*, 9085-9088.

Portions of this work were performed in collaboration with the following persons:
Synthesis was assisted by Sarah Al-Abdullatif

Abstract

We present the design, synthesis, and application of a new family of fluorescent voltage indicators based on isomerically pure tetramethylrhodamines. These new **Rho**damine **V**oltage **R**eporters, or RhoVRs, use photoinduced electron transfer (PeT) as a trigger for voltage sensing, display excitation and emission profiles in the green to orange region of the visible spectrum, demonstrate high sensitivity to membrane potential changes (up to 47% ΔF/F per 100 mV), and employ a tertiary amide derived from sarcosine, which aids in membrane localization and simultaneously simplifies the synthetic route to the voltage sensors. The most sensitive of the RhoVR dyes, RhoVR 1, features a methoxy-substituted diethylaniline donor and phenylenevinylene molecular wire in the 5'-position of the rhodamine aryl ring, the highest voltage-sensitivity to date for red-shifted PeT-based voltage sensors, and is compatible with simultaneous imaging alongside GFP-based indicators. The discoveries that sarcosine-based tertiary amides in the context of molecular wire voltage indicators prevent dye internalization, along with the improved voltage sensitivity of 5'-substituted voltage indicators should be broadly applicable to other types of PeT-based voltage-sensitive fluorophores.

Introduction

Cells expend a large amount of energy to maintain an unequal distribution of ions across the plasma membrane, resulting in a transmembrane voltage or potential (V_m).[1] Fast changes in V_m are responsible for the distinct cellular physiology of neurons and cardiomyocytes, and mounting evidence points to the importance of V_m in shaping fundamental cellular processes, such as differentiation, migration, and division, across a number of cell types.[2] Traditionally, changes in V_m have been monitored using electrodes, which are highly invasive and limited in throughput.[3] Broadly applicable and sensitive optical methods to track V_m would expand our capacity to disentangle the contributions V_m makes to human health and disease.[4-6]

We have recently undertaken a program to design and apply small molecule fluorescent dyes that use photoinduced electron transfer (PeT) as a molecular switch to optically monitor changes in V_m. The parent family of sensors includes VoltageFluors (VF dyes),[7-9] and makes use of PeT[10] through a phenylenevinylene molecular wire to modulate the fluorescence intensity of a sulfonofluorescein-based reporter in a V_m-dependent fashion. More recently, we disclosed the development of BeRST 1 (**Be**rkeley **R**ed **S**ensor of **T**ransmembrane potential),[11] which features the shared phenylenevinylene molecular wire along with a sulfonated silicon-rhodamine fluorophore. Although some members of the VF dye family display high voltage sensitivity (ΔF/F of 48-49% per 100 mV change),[8] excitation and emission profiles in the cyan to green range limit their application alongside many common optical tools like GFP and GCaMP[12] (Ca^{2+}-sensitive GFPs). BeRST 1 partially solves this problem of spectral overlap by use of the far-red/near infra-red Si-rhodamine, but voltage sensitivity is lower compared to VF dyes (24% ΔF/F per 100 mV) and the synthetic route to BeRST 1 is low yielding, due to the inclusion of a sulfonic acid functional group on the *meso* aryl ring of BeRST 1. We hoped to develop a voltage-sensing scaffold that retains the high sensitivity of the VF dye series, expands the spectrum of colors available for high-fidelity voltage sensing, and circumvents the inclusion of the sulfonate group that makes synthetic efforts challenging. Towards this end we disclose the design and synthesis of the RhoVR ("rover", **Rho**damine **V**oltage **R**eporters) family of tetramethylrhodamine-based PeT voltage indicators. We have synthesized four new RhoVR dyes, which display excitation and emission profiles spectrally

distinct from both VF and BeRST-type dyes, feature voltage sensitivities ranging from 3 to 47% ΔF/F per 100 mV, and make use of an *ortho*-tertiary amide instead of a sulfonate to achieve membrane localization.

Results and Discussion

Synthesis and in Vitro *Characterization of RhoVRs*

Tetramethylrhodamine (TMR)-based voltage indicators were synthesized in isomerically pure form from the 4'- and 5'-bromo TMR derivatives (**Scheme 1-1**). We generated isomerically pure rhodamines by condensation of dimethylaminophenol with the corresponding 2-carboxybenzaldehydes (**3** and **5**, **Scheme 1-2**), which were prepared in 79% and 88% yield over a two-step radical bromination followed by hydrolysis of either commercially-available 5-bromophthalide **4** or 6-bromophtalide **2** (prepared from commercially-available phthalide **1** in 62% yield, **Scheme 1-2**).[13,14] Separation of isomers at the 6-bromophthalide stage obviates the need to separate isomers at the rhodamine stage: addition of dimethylaminophenol occurs exclusively at the electrophilic aldehyde carbonyl.[15] Condensation of dimethylaminophenol with carboxybenzaldehyde in propionic acid in the presence of catalytic PTSA[15] gave 4'- and 5'-bromoTMR derivatives in 35% (**6**) and 57% (**7**) yield after purification by silica gel chromatography (**Scheme 1-1**). Subsequent Pd-catalyzed Heck coupling with substituted styrenes **8** or **9** (**Scheme 1-3** and **Scheme 1-4**) gave the TMR-based voltage sensors in yields ranging from 41-55%, following silica gel purification. Formation of an N-methyl glycine-derived tertiary amide mediated by HATU gave the *t*-butyl ester protected voltage sensors in >70% yield, which exists as a mixture of rotamers around the sarcosinyl-amide bond, as determined by VT-NMR (**Figure 1-1**). TFA-catalyzed deprotection of the *t*-butyl ester gave the final voltage sensors in 7-18% yield over two steps after reversed-phase HPLC purification.

Each RhoVR displayed absorption and emission profiles centered at 564-565 nm (ε = 70,000 to 87,000 M^{-1} cm^{-1}, **Figure 1-2**). A strong secondary absorbance band near 400 nm indicated the presence of the phenylenevinylene molecular wire (**Figure 1-2**). Emission from all RhoVRs was centered at 587 nm (Φ = 0.89% to 9.2%, **Table 1-1**). The low Φ values may indicate variable levels of PeT within the compounds.

Characterization of RhoVRs in HEK293T Cells

All sarcosine-substituted RhoVRs (500 nM, imaged in dye-free HBSS) localized well to the plasma membrane of HEK cells, as determined by fluorescence microscopy (**Figures 1-3, 1-6** and **1-7**). Control experiments conducted with TMR derivatives lacking the sarcosine amide (i.e. free carboxylate, **10-13**) show strong internal membrane staining (**Figure 1-3a**). The dramatic change in cellular localization is consistent with our hypothesis that inclusion of a charged tertiary amide in the *ortho* position of the pendant aryl ring prevents formation a neutral spirocycle and subsequent cellular dye uptake. The use of carboxylate derivatives drastically simplifies the synthetic route to make long-wavelength voltage indicators.

The voltage sensitivity of each RhoVR was assessed in HEK cells using patch-clamp electrophysiology in whole-cell, voltage-clamp mode. Hyper- and depolarizing voltage steps spanning a range from -100 mV to +100 mV in 20 mV increments from a holding potential of -60 mV provided voltage sensitivities of 3% to 47%, depending on the dye (**Table 1-1, Figure 1-3c,**

Figure 1-8). Compound **21**, which we dubbed RhoVR 1, emerged as the most voltage-sensitive dye (**Table 1**). Dyes bearing methoxy substitution on the aniline (**17** and **21**) showed improved voltage sensitivity relative to unsubstituted anilines (26% (**17**) vs. 3% (**16**) and 47% (**21**, RhoVR 1) vs. 7% (**20**)), as observed for fluorescein-based voltage indicators.[8] We also observed that voltage indicators derived from 5'-substituted rhodamines were both more voltage-sensitive (47% (**21**, RhoVR 1) vs 26% (**17**) and 7% (**20**) vs. 3% (**16**)) and brighter in cells (**Figure 1-7**, **Figure 1-8**). Studies are underway to probe the nature of this difference. Given the high sensitivity and brightness of RhoVR 1 in cells, we chose this dye to evaluate in subsequent experiments. RhoVR 1 has photostability comparable to VF2.1.Cl (**Figure 1-2**).

Imaging Neuronal Activity in Cultured Rat Hippocampal Neurons

When bath-applied to cultured rat hippocampal neurons, RhoVR1 gave distinct membrane-associated staining. The clear membrane staining, coupled with the high voltage-sensitivity of RhoVR 1 enabled detection of spontaneously firing action potentials with an average $\Delta F/F$ of 15% (N = 27 spikes) and signal-to-noise ratios (SNRs) ranging from 10:1 to 20:1 that were largely dependent on the illumination intensity used (1.7 to 3.1 W/cm^2) (**Figure 1-4**, cells 2-5). To confirm that spiking events we observed arose from action potentials, we treated actively firing cultures with tetrodotoxin (TTX), a sodium channel toxin which inhibits action potential firing, and observed no spiking activity after TTX treatment (**Figure 1-9**).

RhoVR 1 represents the most sensitive red-shifted PeT-based voltage indicator to date: VF2.1(OMe).Cl has a voltage sensitivity of 49%,[8] but emission at 536 nm while BeRST 1 has bathochromic emission at 680 nm, but only a 24% voltage sensitivity.[11] Given the success of far-red voltage dyes like BeRST 1 in integrating multiple functional signals simultaneously, we wondered whether we might be able to perform two-color imaging simultaneously with RhoVR 1, despite the tighter optical overlap between rhodamines and GFP-based chromophores. Expression of cytosolic GFP in HEK cells stained with RhoVR 1 did not result in significant bleed-through of GFP fluorescence into the rhodamine channel and did not substantially diminish the voltage sensitivity of RhoVR-1 in voltage-clamped HEK cells (47±3% without vs. 45±1% with GFP, **Figure 1-10**). Furthermore, cytosolic GFP in cultured neurons did not attenuate our ability to track action potentials in spontaneously firing neurons in culture (**Figure 1-4**). Indeed, when imaging spontaneous activity in cultured rat hippocampal neurons, we were able to clearly distinguish distinct spiking events arising from neighboring cells (**Figure 1-4b-d**; neurons 3 and 4) and clearly resolve spikes in neurons expressing GFP in single trials (**Fig. 1-4b-d**; neuron 1).

Encouraged by these results, we next sought to image voltage and Ca^{2+} dynamics simultaneously[16] by exciting the specimen with green and blue light and splitting the resulting emission to capture rhodamine and GFP fluorescence in parallel (**Scheme 1-5**). Brief rises in intracellular [Ca^{2+}] (Ca^{2+} transients), on the order of hundreds of milliseconds, are used as a surrogate for neuronal membrane depolarizations and are often monitored with green-fluorescent Ca^{2+} sensitive fluorophores like the genetically-engineered, Ca^{2+}-sensitive GFP, GCaMP.[12] We expressed GCaMP6s, on account of its excellent sensitivity to Ca^{2+} released in response to single action potentials,[12] in cultured hippocampal neurons and incubated these neurons with RhoVR 1 (500 nM). Using an image-splitter (**Scheme 1-5**) to separate emitted photons according to wavelength, we recorded Ca^{2+} transients via GCaMP6s fluorescence and voltage spikes via RhoVR 1 fluorescence. Under these conditions, hippocampal neurons again displayed significant

amounts of spontaneous spiking activity in multiple, distinct neurons, as detected by GCaMP6 (**Figure 1-5a**, green) and RhoVR 1 (**Figure 1-5a**, magenta).

The sensitivity of RhoVR 1 to these action potentials was similar to values obtained in experiments recorded at a single wavelength alone (ΔF/F per spike = 9.5%, SNR = 12:1, N = 70 spikes, **Figure1-5a, e-g**). Typically, one neuron expressed high levels of GCaMP6s fluorescence in a field of view (**Figure 1-5d**), which enabled us to directly compare transient rises in Ca^{2+} with fast voltage spikes in the same neuron (**Figure1-5a**). In all cases, the fast voltage spike clearly precedes the subsequent Ca^{2+} transient. RhoVR 1 displays comparable or better ΔF/F values for single spikes relative to the corresponding Ca^{2+} transient in the same cell (**Figure1-5a**). Because of the inherently fast kinetics of V_m relative to Ca^{2+}, monitoring V_m directly via RhoVR 1 enables resolution and precise timing of spikes occurring in quick succession from multiple cells, which would be impossible using more traditional approaches like Ca^{2+} imaging or single-cell electrophysiology (**Figure 1-5f-h**).

Conclusion

In summary, we present the design, synthesis, and application of four members of a new class of voltage-sensitive dyes based on tetramethylrhodamine. All of the new sensors display excitation and emission profiles greater than 550 nm, good photostability, and varying degrees of voltage sensitivity in patch-clamped HEK cells. The best of the new voltage indicators, RhoVR 1, displays a voltage sensitivity of 47% ΔF/F per 100 mV, rivaling the sensitivity of the fluorescein-based VF2.1(OMe).H (49% ΔF/F per 100 mV)[8] and surpassing that of our most red-shifted probe, BeRST 1, (24% ΔF/F per 100 mV).[11] Although the excitation and emission spectrum of RhoVR 1 is blue-shifted relative to BeRST 1, the TMR optical profile still provides ample spectral separation to perform two-color imaging alongside other optical probes, such as GFP and the GCaMP family of sensors. Using a combination of GCaMP6s and RhoVR 1, we simultaneously imaged Ca^{2+} transients and membrane potential depolarizations in cultured hippocampal neurons, establishing that RhoVR 1 and related compounds will be useful for parsing the roles of Ca^{2+} and V_m in living cells.

Taken together, these data demonstrate the utility of sarcosine-substituted rhodamines dyes for voltage sensing in living cells. The incorporation of the 2'-carboxylate simplifies the synthetic route to long wavelength voltage sensors by avoiding highly polar sulfonates, which complicate purification, and subsequent modification with sarcosine prevents the internalization that plagues un-functionalized xanthene-based voltage indicators. Inclusion of the free carboxylate on sarcosine provides a convenient handle for subsequent functionalization and localization to genetically-encoded protein partners or delivery agents. Furthermore, expansion of PeT-based voltage indicators to include rhodamines offers a new optical channel for use in voltage sensing and demonstrates the versatility and generality of a PeT-based approach to voltage sensing. We were pleasantly surprised to find that the 5'-substituted rhodamines showed greater voltage sensitivity than the 4'-substituted dye, which has been the typical substitution pattern for our previous molecular wire voltage sensors and many PeT-based analyte sensors.[17-19] Experiments are underway to probe the nature of this voltage sensitivity enhancement as well as to apply this substitution pattern to future generations of voltage-sensitive dyes and other sensing platforms.

Experimental Section

General Method for Chemical Synthesis and Characterization

Chemical reagents and solvents (dry) were purchased from commercial suppliers and used without further purification. Preparation of phthalaldehydic acids (**3** and **5**) and isomerically pure tetramethylrhodamines (**6** and **7**) were modified from previously reported procedures.[13-15] Synthesis of 4-(diethylamino)-2-methoxybenzaldehyde **22** and (E)-N,N-dimethyl-4-(4-vinylstyryl)aniline **8** were carried out as previously reported.[7,20] Thin layer chromatography (TLC) (Silicycle, F254, 250 μm) and preparative thin layer chromatography (PTLC) (Silicycle, F254, 1000 μm) was performed on glass backed plates pre-coated with silica gel and were visualized by fluorescence quenching under UV light. Flash column chromatography was performed on Silicycle Silica Flash F60 (230–400 Mesh) using a forced flow of air at 0.5–1.0 bar. NMR spectra were measured on Bruker AVB-400 MHz, 100 MHz, AVQ-400 MHz, 100 MHz, Bruker AV-600 MHz, 150 MHz. NMR spectra measured on Bruker AVII-900 MHz, 225 MHz, equipped with a TCI cryoprobe accessory, were performed by Dr. Jeffrey Pelton (QB3). Variable temperature NMR experiments were measured on the Bruker AV-600 with the assistance of Hasan Celik. Chemical shifts are expressed in parts per million (ppm) and are referenced to $CDCl_3$ (7.26 ppm, 77.0 ppm) or DMSO (2.50 ppm, 40 ppm). Coupling constants are reported as Hertz (Hz). Splitting patterns are indicated as follows: s, singlet; d, doublet; t, triplet; q, quartet, dd, doublet of doublet; m, multiplet. High-resolution mass spectra (HR-ESI-MS) were measured by the QB3/Chemistry mass spectrometry service at University of California, Berkeley. High performance liquid chromatography (HPLC) and low resolution ESI Mass Spectrometry were performed on an Agilent Infinity 1200 analytical instrument coupled to an Advion CMS-L ESI mass spectrometer. The column used for the analytical HPLC was Phenomenex Luna C18(2) (4.6 mm I.D. × 150 mm) with a flow rate of 1.0 mL/min. The mobile phases were MQ-H_2O with 0.05% formic acid (eluent A) and HPLC grade acetonitrile with 0.05% formic acid (eluent B). Signals were monitored at 254, 340 and 545 nm over 20 min with a gradient of 10-100% eluent B. The column used for semi-preparative HPLC was Phenomenex Luna 5μ C18(2) (10 mm I.D. x 150 mm) with a flow rate of 5.0 mL/min. The mobile phases were MQ-H_2O with 0.05% formic acid (eluent A) and HPLC grade acetonitrile with 0.05% formic acid (eluent B). Signals were monitored at 254 over 20 min with a gradient of 10-100% eluent B.

Synthetic Procedures

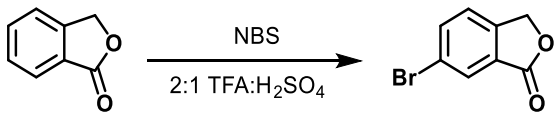

1 **2**

Synthesis of 6-bromoisobenzofuran-1(3H)-one, 2:
Acetic acid (10 mL) and concentrated sulfuric acid (4.5 mL) were added to **1** (5.00 g, 37.3 mmol). *N*-bromosuccinimide (9.95 g, 55.9 mmol) was added portion-wise over 6 h and the reaction was stirred at 22 °C for 5 d, after which the reaction was judged complete by NMR. The reaction mixture was poured over 150 mL of ice, then extracted with dichloromethane (2 x 200 mL), dried with anhydrous magnesium sulfate and the solvent removed by rotary evaporation. The crude solid was purified by flash chromatography (10-30% ethyl acetate in hexanes, linear gradient), yielding

4.95 g (23.2 mmol, 62%) of **2** and 2.18 g of a mixture of other isomers. ^{1}H NMR (400 MHz, $CDCl_3$) δ 8.04 (d, *J* = 1.2 Hz, 1H), 7.79 (dd, *J* = 8.1, 1.6 Hz, 1H), 7.39 (d, *J* = 8.1 Hz, 1H), 5.28 (s, 2H).

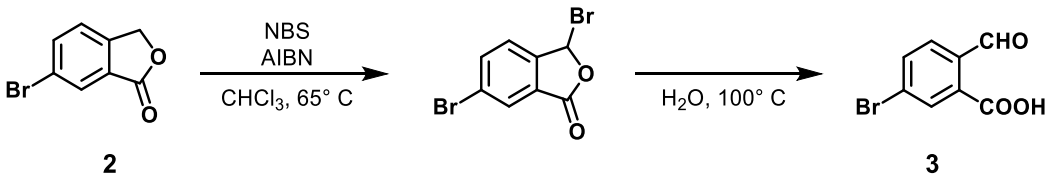

2 **3**

Synthesis of 5-bromo-2-formylbenzoic acid, 3:

2 (1.50 g, 7.04 mmol) was stirred in $CHCl_3$ (40 mL) with *N*-bromosuccinimide (1.38 g, 7.75 mmol) and AIBN (86 mg, 0.35 mmol) at reflux for 8 h, after which a second portion of *N*-bromosuccinimide (1.38 g, 7.75 mmol) and AIBN (86 mg, 0.35 mmol) was added. The reaction was stirred for a further 16 h, after which the bromination was deemed complete by analysis of the crude reaction mixture by NMR. The precipitated solid was filtered off and the filtrate concentrated *in vacuo*. Water (75 mL) was added to the resulting solid and refluxed for 2 h. The resulting white solid was collected by vacuum filtration and washed with water (50 mL) and hexanes (25 mL), affording **3** as a white solid (1.42 g, 6.21 mmol, 88%). ^{1}H NMR (600 MHz, DMSO-d_6) δ 8.28 (s, 1H), 8.01 (s, 1H), 7.97 (d, *J* = 8.1 Hz, 1H), 7.64 (d, *J* = 8.3 Hz, 1H), 6.66 (s, 1H).

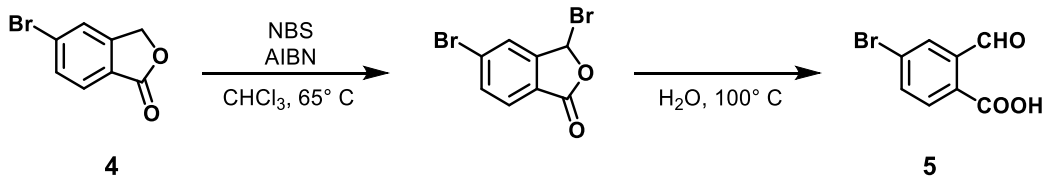

4 **5**

Synthesis of 4-bromo-2-formylbenzoic acid, 5:

4 (1.50 g, 7.04 mmol) was stirred in $CHCl_3$ (40 mL) with *N*-bromosuccinimide (1.38 g, 7.75 mmol) and AIBN (86 mg, 0.35 mmol) at reflux for 8 h, after which a second portion of *N*-bromosuccinimide (1.38 g, 7.75 mmol) and AIBN (86 mg, 0.35 mmol) was added. The reaction was stirred for a further 16 h, after which the bromination was deemed complete by NMR analysis of the crude reaction mixture. The precipitated solid was filtered off and the filtrate concentrated *in vacuo*. Water (75 mL) was added to the resulting solid and refluxed for 2 h. The resulting white solid was collected by vacuum filtration and washed with water (50 mL) and hexanes (25 mL), affording **5** as a white solid (1.27 g, 5.55 mmol, 79%). ^{1}H NMR (400 MHz, DMSO-d_6) δ 8.29 (s, 1H), 7.93 (d, *J* = 1.6 Hz, 1H), 7.86 (dd, *J* = 8.1, 1.7 Hz, 1H), 7.76 (d, *J* = 8.1 Hz, 1H), 6.65 (s, 1H).

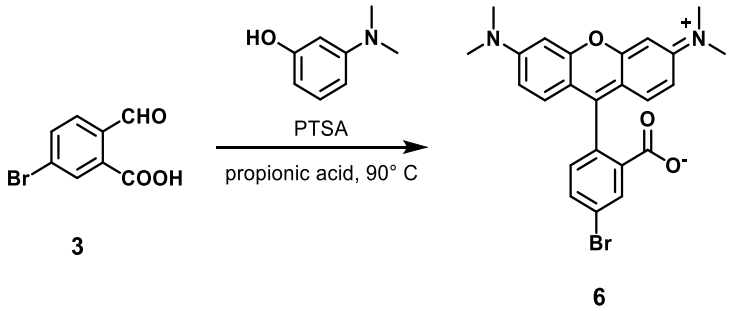

3 **6**

Synthesis of 4'-Br-TMR, 6:

3 (229 mg, 1.00 mmol), 3-dimethylaminophenol (288 mg, 2.01 mmol) and PTSA (35 mg, 0.2 mmol) were stirred in propionic acid (4 mL) at 90 °C for 18 h. The mixture was cooled to 22 °C, then the solvent removed *in vacuo*. The resulting crude residue was purified by flash chromatography (5-10% methanol in DCM, linear gradient), affording **6** as a purple solid (163 mg, 0.350 mmol, 35%). ^{1}H NMR (600 MHz, $CDCl_3$) δ 8.15 (s, 1H), 7.73 (d, *J* = 8.4 Hz, 1H), 7.05 (d, *J* = 8.1 Hz, 1H), 6.64 (d, *J* = 8.6 Hz, 2H), 6.49 (s, 2H), 6.43 (d, *J* = 8.0 Hz, 2H), 3.00 (s, 12H); Analytical HPLC retention time 9.67 min; MS (ESI) Exact mass calcd for $C_{24}H_{22}{}^{79}BrN_2O_3^+$ $[M+H]^+$: 465.1, found: 464.9; HR-ESI-MS m/z for $C_{24}H_{22}{}^{79}BrN_2O_3^+$ calcd: 465.0808 found: 465.0806.

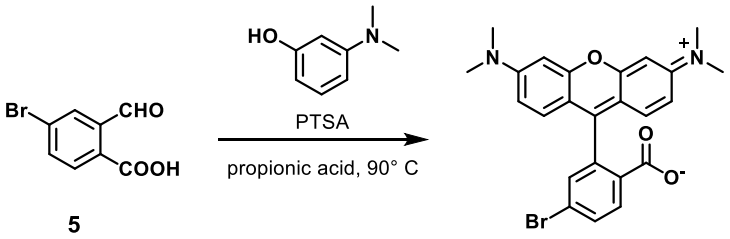

5 **7**

Synthesis of 5'-Br-TMR, 7:

5 (229 mg, 1.00 mmol), 3-dimethylaminophenol (288 mg, 2.01 mmol) and PTSA (35 mg, 0.2 mmol) were stirred in propionic acid (4 mL) at 90 °C for 18 h. The mixture was cooled to 22 °C, then the solvent removed *in vacuo*. The resulting crude residue was purified by flash chromatography (5-10% methanol in DCM, linear gradient), affording **7** as a purple solid (267 mg, 0.574 mmol, 57%). ^{1}H NMR (600 MHz, $CDCl_3$) δ 7.85 (d, *J* = 8.2 Hz, 1H), 7.70 (d, *J* = 8.1 Hz, 1H), 7.32 (s, 1H), 6.62 (d, *J* = 8.8 Hz, 2H), 6.48 (d, *J* = 2.7 Hz, 2H), 6.42 (dd, *J* = 8.9, 2.7 Hz, 2H), 2.99 (s, 12H); Analytical HPLC: retention time 9.97 min; MS (ESI) Exact mass calcd for $C_{24}H_{22}{}^{79}BrN_2O_3^+$ $[M+H]^+$: 465.1, found: 465.2; HR-ESI-MS m/z for $C_{24}H_{22}{}^{79}BrN_2O_3^+$ calcd: 465.0808 found: 465.0807.

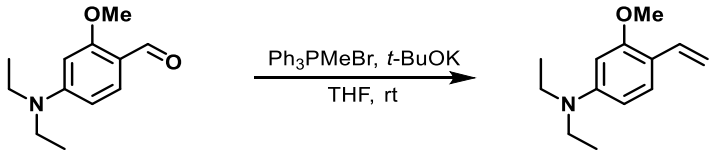

22 **23**

Synthesis of 3-methoxy-N,N-diethyl-4-vinylaniline, 23:

A round-bottom flask was charged with methyltriphenylpohsphonium bromide (1.04 g, 5 mmol) and then evacuated/backfilled with nitrogen (3x). Anhydrous THF (25 mL) was added and the reaction stirred for 15 min, then 1 M potassium *tert*-butoxide (in THF, 10.5 mL, 10.5 mmol) was added via syringe. After stirring for another 15 min, **22** was added and the reaction stirred at 22 °C for 18 h. The solvent was then removed *in vacuo* and the remaining crude material taken up in hexanes and filtered through an alumina plug, washing with hexanes. The combined organics were dried with anhydrous magnesium sulfate and the solvent removed *in vacuo*, affording **23** as a pale yellow oil (927 mg, 4.51 mmol, 90%). ^{1}H NMR (300 MHz, $CDCl_3$) δ 7.33 (d, *J* = 8.6 Hz, 1H), 6.93 (dd, *J* = 17.7, 11.1 Hz, 1H), 6.28 (dd, *J* = 8.6, 2.5 Hz, 1H), 6.17 (d, *J* = 2.4 Hz, 1H), 5.53 (dd, *J* = 17.7, 1.8 Hz, 1H), 5.01 (dd, *J* = 11.1, 1.8 Hz, 1H), 3.84 (s, 3H), 3.37 (q, *J* = 7.1 Hz, 4H), 1.18

(t, J = 7.1 Hz, 6H); Analytical HPLC retention time 8.54 min; HR-ESI-MS m/z for $C_{13}H_{20}NO^+$ calcd: 206.1539 found: 206.1539.

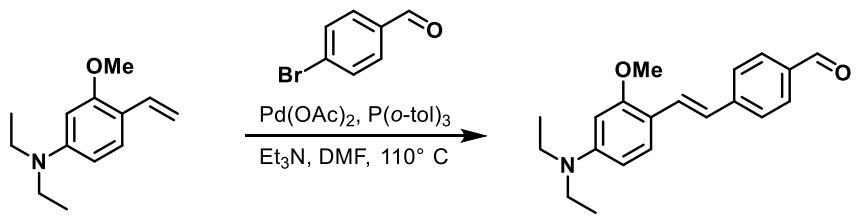

23 **24**

Synthesis of (E)-4-(4-(diethylamino)-2-methoxystyryl)benzaldehyde, 24:
A Schlenk flask was charged with **23** (822 mg, 4.00 mmol), bromobenzaldehyde (815 mg, 4.40 mmol), $Pd(OAc)_2$ (9 mg, 0.04 mmol), and $P(o\text{-tol})_3$ (37 mg, 0.12 mmol). The flask was sealed and evacuated/backfilled with nitrogen (3x). Anhydrous DMF (8 mL) and anhydrous triethylamine (8 mL) were added via syringe and the reaction stirred at 110 °C for 18 h. The reaction was cooled and the solvent removed *in vacuo*. The remaining residue was purified by flash chromatography (0-20% ethyl acetate in hexanes, linear gradient) affording **24** as an orange oil (698 mg, 2.26 mmol, 53%). ^{1}H NMR (300 MHz, $CDCl_3$) δ 9.93 (s, 1H), 7.80 (d, J = 8.3 Hz, 2H), 7.63 – 7.420 (m, 4H), 6.95 (d, J = 16.4 Hz, 1H), 6.31 (dd, J = 8.8, 2.5 Hz, 1H), 6.17 (d, J = 2.4 Hz, 1H), 3.89 (s, 3H), 3.40 (q, J = 7.0 Hz, 4H), 1.20 (t, J = 7.1 Hz, 6H); Analytical HPLC retention time 11.16 min; HR-ESI-MS m/z for $C_{20}H_{24}NO_2^+$ calcd: 310.1802 found: 310.1801.

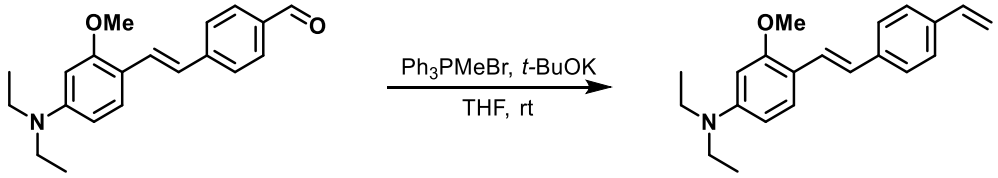

24 **9**

Synthesis of (E)-N,N-diethyl-3-methoxy-4-(4-vinylstyryl)aniline, 9:
A round-bottom flask was charged with methyltriphenylpohsphonium bromide (643 mg, 1.80 mmol) and then evacuated/backfilled with nitrogen (3x). Anhydrous THF (5 mL) was added and the reaction stirred for 15 min, then 1 M potassium *tert*-butoxide (in THF, 2.4 mL, 2.4 mmol) was added via syringe. After stirring for another 15 min, **24** (371 mg, 1.20 mmol) was added and the reaction stirred for 5 h. The reaction was diluted with hexanes, then the solids removed by vacuum filtration, rinsing with hexanes. The organics were concentrated *in vacuo* and the remaining oil was purified by flash chromatography (10% ethyl acetate in hexanes, isocratic) affording **9** as a yellow solid (305 mg, 0.992 mmol, 83%). ^{1}H NMR (400 MHz, $CDCl_3$) δ 7.50 – 7.32 (m, 6H), 6.91 (d, J = 16.4 Hz, 1H), 6.70 (dd, J = 17.6, 10.9 Hz, 1H), 6.31 (dd, J = 8.6, 2.4 Hz, 1H), 6.19 (d, J = 2.4 Hz, 1H), 5.72 (dd, J = 17.6, 1.2 Hz, 1H), 5.19 (dd, J = 10.8, 1.2 Hz, 1H), 3.88 (s, 3H), 3.39 (q, J = 7.1 Hz, 4H), 1.20 (t, J = 7.0 Hz, 6H); Analytical HPLC retention time 13.40 min; HR-ESI-MS m/z for $C_{21}H_{20}NO^+$ calcd: 308.2009 found: 308.2007.

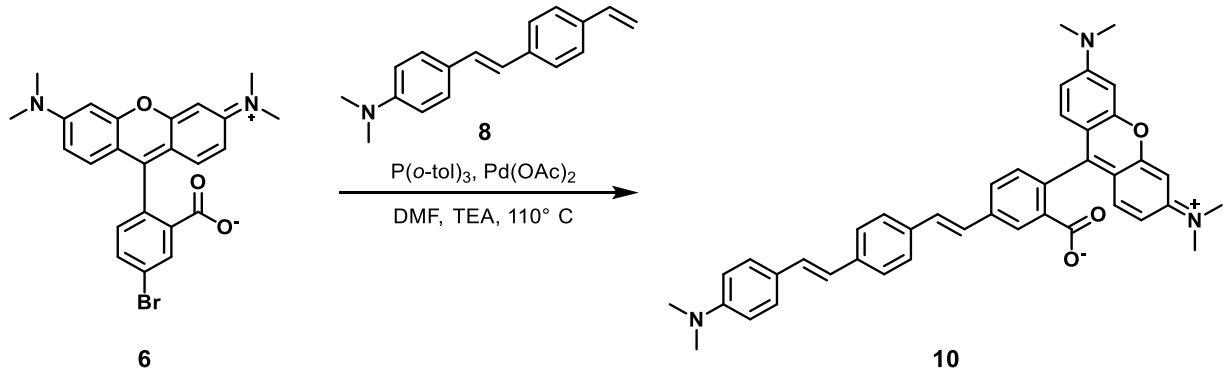

6 10

Synthesis of 10:

A Schlenk flask was charged with **6** (100 mg, 214 μmol), **8** (59.0 mg, 236 μmol), $Pd(OAc)_2$ (0.5 mg, 22 μmol) and P(*o*-tol)$_3$ (1.3 mg, 43 μmol). The flask was sealed and evacuated/backfilled with nitrogen (3x). Anhydrous DMF (3 mL) and anhydrous triethylamine (1.5 mL) were added via syringe and the reaction stirred at 110 °C for 18 h. The reaction was cooled and the solvent removed *in vacuo*. The remaining residue was purified by flash chromatography (5-10% methanol in DCM, linear gradient) affording **10** as a purple solid (65.0 mg, 103 μmol, 48%). ^{1}H NMR (900 MHz, DMSO-d_6) δ 8.17 (s, 1H), 7.99 (d, *J* = 8.0 Hz, 1H), 7.60 (dd, *J* = 55.9, 7.9 Hz, 4H), 7.52 – 7.42 (m, 4H), 7.24 – 7.17 (m, 2H), 7.00 (d, *J* = 16.3 Hz, 1H), 6.73 (d, *J* = 8.3 Hz, 2H), 6.56 (d, *J*= 8.8 Hz, 2H), 6.51 (s, 4H) 2.94 (m, 18H); Analytical HPLC retention time 13.88 min; MS (ESI) Exact mass calcd for $C_{42}H_{41}N_3O_3^+$ $[M+2H]^{2+}$: 317.7, found: 318.3; HR-ESI-MS m/z for $C_{42}H_{40}N_3O_3^+$ calcd: 634.3064 found: 634.3060.

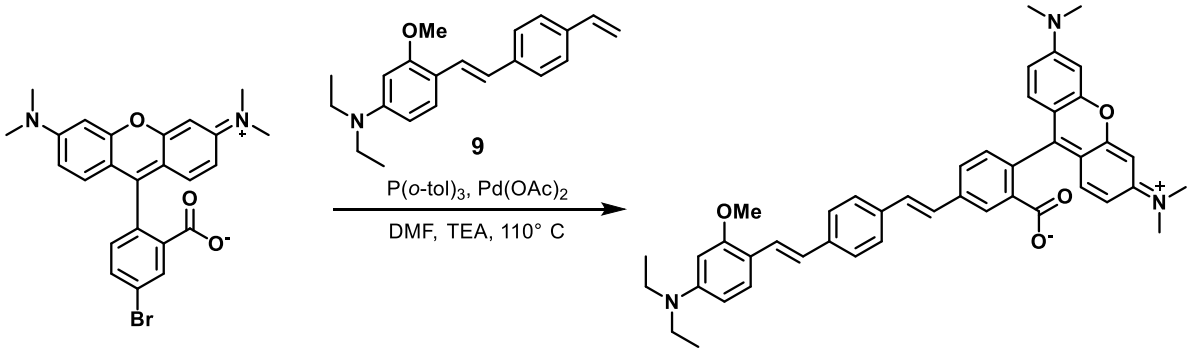

6 11

Synthesis of 11:

A Schlenk flask was charged with **6** (100 mg, 214 μmol), **9** (73.0 mg, 236 μmol), $Pd(OAc)_2$ (0.5 mg, 22 μmol) and P(*o*-tol)$_3$ (1.3 mg, 43 μmol). The flask was sealed and evacuated/backfilled with nitrogen (3x). Anhydrous DMF (3 mL) and anhydrous triethylamine (1.5 mL) were added via syringe and the reaction stirred at 110 °C for 18 h. The reaction was cooled and the solvent removed *in vacuo*. The remaining residue was purified by flash chromatography (5-10% methanol in DCM, linear gradient) affording **11** as a purple solid (62 mg, 89 μmol, 41%). ^{1}H NMR (400 MHz, $CDCl_3$) δ 8.11 (d, *J* = 1.6 Hz, 1H), 7.75 (dd, *J* = 8.0, 1.6 Hz, 1H), 7.51 (s, 4H), 7.47 (d, *J* = 4.0 Hz, 1H), 7.44 (d, *J* = 11.8 Hz, 1H), 7.21 (d, *J* = 12.1 Hz, 2H), 7.14 (d, *J* = 8.1 Hz, 1H), 6.94 (d, *J* = 16.4 Hz, 1H), 6.66 (d, *J* = 8.8 Hz, 2H), 6.49 (d, *J* = 2.6 Hz, 2H), 6.40 (dd, *J* = 8.9, 2.6 Hz, 2H), 6.32 (dd, *J* = 8.7, 2.4 Hz, 1H), 6.20 (d, *J* = 2.4 Hz, 1H), 3.89 (s, 3H), 3.40 (q, *J* = 7.0 Hz, 4H), 2.98 (s, 12H), 1.20 (t, *J* = 7.1 Hz, 6H); Analytical HPLC retention time 12.96 min; Exact mass

calcd for $C_{45}H_{46}N_3O_4^+$ $[M+H]^+$: 692.3, found: 692.5; HR-ESI-MS m/z for $C_{45}H_{46}N_3O_4^+$ calcd: 692.3488 found: 692.3470.

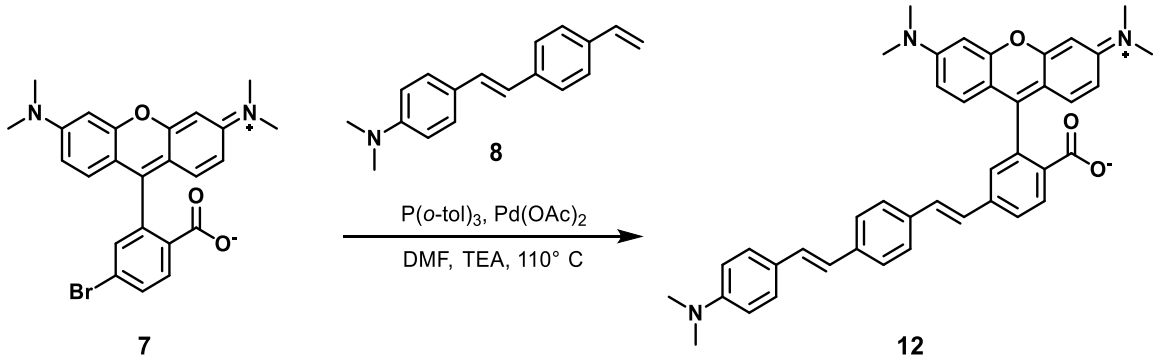

Synthesis of 12:

A Schlenk flask was charged with **7** (100 mg, 214 μmol), **8** (59.0 mg, 236 μmol), $Pd(OAc)_2$ (0.5 mg, 22 μmol) and P(*o*-tol)$_3$ (1.3 mg, 43 μmol). The flask was sealed and evacuated/backfilled with nitrogen (3x). Anhydrous DMF (3 mL) and triethylamine (1.5 mL) were added via syringe and the reaction stirred at 110 °C for 18 h. The reaction was cooled and the solvent removed *in vacuo*. The remaining residue was purified by flash chromatography (5-10% methanol in DCM, linear gradient) affording **12** as a purple solid (91.2 mg, 144 μmol, 67%). ^{1}H NMR (400 MHz, $CDCl_3$) δ 7.75 (d, *J* = 8.0 Hz, 1H), 7.52 (d, *J* = 8.0 Hz, 1H), 7.21 (s, 4H), 7.16 (d, *J* = 8.5 Hz, 2H), 7.07 (s, 1H), 6.87 (m, 3H), 6.65 (d, *J* = 16.3 Hz, 1H), 6.48 (dd, *J* = 12.7, 8.7 Hz, 4H), 6.32 – 6.21 (m, 4H), 2.80 (s, 12H), 2.75 (s, 6H); Analytical HPLC retention time 13.54 min; MS (ESI) Exact mass calcd for $C_{42}H_{40}N_3O_3^+$ $[M+H]^+$: 634.3, found: 634.4; HR-ESI-MS m/z for $C_{42}H_{40}N_3O_3^+$ calcd: 634.3064 found: 634.3055.

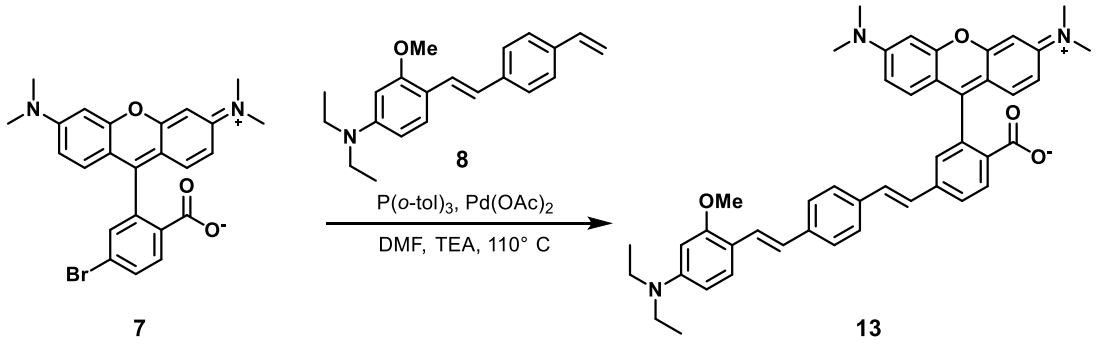

Synthesis of 13:

A Schlenk flask was charged with **7** (100 mg, 214 μmol), **8** (73.0 mg, 236 μmol), $Pd(OAc)_2$ (0.5 mg, 22 μmol) and P(*o*-tol)$_3$ (1.3 mg, 43 μmol). The flask was sealed and evacuated/backfilled with nitrogen (3x). Anhydrous DMF (3 mL) and anhydrous triethylamine (1.5 mL) were added via syringe and the reaction stirred at 110 °C for 18 h. The reaction was cooled and the solvent removed *in vacuo*. The remaining residue was purified by flash chromatography (5-10% methanol in DCM, linear gradient) affording **13** as a purple solid (75 mg, 110 μmol, 47%). ^{1}H NMR (600 MHz, DMSO-d_6) δ 7.91 (dd, *J* =18.1, 8.3 Hz, 2H), 7.53 (d, *J* = 8.3 Hz, 2H), 7.46 – 7.38 (m, 5H), 7.32 (dd, *J* = 16.4, 6.8 Hz, 2H), 6.92 (d, *J* = 16.4 Hz, 1H), 6.60 – 6.48 (m, 6H), 6.28 (dd, *J* = 8.8, 2.4 Hz, 1H), 6.20 (d, *J* = 2.4 Hz, 1H), 3.83 (s, 3H), 3.37 (q, *J* = 6.9 Hz, 4H), 2.94 (s, 12H), 1.12

(d, J = 7.0 Hz, 6H); Analytical HPLC retention time 12.16 min; Exact mass calcd for $C_{45}H_{46}N_3O_4^+$ $[M+H]^+$: 692.3, found: 692.4; HR-ESI-MS m/z for $C_{45}H_{46}N_3O_4^+$ calcd: 692.3483 found: 692.3479.

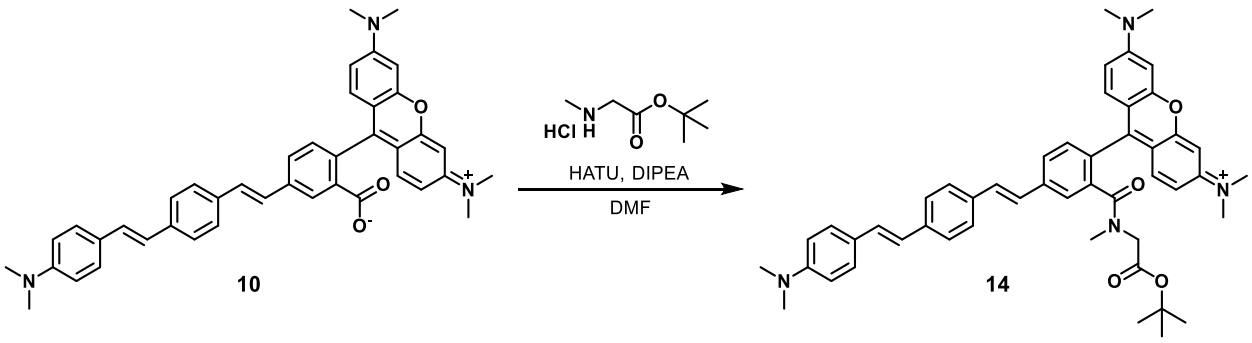

Synthesis of 14:

A vial was charged with **10** (14.0 mg, 22.1 μmol), N-methyl sarcosine *t*-Bu ester hydrochloride (5.0 mg, 28 μmol), and HATU (8.4 mg, 22 μmol). The vial was sealed and evacuated/backfilled with nitrogen (3x). Anhydrous DMF (2 mL) and anhydrous diisopropylethylamine (5.8 μL, 28 μmol) were added and the vial flushed with nitrogen, sealed, and stirred at 22 °C for 18 h. The solvent was removed *in vacuo* and the remaining residue was purified by flash chromatography (2.5% methanol in DCM) affording **14** as a purple solid (13.5 mg, 17.7 μmol, 80%). ^{1}H NMR (only major rotamer peaks reported, 600 MHz, $CDCl_3$) δ 7.78 (dd, J = 7.9, 1.6 Hz, 1H), 7.73 (d, J = 1.6 Hz, 1H), 7.53 (q, J = 8.3 Hz, 4H), 7.50 (s, 1H), 7.44 (d, J = 8.7 Hz, 2H), 7.37 (m, 3H), 7.29 (d, J = 16.2 Hz, 1H), 7.19 (d, J = 16.3 Hz, 1H), 7.11 (d, J = 16.2 Hz, 1H), 6.95 – 6.92 (m, 3H), 6.80 (d, J = 2.6 Hz, 2H), 6.73 (d, J = 8.7 Hz, 2H), 3.78 (s, 2H), 3.30 (s, 12H), 3.00 (s, 6H), 2.80 (s, 3H), 1.33 (s, 9H); Analytical HPLC retention time 14.83 min; HR-ESI-MS m/z for $C_{49}H_{53}N_4O_4^+$ calcd: 761.4061 found: 761.4055.

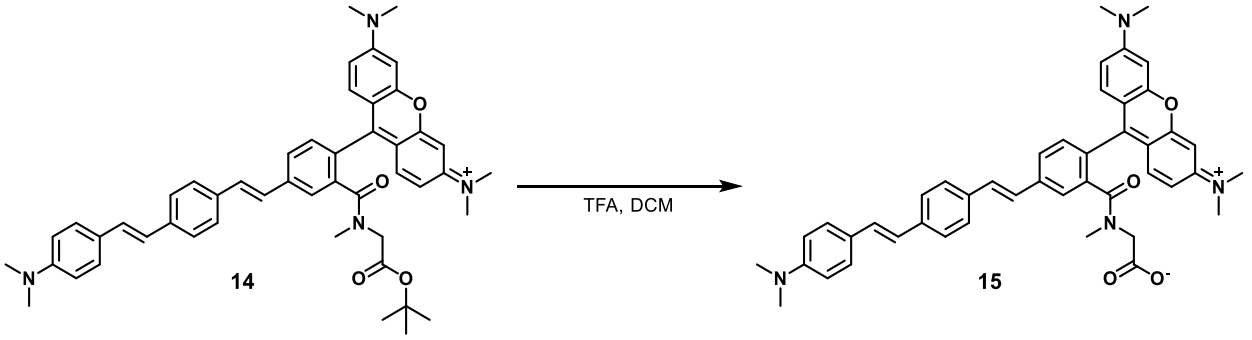

Synthesis of 15:

To a solution of **14** (7.0 mg, 9.2 μmol) in DCM (1 mL) was added trifluoroacetic acid (1 mL). The reaction was stirred at 22 °C for 1 h, then the solvent removed under a stream of nitrogen. The remaining crude solid was purified by semi-preparative HPLC, affording **15** as a purple solid (1.5 mg, 2.1 μmol, 23%). Analytical HPLC retention time 12.83 min; HR-ESI-MS m/z for $C_{45}H_{45}N_4O_4^+$ calcd: 705.3435 found: 705.3441.

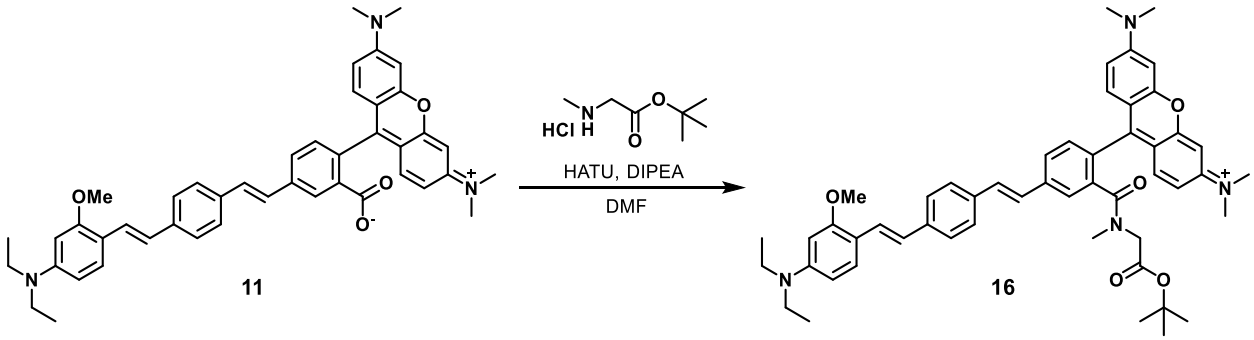

Synthesis of 16:

A vial was charged with **11** (20.0 mg, 28.9 μmol), N-methyl sarcosine *t*-Bu ester hydrochloride (6.0 mg, 33 μmol), and HATU (11.0 mg, 28.9 μmol). The vial was sealed and evacuated/backfilled with nitrogen (3x). Anhydrous DMF (4 mL) and anhydrous diisopropylethylamine (5.0 μL, 29 μmol) were added and the vial flushed with nitrogen, sealed, and stirred at 22 °C for 18 h. The solvent was removed *in vacuo* and the remaining residue was purified by flash chromatography (2.5% methanol in DCM) affording **16** as a purple solid (21.4 mg, 26.1 μmol, 91%). LC-MS showed this material to be approximately 95% pure. This material was used without further purification for further reactions. ^{1}H NMR (only major rotamer peaks reported, 600 MHz, $CDCl_3$) δ 7.77 (dd, *J* = 8.0, 1.7 Hz, 1H), 7.71 (d, *J* = 1.8 Hz, 1H), 7.51 (s, 4H), 7.47 – 7.43 (m, 2H), 7.36 (d, *J* = 9.7 Hz, 3H), 7.28 (d, *J* = 7.5 Hz, 1H), 7.17 (d, *J* = 16.2 Hz, 1H), 6.95 – 6.91 (m, 3H), 6.78 (d, *J* = 2.6 Hz, 2H), 6.32 (dd, *J* = 8.7, 2.4 Hz, 1H), 6.20 (d, *J* = 2.5 Hz, 1H), 3.90 (s, 3H), 3.78 (s, 2H), 3.40 (q, *J* = 7.1 Hz, 4H), 3.29 (s, 12H), 2.80 (s, 3H), 1.33 (s, 9H), 1.21 (t, *J* = 7.0 Hz, 6H); Analytical HPLC retention time 13.61 min; HR-ESI-MS m/z for $C_{52}H_{59}N_4O_5^+$ calcd: 819.4485 found: 819.4490.

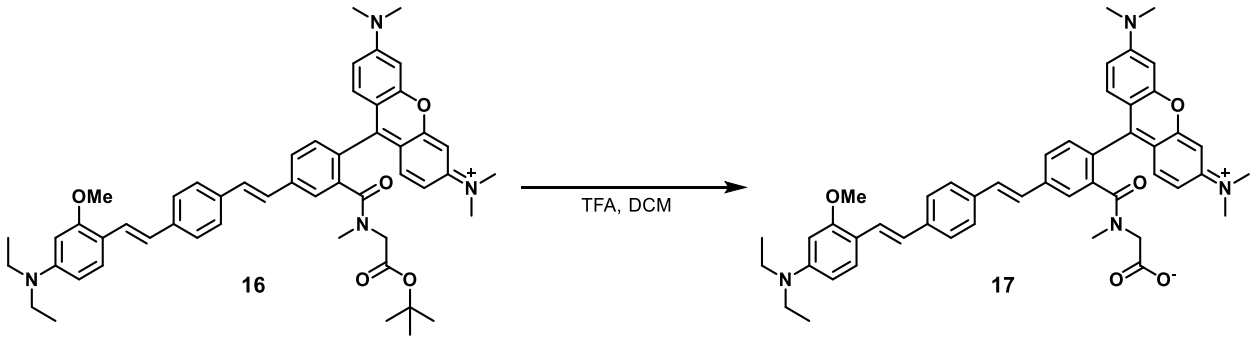

Synthesis 17:

To a solution of **16** (7.0 mg, 8.5 μmol) in DCM (1 mL) was added trifluoroacetic acid (1 mL). The reaction was stirred at 22 °C for 1 h, then the solvent removed under a stream of nitrogen. The remaining crude solid was purified by semi-preparative HPLC, affording **17** as a purple solid (1.2 mg, 1.6 μmol, 18%). Analytical HPLC retention time 11.65 min; HR-ESI-MS m/z for $C_{48}H_{51}N_4O_5^+$ calcd: 763.3859 found: 763.3849.

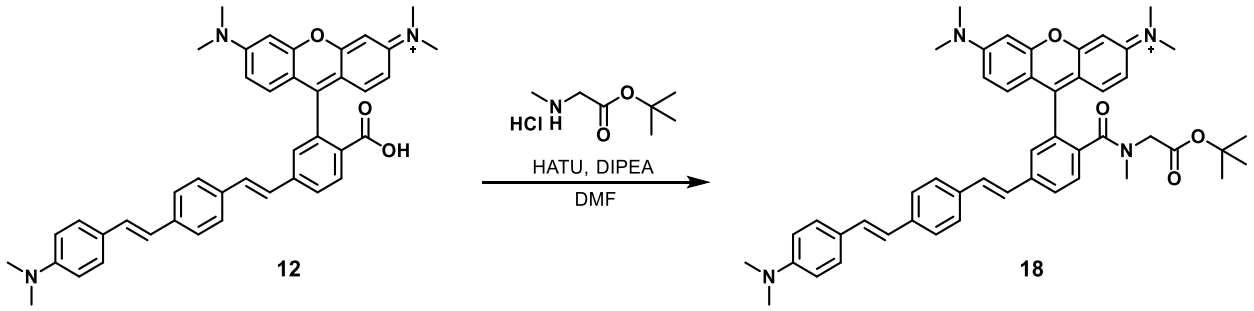

Synthesis of 18:

A vial was charged with **12** (53.0 mg, 83.5 μmol), N-methyl sarcosine *t*-Bu ester hydrochloride (16.7 mg, 91.8 μmol), and HATU (31.8 mg, 83.5 μmol). The vial was sealed and evacuated/backfilled with nitrogen (3x). Anhydrous DMF (4 mL) and anhydrous diisopropylethylamine (15.0 μL, 86 μmol) were added and the vial flushed with nitrogen, sealed, and stirred at 22 °C for 18 h. The solvent was removed *in vacuo* and the remaining residue was purified by flash chromatography (2.5% methanol in DCM) affording **18** as a purple solid (46.0 mg, 60.4 μmol, 72%). LCMS showed this material to be approximately 95% pure. This material was used without further purification for further reactions. ^{1}H NMR (only major rotamer peaks reported, 600 MHz, $CDCl_3$) δ 7.77 (d, *J* = 8.2 Hz, 1H), 7.60 (d, *J* = 8.0 Hz, 1H), 7.46 (m, 5H), 7.41 (d, *J* = 8.3 Hz, 2H), 7.33 (d, *J* = 9.5 Hz, 2H), 7.23 – 7.11 (m, 2H), 7.06 (d, *J* = 16.2 Hz, 1H), 6.93 (dd, *J* = 9.7, 2.5 Hz, 2H), 6.88 (d, *J* = 16.2 Hz, 1H), 6.77 (d, *J* = 2.5 Hz, 2H), 6.71 (d, *J* = 8.6 Hz, 2H), 3.78 (s, 2H), 3.29 (s, 12H), 2.99 (s, 6H), 2.86 (s, 3H), 1.32 (s, 9H), 1.25 (s, 3H); Analytical HPLC retention time 14.51 min; HR-ESI-MS m/z for $C_{49}H_{53}N_4O_4^+$ calcd: 761.4061 found: 761.4051.

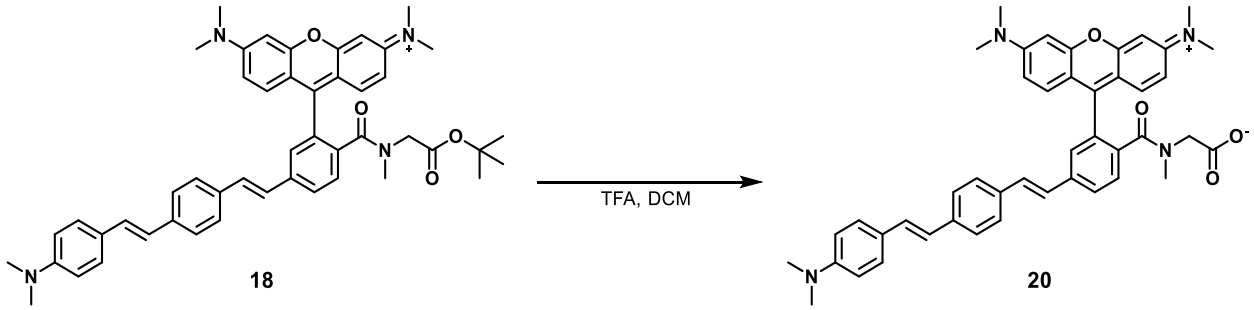

Synthesis of 20:

To a solution of **18** (7.5 mg, 9.9 μmol) in DCM (1 mL) was added trifluoroacetic acid (1 mL). The reaction was stirred at 22 °C for 1 h, then the solvent removed under a stream of nitrogen. The remaining crude solid was purified by semi-preparative HPLC affording **20** as a purple solid (1.5 mg, 2.1 μmol, 21%). Analytical HPLC retention time 12.48 min; HR-ESI-MS m/z for $C_{44}H_{41}N_4O_4^+$ calcd: 705.3435 found: 705.3431.

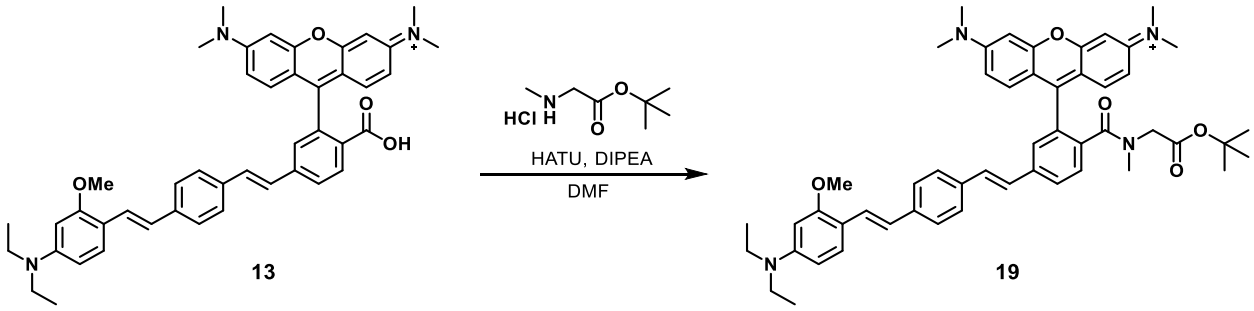

Synthesis of RhoVR 1 N-methyl sarcosine *t*-Bu ester, 19:

A vial was charged with **13** (35 mg, 51 μmol), N-methyl sarcosine *t*-Bu ester hydrochloride (14 mg, 77 μmol), and HATU (20 mg, 53 μmol). The vial was sealed and evacuated/backfilled with nitrogen (3x). Anhydrous DMF (2 mL) and anhydrous diisopropylethylamine (16 μL, 76 μmol) were added and the vial flushed with nitrogen, sealed, and stirred at 22 °C for 18 h. The solvent was removed *in vacuo* and the remaining residue was purified by flash chromatography (2.5% methanol in DCM) affording **19** as a purple solid (29 mg, 35.4 μmol, 70%). ^{1}H NMR (only major rotamer peaks reported, 600 MHz, DMSO-d_6) δ 7.96 (d, J = 8.2 Hz, 1H), 7.79 (s, 1H), 7.62 (d, J = 8.0 Hz, 1H), 7.56 (d, J = 8.0 Hz, 2H), 7.52 – 7.41 (m, 4H), 7.40 – 7.24 (m, 4H), 7.12 (dd, J = 9.8, 2.6 Hz, 2H), 7.00 – 6.89 (m, 3H), 6.29 (d, J = 10.3 Hz, 1H), 6.21 (s, 1H), 3.84 (s, 3H), 3.76 (s, 2H), 3.38 (q, J = 7.0 Hz, 4H), 3.33 (s, 12H), 2.81 (s, 3H), 1.25 (s, 9H), 1.12 (t, J = 7.0 Hz, 6H); Analytical HPLC retention time 13.40 min; HR-ESI-MS m/z for $C_{52}H_{59}N_4O_5^+$ calcd: 819.4480 found: 819.4484.

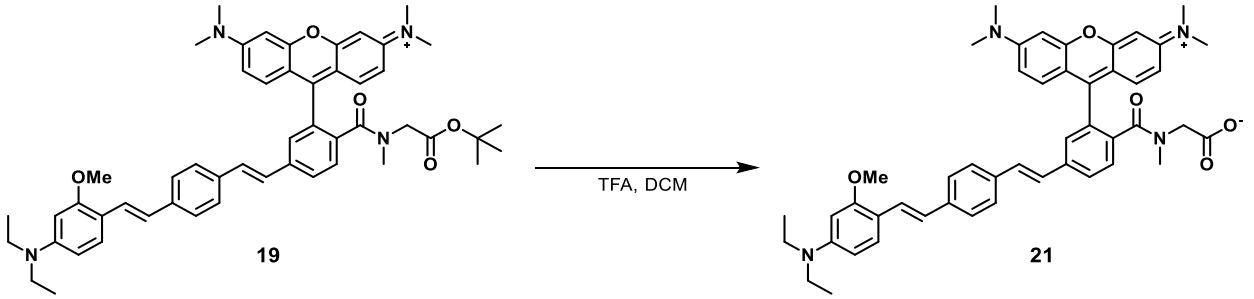

Synthesis of RhoVR 1, 21:

To a solution of **19** (16.4 mg, 20.0 μmol) in DCM (1 mL) was added trifluoroacetic acid (1 mL). The reaction was stirred at 22 °C for 1 h, then the solvent removed under a stream of nitrogen. The remaining crude solid was purified by semi-preparative HPLC affording **21** as a purple solid (1.6 mg, 2.1 μmol, 10%). Analytical HPLC retention time 11.52 min; HR-ESI-MS m/z for $C_{52}H_{59}N_4O_5^+$ calcd: 763.3854 found: 763.3856.

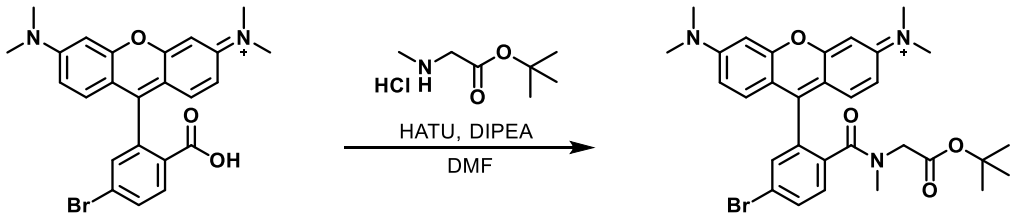

7 22

Synthesis of 22:

A vial was charged with **7** (20.0 mg, 42.9 μmol), N-methyl sarcosine *t*-Bu ester hydrochloride (9.7 mg, 54 μmol), and HATU (16.3 mg, 42.9 μmol). The vial was sealed and evacuated/backfilled with nitrogen (3x). Anhydrous DMF (1 mL) and anhydrous diisopropylethylamine (12 μL, 57 μmol) were added and the vial flushed with nitrogen, sealed, and stirred at 22 °C for 18 h. The solvent was removed *in vacuo* and the remaining residue was purified by preparative TLC (5% methanol in DCM) affording **22** as a purple solid (16.0 mg, 27.0 μmol, 63%). LCMS showed this material to be approximately 98% pure. This material was used without further purification for further reactions. ^{1}H NMR (only major rotamer peaks reported, ^{1}H NMR (600 MHz, DMSO-d_6) δ 7.98 (dd, *J* = 8.3, 2.0 Hz, 1H), 7.86 (d, *J* = 2.0 Hz, 1H), 7.57 (d, *J* = 8.3 Hz, 1H), 7.23 (d, *J* = 9.5 Hz, 2H), 7.09 (dd, *J* = 9.6, 2.4 Hz, 2H), 6.93 (d, *J* = 2.5 Hz, 2H), 3.74 (s, 2H), 3.27 (s, 12H), 2.74 (s, 3H), 1.23 (s, 9H); Analytical HPLC retention time 13.56 min; HR-ESI-MS m/z for $C_{31}H_{35}N_3O_4{}^{79}Br_1{}^+$ calcd: 592.1805 found: 592.1797.

22 23

Synthesis of 23:

To a solution of **22** (10.0 mg, 16.9 μmol) in DCM (1 mL) was added trifluoroacetic acid (1 mL). The reaction was stirred at 22 °C for 2 h, then the solvent removed under a stream of nitrogen. The remaining crude solid was purified by preparative TLC (7.5% methanol in DCM) affording **23** as a purple solid (4.5 mg, 8.4 μmol, 50%). Analytical HPLC retention time 10.92 min; HR-ESI-MS m/z for $C_{27}H_{27}N_3O_4{}^{79}Br_1{}^+$ calcd: 536.1179 found: 536.1176.

Spectroscopic Studies

Stock solutions of RhoVRs were prepared in DMSO (1-5 mM) and diluted with PBS (10 mM KH_2PO_4, 30 mM $Na_2HPO_4 \cdot 7H_2O$, 1.55 M NaCl, pH 7.2) solution containing 0.10 % (w/w) SDS (1:100-1:1000 dilution). UV-Vis absorbance and fluorescence spectra were recorded using a Shimadzu 2501 Spectrophotometer (Shimadzu) and a Quantamaster Master 4 L-format scanning spectrofluorometer (Photon Technologies International). The fluorometer is equipped with an LPS-220B 75-W xenon lamp and power supply, A-1010B lamp housing with integrated igniter, switchable 814 photon-counting/analog photomultiplier detection unit, and MD5020 motor driver. Samples were measured in 1-cm path length quartz cuvettes (Starna Cells).

Quantum yields were measured according to the procedure outlined in **Appendix 4**.

Cell Culture

All animal procedures were approved by the UC Berkeley Animal Care and Use Committees and conformed to the NIH Guide for the Care and Use and Laboratory Animals and the Public Health Policy.

Human embryonic kidney 293T (HEK) cells were passaged and plated onto 12 mm glass coverslips pre-coated with Poly-D-Lysine (PDL; 1 mg/ml; Sigma-Aldrich) to provide a confluency of ~15% and 50% for electrophysiology and imaging, respectively. HEK cells were plated and maintained in Dulbecco's modified eagle medium (DMEM) supplemented with 4.5 g/L D-glucose, 10% FBS and 1% Glutamax. Transfection of genetic tools was carried out using Lipofectamine 3000 24 h after plating. Imaging was performed 18-24 h following transfection.

Hippocampi were dissected from embryonic day 18 Sprague Dawley rats (Charles River Laboratory) in cold sterile HBSS (zero Ca^{2+}, zero Mg^{2+}). All dissection products were supplied by Invitrogen, unless otherwise stated. Hippocampal tissue was treated with trypsin (2.5%) for 15 min at 37 °C. The tissue was triturated using fire polished Pasteur pipettes, in minimum essential media (MEM) supplemented with 5% fetal bovine serum (FBS; Thermo Scientific), 2% B-27, 2% 1M D-glucose (Fisher Scientific) and 1% glutamax. The dissociated cells were plated onto 12 mm diameter coverslips (Fisher Scientific) pre-treated with PDL (as above) at a density of 30-40,000 cells per coverslip in MEM supplemented media (as above). Neurons were maintained at 37 °C in a humidified incubator with 5 % CO_2. At 1 day in vitro (DIV) half of the MEM supplemented media was removed and replaced with Neurobasal media containing 2% B-27 supplement and 1% glutamax. Transfection of genetic tools was carried out using Lipofectamine 3000 at 7 DIV. Functional imaging was performed on mature neurons 13-20 DIV, except electrophysiological experiments which were performed on 12-15 DIV neurons. Unless stated otherwise, for loading of HEK cells and hippocampal neurons, RhoVRs were diluted in DMSO to 500 μM, and then diluted 1:1000 in HBSS. All imaging experiments were performed in HBS (in mM) 140 NaCl, 2.5 KCl, 10 HEPES, 10 D-glucose 1.3 $MgCl_2$ and 2 $CaCl_2$; pH 7.3 and 290 mOsmol.

DNA Constructs

GCaMP6s was a gift from Douglas Kim (Addgene plasmid # 40753) and was driven in mammalian cells by the cytomegalovirus promoter.

Imaging Parameters

Epifluorescence imaging was performed on an AxioExaminer Z-1 (Zeiss) equipped with a Spectra-X Light engine LED light (Lumencor), controlled with Slidebook (v6, Intelligent Imaging Innovations). Co-incident excitation with multiple LEDs was controlled by Lumencor software triggered through a Digidata 1332A digitizer and pCLAMP 10 software (Molecular Devices). Images were acquired with either a W-Plan-Apo 20x/1.0 water objective (20x; Zeiss) or a W-Plan-Apo 63x/1.0 water objective (63x; Zeiss). Images were focused onto either an OrcaFlash4.0 sCMOS camera (sCMOS; Hamamatsu) or an eVolve 128 EMCCD camera (EMCCD; Photometrix). More detailed imaging information for each experimental application is expanded below.

Confocal imaging was performed with a Zeiss LSM 880 NLO AxioExaminer equipped with a Diode 405 nm laser line, Argon 458, 488, and 514 laser lines, and a DPSS 561 nm laser line. Images were acquired using a W-Plan-Apo 40x/1.0 DIC objective and a Zeiss Airyscan detector.

Multicolor imaging of RhoVR 1 in HEK cells and photostability

EGFP transfected HEK cells were incubated with a HBSS solution (Gibco) containing RhoVR 1 (500 nM) at 37 °C for 20 min prior to transfer to fresh HBSS (no dye) for imaging. Microscopic images were acquired with a W-Plan-Apo 20x/1.0 water objective (Zeiss) and OrcaFlash4.0 sCMOS camera (Hamamatsu). For RhoVR 1 images, the excitation light was delivered from a LED (9.72 W/cm^2; 100 ms exposure time) at 542/33 (bandpass) nm and emission was collected with a quadruple emission filter (430/32, 508/14, 586/30, 708/98 nm) after passing through a quadruple dichroic mirror (432/38, 509/22, 586/40, 654 nm LP). For eGFP images, the excitation light was delivered from a LED (5.77 W/cm^2; 20 ms exposure time) at 475/34 nm and emission was collected with a quadruple emission filter (430/32, 508/14, 586/30, 708/98 nm) after passing through a quadruple dichroic mirror (432/38, 509/22, 586/40, 654 nm LP). For photostability experiments HEK cells were incubated separately with RhoVR 1 (500 nM) and VF2.1.Cl (500 nM) in HBSS at 37°C for 20 min and then the dye loading buffer was exchanged for fresh HBSS. Data were acquired with a W-Plan-Apo 63x/1.0 objective (Zeiss) and OracFlash4.0 sCMOS camera (Hamamatsu). Images (pixel size 0.38 μm × 0.38 μm) were taken every 3 sec for 10 min with constant illumination of LED (60 W/cm^2; 10 ms exposure time). For RhoVR images, the excitation light was delivered at 542/33 nm and emission was collected with a quadruple emission filter (430/32, 508/14, 586/30, 708/98 nm) after passing through a quadruple dichroic mirror (432/38, 509/22, 586/40, 654 nm LP). For VF2.1.Cl images, the excitation light was delivered at 475/34 nm and emission was collected with an emission filter (540/50 nm) after passing through a dichroic mirror (510 nm LP). The obtained fluorescence curves (background subtracted) were normalized with the fluorescence intensity at t = 0 and averaged (three different cells of each dye).

Voltage sensitivity in HEK cells

Functional imaging of the RhoVR voltage dyes was performed using a 20x objective paired with image capture from the EMCCD camera at a sampling rate of 0.5 kHz. RhoVRs were excited using the 542 nm LED with an intensity of 9.73 W/cm^2. For initial voltage characterization emission was collection with the QUAD filter and dichroic (see above).

Imaging groups of neurons

Imaging experiments looking at functional responses from many (>5) neurons (**Figure 1-4** and **Figure 1-9**) required a larger field of view which were obtained using the sCMOS camera with a 20x objective. RhoVR 1 was excited using the 542 nm LED with an intensity of 1.73-3.07 W/cm^2 and emission was collected with a QUAD filter and dichroic (see above). Images were binned 4x4 to allow sampling rates of 0.5 kHz. EGFP was excited by the 475 nm LED with an intensity of 0.82-1.20 W/cm^2 and emission was collected with the same QUAD filter and dichroic.

Dual-View imaging

Dual-view imaging was preformed using a 20x objective paired with the sCMOS camera. RhoVR 1 was excited using the 542 nm LED with a light intensity of 2.40-4.82 W/cm^2 while GCaMP6s was excited simultaneously using a 475 nm LED with a light intensity of 0.82-1.20 W/cm^2. Emission was collected with a QUAD filter and dichroic (see above) used in conjunction with a Dual-View emission splitter (Optical Insights). The Dual-View was equipped with a 585dcxr dichroic (Chroma) and 520/28 nm (Semrock) and 610/75 nm (Chroma) emission filters which separated the GCaMP6s and RhoVR 1 signals.

Cellular localization of rhodamines by confocal microscopy

EGFP transfected HEK cells were incubated with a HBSS solution (Gibco) containing 500 nM of either RhoVR 1, **12**, **18**, **7**, or **23** at 37°C for 20 min prior to transfer to fresh HBSS (no dye) for imaging. Rhodamine derivatives **7** and **23** were excited at 561 nm at 7% laser power while RhoVR 1, **12** and **18** were imaged at 11% laser power. Emission for all rhodamines was collected from 580-695 nm. EGFP was excited at 488 nm and the emission was collected from 500-560 nm.

Image Analysis

Analysis of voltage sensitivity in HEK cells was performed using ImageJ (FIJI). Briefly, a region of interest (ROI) was selected automatically based on fluorescence intensity and applied as a mask to all image frames. Fluorescence intensity values were calculated at known baseline and voltage step epochs. For analysis of RhoVR 1 voltage responses in neurons, regions of interest encompassing cell bodies (all of approximately the same size) were drawn in ImageJ and the mean fluorescence intensity for each frame extracted. ΔF/F values were calculated by first subtracting a mean background value from all raw fluorescence frames, bypassing the noise amplification which arises from subtracting background for each frame, to give a background subtracted trace (bkgsub). A baseline fluorescence value (F_{base}) is calculated either from the first several (10-20) frames of the experiment for evoked activity, or from the median for spontaneous activity, and was subtracted from each timepoint of the bkgsub trace to yield a ΔF trace. The ΔF was then divided by F_{base} to give ΔF/F traces. No averaging has been applied to any voltage traces.

Movies were created using FIJI according to the following protocol. In FIJI, a substack of the first 70 images were averaged to create a single baseline or "F" image. The full stack was then divided by this image to give a 32-bit floating decimal result, whose scale ranged from 0.92 and 1.18. The images were multiplied by 50,000 (56,000 for Ca image) to give an image that was within the 16-bit range. After this transformation, the scale was between approximately 46,000 and 59,000. The full 16-bit range was applied, a 3D Gaussian blur (1.0 pixels in x, y, and z dimensions) was applied, and the baseline/bleaching was corrected using the built-in ratio method. The images were converted to 8-bit .AVI files.

Analysis of cellular localization was performed in FIJI. Briefly, a line segment was drawn across the width of an eGFP transfected HEK cell and the normalized fluorescence intensity plotted against the normalized length of the line segment (0-100). The fluorescence of the interior of the cell was taken to be the average fluorescence from the rhodamine channel across the 20^{th}-80^{th} percentile of the line segment. The edge of the cell was then defined by the point at which the eGFP fluorescence fell below one half of the average fluorescence of the center of the cell. "Edge fluorescence" was then calculated by averaging the intensities of the line segment ± .2 microns from the cell edge in the rhodamine channel.

Electrophysiology

For electrophysiological experiments, pipettes were pulled from borosilicate glass (Sutter Instruments, BF150-86-10), with a resistance of 5–8 MΩ, and were filled with an internal solution; 115 mM potassium gluconate, 10 mM BAPTA tetrapotassium salt, 10 mM HEPES, 5 mM NaCl, 10 mM KCl, 2 mM ATP disodium salt, 0.3 mM GTP trisodium salt (pH 7.25, 275 mOsm). Recordings were obtained with an Axopatch 200B amplifier (Molecular Devices) at room temperature. The signals were digitized with Digidata 1440A, sampled at 50 kHz and recorded with pCLAMP 10 software (Molecular Devices) on a PC. Fast capacitance was compensated in the on-cell configuration. For all electrophysiology experiments, recordings were only pursued if series resistance in voltage clamp was less than 30 MΩ. For whole-cell, voltage clamp recordings in HEK 293T cells, cells were held at -60 mV and 100 ms hyper- and de- polarizing steps applied from -100 to +100 mV in 20 mV increments.

Figures and Schemes

Scheme 1-1: *Synthesis of 4'- and 5'-Br-TMR* ***6*** *and* ***7***

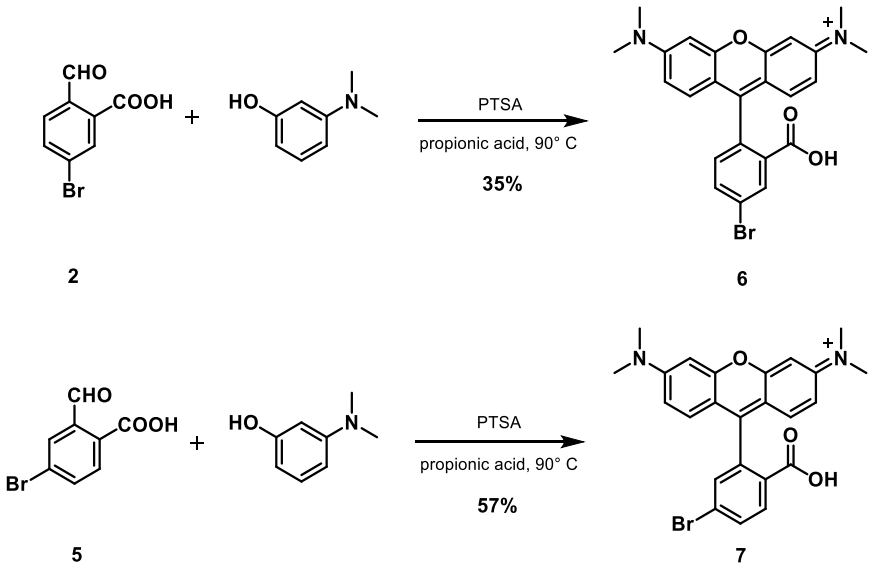

Scheme 1-1: Synthesis of 4'- and 5'-Br-TMR from 2-carboxybenzaldehydes.

Scheme 1-2: *Synthesis of 2-carboxybenzaldehydes* ***3*** *and* ***5***

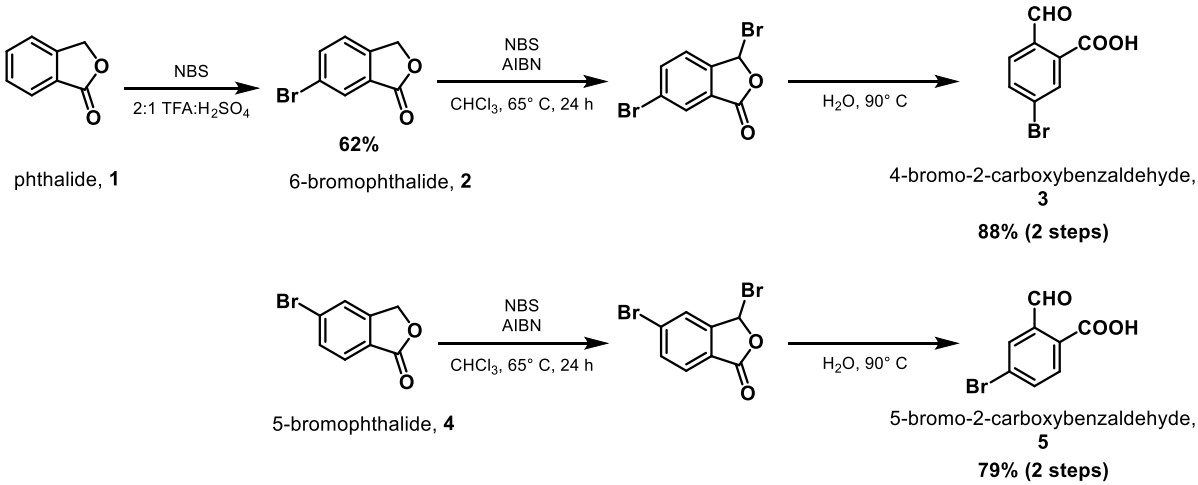

Scheme 1-2: Synthesis of 2-carboxybenzaldehydes.

Scheme 1-3: *Synthesis of isomerically pure rhodamine voltage sensors (RhoVRs)*

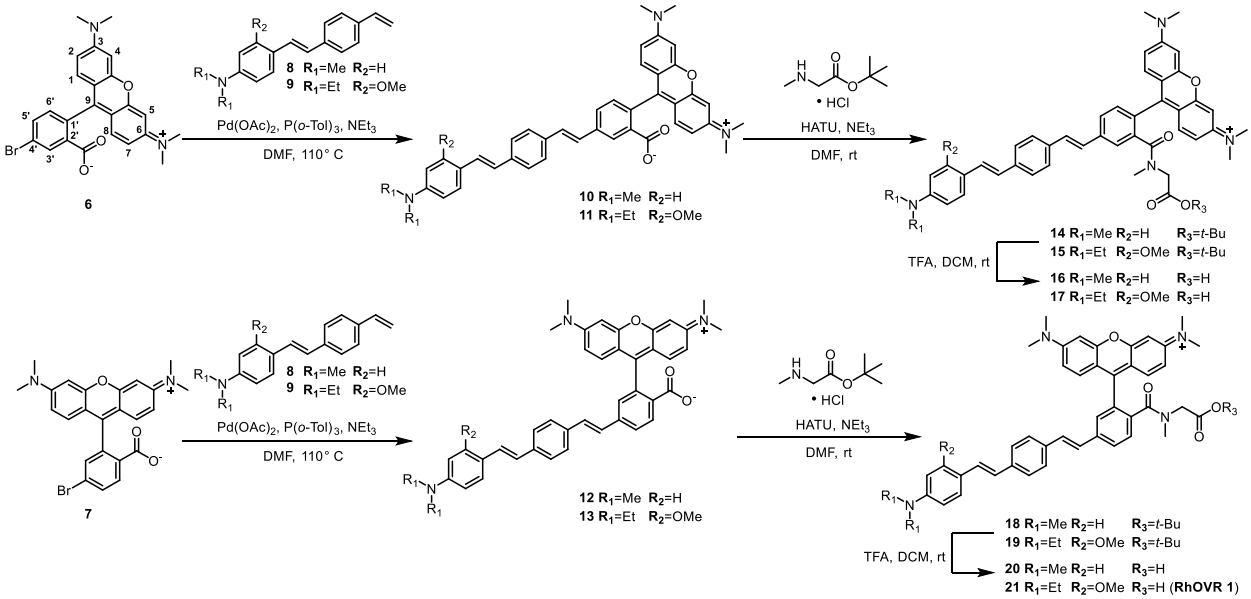

Scheme 1-3: Synthesis of isomerically pure rhodamine voltage sensors.

Scheme 1-4: *Synthesis of styrene 9*

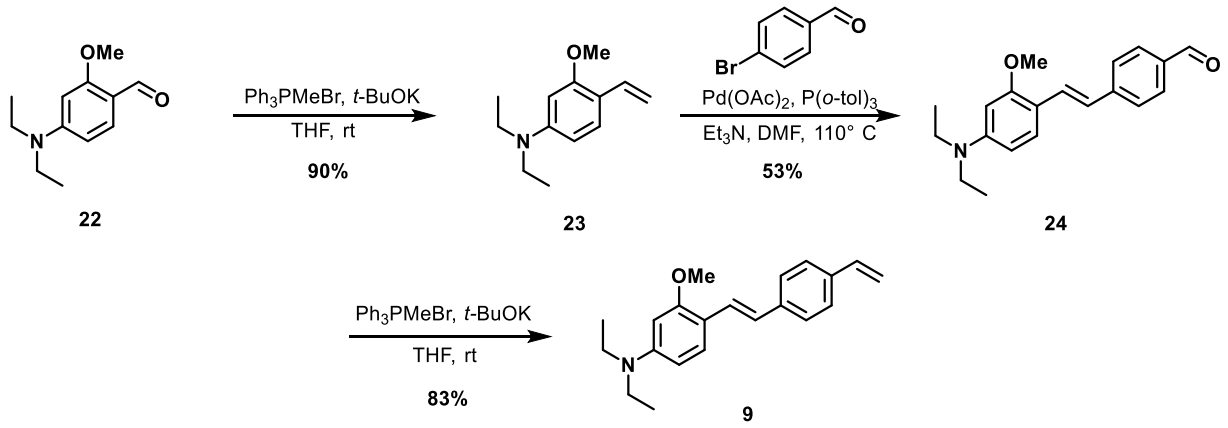

Scheme 1-4: Synthesis of styrene **9**.

Scheme 1-5: *Optical path for two-color voltage and Ca^{2+} imaging.*

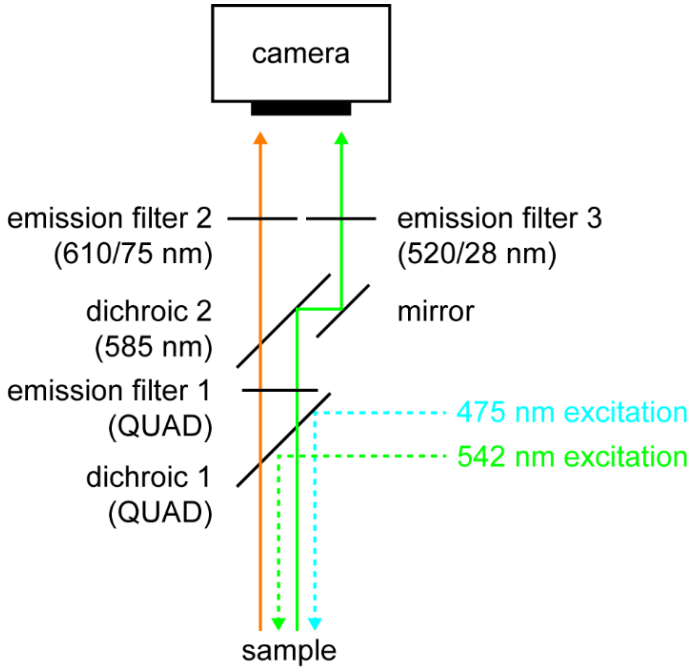

Scheme 1-5: Cyan excitation: 475/34. Green excitation: 542/33. Dichroic 1: "QUAD", 432/38, 509/22, 586/40, 654LP. Emission filter 1: 430/32, 508/14, 586/30, 708/98. Dichroic 2 (DualView): 585LP. Emission filter 2 (DualView): 610/75 or 593/40. Emission filter 3 (DualView): 520/28. All values in nm.

Table 1-1: *Properties of RhoVRs*

Compound	ε ($M^{-1}cm^{-1}$)[a]	Φ (λ_{max})[a]	ΔF/F (100 mV)[b]	SNR (100 mV)[b]
16	75,000 (565 nm)	0.036 (586 nm)	3% (±0.2%)	19:1
17	70,000 (565 nm)	0.092 (588 nm)	26% (±3%)	37:1
20	77,000 (564 nm)	0.0089 (586 nm)	7% (±1%)	96:1
21 (RhoVR 1)	87,000 (564 nm)	0.045 (588 nm)	47% (±3%)	160:1

[a] PBS, pH 7.2, 0.1% SDS [b] voltage-clamped HEK cells

Figure 1-1: *Variable temperature NMR study of compound* ***20***

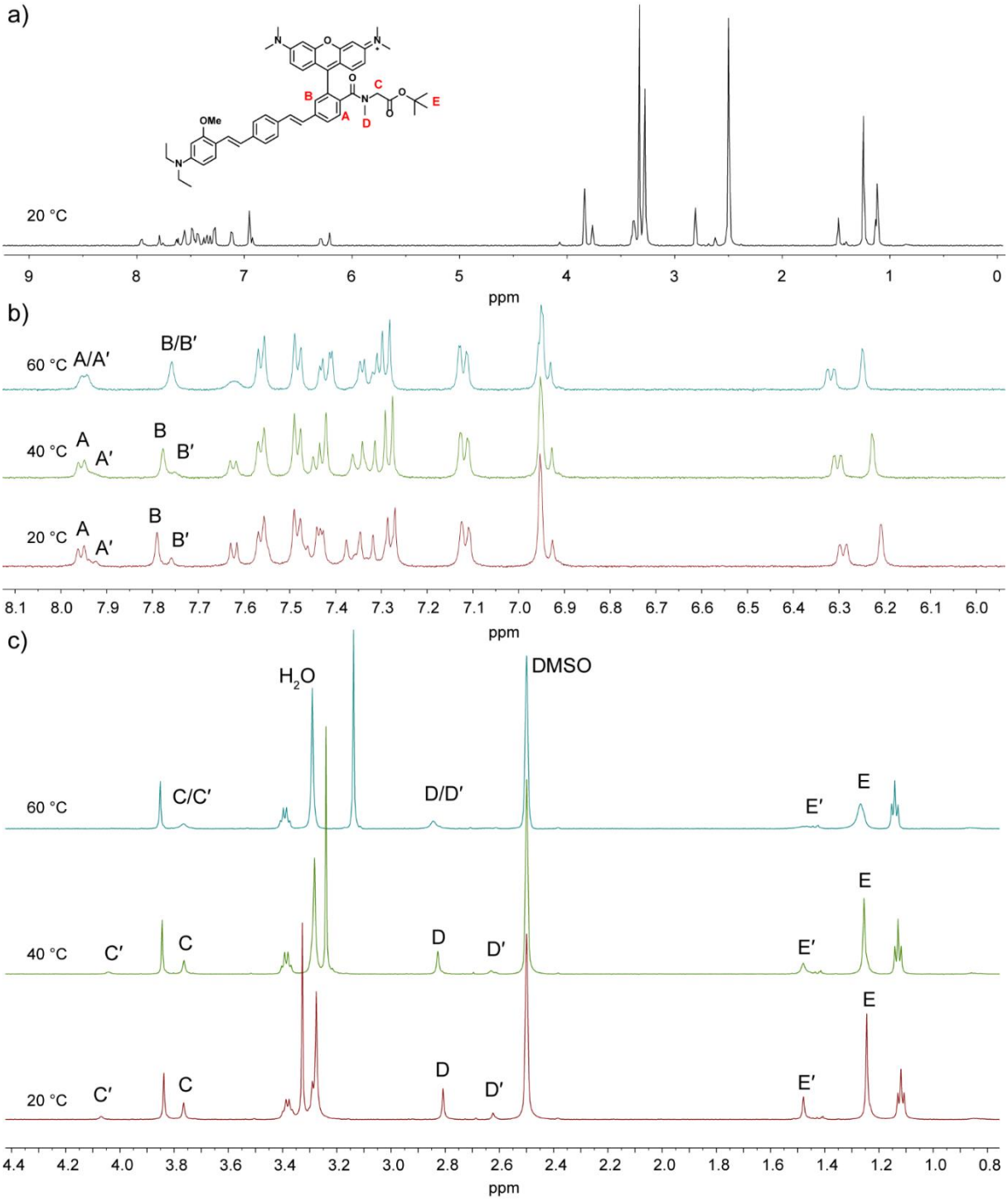

Figure 1-1: Variable temperature NMR study of compound **20**. (a) Full spectrum of **20** at 20 °C in d_6-DMSO. (b) Expanded aromatic region. The prime peaks correlate to the minor rotamer. A/A' and B/B' peaks are split due to their proximity to the amide bond, while more distant protons undergo minor changes in δ. (c) Expanded alkyl region. The prime peaks correlate to the minor rotamer. Unlabeled peaks correlate to the distant molecular wire protons, which display only minor changes in δ. Integration reveals the ratio of the major to minor rotamers is approximately 4:1.

Figure 1-2: Cellular localization and photophysical properties of RhoVR derivatives

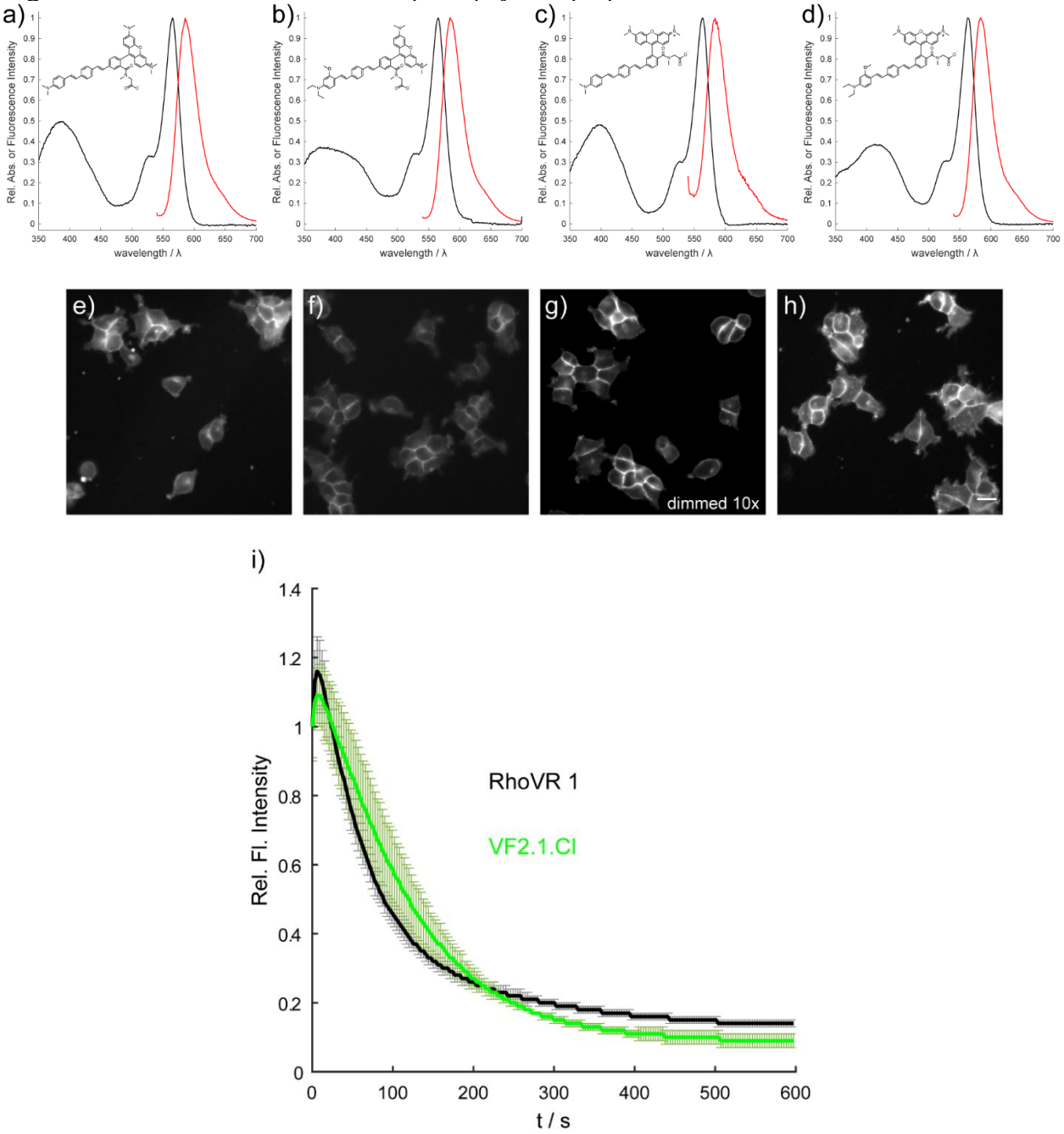

Figure 1-2: Normalized absorbance and emission profiles of **15** (a), **17** (b), **19** (c), and **21** (RhoVR 1) (d). All spectra were acquired at a dye concentration of 1 μM in PBS with 0.1% SDS. Widefield fluorescence microscopy images of RhoVRs (500 nM) in HEK cells. **15** (e), **17** (f), **19** (g), and **21** (RhoVR 1) (h). All acquisition and processing parameters are identical, to permit a comparison of loading efficacy and cellular brightness. The exception is **19** (panel c), which has been dimmed 10x (grey values in each pixel divided by 10) so that the displayed values are similar to panels a, b, and d. (i) Relative photostability of RhoVR 1 (black) and VF2.1.Cl (green). Plot shows the relative fluorescence intensity decay under high-powered illumination (illumination intensities matched at 60 W/cm^2). Error bars are ±S.E.M. for 3 separate cells. There is no significant difference between the relative fluorescence values of RhoVR 1 and VF2.1.Cl prior to 300 seconds ($p > 0.05$, two-tailed Student's t-test). After 300 seconds, RhoVR 1 is significantly brighter than VF2.1.Cl ($p < 0.05$, two-tailed Student's t-test).

Figure 1-3: Characterization of RhoVRs in HEK293T Cells

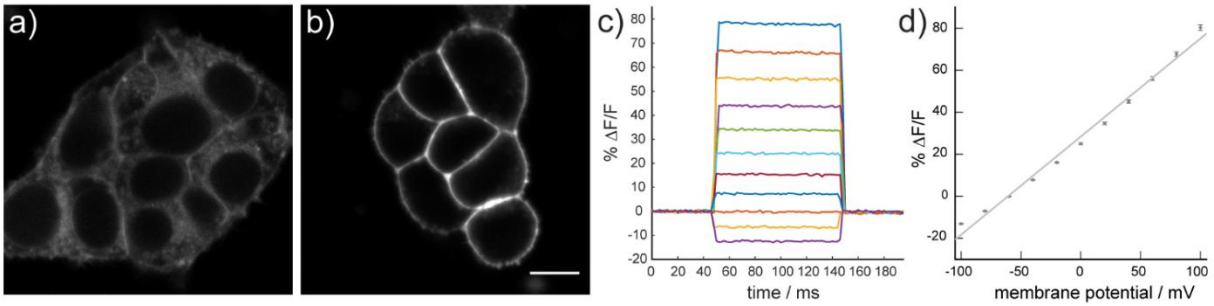

Figure 1-3: Cellular characterization of rhodamine-based voltage indicators. Confocal fluorescence images of HEK cells stained with (a) compound **13** (no sarcosine amide) or (b) RhoVR 1 (compound **21**, with sarcosine amide). Incorporation of the tertiary amide based on sarcosine results in a clear enhancement of membrane-localized fluorescence (panels a vs b). Membrane-localized RhoVR 1 fluorescence is voltage-sensitive. (c) The fractional change in fluorescence is plotted vs. time for 100 ms hyper- and depolarizing steps (±100 mV, 20 mV increments) from a holding potential of -60 mV for a single HEK cells under whole-cell voltage-clamp mode. (d) A plot of % ΔF/F vs. final membrane potential (mV), summarizing data from 9 separate cells, reveals a voltage sensitivity of approximately 47% per 100 mV. Error bars are ±S.E.M. Scale bar is 10 μm.

Figure 1-4: *Imaging spontaneous neuronal activity with RhoVR 1*

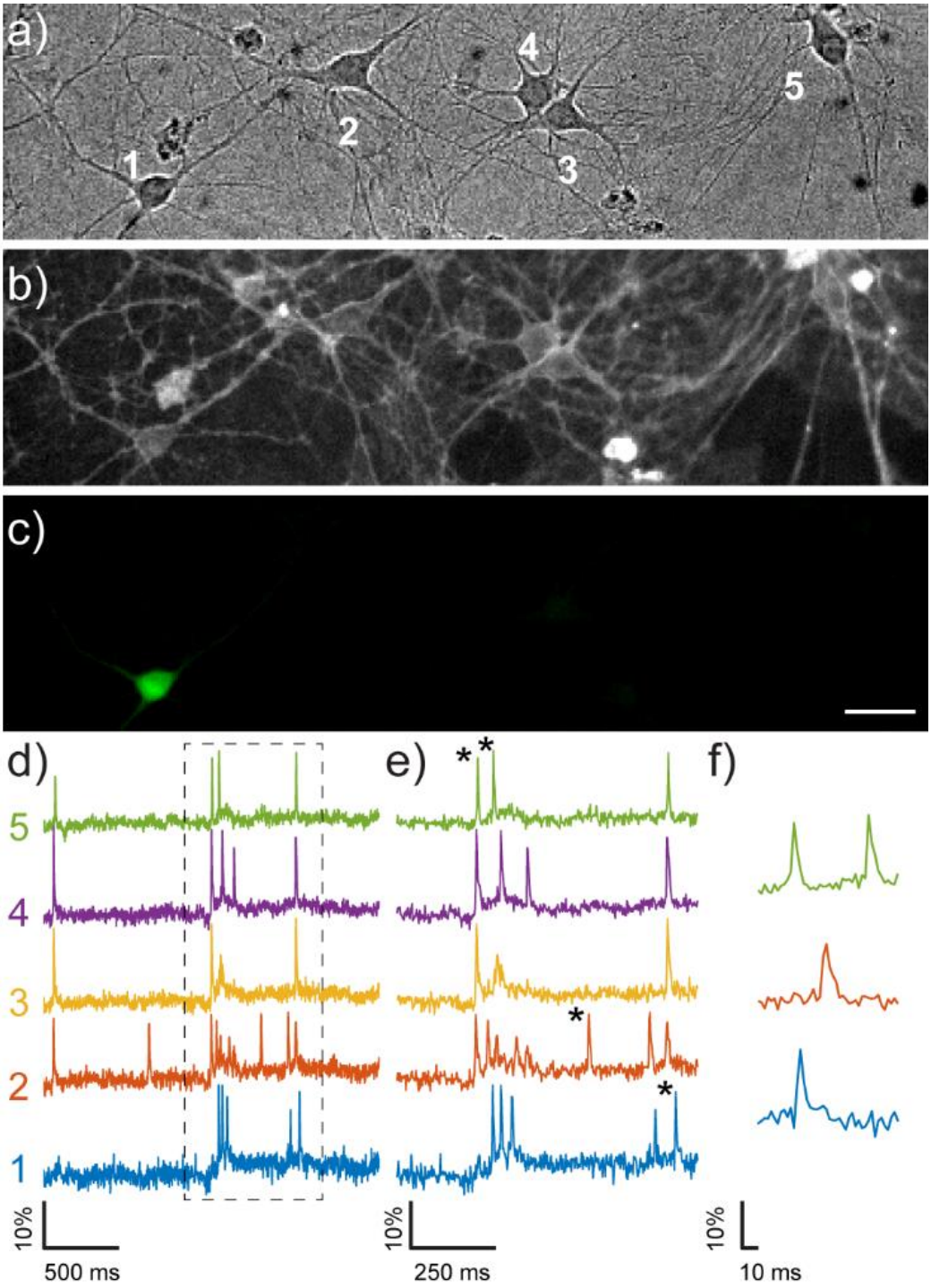

Figure 1-4: Imaging spontaneous neuronal activity with RhoVR 1 and EGFP. Rat hippocampal neurons (DIC, a) were stained with 500 nM RhoVR (fluorescence, b). A small number of neurons transiently expressed EGFP (fluorescence, c). Scale bar is 20 µm. (d) The spontaneous activity of neurons in panel a/b were recorded optically at 500 Hz using RhoVR 1. The activity of each neuron (1-5, panel a) is displayed as a trace of fluorescence intensity vs. time. The boxed regions in panel (d) are shown on an expanded scale in part e. Asterisks indicate traces expanded in panel f.

Figure 1-5: *Simultaneous, two-color imaging of voltage and Ca^{2+} in hippocampal neurons*

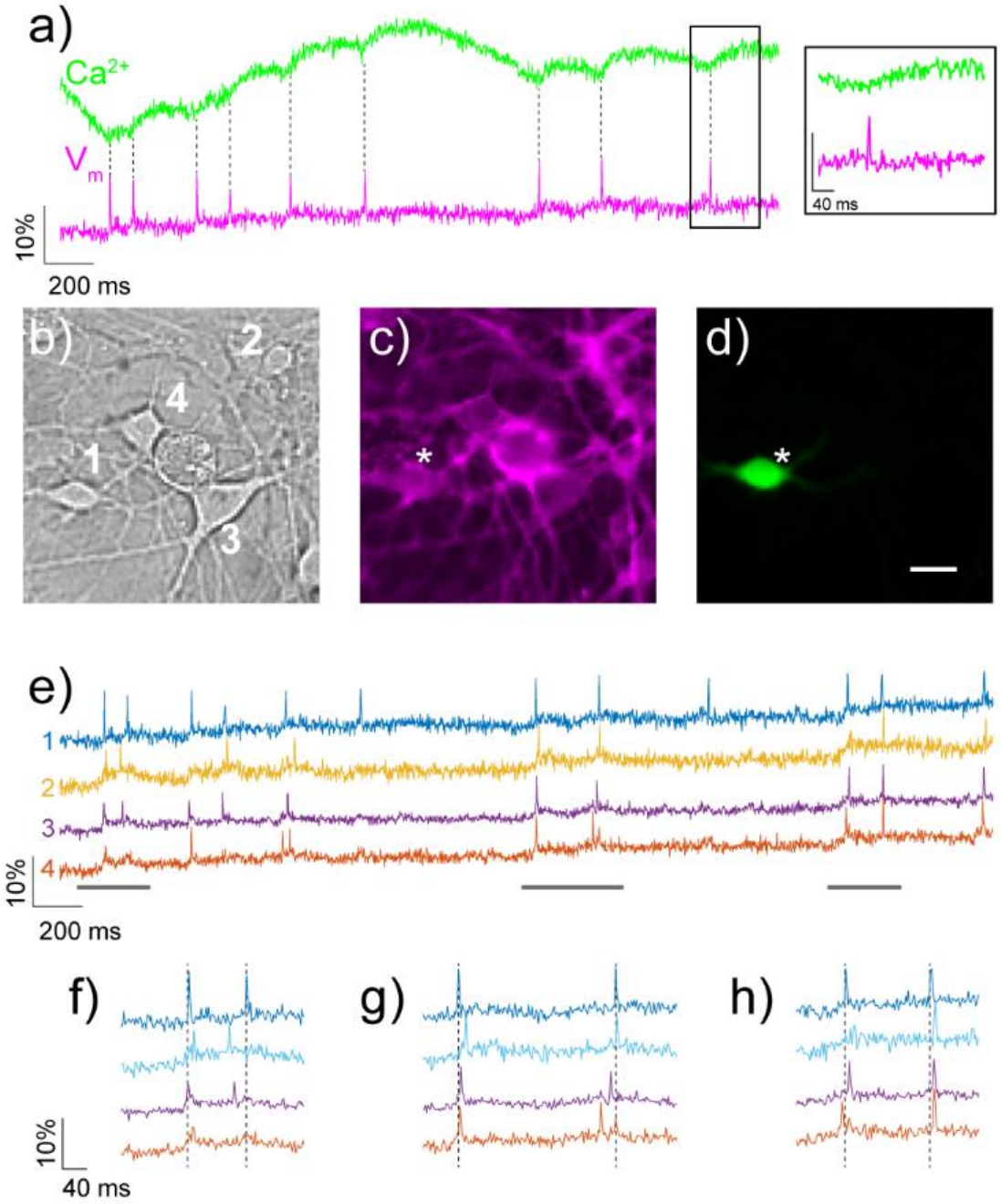

Figure 1-5: Simultaneous, two-color imaging of voltage and Ca^{2+} in hippocampal neurons using RhoVR 1 and GCaMP6s. (a) The green trace shows the relative change in fluorescence from Ca^{2+}-sensitive GCaMP6s, while the magenta trace depicts relative fluorescence changes in RhoVR 1 fluorescence from neuron "1" in panel b. Inset shows an expand time scale of the boxed region. (b) DIC image of neurons expressing GCaMP6s and stained with RhoVR 1. (c) Fluorescence image showing membrane localization of RhoVR 1 fluorescence from neurons in panel b. (d) Fluorescence image of neurons in (b) showing GCaMP6s fluorescence. Scale bar is 20 μm. (e) Traces show the activity of each neuron in panels b-d, displayed as the fractional change in voltage-sensitive RhoVR 1 fluorescence vs. time. (f-g) Regions of traces in panel e are shown in an expanded time scale to compare the spike timing of imaged neurons.

Figure 1-6: *Analysis of celular localization of rhodamines by confocal microscopy*

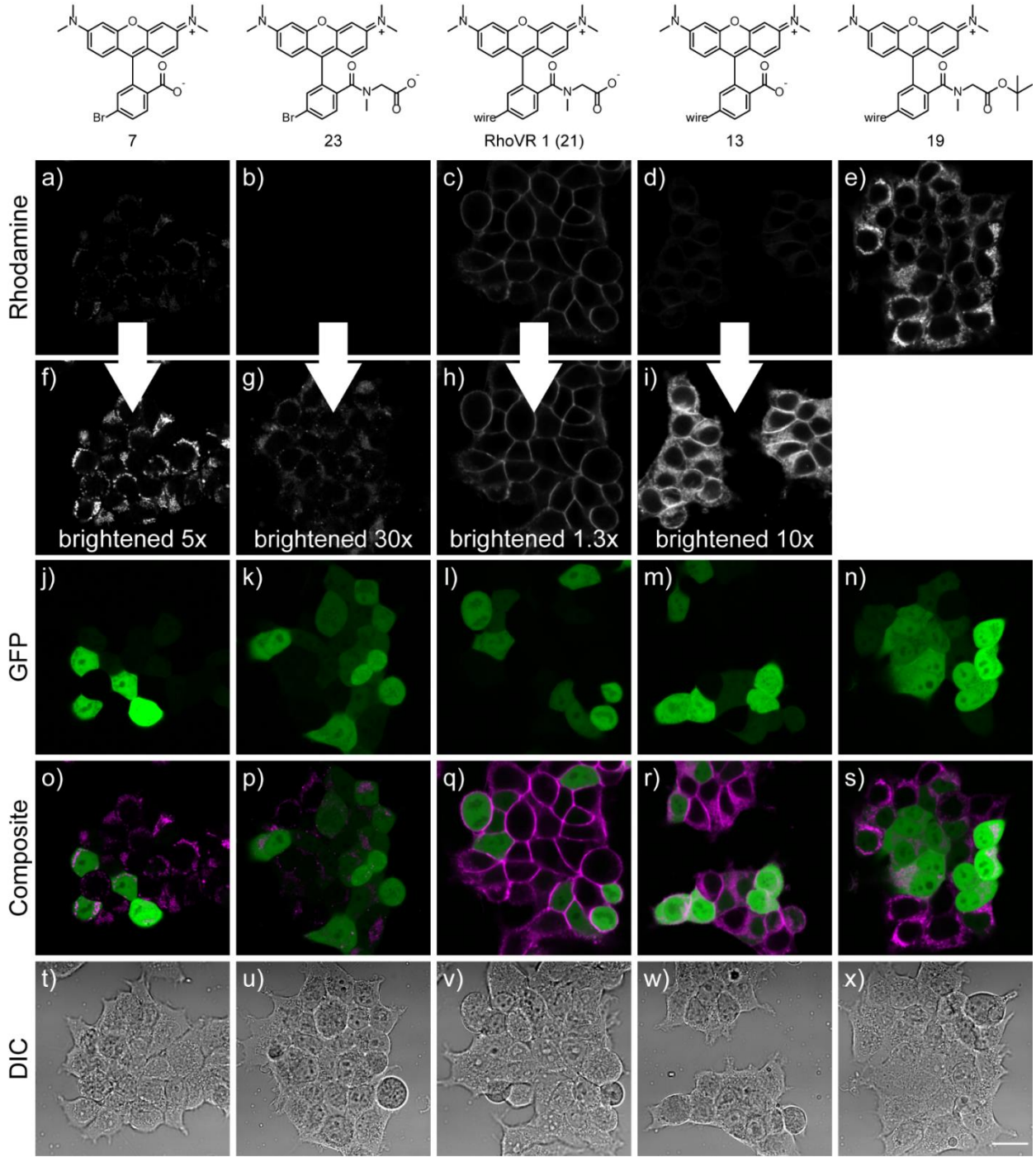

Figure 1-6: Analysis of cellular localization of rhodamines by confocal microscopy. The indicated rhodamine derivatives were loaded in HEK cells (500 nM, then washed with fresh HBSS) expressing cytosolic EGFP. (a-e) All display settings are identical to enable comparison of rhodamine loading efficiency. (f-i) Images of compounds **7**, **23**, **21**, and **13** were brightened by the indicated amount to enable visual inspection of cellular localization. (j-n) Images showing EGFP fluorescence (all display settings identical). (o-s) Composite images showing localization of rhodamines and GFP. Each image's display settings are individually optimized to facilitate comparison of EGFP and rhodamine staining. (t-x) Transmitted light images. Scale bar is 20 μm.

Figure 1-7: *Quantification of RhoVR 1 and rhodamine cellular localization*

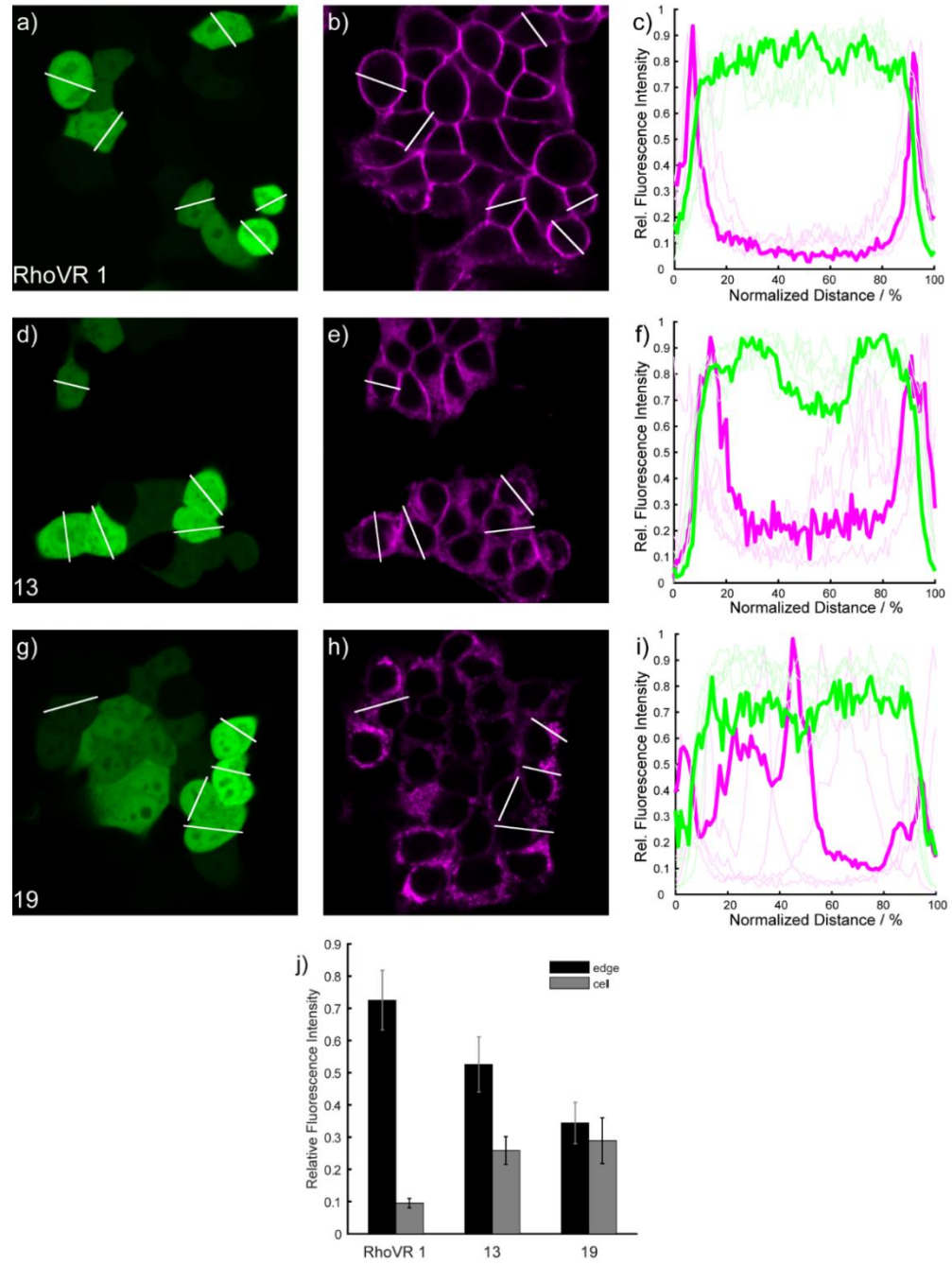

Figure 1-7: Quantification of RhoVR 1 and rhodamine cellular localization. The fluorescence intensity of rhodamine signal was measured relative to cytosolic EGFP by measuring the pixel intensity across a line segment spanning cytosolic EGFP. Images are shown for RhoVR 1 (compound **21**, a-b), compound **13** (free carboxylate, no sarcosine, d-e), and compound **19** (*t*Bu ester of RhoVR 1, g-h). Plots c, f, and i show the normalized fluorescence intensity for EGFP (green) or rhodamine derivative (magenta) vs. the normalized widths of the white line segments in the fluorescence images on the left. Thick traces represent the average of 5-6 cells for each condition. Light traces represent individual intensity profiles. Plot j depicts the relative fluorescence intensity of rhodamine derivatives at the edge of the cell ("edge", black bars) vs. the cytosol ("cell", grey bars). Error bars are ± S.E.M.

Figure 1-8: *Voltage sensitivity of RhoVR derivatives*

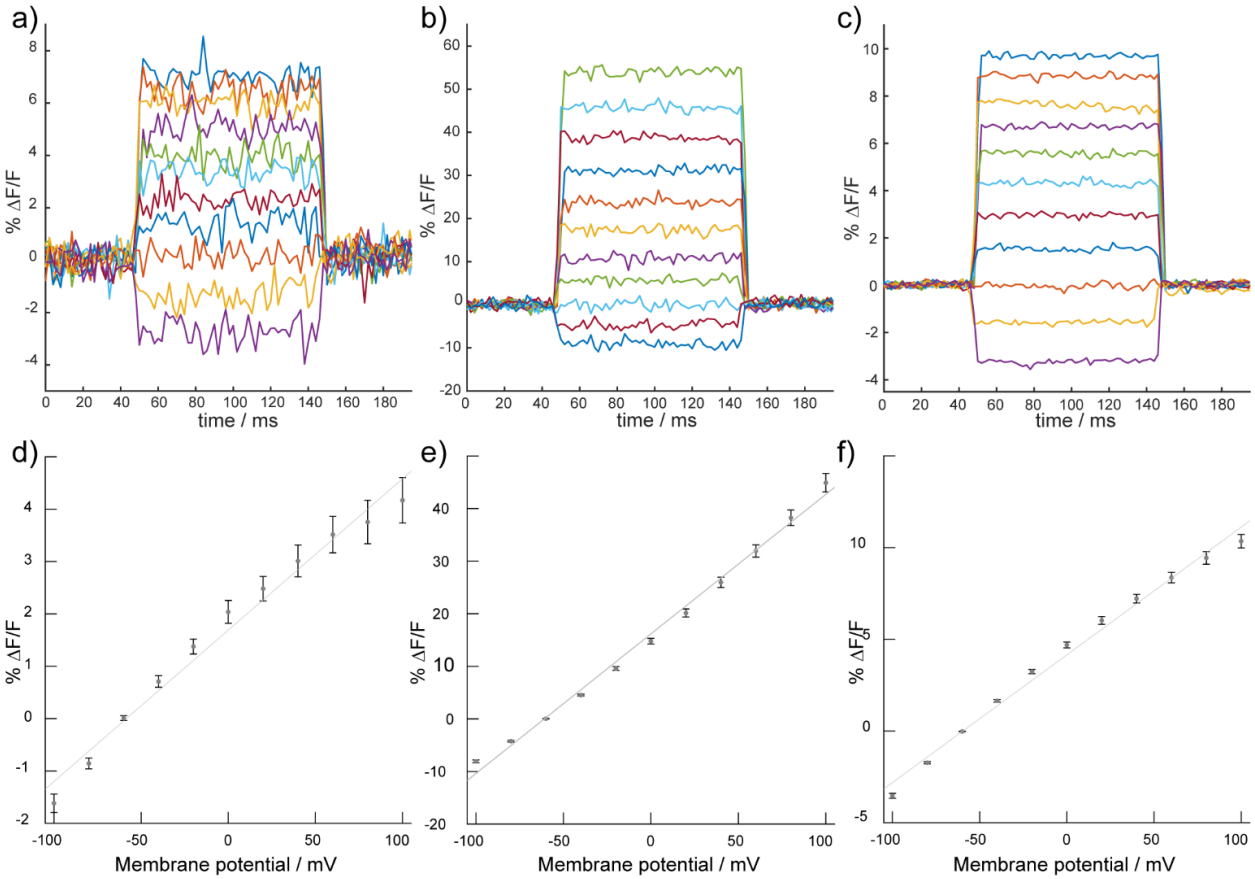

Figure 1-8: Voltage sensitivity of RhoVR derivatives. **15** (a,d); **17** (b,e); and **19** (c,f). (upper row) The fractional change in fluorescence is plotted vs. time for 100 ms hyper- and depolarizing steps (±100 mV, 20 mV increments) from a holding potential of -60 mV for a single HEK cells under whole-cell voltage-clamp mode. (lower row) A plot of % ΔF/F vs. final membrane potential (mV), summarizing data from 9 separate cells, reveals a voltage sensitivity of approximately 47% per 100 mV. Error bars are ±S.E.M.

Figure 1-9: *TTX treatment abolishes neuronal activity as measured by RhoVR 1*

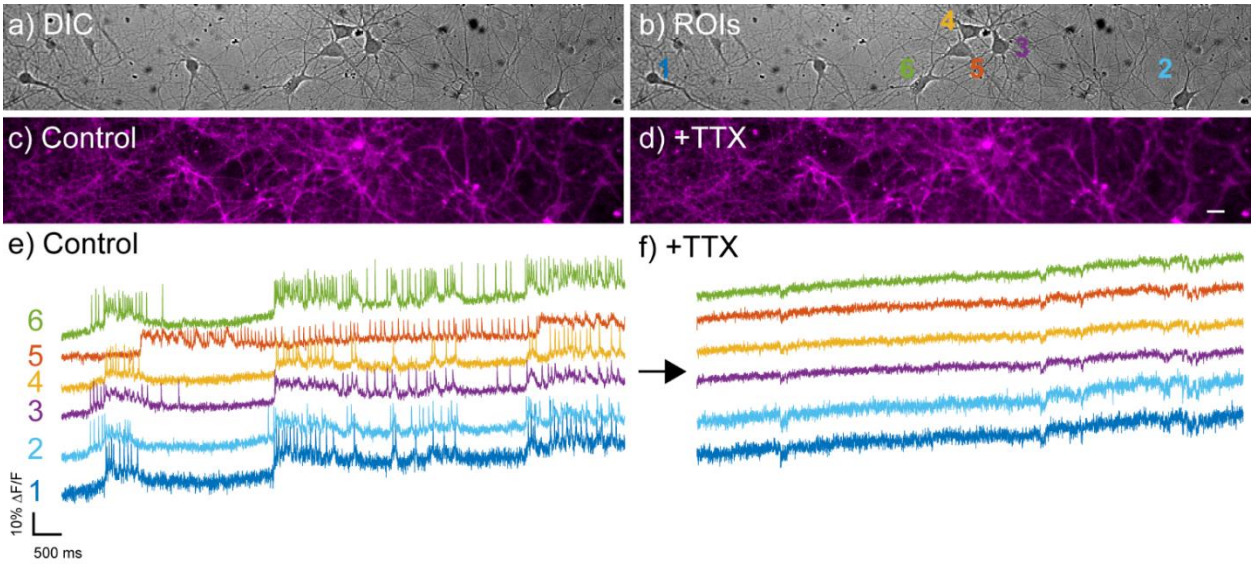

Figure 1-9: TTX treatment abolishes neuronal activity as measured by RhoVR 1. (a) Transmitted light/DIC image of cultured rat hippocampal neurons stained with RhoVR 1 (500 nM) and imaged at 500 Hz. (b) Regions of interest (ROIs) around the indicated cell bodies were examined before (c) and after (d) addition of TTX (1 µm). The relative change in fluorescence vs. time is plotted for the control (e) and TTX-treated neurons (f). TTX treatment causes a clear loss of activity, as measured by RhOVR 1 fluorescence. Image scale bar is 20 µm.

Figure 1-10: *RhoVR 1 and GFP display minimal excitation and emission cross-talk*

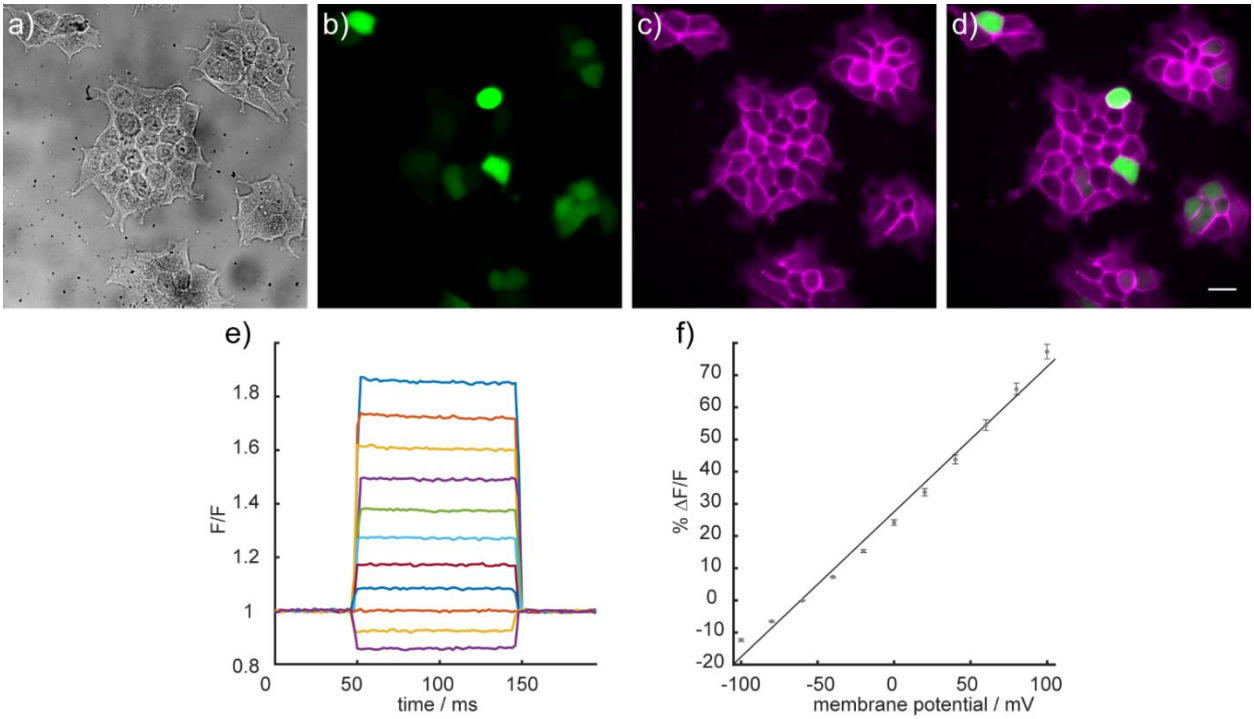

Figure 1-10: RhoVR 1 and GFP display minimal excitation and emission cross-talk. (a) DIC image of HEK cells expressing GFP and stained with 500 nM RhoVR 1. (b) EGFP and (c) RhoVR 1 fluorescence are collected in separate channels. Panel d shows an overlay of the images from panels b and c. HEK cells that are positive for cytosolic EGFP (panel b; GFP+) display similar levels of cytosolic fluorescence in the RhoVR 1 channel (panels c and d). Scale bar is 20 µm. (e) Voltage sensitivity of a single EGFP+, RhoVR 1-stained HEK cells. (f) Plots of ΔF/F vs mV reveal a 45±1.3% ΔF/F per 100 mV, which is comparable to the voltage-sensitivity in the absence of EGFP. Error bars are ±S.E.M for n = 5 cells.

References

(1) Engl, E.; Attwell, D. *J Physiol-London* **2015**, *593*, 3417.
(2) Levin, M. *Mol Biol Cell* **2014**, *25*, 3835.
(3) Peterka, D. S.; Takahashi, H.; Yuste, R. *Neuron* **2011**, *69*, 9.
(4) Braubach, O.; Cohen, L. B.; Choi, Y. In *Adv Exp Med Biol*; Canepari, M., Zecevic, D., Bernus, O., Eds.; **2015**; *859*, 3.
(5) Loew, L. M. In *Adv Exp Med Biol*; Canepari, M., Zecevic, D., Bernus, O., Eds.; **2015**; *859*, 27.
(6) Miller, E. W. *Curr Opin Chem Biol* **2016**, *33*, 74.
(7) Miller, E. W.; Lin, J. Y.; Frady, E. P.; Steinbach, P. A.; Kristan, W. B., Jr.; Tsien, R. Y. *Proc Natl Acad Sci U S A* **2012**, *109*, 2114.
(8) Woodford, C. R.; Frady, E. P.; Smith, R. S.; Morey, B.; Canzi, G.; Palida, S. F.; Araneda, R. C.; Kristan, W. B., Jr.; Kubiak, C. P.; Miller, E. W.; Tsien, R. Y. *J Am Chem Soc* **2015**, *137*, 1817.
(9) Grenier, V.; Walker, A. S.; Miller, E. W. *J Am Chem Soc* **2015**, *137*, 10894.
(10) Li, L. S. *Nano Lett* **2007**, *7*, 2981.
(11) Huang, Y. L.; Walker, A. S.; Miller, E. W. *J Am Chem Soc* **2015**, *137*, 10767.
(12) Chen, T. W.; Wardill, T. J.; Sun, Y.; Pulver, S. R.; Renninger, S. L.; Baohan, A.; Schreiter, E. R.; Kerr, R. A.; Orger, M. B.; Jayaraman, V.; Looger, L. L.; Svoboda, K.; Kim, D. S. *Nature* **2013**, *499*, 295.
(13) Mirabdolbaghi, R.; Dudding, T. *Org Lett* **2012**, *14*, 3748.
(14) Clark, R. B.; Hunt, D. K.; Plamondon, L.; Sun, C.; Xiao, X.-Y.; Roenn, M. (*Tetraphase Pharmaceuticals, Inc., USA .)*, **2010**, *WO2010132670A2*.
(15) Mudd, G.; Perez Pi, I.; Fethers, N.; Dodd, P. G.; Barbeau, O. R.; Auer, M. *Methods Appl Fluoresc* **2015**, *3*, 045002 (6 pp.).
(16) Jaafari, N.; Vogt, K. E.; Saggau, P.; Leslie, L. M.; Zecevic, D.; Canepari, M. In *Adv Exp Med Biol*; Canepari, M., Zecevic, D., Bernus, O., Eds.; **2015**; *859*, 103.
(17) Minta, A.; Kao, J. P. Y.; Tsien, R. Y. *J Biol Chem* **1989**, *264*, 8171.
(18) Dodani, S. C.; He, Q. W.; Chang, C. J. *J Am Chem Soc* **2009**, *131*, 18020.
(19) Egawa, T.; Hirabayashi, K.; Koide, Y.; Kobayashi, C.; Takahashi, N.; Mineno, T.; Terai, T.; Ueno, T.; Komatsu, T.; Ikegaya, Y.; Matsuki, N.; Nagano, T.; Hanaoka, K. *Angew Chem Int Edit* **2013**, *52*, 3874.
(20) Cheng, Y. M.; Pu, S. C.; Yu, Y. C.; Chou, P. T.; Huang, C. H.; Chen, C. T.; Li, T. H.; Hu, W. P. *Journal of Physical Chemistry A* **2005**, *109*, 11696.

Chapter 2:
Genetically Targeted Tetramethylrhodamine Voltage Reporters for Imaging Neuronal Activity

Portions of this work were performed in collaboration with the following persons:

Synthesis was assisted by Sarah Al-Abdullatif
Confocal microscopy and brain slice imaging was assisted by Pei Liu
In utero electroporation was performed by Kiarash Shamardani

Abstract

Voltage-sensitive fluorescent dyes (VSDs) are powerful tools that enable the recording of millisecond-scale neuronal dynamics. VSDs are attractive for such measurements due to their extremely fast kinetics, high sensitivities to membrane potential changes, and easily tunable absorbance and emission profiles. Despite these advantages, previously developed VSDs have found limited use in complex tissues preparations, such as brain slice and *in vivo*, because of the indiscriminate nature by which they label cellular membranes. We addressed this limitation by developing genetically targeted tetramethylrhodamine-based voltage reporters (RhoVRs) using the protein tag HaloTag. The system is comprised of a photoinduced electron transfer (PeT) triggered RhoVR voltage dye coupled to a chloroalkane ligand through a long, water-soluble linker (RhoVR-Halos). When applied to cells, RhoVR-Halos selectively and covalently bind to surface-expressed HaloTag protein on genetically modified cells. RhoVR-Halos possess high voltage sensitivities (up to 34% $\Delta F/F$ per 100 mV) and fast response times typical of RhoVRs, while gaining the selectivity typical of genetically encodable voltage indicators. We demonstrated that RhoVR-Halos can record activity from cultured rat hippocampal neurons and in brain slice with single cell and single-trial resolution. In addition, RhoVR-Halos possess high two-photon cross sections (σ_{TPA} up to 190 GM at 830 nm), enabling fast, two-photon voltage imaging. These results demonstrate the potential of hybrid chemogenetic voltage indicators to combine the optical performance of small-molecule chromophores with the inherent selectivity of genetically-encodable systems, permitting imaging modalities inaccessible to either technique individually.

Introduction

Rapid changes in neuronal membrane potential (V_m) are fundamental to signaling in the brain. Classically, V_m dynamics have been studied through electrode-based methods which, despite possessing unmatched speed and SNR, are typically limited to studying single neurons with low spatial resolution.[1,2] To address this limitation both chemical- and genetic-based fluorescence voltage imaging techniques have been developed that enable the study of V_m without invasive electrodes. Small molecule voltage sensitive dyes (VSDs) were first reported over 40 years ago and have served as a critical tool for neuroscientists probing the mechanisms of high-speed neuronal signaling.[3] VSDs have been continually improved over this time and next-generation VSDs, such as VoltageFluors developed in our lab, possess exceptional and readily tunable photophysical properties (i.e. absorption and emission profiles, photostability, brightness, voltage sensitivity, etc.).[4,5]

Despite their outstanding optical properties, VSDs have found limited use in complex tissues such as brain slice or *in vivo* due to their indiscriminate labeling of all membranes, leading to unproductive fluorescence dominating the desired voltage readout.[1] In an attempt to improve the selectivity of VSD labeling, our lab has developed both photoactivatable and enzymatically uncaged VoltageFluors that reduce off-target fluorescence through fluorogenic activation of the dye at cells of interest.[6,7] While effective in culture, we found these systems still lacked the specificity necessary to enable *in vivo* voltage imaging. In addition, these strategies use the phenolic oxygen of fluorescein-based VoltageFluors to impart fluorogenicity and are therefore untranslatable to red-shifted rhodamine-based VoltageFluors RhoVR 1 and BeRST 1.[4,8] Another chemical targeting strategy utilizing dextran polymer conjugated VSDs targeted to monoaminergic

neurons was also recently reported.[9] Unfortunately, while selective staining in slice and *in vivo* was observed, they were unable to record neuronal activity.

In response to the lack of targetable VSDs, genetically encodable voltage indicators (GEVIs) have been developed that can be selectively targeted to many different neuronal cell types through promoter-based methods.[10,11] The intense pursuit of improved GEVIs over the past decade has led to highly optimized GEVIs capable of recording neuronal activity from single cells with high selectivity *in vivo*.[12–15] While progress in GEVI development has led to several classes of proteins with varying spectral and kinetic properties,[16] they in general have distinct disadvantages when compared to VSDs. For example, two of the fastest GEVIs developed, ASAP2f and QuasAr2, respond to membrane potential changes on the order of milliseconds.[13] In comparison, VoltageFlours such as VF2.1.Cl respond to membrane potential changes nearly instantaneously (<<140 μs) due to the unique photoinduced electron transfer (PeT) mechanism of voltage sensing.[17] While GEVIs have now been developed which span the visible spectrum,[13] the use of protein-based chromophores can restrict the design space when compared to VSDs. This is especially apparent with opsin-based GEVIs, which due to their complex photocycle are not conducive to two-photon (2P) microscopy techniques preferred for imaging *in vivo*.[18] In contrast small molecule chromophores are readily optimized for 2P excitation and can possess 2P cross-sections an order of magnitude larger than protein-based chromophores.[19,20]

In attempt to combine the selectivity of genetically encodable systems with the favorable photophysics and tunability of VSDs, we aimed to design a hybrid chemogenetic system using a rhodamine-based voltage reporter (RhoVR) genetically targeted to cells of interest utilizing the protein tagging system HaloTag.[21] We choose to target RhoVRs due to their red-shifted absorption/emission and high 2P cross section, large voltage sensitivities (up to 47% ΔF/F per 100 mV) and ease of synthesis and functionalization.[8,19] By expressing Halotag extracellularly, then adding RhoVR linked to the HaloTag ligand via a flexible polyethene glycol linker (PEG), we hoped to gain selectivity through the protein component while maintaining the favorable photophysical properties of VSDs (**Scheme 2-1**).

Results and Discussion

Development of a surface expressed HaloTag

To design the protein component of the hybrid system, we selected the HaloTag system due to its remarkable affinity and selectivity, ease of ligand synthesis and extremely fast kinetics.[21] In order to express the HaloTag enzyme on the cell surface, we fused a transmembrane domain (pDisplay) derived from platelet-derived growth factor receptor (PDGFR) or a glycophosphatidyl inositol (GPI) signal peptide derived from decay accelerating factor (DAF) to the C-terminal of the HaloTag sequence. We also appended a secretion signal peptide from immunoglobulin K (IgK) to the N-terminal to enhance extracellular trafficking (**Figure 2-1a**). These modifications successfully resulted in cell surface expression of HaloTag in HEK cells, as shown by immunostaining in fixed cells under non-permeable conditions. To track the protein expression in live cells, we included a nuclear-localized EGFP downstream of HaloTag, separated by an internal ribosome entry site (IRES). We tested the effectiveness of the pDisplay and DAF constructs in live HEK cells using a cell-impermeant tetramethylrodamine (TMR)-HaloTag ligand **44** (**Scheme 2-2**). Bath application of TMR-HaloTag at 50 nM for 30 minutes showed clear membrane-bound fluorescence, which matched EGFP signal in transfected cells (**Figure 2-1b-e**). In HEK cells, use

of pDisplay-based constructs results in higher RhoVR fluorescence than the analogous DAF constructs (**Figure 2-4g,h**).

*Synthesis of Piperazine-functionalized RhoVR 1, **7***

Synthesis of HaloTag functionalized RhoVR 1 (RhoVR1-Halos) begins from Tetramethylrhodamine voltage dye **3**, which was synthesized in 70% yield via a Heck coupling between isomerically pure Br-TMR **1** and phenylenevinylene wire **2**.[8] Previous studies in our lab have shown that a negatively charged functional group on the chromophore is necessary for the proper localization and function of the voltage dye.[22] In order to both maintain a negatively charged anchor and provide a functional handle for the attachment of the HaloTag ligand, we modified the substitution at the 2' position of our typical RhoVRs in order to incorporate an L-cysteic acid amino acid linker.[23] This was accomplished through a HATU mediated coupling between **3** and 1-Boc-piperazine, followed by a TFA-catalyzed deprotection of the Boc-protected amine to afford **5** in 62% yield over two steps (**Scheme 2-3**).[24] A second HATU-mediated coupling between **5** and Boc-L-cysteic acid and subsequent TFA deprotection afforded **7** in 78% yield over two steps.

7 localizes well to the plasma membrane of HEK293T cells; however, **7** was slightly dimmer than RhoVR 1 when loaded at the same concentration (**Figure 2-2a-e**). The voltage sensitivity of **7** was evaluated using patch-clamp electrophysiology in whole-cell voltage clamp mode. Hyper-polarizing and depolarizing voltage steps spanning a range from -100 mV to +100 mV in 20 mV increments from a holding potential of -60 mV showed **7** possessed a voltage sensitivity of 38% per 100 mV (**Table 2-1**, **Figure 2-2f,g**). The optical properties of **7** were similar to RhoVR 1, with a λ_{max} at 565 nm (ε = 82,000 $M^{-1}cm^{-1}$) and emission maximum at 585 nm (**Table 2-1**, **Figure 2-3g**).

*Synthesis and Characterization of RhoVR1-PEG$_x$-Halos **12-16** in HEK Cells*

Due to the covalent nature of HaloTag labeling, we hypothesized that a long linker might be required to allow the voltage dye to properly insert into the plasma membrane while covalently bound to the active site of HaloTag. We therefore synthesized a library of RhoVR1-Halo derivatives with varying lengths of PEG linkers in order to determine its effect on voltage sensitivity. From **7**, NHS-ester activated dPEG® linkers between 5-25 ethylene units long were coupled to the free amine of the L-cysteic acid moiety (**Scheme 2-4**). Subsequent HATU-mediated coupling of the HaloTag-amine ligand and purification by preparative HPLC afforded compounds **12-15** in 24-53% yield. In addition, we synthesized a "PEG$_0$" RhoVR1-Halo derivative **16** using a succinic anhydride-derived linker.

All of the synthesized RhoVR1-PEG$_x$-Halo derivatives showed highly selective labeling of only HaloTag expressing HEK293T cells (**Figure 2-4d-f**). Labeling of HaloTag positive cells was observed with RhoVR1-Halo concentrations as low as 5 nM, indicating the fast kinetics of HaloTag labeling leads to rapid sequestration of the dye.[21] In addition, we observed highly selective labeling at concentrations as high as 500 nM (**Figure 2-4d-f**). We hypothesize the minimal off-target labeling is due to the increased water solubility of RhoVR1-PEG$_x$-Halos afforded by the L-cysteic acid and PEG linkers.[23] Knowing that we could selectively label HaloTag expressing HEK293T cells, patch-clamp electrophysiology was used to measure the voltage sensitivities of the RhoVR1-PEG$_x$-Halo library. RhoVR-Halo **16**, incorporating a very short succinic anhydride-derived linker, was completely insensitive to membrane potential changes.

This was likely caused by the short linker of **16** preventing the RhoVR component from spanning the distance between the HaloTag active site and the plasma membrane (**Figure 2-5e, Table 2-1**). When the length of the dPEG® linkers was increased, the voltage sensitivity of the RhoVR-Halos also increased. RhoVR1-PEG_{25}-Halo **15**, possessing the longest dPEG® used, had the highest measured voltage sensitivity at 34% ΔF/F per 100 mV (**Figure 2-5e,f**). We hypothesize that the increase in sensitivity with linker length is representative of both a larger portion of voltage dye reaching the plasma membrane as well as improved orientation of RhoVR1-PEG_x-Halos in the membrane.

*Synthesis of RhoVR(Me) **21** and RhoVR(Me)-PEG_{25}-Halo **27***

One potential limitation to the covalent labeling strategy is that the concentration of RhoVR in the membrane is directly correlated to the expression levels of HaloTag on the plasma membrane (**Figure 2-4a**). Loading screens showed that RhoVR1-PEG_x-Halo compounds were 3-4 fold dimmer than bath applied RhoVR 1 under normal loading conditions (**Figure 2-6**, **Table 2-1**). In attempt to address this limitation, we synthesized a new RhoVR derivative, dubbed RhoVR(Me), which includes a methyl-substituted molecular wire as opposed to the methoxy-substituted wire of RhoVR 1 (**Scheme 2-5a,b**). The synthesis of the untargeted RhoVR(Me) was analogous to RhoVR 1, starting with a Heck coupling between isomerically pure Br-TMR **1** and phenylenevinylene wire **18** to generate voltage dye **19** in 80% yield. Formation of an N-methyl glycine-derived tertiary amide at the 2' position of the pendant aryl ring gave the untargeted RhoVR(Me) **21** in 77% yield over two steps (**Scheme 2-5b**).

In cells, RhoVR(Me) is approximately 4-fold brighter than RhoVR 1 (**Figure 2-6**, **Table 2-1**). Patch-clamp electrophysiology revealed the increased brightness came at the cost of voltage sensitivity, with RhoVR(Me) possessing a modest 13% ΔF/F per 100 mV (**Figure 2-7c,d**, **Table 2-1**). When accounting for both the brightness and voltage sensitivity of the dyes, RhoVR(Me) performs as well or better than RhoVR 1, and in particular is an ideal VoltageFluor when the photon budget is a limiting factor for imaging.

We then synthesized RhoVR(Me)-PEG_{25}-Halo **27** from the L-cysteic acid functionalized **25** (**Scheme 2-6a**). Coupling of the NHS-ester activated NHS-PEG_{25}-Acid linker followed by HATU-mediated coupling of HaloTag-amine **8** afforded **27** in 28% yield over two steps. Patch-clamp electrophysiology in HEK293T cells revealed that **27** had a voltage sensitivity of 16% ΔF/F per 100 mV, higher than the parent RhoVR(Me) (**Figure 2-7g,h**). Loading screens with **27** showed the new dye was 3-4 fold brighter than RhoVR1-PEG_x-Halo, confirming that the increased brightness of RhoVR(Me) over RhoVR 1 is the result of reduced PeT quenching, and not due to higher concentrations of the dye in the membrane (**Figure 2-6**).

Recording Neuronal Activity with RhoVR-Halos in Rat Hippocampal Neurons

Having validated both **15** and **27** in HEK293T cells, we next evaluated the system in cultured rat hippocampal neurons. The HaloTag constructs were modified by replacing the CMV promoter with a neuron-specific synapsin promoter. A regulatory element from the woodchuck hepatitis virus (WPRE) was also added to improve protein expression (**Figure 2-1a**). Sparsely transfected neurons were labeled with either **15** or **27** at 50 nM. Similar to HEK293T cells, both dyes labeled HaloTag expressing neurons with high selectivity (**Figure 2-8a-h**). Unlike in HEK cells, HaloTag incorporating either the pDisplay or DAF transmembrane domains resulted in

similar RhoVR staining in neurons. We then used **15** to monitor spontaneous neuronal activity. Spontaneously firing action potentials were detected with an average ΔF/F of 6.7 ± 0.2% (N = 71 spikes) and signal-to-noise ratios (SNRs) of 25.0 ± 7.0 that were largely dependent on the expression levels of HaloTag (**Figure 2-8k**). Patch clamp electrophysiology showed that **15** had little to no impact on the action potential waveforms (**Figure 2-9**).

Having confirmed the ability of our chemogenetic system to record spontaneous neuronal activity, we then compared the performance of **15** to the commonly used GEVIs ASAP1,[25] based on circularly permuted green fluorescent protein (cpGFP), and Ace2N-mNeon (Ace2N),[12] which uses the mNeon fluorescent protein appended to the *Acetabularia acetabulum* rhodopsin (Ace) voltage sensitive domain. Neurons labeled with **15** compared favorably to both ASAP1 and Ace2N expressing neurons, displaying brighter and red-shifted membrane fluorescence at matched light powers (**Figure 2-10a**), turn-on responses to action potentials (ASAP1 and Ace2N-mNeon both possess turn-off responses) (**Figure 2-10a**) and an average ΔF/F per spike of 10.4% ± 0.2% (SNR= 16.5:1) for evoked action potentials, compared to -4.4% ± 0.1% (SNR= 10:1) per spike for ASAP1 and -1.7% ± 0.1% per spike for Ace2N (SNR= 8:1) (**Figure 2-10b,c**). Another advantage of our chemogenetic approach is greatly improved membrane localization of fluorescence. Because the genetically encoded HaloTag protein is non-fluorescent and the RhoVR-Halo dye is impermeable to the plasma membrane, we only observe RhoVR staining when both components are present at the cell surface (**Figure 2-4a-d**). In contrast, GEVIs rely on genetically encoded fluorescent proteins that can contribute high amounts of unresponsive background fluorescence during the various stages of their assembly/export to the plasma membrane.

Since the red-shifted absorbance/emission profile of RhoVR-Halos allows their use alongside green fluorescent tools, we demonstrated our ability carry out dual-color calcium and voltage imaging in genetically defined cells by replacing the nuclear EGFP marker with a genetically encode calcium sensor GCaMP6s (**Figure 2-1**).[26] Neurons expressing the HaloTag-GCaMP6s construct were selectively labeled with **15** with the same efficiency as the HaloTag-EGFP constructs. Using an image splitter (**Scheme 1-5**) and simultaneously exciting with both blue and green light, then splitting the resulting emission into GCaMP6s and RhoVR fluorescence channels, we were able to visualize both the rapid changes in membrane potential and the corresponding slower increase in [Ca^{2+}] during spontaneous spiking events (**Figure 2-11**). The sensitivity of **15** to these action potentials was similar to those obtained at a single wavelength (ΔF/F per spike = 5.3 ± 0.9%, SNR = 15.6:1, N = 18 spikes, **Figure 2-11**). In all cases, the fast voltage spike precedes the subsequent Ca^{2+} transient. Because of the fast kinetics of V_m compared to Ca^{2+} transients, monitoring V_m directly enables better resolution of spike timing than Ca^{2+}, especially when spikes occur in quick succession.

Two-photon Imaging with RhoVR-Halos

Two-photon (2P) excitation microscopy has become the preferred methodology for imaging deep within tissue, as the longer wavelength excitation light decreases phototoxicity and increases the depth at which imaging can be performed.[27] 2P voltage imaging poses additional difficulties, due to the need for high acquisition rates (≥500 Hz) and membrane-localized indicators that greatly reduces the available photon budget. Despite these challenges, voltage indicators compatible with 2P imaging techniques are highly desired and have been the subject of many recent publications.[5,27–31] The advances in both voltage indicators and microscopy techniques are now enabling 2P voltage imaging *in vivo*, albeit with either/or low SNR and

specificity.[29] Due to the relatively high 2P absorption cross-section (σ_{TPA}) of rhodamines, we believed RhoVR-Halos could potentially serve as bright, sensitive 2P voltage indicators. We measured the σ_{TPA} of **15** and **27** in solution by normalizing to a rhodamine B standard.[32] Plotting 2P absorption cross-section vs excitation wavelength revealed a σ_{TPA} maxima of approximately 180 GM at 830 nm for **15** and 190 GM at 830 nm for **27** (**Figure 2-12a,b**), which was in good agreement with literature values for rhodamine B (a similar chromophore) and other RhoVR derivatives (**Figure 2-12c**).[19,32] Similar to 1P microscopy, we saw highly selective staining of only HaloTag expressing rat hippocampal neurons under 2P illumination between 840 and 1060 nm (**Figure 2-12d-f**).

Monitoring Neuronal Activity with RhoVR-Halos in Slice

Having shown that RhoVR-Halos label HaloTag expressing cells with great selectivity in culture, we next tested the ability of RhoVR-Halos to selectively label HaloTag expressing neurons in brain slice. We first generated transgenic mice through *in utero* electroporation using a construct in which EGFP was replaced with a blue fluorescent protein (BFP) (**Figure 2-1a**). HaloTag expressing brains were then sliced and loaded with 250 nM of either **15** or **27**. While off-target staining was observed near the surface of the slice where dye concentrations were presumably highest, HaloTag expressing neurons were clearly labeled at tissue depths up to 100 μm (**Figure 2-13a**). In addition to 1P excitation, we also looked at RhoVR-Halo labeling with 2P excitation, illuminating at 860 nm. **15** was bright under 2P illumination, allowing imaging at depths past 100 μm (**Figure 2-13b**)

While selective labeling was achieved, the amount of fluorescence from transfected cells was low. We hypothesize that this was caused by the low transfection efficiency of *in utero* electroporation. This was corroborated by the low number of HaloTag positive cells found per slice as well as the weak fluorescence of the BFP marker. We improved transfection efficiency by removal of the FP component of the HaloTag plasmid (**Figure 2-1**), however overall brightness was still low, leading to poor SNR when measuring membrane potential changes. In order to increase expression efficiency, we are currently carrying out viral infection of HaloTag constructs in mice. We anticipate a large improvement in brightness will enable 2P photon imaging in slice.

Conclusion

We have presented the design, synthesis, and application of genetically targetable tetramethylrhodamine voltage indicators (RhoVR-Halos) that combine the specificity of self-labeling proteins with the favorable photophysics of small-molecule VFs. RhoVR-Halos were shown to label HaloTag expressing neurons with exceptional selectivity ($\geq$30-fold selectivity over untransfected neurons in culture) and record membrane potential changes with high sensitivities (up to 34% ± 2% $\Delta F/F$ per 100 mV in HEK cells, 6.7% ± 0.2% $\Delta F/F$ per spike in neurons). We demonstrated the utility of RhoVR-Halos for simultaneous dual-color imaging, for example enabling simultaneous V_m and Ca^{2+}, and their compatibility with 2P excitation (σ_{TPA} = 180-190 GM at 830 nm). Finally, we demonstrated the ability to selectively label and record neuronal activity in brain slice with RhoVR-Halos, a feat not previously possible with RhoVRs.

Taken together, these results demonstrate the power of a chemical/genetic voltage indicator to combine the favorable photophysics of small-molecule probes with the selectivity afforded to genetically encoded proteins. Due to the modularity of this approach, we envision developing

hybrid voltage sensors using other VoltageFluors developed in our lab (i.e. BeRST) as well as orthogonal self-labeling enzymes or targeting motifs (i.e. SNAP-tag, Spy-tag, antibodies/ nanobodies, etc.). These future probes will enable multi-dimensional experiments, for example dual-color voltage imaging of excitatory and inhibitory neurons. Finally, we are currently working to demonstrate the utility of RhoVR-Halos in alive, behaving mice using holographic imaging techniques in collaboration with the Adesnik Lab.

Experimental Section

General Method for Chemical Synthesis and Characterization

Chemical reagents and solvents (dry) were purchased from commercial suppliers and used without further purification. NHS-PEG$_x$-Acid dPEG® linkers were purchased from Quanta Biodesign. Synthesis of HaloTag succinimidyl ester (O2), tetramethyl rhodamine **1**, (E)-N,N-diethyl-3-methoxy-4-(4-vinylstyryl)aniline **2** and RhoVR 1 free carboxy **3** were carried out as previously reported.[8] Thin layer chromatography (TLC) (Silicycle, F254, 250 μm) and preparative thin layer chromatography (PTLC) (Silicycle, F254, 1000 μm) was performed on glass backed plates pre-coated with silica gel and were visualized by fluorescence quenching under UV light. Flash column chromatography was performed on Silicycle Silica Flash F60 (230–400 Mesh) using a forced flow of air at 0.5–1.0 bar. NMR spectra were measured on Bruker AVB-400 MHz, 100 MHz, AVQ-400 MHz, 100 MHz, Bruker AV-600 MHz, 150 MHz. NMR spectra measured on Bruker AVII-900 MHz, 225 MHz, equipped with a TCI cryoprobe accessory, were performed by Dr. Jeffrey Pelton (QB3). Chemical shifts are expressed in parts per million (ppm) and are referenced to $CDCl_3$ (7.26 ppm, 77.0 ppm) or DMSO (2.50 ppm, 40 ppm). Coupling constants are reported as Hertz (Hz). Splitting patterns are indicated as follows: s, singlet; d, doublet; t, triplet; q, quartet, dd, doublet of doublet; m, multiplet. High-resolution mass spectra (HR-ESI-MS) were measured by the QB3/Chemistry mass spectrometry service at University of California, Berkeley. High performance liquid chromatography (HPLC) and low resolution ESI Mass Spectrometry were performed on an Agilent Infinity 1200 analytical instrument coupled to an Advion CMS-L ESI mass spectrometer. The column used for the analytical HPLC was Phenomenex Luna C18(2) (4.6 mm I.D. × 75 mm) with a flow rate of 1.0 mL/min. The mobile phases were MQ-H_2O with 0.05% trifluoroacetic acid (eluent A) and HPLC grade acetonitrile with 0.05% trifluoroacetic acid (eluent B). Signals were monitored at 254, 340 and 545 nm over 10 min with a gradient of 10-100% eluent B. Preparative HPLC was performed using a Waters Acquity Autopurification system (prep UHPLC-MS). The column used for preparative HPLC was an XBridge OBD Prep Column (5 μm, 19mm I.D. x 250 mm) with a flow rate of 30.0 mL/min. The mobile phases were MQ-H_2O with 0.05% trifluoroacetic acid (eluent A) and HPLC grade acetonitrile with 0.05% trifluoroacetic acid (eluent B). Signals were monitored at 545 over 20 min with a gradient of 30-70% eluent B and by ESI-MS. The collected fractions were concentrated *in vacuo*, neutralized with dilute sodium bicarbonate and then extracted with DCM. The combined organics were dried with sodium sulfate, filtered and concentrated *in vacuo*. This procedure was necessary as decomposition of the products was sometimes observed when prepared as the TFA salt.

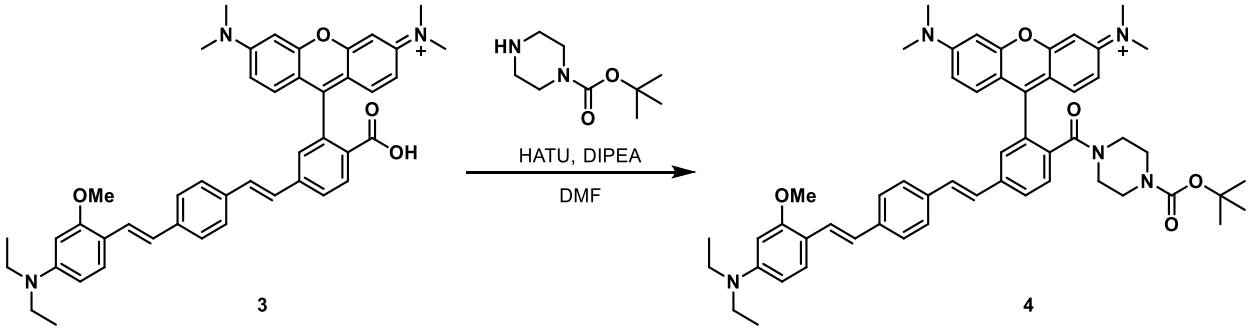

Synthesis of 4:

A vial was charged with **3** (60.8 mg, 87.8 μmol), 1-Boc piperazine (20.4 mg, 110 μmol), and HATU (41.7 mg, 110 μmol). Anhydrous DMF (3 mL) and anhydrous diisopropylethylamine (23.2 μL, 110 μmol) were added and the vial was flushed with nitrogen, sealed, and stirred at 22 °C for 18 h. The solvent was removed *in vacuo* and the remaining residue was purified by flash chromatography (0-5% methanol in DCM, linear gradient) affording **4** as a purple solid **(**62.3 mg, 72.3 μmol, 83%). ^{1}H NMR (600 MHz, DMSO-d_6) δ 7.93 (d, J = 8.1 Hz, 1H), 7.76 (s, 1H), 7.68 (d, J = 8.0 Hz, 1H), 7.56 (d, J = 8.1 Hz, 2H), 7.51-7.39 (m, 4H), 7.39-7.30 (m, 2H), 7.26 (d, J = 9.5 Hz, 2H), 7.14 (dd, J = 9.6, 2.5 Hz, 2H), 6.99-6.90 (m, 3H), 6.29 (d, J = 9.1 Hz, 1H), 6.21 (d, J = 2.2 Hz, 1H), 3.84 (s, 3H), 3.38 (m, J = 7.1 Hz, 6H), 3.29 (s, 12H), 3.23 (br s, 4H), 3.16 (br s, 2H), 1.38 (s, 9H), 1.12 (t, J = 7.0 Hz, 6H); Analytical HPLC retention time 13.23 min; MS (ESI) exact mass for $C_{54}H_{54}N_5O_5^+$ $[M+H]^+$ calcd: 860.5 found: 860.8; HR-ESI-MS m/z for $C_{54}H_{56}N_5O_5^+$ calcd: 860.4745 found: 860.4750.

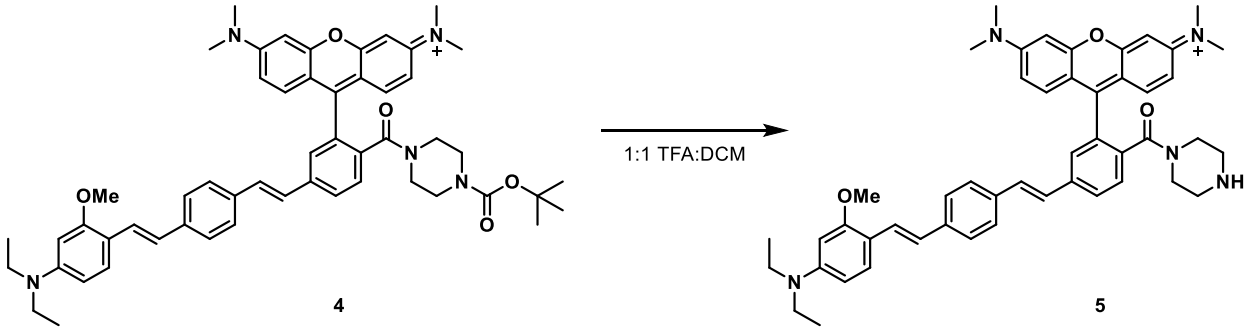

Synthesis of 5:

Trifluoroacetic acid (2 mL) was added to a solution of **4** (60.0 mg, 69.7 μmol) in DCM (2 mL). The reaction was stirred at 22 °C for 1 h, then the solvent removed under a stream of nitrogen. The remaining residue was purified by flash chromatography (5-10% methanol in DCM, linear gradient) affording **5** as a purple solid (39.5 mg, 51.9 μmol, 75%). ^{1}H NMR (600 MHz, DMSO-d_6) δ 8.96 (br s, 1H), 7.96 (d, J = 7.4 Hz, 1H), 7.83 – 7.73 (m, 2H), 7.59 – 7.46 (m, 4H), 7.46 – 7.24 (m, 6H), 7.11 (dd, J = 9.7, 2.4 Hz, 2H), 7.02 – 6.89 (m, 3H), 6.29 (d, J = 8.3 Hz, 1H), 6.21 (s, 1H), 3.84 (s, 3H), 3.63 (br s, 2H), 3.44 (br s, 2H), 3.38 (q, J = 6.9 Hz, 4H), 3.30 (s, 12H), 3.00 (br s, 2H), 2.93 (br s, 2H), 1.12 (t, J = 7.0 Hz, 6H); Analytical HPLC retention time 9.53 min; MS (ESI) exact mass for $C_{49}H_{54}N_5O_3^+$ $[M+H]^+$ calcd: 760.4 found: 760.7; HR-ESI-MS m/z for $C_{49}H_{54}N_5O_3^+$ calcd: 760.4221 found: 760.4228.

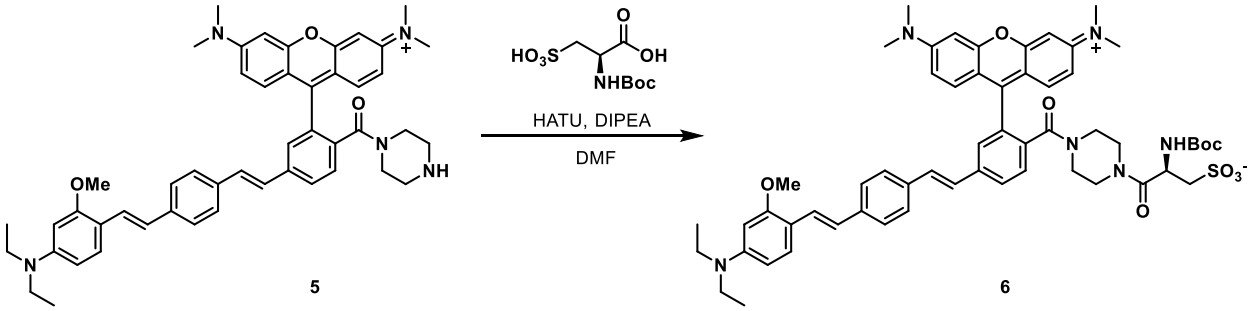

Synthesis of 6:

A vial was charged with **5** (5.0 mg, 72.3 μmol), Boc-L-cysteic acid (24.3 mg, 90.3 μmol), and HATU (34.4mg, 90.3 μmol). Anhydrous DMF (2 mL) and anhydrous diisopropylethylamine (21.8 μL, 108.4 μmol) were added and the vial was flushed with nitrogen, sealed, and stirred at 22 °C for 18 h. The solvent was removed *in vacuo* and the remaining residue diluted with DCM/*i*-PrOH (40 mL) and washed with water (2 x 50 mL). The combined organics were dried with anhydrous sodium sulfate, filtered and the solvent removed *in vacuo*. The remaining solid was purified by preparative TLC (10% methanol in DCM) affording **6** as a purple solid (57.0 mg, 56.4 μmol, 78%). Analytical HPLC retention time 5.92 min; MS (ESI) exact mass for $C_{57}H_{67}N_6O_9S^{2+}$ $[M+2H]^{2+}$ calcd: 506.2 found: 506.4; HR-ESI-MS m/z for $C_{57}H_{66}N_6O_9S^+$ calcd: 1011.4685 found: 1011.4687.

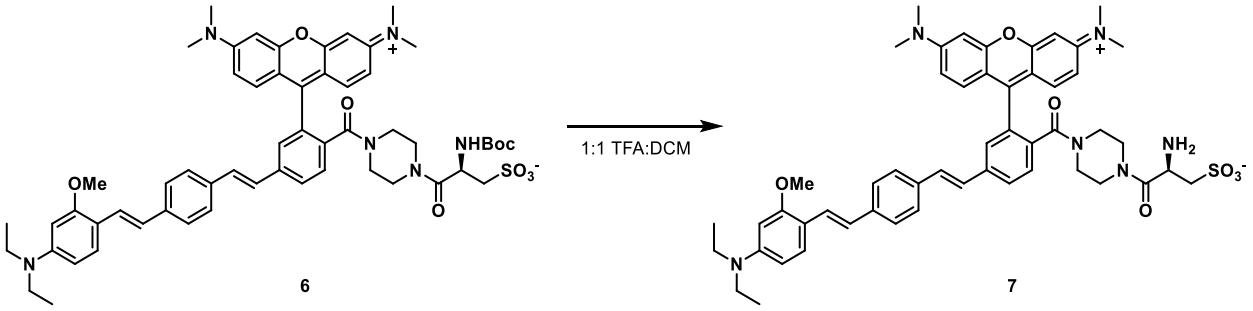

Synthesis of 7:

Trifluoroacetic acid (2 mL) was added to a solution of **6** (57 mg, 56 μmol) in DCM (2 mL). The reaction was stirred at 22 °C for 3 h, then the solvent removed under a stream of nitrogen. The remaining residue was co-evaporated with toluene (1 x 10 mL) and acetonitrile (2 x 10 mL) affording **7** as a purple solid (57 mg, 56 μmol, 100%). Analytical HPLC retention time 5.09 min; MS (ESI) exact mass for $C_{52}H_{59}N_6O_7S^+$ $[M+H]^+$ calcd: 911.4 found: 911.1; HR-ESI-MS m/z for $C_{52}H_{59}N_6O_7S^+$ calcd: 911.4160 found: 911.4152.

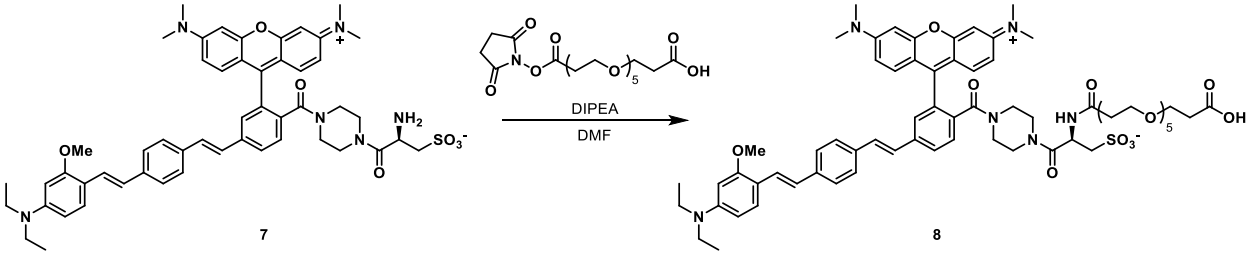

Synthesis of RhoVR1-PEG5-Acid, 8:

A vial was charged with **7** (8.00 mg, 8.78 µmol) and NHS-PEG$_5$-Acid (3.82 mg, 8.78 µmol). Anhydrous DMF (1 mL) and anhydrous diisopropylethylamine (3.0 uL, 17.6 µmol) were added and the vial was flushed with nitrogen, sealed and stirred at 22 ºC for 16 h. The solvent was removed *in vacuo* and the remaining crude solid was diluted in DCM (10 mL) and washed with water (3 x 20 mL). The combined organics were dried with anhydrous sodium sulfate, filtered and the solvent removed *in vacuo* affording **8** as a purple solid which was used without further purification for the next reaction. Analytical HPLC retention time 5.40 min; MS (ESI) exact mass for $C_{66}H_{84}N_8O_{16}S^+$ $[M+H]^+$ calcd: 616.3, found: 616.5.

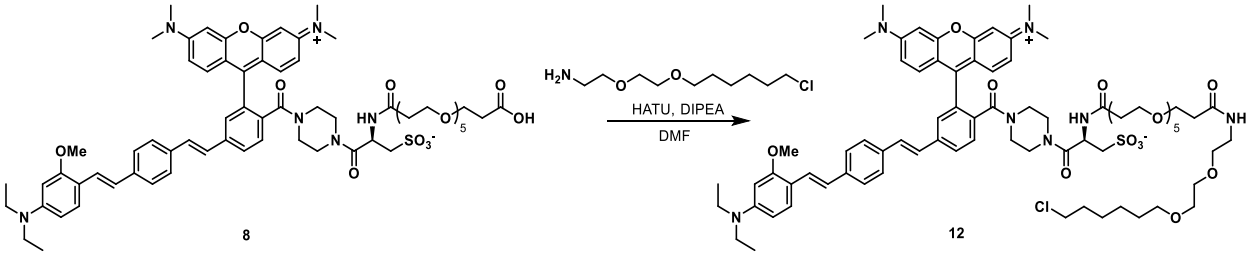

Synthesis of RhoVR1-PEG$_5$-Halo, 12:

A vial was charged with crude **8** (8.78 µmol), Halotag-Amine (3.93 mg, 17.6 µmol) and HATU (6.68 mg, 17.6 µmol). Anhydrous DMF (1 mL) and anhydrous diisopropylethylamine (4.6 uL, 22.0 µmol) were added and the vial flushed with nitrogen, sealed and stirred at 22 ºC for 18 h. The solvent was removed *in vacuo* and the crude product purified by preparative HPLC affording **12** as a purple solid (6.46 mg, 4.5 µmol, 51% over two steps). Analytical HPLC retention time 6.18 min; MS (ESI) exact mass for $C_{76}H_{104}ClN_7O_{18}S_2^+$ $[M+2H]^{2+}$ calcd: 718.8, found: 718.8; HR-ESI-MS m/z for $C_{76}H_{102}ClN_7NaO_{16}S^+$ $[M+H]^+$ calcd: 1458.6684 found: 1458.6691.

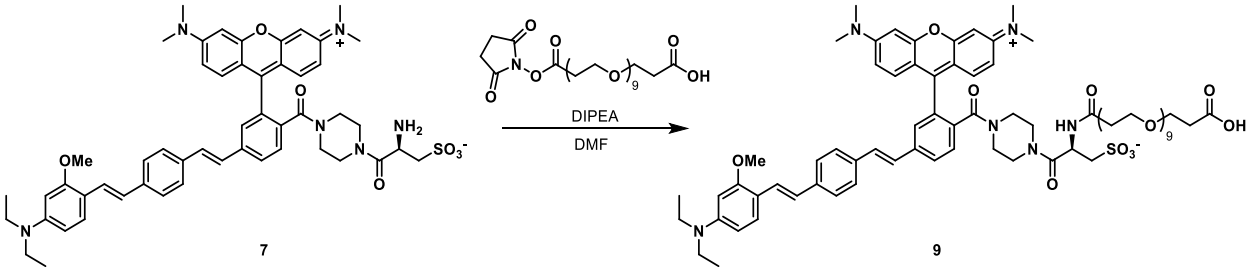

Synthesis of RhoVR1-PEG$_9$-Acid, 9:

A vial was charged with 7 (15.0 mg, 16.5 µmol) and NHS-PEG$_9$-Acid (10.1 mg, 16.5 µmol, 1.0 equiv.). Anhydrous DMF (1 mL) and anhydrous diisopropylethylamine (4.6 uL, 33 µmol, 2.0 equiv.) were added and the vial was flushed with nitrogen, sealed and stirred at 22 ºC for 18 h. The solvent was removed *in vacuo* and the remaining crude solid was diluted in DCM (10 mL) and washed with water (3 x 20 mL). The combined organics were dried with anhydrous sodium sulfate, filtered and the solvent removed *in vacuo* affording 9 as a purple solid which was used without further purification for the next reaction. Analytical HPLC retention time 5.48 min; MS (ESI) exact mass for $C_{74}H_{100}N_6O_{19}S^{2+}$ $[M+2H]^{2+}$ calcd: 704.3, found: 704.3.

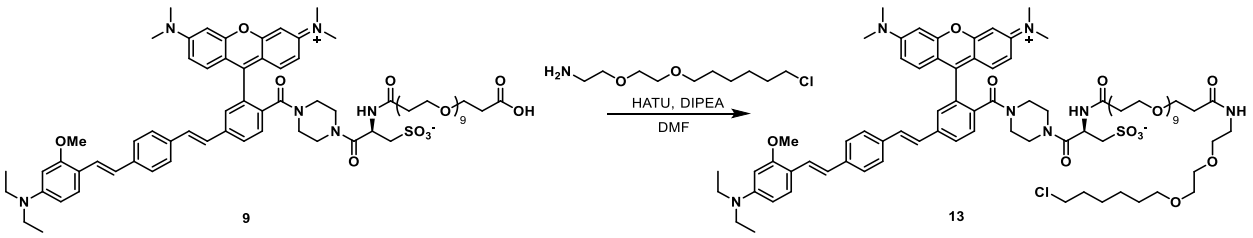

Synthesis of RhoVR1-PEG$_9$-Halo, 13:
A vial was charged with crude 9 (16.5 µmol), Halotag-Amine (7.4 mg, 33.0 µmol) and HATU (12.5 mg, 33.0 µmol). Anhydrous DMF (2 mL) and anhydrous diisopropylethylamine (8.7 uL, 41 µmol) were added and the vial was flushed with nitrogen, sealed and stirred at 22 ºC for 16 h. The solvent was removed *in vacuo* and the crude product purified by preparative HPLC affording 13 as a purple solid (11.5 mg, 7.10 µmol, 43% over two steps). Analytical HPLC retention time 6.14 min; MS (ESI) exact mass for $C_{84}H_{121}ClN_7O_{20}S^{3+}$ $[M+3H]^{3+}$ calcd: 538.3, found: 538.3; HR-ESI-MS m/z for $C_{84}H_{120}ClN_7O_{20}S^{2+}$ $[M+2H]^{2+}$ calcd: 806.8993 found: 806.9007.

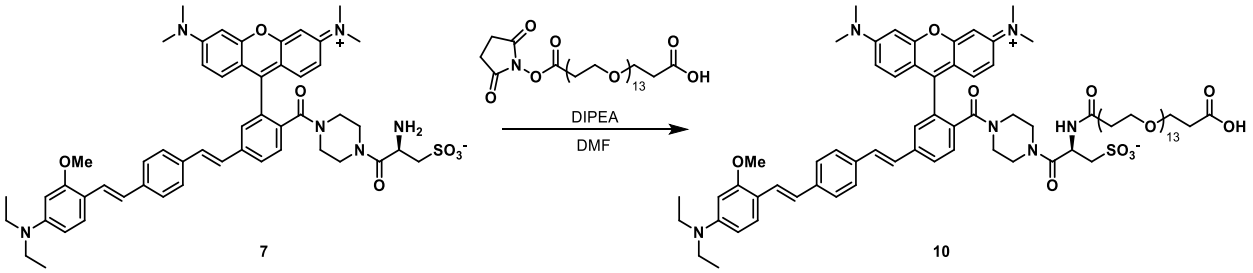

Synthesis of RhoVR1-PEG$_{13}$-Acid, 10:
A vial was charged with **7** (17.4 mg, 19.1 µmol) and NHS-PEG$_{13}$-Acid (15.1 mg, 19.1 µmol). Anhydrous DMF (1 mL) and anhydrous diisopropylethylamine (5.3 uL, 38.2 µmol) were added and the was vial flushed with nitrogen, sealed and stirred at 22 ºC for 18 h. The solvent was removed *in vacuo* and the remaining crude solid was diluted in DCM (10 mL) and washed with water (3 x 20 mL). The combined organics were dried with anhydrous sodium sulfate, filtered and the solvent removed *in vacuo* affording **10** as a purple solid which was used without further purification for the next reaction. Analytical HPLC retention time 5.38 min; MS (ESI) exact mass for $C_{82}H_{116}N_6O_{23}S^{2+}$ $[M+2H]^{2+}$ calcd: 792.4, found: 792.1.

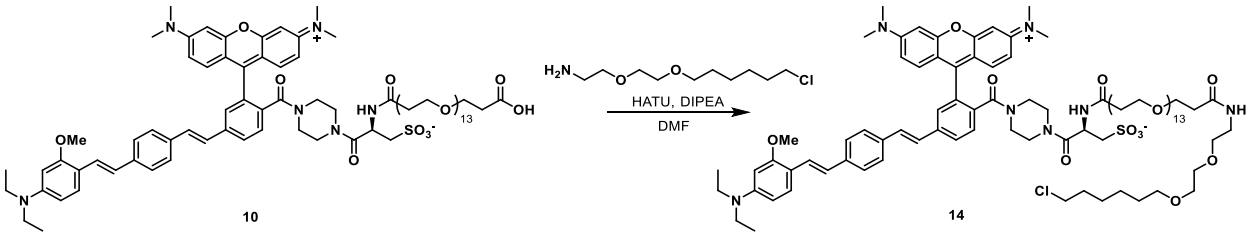

Synthesis of RhoVR1-PEG$_{13}$-Halo, 14:
A vial was charged with crude **10** (19.1 µmol), Halotag-Amine (8.6 mg, 38.2 µmol) and HATU (14.5 mg, 38.2 µmol). Anhydrous DMF (2 mL) and anhydrous diisopropylethylamine (8.3 uL, 48 µmol) were added and the vial was flushed with nitrogen, sealed and stirred at 22 ºC for 16 h. The solvent was removed *in vacuo* and the crude product purified by preparative HPLC affording **14** as a purple solid (8.33 mg, 4.65 µmol, 24.3% over two steps). Analytical HPLC retention time

6.18 min; MS (ESI) exact mass for $C_{92}H_{137}ClN_7O_{24}S^{3+}$ $[M+3H]^{3+}$ calcd: 597.0, found: 597.3; HR-ESI-MS m/z for $C_{92}H_{136}ClN_7O_{24}S^{2+}$ $[M+2H]^{2+}$ calcd: 894.9518 found: 894.9522.

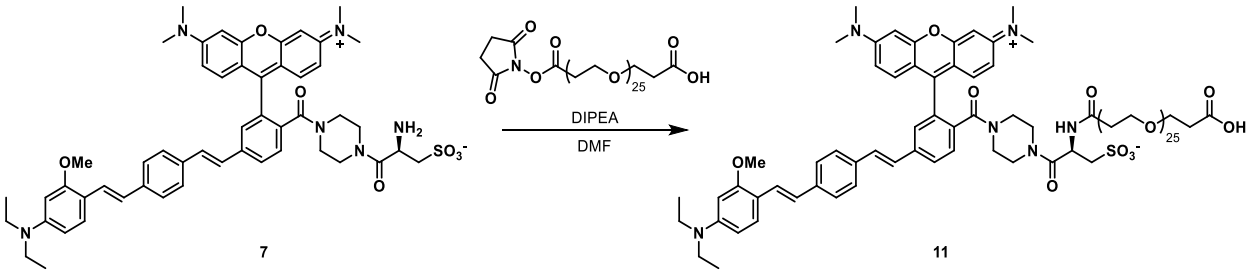

Synthesis of RhoVR1-PEG$_{25}$-Acid, 11:

A vial was charged with **7** (20.0 mg, 21.9 µmol) and NHS-PEG$_{25}$-Acid (29.2 mg, 21.9 µmol). Anhydrous DMF (1 mL) and anhydrous diisopropylethylamine (6.1 uL, 44 µmol) were added and the vial was flushed with nitrogen, sealed and stirred at 22 ºC for 18 h. The solvent was removed *in vacuo* and the remaining crude solid was diluted in DCM (10 mL) and washed with water (3 x 20 mL). The combined organics were dried with anhydrous sodium sulfate, filtered and the solvent removed *in vacuo* affording **11** as a purple solid which was used without further purification for the next reaction. Analytical HPLC retention time 5.46 min; MS (ESI) exact mass for $C_{106}H_{164}ClN_6O_{35}S^{2+}$ $[M+2H]^{2+}$ calcd: 1057.0, found: 1056.8.

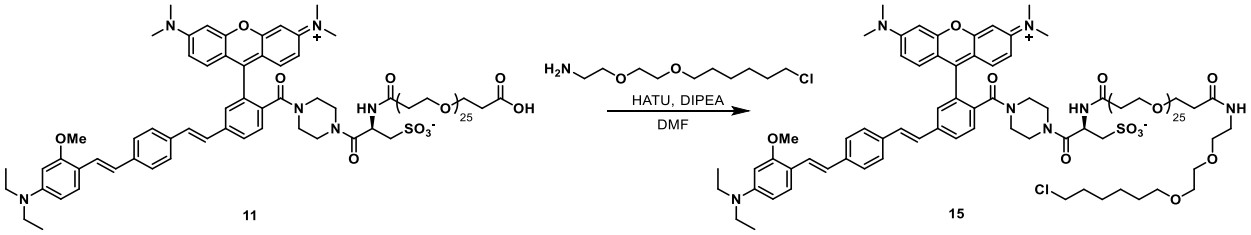

Synthesis of RhoVR1-PEG$_{25}$-Halo, 15:

A vial was charged with crude **11** (8.0 mg, 3.8 µmol), Halotag-Amine (1.7 mg, 7.5 µmol) and HATU (2.9 mg, 7.5 µmol). Anhydrous DMF (1 mL) and anhydrous diisopropylethylamine (2.0 uL, 9.4 µmol) were added and the was vial flushed with nitrogen, sealed and stirred at 22 ºC for 7 h. The solvent was removed *in vacuo* and the crude product purified by preparative HPLC affording **15** as a purple solid (3.5 mg, 1.5 µmol, 40.0% over two steps). Analytical HPLC retention time 6.11 min; MS (ESI) exact mass for $C_{106}H_{165}ClN_6O_{35}S^{3+}$ $[M+3H]^{3+}$ calcd: 773.1, found: 773.1; HR-ESI-MS m/z for $C_{116}H_{184}ClN_7O_{36}S^{2+}$ $[M+2H]^{2+}$ calcd: 1159.6107 found: 1159.6129.

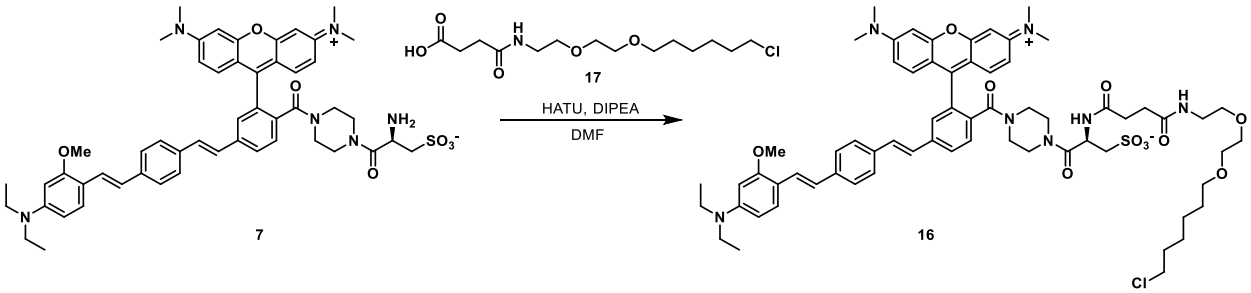

Synthesis of RhoVR1-PEG$_0$-Halo, 16:

A vial was charged with **7** (10.0 mg, 11.0 µmol), HaloTag succinimidyl ester (O2) **17** (7.1 mg, 21.9 µmol) and HATU (8.3 mg, 21.9 µmol). Anhydrous DMF (2 mL) and anhydrous diisopropylethylamine (7.0 µL, 33 µmol) were added and the vial was flushed with nitrogen, sealed and stirred at 22 ºC for 16 h. The solvent was removed *in vacuo* and the remaining crude solid was purified by preparative HPLC affording **16** as a purple solid (3.53 mg, 2.88 mmol, 26.5%). Analytical HPLC retention time 7.23 min; MS (ESI) exact mass for $C_{66}H_{84}N_7O_{11}S^+$ $[M+2H]^{2+}$ calcd: 608.8, found: 609.0; HR-ESI-MS m/z for $C_{66}H_{83}ClN_7O_{11}S^+$ $[M+H]^+$ calcd: 1216.5554 found: 1216.5544.

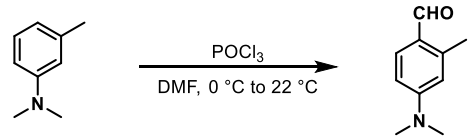

S1

Synthesis of 4-(dimethylamino)-2-methylbenzaldehyde, S1:
A round-bottom flask was charged with N,N,3-trimethylaniline (1.35 g, 10.0 mmol) and evacuated/backfilled with nitrogen (3x). Anhydrous DMF (20 mL) was added and the reaction cooled to 0 °C before the dropwise addition of phosphoryl chloride (1.64 mL, 18.0 mmol) via syringe. The reaction was allowed to warm to 22 °C and stirred for 18 h. The reaction was poured over ice water (250 mL) and the pH adjusted to between 8 and 9 with sodium hydroxide (1 M) at which point a white precipitant formed. The solid was collected by vacuum filtration, rinsing with water, providing **S1** as a white solid (1.21 g, 7.40 mmol, 74%). ^{1}H NMR (400 MHz, $CDCl_3$) δ 9.98 (s, 1H), 7.66 (d, *J* = 8.7 Hz, 1H), 6.57 (dd, *J* = 8.7, 2.6 Hz, 1H), 6.43 (d, *J* = 2.6 Hz, 1H), 3.07 (s, 6H), 2.62 (d, *J* = 0.7 Hz, 3H); HR-ESI-MS m/z for $C_{10}H_{14}NO^+$ calcd: 164.1070 found: 164.1069.

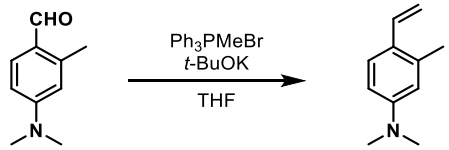

S1 **S2**

Synthesis of N,N,3-trimethyl-4-vinylaniline, S2:
A round-bottom flask was charged with methyltriphenylphosphonium bromide (4.14 g, 11.6 mmol) and then evacuated/backfilled with nitrogen (3x). Anhydrous THF (5 mL) was added and the reaction stirred for 15 min, then potassium *tert*-butoxide (1.3 g, 11.6 mmol) was added. After stirring for another 15 min, **S1** was added in anhydrous THF (5 mL) via syringe and the reaction stirred for 18 h. The solvent was then removed *in vacuo* and the remaining crude material taken up in hexanes and filtered through an alumina plug, washing with hexanes. The solvent was removed *in vacuo*, affording **S2** as a yellow oil (841 mg, 4.51 mmol, 95%). ^{1}H NMR (400 MHz, $CDCl_3$) δ 7.41 (d, *J* = 8.6 Hz, 1H), 6.88 (dd, *J* = 17.4, 11.0 Hz, 1H), 6.59 (dd, *J* = 8.6, 2.8 Hz, 1H), 6.51 (d, *J* = 2.7 Hz, 1H), 5.49 (dd, *J* = 17.4, 1.6 Hz, 1H), 5.08 (dd, *J* = 11.0, 1.5 Hz, 1H), 2.95 (s, 6H), 2.34 (s, 3H); HR-ESI-MS m/z for $C_{10}H_{16}N^+$ calcd: 162.1277 found: 162.1278.

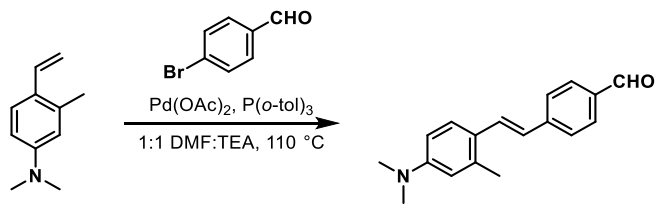

S2 S3

Synthesis of (E)-4-(4-(diethylamino)-2-methylstyryl)benzaldehyde, S3:
A Schlenk flask was charged with **S2** (821 mg, 5.09 mmol), bromobenzaldehyde (942 mg, 5.09 mmol), $Pd(OAc)_2$ (11.4 mg, 0.051 mmol), and P(*o*-tol)$_3$ (31 mg, 0.11 mmol). The flask was sealed and evacuated/backfilled with nitrogen (3x). Anhydrous DMF (5 mL) and anhydrous triethylamine (5 mL) were added via syringe and the reaction stirred at 110 °C for 16 h. The reaction was cooled and the solvent removed *in vacuo*. The remaining residue was diluted with ethyl acetate (50 mL) and washed with water (2 x 50 mL). The combined organics were dried with anhydrous sodium sulfate, filtered and the solvent removed *in vacuo.* The remaining solid was then triturated with hexanes and a small amount of diethyl ether to afford **S3** as a yellow solid (970 mg, 3.66 mmol, 72%). ^{1}H NMR (400 MHz, $CDCl_3$) δ 9.97 (s, 1H), 7.87 – 7.80 (m, 2H), 7.64 – 7.58 (m, 2H), 7.56 (d, *J* = 8.7 Hz, 1H), 7.47 (d, *J* = 16.1 Hz, 1H), 6.89 (d, *J* = 16.1 Hz, 1H), 6.61 (dd, *J* = 8.8, 2.8 Hz, 1H), 6.53 (d, *J* = 2.7 Hz, 1H), 2.99 (s, 6H), 2.44 (s, 3H); Analytical HPLC retention time 8.91 min; HR-ESI-MS m/z for $C_{18}H_{20}NO^+$ calcd: 266.1539 found: 266.1537.

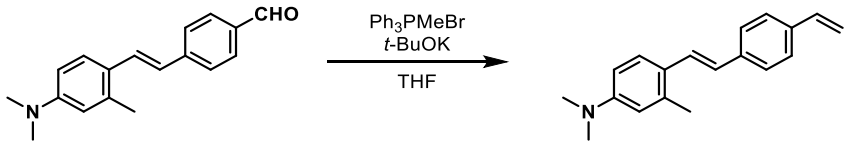

S3 18

Synthesis of (E)-N,N,3-trimethyl-4-(4-vinylstyryl)aniline, 18:
A round-bottom flask was charged with methyltriphenylphosphonium bromide (2.71 g, 7.60 mmol) and then evacuated/backfilled with nitrogen (3x). Anhydrous THF (8 mL) was added and the reaction stirred for 15 min, then potassium *tert*-butoxide (852 mg, 7.60 mmol) was added. After stirring for another 15 min, **S3** (960 mg, 3.62 mmol) was added portion-wise and the reaction stirred for 18 h. The reaction was diluted with hexanes, then the solids removed by vacuum filtration through diatomaceous earth, rinsing with hexanes. The organics were concentrated *in vacuo* and the remaining oil was purified by flash chromatography (10% ethyl acetate in hexanes, isocratic) affording **18** as a yellow solid (655 mg, 2.49 mmol, 69%). ^{1}H NMR (400 MHz, $CDCl_3$) δ 7.53 (d, *J* = 8.7 Hz, 1H), 7.48 – 7.35 (m, 4H), 7.29 (d, *J* = 16.1 Hz, 1H), 6.85 (d, *J* = 16.1 Hz, 1H), 6.72 (dd, *J* = 17.6, 10.9 Hz, 1H), 6.62 (dd, *J* = 8.7, 2.8 Hz, 1H), 6.54 (d, *J* = 2.7 Hz, 1H), 5.75 (dd, *J* = 17.6, 0.9 Hz, 1H), 5.22 (dd, *J* = 10.9, 0.9 Hz, 1H), 2.98 (s, 6H), 2.42 (s, 3H); Analytical HPLC retention time 5.12 min; HR-ESI-MS m/z for $C_{19}H_{22}N^+$ calcd: 264.1747 found: 264.1743.

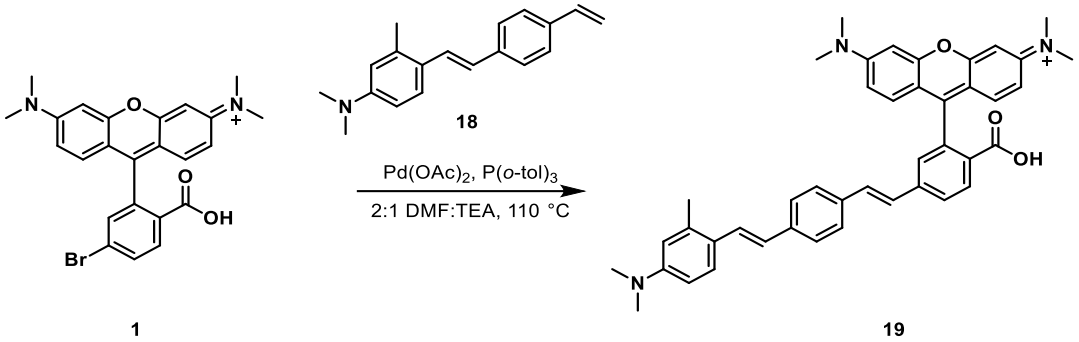

Synthesis of 19:

A Schlenk flask was charged with **1** (100 mg, 0.214 mmol), **18** (69.0 mg, 0.236 mmol), $Pd(OAc)_2$ (0.5 mg, 0.02 mmol) and P(*o*-tol)$_3$ (1.3 mg, 0.04 mmol). The flask was sealed and evacuated/backfilled with nitrogen (3x). Anhydrous DMF (3 mL) and triethylamine (1.5 mL) were added via syringe and the reaction stirred at 110 °C for 18 h. The reaction was cooled and the solvent removed *in vacuo*. The remaining residue was purified by flash chromatography (0-10% methanol in DCM, linear gradient) affording **19** as a purple solid (119 mg, 0.172 mmol, 80%). ^{1}H NMR (900 MHz, DMSO-d_6) δ 7.94 (d, *J* = 8.1 Hz, 1H), 7.90 (d, *J* = 8.1 Hz, 1H), 7.57-7.53 (m, 4H), 7.52 (d, *J* = 8.8 Hz, 1H), 7.46-7.42 (m, 2H), 7.34 (dd, *J* = 16.2, 9.5 Hz, 2H), 6.89 (d, *J* = 16.1 Hz, 1H), 6.60-6.56 (m, 3H), 6.53 (d, *J* = 2.7 Hz, 1H), 6.51 (d, *J* = 1.1 Hz, 3H), 6.50 (d, *J* = 2.6 Hz, 1H), 2.94 (s, 12H), 2.91 (s, 6H), 2.36 (s, 3H); ^{13}C NMR (226 MHz, DMSO-d_6) δ 168.6, 153.7, 152.2, 152.1, 151.9, 149.9, 144.4, 138.4, 136.6, 134.7, 132.1, 128.5, 128.2, 127.3, 126.5, 126.23, 126.1, 125.9, 125.0, 124.8, 124.2, 123.6, 120.8, 113.6, 110.4, 109.0, 106.2, 98.0, 83.0, 39.9, 39.8, 20.1; Analytical HPLC retention time 6.70 min; MS (ESI) exact mass for $C_{42}H_{40}N_3O_3^+$ $[M+H]^+$ calcd: 648.3 found: 648.6; HR-ESI-MS m/z for $C_{42}H_{40}N_3O_3^+$ calcd: 648.3211 found: 648.3212.

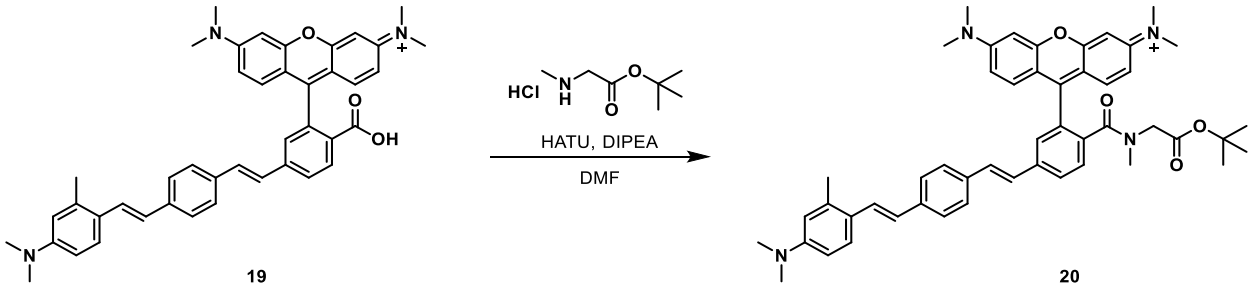

Synthesis of 20:

A vial was charged with **19** (25.0 mg, 38.5 μmol), N-methyl sarcosine *t*-Bu ester hydrochloride (7.0 mg, 48 μmol), and HATU (18.3 mg, 48.1 μmol). Anhydrous DMF (3 mL) and anhydrous diisopropylethylamine (16 μL, 77 μmol) were added and the vial was flushed with nitrogen, sealed, and stirred at 22 °C for 18 h. The solvent was removed *in vacuo* affording **20** as a purple solid which was used without further purification for the next reaction. A portion of the material was purified by Preparative TLC (5% methanol in DCM) for characterization. ^{1}H NMR (600 MHz, $CDCl_3$) δ 7.78 (dd, *J* = 8.1, 1.7 Hz, 1H), 7.60 (d, *J* = 8.0 Hz, 1H), 7.53 (d, *J* = 8.7 Hz, 1H), 7.50-7.44 (m, 5H), 7.36-7.27 (m, 3H), 7.24 – 7.08 (m, 2H), 6.93 (dd, *J* = 9.5, 2.5 Hz, 2H), 6.84 (d, *J* = 16.0 Hz, 1H), 6.76 (d, *J* = 2.4 Hz, 2H), 6.67 (d, *J* = 7.5 Hz, 1H), 6.60 (d, *J* = 2.6 Hz, 1H), 3.78 (s, 2H), 3.28 (s, 12H), 2.99 (s, 6H), 2.86 (s, 3H), 2.42 (s, 3H), 1.32 (s, 9H); Analytical HPLC retention

time 7.24 min; MS (ESI) exact mass for $C_{50}H_{55}N_4O_4^+$ $[M+H]^+$ calcd: 775.4 found: 775.6; HR-ESI-MS m/z for $C_{43}H_{48}N_3O_4^+$ calcd: 775.4218 found: 775.4212.

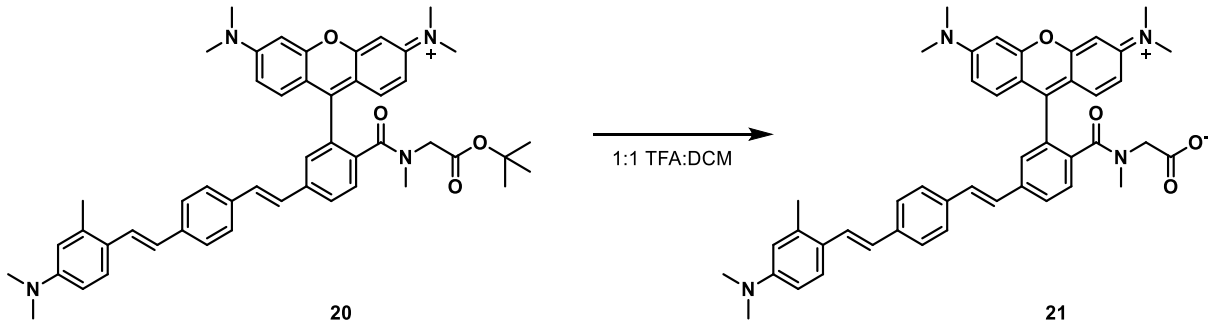

20 21

Synthesis of 21:

Trifluoroacetic acid (2 mL) was added to a solution of **20** (15.6 mg, 20.1 μmol) in DCM (2 mL). The reaction was stirred at 22 °C for 1 h, then the solvent removed under a stream of nitrogen. The remaining residue was co-evaporated with toluene (1 x 10 mL) and acetonitrile (2 x 10 mL) and then purified by preparative HPLC affording **21** as a purple solid (11.2 mg, 15.6 μmol, 77%). ^{1}H NMR (only major rotomer peaks reported, 600 MHz, DMSO-d_6) δ 7.95 (d, J = 8.2 Hz, 1H), 7.77 (s, 1H), 7.63 (d, J = 8.0 Hz, 1H), 7.59 (s, 5H), 7.54-7.33 (m, 3H), 7.30-7.23 (m, 2H), 7.11 (dd, J = 9.6, 2.5 Hz, 2H), 7.00-6.86 (m, 3H), 6.73 (d, J = 23.2 Hz, 2H), 3.82 (s, 2H), 3.28 (s, 12H), 2.96 (s, 6H), 2.81 (s, 3H), 2.39 (s, 3H); Analytical HPLC retention time 9.73 min; MS (ESI) exact mass for $C_{46}H_{47}N_4O_4^+$ calcd: 719.4 found: 719.5; HR-ESI-MS m/z for $C_{46}H_{47}N_4O_4^+$ calcd: 719.3592 found: 719.3602.

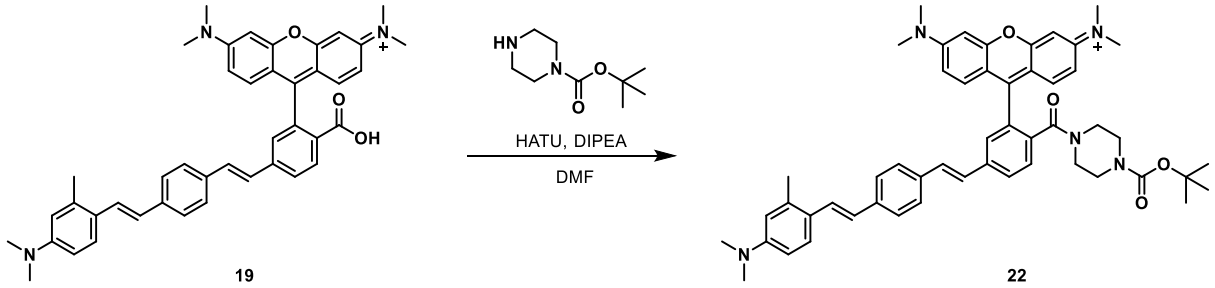

19 22

Synthesis of 22:

A vial was charged with **19** (30.0 mg, 46.2 μmol), 1-Boc piperazine (10.8 mg, 57.8 μmol), and HATU (22.0 mg, 57.8 μmol). Anhydrous DMF (3 mL) and anhydrous diisopropylethylamine (19.6 μL, 92.5 μmol) were added and the vial was flushed with nitrogen, sealed, and stirred at 22 °C for 18 h. The solvent was removed *in vacuo* and the remaining residue was purified by preparative TLC (5% methanol in DCM) affording **22** as a purple solid (25.2 mg, 30.8 μmol, 67%). ^{1}H NMR (600 MHz, CD_3OD and $CDCl_3$) δ 7.85 (dd, J = 8.2, 1.7 Hz, 1H), 7.56 (d, J = 8.1 Hz, 1H), 7.52-7.44 (m, 6H), 7.35-7.28 (m, 3H), 7.26-7.13 (m, 2H), 7.00 (dd, J = 9.5, 2.5 Hz, 2H), 6.85 (d, J = 2.5 Hz, 2H), 6.83 (d, J = 16.0 Hz, 1H), 6.61 (dd, J = 8.7, 2.7 Hz, 1H), 6.53 (d, J = 2.6 Hz, 1H), 3.39 (m, 4H), 3.32 (s, 12H), 3.24 (m, 4H), 2.94 (s, 6H), 2.39 (s, 3H), 1.41 (s, 9H); Analytical HPLC retention time 7.23 min; MS (ESI) exact mass for $C_{52}H_{58}N_5O_4^+$ $[M+H]^+$ calcd: 816.4 found: 816.5; HR-ESI-MS m/z for $C_{52}H_{58}N_5O_4^+$ calcd: 816.4483 found: 816.4488.

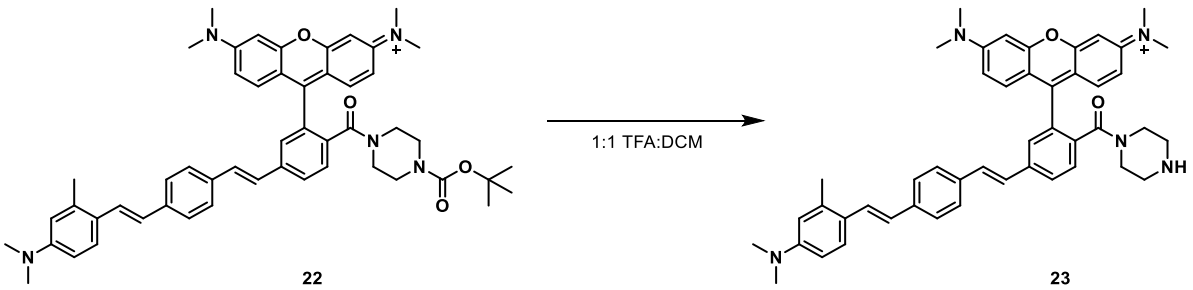

Synthesis of 23:

Trifluoroacetic acid (2 mL) was added to a solution of **22** (25.2 mg, 30.8 μmol) in DCM (2 mL). The reaction was stirred at 22 °C for 1 h, then the solvent removed under a stream of nitrogen. The remaining residue was co-evaporated with toluene (1 x 10 mL) and acetonitrile (2 x 10 mL) affording **23** as a purple solid (16.1 mg, 22.5 μmol, 73%). ^{1}H NMR (600 MHz, DMSO-d_6) δ 9.06 (br s, 1H), 7.96 (dd, *J* = 8.1, 1.7 Hz, 1H), 7.80 – 7.77 (m, 2H), 7.58 (s, 4H), 7.56 (d, *J* = 8.8 Hz, 1H), 7.50 – 7.38 (m, 2H), 7.35 (d, *J* = 16.2 Hz, 1H), 7.28 (d, *J* = 9.5 Hz, 2H), 7.11 (dd, *J* = 9.6, 2.5 Hz, 2H), 6.96 (d, *J* = 2.4 Hz, 2H), 6.94 (d, *J* = 16.1 Hz, 1H), 6.66 (d, *J* = 8.8 Hz, 1H), 6.61 (s, 1H), 3.65 (br s, 2H), 3.43 (br s, 2H), 3.29 (s, 12H), 3.09 (br s, 2H), 3.04 (br s, 2H), 2.94 (s, 6H), 2.38 (s, 3H). Analytical HPLC retention time 5.33 min; MS (ESI) exact mass for $C_{47}H_{50}N_5O_2^+$ $[M+H]^+$ calcd: 716.4 found: 716.2; HR-ESI-MS m/z for $C_{47}H_{50}N_5O_2^+$ calcd: 716.3972 found: 716.3970.

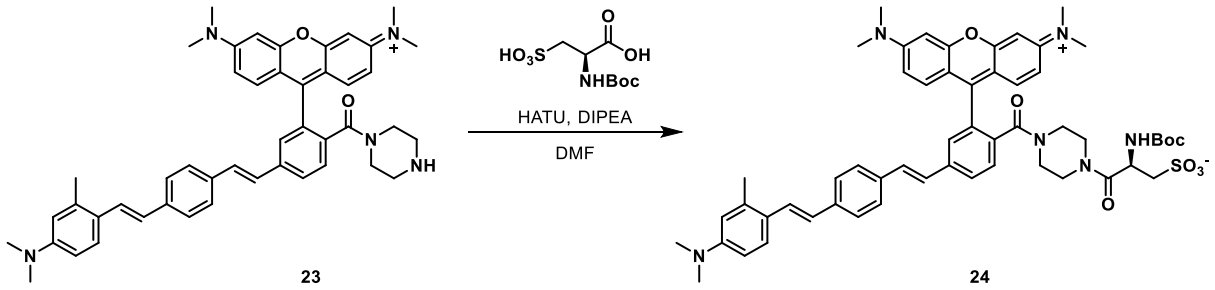

Synthesis of 24:

A vial was charged with **23** (55.3 mg, 77.1 μmol), Boc-L-cysteic acid (26.0 mg, 96.4 μmol), and HATU (36.7mg, 96.4 μmol). Anhydrous DMF (3 mL) and anhydrous diisopropylethylamine (32.7 μL, 154.2 μmol) were added and the vial was flushed with nitrogen, sealed, and stirred at 22 °C for 16 h. The solvent was removed *in vacuo* and the remaining residue was purified by preparative TLC (10% methanol in DCM) affording **24** as a purple solid (55.8 mg, 57.7 μmol, 75%); Analytical HPLC retention time 6.10 min; MS (ESI) exact mass for $C_{55}H_{63}N_6O_8S^+$ $[M+H]^+$ calcd: 967.4, found: 966.9; HR-ESI-MS m/z for $C_{55}H_{63}N_6O_8S^+$ calcd: 967.4423 found: 967.4454.

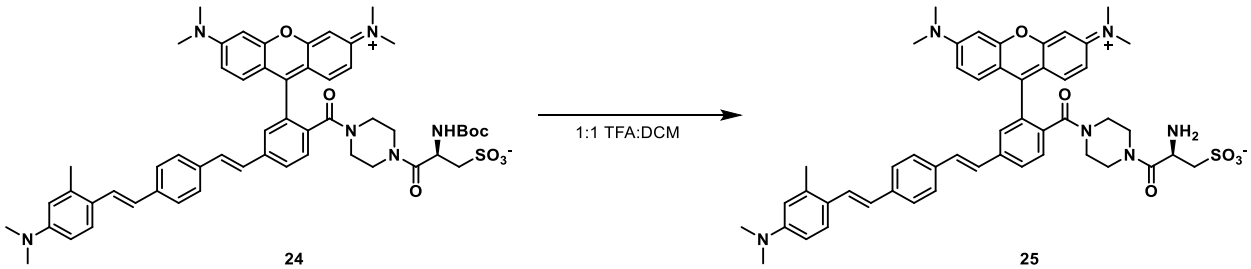

Synthesis of 25:

Trifluoroacetic acid was added to a solution of **24** (55.8 mg, 57.7 µmol) in DCM (2 mL). The reaction was stirred at 22 °C for 2 h, then the solvent removed under a stream of nitrogen. The remaining residue was co-evaporated with toluene (1 x 10 mL) and acetonitrile (2 x 10 mL) affording **25** as a purple solid (19.2 mg, 22.1 µmol, 38%). Analytical HPLC retention time 5.35 min; (ESI) exact mass for $C_{50}H_{56}N_6O_6S^+$ $[M+2H]^{2+}$ calcd: 434.2, found: 434.3; HR-ESI-MS m/z for $C_{50}H_{55}N_6O_6S^+$ calcd: 867.3898 found: 867.3899.

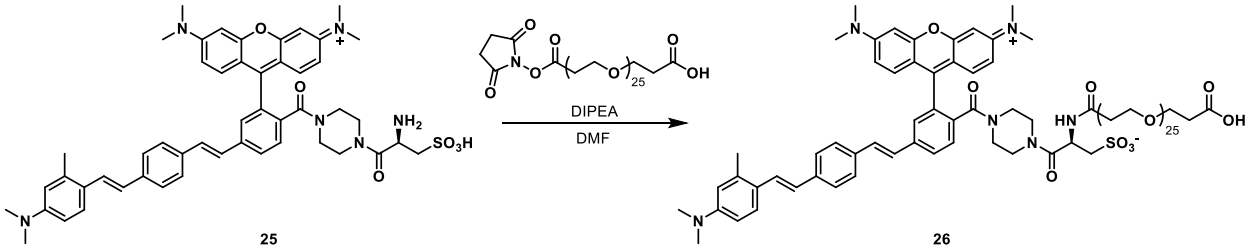

25 26

Synthesis of RhoVR(Me)-PEG$_{25}$-Acid, 26:

A vial was charged with **25** (10.0 mg, 11.5 µmol) and NHS-PEG$_{25}$-Acid (14.7 mg, 11.5 µmol). Anhydrous DMF (1 mL) and anhydrous diisopropylethylamine (3.1 uL, 23 µmol) were added and the vial was flushed with nitrogen, sealed and stirred at 22 ºC for 18 h. The solvent was removed *in vacuo* and the remaining crude solid was diluted in DCM (10 mL) and washed with water (3 x 20 mL). The combined organics were dried with anhydrous sodium sulfate, filtered and the solvent removed *in vacuo* affording **26** as a purple solid which was used without further purification for the next reaction. Analytical HPLC retention time 5.57 min; MS (ESI) exact mass for $C_{104}H_{160}ClN_6O_{34}S^{2+}$ $[M+2H]^{2+}$ calcd: 1035.0, found: 1035.5.

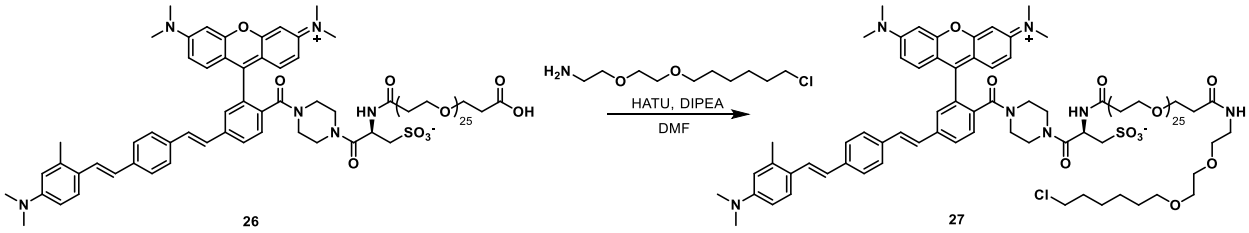

26 27

Synthesis of RhoVR(Me)-PEG$_{25}$-Halo, 27:

A vial was charged with crude **26** (23.1 mg, 11.5 µmol), Halotag-Amine (6.3 mg, 28.8 µmol) and HATU (10.6 mg, 28.8 µmol). Anhydrous DMF (1 mL) and anhydrous diisopropylethylamine (7.1 uL, 34 µmol) were added and the vial was flushed with nitrogen, sealed and stirred at 22 ºC for 16 h. The solvent was removed *in vacuo* and the crude product purified by preparative HPLC affording **27** as a purple solid (7.0 mg, 3.1 µmol, 28% over two steps). Analytical HPLC retention time 6.26 min; MS (ESI) exact mass for $C_{114}H_{180}ClN_6O_{35}S^{2+}$ $[M+2H]^{2+}$ calcd: 1137.6, found: 1137.9; HR-ESI-MS m/z for $C_{114}H_{180}ClN_7O_{35}S^{2+}$ $[M+2H]^{2+}$ calcd: 1137.5976 found: 1137.5970.

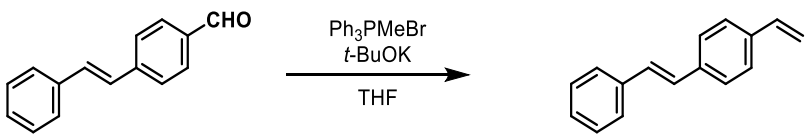

28 29

Synthesis of (E)-1-styryl-4-vinylbenzene, 29:

A round-bottom flask was charged with methyltriphenylphosphonium bromide (3.60 g, 10.1 mmol) and then evacuated/backfilled with nitrogen (3x). Anhydrous THF (10 mL) was added and the reaction stirred for 15 min, then potassium *tert*-butoxide (1.13 mg, 10.1 mmol) was added. After stirring for another 15 min, *trans*-4-stilbenecarboxaldehyde **28** (1.00 g, 4.80 mmol) was added portion-wise and the reaction stirred for 18 h. The reaction was diluted with hexanes, then the solids removed by vacuum filtration through diatomaceous earth, rinsing with hexanes. The organics were concentrated *in vacuo* and the remaining oil was purified by flash chromatography (hexanes, isocratic) affording **29** as a white solid (840 mg, 4.08 mmol, 85%). ^{1}H NMR (400 MHz, $CDCl_3$) δ 7.52 (d, *J* = 7.3 Hz, 2H), 7.50 – 7.39 (m, 4H), 7.37 (t, *J* = 7.6 Hz, 2H), 7.30 – 7.24 (m, 2H), 7.11 (s, 2H), 6.72 (dd, *J* = 17.6, 10.9 Hz, 1H), 5.77 (d, *J* = 17.6 Hz, 1H), 5.26 (d, *J* = 10.9 Hz, 1H); Analytical HPLC retention time 10.24 min; EI-MS m/z for $C_{16}H_{14}^+$ calcd: 206 found: 206.

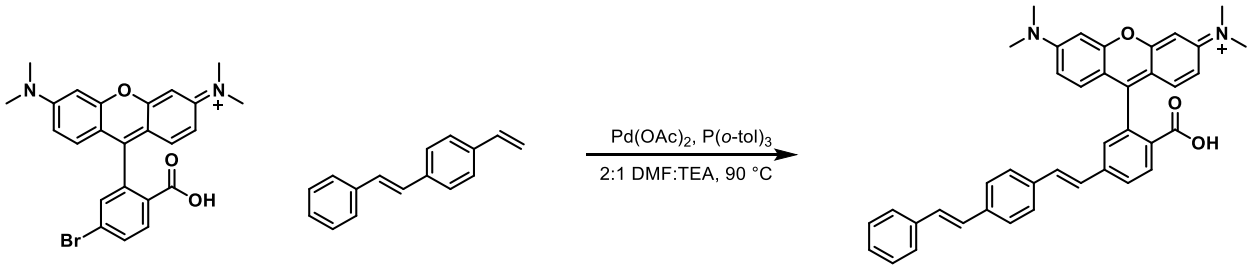

1 29 30

Synthesis of 30:

A Schlenk flask was charged with **1** (100 mg, 0.214 mmol), **29** (48.0 mg, 0.236 mmol), $Pd(OAc)_2$ (0.5 mg, 0.02 mmol) and P(*o*-tol)$_3$ (1.3 mg, 0.04 mmol). The flask was sealed and evacuated/backfilled with nitrogen (3x). Anhydrous DMF (3 mL) and triethylamine (1.5 mL) were added via syringe and the reaction stirred at 90 °C for 18 h. The reaction was cooled and the solvent removed *in vacuo*. The remaining residue was purified by flash chromatography (0-10% methanol in DCM, linear gradient) affording **30** as a purple solid (82 mg, 0.139 mmol, 65%). ^{1}H NMR (900 MHz, DMSO-d_6) δ 7.96 (d, *J* = 8.0 Hz, 1H), 7.91 (d, *J* = 7.8 Hz, 1H), 7.60 (s, 4H), 7.59 (s, 2H), 7.48-7.42 (m, 2H), 7.41-7.35 (m, 3H), 7.30-7.23 (m, 3H), 6.57 (d, *J* = 8.7 Hz, 2H), 6.52-6.49 (m, 4H), 2.94 (s, 12H); ^{13}C NMR (226 MHz, DMSO-d_6) δ 168.6, 153.7, 152.1, 151.9, 144.3, 137.2, 137.0, 135.8, 131.9, 128.8, 128.7, 128.5, 128.3, 127.9, 127.7, 127.3, 126.9, 126.7, 126.5, 125.1, 124.8, 120.9, 109.0, 106.2, 98.0, 84.0, 39.8; Analytical HPLC retention time 8.56 min; MS (ESI) exact mass for $C_{40}H_{35}N_2O_3^+$ $[M+H]^+$ calcd: 591.3 found: 591.5; HR-ESI-MS m/z for $C_{40}H_{35}N_2O_3^+$ calcd: 591.2642 found: 591.2637.

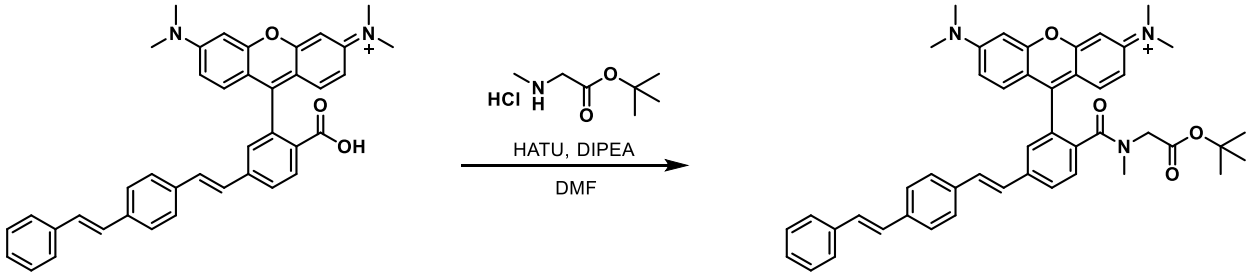

30 31

Synthesis of 31:

A vial was charged with **30** (40.0 mg, 67.6 μmol), N-methyl sarcosine *t*-Bu ester hydrochloride (18.5 mg, 101 μmol), and HATU (38.5 mg, 101 μmol). Anhydrous DMF (3 mL) and anhydrous diisopropylethylamine (17.7 μL, 101 μmol) were added and the vial was flushed with nitrogen, sealed, and stirred at 22 °C for 18 h. The solvent was removed *in vacuo* affording **31** as a purple solid which was used without further purification for the next reaction. A portion of the material was further purified by Preparative TLC (5% methanol in DCM) for characterization. ^{1}H NMR (only major rotamer peaks reported, 600 MHz, $CDCl_3$) δ 7.78 (dd, *J* = 8.1, 1.7 Hz, 1H), 7.60 (d, *J* = 8.0 Hz, 1H), 7.52-7.45 (m, 7H), 7.35 (t, *J* = 7.6 Hz, 2H), 7.32 (d, *J* = 9.5 Hz, 2H), 7.27-7.23 (m, 2H), 7.18 (m, 2H), 7.13-7.03 (m, 1H), 6.92 (dd, *J* = 9.5, 2.5 Hz, 2H), 6.74 (d, *J* = 2.5 Hz, 2H), 3.78 (s, 2H), 3.27 (s, 12H), 2.86 (s, 3H), 1.31 (s, 9H); Analytical HPLC retention time 9.12 min; MS (ESI) exact mass for $C_{47}H_{48}N_3O_4^+$ $[M+H]^+$ calcd: 718.4 found: 718.5.

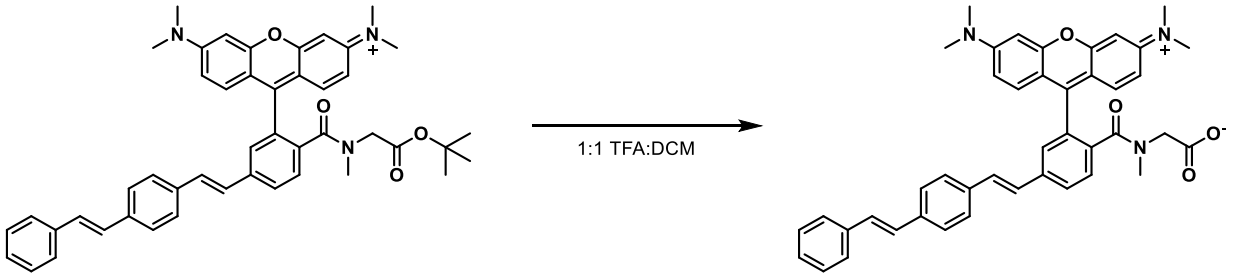

31 32

Synthesis of 32:

Trifluoroacetic acid (2 mL) was added to a solution of **31** (28.6 mg, 39.8 μmol) in DCM (2 mL). The reaction was stirred at 22 °C for 1 h, then the solvent removed under a stream of nitrogen. The remaining residue was co-evaporated with toluene (1 x 10 mL) and acetonitrile (2 x 10 mL) to remove any remaining trifluoroacetic acid and was then purified by preparative HPLC affording **32** as a purple solid (19.6 mg, 29.6 μmol, 74%). ^{1}H NMR (only major rotamer peaks reported, 600 MHz, DMSO-d_6) δ 7.95 (dd, *J* = 8.1, 1.7 Hz, 1H), 7.75 (d, *J* = 1.7 Hz, 1H), 7.67-7.50 (m, 7H), 7.48-7.36 (m, 4H), 7.32-7.23 (m, 5H), 7.10 (dd, *J* = 9.6, 2.4 Hz, 2H), 6.89 (d, *J* = 2.4 Hz, 2H), 3.82 (s, 2H), 3.27 (s, 12H), 2.81 (s, 3H); Analytical HPLC retention time 8.19 min; MS (ESI) exact mass for $C_{43}H_{40}N_3O_4^+$ $[M+H]^+$ calcd: 662.3 found: 662.4; HR-ESI-MS m/z for $C_{43}H_{48}N_3O_4^+$ calcd: 662.3013 found: 662.3008.

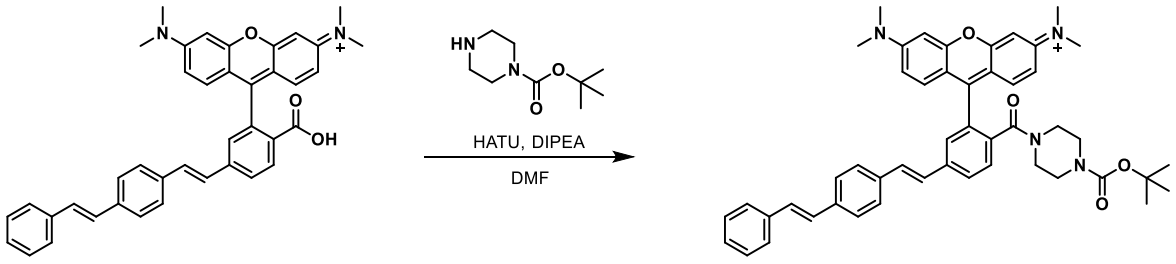

30 33

Synthesis of 33:

A vial was charged with **30** (25.0 mg, 42.2 μmol), 1-Boc piperazine (9.9 mg, 53 μmol), and HATU (20.1 mg, 53 μmol). Anhydrous DMF (2 mL) and anhydrous diisopropylethylamine (18 μL, 85 μmol) were added and the vial was flushed with nitrogen, sealed, and stirred at 22 °C for 2 h. The solvent was removed *in vacuo* affording **33** as a purple solid which was used without further

purification for the next reaction. A portion of the material was purified by Preparative TLC (5% methanol in DCM) for characterization. ^{1}H NMR (600 MHz, DMSO-d_6) δ 7.94 (dd, *J*=1.7 Hz, 1H), 7.77 (d, *J* = 1.7 Hz, 1H), 7.69 (d, *J* = 8.0 Hz, 1H), 7.66 – 7.59 (m, 6H), 7.44 (q, *J* = 16.4 Hz, 2H), 7.38 (t, *J* = 7.7 Hz, 2H), 7.27 (dd, *J* = 17.0, 9.0 Hz, 5H), 7.13 (dd, *J* = 9.5, 2.5 Hz, 2H), 6.95 (d, *J* = 2.5 Hz, 2H), 3.28 (s, 12H), 3.22 (br s, 4H), 3.16 (br s, 3H), 3.11 (br s, 1H), 1.38 (s, 9H); Analytical HPLC retention time 9.01 min; MS (ESI) exact mass for $C_{49}H_{51}N_4O_4^+$ $[M+H]^+$ calcd: 759.4, found: 759.5. HR-ESI-MS m/z for $C_{49}H_{51}N_4O_4^+$ calcd: 759.3918 found: 759.3905.

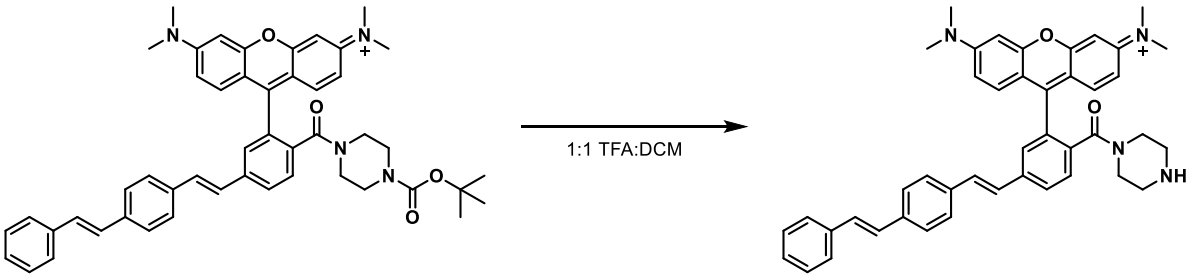

33 34

Synthesis of 34:

Trifluoroacetic acid (2 mL) was added to a solution of **33** (32.1 mg, 42.2 µmol) in DCM (2 mL). The reaction was stirred at 22 °C for 1 h, then the solvent removed under a stream of nitrogen. The remaining residue was diluted into DCM (40 mL) and washed with saturated sodium bicarbonate (40 mL) and water (40 mL), then dried with anhydrous sodium sulfate and the solvent removed *in vacuo* affording **34** as a pink solid (25.0 mg, 37.9 µmol, 90%). A portion of the material was purified by preparative TLC (10% methanol in DCM w/ 0.1% triethylamine) for characterization. ^{1}H NMR (600 MHz, DMSO-d_6) δ 9.22 (br s, 1H), 7.97 (dd, *J* = 8.2, 1.7 Hz, 1H), 7.82 – 7.77 (m, 2H), 7.65 – 7.59 (m, 6H), 7.46 (q, *J* = 16.4 Hz, 2H), 7.39 (t, *J* = 7.6 Hz, 2H), 7.33 – 7.23 (m, 5H), 7.11 (dd, *J* = 9.5, 2.5 Hz, 2H), 6.97 (d, *J* = 2.5 Hz, 2H), 3.67 (br s, 2H), 3.48 (br s, 2H), 3.30 (s, 12H), 3.01 (br s, 2H), 2.92 (br s, 2H); Analytical HPLC retention time 9.73 min; MS (ESI) exact mass for $C_{44}H_{43}N_4O_2^+$ $[M+H]^+$ calcd: 659.3, found: 659.7; HR-ESI-MS m/z for $C_{44}H_{43}N_4O_2^+$ calcd: 659.3381 found: 659.3375.

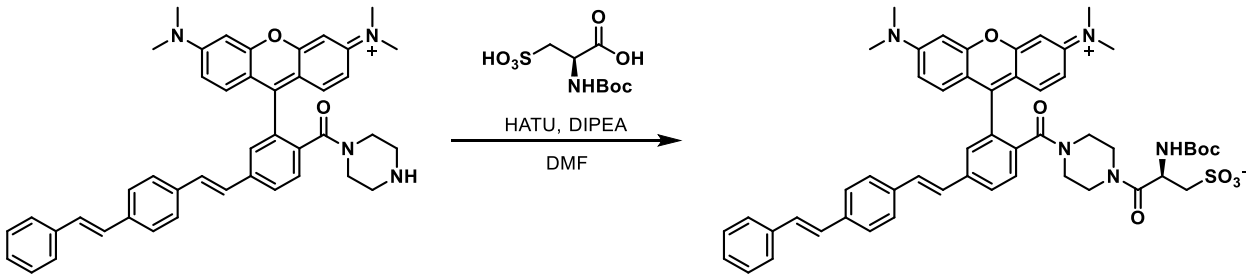

34 35

Synthesis of 35:

A vial was charged with **34** (15 mg, 20.9 µmol), Boc-L-cysteic acid (7.0 mg, 26.2 µmol), and HATU (9.9 mg, 26.2 µmol). Anhydrous DMF (2 mL) and anhydrous diisopropylethylamine (8.9 µL, 41.8 µmol) were added and the vial was flushed with nitrogen, sealed, and stirred at 22 °C for 16 h. The solvent was removed *in vacuo* affording **35** as a purple solid which was used without further purification for the next reaction. Analytical HPLC retention time 8.37 min.

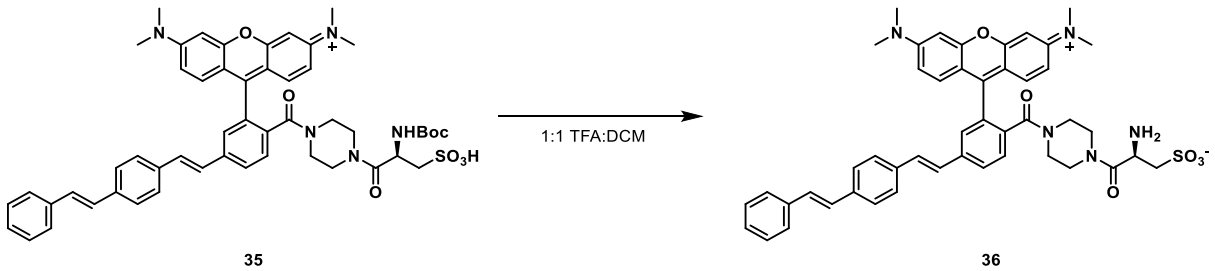

35 36

Synthesis of 36:

Trifluoroacetic acid (2 mL) was added to a solution of **35** (27.6 mg, 30.3 µmol) in DCM (2 mL). The reaction was stirred at 22 °C for 2 h, then the solvent removed under a stream of nitrogen. The remaining residue was diluted into DCM (40 mL) and washed with 1M hydrochloric acid (40 mL), saturated sodium bicarbonate (40 mL) and water (40 mL), then dried with anhydrous sodium sulfate and the solvent removed *in vacuo* affording **36** as a pink solid (20.0 mg, 24.7 µmol, 81%). Analytical HPLC retention time 6.94 min; MS (ESI) exact mass for $C_{47}H_{47}N_5O_6S^+$ $[M+H]^+$ calcd: 810.3, found: 810.5; HR-ESI-MS m/z for $C_{47}H_{47}N_5O_6S^+$ calcd: 810.3320 found: 810.3338.

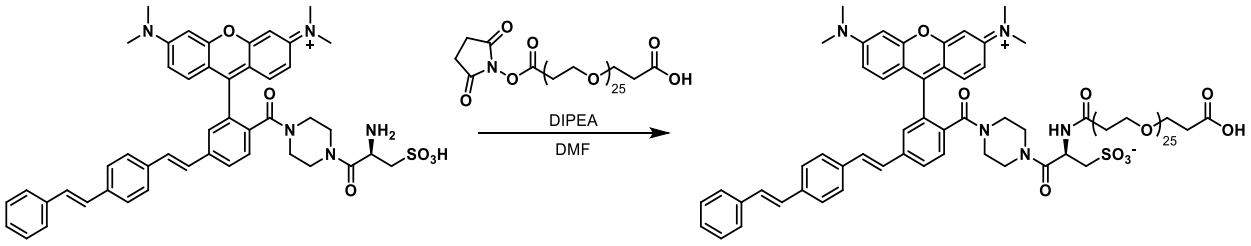

36 37

Synthesis of RhoVR(0)-PEG$_{25}$-Acid, 37:

A vial was charged with **36** (10.0 mg, .012 mmol, 1.0 equiv.) and NHS-PEG$_{25}$-Acid (16.3 mg, .012 mmol, 1.0 equiv.). Anhydrous DMF (1 mL) and anhydrous diisopropylethylamine (3.4 uL, .025 mmol, 2.0 equiv.) were added and the vial was flushed with nitrogen, sealed and stirred at 22 ºC for 18 h. The solvent was removed *in vacuo* and the remaining crude solid was diluted in DCM (10 mL) and washed with water (3 x 20 mL). The combined organics were dried with anhydrous sodium sulfate, filtered and the solvent removed *in vacuo* affording **37** as a purple solid which was used without further purification for the next reaction. Analytical HPLC retention time 7.10 min; MS (ESI) exact mass for $C_{101}H_{153}ClN_5O_{34}S^{2+}$ $[M+2H]^+$ calcd: 1006.5, found: 1006.5.

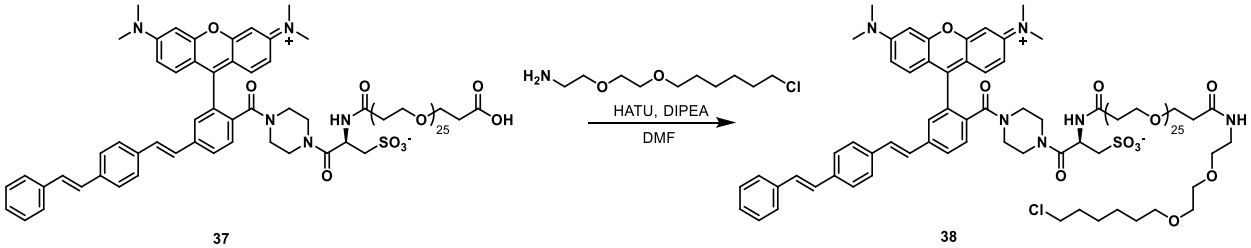

37 38

Synthesis of RhoVR(0)-PEG$_{25}$-Halo, 38:

A vial was charged with crude **37** (24.8 mg, .012 mmol, 1.0 equiv.), Halotag-Amine (6.9 mg, .031 mmol, 2.0 equiv.) and HATU (11.7 mg, .031 mmol, 2.0 equiv.). Anhydrous DMF (1 mL) and anhydrous diisopropylethylamine (8.6 uL, .049 mmol, 3.0 equiv.) were added and the vial was flushed with nitrogen, sealed and stirred at 22 ºC for 16 h. The solvent was removed *in vacuo* and

the crude product purified by preparative HPLC affording **38** as a purple solid (7.7 mg, 3.5 μmol, 28% over two steps). Analytical HPLC retention time 7.83 min; MS (ESI) exact mass for $C_{111}H_{173}ClN_6O_{35}S^{3+}$ $[M+2H]^{2+}$ calcd: 1109.6, found: 1109.5; HR-ESI-MS m/z for $C_{111}H_{170}ClN_6Na_3O_{35}S^{2+}$ $[M+3Na]^{3+}$ calcd: 761.3624 found: 761.3633.

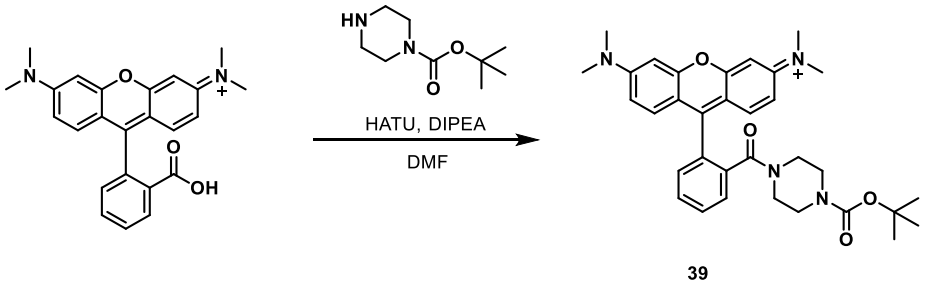

39

Synthesis of 39:

A vial was charged with tetramethylrhodamine (34.5 mg, 89.0 μmol), 1-Boc piperazine (19.1 mg, 102 μmol), and HATU (38.9 mg, 102 μmol). Anhydrous DMF (3 mL) and anhydrous diisopropylethylamine (37.7 μL, 178 μmol) were added and the vial was flushed with nitrogen, sealed, and stirred at 22 °C for 18 h. The solvent was removed *in vacuo* and the remaining residue diluted with ethyl acetate (35 mL), washed with water (3 x 30 mL), and then dried with anhydrous sodium sulfate and the solvent removed *in vacuo* affording **39** as a purple solid which was used without further purification for the next reaction. Analytical HPLC retention time 6.52 min; MS (ESI) exact mass for $C_{33}H_{39}N_4O_4^+$ $[M+H]^+$ calcd: 555.7 found: 555.1.

39 40

Synthesis of 40:

Trifluoroacetic acid (2 mL) was added to a solution of **39** (49.5 mg, 89.0 μmol) in DCM (2 mL). The reaction was stirred at 22 °C for 2 h, then the solvent removed under a stream of nitrogen. The remaining residue was diluted into DCM (40 mL) and washed with saturated sodium bicarbonate (40 mL) and water (40 mL), then dried with anhydrous sodium sulfate and the solvent removed *in vacuo* affording **40** as a purple solid which was used without further purification for the next reaction. Analytical HPLC retention time 4.19 min; MS (ESI) exact mass for $C_{28}H_{31}N_4O_2^+$ $[M+H]^+$ calcd: 455.2, found: 455.0.

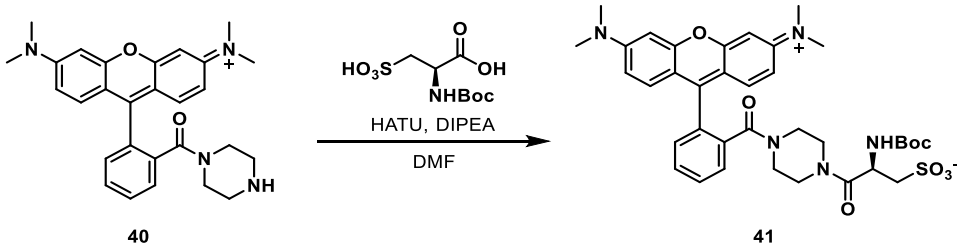

40 41

Synthesis of 41:

A vial was charged with **40** (41.1 mg, 89 µmol), Boc-L-cysteic acid (30.3 mg, 113 µmol), and HATU (42.8 mg, 113 µmol). Anhydrous DMF (2 mL) and anhydrous diisopropylethylamine (38.2 µL, 180 µmol) were added and the vial was flushed with nitrogen, sealed, and stirred at 22 °C for 16 h. The solvent was removed *in vacuo* and the remaining residue was purified by flash chromatography (0-20% methanol in DCM, linear gradient) affording **41** as a purple solid (54.2 mg, 76.8 µmol, 86%). Analytical HPLC retention time 5.20 min; MS (ESI) exact mass for $C_{36}H_{44}N_5O_8S_1^+$ $[M+H]^+$ calcd: 706.3, found: 706.0.

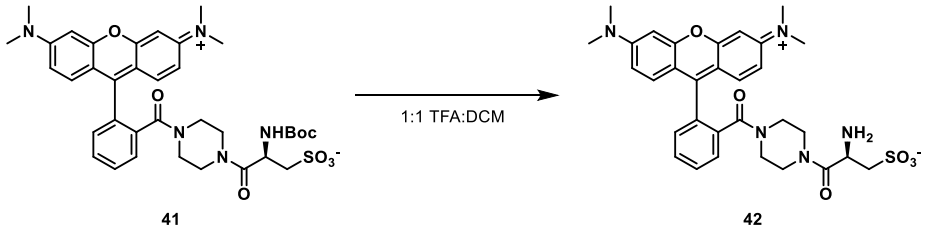

41 42

Synthesis of 42:

Trifluoroacetic acid (2 mL) was added to a solution of **41** (54.0 mg, 76.5 µmol) in DCM (2 mL). The reaction was stirred at 22 °C for 2 h, then the solvent removed under a stream of nitrogen. The remaining residue was diluted into DCM (40 mL) and washed with saturated sodium bicarbonate (40 mL) and water (40 mL), then dried with anhydrous sodium sulfate and the solvent removed *in vacuo*. The remaining material was purified by preparative TLC (15% methanol in DCM) affording **42** as a purple solid (38.6 mg, 63.7 µmol, 83%). Analytical HPLC retention time 4.48 min; MS (ESI) exact mass for $C_{44}H_{43}N_4O_2^+$ $[M+H]^+$ calcd: 606.7, found: 606.0.

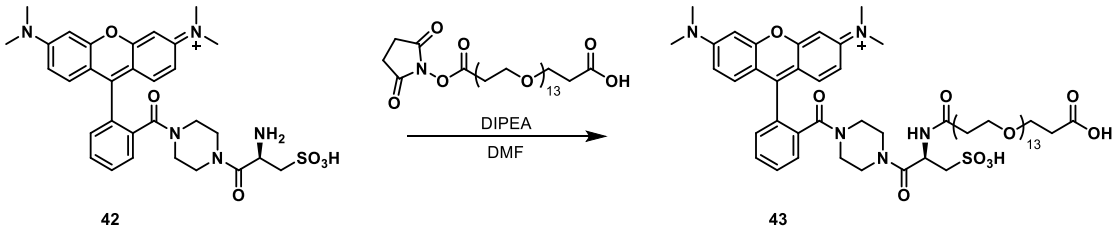

42 43

Synthesis of TMR-PEG$_{13}$-Acid, 43:

A vial was charged with **42** (10.0 mg, 16.5 µmmol and NHS-PEG$_{13}$-Acid (14.2 mg, 18.3 µmol). Anhydrous DMF (1 mL) and anhydrous diisopropylethylamine (5.9 uL, .033 µmol) were added and the vial was flushed with nitrogen, sealed and stirred at 22 ºC for 18 h. The solvent was removed *in vacuo* affording **43** as a purple solid which was used without further purification for the next reaction. Analytical HPLC retention time 4.77 min; MS (ESI) exact mass for

$C_{61}H_{93}N_5O_{22}S^{2+}$ $[M+2H]^{2+}$ calcd: 638.8, found: 638.6; HR-ESI-MS m/z for $C_{61}H_{91}N_5Na_2O_{22}S^{2+}$ $[M+2Na]^{2+}$ calcd: 661.7830 found: 661.7830.

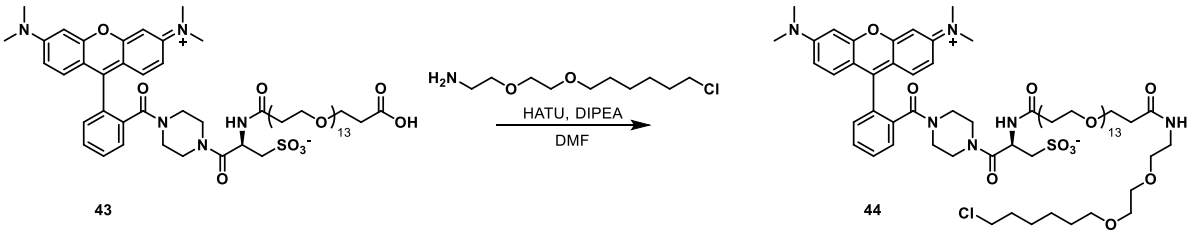

43 44

Synthesis of TMR-PEG$_{13}$-Halo, 44:
A vial was charged with crude **43** (16.5 µmmol), Halotag-Amine (4.6 mg, 20.6 µmol) and HATU (14.5 mg, 20.6 µmol). Anhydrous DMF (2 mL) and anhydrous diisopropylethylamine (5.2 uL, 24.7 µmol, 1.5 equiv.) were added and the vial flushed with nitrogen, sealed and stirred at 22 ºC for 16 h. The solvent was removed *in vacuo* and the crude product purified by preparative HPLC affording **44** as a purple solid (12.0 mg, 8.1 µmol, 49.1% over two steps). Analytical HPLC retention time 5.93 min; MS (ESI) exact mass for $C_{71}H_{113}ClN_6O_{23}S^{2+}$ $[M+2H]^{2+}$ calcd: 742.4, found: 742.4; HR-ESI-MS m/z for $C_{71}H_{111}ClN_6Na_2O_{23}S^{2+}$ $[M+2Na]^{2+}$ calcd: 764.3447 found: 764.3456.

Spectroscopic Studies

Stock solutions of RhoVRs were prepared in DMSO (500-5000 µM) and diluted with either dPBS (10 mM KH_2PO_4, 30 mM $Na_2HPO_4{\cdot}7H_2O$, 1.55 M NaCl, pH 7.2) solution containing 0.10 % (w/w) SDS (1:100-1:1000 dilution), HBSS (140 mM NaCl, 2.5 mM KCl, 10 mM HEPES, 10 mM D-glucose 1.3 mM $MgCl_2$ and 2 mM $CaCl_2$; pH 7.3 and 290 mOsmol) or EtOH. UV-Vis absorbance and fluorescence spectra were recorded using a Shimadzu 2501 Spectrophotometer (Shimadzu) and a Quantamaster Master 4 L-format scanning spectrofluorometer (Photon Technologies International). The fluorometer is equipped with an LPS-220B 75-W xenon lamp and power supply, A-1010B lamp housing with integrated igniter, switchable 814 photon-counting/analog photomultiplier detection unit, and MD5020 motor driver. Samples were measured in 1-cm path length quartz cuvettes (Starna Cells).

The two-photon excitation (TPE) cross section of RhoVR1-PEG$_{25}$-Halo and RhoVR(Me)-PEG$_{25}$-Halo were determined according to previously reported procedures. We first measured the fluorescence signal generated by two-photon excitation of a rhodamine B standard using a Zeiss BiG-2 GaAsP detector on a Zeiss LSM 880 NLO AxioExaminer equipped with a Chameleon Ultra I laser. We then determined the one-photon quantum yield of the dyes of interest and measured the fluorescence signal generated by two-photon excitation of the dyes of interest. We then calculated the TPE of the dyes of interest via the following equation:

$$\sigma_{TPE\ Dye} = \frac{\Phi_{Rho\ B} * \sigma_{TPE\ Dye}}{\Phi_{Dye}} * \frac{F_{Dye}}{F_{Rho\ B}}$$

Where F_{dye} and $F_{Rho\ B}$ are the measured fluorescence signal from the dye of interest and rhodamine b, respectively. The values for σ_{TPE} at different wavelengths for rhodamine b were obtained from Xu and Webb.[32]

Quantum yields were measured according to the procedure outlined in **Appendix 3**.

Cell Culture

All animal procedures were approved by the UC Berkeley Animal Care and Use Committees and conformed to the NIH Guide for the Care and Use and Laboratory Animals and the Public Health Policy.

Human embryonic kidney 293T (HEK) cells were passaged and plated onto 12 mm glass coverslips pre-coated with Poly-D-Lysine (PDL; 1 mg/ml; Sigma-Aldrich) to provide a confluency of ~15% and 50% for electrophysiology and imaging, respectively. HEK cells were plated and maintained in Dulbecco's modified eagle medium (DMEM) supplemented with 4.5 g/L D-glucose, 10% FBS and 1% Glutamax. Transfection of genetic tools was carried out using Lipofectamine 3000 24 h after plating. Imaging was performed 18-24 h following transfection.

Hippocampi were dissected from embryonic day 18 Sprague Dawley rats (Charles River Laboratory) in cold sterile HBSS (zero Ca^{2+}, zero Mg^{2+}). All dissection products were supplied by Invitrogen, unless otherwise stated. Hippocampal tissue was treated with trypsin (2.5%) for 15 min at 37 °C. The tissue was triturated using fire polished Pasteur pipettes, in minimum essential media (MEM) supplemented with 5% fetal bovine serum (FBS; Thermo Scientific), 2% B-27, 2% 1M D-glucose (Fisher Scientific) and 1% glutamax. The dissociated cells were plated onto 12 mm diameter coverslips (Fisher Scientific) pre-treated with PDL (as above) at a density of 30-40,000 cells per coverslip in MEM supplemented media (as above). Neurons were maintained at 37 °C in a humidified incubator with 5 % CO_2. At 1 day in vitro (DIV) half of the MEM supplemented media was removed and replaced with Neurobasal media containing 2% B-27 supplement and 1% glutamax. Transfection of genetic tools was carried out using Lipofectamine 3000 at 7 DIV. Functional imaging was performed on mature neurons 13-20 DIV, except electrophysiological experiments which were performed on 12-15 DIV neurons.

In utero *electroporation*

Pregnant mice at E15-16 were anaesthetized with 2.0% isoflurane, the abdomen was cleaned with 70% ethanol and swabbed with iodine, and a small vertical incision was made in the skin and abdominal wall and 8–12 embryos gently exposed. Each embryo was injected with 0.5–1 μl of DNA solution and 0.05% Fast Green dye. We used a pressure-controlled beveled glass pipette (Drummond, Custom Microbeveller) for injection. After each injection, the embryos were moistened with saline and voltage steps via tweezertrodes (BTX, 5 mm round, platinum, BTX electroporator) were applied with the positive electrode placed over the visual cortex and the negative electrode placed under the head of the embryo. Voltage was 40 V for 5 pulses at 1 Hz, each pulse lasting 50 ms. The embryos were returned to the abdomen, which was sutured, followed by suturing of the skin. The procedure typically lasted under 30 min.

Acute brain slice preparation

Mice were deeply anesthetized with isoflurane and quickly decapitated. After removing the scalp and skull, ice cold sucrose cutting solution (in mM: NaCl, 83; KCl, 2.5; $MgSO_4$, 3.3; NaH_2PO_4, 1; $NaHCO_3$, 26.2; D-glucose, 22; sucrose, 72; and $CaCl_2$, 0.5) was applied to the brain. BFP fluorescence was checked with a hand held 405 nm laser before the brain was taken out. The

brain was cut into 300 µm thick slices with a DTK-1000 slicer in ice cold sucrose cutting solution. The cut slices were incubated in sucrose cutting solution, bubbled with 95% O_2 and 5% CO_2, first at 31 °C for about 30 min and then at room temperature until further use. For bath application of the dye and cell staining, a slice was transferred to a 35 mm dish with sucrose cutting solution bubbled with 95% O_2 and 5% CO_2 to which dye stock solution was added (250 nM final concentration). The slice was incubated with the dye at room temperature for 15 min.

Imaging Parameters

Epifluorescence imaging was performed on an AxioExaminer Z-1 (Zeiss) equipped with a Spectra-X Light engine LED light (Lumencor), controlled with Slidebook (v6, Intelligent Imaging Innovations). Co-incident excitation with multiple LEDs was controlled by Lumencor software triggered through a Digidata 1332A digitizer and pCLAMP 10 software (Molecular Devices). Images were acquired with either a W-Plan-Apo 20x/1.0 water objective (20x; Zeiss) or a W-Plan-Apo 63x/1.0 water objective (63x; Zeiss). Images were focused onto either an OrcaFlash4.0 sCMOS camera (sCMOS; Hamamatsu) or an eVolve 128 EMCCD camera (EMCCD; Photometrix). More detailed imaging information for each experimental application is expanded below. For RhoVR images, the excitation light was delivered from a LED (1.73-9.72 W/cm^2) at 542/33 (bandpass) nm and emission was collected with a quadruple emission filter (430/32, 508/14, 586/30, 708/98 nm) after passing through a quadruple dichroic mirror (432/38, 509/22, 586/40, 654 nm LP). For EGFP images, excitation light was delivered from a LED (0.82-5.77 W/cm^2) at 475/34 nm and emission was collected with a quadruple emission filter (430/32, 508/14, 586/30, 708/98 nm) after passing through a quadruple dichroic mirror (432/38, 509/22, 586/40, 654 nm LP).

Confocal imaging was performed with a Zeiss LSM 880 NLO AxioExaminer equipped with a Diode 405 nm laser line, Argon 458, 488, and 514 laser lines, and a DPSS 561 nm laser line and a BiG-2 detector with a 690+ dichroic. Images were acquired using a W-Plan-Apo 40x/1.0 DIC objective and a Zeiss Airyscan detector. For 2P imaging RhoVR-halos were excited using 820-1060 nm light with a laser attenuation percentage between 2 and 5% between 820-860 nm and 100% at 1060 nm.

Unless stated otherwise, for loading of HEK cells and hippocampal neurons, 50 µM DMSO stock solutions of were diluted 1:1000 in HBSS for loading. All imaging experiments were performed in HBSS (in mM) 140 NaCl, 2.5 KCl, 10 HEPES, 10 D-glucose 1.3 $MgCl_2$ and 2 $CaCl_2$; pH 7.3 and 290 mOsmol.

Multicolor imaging of RhoVR 1 in HEK cells and photostability

EGFP transfected HEK cells were incubated with a HBSS solution (Gibco) containing **15** (50 nM) at 37 °C for 30 min prior to transfer to fresh HBSS (no dye) for imaging. Microscopic images were acquired with a W-Plan-Apo 20x/1.0 water objective (Zeiss) and OrcaFlash4.0 sCMOS camera (Hamamatsu). For RhoVR 1 images, the excitation light was delivered from a LED (9.72 W/cm^2; 100 ms exposure time) at 542/33 (bandpass) nm and emission was collected with a quadruple emission filter (430/32, 508/14, 586/30, 708/98 nm) after passing through a quadruple dichroic mirror (432/38, 509/22, 586/40, 654 nm LP). For eGFP images, the excitation light was delivered from a LED (5.77 W/cm^2; 20 ms exposure time) at 475/34 nm and emission was collected with a quadruple emission filter (430/32, 508/14, 586/30, 708/98 nm) after passing through a quadruple dichroic mirror (432/38, 509/22, 586/40, 654 nm LP).

Voltage sensitivity in HEK cells

Functional imaging of the RhoVR voltage dyes was performed using a 20x objective paired with image capture from the EMCCD camera at a sampling rate of 0.5 kHz. RhoVRs were excited using the 542 nm LED with an intensity of 9.73 W/cm^2. For initial voltage characterization emission was collection with the QUAD filter and dichroic (see above).

Imaging spontaneous activity in cultured neurons

Imaging experiments looking at functional responses from neurons were obtained using the sCMOS camera with a 20x objective. RhoVR-Halos were excited using the 542 nm LED with an intensity of 1.73-9.73 W/cm^2 and emission was collected with a QUAD filter and dichroic (see above). Images were binned 4x4 to allow sampling rates of 0.5 kHz. eGFP was excited by the 475 nm LED with an intensity of 0.82-1.20 W/cm^2 and emission was collected with the same QUAD filter and dichroic.

Imaging evoked activity in cultures neurons

Coverslips of cultured hippocampal neurons were placed in a recording chamber containing two platinum electrodes (Warner), which were connected to a SD9 Grass Stimulator which delivered the extracellular field stimulation. The triggering was provided through the same Digidata 1332A digitizer and pCLAMP 9 software (Molecular Devices) that ran the electrophysiology. Action potentials were triggered by 1 ms 60 V field potentials delivered at 5 Hz. Synaptic blockers including 10 μM 2,3-Dioxo-6-nitro-1,2,3,4-tetrahydrobenzo[f]quinoxaline-7-sulfonamide (NBQX; Santa Cruz Biotechnology) and 25 μM DL-2-Amino-5-phosphonopentanoic acid (APV; Sigma-Aldrich) were added to the HBSS solution to prevent recurrent activity. For both evoked action potentials and spontaneous activity, images were binned 4x4 to allow sampling rates of 0.5 kHz and 2500 frames (5 s) were acquired for each recording.

Simultaneous electrophysiology and fluorescence voltage imaging in cultured neurons

Functional imaging of patched neurons was performed using an EMCCD camera and a 20x objective. This objective has a larger working distance and allowed for positioning of the patch electrode. RhoVR-PEG$_{25}$-Halo **15** was excited by a 542 nm LED with an intensity of 9.73 W/cm^2 and emission was collected with a QUAD filter and dichroic (see above). For optical assessment of the action potential waveform the sampling rate was increased to 1.8 kHz.

Dual-View imaging

Dual-view imaging was preformed using a 20x objective paired with the sCMOS camera. RhoVR-PEG$_{25}$-Halo **15** was excited using the 542 nm LED with a light intensity of 2.40-9.73 W/cm^2 while GCaMP6s was excited simultaneously using a 475 nm LED with a light intensity of 0.82-1.20 W/cm^2. Emission was collected with a QUAD filter and dichroic (see above) used in conjunction with a Dual-View emission splitter (Optical Insights). The Dual-View was equipped with a 585dcxr dichroic (Chroma) and 520/28 nm (Semrock) and 610/75 nm (Chroma) emission filters which separated the GCaMP6s and RhoVR signals.

Image Analysis

Analysis of voltage sensitivity in HEK cells and neurons was performed using ImageJ (FIJI). Briefly, a region of interest (ROI) was selected automatically based on fluorescence intensity and applied as a mask to all image frames. Fluorescence intensity values were calculated at known baseline and voltage step epochs. For analysis of RhoVR-PEG$_x$-Halo voltage responses in neurons, regions of interest encompassing cell bodies (all of approximately the same size) were drawn in ImageJ and the mean fluorescence intensity for each frame extracted. ΔF/F values were calculated by first subtracting a mean background value from all raw fluorescence frames, bypassing the noise amplification which arises from subtracting background for each frame, to give a background subtracted trace (bkgsub). A baseline fluorescence value (F_{base}) is calculated either from the first several (10-20) frames of the experiment for evoked activity, or from the median for spontaneous activity, and was subtracted from each timepoint of the bkgsub trace to yield a ΔF trace. The ΔF was then divided by F_{base} to give ΔF/F traces. No averaging has been applied to any voltage traces.

Electrophysiology

For electrophysiological experiments, pipettes were pulled from borosilicate glass (Sutter Instruments, BF150-86-10), with a resistance of 4–8 MΩ, and were filled with an internal solution; 115 mM potassium gluconate, 10 mM BAPTA tetrapotassium salt, 10 mM HEPES, 5 mM NaCl, 10 mM KCl, 2 mM ATP disodium salt, 0.3 mM GTP trisodium salt (pH 7.25, 275 mOsm). Recordings were obtained with an Axopatch 200B amplifier (Molecular Devices) at room temperature. The signals were digitized with Digidata 1440A, sampled at 50 kHz and recorded with pCLAMP 10 software (Molecular Devices) on a PC. Fast capacitance was compensated in the on-cell configuration. For all electrophysiology experiments, recordings were only pursued if series resistance in voltage clamp was less than 30 MΩ. For whole-cell, voltage clamp recordings in HEK 293T cells, cells were held at -60 mV and 100 ms hyper- and de- polarizing steps applied from -100 to +100 mV in 20 mV increments.

For whole-cell, current clamp recordings in hippocampal neurons, following membrane rupture, resting membrane potential was assessed and recorded at I = 0 and monitored during the data acquisition. Neurons were switched to current clamp mode if they displayed series resistance in voltage clamp <30 MΩ. Pipette tip resistance was corrected by performing a bridge balance compensation.

To test if loading of RhoVR-PEG$_{25}$-Halo onto the membrane of neurons has any effect on their action potential firing, ten 500 ms current steps (0.05-0.20 pA) were injected into neurons. The action potential from each sweep was analyzed in Clampfit 10 software (Molecular Devices) to give amplitude and kinetic data. The cell capacitance determined by the Clampex software during recording. To evoke single action potentials for electrophysiological and imaging comparisons, short (10 ms) current injections were applied which were 2x the threshold required to evoke a single action potential. Analysis of action potentials was performed using spike detection algorithms in the Clampfit 10 software.

DNA constructs

To express the HaloTag protein on the cell surface, an IgK leader sequence was fused to the N-terminal and either a signal peptide for GPI addition (DAF) or a transmembrane domain (pDisplay) was added to the C-terminal of the HaloTag sequence. For the purpose of inmmunostaining, an HA tag was inserted. Mammalian expression vector pcDNA3 with either a cytomegalovirus (CMV) promoter or human synapsin promoter (Syn) was used for protein expression in HEK cells and cultured neurons, respectively. To increase expression in neurons, a regulatory element from the woodchuck hepatitis virus (WPRE) was used. In some constructs, nuclear-targeted EGFP (NLS-EGFP) was inserted down stream of HaloTag, separated by an internal ribosome entry site (IRES) sequence, in order to track the expression of HaloTag in live cells. For dual voltage and calcium imaging, a GCaMP6s with an IRES sequence was inserted down stream of HaloTag. The cloned constructs were verified by sequencing. All the constructs were prepared using Qiagen Maxiprep kit, except those with CMV promoter. The following sequences were used (5' to 3'):

IgK
ATGGAGACAGACACACTCCTGCTATGGGTACTGCTGCTCTGGGTTCCAGGTTCCACT
GGTGAC

HaloTag
GCAGAAATCGGTACTGGCTTTCCATTCGACCCCCATTATGTGGAAGTCCTGGGCGAG
CGCATGCACTACGTCGATGTTGGTCCGCGCGATGGCACCCCTGTGCTGTTCCTGCAC
GGTAACCCGACCTCCTCCTACGTGTGGCGCAACATCATCCCGCATGTTGCACCGACC
CATCGCTGCATTGCTCCAGACCTGATCGGTATGGGCAAATCCGACAAACCAGACCTG
GGTTATTTCTTCGACGACCACGTCCGCTTCATGGATGCCTTCATCGAAGCCCTGGGTC
TGGAAGAGGTCGTCCTGGTCATTCACGACTGGGGCTCCGCTCTGGGTTTCCACTGGG
CCAAGCGCAATCCAGAGCGCGTCAAAGGTATTGCATTTATGGAGTTCATCCGCCCTA
TCCCGACCTGGGACGAATGGCCAGAATTTGCCCGCGAGACCTTCCAGGCCTTCCGCA
CCACCGACGTCGGCCGCAAGCTGATCATCGATCAGAACGTTTTTATCGAGGGTACGC
TGCCGATGGGTGTCGTCCGCCCGCTGACTGAAGTCGAGATGGACCATTACCGCGAG
CCGTTCCTGAATCCTGTTGACCGCGAGCCACTGTGGCGCTTCCCAAACGAGCTGCCA
ATCGCCGGTGAGCCAGCGAACATCGTCGCGCTGGTCGAAGAATACATGGACTGGCT
GCACCAGTCCCCTGTCCCGAAGCTGCTGTTCTGGGGCACCCCAGGCGTTCTGATCCC
ACCGGCCGAAGCCGCTCGCCTGGCCAAAAGCCTGCCTAACTGCAAGGCTGTGGACA
TCGGCCCGGGTCTGAATCTGCTGCAAGAAGACAACCCGGACCTGATCGGCAGCGAG
ATCGCGCGCTGGCTGTCGACGCTCGAGATTTCCGGC

HA
TATCCATATGATGTTCCAGATTATGCT

DAF
CCAAATAAAGGAAGTGGAACCACTTCAGGTACTACCCGTCTTCTATCTGGGCACACG
TGTTTCACGTTGACAGGTTTGCTTGGGACGCTAGTAACCATGGGCTTGCTGACTTAG

pDisplay

GCTGTGGGCCAGGACACGCAGGAGGTCATCGTGGTGCCACACTCCTTGCCCTTTAAG
GTGGTGGTGATCTCAGCCATCCTGGCCCTGGTGGTGCTCACCATCATCTCCCTTATCA
TCCTCATCATGCTTTGGCAGAAGAAGCCACGT

IRES

GCCCCTCTCCCTCCCCCCCCCCTAACGTTACTGGCCGAAGCCGCTTGGAATAAGGCC
GGTGTGCGTTTGTCTATATGTTATTTTCCACCATATTGCCGTCTTTTGGCAATGTGAG
GGCCCGGAAACCTGGCCCTGTCTTCTTGACGAGCATTCCTAGGGGTCTTTCCCCTCTC
GCCAAAGGAATGCAAGGTCTGTTGAATGTCGTGAAGGAAGCAGTTCCTCTGGAAGC
TTCTTGAAGACAAACAACGTCTGTAGCGACCCTTTGCAGGCAGCGGAACCCCCCACC
TGGCGACAGGTGCCTCTGCGGCCAAAAGCCACGTGTATAAGATACACCTGCAAAGG
CGGCACAACCCCAGTGCCACGTTGTGAGTTGGATAGTTGTGGAAAGAGTCAAATGG
CTCTCCTCAAGCGTATTCAACAAGGGGCTGAAGGATGCCCAGAAGGCACCCCATTG
TATGGGATCTGATCTGGGGCCTCGGTGCACATGCTTTACATGTGTTTAGTCGAGGTT
AAAAAAACGTCTAGGCCCCCCGAACCACGGGGACGTGGTTTTCCTTTGAAAAACAC
GATGATAATATGGCCACA

NLS-EGFP

ATGGTGCCCAAGAAGAAGAGGAAAGTCAGCAAGGGCGAGGAGCTGTTCACGGGGT
GGTGCCCATCCTGGTCGAGCTGGACGGCGACGTAAACGGCCACAAGTTCAGCGTGT
CCGGCGAGGGCGAGGGCGATGCCACCTACGGCAAGCTGACCCTGAAGTTCATCTGC
ACCACCGGCAAGCTGCCCGTGCCCTGGCCCACCCTCGTGACCACCCTGACCTACGGC
GTGCAGTGCTTCAGCCGCTACCCCGACCACATGAAGCAGCACGACTTCTTCAAGTCC
GCCATGCCCGAAGGCTACGTCCAGGAGCGCACCATCTTCTTCAAGGACGACGGCAA
CTACAAGACCCGCGCCGAGGTGAAGTTCGAGGGCGACACCCTGGTGAACCGCATCG
AGCTGAAGGGCATCGACTTCAAGGAGGACGGCAACATCCTGGGGCACAAGCTGGAG
TACAACTACAACAGCCACAACGTCTATATCATGGCCGACAAGCAGAAGAACGGCAT
CAAGGTGAACTTCAAGATCCGCCACAACATCGAGGACGGCAGCGTGCAGCTCGCCG
ACCACTACCAGCAGAACACCCCCATCGGCGACGGCCCCGTGCTGCTGCCCGACAAC
CACTACCTGAGCACCCAGTCCGCCCTGAGCAAAGACCCCAACGAGAAGCGCGATCA
CATGGTCCTGCTGGAGTTCGTGACCGCCGCCGGGATCACTCTCGGCATGGACGAGCT
GTACAAG

GCaMP6s

ATGGGTTCTCATCATCATCATCATCATGGTATGGCTAGCATGACTGGTGGACAGCAA
ATGGGTCGGGATCTGTACGACGATGACGATAAGGATCTCGCCACCATGGTCGACTC
ATCACGTCGTAAGTGGAATAAGACAGGTCACGCAGTCAGAGCTATAGGTCGGCTGA
GCTCACTCGAGAACGTCTATATCAAGGCCGACAAGCAGAAGAACGGCATCAAGGCG
AACTTCCACATCCGCCACAACATCGAGGACGGCGGCGTGCAGCTCGCCTACCACTA
CCAGCAGAACACCCCCATCGGCGACGGCCCCGTGCTGCTGCCCGACAACCACTACC
TGAGCGTGCAGTCCAAACTTTCGAAAGACCCCAACGAGAAGCGCGATCACATGGTC
CTGCTGGAGTTCGTGACCGCCGCCGGGATCACTCTCGGCATGGACGAGCTGTACAA
GGGCGGTACCGGAGGGAGCATGGTGAGCAAGGGCGAGGAGCTGTTCACCGGGGTG
GTGCCCATCCTGGTCGAGCTGGACGGCGACGTAAACGGCCACAAGTTCAGCGTGTC
CGGCGAGGGTGAGGGCGATGCCACCTACGGCAAGCTGACCCTGAAGTTCATCTGCA
CCACCGGCAAGCTGCCCGTGCCCTGGCCCACCCTCGTGACCACCCTGACCTACGGCG

TGCAGTGCTTCAGCCGCTACCCCGACCACATGAAGCAGCACGACTTCTTCAAGTCCG
CCATGCCCGAAGGCTACATCCAGGAGCGCACCATCTTCTTCAAGGACGACGGCAAC
TACAAGACCCGCGCCGAGGTGAAGTTCGAGGGCGACACCCTGGTGAACCGCATCGA
GCTGAAGGGCATCGACTTCAAGGAGGACGGCAACATCCTGGGGCACAAGCTGGAGT
ACAACCTGCCGGACCAACTGACTGAAGAGCAGATCGCAGAATTTAAAGAGGCTTTC
TCCCTATTTGACAAGGACGGGGATGGGACAATAACAACCAAGGAGCTGGGGACGGT
GATGCGGTCTCTGGGGCAGAACCCCACAGAAGCAGAGCTGCAGGACATGATCAATG
AAGTAGATGCCGACGGTGACGGCACAATCGACTTCCCTGAGTTCCTGACAATGATG
GCAAGAAAAATGAAATACAGGGACACGGAAGAAGAAATTAGAGAAGCGTTCGGTG
TGTTTGATAAGGATGGCAATGGCTACATCAGTGCAGCAGAGCTTCGCCACGTGATGA
CAAACCTTGGAGAGAAGTTAACAGATGAAGAGGTTGATGAAATGATCAGGGAAGCA
GACATCGATGGGGATGGTCAGGTAAACTACGAAGAGTTTGTACAAATGATGACAGC
GAAGTGA

WPRE

GCTTATCGATAATCAACCTCTGGATTACAAAATTTGTGAAAGATTGACTGGTATTCT
TAACTATGTTGCTCCTTTTACGCTATGTGGATACGCTGCTTTAATGCCTTTGTATCAT
GCTATTGCTTCCCGTATGGCTTTCATTTTCTCCTCCTTGTATAAATCCTGGTTGCTGTC
TCTTTATGAGGAGTTGTGGCCCGTTGTCAGGCAACGTGGCGTGGTGTGCACTGTGTT
TGCTGACGCAACCCCCACTGGTTGGGGCATTGCCACCACCTGTCAGCTCCTTTCCGG
GACTTTCGCTTTCCCCCTCCCTATTGCCACGGCGGAACTCATCGCCGCCTGCCTTGCC
CGCTGCTGGACAGGGGCTCGGCTGTTGGGCACTGACAATTCCGTGGTGTTGTCGGGG
AAATCATCGTCCTTTCCTTGGCTGCTCGCCTGTGTTGCCACCTGGATTCTGCGCGGGA
CGTCCTTCTGCTACGTCCCTTCGGCCCTCAATCCAGCGGACCTTCCTTCCCGCGGCCT
GCTGCCGGCTCTGCGGCCTCTTCCGCGTCTTCGCCTTCGCCCTCAGACGAGTCGGAT
CTCCCTTTGGGCCGCCTCCCCGCATCGATACCG

CMV promoter

GACATTGATTATTGACTAGTTATTAATAGTAATCAATTACGGGGTCATTAGTTCATA
GCCCATATATGGAGTTCCGCGTTACATAACTTACGGTAAATGGCCCGCCTGGCTGAC
CGCCCAACGACCCCCGCCCATTGACGTCAATAATGACGTATGTTCCCATAGTAACGC
CAATAGGGACTTTCCATTGACGTCAATGGGTGGACTATTTACGGTAAACTGCCCACT
TGGCAGTACATCAAGTGTATCATATGCCAAGTACGCCCCCTATTGACGTCAATGACG
GTAAATGGCCCGCCTGGCATTATGCCCAGTACATGACCTTATGGGACTTTCCTACTT
GGCAGTACATCTACGTATTAGTCATCGCTATTACCATGGTGATGCGGTTTTGGCAGT
ACATCAATGGGCGTGGATAGCGGTTTGACTCACGGGGATTTCCAAGTCTCCACCCCA
TTGACGTCAATGGGAGTTTGTTTTGGCACCAAAATCAACGGGACTTTCCAAAATGTC
GTAACAACTCCGCCCCATTGACGCAAATGGGCGGTAGGCGTGTACGGTGGGAGGTC
TATATAAGCAGAGCT

Synapsin Promoter

GTGTCTAGACTGCAGAGGGCCCTGCGTATGAGTGCAAGTGGGTTTTAGGACCAGGA
TGAGGCGGGGTGGGGGTGCCTACCTGACGACCGACCCCGACCCACTGGACAAGCAC
CCAACCCCCATTCCCCAAATTGCGCATCCCCTATCAGAGAGGGGGAGGGGAAACAG
GATGCGGCGAGGCGCGTGCGCACTGCCAGCTTCAGCACCGCGGACAGTGCCTTCGC
CCCCGCCTGGCGGCGCGCGCCACCGCCGCCTCAGCACTGAAGGCGCGCTGACGTCA

CTCGCCGGTCCCCCGCAAACTCCCCTTCCCGGCCACCTTGGTCGCGTCCGCGCCGCC
GCCGGCCCAGCCGGACCGCACCACGCGAGGCGCGAGATAGGGGGGCACGGGCGCG
ACCATCTGCGCTGCGGCGCCGGCGACTCAGCGCTGCCTCAGTCTGCGGTGGGCAGC
GGAGGAGTCGTGTCGTGCCTGAGAGCGCAGTCGAGA

Immunohistochemistry

In addition to sequencing, immunostaining was performed to confirm the expression and localization of HaloTag protein. Following plasmid transfection HEK cells (~20-24 h) or neurons (~7-8 days) were fixed with 4% paraformaldehyde in PBS for 10 min at room temperature (RT). Permeabilization (if stated) was carried out with 0.3% v/v Triton-X100 (Sigma Aldrich) in PBS for 2 min. The fixed cells were then blocked in 5% w/v bovine serum albumin (BSA; Sigma Aldrich) in PBS at RT for 1 h. Primary antibody was incubated at 4 °C overnight, followed by AlexaFluor secondary antibody (Life Technologies) and Hoechst 33342 (Thermo Scientific) at RT for 2 h. All antibodies were used at 1:1000 dilution.

Figures and Schemes

Scheme 2-1: *Covalently targeted rhodamine-based VoltageFluors using HaloTag*

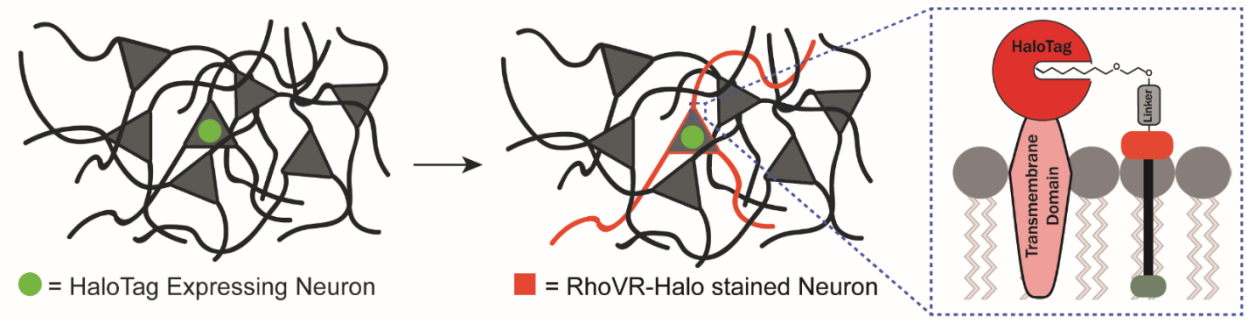

Scheme 2-1: Genetically-modified neurons express a membrane-anchored HaloTag, as indicated by nuclear GFP marker. Bath-application of RhoVR-Halo results in the chloroalkane ligand selectively and irreversibly binding to the HaloTag expressing neurons, tethering the voltage dye and facilitating its intercalation into the outer membrane.

Scheme 2-2**: Synthesis of TMR-Halo **44

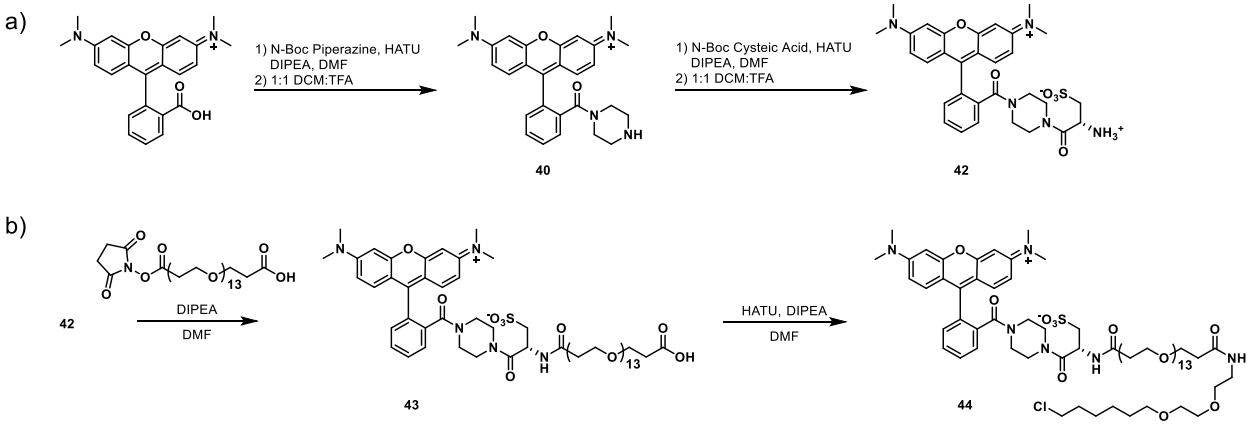

Scheme 2-2: Synthesis of **44**. (a) From tetramethylrhodamine, a HATU-mediated coupling of N-Boc-piperazine followed by TFA deprotection afforded **40**. A second HATU-assisted coupling to L-cysteic acid and subsequent TFA deprotection afforded **42**. (b) Activated linker NHS-PEG_{13}-Acid linker was coupled to **42** to afford **43**. The crude product was then coupled to HaloTag-amine through a HATU-mediated reaction.

Scheme 2-3**: Synthesis of **7

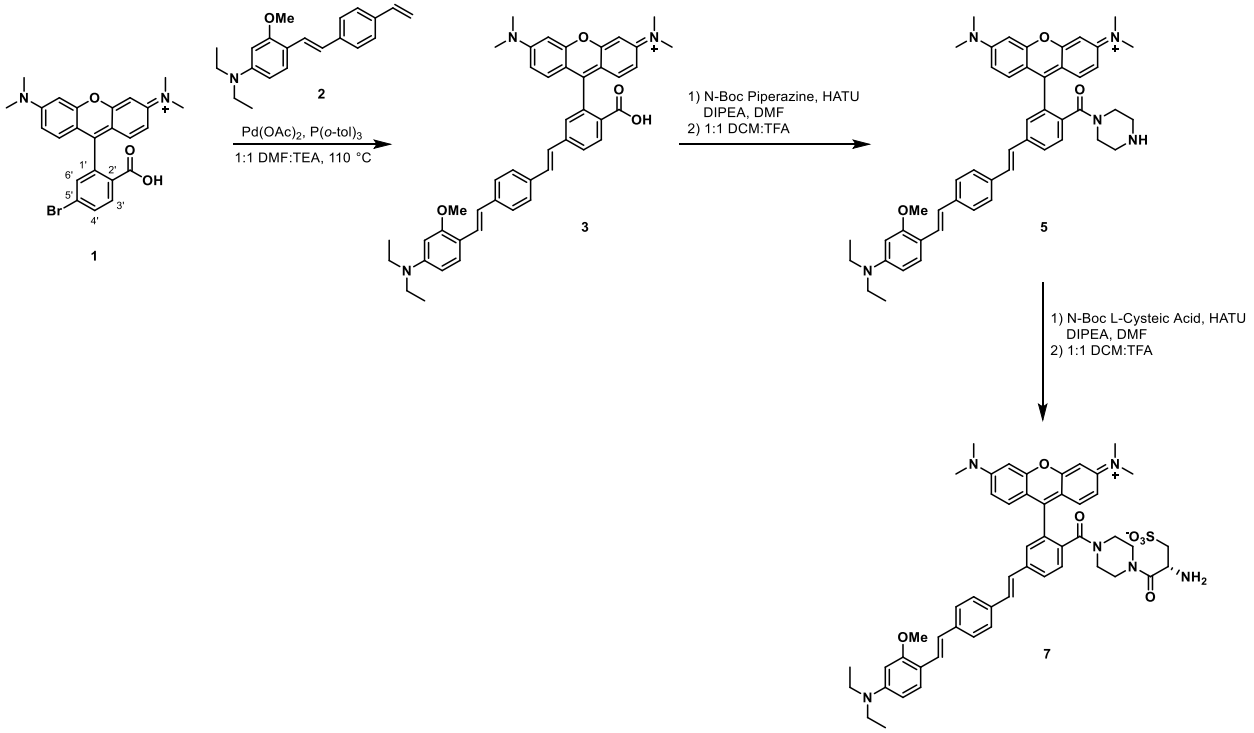

Scheme 2-3: Synthesis of **7**. A Heck coupling between isomerically pure Br-TMR **1** and methoxy-substituted wire **2** afforded RhoVR **3**. HATU-mediated coupling of N-Boc Piperazine followed by subsequent TFA deprotection gave the piperazine-functionalized RhoVR **5**. A second HATU-mediated coupling to N-Boc L-cysteic acid and subsequent TFA deprotection afforded **7**, which was used for the synthesis of the RhoVR-PEG$_x$-Halo library.

Scheme 2-4: *Synthesis of RhoVR1-PEG$_x$-Halos* ***12-16***

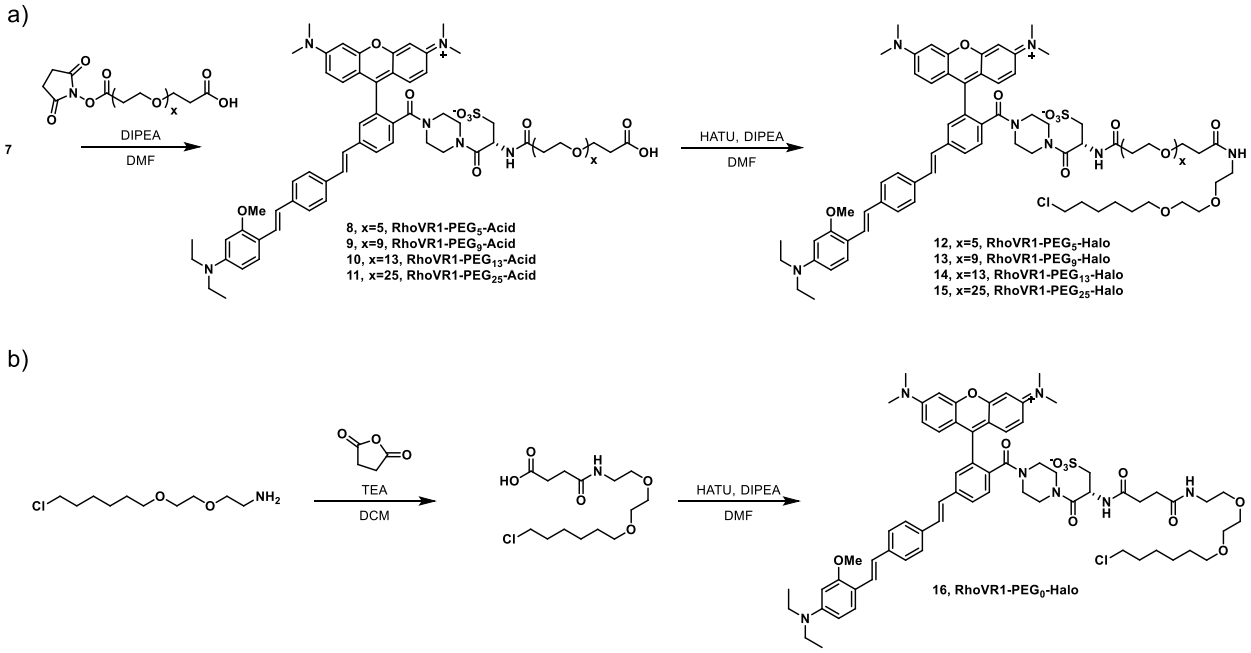

Scheme 2-4. Synthesis of RhoVR1-PEG$_x$-Halo Derivatives **12**-**16**. (a) From **7**, commercially available NHS-PEG$_x$-Acid linkers were coupled to the free-amine of the L-cysteic acid linker. The crude RhoVR-PEG$_x$-Acids were then subjected to a HATU-mediated coupling to HaloTag-amine. (b) RhoVR-PEG$_0$-Halo **16** was synthesized by first coupling HaloTag-amine to succinic anhydride, affording HaloTag-succinimidyl ester. A subsequent HATU-mediated coupling between **7** and HaloTag-succinimidyl ester afforded **17**.

Scheme 2-5: *Synthesis of untargeted RhoVR(Me)* ***21*** *and RhoVR(0)* ***32***

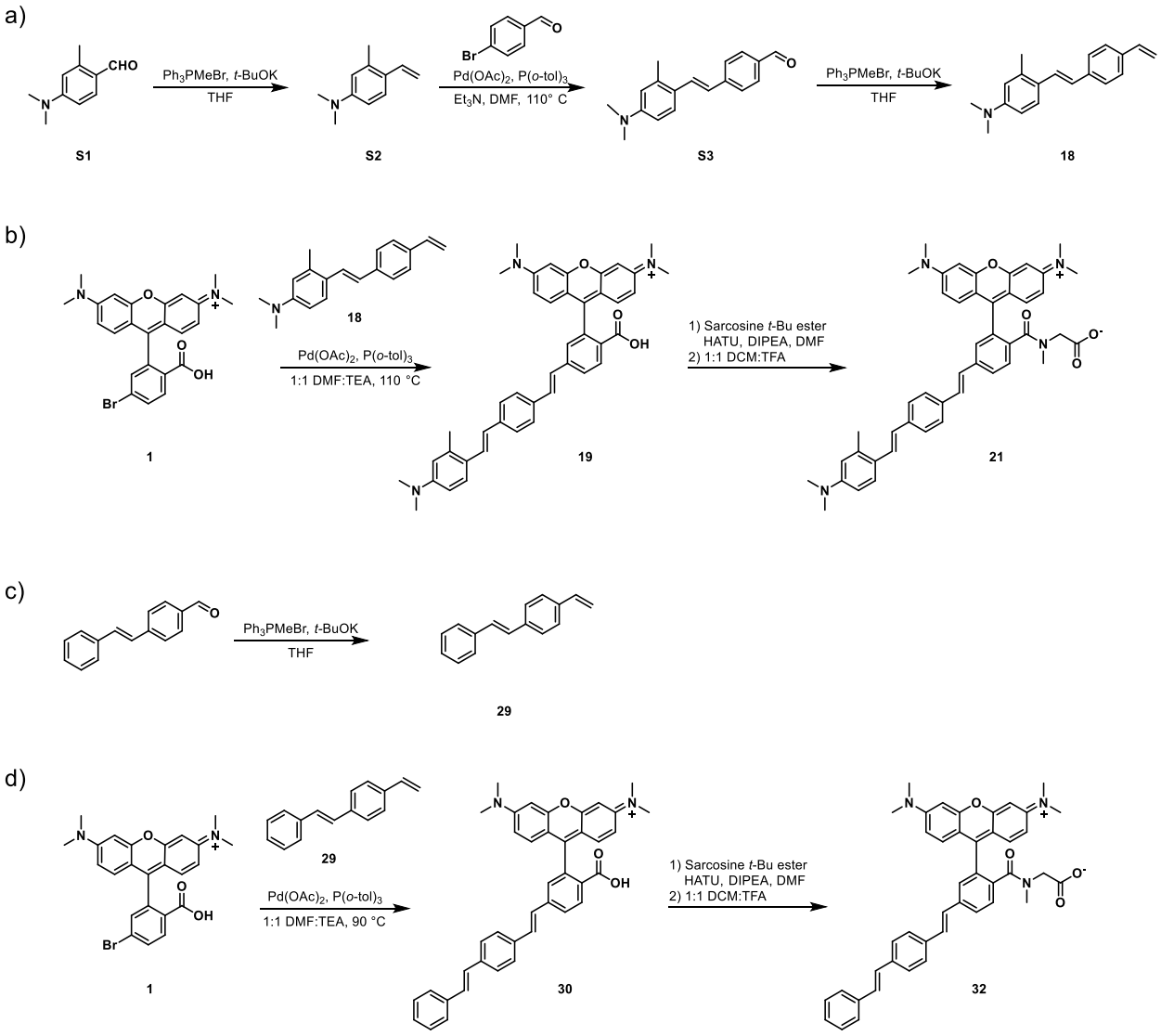

Scheme 2-5: Synthesis of untargeted RhoVR derivatives RhoVR(Me) and RhoVR(0). (a) Synthesis of methyl-substituted wire **18**. (b) Synthesis of untargeted RhoVR(Me) **21**. (c) Synthesis of phenylene vinylene wire **20**. (d) Synthesis of untargeted RhoVR(0) **32**. Due to its lack of aniline moiety, **32** is insensitive to changes in membrane potential, but is also very bright (due to lack of PeT quenching). RhoVR(0) was used as a negative control for voltage imaging experiments in slice.

Scheme 2-6: *Synthesis of genetically targeted RhoVR(Me)-PEG$_{25}$-Halo* ***27*** *and RhoVR(0)-PEG$_{25}$-Halo,* ***38***

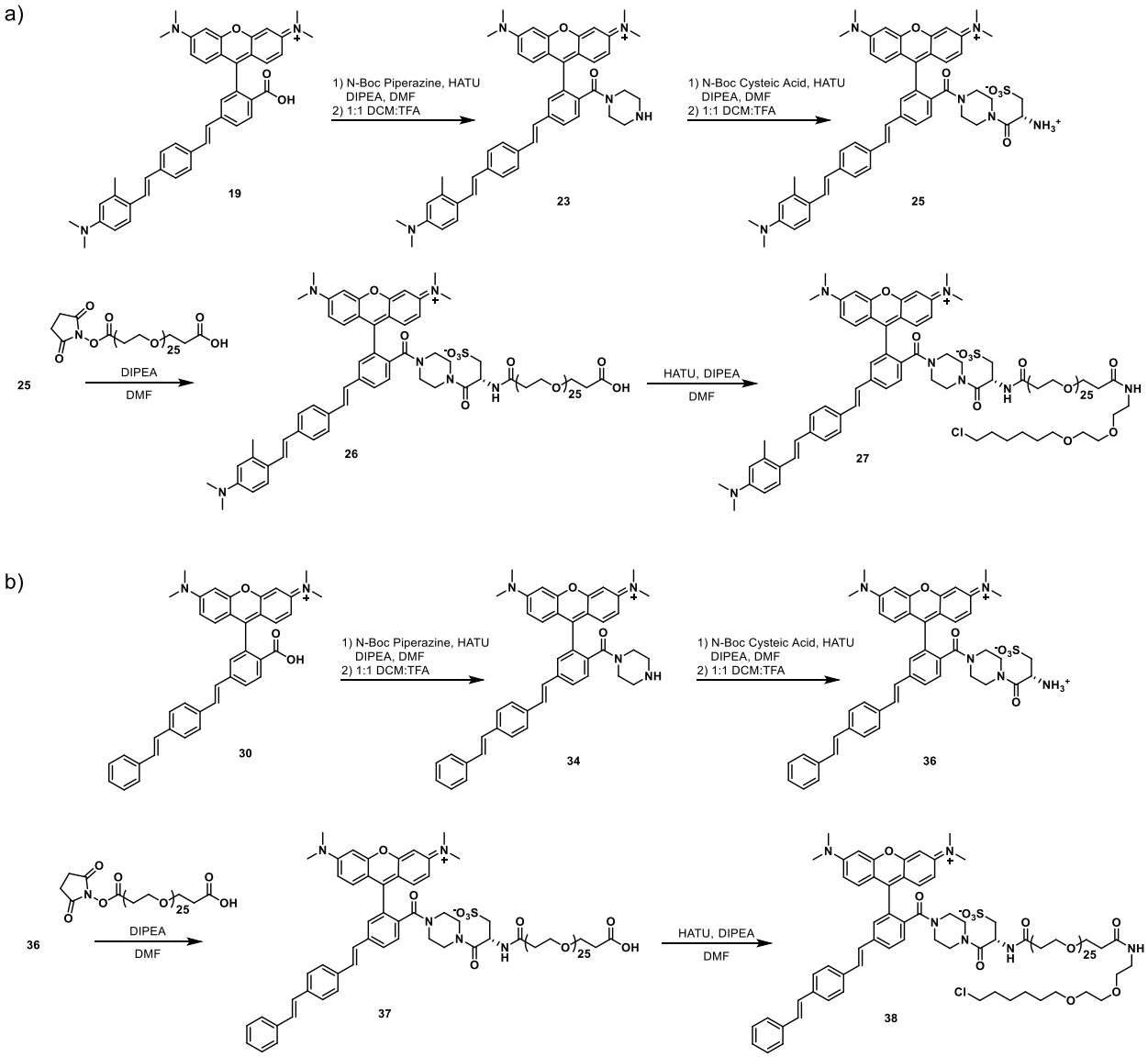

Scheme 2-6: Synthesis of (a) genetically targeted RhoVR(Me)-PEG$_{25}$-Halo, **27** and (b) RhoVR(0)-PEG$_{25}$-Halo, **38**.

Table 2-1: *Properties of RhoVR-Halo compounds*

RhoVR-Halo Derivative	ε_{565}[a] M^{-1} cm^{-1}	Φ_{Fl}	$\Delta F/F$[c] (100 mV)	Rel. Brightness[c]	SNR[c] (100 mV)
RhoVR 1 (500 nM)	87,000	0.045[a]	47%	100%	90
7	82,000	0.026[a]	38%	18%	30
RhoVR1-PEG_{25}-Halo, **15**	74,000	0.050[a], 0.017[b]	34%	30%	34
RhoVR1-PEG_{13}-Halo, **14**	-	-	26%	29%	30
RhoVR1-PEG_{9}-Halo, **13**	-	-	20%	34%	14
RhoVR1-PEG_{5}-Halo, **12**	-	-	11%	32%	11
RhoVR1-PEG_{0}-Halo, **16**	-	-	0%	61%	-
RhoVR(Me) (500 nM), **21**	81,000	0.022[a]	13%	220%	77
RhoVR(Me)-PEG_{25}-Halo, **27**	85,000	0.038[a], 0.009[b]	16%	118%	40
RhoVR(0), **32**	71,000	0.219[a]	0%	-	-
RhoVR(0)-PEG_{25}-Halo, **38**	83,000	0.214[a]	0%	-	-

[a] PBS, pH 7.2, 0.1% SDS [b] HBSS [c] voltage-clamped HEK cells

Table 2-1: Photophysical properties of RhoVR-Halos.

***Figure 2-1**: Extracellular HaloTag constructs*

a)

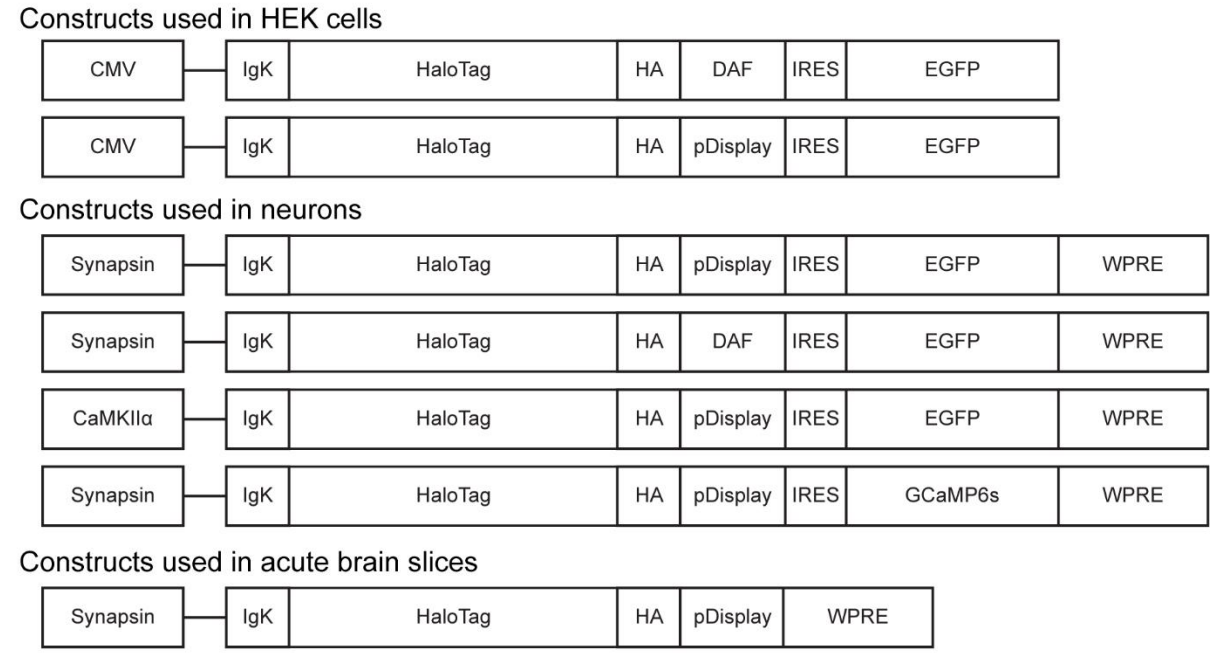

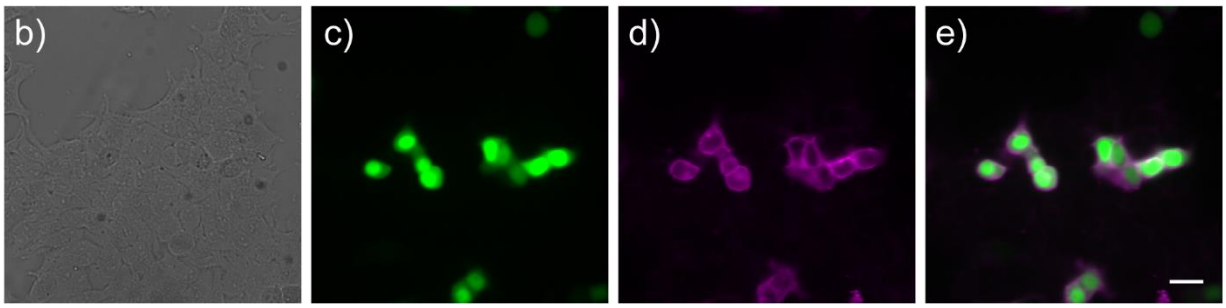

Figure 2-1: Evaluation of HaloTag constructs in HEK cells. (a) HaloTag constructs used for imaging experiments. The initial construct design was first evaluated in HEK cells. Modifications to promoters or fluorescent protein markers were made to facilitate expression in neurons. (b) DIC image of CMV-Igk-HaloTag-Ha-pDisplay-IRES-EGFP transfected HEK Cells. (c) EGFP fluorescence channel. EGFP serves as a marker for HaloTag expression. (d) TMR fluorescence channel. Application of 200 nM TMR-PEG_{13}-Halo **44** for 30 min at 37 °C resulted in selective localization of TMR to only HaloTag expressing cells. (e) Merge of panels c and d. The expression levels of HaloTag, as indicated by EGFP fluorescence intensity, correlates to higher TMR brightness. Scale bar is 20 µm.

Figure 2-2: *Localization and staining of* ***7***

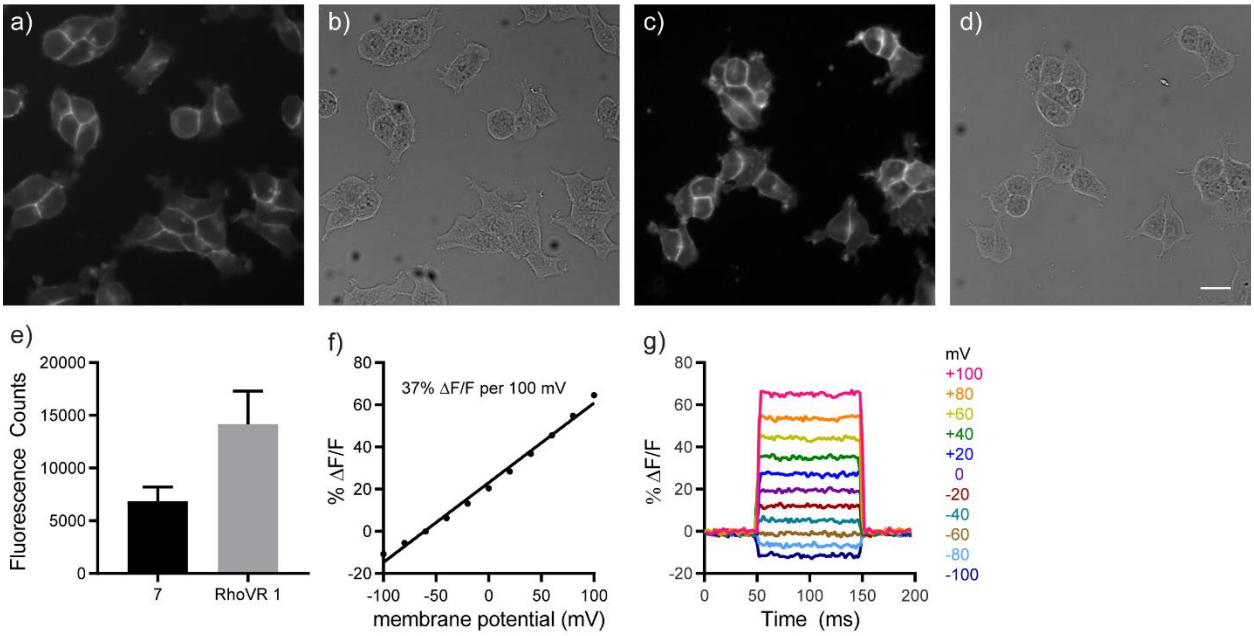

Figure 2-2: Cellular localization and voltage sensitivity of **7** in HEK293T cells. (a-d) Comparison of the brightness and localization of **7** with RhoVR 1. Both dyes were loaded at 500 nM for for 30 minutes at 37 °C and were imaged with identical settings to enable the comparison of dye loading efficiency. Scale bar is 20 μm; a) Fluorescence image of **7** shows the dye localizes well to the plasma membrane. (b) DIC image of cells labeled with **7**. (c) Fluorescence image of RhoVR 1 shows the dye localizes well to the plasma membrane. (d) DIC image of cells labeled with RhoVR 1. (e) Quantification of the brightness of cells labeled with **7** and RhoVR 1. RhoVR 1 labeled cells were approximately 2-fold brighter than cells labeled with **7**. We hypothesize this difference in loading efficiency is due to the increased water solubility of **7**. (f) A plot of % ΔF/F vs. final membrane potential (mV), summarizing data from 4 separate cells loaded with **7**, reveals a voltage sensitivity of approximately 37% per 100 mV. (g) The fractional change in fluorescence of **7** is plotted vs. time for 100 ms hyper- and depolarizing steps (±100 mV, 20 mV increments) from a holding potential of -60 mV for a single HEK cells under whole-cell voltage-clamp mode.

Figure 2-3: *Absorbance and emission profiles for RhoVR derivatives*

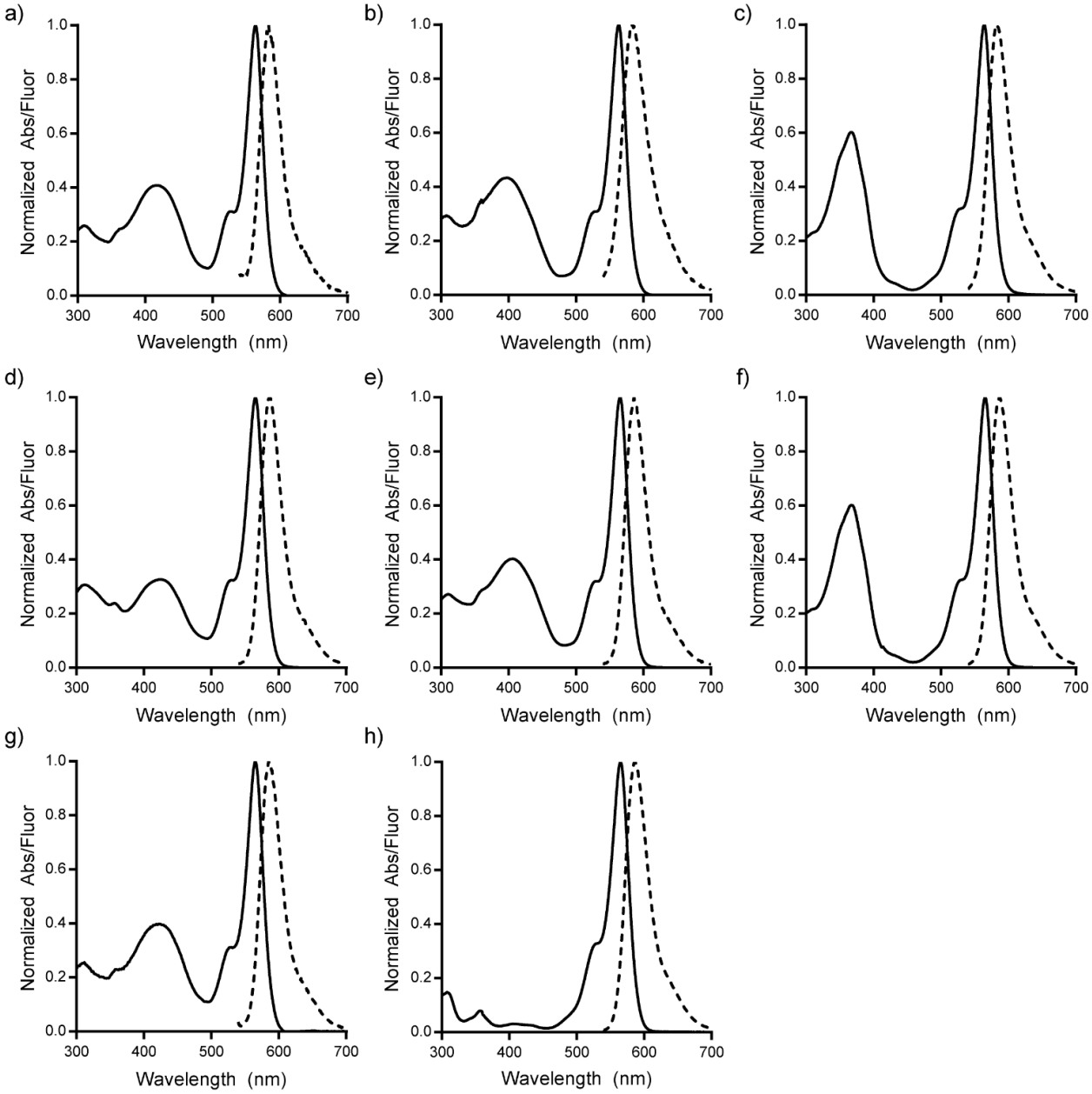

Figure 2-3: Normalized absorbance and fluorescence profiles for: (a) RhoVR 1; (b) RhoVR(Me) **21**; (c) RhoVR(0) **32**; (d) RhoVR1-PEG_{25}-Halo **15**; **(**e) RhoVR(Me)-PEG_{25}-Halo **27**; (f) RhoVR(0)-PEG_{25}-Halo **38**; (g) RhovR.Pip.Cys, **7**; (h) TMR-PEG_{13}-Halo **44**. Spectra were obtained at 500 nM in dPBS with 0.1% SDS.

Figure 2-4: *Screen of loading conditions for RhoVR-Halos*

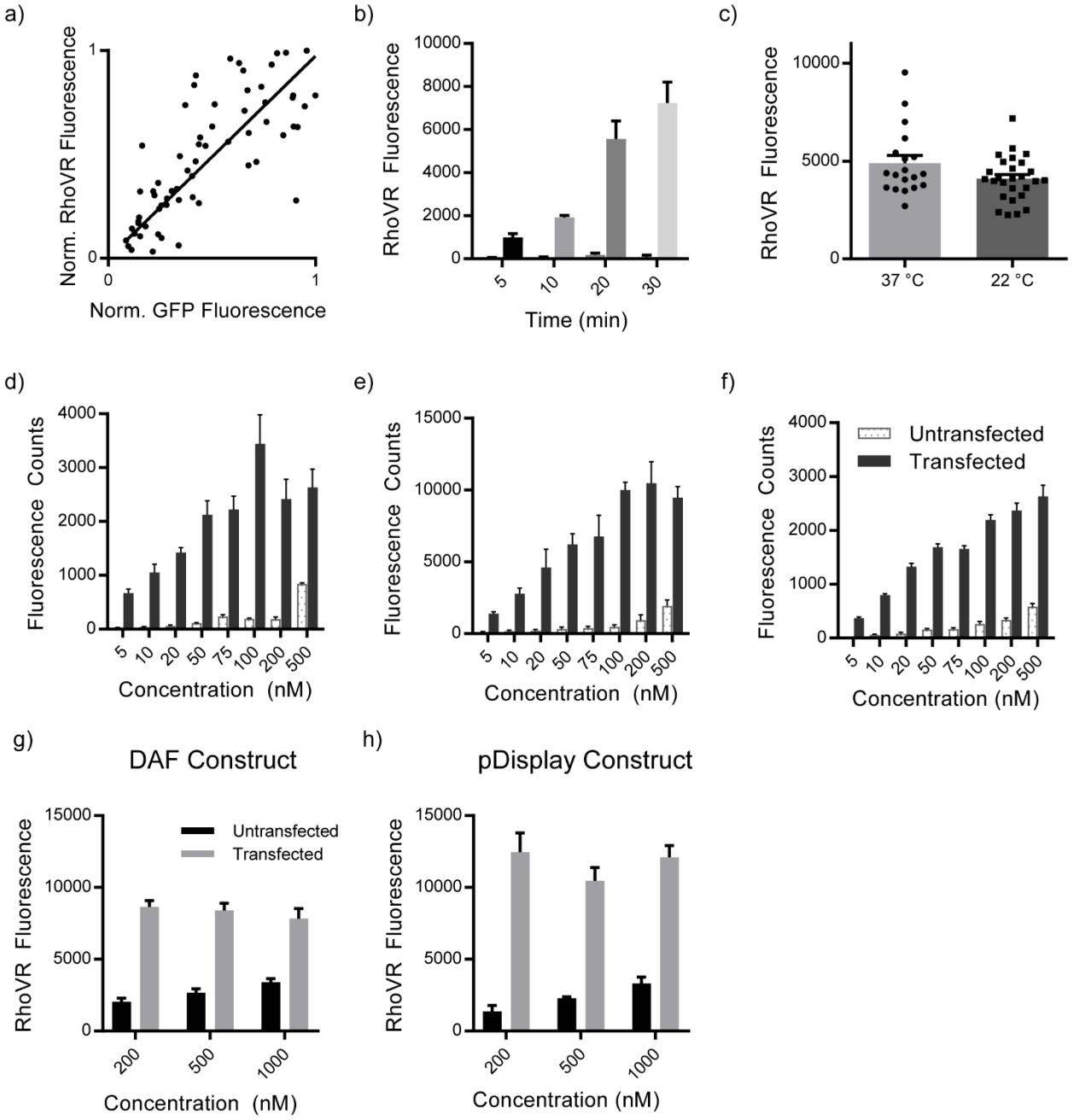

Figure 2-4: Loading condition screens for RhoVR-Halos. (a) RhoVR fluorescence from cells labeled with **15** were shown to correlate to the fluorescence of nuclear EGFP. (b) Loading of **15** at 50 nM at 37 °C for increasing amounts of time. (c) Loading of **15** in neurons did not depend on temperature. Concentration screens for (d) **16**; (e) **27**; (f) **15**. All RhoVR-Halo derivatives displayed very selective labeling of transfected cells over untransfected cells, with the highest contrast ratios around 50 nM. Loading screens for (g) CMV-IgK-HaloTag-HA-DAF-IRES-EGFP construct and (h) CMV-IgK-HaloTag-HA-DAF-pDisplay-IRES-EGFP construct revealed the pDisplay construct gave brighter cells than the DAF construct.

Figure 2-5: *Labeling and voltage sensitivities of RhoVR1-PEGx-Halo compounds*

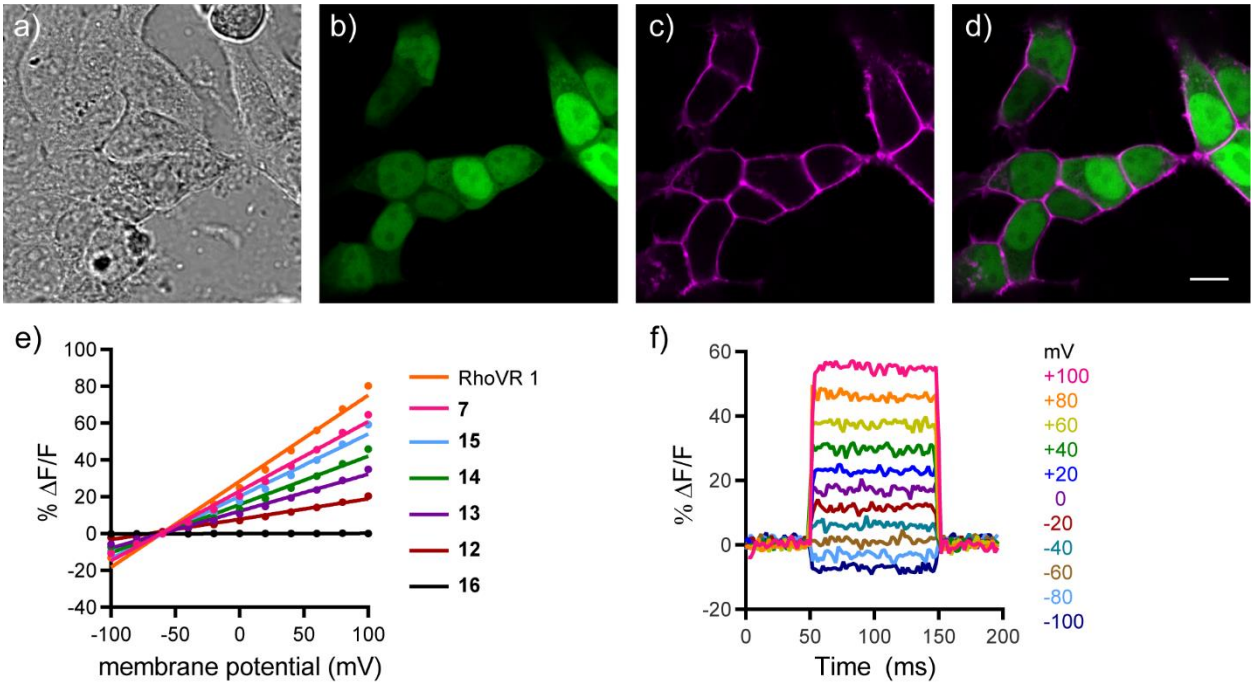

Figure 2-5: Selective labeling and voltage sensitivities of RhoVR1-PEG$_x$-Halo Compounds in HEK cells. (a) DIC image of HEK cells expressing nuclear EGFP stained with **15**. (b) Confocal fluorescence image of HaloTag expressing cells from (a) as indicated by nuclear EGFP fluorescence. (c) Confocal fluorescence image showing the fluorescence of **15** from cells in panel a. (d) Merge of fluorescence from EGFP (green) and **15** (magenta), demonstrating the highly selective localization of **15** to HaloTag expressing cells. Scale bar is 10 μm. (e) Plot of % ΔF/F vs final membrane potential for RhoVR 1, **7** and RhoVR-PEG$_x$-Halo derivatives **12-16** (n=3-9, error bars not shown). Increasing linker length was shown to increase voltage sensitivity with a maximum of 34% ΔF/F per 100 mV for **15**. (f) Plot of the fractional change in fluorescence of **15** vs time for 100 ms hyper- and depolarizing steps (±100 mV in 20 mV increments) from a holding potential of -60 mV for single HEK cells under whole-cell voltage clamp mode.

Figure 2-6: *Relative brightness of RhoVRs*

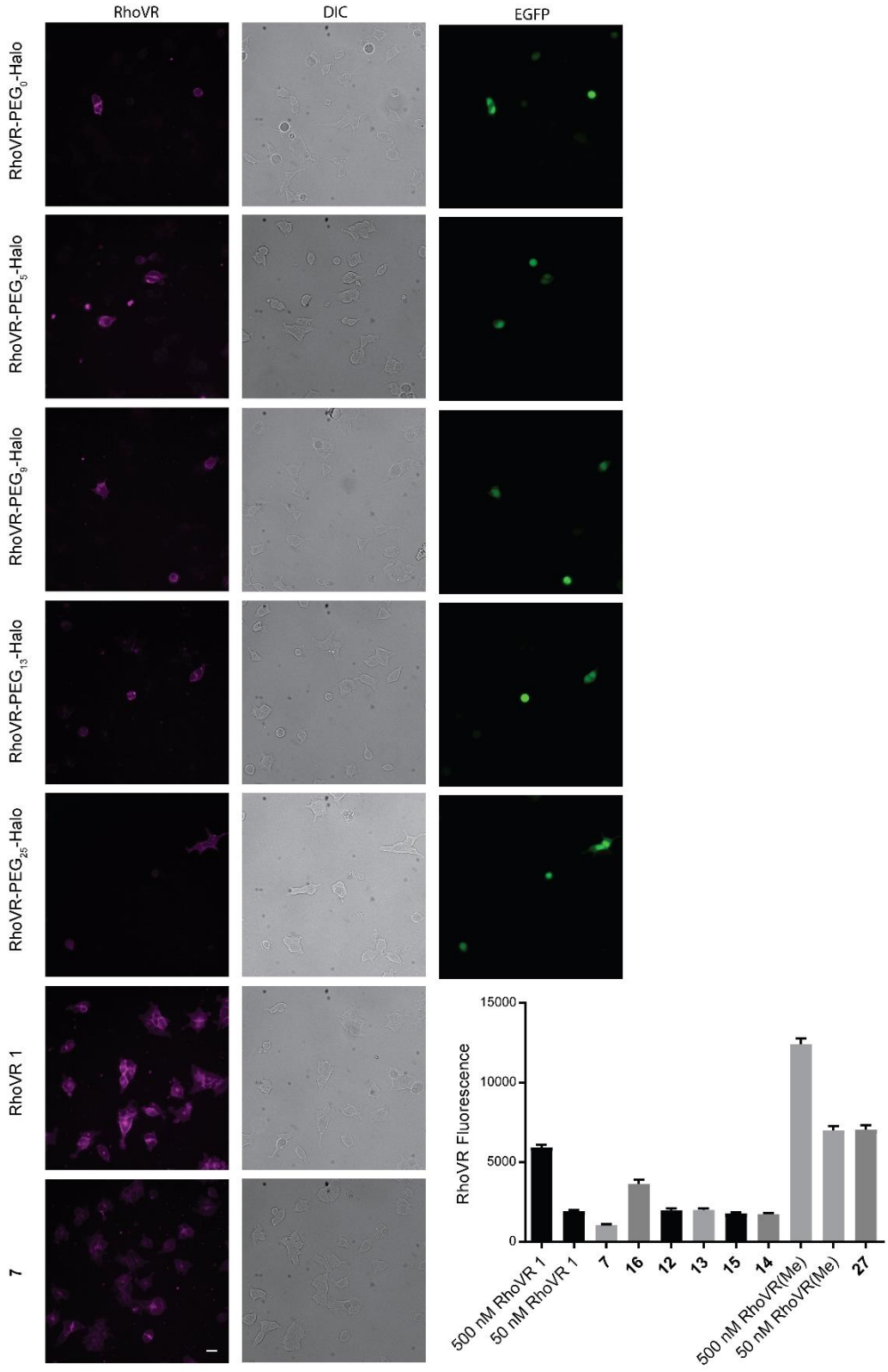

Figure 2-6: Comparison of the brightness of RhoVR-Halos. Relative fluorescence values are summarized in **Table 2-1**. Scale bar is 20 μm.

Figure 2-7: *RhoVR(Me)* ***21*** *and RhoVR(Me)-PEG$_{25}$-Halo* ***27*** *loading and patching*

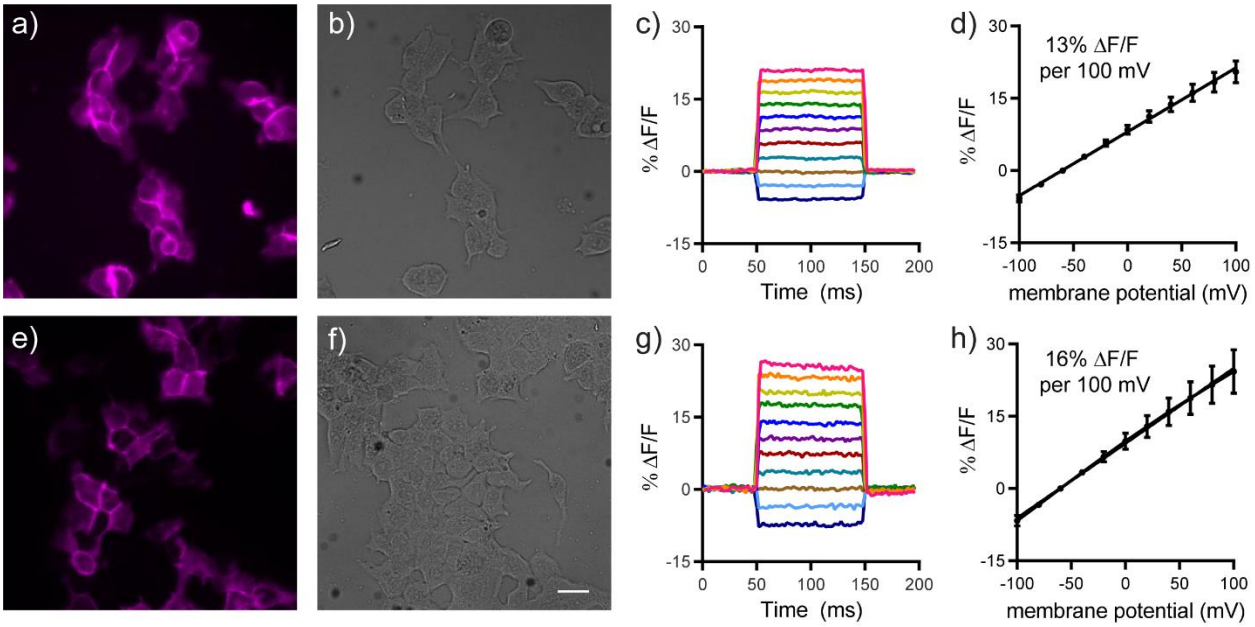

Figure 2-7: RhoVR(Me) **21** and RhoVR(Me)-PEG$_{25}$-Halo **27** loading and voltage sensitivities in HEK cells. (a) RhoVR Fluorescence channel showing **21** labeling all cellular membranes. (b) DIC image of cells labeled in panel a. (c) Plot of the fractional change in fluorescence of **21** vs time for 100 ms hyper- and depolarizing steps (±100 mV in 20 mV increments) from a holding potential of -60 mV for single HEK cells under whole-cell voltage clamp mode. (d) Plot of % ΔF/F vs final membrane potential for **21** (n=9). (e) RhoVR Fluorescence channel showing **27** selectively labeling HaloTag expressing cells. (f) DIC image of cells in panel e. (g) Plot of the fractional change in fluorescence of **27** vs time for 100 ms hyper- and depolarizing steps (±100 mV in 20 mV increments) from a holding potential of -60 mV for single HEK cells under whole-cell voltage clamp mode; h) Plot of % ΔF/F vs final membrane potential for **27** (n=11).

Figure 2-8: *Monitoring neuronal activity with RhoVR-Halos in cultured hippocampal neurons*

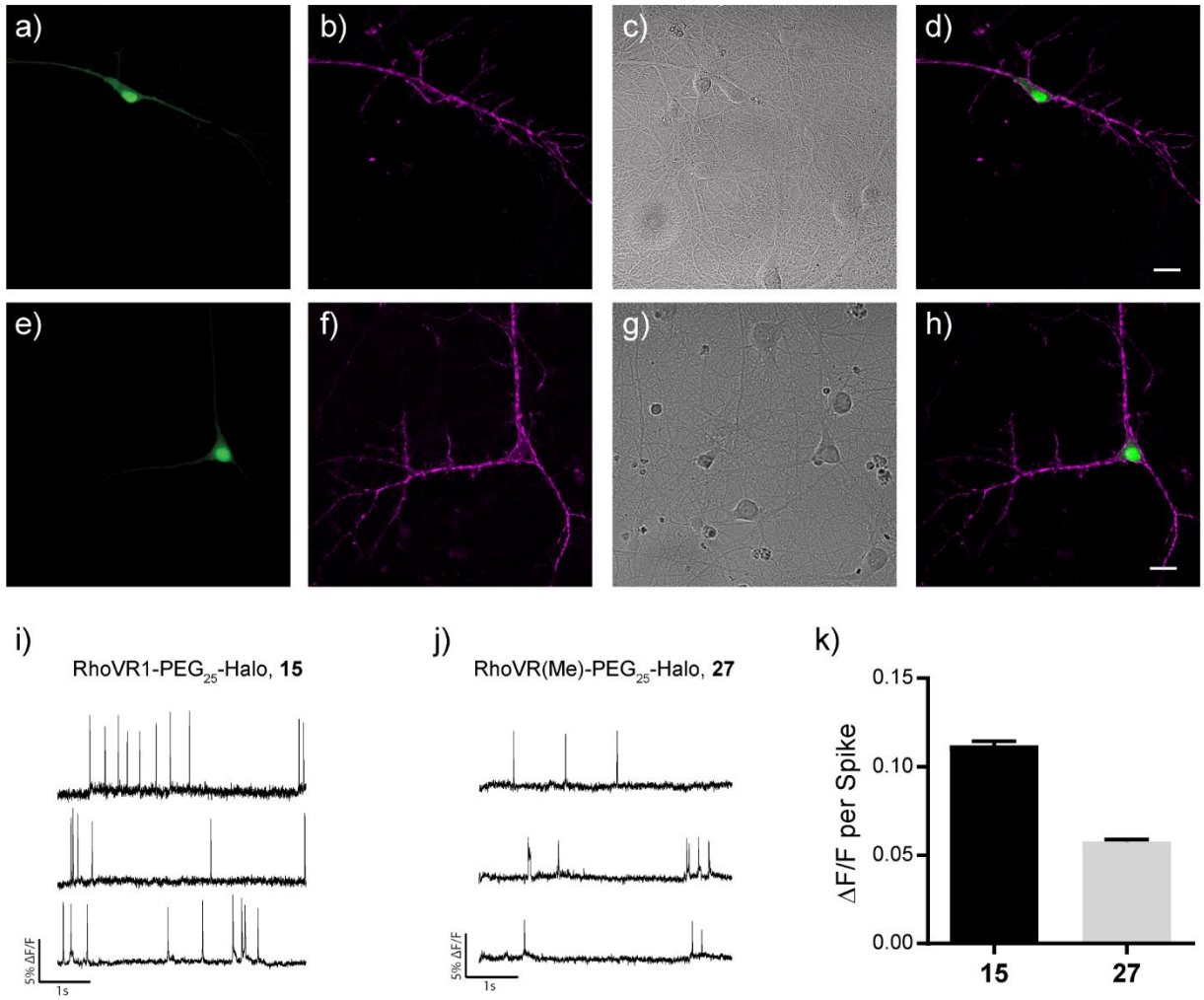

Figure 2-8: Evaluation of RhoVR-Halos **15** and **27** in cultured rat hippocampal neurons. (a-d) Confocal images depicting the selective labeling of HaloTag expressing neurons with **15**. (a) EGFP fluorescence serves as a marker for HaloTag expression. (b) RhoVR fluorescence is localized to the plasma membrane of the HaloTag expressing neuron. (c) DIC image of the images in panels a and b. (d) Merge of panels a and b confirms the colocalization of **15** with EGFP. (e-f) Confocal images depicting the labeling of **27**. (e) EGFP Fluorescence. (f) RhoVR fluorescence. (g) DIC image of the neurons in panels e and f. (h) Merge of panels e and f. (i) Examples of voltage recordings from spontaneously firing neurons labeled with **15**. (j) Example voltage recordings from spontaneously firing neurons labeled with **27**. (k) Average ΔF/F per spike for RhoVR-Halos. While **15** has a higher voltage sensitivity, **27** is much brighter, leading to similar SNRs for spike detection. Error bars are ±S.E.M.

***Figure 2-9**: Membrane properties of cultured primary mouse hippocampal neurons*

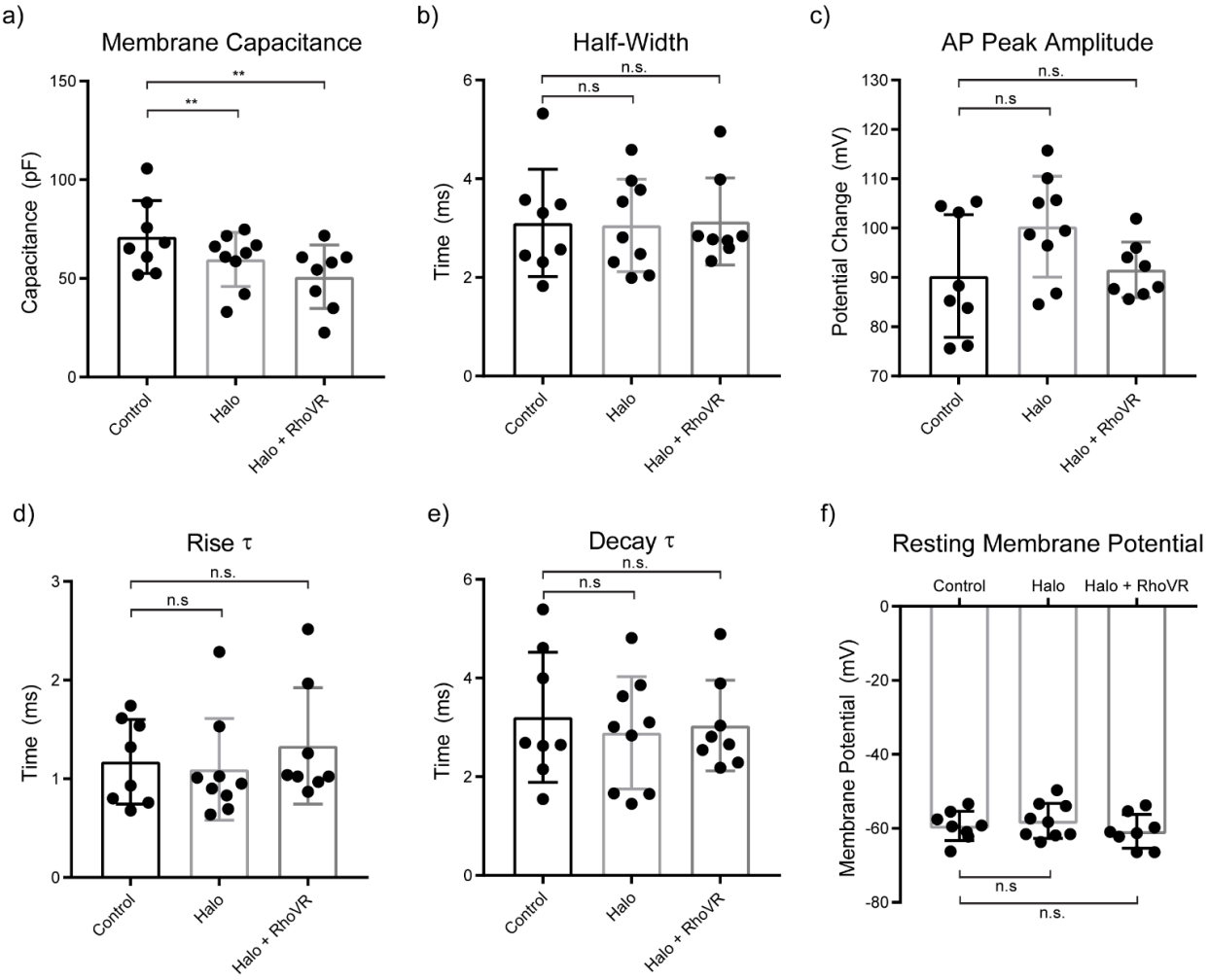

Figure 2-9: Membrane properties of cultured primary mouse hippocampal neurons as determined by patch-clamp electrophysiology. Wild-type neurons with no **15** present (Control) were compared to neurons transfected with CMV-IgK-HaloTag-HA-pDisplay-IRES-EGFP without **15** present (Halo) and loaded with 50 nM **15** loaded for 30 minutes at 37 °C (Halo + RhoVR). Expression of HaloTag and application of **15** had minimal effect on the kinetics and cell health of neurons. Transfected neurons displayed a statistically significant lower membrane capacitance than wild-type neurons, however the presence of **15** did not lead to any difference in capacitance.

***Figure 2-10**: Comparison of RhoVR1-PEG$_{25}$-Halo to GEVIs ASAP1 and Ace2N-mNeon*

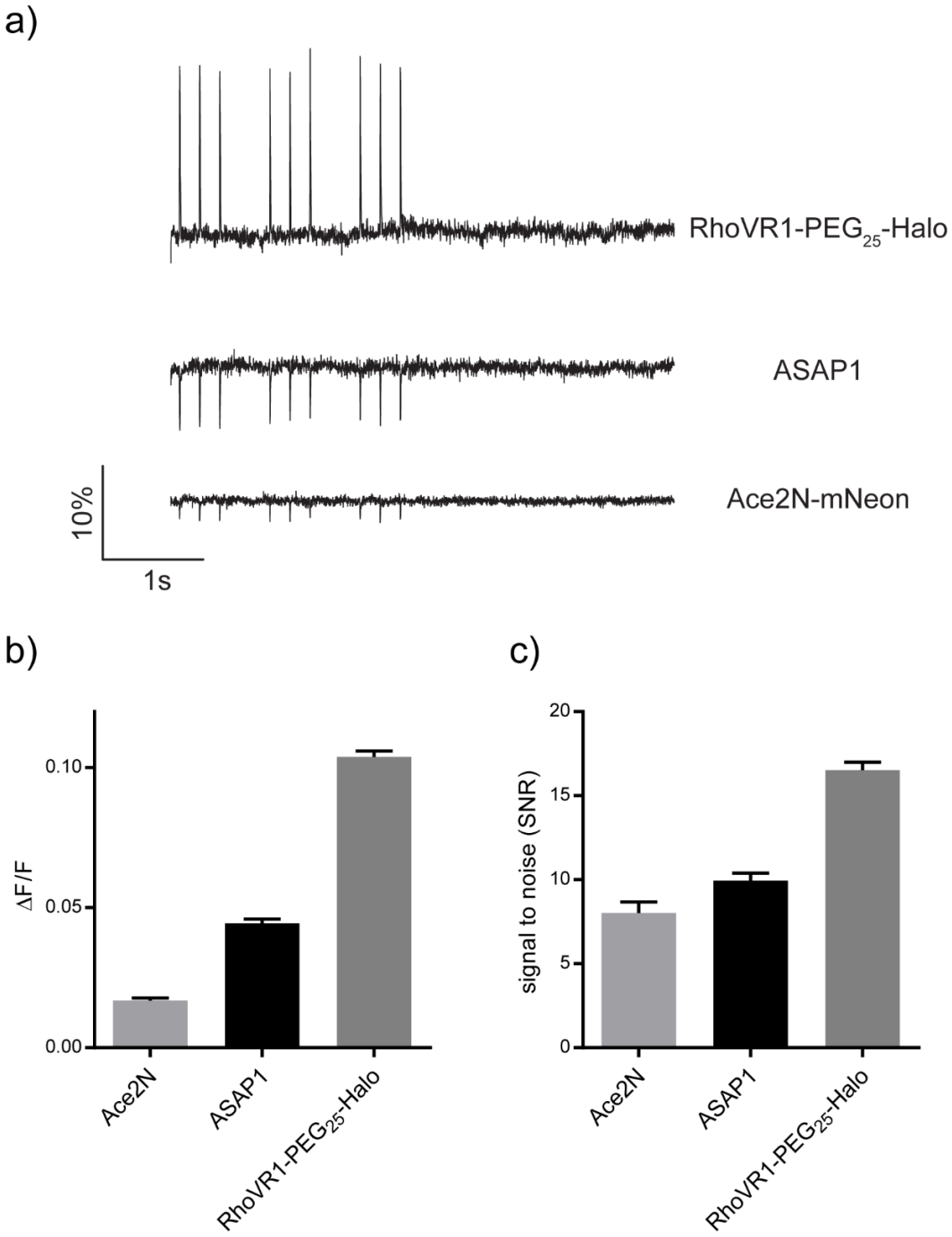

Figure 2-10: Comparison of RhoVR1-PEG$_{25}$-Halo **15** to GEVIs ASAP1 and Ace2N-mNeon. (a) Representative voltage recordings of evoked activity measured with **15**, ASAP1 and Ace2N-mNeon. Voltage traces were acquired with identical parameters and matched light power. (b) Average voltage sensitivities per spike (evoked) for **15**, ASAP1 and Ace2N-mNeon (n=77-205). (c) Average SNRs for individual spikes (evoked) for **15**, ASAP1 and Ace2N-mNeon (n=77-205). Error bars are ±S.E.M.

***Figure 2-11**: Simultaneous two-color voltage and Ca^{2+} imaging with **15** and GCaMP6s*

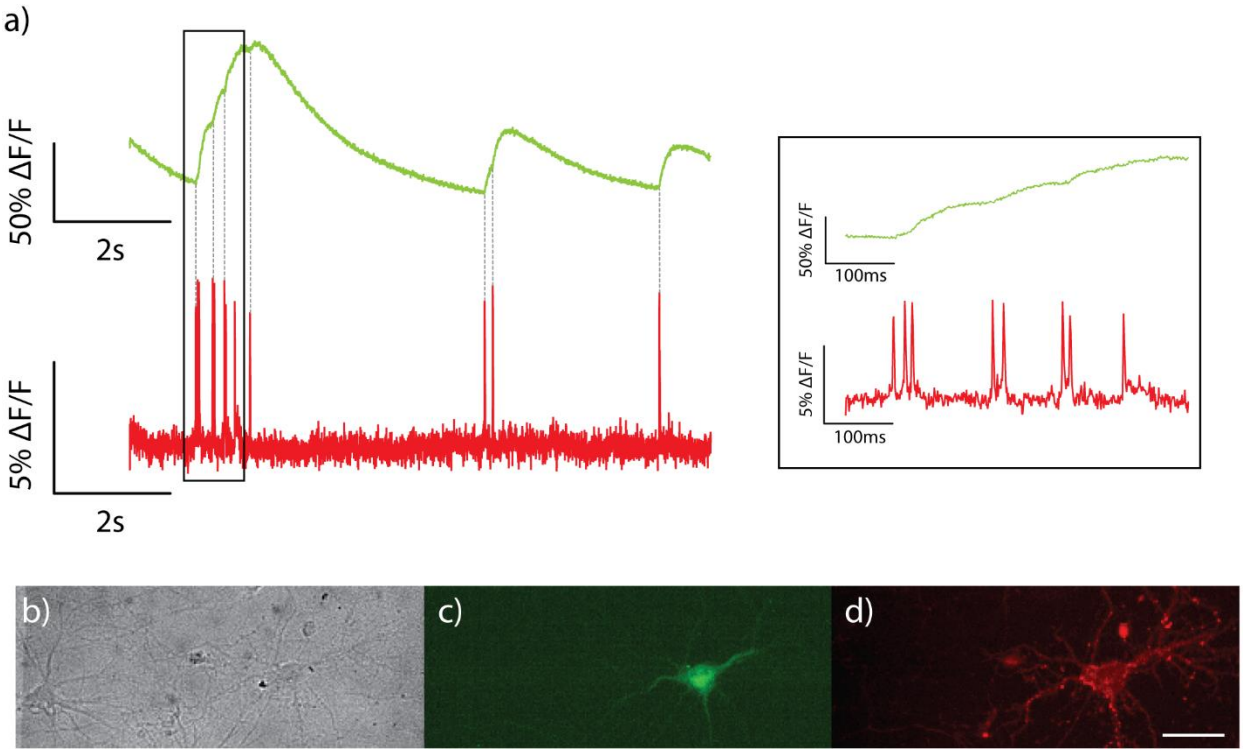

Figure 2-11: Simultaneous, two-color imaging of voltage and Ca^{2+} in hippocampal neurons **15** and GCaMP6s. (a) The green trace shows the relative change in fluorescence from Ca^{2+}-sensitive GCaMP6s, while the red trace depicts relative fluorescence changes from **15**. The inset shows an expanded time scale of the boxed region. (b) DIC image of neurons expressing GCaMP6s and stained with RhoVR. (c) Fluorescence image of neurons in panel b showing GCaMP6s fluorescence. (d) Fluorescence image of neurons shows **15** is localized to the GCaMP6s expressing neuron. Scale bar is 50 μm.

***Figure 2-12**: Two-photon imaging with RhoVR-Halos*

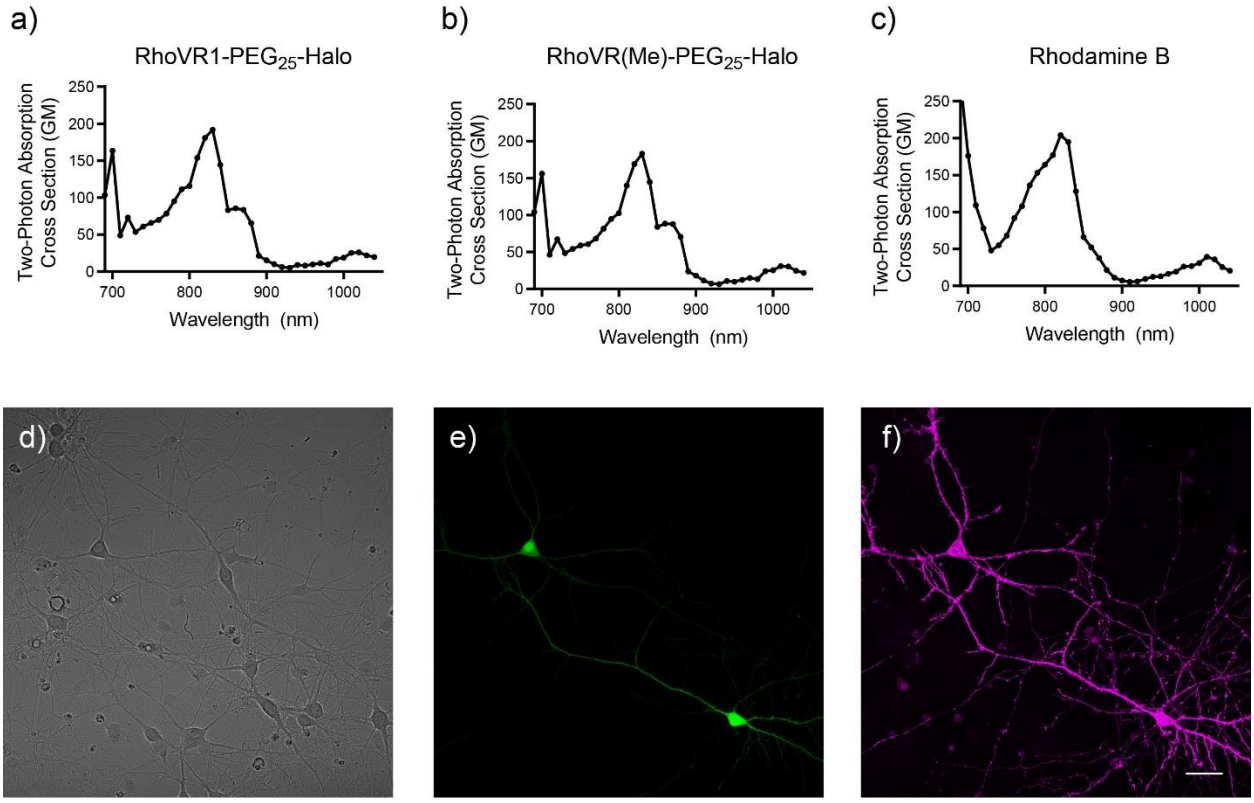

Figure 2-12: Two-photon absorption cross sections for (a) RhoVR1-PEG_{25}-Halo **15** and (b) RhoVR(Me)-PEG_{25}-Halo **27** relative to the reported cross section of (c) rhodamine B, acquired in HBSS.[32] Both RhoVR-Halos possessed a σ_{TPA} maxima of approximately 190 GM (830 nm). (d) DIC image of rat hippocampal neurons sparsely transfected with HaloTag and loaded with **27**. (e) EGFP fluorescence image revealing the presence of two HaloTag expressing neurons. (f) **F**luorescence image of **27** under two-photon illumination (860 nm). Scale bar is 40 µm.

***Figure 2-13**: Fluorescence imaging of RhoVR-PEG$_{25}$-Halo in brain slice*

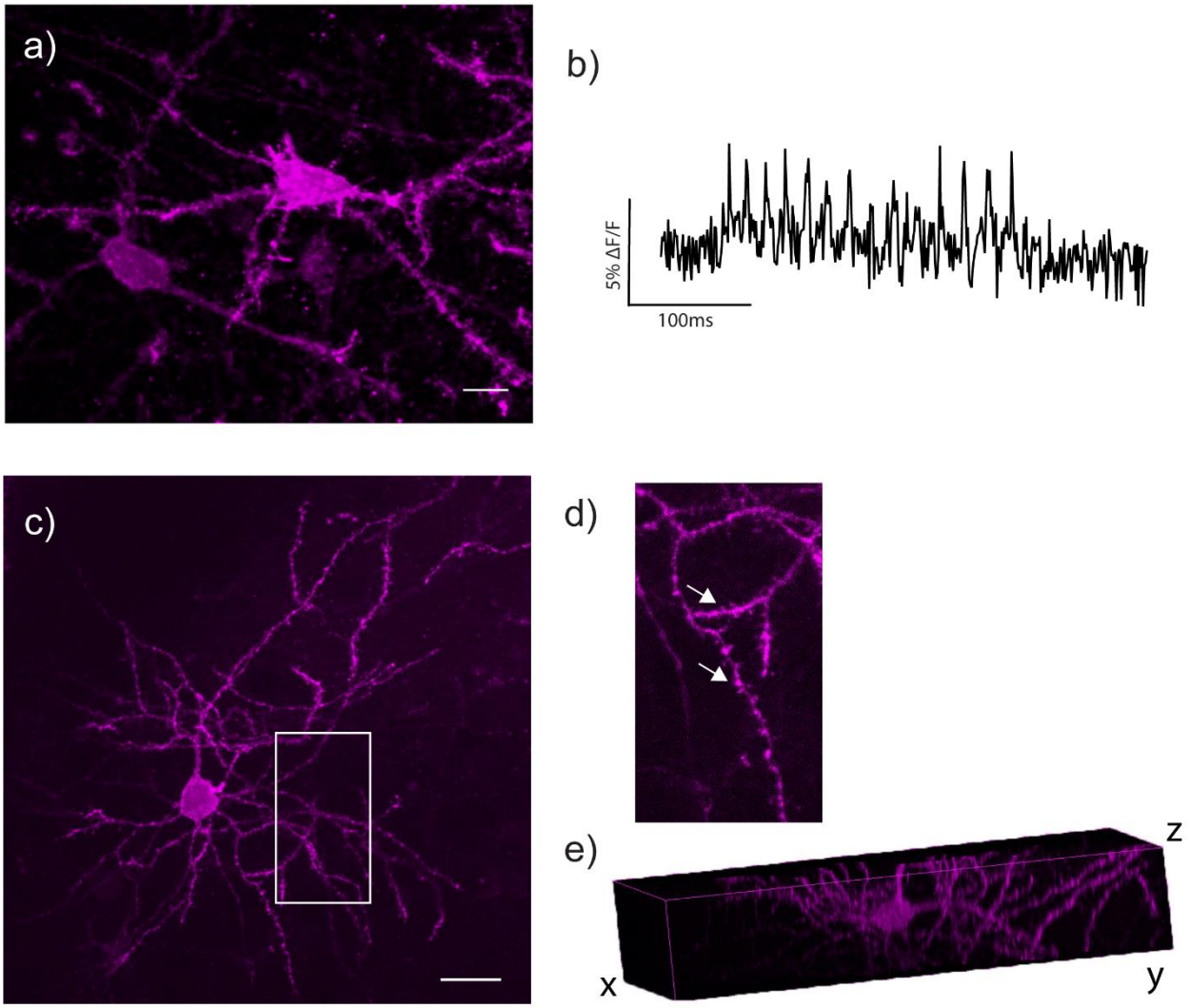

Figure 2-13: Fluorescence imaging of **15** in brain slice. (a) Fluorescence image of a brain slice labeled with **15**. The image is a max projection of a 50 µm z-stack under 1P confocal illumination. (b) Epifluorescence voltage trace of evoked activity from a patched HaloTag expressing neuron in a slice loaded with **15**. **(**c) Fluorescence image of a neuron under 2P illumination (860 nm) labeled with **15**. The image is a max projection of an 80 µm z-stack. (d) Zoom in of the region indicated by the white rectangle in panel c. Clear labeling of synapses can be seen. (e) An orthogonal view of the z-stack taken for panel c. Projections from the labeled neuron can be seen extending deeper into the tissue and out of the field of view.

References

(1) Peterka, D. S.; Takahashi, H.; Yuste, R. Imaging Voltage in Neurons. *Neuron* **2011**, *69* (1), 9–21.

(2) Miller, E. W. Small Molecule Fluorescent Voltage Indicators for Studying Membrane Potential. *Curr. Opin. Chem. Biol.* **2016**, *33*, 74–80.

(3) Canepari, M.; Zecevic, D.; Bernus, O. Membrane Potential Imaging in the Nervous System and Heart. *Membr. Potential Imaging Nerv. Syst. Hear.* **2015**, 1–509.

(4) Huang, Y. L.; Walker, A. S.; Miller, E. W. A Photostable Silicon Rhodamine Platform for Optical Voltage Sensing. *J. Am. Chem. Soc.* **2015**, *137* (33), 10767–10776.

(5) Kulkarni, R. U.; Kramer, D. J.; Pourmandi, N.; Karbasi, K.; Bateup, H. S.; Miller, E. W. Voltage-Sensitive Rhodol with Enhanced Two-Photon Brightness. *Proc. Natl. Acad. Sci.* **2017**, *114* (11), 2813–2818.

(6) Grenier, V.; Walker, A. S.; Miller, E. W. A Small-Molecule Photoactivatable Optical Sensor of Transmembrane Potential. *J. Am. Chem. Soc.* **2015**, *137* (34), 10894–10897.

(7) Liu, P.; Grenier, V.; Hong, W.; Muller, V. R.; Miller, E. W. Fluorogenic Targeting of Voltage-Sensitive Dyes to Neurons. *J. Am. Chem. Soc.* **2017**, *139* (48), 17334–17340.

(8) Deal, P. E.; Kulkarni, R. U.; Al-Abdullatif, S. H.; Miller, E. W. Isomerically Pure Tetramethylrhodamine Voltage Reporters. *J. Am. Chem. Soc.* **2016**, *138* (29), 9085–9088.

(9) Fiala, T.; Wang, J.; Dunn, M.; Šebej, P.; Nwadibia, E.; Martinez, D. M.; Claire, E.; Fogle, K. J.; Palladino, M. J.; Bando, Y.; et al. Chemical Targeting of Voltage Sensitive Dyes to Specific Cell Types in the Brain. *ChemRxiv* **2018**.

(10) Knöpfel, T. Genetically Encoded Optical Indicators for the Analysis of Neuronal Circuits. *Nat. Rev. Neurosci.* **2012**, *13* (10), 687–700.

(11) Lin, M. Z.; Schnitzer, M. J. Genetically Encoded Indicators of Neuronal Activity. *Nat. Neurosci.* **2016**, *19* (9), 1142–1153.

(12) Gong, Y.; Huang, C.; Li, J. Z.; Grewe, B. F.; Zhang, Y.; Eismann, S.; Schnitzer, M. J. High-Speed Recording of Neural Spikes in Awake Mice and Flies with a Fluorescent Voltage Sensor. *Science* **2015**, *350* (6266), 1361–1366.

(13) Zou, P.; Zhao, Y.; Douglass, A. D.; Hochbaum, D. R.; Brinks, D.; Werley, C. A.; Harrison, D. J.; Campbell, R. E.; Cohen, A. E. Bright and Fast Multicoloured Voltage Reporters via Electrochromic FRET. *Nat. Commun.* **2014**, *5*, 1–10.

(14) Piatkevich, K. D.; Jung, E. E.; Boyden, ...E. S. A Robotic Multidimensional Directed Evolution Approach Applied to Fluorescent Voltage Reporters. *Nat. Chem. Biol.* **2018**, *14*, 350–360.

(15) Brinks, D.; Klein, A. J.; Cohen, A. E. Two-Photon Lifetime Imaging of Voltage Indicating Proteins as a Probe of Absolute Membrane Voltage. *Biophys. J.* **2015**, *109* (5), 914–921.

(16) Xu, Y.; Zou, P.; Cohen, A. E. Voltage Imaging with Genetically Encoded Indicators. *Curr. Opin. Chem. Biol.* **2017**, *39*, 1–10.

(17) Miller, E. W.; Lin, J. Y.; Frady, E. P.; Steinbach, P. a.; Kristan, W. B.; Tsien, R. Y. Optically Monitoring Voltage in Neurons by Photo-Induced Electron Transfer through Molecular Wires. *Proc. Natl. Acad. Sci.* **2012**, *109* (6), 2114–2119.

(18) Bayraktar, H.; Fields, A. P.; Kralj, J. M.; Spudich, J. L.; Rothschild, K. J.; Cohen, A. E. Ultrasensitive Measurements of Microbial Rhodopsin Photocycles Using Photochromic FRET. *Photochem. Photobiol.* **2012**, *88* (1), 90–97.

(19) Kulkarni, R. U.; Vandenberghe, M.; Thunemann, M.; James, F.; Andreassen, O. A.; Djurovic, S.; Devor, A.; Miller, E. W. In Vivo Two-Photon Voltage Imaging with Sulfonated Rhodamine Dyes. *ACS Cent. Sci.* **2018**, *4* (10), 1371–1378.

(20) Bort, G.; Gallavardin, T.; Ogden, D.; Dalko, P. I. From One-Photon to Two-Photon Probes: "Caged" Compounds, Actuators, and Photoswitches. *Angew. Chemie - Int. Ed.* **2013**, *52* (17), 4526–4537.

(21) Los, G. V; Encell, L. P.; Mcdougall, M. G.; Hartzell, D. D.; Karassina, N.; Simpson, D.; Mendez, J.; Zimmerman, K.; Otto, P.; Vidugiris, G.; et al. HaloTag: A Novel Protein Labeling Technology for Cell Imaging and Protein Analysis. *ACS Chem. Biol.* **2008**, *3* (6), 373–382.

(22) Kulkarni, R. U.; Yin, H.; Pourmandi, N.; James, F.; Adil, M. M.; Schaffer, D. V.; Wang, Y.; Miller, E. W. A Rationally Designed, General Strategy for Membrane Orientation of Photoinduced Electron Transfer-Based Voltage-Sensitive Dyes. *ACS Chem. Biol.* **2017**, *12* (2), 407–413.

(23) Roubinet, B.; Bischoff, M.; Nizamov, S.; Yan, S.; Geisler, C.; Stoldt, S.; Mitronova, G. Y.; Belov, V. N.; Bossi, M. L.; Hell, S. W. Photoactivatable Rhodamine Spiroamides and Diazoketones Decorated with

"Universal Hydrophilizer" or Hydroxyl Groups. *J. Org. Chem.* **2018**, *83* (12), 6466–6476.
(24) Nguyen, T.; Francis, M. B. Practical Synthetic Route to Functionalized Rhodamine Dyes. *Org. Lett.* **2003**, *5* (18), 3245–3248.
(25) St-Pierre, F.; Marshall, J. D.; Yang, Y.; Gong, Y.; Schnitzer, M. J.; Lin, M. Z. High-Fidelity Optical Reporting of Neuronal Electrical Activity with an Ultrafast Fluorescent Voltage Sensor. *Nat. Neurosci.* **2014**, *17* (6), 884–889.
(26) Chen, T. W.; Wardill, T. J.; Sun, Y.; Pulver, S. R.; Renninger, S. L.; Baohan, A.; Schreiter, E. R.; Kerr, R. A.; Orger, M. B.; Jayaraman, V.; et al. Ultrasensitive Fluorescent Proteins for Imaging Neuronal Activity. *Nature* **2013**, *499* (7458), 295–300.
(27) Kazemipour, A.; Novak, O.; Flickinger, D.; Marvin, J. S.; King, J.; Borden, P.; Druckmann, S.; Svoboda, K.; Looger, L. L.; Podgorski, K. Kilohertz Frame-Rate Two-Photon Tomography. *bioRxiv* **2018**, 357269.
(28) Abdelfattah, A. S.; Farhi, S. L.; Zhao, Y.; Brinks, D.; Zou, P.; Ruangkittisakul, A.; Platisa, J.; Pieribone, V. A.; Ballanyi, K.; Cohen, A. E.; et al. A Bright and Fast Red Fluorescent Protein Voltage Indicator That Reports Neuronal Activity in Organotypic Brain Slices. *J. Neurosci.* **2016**, *36* (8), 2458–2472.
(29) Chavarha, M.; Villette, V.; Dimov, I.; Pradhan, L.; Evans, S.; Shi, D.; Yang, R.; Chamberland, S.; Bradley, J.; Mathieu, B.; et al. Fast Two-Photon Volumetric Imaging of an Improved Voltage Indicator Reveals Electrical Activity in Deeply Located Neurons in the Awake Brain. *bioRxiv* **2018**, 445064.
(30) Acker, C. D.; Yan, P.; Loew, L. M. Single-Voxel Recording of Voltage Transients in Dendritic Spines. *Biophys. J.* **2011**, *101* (2), L11–L13.
(31) Fisher, J. A. N.; Barchi, J. R.; Welle, C. G.; Kim, G.-H.; Kosterin, P.; Obaid, A. L.; Yodh, A. G.; Contreras, D.; Salzberg, B. M. Two-Photon Excitation of Potentiometric Probes Enables Optical Recording of Action Potentials From Mammalian Nerve Terminals In Situ. *J. Neurophysiol.* **2008**, *99* (3), 1545–1553.
(32) Xu, C.; Webb, W. W. Measurement of Two-Photon Excitation Cross Sections of Molecular Fluorophores with Data from 690 to 1050 Nm. *J. Opt. Soc. Am. B* **1996**, *13* (3), 481.

Chapter 3:
Design and Synthesis of RhoVRs with Improved Brightness and Voltage Sensitivities

Portions of this work were performed in collaboration with the following persons:
Synthesis was assisted by Sarah Al-Abdullatif
Synthesis was assisted by Rishi Kulkarni

Abstract

We report the synthesis of second-generation rhodamine-based voltage reporters (RhoVRs). These RhoVR derivatives were synthesized to improve the brightness, voltage sensitivity and photostability of the previously reported RhoVR 1, as well as to develop a better understanding of the structure-function relationships important to VoltageFluor performance. We first looked to modulate the rate of photo-induced electron transfer (PeT) through the synthesis of RhoVRs with various donor moieties. We found that RhoVR 1, while possessing a high voltage sensitivity (47% ΔF/F per 100 mV), is highly PeT quenched and therefore dim. Significantly brighter RhoVRs were synthesized from less electron-rich donors, with the best performance coming from the methyl-substituted donor, RhoVR(Me). RhoVR(Me) is 4-fold brighter than RhoVR 1, but exhibited a lower voltage sensitivity (13% ΔF/F per 100 mV). We next looked to improve the performance of RhoVRs through the incorporation of 4-membered azetidine rings into the rhodamine fluorophore (az-RhoVRs). az-RhoVRs were synthesized from isomerically pure fluorescein-based VoltageFluors through a Pd-catalyzed cross-coupling approach. az-RhoVR1 possesses nearly identical voltage sensitivities as RhoVR 1 (49% vs. 47% ΔF/F per 100 mV, respectively), but is 2-fold dimmer. Finally, we improved the membrane loading of RhoVRs by exchanging the sarcosine-derived *ortho*-tertiary amide with a sulfonated piperazine moiety that increased brightness by 50% with minimal effect on voltage sensitivity. These results demonstrate the tunability of RhoVRs, as minor synthetic changes can greatly influence the sensitivity, brightness, photostability and membrane localization of VoltageFluors.

Introduction

Optical methods for interrogating membrane potential provide an alternative to the highly invasive and low-throughput patch-clamp electrophysiology.[1] Our lab has worked to develop a new class of voltage sensitive dyes, VoltageFluors (VFs), which utilize photo-induced electron transfer (PeT) as a trigger for voltage sensing (**Scheme 3-1**).[2,3] This PeT-based sensing mechanism affords VFs with incredibly fast response times to membrane potential changes (<<140 μs),[2] operates independently of excitation wavelength, allowing VFs spanning the visible spectrum,[3–5] and can lead to highly sensitive voltage indicators (up to 63% ΔF/F per 100 mV).[6] A consequence of PeT-based sensing is that as voltage sensitivity increases with the rate of electron-transfer, Φ_{Fl} decreases, leading to dimmer VoltageFluors.[7] A compromise between voltage sensitivity and Φ_{Fl} is therefore necessary in order to maximize VF performance (i.e. SNR).

While there has been some success estimating the driving force of PeT (ΔG_{PeT}) in fluorescein-based VFs,[8] The discovery and optimization of new classes of VFs is still largely empirical. During the development of first-generation tetramethylrhodamine-based voltage reporters (RhoVRs), four derivatives were synthesized before the bright and sensitive RhoVR 1 was identified.[3] The original RhoVR library focused on modifications to the molecular wire and revealed two key modifications that significantly increased RhoVR performance. First, moving the phenylenevinylene wire from the 4' to 5' position of the *meso*-aryl ring increased both the brightness and voltage sensitivity.[3] Interestingly, this modification also increases performance in fluorescein-based VFs, but not in Si-rhodamine-based VFs (unpublished results). Second, using an electron-rich, methoxy-substituted donor increased voltage sensitivity significantly (**Figure 1-8**). While RhoVR 1 is an excellent and versatile VF, one major limitation is its relatively low brightness in cells. This is likely a result of increased PeT-quenching from the methoxy-substituted

wire leading to a low Φ_{Fl}. Based on previous synthetic studies with fluorescein-based VFs, we believed that further structural modification of the aniline donor moiety could result in significant improvements in RhoVR performance.[5,8] These second-generation RhoVRs would incorporate donors with both higher and lower electron-richness in attempt to develop brighter RhoVR derivatives and gain a better understanding of donor-acceptor relationships as they pertain to PeT sensing in RhoVRs.

In addition to modifications to the electron donor, we were also interested in improving RhoVR performance at the tetramethylrhodamine (TMR) acceptor. Recent work by Grimm *et al.* showed that the brightness and photostability of TMRs could be significantly improved by replacing the N,N-dimethylamino substituents with 4-membered azetidine rings.[9] This modification was found to double the quantum efficiency of rhodamine fluorescence by disfavoring the formation of a twisted internal charge transfer (TICT) state following excitation, a process which is a significant contributor to the non-radiative decay of the fluorophore.[10] The development of azetidine-based RhoVRs (az-RhoVRs) was particularly attractive as azetidines have minimal effect on the absorption/emission profile of the parent dye and result in the net addition of only 2 carbons.[9] We therefore believed this modification would not perturb the PeT quenching voltage sensing mechanism, thus have minimal impact on voltage sensitivity while increasing brightness. Finally, we looked to modify the solubilizing group at the *ortho*-tertiary amide of RhoVR 1 in order to improve membrane loading of RhoVRs. Piperazine-derived tertiary amides were of particular interest as they provided greater flexibility for synthesizing functionalized RhoVRs.

Results and Discussion

*Synthesis of RhoVR Derivatives **9-12***

The modular nature of RhoVR synthesis enabled the rapid construction of several new derivatives from substituted phenylenevinylene molecular wires (**Scheme 3-2**).[3] In general, these molecular wires were synthesized from commercially available N,N-dimethylaniline derivatives. Formylation via a Vilsmeyer-Haack reaction followed by a Wittig reaction provided styrene intermediates that were then coupled to bromobenzaldehyde through a Pd-catalyzed Heck coupling. A final Wittig reaction afforded phenylenevinylene wires **1-6**, which were subsequently coupled to isomerically pure 5'-bromotetramethylrhodamine (Br-TMR, **Scheme 3-3**). Only 5'-substituted RhoVRs, and not 4'-substituted RhoVRs, were synthesized due to previous studies showing the 5'-substitution pattern resulted in both brighter and more voltage sensitive RhoVRs.[3] Formation of an N-methyl glycine-derived tertiary amide mediated by HATU gave *t*-butyl ester protected voltage sensors. Subsequent TFA-catalyzed deprotection of the *t*-butyl ester followed by reversed-phase HPLC purification gave final voltage sensors **7-12** in >14% yield over two steps (**Scheme 3-3**).

*Characterization of RhoVR Derivatives **9-12** in HEK Cells*

We evalulated the performance of RhoVR derivatives **7-12** in HEK cells by comparison of their brightness and voltage sensitivity. RhoVRs with more electron-rich donors (RhoVR 1, **9**) were much dimmer than RhoVRs with relatively electron-poor donors (**7**, **10**, **11**, **Table 3-1**, **Figure 3-1**). The dimmest RhoVR was dianiline-substituted **9**, which was 86% as bright as RhoVR

1 (**Figure 3-1**). Interestingly, patch-clamp electrophysiology revealed that **9** was also less voltage sensitive than RhoVR 1, with a 22% ΔF/F per 100 mV (**Figure 3-2e**). This reduced sensitivity with increased donor electron-richness suggests that the driving force of PeT (ΔG_{PeT}) for **9** is large, and that the dye is too quenched for efficient voltage sensing in the physiologically relevant ±100 mV window.[7] This hypothesis is supported by the non-linear voltage sensitivity recorded for **9**, where hyperpolarizing voltage steps in voltage-clamped HEK cells resulted in much smaller fluorescence changes than depolarizing steps (**Figure 3-2f**). This non-linearity was also observed for RhoVR 1, with hyperpolarizing steps displaying a nearly 2-fold greater change in fluorescence than depolarizing steps (**Figure 3-2d**). Taken together these results suggest that, while RhoVR 1 possesses a high voltage sensitivity, its ΔG_{PeT} is likely too large and that increased performance could be achieved through the incorporation of a less electron-rich donor moiety. In contrast to **9**, unsubstituted **7** was the brightest of all RhoVRs (9-fold brighter than RhoVR 1), but was also the least voltage sensitivity (7% ΔF/F per 100 mV). Interestingly, the voltage response of **7** was also observed to be non-linear over the ±100 mV range and displayed 2-fold larger fluorescence changes during hyperpolarizing steps than depolarizing steps (**Figure 3-2b**). This supports our hypothesis that the unsubstituted aniline donor possesses a small ΔG_{PeT} and explains why **7** is a bright, yet relatively insensitive dye.

In attempt to synthesize RhoVR derivatives with moderate ΔG_{PeT} and linear responses to voltage changes in the ±100 mV range, we synthesized RhoVR derivatives **10-12** (**Scheme 3-2**). RhoVR **10**, replaces the aniline motif with a dimethoxy donor, demonstrated very poor membrane staining and its voltage sensitivity was therefore not measured. Methyl-substituted and dimethyl-substituted RhoVRs **11** and **12** were both brighter than RhoVR 1 (4-fold and 5-fold, respectively). In addition, **11** and **12** exhibited moderate voltage sensitivities (13% and 12% ΔF/F per 100 mV, respectively) with a more linear responses over the ±100 mV range (**Figure 3-2h,j**), suggesting a more favorable ΔG_{PeT} for these donor/acceptor pairs. RhoVRs **11** and **12** moderate voltage sensitivities and increased brightness meant voltage changes in HEK cells were measured with SNRs rivaling or surpassing that of RhoVR 1 (**Table 3-1**). While not strictly superior to RhoVR 1, we have begun using **11**, now dubbed RhoVR(Me), to record neuronal activity in neurons and in brain slice. In particular, we have found the additional brightness of RhoVR(Me) to be useful in imaging settings where the photon budget is a limiting factor.[11]

Synthesis of Azetidine-substituted RhoVRs (az-RhoVRs)

In addition to improving RhoVR function through synthetic modifications at the donor moiety, we hoped to improve RhoVR brightness and photostability without sacrificing voltage sensitivity by incorporating 4-membered azetidine rings into the rhodamine chromophore. Azetidine-functionalized rhodamines are synthesized from fluoresceins through a Pd-catalyzed Buchwald-Hartwig cross-coupling.[9] In order to avoid potential cross reactivity with the halogenated xanthenes necessary for attachment of the molecular wire, we first synthesized isomerically pure carboxy-fluorescein VoltageFluors (carboxyVFs, **Scheme 3-4,5**). CarboxyVFs were synthesized from isomerically pure 5'- and 4'-Br-fluoresceins that were isolated from the condensation of resorcinol with 4-bromophthalic anhydride.[12] Pd-catalyzed Heck couplings between either the 5'- or 4'-Br-fluorescein and methoxy-substituted molecular wire **2** generated carboxyVFs **15** and **16** in 84% and 66% yields, respectively. The phenolic oxygens of the **15** and **16** were then reacted with triflic anhydride and a subsequent Buckwald-Hartwig amination with azetidine afforded RhoVRs **19** and **20** (30% and 29% yield over two steps, respectively). Finally,

the formation of an N-methyl glycine-derived tertiary amide with HATU followed by TFA-catalyzed deprotection of the *t*-butyl esters afforded az-RhoVRs **23** and **24**.

Characterization of az-RhoVRs in HEK Cells

HEK cells were loaded with either **23** or **24** and their brightness and voltage sensitivities compared to their TMR counterparts RhoVR 1 and RhoVR(OMe) (**Figure 3-3**). Both az-RhoVRs possessed voltage sensitivities slightly higher than their TMR-RhoVR counterparts (29% vs 26% for **23**, 49% vs. 47% for **24**) with the same non-linear responses to voltage steps over the ±100 mV range (**Table 3-1**, **Figure 3-3i-l**). In addition, the absorption and emission profiles of az-RhoVRs were very similar to their TMR-based RhoVRs, suggesting the incorporation of azetidines had little effect on the ΔG_{PeT} (**Table 3-1**).

While the voltage sensitivities of az-RhoVRs were virtually unchanged, both **23** and **24** were found to be much dimmer than their TMR-RhoVR counterparts when applied to HEK cells (**Figure 3-3e-h**). This result was somewhat surprising as az-RhoVRs were found to be approximately 50% brighter than TMR-RhoVRs in solution (**Table 3-1**). One possible explanation is that the rate of PeT quenching (k_{PeT}) in RhoVRs is much faster than the rate of TICT (k_{TICT}). This is plausible, as RhoVRs possess much lower Φ_{Fl} than their parent chromophores. With k_{PeT} dominating the decay of the excited state, the observed gains in brightness from the reduction of TICT are attenuated. It has also been shown that the k_{TICT} is much faster in polar solvents than non-polar solvents.[9] As RhoVRs intercalate into the lipid bilayer, it is possible the rate of k_{TICT} for RhoVRs may already be quite slow. Finally, it is possible the reduced brightness is unrelated to k_{TICT}, but is a result of less az-RhoVR loading into the membrane. In order to test this hypothesis, fluorescence lifetime imaging (FLIM) could be used to compare az-RhoVRs to RhoVRs independent of fluorescence intensity.

Synthesis and Characterization of an Alkyl Sulfonate-Functionalized RhoVR

Modifications to the donor and acceptor of RhoVRs both aimed to improve performance by increasing the photon yield of the sensor. Alternatively, modifications to the *ortho* solubilizing group could be made that increase brightness by increasing the concentration of RhoVR in the plasma membrane. We hypothesized that improved membrane staining could be achieved by increasing the amphiphilicity of the *ortho*-tertiary amide used to anchor RhoVRs in the outer leaflet of the membrane. During the development of genetically targetable RhoVR-Halos, we showed that the N-methyl glycine-derived tertiary-amide of RhoVR 1 could be replaced with a piperazine (RhoVR.Pip). This provided a nucleophilic handle for further functionalization with the HaloTag ligand (**Chapter 2**). To synthesize a more amphiphilic RhoVR, we instead envisioned functionalizing RhoVR.Pip with an alkyl sulfonate (**Scheme 3-6**).

In order to minimize the number of synthetic steps carried out on the RhoVR voltage dye, 1-Boc-piperazine was first alkylated with 1,3-propanesultone, yielding **25** in 86% yield. TFA catalyzed deprotection of the Boc group then afforded the sulfonated piperazine **26** in 89% yield. **26** was then added to RhoVR **S15** through a HATU-mediated coupling, affording the alkyl sulfonate-functionalized RhoVR **27**, or RhoVR.Pip.Sulf, in 68% yield following reverse-phase HPLC purification (**Scheme 3-6**). Bath application of RhoVR.Pip.Sulf onto HEK cells showed it localized well to the plasma membrane. When loaded at the same concentration as RhoVR 1, RhoVR.Pip.Sulf was 50% brighter, indicating it loads membranes more efficiently (**Figure 3-4a-**

d). In order to determine if RhoVR.Pip.Sulf was properly oriented in the membrane (i.e. roughly perpendicular to the plasma membrane),[6] we measured the voltage sensitivity of the dye. Since RhoVR.Pip.Sulf and RhoVR 1 have identical donors and acceptors, we expected any change in ΔG_{PeT}, and therefore voltage sensitivity, would be the result of tilting of RhoVR.Pip.Sulf in the membrane.[6] Patch-clamp electrophysiology revealed RhoVR.Pip.Sulf had a voltage sensitivity of 44 ±1% ΔF/F per 100 mV, nearly identical to that of RhoVR 1 (47 ± 3% ΔF/F per 100 mV, **Figure 3-4e,f**).

Conclusion

In summary, we synthesized a library of RhoVR derivatives in attempt to improve their brightness, sensitivity and SNR. We first looked to tune the ΔG_{PeT} of RhoVRs through the incorporation of novel electron donors. These modifications revealed that, while RhoVR 1 is highly voltage sensitive in the ±100 mV range, its fluorescence is also overly quenched and therefore dim. New methyl-substituted derivatives RhoVR(Me) and **12** increase the brightness (approximately 5-fold brighter than RhoVR 1), but displayed moderate sensitivities (13% and 12% ΔF/F per 100 mV, respectively). While the increased brightness of these dyes has made them attractive for use in photon-limiting experiments, their performance (i.e. SNR) is comparable to RhoVR 1. Future work will focus on further optimization of electron donor, as both RhoVR 1 and RhoVR(Me) display non-linear responses to voltage steps over the ±100 mV range, implying an "ideal" ΔG_{PeT} has yet to be reached.

In addition to modifications of the donor, we sought to improve performance at the acceptor/chromophore by synthesizing az-RhoVRs. Both az-RhoVRs **23** and **24** showed similar voltage sensitivities to their TMR-RhoVR counterparts (29% vs 26% for **23**, 49% vs. 47% for **24**), however they were surprisingly dimmer when loaded on cells. To determine if this reduced brightness is an intrinsic property of az-RhoVRs or an issue with membrane loading, the fluorescence lifetimes of az-RhoVRs could be measured. Longer fluorescence lifetimes relative to TMR-RhoVRs would suggest the azetidine modification is indeed lowering k_{TICT} and the reduced brightness of az-RhoVRs is a loading effect. The synthesis of genetically targetable az-RhoVRs could also be used to normalize for loading efficiency, as the brightness of genetically targeted RhoVRs can be normalized to the expression levels of the protein tag. Finally, az-RhoVR(Me) derivatives could be synthesized to determine if the reduced performance of **23** and **24** is a result of k_{PeT} dominating k_{TICT}. Az-RhoVR(Me) would have a smaller k_{PeT} due to the less e-rich donor. With k_{PeT} no longer dominating the decay of the excited state, the effect of azetidine incorporation may be more apparent, leading to brighter, more photostable RhoVRs.

We also synthesized an alkyl sulfonate substituted RhoVR, RhoVR.Pip.Sulf, which showed a 50% increase in brightness over RhoVR 1 when loaded at the same concentrations. In order to further investigate the effect *ortho*- solubilizing groups can have on RhoVR performance, more derivatives must be synthesized. For example, the incorporation of sulfonates with longer alkyl chains or the use of other polar groups such as phosphonates, is of interest. We are also interested in examining how different solubilizing groups can affect the loading of RhoVRs into different cellular membranes, such as gram-positive or gram-negative bacterial membranes.

Experimental Section

General Method for Chemical Synthesis and Characterization

Chemical reagents and solvents (dry) were purchased from commercial suppliers and used without further purification. Azetidine was purchased specifically from Sigma-Aldrich (250 mg ampules), as azetidine sourced from other suppliers significantly reduced yields for Buchwald-Hartwig couplings. Synthesis of **1**, **2**, **5**, **7**, **S15**, RhoVR 1 and RhoVR(Me) were carried out as previously reported in this thesis or in the literature.[3,4] Compounds **3** and **4** were synthesized by Rishi Kulkarni. Thin layer chromatography (TLC) (Silicycle, F254, 250 μm) and preparative thin layer chromatography (PTLC) (Silicycle, F254, 1000 μm) was performed on glass backed plates pre-coated with silica gel and were visualized by fluorescence quenching under UV light. Flash column chromatography was performed on Silicycle Silica Flash F60 (230–400 Mesh) using a forced flow of air at 0.5–1.0 bar. NMR spectra were measured on Bruker AVB-400 MHz, 100 MHz, AVQ-400 MHz, 100 MHz, Bruker AV-600 MHz, 150 MHz. Chemical shifts are expressed in parts per million (ppm) and are referenced to $CDCl_3$ (7.26 ppm, 77.0 ppm) or DMSO (2.50 ppm, 40 ppm). Coupling constants are reported as Hertz (Hz). Splitting patterns are indicated as follows: s, singlet; d, doublet; t, triplet; q, quartet; dd, doublet of doublet; m, multiplet; br, broad singlet. High-resolution mass spectra (HR-ESI-MS) were measured by the QB3/Chemistry mass spectrometry service at University of California, Berkeley. High performance liquid chromatography (HPLC) and low resolution ESI Mass Spectrometry were performed on an Agilent Infinity 1200 analytical instrument coupled to an Advion CMS-L ESI mass spectrometer. Two columns were used for the analytical HPLC, a Phenomenex Luna C18(2) (4.6 mm I.D. × 150 mm, 20 min runs) and a Phenomenex Luna C18(2) (4.6 mm I.D. × 50 mm, 12 min runs) with a flow rate of 1.0 mL/min. The mobile phases were MQ-H_2O with 0.05% formic acid (eluent A) and HPLC grade acetonitrile with 0.05% formic acid (eluent B). Signals were monitored at 254, 340 and 545 nm over 10-20 min with a gradient of 10-100% eluent B. The column used for semi-preparative HPLC was Phenomenex Luna 5μ C18(2) (10 mm I.D. x 150 mm) with a flow rate of 5.0 mL/min. The mobile phases were MQ-H_2O with 0.05% formic acid (eluent A) and HPLC grade acetonitrile with 0.05% formic acid (eluent B). Signals were monitored at 254 over 20 min with a gradient of 10-100% eluent B.

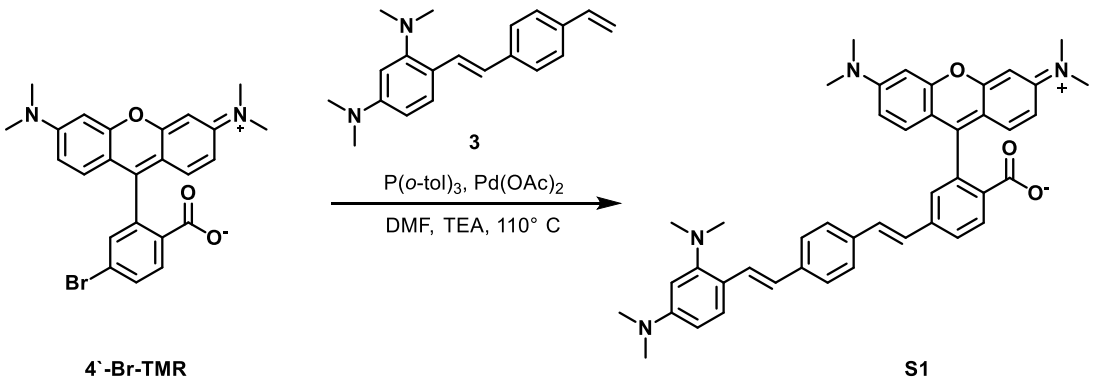

Synthesis of S1:

A Schlenk flask was charged with **4'-Br-TMR** (150 mg, 0.322 mmol), **3** (103 mg, 0.354 mmol), $Pd(OAc)_2$ (0.7 mg, 0.03 mmol) and P(*o*-tol)$_3$ (2.0 mg, 0.064 mmol). The flask was sealed and evacuated/backfilled with nitrogen (3x). Anhydrous DMF (5 mL) and anhydrous triethylamine (3 mL) were added via syringe and the reaction stirred at 110 °C for 18 h. The reaction was cooled and the solvent removed *in vacuo*. The remaining residue was purified by flash chromatography (5-10% methanol in DCM, linear gradient) affording **S1** as a purple solid (70 mg, 0.103 mmol, 32%). Analytical HPLC retention time 6.00 min; Exact mass calcd for $C_{44}H_{46}N_4O_3^{2+}$ $[M+2H]^{2+}$: 339.2, found: 339.5.

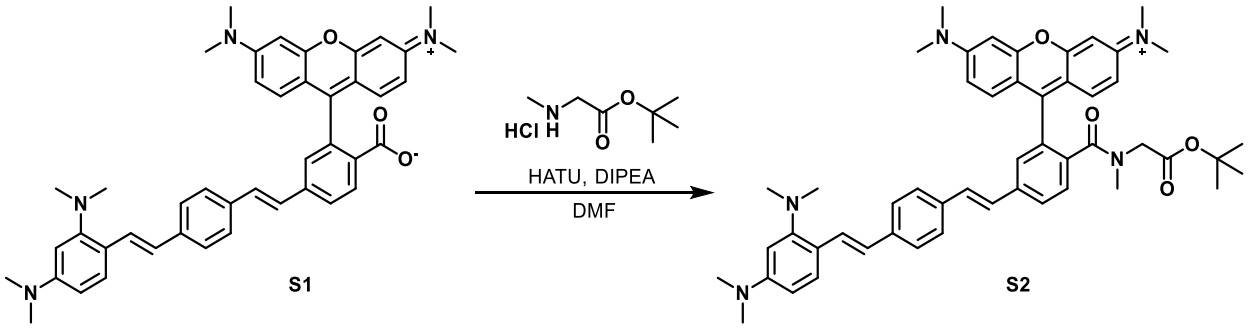

Synthesis of S2:

A vial was charged with **S1** (70.0 mg, 103 μmol), N-methyl sarcosine *t*-Bu ester hydrochloride (21.7 mg, 119 μmol), and HATU (43.2 mg, 114 μmol). The vial was sealed and evacuated/backfilled with nitrogen (3x). Anhydrous DMF (2 mL) and anhydrous diisopropylethylamine (22 μL, 103 μmol) were added and the vial was flushed with nitrogen, sealed, and stirred at 22 °C for 18 h. The solvent was removed *in vacuo* affording crude **S2** which was used without further purification for the next reaction. A portion of the material was purified by Preparative TLC (5% methanol in DCM) for characterization. ^{1}H NMR (only major rotamer peaks reported, 300 MHz, $CDCl_3$) δ 7.77 (d, *J* = 7.9 Hz, 1H), 7.60 (d, *J* = 8.1 Hz, 1H), 7.52 – 7.39 (m, 7H), 7.34 (d, *J* = 9.5 Hz, 2H), 7.20 – 7.08 (m, 2H), 6.93 (dd, *J* = 9.5, 2.5 Hz, 2H), 6.86 (d, *J* = 16.3 Hz, 1H), 6.78 (d, *J* = 2.5 Hz, 2H), 6.42 (d, *J* = 8.1 Hz, 1H), 6.36 (d, *J* = 2.5 Hz, 1H), 3.77 (s, 2H), 3.29 (s, 12H), 2.98 (s, 6H), 2.76 (s, 6H), 1.57 (s, 3H), 1.31 (s, 9H); Analytical HPLC retention time 6.84 min; MS (ESI) Exact mass for $C_{51}H_{59}N_5O_4^{2+}$ $[M+H]^{2+}$ calc: 402.7, found: 403.1; HR-ESI-MS m/z for $C_{51}H_{58}N_5O_4^{+}$ $[M+H^{+}]$ calcd: 804.4483 found: 804.4469.

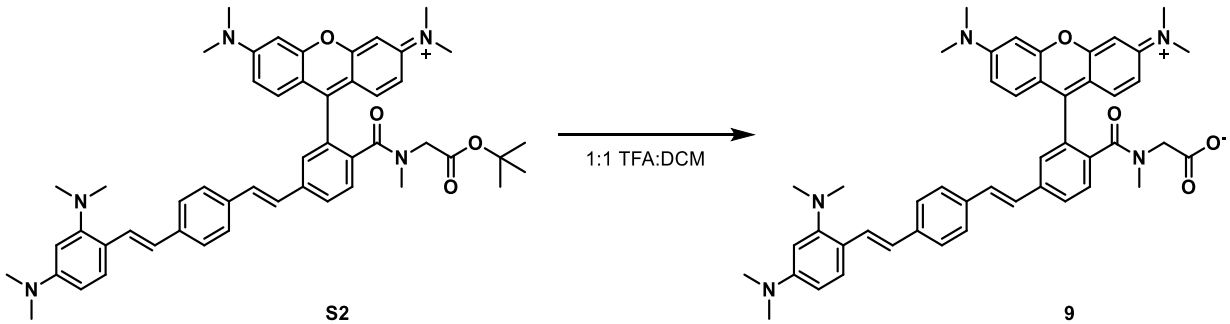

Synthesis of 9:

Trifluoroacetic acid (3 mL) was added to a solution of **S2** (45 mg, 56 μmol) in DCM (3 mL). The reaction was stirred at 22 °C for 1 h, then the solvent removed under a stream of nitrogen. The remaining residue was co-evaporated with toluene (1 x 10 mL) and acetonitrile (2 x 10 mL) and then purified by preparative TLC (10% methanol in DCM) affording **9** as a purple solid (6 mg, 8.0 μmol, 14.3%); Analytical HPLC retention time 5.88 min; MS (ESI) exact mass for $C_{47}H_{50}N_5O_4^+$ $[M+H]^+$ calcd: 748.4 found: 748.9; HR-ESI-MS m/z for $C_{47}H_{50}N_5O_4^+$ $[M+H]^+$ calcd: 748.3844 found: 748.3845.

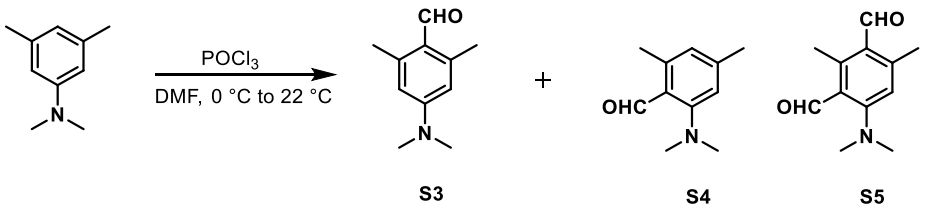

Synthesis of 4-(dimethylamino)-2,6-dimethylbenzaldehyde, S3:

A round-bottom flask was charged with N,N,3,5-tetramethylaniline (1.50 g, 10.0 mmol) and evacuated/backfilled with nitrogen (3x). Anhydrous DMF (20 mL) was added and the reaction cooled to 0 °C before the dropwise addition of phosphoryl chloride (1.64 mL, 18.0 mmol) via syringe. The reaction was allowed to warm to 22 °C and stirred for 18 h. The reaction was poured over ice water (250 mL) and the pH of the solution was adjusted to 8-9 with a 1 M solution of sodium hydroxide, at which point a white precipitant formed. The aqueous mixture was extracted with ethyl acetate (3 x 75 mL) and the combined organics dried with anhydrous magnesium sulfate, filtered and the solvent removed *in vacuo*. The remaining solid was purified by flash chromatography (10-25% ethyl acetate in hexanes). Three major benzaldehyde products were isolated. The first fraction (R_f = 0.5, 493 mg, 27.7%) corresponded to the ortho substituted aldehyde **S4**, the second fraction (R_f = 0.25, 586 mg, 33%) corresponded to desired product **S3**, and the third fraction (R_f = 0.1, 180 mg, 8.9%) corresponded to the isophthalaldehyde **S5**. ^{1}H NMR **S3** (400 MHz, $CDCl_3$) δ 10.39 (s, 1H), 6.35 (s, 2H), 3.09 (s, 6H), 2.64 (s, 6H); ^{1}H NMR **S4** (400 MHz, $CDCl_3$) δ 10.33 (s, 1H), 6.79 (s, 1H), 6.69 (s, 1H), 2.90 (s, 6H), 2.56 (s, 3H), 2.37 (s, 3H); ^{1}H NMR **S5** (400 MHz, $CDCl_3$) δ 10.56 (s, 1H), 10.19 (s, 1H), 6.72 (s, 1H), 3.03 (s, 6H), 2.85 (s, 3H), 2.64 (s, 3H).

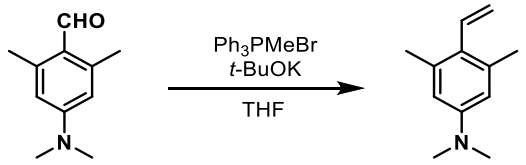

S3 S6

Synthesis of N,N,3,5-tetramethyl-4-vinylaniline, S6:

A round-bottom flask was charged with methyltriphenylpohsphonium bromide (2.33 g, 6.52 mmol) and then evacuated/backfilled with nitrogen (3x). Anhydrous THF (3 mL) was added and the reaction stirred for 15 min, then potassium *tert*-butoxide (730 mg, 6.52 mmol) was added. After stirring for another 15 min, **S3** (550 mg, 3.10 mmol) was added in anhydrous THF (5 mL) via syringe and the reaction stirred for 18 h. The reaction was diluted with hexanes (100 mL) and filtered through a diatomaceous earth. The solvent was then removed *in vacuo* and the remaining crude material purified by flash chromatography (15% ethyl acetate in hexanes, isocratic) affording **S6** as a yellow oil. (484 mg, 2.76 mmol, 89%). ^{1}H NMR (400 MHz, $CDCl_3$) δ 6.72 (dd, *J* = 17.9, 11.5 Hz, 1H), 6.50 (s, 2H), 5.46 (dd, *J* = 11.5, 2.2 Hz, 1H), 5.24 (dd, *J* = 17.9, 2.2 Hz, 1H), 2.97 (s, 6H), 2.36 (s, 6H).

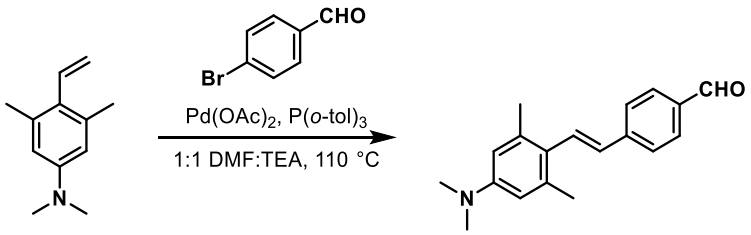

S6 S7

Synthesis of (E)-4-(4-(diethylamino)-2,6-dimethylstyryl)benzaldehyde, S7:

A Schlenk flask was charged with **S6** (450 mg, 2.57 mmol), bromobenzaldehyde (475 mg, 2.57 mmol), $Pd(OAc)_2$ (5.8 mg, 0.026 mmol), and P(*o*-tol)$_3$ (16 mg, 0.051 mmol). The flask was sealed and evacuated/backfilled with nitrogen (3x). Anhydrous DMF (2 mL) and anhydrous triethylamine (1 mL) were added via syringe and the reaction stirred at 110 °C for 16 h. The reaction was cooled and the solvent removed *in vacuo*. The remaining residue was diluted with ethyl acetate (50 mL) and washed with water (2 x 50 mL). The combined organics were dried with anhydrous sodium sulfate, filtered and the solvent removed *in vacuo.* The remaining solid was then triturated with hexanes and a small amount of diethyl ether to afford **S7** as a yellow solid (298 mg, 1.07 mmol, 41.6%). ^{1}H NMR (600 MHz, $CDCl_3$) δ 10.03 (s, 1H), 7.91 – 7.87 (m, 2H), 7.67 – 7.62 (m, 2H), 7.37 (d, *J* = 16.5 Hz, 1H), 6.67 (d, *J* = 16.5 Hz, 1H), 6.52 (s, 2H), 3.01 (s, 6H), 2.44 (s, 6H); Analytical HPLC retention time 5.64 min; MS (ESI) Exact mass calcd for $C_{19}H_{22}NO^+$ $[M+H]^+$: 280.4, found: 280.1; HR-ESI-MS m/z for $C_{19}H_{22}NO^+$ calcd: 280.1696 found: 280.1696.

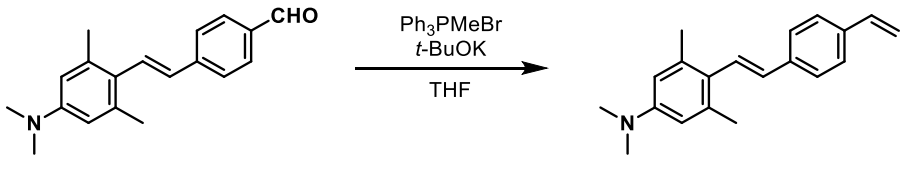

S7 6

Synthesis of (E)-N,N-diethyl-3-methoxy-4-(4-vinylstyryl)aniline, 6:

A round-bottom flask was charged with methyltriphenylphosphonium bromide (752 mg, 2.10 mmol) and then evacuated/backfilled with nitrogen (3x). Anhydrous THF (3 mL) was added and the reaction stirred for 15 min, then potassium *tert*-butoxide (236 mg, 2.10 mmol) was added. After stirring for another 15 min, **S7** (280 mg, 1.00 mmol) was added portion-wise and the reaction stirred for 18 h. The reaction was diluted with hexanes, then the solids removed by vacuum filtration through diatomaceous earth, rinsing with hexanes. The organics were concentrated *in vacuo* and the remaining oil was purified by flash chromatography (10% ethyl acetate in hexanes, isocratic) affording **6** as a yellow solid (250 mg, 0.90 mmol, 90%). ^{1}H NMR (600 MHz, $CDCl_3$) δ 7.50 – 7.42 (m, 4H), 7.17 (d, *J* = 16.5 Hz, 1H), 6.76 (dd, *J* = 17.6, 10.9 Hz, 1H), 6.59 (d, *J* = 16.5 Hz, 1H), 6.52 (s, 2H), 5.79 (d, *J* = 17.6 Hz, 1H), 5.27 (d, *J* = 10.9 Hz, 1H), 2.99 (s, 6H), 2.42 (s, 6H); Analytical HPLC retention time 9.09 min; MS (ESI) Exact mass calcd for $C_{20}H_{24}NO^+$ $[M+H]^+$: 278.2, found: 278.1; HR-ESI-MS m/z for $C_{20}H_{24}N^+$ $[M+H]^+$ calcd: 278.1903 found: 278.1901.

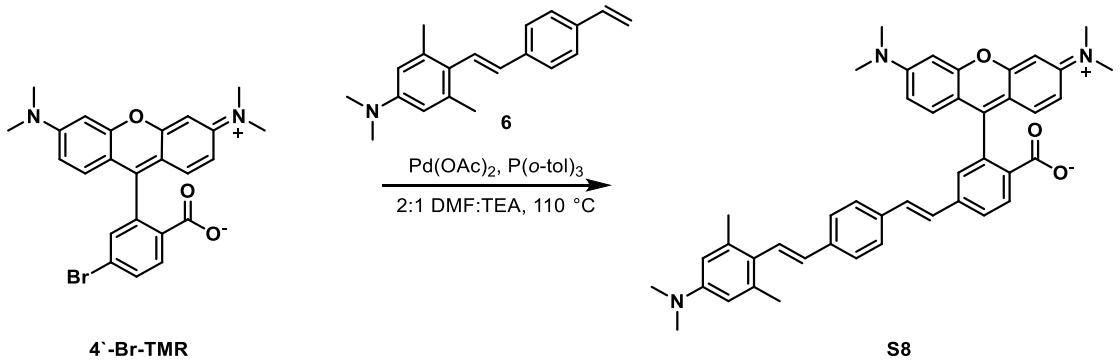

4`-Br-TMR S8

Synthesis of S8:

A Schlenk flask was charged with **4'-Br-TMR** (100 mg, 0.214 mmol), **6** (65.4 mg, 0.236 mmol), $Pd(OAc)_2$ (0.5 mg, 0.02 mmol) and P(*o*-tol)$_3$ (1.3 mg, 0.04 mmol). The flask was sealed and evacuated/backfilled with nitrogen (3x). Anhydrous DMF (2 mL) and triethylamine (1 mL) were added via syringe and the reaction stirred at 110 °C for 18 h. The reaction was cooled and the solvent removed *in vacuo*. The remaining residue was purified by flash chromatography (0-10% methanol in DCM, linear gradient) affording **S8** as a purple solid (105 mg, 0.158 mmol, 74%). ^{1}H NMR (400 MHz, $CDCl_3$) δ 8.04 (d, *J* = 8.0 Hz, 1H), 7.74 (d, *J* = 9.6 Hz, 1H), 7.49 (s, 4H), 7.34 (s, 1H), 7.24 – 7.07 (m, 3H), 6.78 (d, *J* = 8.8 Hz, 2H), 6.66 – 6.44 (m, 7H), 3.06 (s, 12H), 3.00 (s, 6H), 2.42 (s, 6H); Analytical HPLC retention time 6.53 min; MS (ESI) exact mass for $C_{44}H_{44}N_3O_3^+$ $[M+H]^+$ calcd: 662.3 found: 662.1. HR-ESI-MS m/z for $C_{44}H_{44}N_3O_3^+$ $[M+H]^+$ calcd: 662.3377 found: 662.3384.

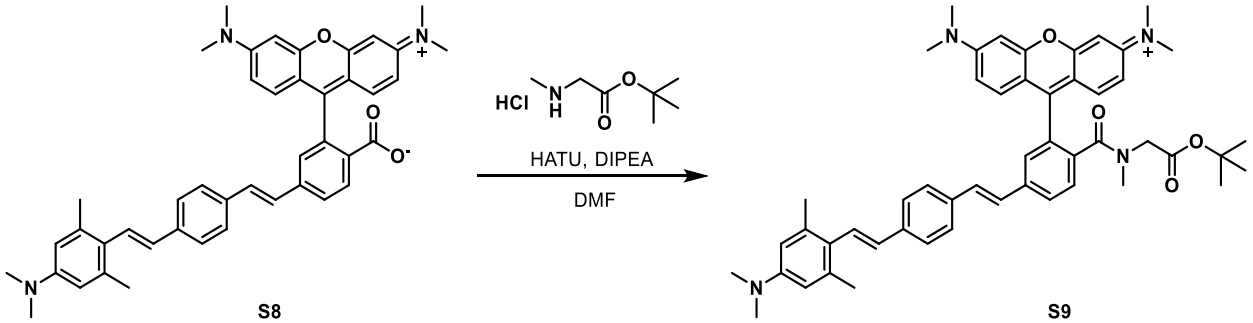

Synthesis of S9:

A vial was charged with **S8** (49.0 mg, 74 μmol), N-methyl sarcosine *t*-Bu ester hydrochloride (16.7 mg, 92.4 μmol), and HATU (35.1 mg, 92.4 μmol). Anhydrous DMF (5 mL) and anhydrous diisopropylethylamine (23.5 μL, 92.4 μmol) were added and the vial was flushed with nitrogen, sealed, and stirred at 22 °C for 3 h. The solvent was removed *in vacuo* and the remaining residue was purified by flash chromatography (0-2.5% methanol in DCM, linear gradient) affording **S9** as a purple solid (43.4 mg, 54.9 μmol, 74%). ^{1}H NMR (only major rotomer peaks reported, 400 MHz, $CDCl_3$) δ 8.05 (s, 1H), 7.83 (d, *J* = 7.0 Hz, 1H), 7.65 (d, *J* = 8.1 Hz, 1H), 7.53 (q, *J* = 8.3 Hz, 5H), 7.38 (d, *J* = 9.5 Hz, 2H), 7.22 (dd, *J* = 17.4, 8.8 Hz, 2H), 6.98 (dd, *J* = 9.5, 2.5 Hz, 2H), 6.82 (d, *J* = 2.5 Hz, 2H), 6.59 (d, *J* = 16.5 Hz, 1H), 6.51 (s, 2H), 3.82 (s, 2H), 3.34 (d, *J* = 3.6 Hz, 12H), 2.98 (s, 5H), 2.90 (s, 2H), 2.84 (s, 3H), 2.42 (s, 6H), 1.36 (s, 9H); Analytical HPLC retention time 7.09 min; MS (ESI) exact mass for $C_{51}H_{57}N_4O_4^+$ calcd: 789.4 found: 789.2; HR-ESI-MS m/z for $C_{51}H_{57}N_4O_4^+$ $[M+H]^+$ calcd: 789.4374 found: 789.4364.

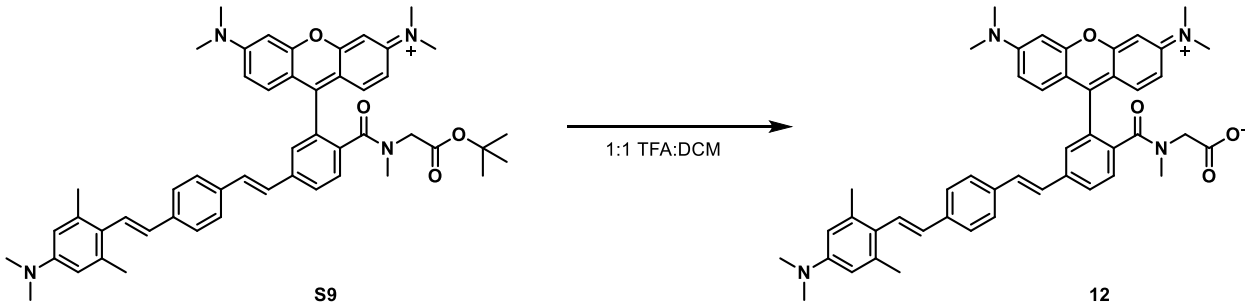

Synthesis of 12:

Trifluoroacetic acid (2 mL) was added to a solution of **S9** (15.6 mg, 20.1 μmol) in DCM (2 mL). The reaction was stirred at 22 °C for 1 h, then the solvent removed under a stream of nitrogen. The remaining residue was co-evaporated with toluene (1 x 10 mL) and acetonitrile (2 x 10 mL) and then purified by preparative TLC (10% methanol in DCM) affording **12** as a purple solid (19.0 mg, 25.9 μmol, 49%); Analytical HPLC retention time 5.99 min; MS (ESI) exact mass for $C_{47}H_{49}N_4O_4^+$ $[M+H]^+$ calcd: 733.4 found: 733.4; HR-ESI-MS m/z for $C_{47}H_{49}N_4O_4^+$ $[M+H]^+$ calcd: 733.3748.

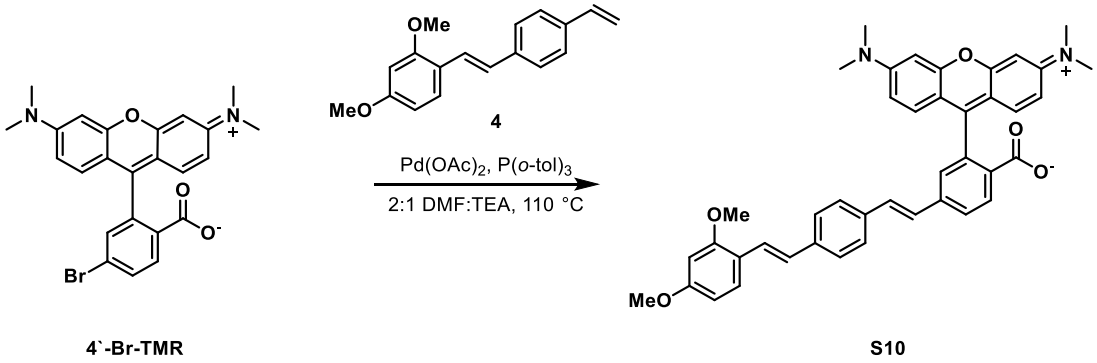

4`-Br-TMR S10

Synthesis of S10:

A Schlenk flask was charged with **4'-Br-TMR** (100 mg, 0.214 mmol), **4** (62.3 mg, 0.236 mmol), $Pd(OAc)_2$ (0.5 mg, 0.02 mmol) and P(*o*-tol)$_3$ (1.3 mg, 0.04 mmol). The flask was sealed and evacuated/backfilled with nitrogen (3x). Anhydrous DMF (3 mL) and triethylamine (1.5 mL) were added via syringe and the reaction stirred at 110 °C for 18 h. The reaction was cooled and the solvent removed *in vacuo*. The remaining residue was purified by flash chromatography (0-10% methanol in DCM, linear gradient) affording **S10** as a purple solid (104 mg, 0.150 mmol, 74%). ^{1}H NMR (400 MHz, DMSO-d_6) δ 7.93 (q, J = 8.0 Hz, 2H), 7.65 – 7.47 (m, 5H), 7.44 (s, 2H), 7.36 (d, J = 18.6 Hz, 2H), 7.08 (d, J = 16.5 Hz, 1H), 6.62 – 6.45 (m, 8H), 3.85 (s, 3H), 3.79 (s, 3H), 2.95 (s, 12H); Analytical HPLC retention time 6.90 min; MS (ESI) exact mass for $C_{42}H_{39}N_2O_5^+$ [M+H] $^+$ calcd: 651.3 found:651.3; HR-ESI-MS m/z for $C_{42}H_{39}N_2O_5^+$ $[M+H]^+$ calcd: 651.2853 found: 651.2847.

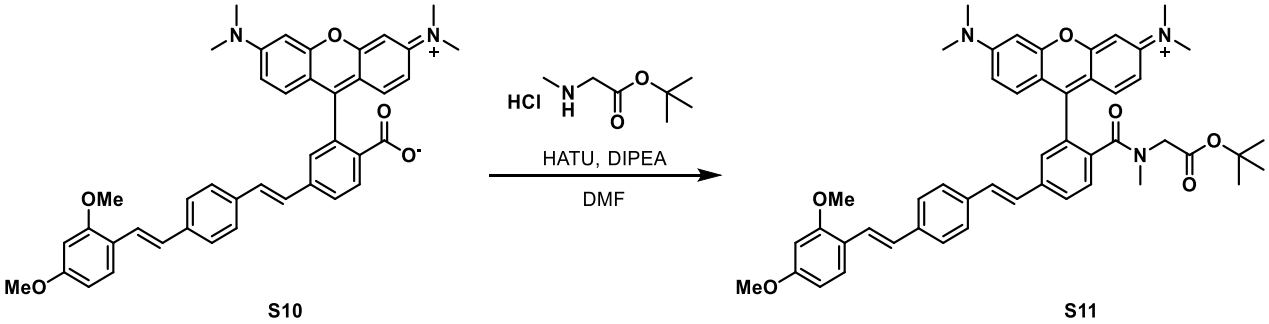

S10 S11

Synthesis of S11:

A vial was charged with **S10** (32.5 mg, 49.9 μmol), N-methyl sarcosine *t*-Bu ester hydrochloride (11.3 mg, 62.3 μmol), and HATU 23.7 mg, 62.3 μmol). Anhydrous DMF (3 mL) and anhydrous diisopropylethylamine (15.9 μL, 74.8 μmol) were added and the vial was flushed with nitrogen, sealed, and stirred at 22 °C for 3 h. The solvent was removed *in vacuo* and the remaining residue was purified by preparative TLC (5% methanol in DCM) affording **S11** as a purple solid (29.6 mg, 38.0 μmol, 76%). ^{1}H NMR (only major rotomer peaks reported, 400 MHz, DMSO-d_6) δ 7.96 (s, 1H), 7.80 (s, 1H), 7.68 – 7.53 (m, 6H), 7.52 – 7.33 (m, 3H), 7.28 (d, J = 9.5 Hz, 2H), 7.17 – 7.06 (m, 3H), 6.96 (d, J = 2.4 Hz, 2H), 6.64 – 6.53 (m, 2H), 3.86 (s, 3H), 3.80 (s, 3H), 3.28 (s, 12H), 2.81 (s, 3H), 2.69 (s, 2H), 1.25 (s, 9H); Analytical HPLC retention time 7.19 min; MS (ESI) exact mass for $C_{49}H_{52}N_3O_6^+$ calcd: 778.4 found: 778.3; HR-ESI-MS m/z for $C_{49}H_{52}N_3O_6^+$ calcd: 778.3851 found: 778.3843.

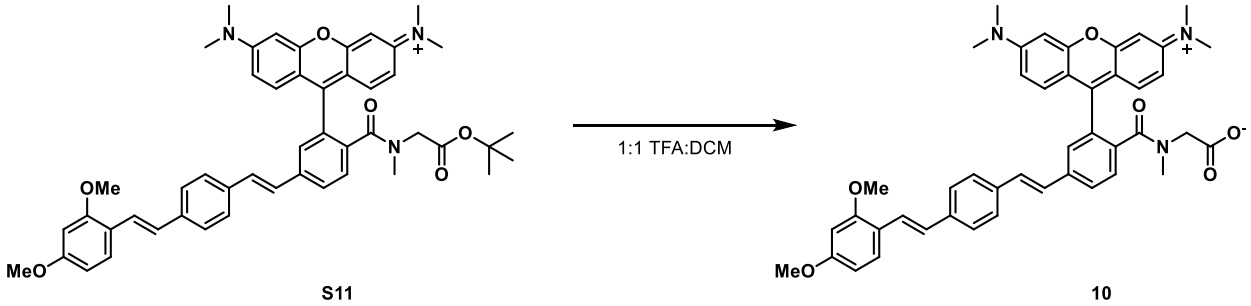

Synthesis of 10:

Trifluoroacetic acid (2 mL) was added to a solution of **S11** (15.6 mg, 20.1 μmol) in DCM (2 mL). The reaction was stirred at 22 °C for 1 h, then the solvent removed under a stream of nitrogen. The remaining residue was purified by preparative TLC (10% methanol in DCM) affording **10** as a purple solid (11.1 mg, 15.4 μmol, 57%); Analytical HPLC retention time 8.01 min; MS (ESI) exact mass for $C_{47}H_{49}N_4O_4^+$ $[M+H]^+$ calcd: 722.3 found: 721.9; HR-ESI-MS m/z for $C_{45}H_{45}N_3O_6^+$ $[M+H]^+$ calcd: 722.3225 found: 721.5566

Synthesis of Isomerically Pure Bromofluoresceins

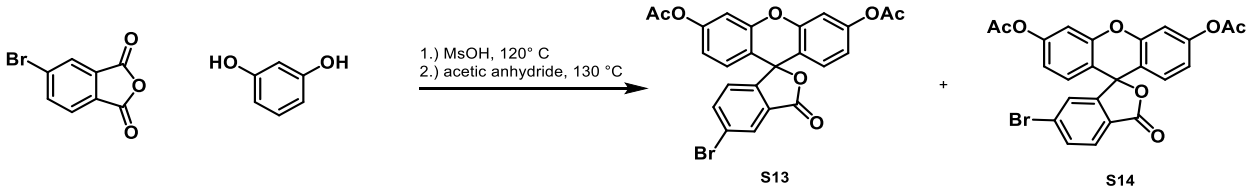

Synthesis of isomerically pure 5'- and 4'- Bromo Fluoresceins S13 and S14:[12]

A mixture of 4-bromophthalic anhydride (10.0 g, 44.0 mmol), resorcinol (9.70 g, 88.0 mmol) and methanesulfonic acid (20 mL) was heated at 120 °C with stirring for 4 h. The reaction was poured over 300 mL of ice-water, forming a yellow solid which was collected by vacuum filtration. This crude mixture was then refluxed in 120 mL of acetic anhydride (50 mL) for 3 h and then slowly cooled to 22 °C to induce recrystallization. The pale-yellow crystals which formed were poured over a fritted funnel and washed with ice-cold acetic anhydride (20 mL) and EtOH (20 mL) to afford 9.21 g of solid, which was determined to be a 3:1 ratio of **S13**:**S14** bromofluorescein, while the remaining mother liquor was a 1:2 ratio of **S13**:**S14** bromofluorescein (by ^{1}H NMR). Repeated recrystallizations of the **S13** enriched crystals from acetic anhydride afforded pure **S13** as colorless crystals (5.28 g, 10.7 mmol, 20.6%). ^{1}H NMR (300 MHz, $CDCl_3$) δ 8.20 (d, J = 1.8, 1H), 7.84 (dd, J = 8.2, 1.8 Hz, 1H), 7.17 – 7.08 (m, 3H), 6.87 (d, J = 1.4 Hz, 4H), 2.36 (s, 6H). Analytical HPLC retention time 17.70 min; MS (ESI) exact mass for $C_{24}H_{16}BrO_7^+$ $[M+H]^+$ calcd: 495.0 found: 495.1.

Initial recrystallizations of the **S14** enriched mother liquor from acetic anhydride were unsuccessful in removing **S13**. Instead, the crude material was added to boiling EtOH (500 mL) and acetic anhydride was added dropwise until the solid material was fully dissolved. The solution was then cooled to 22 °C, affording colorless crystals that were determined to be a 1:5 ratio of **S13:S14**. Further recrystallizations from ethanol afforded colorless crystals that were a 1:9 ratio of **S13:S14** (613 mg, 1.24 mmol, 2.8%). ^{1}H NMR (300 MHz, $CDCl_3$) δ 7.93 (d, J = 8.0 Hz, 1H),

7.81 (dd, *J* = 8.2, 1.6 Hz, 1H), 7.38 (d, *J* = 1.6 Hz, 1H), 7.15 (t, *J* = 1.3 Hz, 2H), 6.90 (d, *J* = 1.3 Hz, 4H), 2.37 (s, 6H). Analytical HPLC retention time 17.50 min; MS (ESI) exact mass for $C_{24}H_{16}BrO_7^+$ $[M+H]^+$ calcd: 495.0 found: 495.1.

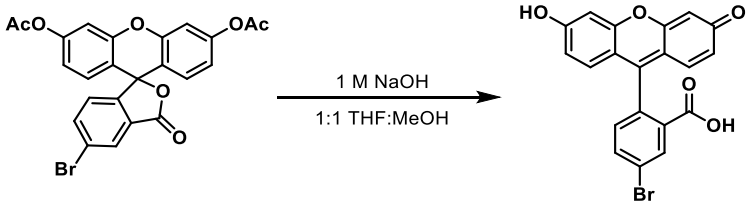

S13 13

Synthesis of 5'-bromofluorescein 13:

A round-bottom flask was charged with **S13** (2.00 g, 4.04 mmol), methanol (20 mL) and THF (20 mL). A 1 M solution of sodium hydroxide (9.7 mL, 9.7 mmol) was added and the reaction stirred at 22 °C for 18 hours. The reaction mixture was acidified by the addition of 2 M hydrochloric acid (10 mL), then extracted with ethyl acetate (2 x 100 mL). The combined organics were dried with anhydrous magnesium sulfate, filtered and the solvent removed *in vacuo* affording **13** as an orange solid (1.65 g, 4.02 mmol, 99%). ^{1}H NMR (300 MHz, MeOD) δ 8.13 (d, *J* = 1.8 Hz, 1H), 7.89 (dd, *J* = 8.3, 1.8 Hz, 1H), 7.13 (d, *J* = 8.3 Hz, 1H), 6.66 (d, *J* = 2.2 Hz, 2H), 6.63 – 6.50 (m, 4H); Analytical HPLC retention time 12.92 min; MS (ESI) exact mass for $C_{20}H_{12}{}^{81}BrO_5^+$ $[M+H]^+$ calcd: 413.0 found: 413.1; HR-ESI-MS m/z for $C_{20}H_{12}{}^{81}BrO_5^+$ $[M+H]^+$ calcd: 412.9835 found: 412.9803.

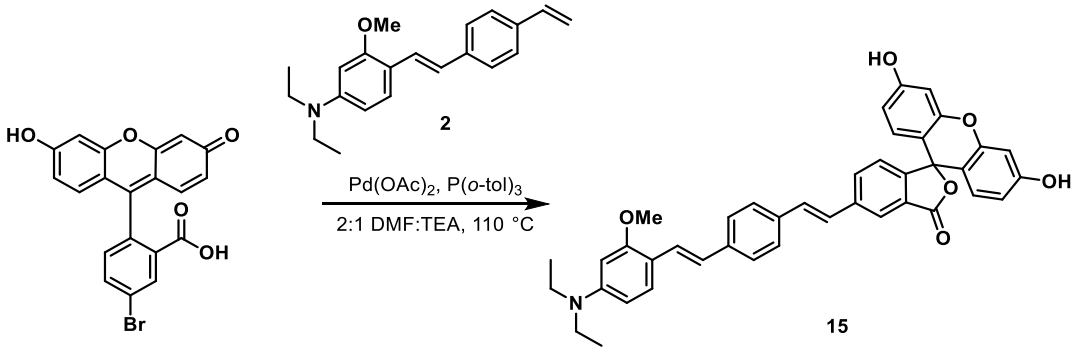

13 15

Synthesis of 15:

A Schlenk flask was charged with **13** (150 mg, 0.365 mmol), **2** (123 mg, 0.401 mmol), $Pd(OAc)_2$ (0.82 mg, 0.037 mmol) and P(*o*-tol)$_3$ (2.2 mg, 0.073 mmol). The flask was sealed and evacuated/backfilled with nitrogen (3x). Anhydrous DMF (3 mL) and triethylamine (1.5 mL) were added via syringe and the reaction stirred at 110 °C for 18 h. The reaction was cooled and the solvent removed *in vacuo*. The remaining residue was purified by flash chromatography (0-5% methanol in DCM, linear gradient) affording **15** as a yellow-orange solid (195 mg, 0.306 mmol, 84%). ^{1}H NMR (600 MHz, DMSO-d_6) δ 10.13 (s, 2H), 8.18 (s, 1H), 8.01 (dd, *J* = 7.9, 1.3 Hz, 1H), 7.62 (d, *J* = 8.0 Hz, 2H), 7.55 – 7.41 (m, 5H), 7.35 (d, *J* = 16.5 Hz, 1H), 7.26 (d, *J* = 8.0 Hz, 1H), 6.96 (d, *J* = 16.5 Hz, 1H), 6.68 (d, *J* = 2.4 Hz, 2H), 6.63 (d, *J* = 8.7 Hz, 2H), 6.56 (dd, *J* = 8.7, 2.4 Hz, 2H), 6.30 (dd, *J* = 8.9, 2.3 Hz, 1H), 6.22 (d, *J* = 2.3 Hz, 1H), 3.85 (s, 3H), 3.39 (q, *J* = 7.0 Hz, 4H), 1.13 (t, *J* = 7.0 Hz, 6H); Analytical HPLC retention time 12.61 min; MS (ESI) exact mass for

$C_{41}H_{37}NO_6^+$ [M+2H]$^+$ calcd: 319.6 found: 319.4; HR-ESI-MS m/z for $C_{41}H_{36}NO_6^+$ [M+H]$^+$ calcd: 638.2537 found: 638.2522.

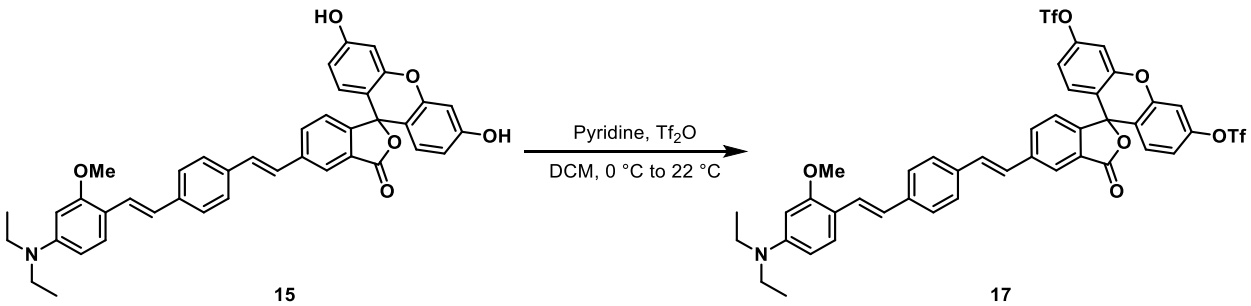

15 17

Synthesis of 17:

A round-bottom flask was charged with **15** (132 mg, 0.207 mmol), DCM (10 mL) and pyridine (133 µL, 1.66 mmol) and the reaction cooled to 0 °C while stirring. Triflic anhydride (139 µL, 0.828 mmol) was added dropwise, then the ice-bath was removed and the reaction was stirred for 3 h, after which the reaction was judged to be complete. The reaction mixture was diluted with water (50 mL) and DCM (50 mL). The combined organics were washed with brine (2 x 75 mL), dried with anhydrous magnesium sulfate, filtered and the solvent removed *in vacuo*. The remaining residue was purified by flash chromatography (20-50% ethyl acetate in hexanes, linear gradient) affording **17** as a yellow oil (105 mg, 0.116 mmol, 56%). ^{1}H NMR (600 MHz, $CDCl_3$) δ 8.20 (s, 1H), 7.87 (d, *J* = 8.1 Hz, 1H), 7.59 – 7.52 (m, 4H), 7.52 – 7.46 (m, 2H), 7.36 – 7.32 (m, 3H), 7.21 (d, *J* = 17.2 Hz, 2H), 7.10 – 7.05 (m, 4H), 6.98 (d, *J* = 16.3 Hz, 1H), 6.36 (d, *J* = 8.5 Hz, 1H), 6.24 (s, 1H), 3.94 (s, 3H), 3.44 (q, *J* = 6.3 Hz, 4H), 1.27 – 1.22 (t, *J* = 6.3 Hz, 6H); Analytical HPLC retention time 18.53 min; MS (ESI) exact mass for $C_{43}H_{34}F_6NO_{10}S_2^+$ [M+H]$^+$ calcd: 902.2 found: 902.5; HR-ESI-MS m/z for $C_{43}H_{34}F_6NO_{10}S_2^+$ [M+H]$^+$ calcd: 902.1509 found: 902.1512.

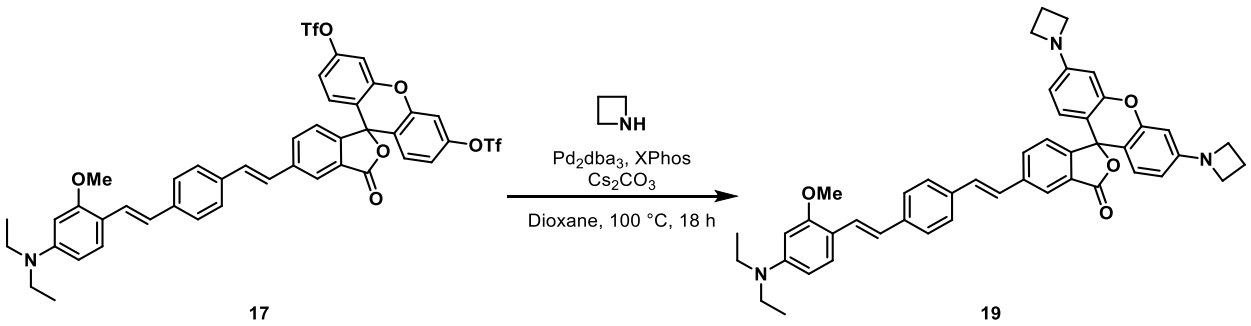

17 19

Synthesis of 19:

A 4 mL vial was charged with **17** (50.0 mg, 55.4 µmol), Pd_3dba_3 (5.1 mg, 5.5 µmol), XPhos (8.0 mg, 16.6 µmol) and cesium carbonate (51 mg, 155 µmol). The flask was sealed and evacuated/backfilled with nitrogen (3x). Anhydrous dioxane (220 µL) and a 0.6 M stock solution of azetidine in anhydrous dioxane (220 µL, 133 µmol) were added via syringe and the reaction stirred at 100 °C for 18 h. The reaction was cooled and the solvent removed *in vacuo*. The remaining residue was purified by flash chromatography (0-10% methanol in DCM, linear gradient) affording **19** as a purple solid (21.5 mg, 30 µmol, 54%). ^{1}H NMR (600 MHz, DMSO-d_6) δ 8.18 (s, 1H), 7.99 (d, *J* = 7.9 Hz, 1H), 7.60 (d, *J* = 8.1 Hz, 2H), 7.55 – 7.37 (m, 5H), 7.33 (m, 1H), 7.23 (s, 1H), 6.94 (d, *J* = 16.4 Hz, 1H), 6.57 (d, *J* = 35.3 Hz, 2H), 6.34 – 6.10 (m, 5H), 3.83

(s, 8H), 3.37 (q, *J* = 7.0 Hz, 4H), 2.32 (s, 4H), 1.11 (t, *J* = 7.0 Hz, 6H); Analytical HPLC retention time 13.27 min MS (ESI) exact mass for $C_{47}H_{46}N_3O_4^+$ $[M+H]^+$ calcd: 716.3 found: 716.8; HR-ESI-MS m/z for $C_{47}H_{46}N_3O_4^+$ $[M+H]^+$ calcd: 716.3483 found: 716.3464.

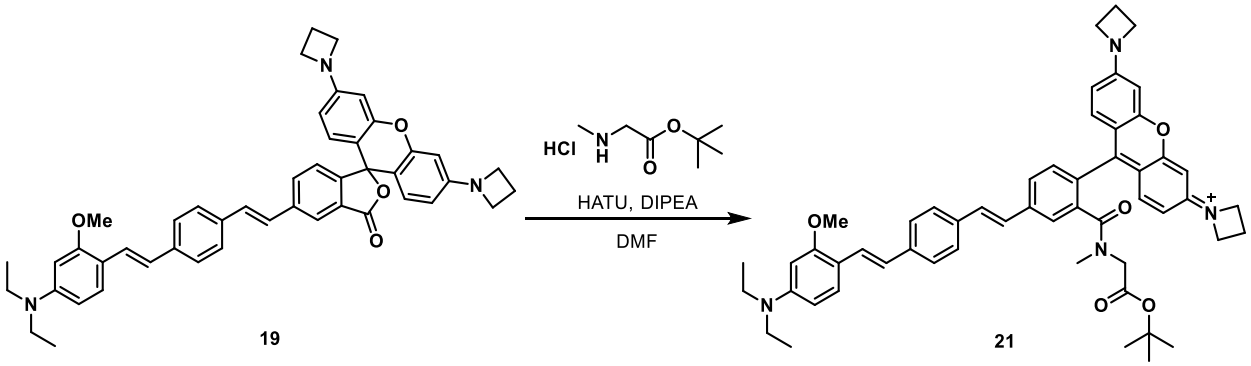

Synthesis of 21:

A vial was charged with **19** (16.7 mg, 23.3 μmol), N-methyl sarcosine *t*-Bu ester hydrochloride (5.1 mg, 35.0 μmol), and HATU 11.1 mg, 29.1 μmol). Anhydrous DMF (500 μL) and anhydrous diisopropylethylamine (6.2 μL, 29.1 μmol) were added and the vial was flushed with nitrogen, sealed, and stirred at 22 °C for 18 h. The solvent was removed *in vacuo* and the remaining residue was purified by preparative TLC (5% methanol in DCM) affording **21** as a purple solid (9.6 mg, 11.4 μmol, 50%). Analytical HPLC retention time 14.37 min; MS (ESI) exact mass for $C_{54}H_{60}N_4O_5^{2+}$ $[M+H]^{2+}$ calcd: 422.2 found: 422.3; HR-ESI-MS m/z for $C_{54}H_{59}N_4O_5^+$ $[M+H]^+$ calcd: 843.4480 found: 843.4464.

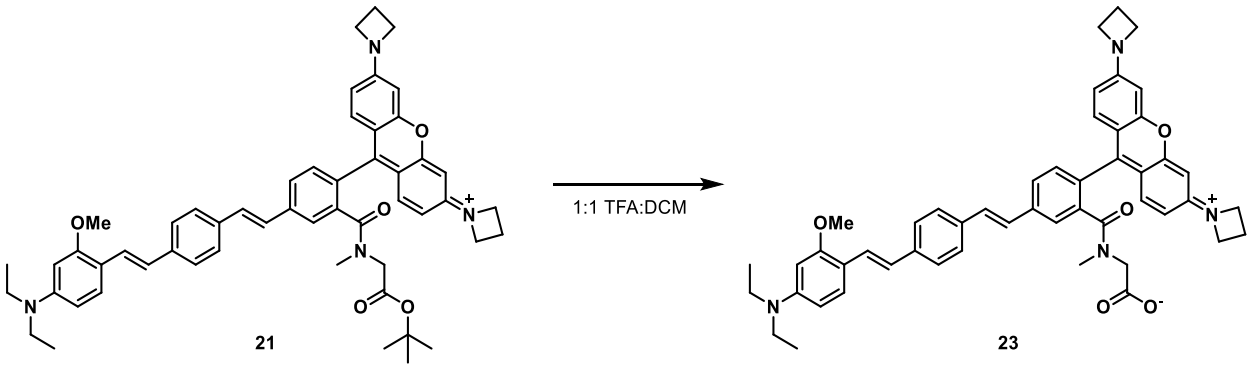

Synthesis of 23:

Trifluoroacetic acid (1 mL) was added to a solution of **21** (9.6 mg, 11.4 μmol) in DCM (1 mL). The reaction was stirred at 22 °C for 2 h, then the solvent removed under a stream of nitrogen. The remaining residue was purified by preparative TLC (10% methanol in DCM) affording **23** as a purple solid (7.0 mg, 8.9 μmol, 74%). Analytical HPLC retention time 6.17 min;, MS (ESI) exact mass for $C_{50}H_{52}N_4O_5^{2+}$ $[M+H]^{2+}$ calcd: 394.2 found: 394.5; HR-ESI-MS m/z for $C_{50}H_{51}N_4O_5^+$ calcd: 787.3854 found: 787.3854.

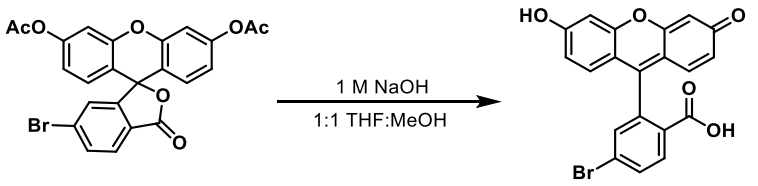

S14 14

Synthesis of 6-bromofluorescein 14:

A vail was charged with **S14** (118 mg, 238 µmol), methanol (1 mL) and THF (1 mL). A 1 M solution of sodium hydroxide (570 µL, 571 µmol) was added and the reaction stirred at 22 °C for 18 hours. The reaction mixture was acidified by the addition of 2 M hydrochloric acid (1 mL) and diluted with water (10 mL), then extracted with ethyl acetate (2 x 25 mL). The combined organics were dried with anhydrous magnesium sulfate, filtered and the solvent removed *in vacuo* affording **14** as an orange solid (98 mg, 238 µmol, quantitative). Analytical HPLC retention time 11.67 min; MS (ESI) exact mass for $C_{20}H_{12}N^{81}BrO_5^+$ $[M+H]^+$ calcd: 413.0 found: 413.0; HR-ESI-MS m/z for $C_{20}H_{12}{}^{81}BrO_5^+$ $[M+H]^+$ calcd: 412.9842 found: 412.9835.

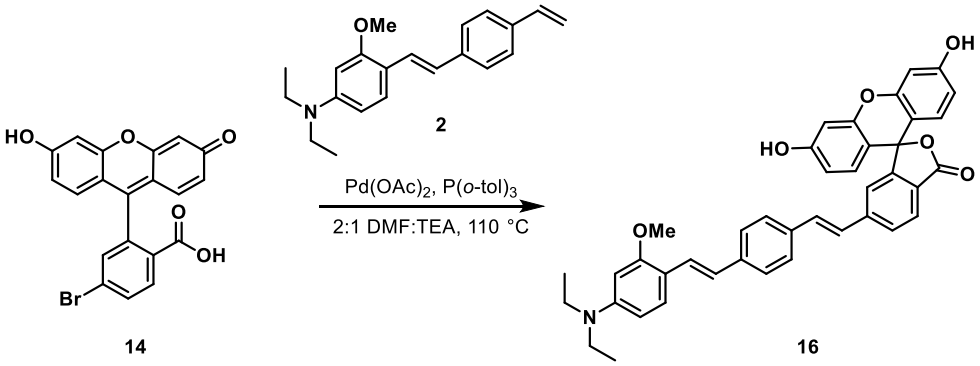

14 16

Synthesis of 16:

A Schlenk flask was charged with **14** (98.0 mg, 238 µmol), **2** (132 mg, 429 µmol), $Pd(OAc)_2$ (0.54 mg, 2.38 µmol) and P(*o*-tol)$_3$ (1.5 mg, 4.78 µmol). The flask was sealed and evacuated/backfilled with nitrogen (3x). Anhydrous DMF (2 mL) and triethylamine (1 mL) were added via syringe and the reaction stirred at 110 °C for 18 h. The reaction was cooled and the solvent removed *in vacuo*. The remaining residue was purified by flash chromatography (0-5% methanol in DCM, linear gradient) affording **16** as a yellow-orange solid (100.2 mg, 157 µmol, 66%). Analytical HPLC retention time 8.14 min; MS (ESI) exact mass for $C_{41}H_{36}NO_6^+$ $[M+H]^+$ calcd: 638.3 found: 638.2; HR-ESI-MS m/z for $C_{41}H_{34}NO_6^-$ $[M-H]^-$ 636.2378 found: 636.2379.

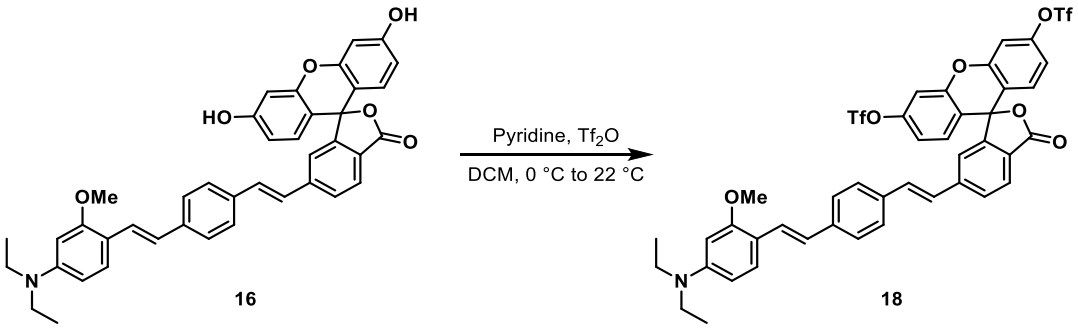

16 18

Synthesis of 18:

A round-bottom flask was charged with **16** (200 mg, 0.314 mmol), DCM (10 mL) and pyridine (202 µL, 2.51 mmol) and the reaction cooled to 0 °C while stirring. Triflic anhydride (211 µL, 1.25 mmol) was added dropwise, then the ice-bath was removed and the reaction was stirred for 2 h, after which the reaction was judged to be complete. The reaction mixture was diluted with water (50 mL) and DCM (50 mL). The combined organics were washed with brine (2 x 75 mL), dried with anhydrous magnesium sulfate, filtered and the solvent removed *in vacuo*. The remaining residue was purified by flash chromatography (10-30% ethyl acetate in hexanes, linear gradient) affording **18** as a yellow oil (92.7 mg, 0.103 mmol, 33%). ^{1}H NMR (400 MHz, $CDCl_3$) δ 8.06 (d, *J* = 8.0 Hz, 1H), 7.54 – 7.41 (m, 6H), 7.36 (dd, *J* = 1.9, 0.9 Hz, 2H), 7.28 – 7.19 (m, 2H), 7.14 – 7.05 (m, 5H), 6.94 (d, *J* = 16.4 Hz, 1H), 6.35 (dd, *J* = 8.7, 2.4 Hz, 1H), 6.22 (d, *J* = 2.4 Hz, 1H), 3.92 (s, 3H), 3.43 (q, *J* = 7.1 Hz, 4H), 1.24 (t, *J* = 7.1 Hz, 6H); Analytical HPLC retention time 6.36 min; MS (ESI) exact mass for $C_{43}H_{34}F_6NO_{10}S_2^+$ $[M+H]^+$ calcd: 902.2 found: 901.9; HR-ESI-MS m/z for $C_{43}H_{34}F_6NO_{10}S_2^+$ $[M+H]^+$ calcd: 902.1523 found: 902.1521.

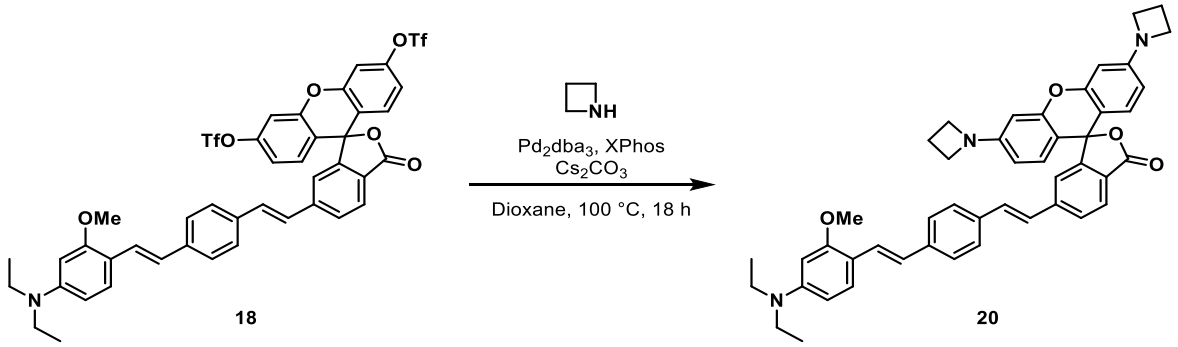

Synthesis of 20:

A 4 mL vial was charged with **18** (72.0 mg, 79.8 µmol), Pd_3dba_3 (7.3 mg, 8.0 µmol), XPhos (11.4 mg, 24.0 µmol) and cesium carbonate (72.8 mg, 223 µmol). The flask was sealed and evacuated/backfilled with nitrogen (3x). Anhydrous dioxane (350 µL) and a .6 M stock solution of azetidine in anhydrous dioxane (350 µL, 192 µmol) were added via syringe and the reaction stirred at 100 °C for 18 h. The reaction was cooled and the solvent removed *in vacuo*. The remaining residue was purified by flash chromatography (0-10% methanol in DCM, linear gradient) affording **20** as a purple solid (50.1 mg, 69.9 µmol, 88%). ^{1}H NMR (600 MHz, DMSO-d_6) δ 8.03 (s, 1H), 7.91 (d, *J* = 8.2 Hz, 1H), 7.53 (d, *J* = 8.2 Hz, 2H), 7.48 – 7.38 (m, 4H), 7.31 (dd, *J* = 16.4, 4.2 Hz, 2H), 6.91 (d, *J* = 16.4 Hz, 1H), 6.37 (s, 4H), 6.27 (d, *J* = 8.6 Hz, 1H), 6.19 (d, *J* = 2.4 Hz, 1H), 3.93 (s, 8H), 3.81 (s, 3H), 3.36 (q, *J* = 7.0 Hz, 4H), 2.36 (s, 4H), 1.10 (t, *J* = 7.0 Hz, 6H); Analytical HPLC retention time 6.65 min; MS (ESI) exact mass for $C_{47}H_{46}N_3O_4^+$ $[M+H]^+$ calcd: 716.3 found: 716.1; HR-ESI-MS m/z for $C_{47}H_{46}N_3O_4^+$ $[M+H]^+$ calcd: 716.3483 found: 716.3487.

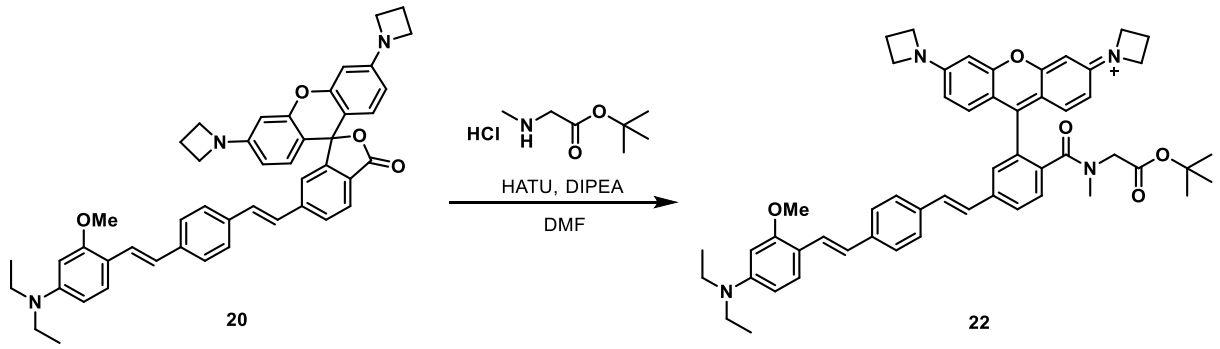

Synthesis of 22:

A vial was charged with **20** (42.0 mg, 58.6 μmol), N-methyl sarcosine *t*-Bu ester hydrochloride (12.8 mg, 87.9 μmol), and HATU 27.9 mg, 73.2 μmol). Anhydrous DMF (1 mL) and anhydrous diisopropylethylamine (18.6 μL, 87.9 μmol) were added and the vial was flushed with nitrogen, sealed, and stirred at 22 °C for 2 h. The solvent was removed *in vacuo* and the remaining residue was purified by preparative TLC (7.5% methanol in DCM) affording **22** as a purple solid (36.6 mg, 43.4 μmol, 73%). ^{1}H NMR (400 MHz, $CDCl_3$) δ 7.80 (d, *J* = 8.1 Hz, 1H), 7.63 (d, *J* = 8.1 Hz, 1H), 7.54 – 7.42 (m, 6H), 7.30 – 7.12 (m, 5H), 6.95 (d, *J* = 16.3 Hz, 1H), 6.55 (dd, *J* = 9.4, 2.1 Hz, 2H), 6.41 (d, *J* = 2.1 Hz, 2H), 6.35 (d, *J* = 8.7 Hz, 1H), 6.23 (d, *J* = 2.2 Hz, 1H), 4.34 (q, *J* = 8.6 Hz, 8H), 3.93 (s, 3H), 3.83 (s, 2H), 3.44 (q, *J* = 7.1 Hz, 4H), 2.89 (s, 3H), 2.61 (m, 4H), 1.39 (s, 9H), 1.24 (t, *J* = 7.1 Hz, 6H); Analytical HPLC retention time 7.24 min; MS (ESI) exact mass for $C_{54}H_{59}N_4O_5^+$ $[M+H]^+$ calcd: 843.4 found: 843.0.

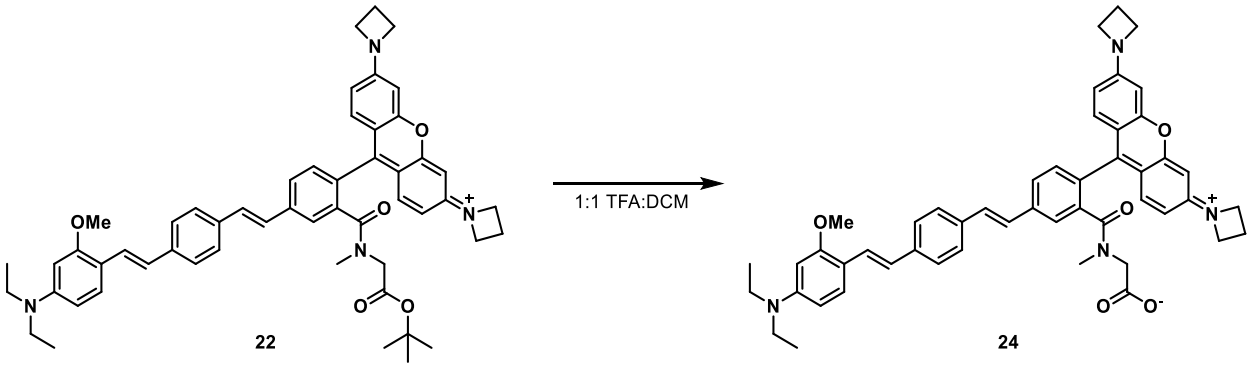

Synthesis of 24:

Trifluoroacetic acid (1 mL) was added to a solution of **22** (28.0 mg, 33.2 μmol) in DCM (1 mL). The reaction was stirred at 22 °C for 2 h, then the solvent removed under a stream of nitrogen. The remaining residue was purified by preparative TLC (10% methanol in DCM) affording **24** as a purple solid (23.8 mg, 30.2 μmol, 91%); Analytical HPLC retention time 6.57 min; MS (ESI) exact mass for $C_{50}H_{52}N_4O_5^{2+}$ $[M+H]^{2+}$ calcd: 394.2 found: 394.3; HR-ESI-MS m/z for $C_{50}H_{51}N_4O_5^+$ calcd: 787.3854 found: 787.3854.

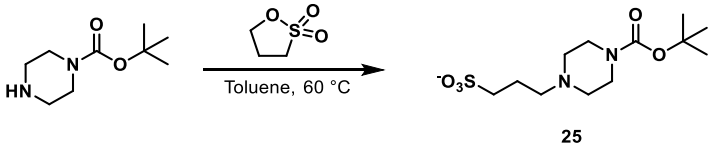

Synthesis of 25:

A vial was charged with N-Boc piperazine (200 mg, 1.07 mmol) and toluene (2 mL). 1,3-propanesultone (104 µL, 1.18 mmol) was added dropwise and the reaction stirred at 60 °C for 16 h. The reaction was diluted with DCM (3 mL), then hexanes (25 mL). The resulting solid was collected by vacuum filtration, affording **25** as a white solid (283 mg, 0.92 mmol, 86%). ^{1}H NMR (400 MHz, DMSO-d_6) δ 9.96 (s, 1H), 4.02 (d, *J* = 13.8 Hz, 2H), 3.48 (d, *J* = 11.7 Hz, 2H), 3.23 (dd, *J* = 11.5, 6.6 Hz, 2H), 3.10 – 2.99 (m, 2H), 2.98 – 2.89 (m, 2H), 2.67 – 2.61 (m, 2H), 2.00 (p, *J* = 6.8 Hz, 2H), 1.41 (s, 9H).

25 26

Synthesis of 26:

Trifluoroacetic acid (1 mL) was added to a solution of **25** (25.0 mg, 81.3 µmol) in DCM (1 mL). The reaction was stirred at 22 °C for 2 h, then the solvent removed under a stream of nitrogen. The remaining residue was triturated with DCM (3 x 5 mL) with sonication, then dried *in vacuo*, affording **26** as a colorless solid (23.5 mg, 72. µmol, 89%). ^{1}H NMR (400 MHz, D_2O) δ 3.72-3.54 (m, 8H), 3.47 – 3.38 (m, 2H), 3.00 (t, *J* = 7.2 Hz, 2H), 2.20 (dt, *J* = 15.1, 7.4 Hz, 2H).

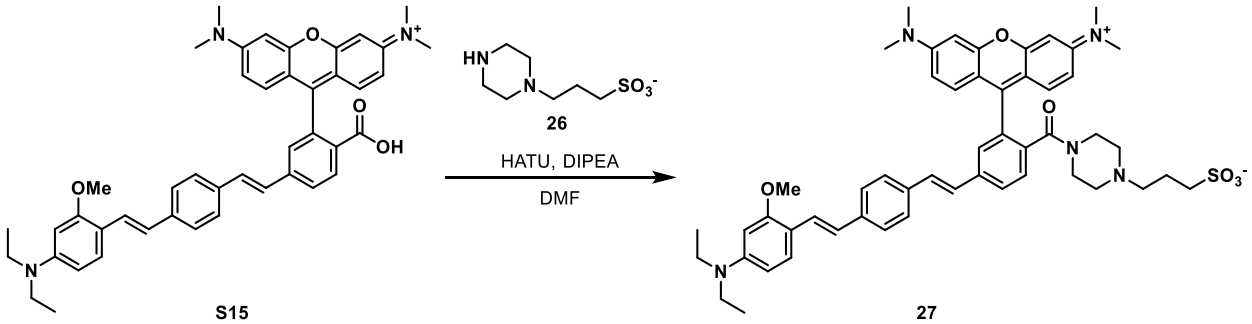

S15 27

Synthesis of 27:

A vial was charged with **S15** (9.6 mg, 13.9 µmol), **26** (7.2 mg, 34.6 µmol), and HATU 10.5 mg, 27.7 µmol). Anhydrous DMF (2 mL) and anhydrous diisopropylethylamine (14.7 µL, 69.3 µmol) were added and the vial was flushed with nitrogen, sealed, and stirred at 22 °C for 16 h. The solvent was removed *in vacuo* and the remaining residue was purified by preparative HPLC affording **22** as a purple solid (8.3 mg, 9.4 µmol, 68%). ^{1}H NMR (600 MHz, DMSO-d_6) δ 7.92 (d, *J* = 8.1 Hz, 1H), 7.75 (s, 1H), 7.63 (d, *J* = 8.0 Hz, 1H), 7.52 (dd, *J* = 47.6, 8.1 Hz, 4H), 7.45 – 7.39 (m, 2H), 7.38 – 7.30 (m, 2H), 7.27 (d, *J* = 9.5 Hz, 2H), 7.14 (dd, *J* = 9.5, 2.5 Hz, 2H), 7.02 – 6.90 (m, 3H), 6.29 (d, *J* = 8.0 Hz, 1H), 6.21 (s, 1H), 3.84 (s, 3H), 3.38 (q, *J* = 7.1 Hz, 4H), 3.29 (s, 12H), 3.24 (br, 2H), 2.34 (t, *J* = 7.7 Hz, 2H), 2.23 (br, 2H), 2.09 (br, 4H), 1.62 (br, 2H), 1.23 (s, 2H), 1.12 (t, *J* = 7.0 Hz, 6H); Analytical HPLC retention time 5.18 min; MS (ESI) exact mass for $C_{52}H_{61}N_5O_6^{2+}$ $[M+2H]^{2+}$ calcd: 441.7 found: 441.9; HR-ESI-MS m/z for $C_{52}H_{60}N_5O_6S^+$ $[M+H]^+$ calcd: 882.4259 found: 882.4251.

Spectroscopic Studies

Stock solutions of RhoVRs were prepared in DMSO (1-5 mM) and diluted with PBS (10 mM KH_2PO_4, 30 mM $Na_2HPO_4 \cdot 7H_2O$, 1.55 M NaCl, pH 7.2) solution containing 0.10 % (w/w) SDS (1:100-1:1000 dilution). UV-Vis absorbance and fluorescence spectra were recorded using a Shimadzu 2501 Spectrophotometer (Shimadzu) and a Quantamaster Master 4 L-format scanning spectrofluorometer (Photon Technologies International). The fluorometer is equipped with an LPS-220B 75-W xenon lamp and power supply, A-1010B lamp housing with integrated igniter, switchable 814 photon-counting/analog photomultiplier detection unit, and MD5020 motor driver. Samples were measured in 1-cm path length quartz cuvettes (Starna Cells).

Quantum yields were measured according to the procedure described in **Appendix 4**.

Cell Culture

All animal procedures were approved by the UC Berkeley Animal Care and Use Committees and conformed to the NIH Guide for the Care and Use and Laboratory Animals and the Public Health Policy.

Human embryonic kidney 293T (HEK) cells were passaged and plated onto 12 mm glass coverslips pre-coated with Poly-D-Lysine (PDL; 1 mg/ml; Sigma-Aldrich) to provide a confluency of ~15% and 50% for electrophysiology and imaging, respectively. HEK cells were plated and maintained in Dulbecco's modified eagle medium (DMEM) supplemented with 4.5 g/L D-glucose, 10% FBS and 1% Glutamax. Transfection of genetic tools was carried out using Lipofectamine 3000 24 h after plating. Imaging was performed 18-24 h following transfection.

Imaging Parameters

Epifluorescence imaging was performed on an AxioExaminer Z-1 (Zeiss) equipped with a Spectra-X Light engine LED light (Lumencor), controlled with Slidebook (v6, Intelligent Imaging Innovations). Images were acquired with either a W-Plan-Apo 20x/1.0 water objective (20x; Zeiss) or a W-Plan-Apo 63x/1.0 water objective (63x; Zeiss). Images were focused onto either an OrcaFlash4.0 sCMOS camera (sCMOS; Hamamatsu) or an eVolve 128 EMCCD camera (EMCCD; Photometrix). More detailed imaging information for each experimental application is expanded below. For RhoVR images, the excitation light was delivered from a LED (1.73-9.72 W/cm^2) at 542/33 (bandpass) nm and emission was collected with a quadruple emission filter (430/32, 508/14, 586/30, 708/98 nm) after passing through a quadruple dichroic mirror (432/38, 509/22, 586/40, 654 nm LP). For EGFP images, excitation light was delivered from a LED (0.82-5.77 W/cm^2) at 475/34 nm and emission was collected with a quadruple emission filter (430/32, 508/14, 586/30, 708/98 nm) after passing through a quadruple dichroic mirror (432/38, 509/22, 586/40, 654 nm LP). Functional imaging of the RhoVR voltage dyes was performed using a 20x objective paired with image capture from the EMCCD camera at a sampling rate of 0.5 kHz. RhoVRs were excited using the 542 nm LED with an intensity of 9.73 W/cm^2. Unless stated otherwise, for loading of HEK cells and hippocampal neurons, RhoVRs were diluted in DMSO to 500 μM, and then diluted 1:1000 in HBSS. All imaging experiments were performed in HBsS (in mM) 140 NaCl, 2.5 KCl, 10 HEPES, 10 D-glucose 1.3 $MgCl_2$ and 2 $CaCl_2$; pH 7.3 and 290 mOsmol.

Image Analysis

Analysis of voltage sensitivity in HEK cells was performed using ImageJ (FIJI). Briefly, a region of interest (ROI) was selected automatically based on fluorescence intensity and applied as a mask to all image frames. Fluorescence intensity values were calculated at known baseline and voltage step epochs. For analysis of RhoVR 1 voltage responses in neurons, regions of interest encompassing cell bodies (all of approximately the same size) were drawn in ImageJ and the mean fluorescence intensity for each frame extracted. ΔF/F values were calculated by first subtracting a mean background value from all raw fluorescence frames, bypassing the noise amplification which arises from subtracting background for each frame, to give a background subtracted trace (bkgsub). A baseline fluorescence value (F_{base}) is calculated either from the first several (10-20) frames of the experiment for evoked activity, or from the median for spontaneous activity, and was subtracted from each timepoint of the bkgsub trace to yield a ΔF trace. The ΔF was then divided by F_{base} to give ΔF/F traces. No averaging has been applied to any voltage traces.

Electrophysiology

For electrophysiological experiments, pipettes were pulled from borosilicate glass (Sutter Instruments, BF150-86-10), with a resistance of 5–8 MΩ, and were filled with an internal solution; 115 mM potassium gluconate, 10 mM BAPTA tetrapotassium salt, 10 mM HEPES, 5 mM NaCl, 10 mM KCl, 2 mM ATP disodium salt, 0.3 mM GTP trisodium salt (pH 7.25, 275 mOsm). Recordings were obtained with an Axopatch 200B amplifier (Molecular Devices) at room temperature. The signals were digitized with Digidata 1440A, sampled at 50 kHz and recorded with pCLAMP 10 software (Molecular Devices) on a PC. Fast capacitance was compensated in the on-cell configuration. For all electrophysiology experiments, recordings were only pursued if series resistance in voltage clamp was less than 30 MΩ. For whole-cell, voltage clamp recordings in HEK 293T cells, cells were held at -60 mV and 100 ms hyper- and de- polarizing steps applied from -100 to +100 mV in 20 mV increments.

Figures and Schemes

Scheme 3-1: *VoltageFluors utilize photo-induced electron transfer mechanism to report membrane potential*

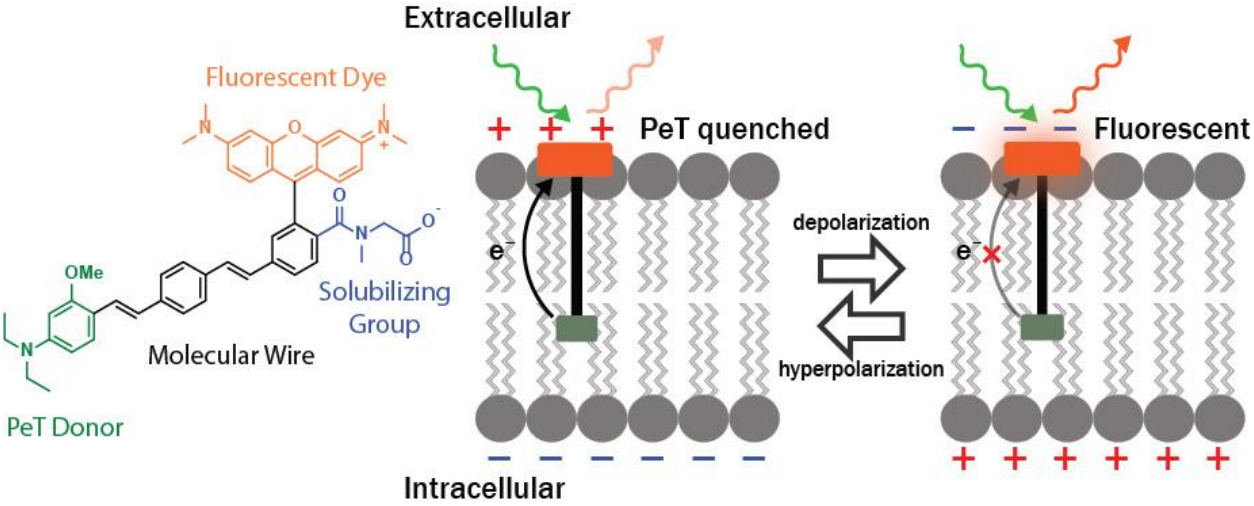

Scheme 3-1: (Left) The structure of RhoVR 1. The highlighted portions indicate where synthetic modifications were focused. (Center) Hyperpolarized membrane potentials (negative inside cell) promote photo-induced electron transfer (PeT) and quench fluorescence. (Right) Depolarization (positive inside cell) decreases the rate of PeT and increases fluorescence (right). Thus, the quantum yields of VF dyes are related to the local membrane potential.

Scheme 3-2: *General synthesis of molecular wires* ***1-6***

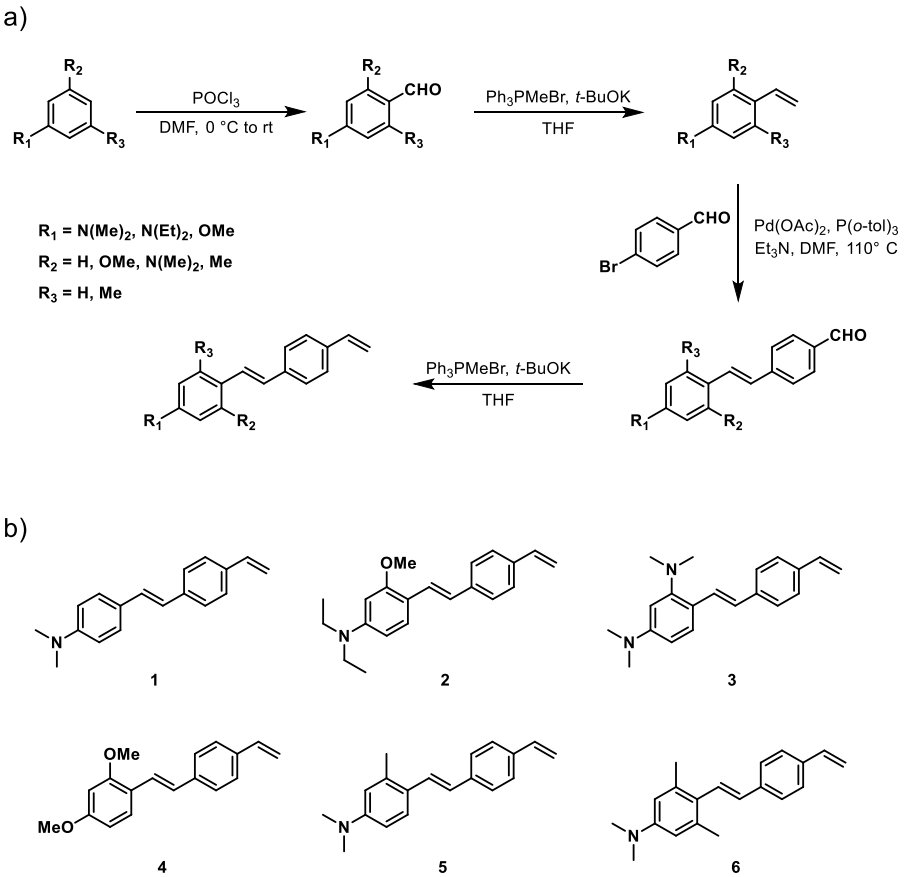

Scheme 3-2: General synthesis of molecular wires **1-6**. (a) general synthetic route to phenylenevinylene wires with varying donors. Wire **6** was synthesized from the commercially available 2,4-dimethoxybenzaldehyde (b) Library of synthesized phenylenevinylene wires **1-6**.

Scheme 3-3: *General synthesis of RhoVRs* ***7-12***

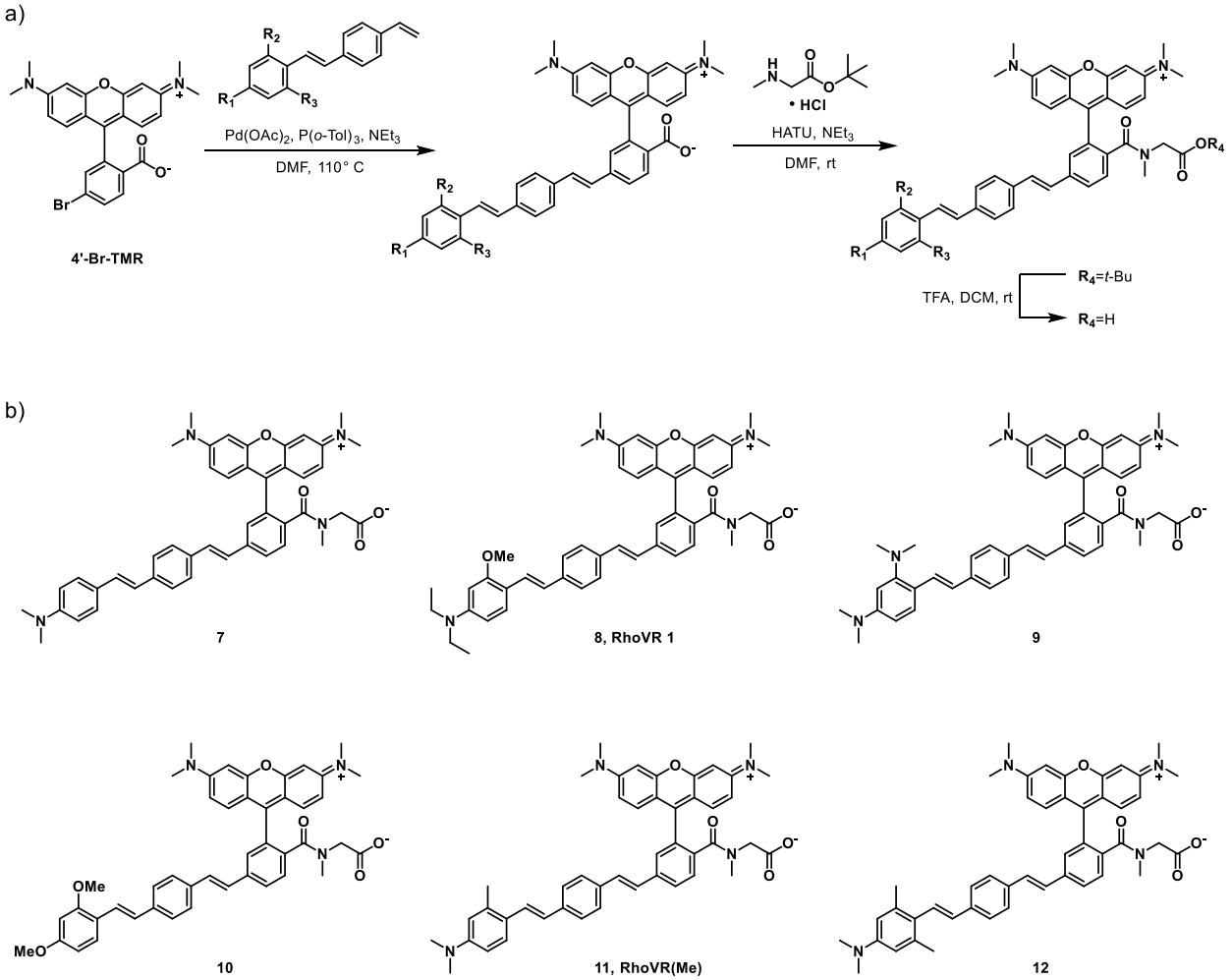

Scheme 3-3: Synthesis of 4'-RhoVR derivatives. (a) General synthesis of RhoVRs **7-12**. A Pd-catalyzed Heck coupling between 4-Br-TMR and a phenylenevinylene molecular wire provides a carboxy-functionalized RhoVR. In order to prevent spirolactonization and internalization, an N-methyl glycine-derived tertiary amide is formed. A TFA-catalyzed deprotection of the *t*-butyl ester affords the final RhoVR **7-12**; b) Library of 4'-RhoVR derivatives with varying electron donors.

Scheme 3-4: *Synthesis of az-RhoVR* ***23***

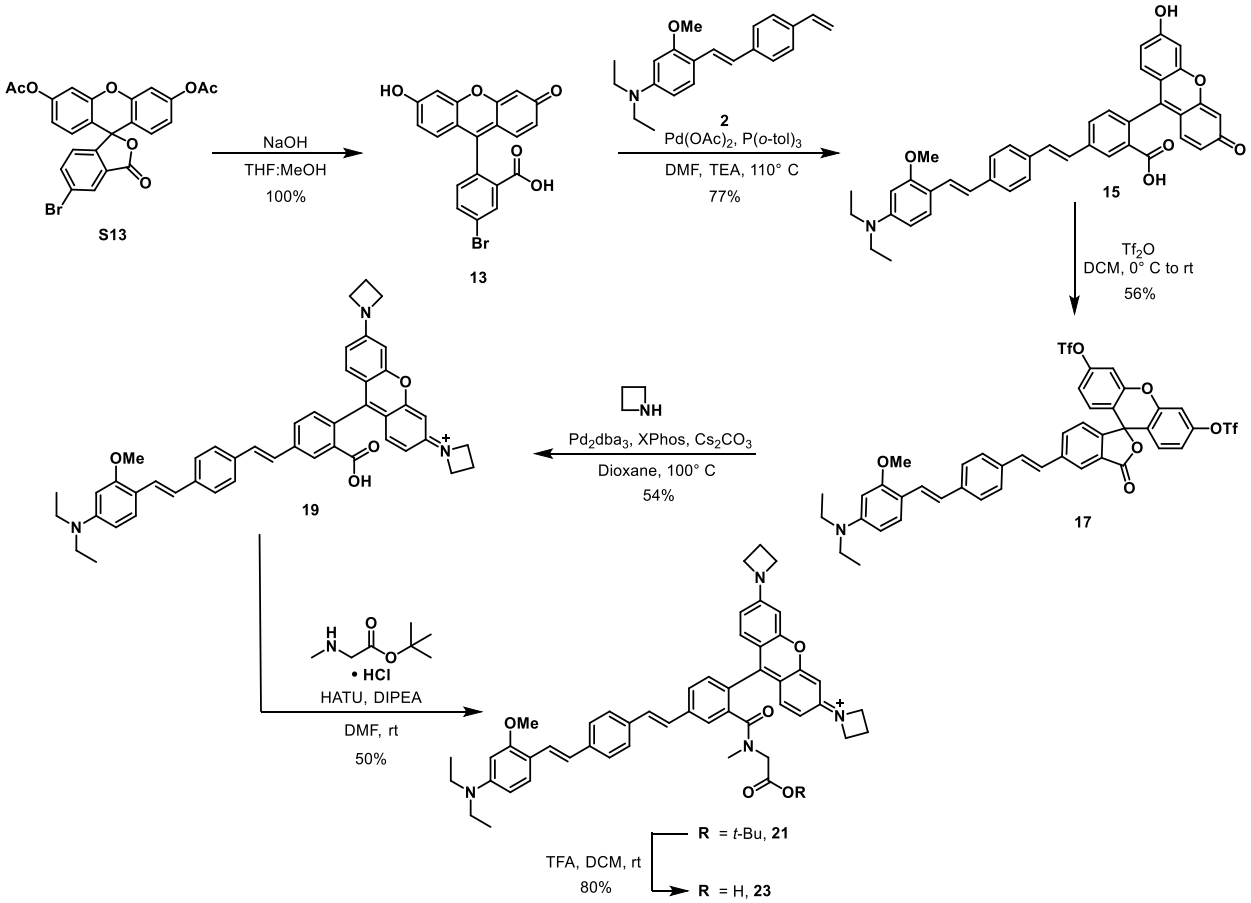

Scheme 3-4: Synthesis of az-RhoVR **23**. In order to prevent cross reactivity between the 5'-Br of **13** and triflates during the Buchwald-Hartwig amination, we choose to first carry out a Pd-catalyzed Heck coupling to attach the molecular wire **2**. Subsequent triflation and Buchwald-Hartwig amination afforded the azetidine-substituted carboxy-RhoVR **19**. Finally, formation of an N-methyl glycine-derived tertiary amide and subsequent TFA deprotection of the *t*-butyl ester afforded az-RhoVR **23**.

Scheme 3-5: *Synthesis of az-RhoVR* ***24***

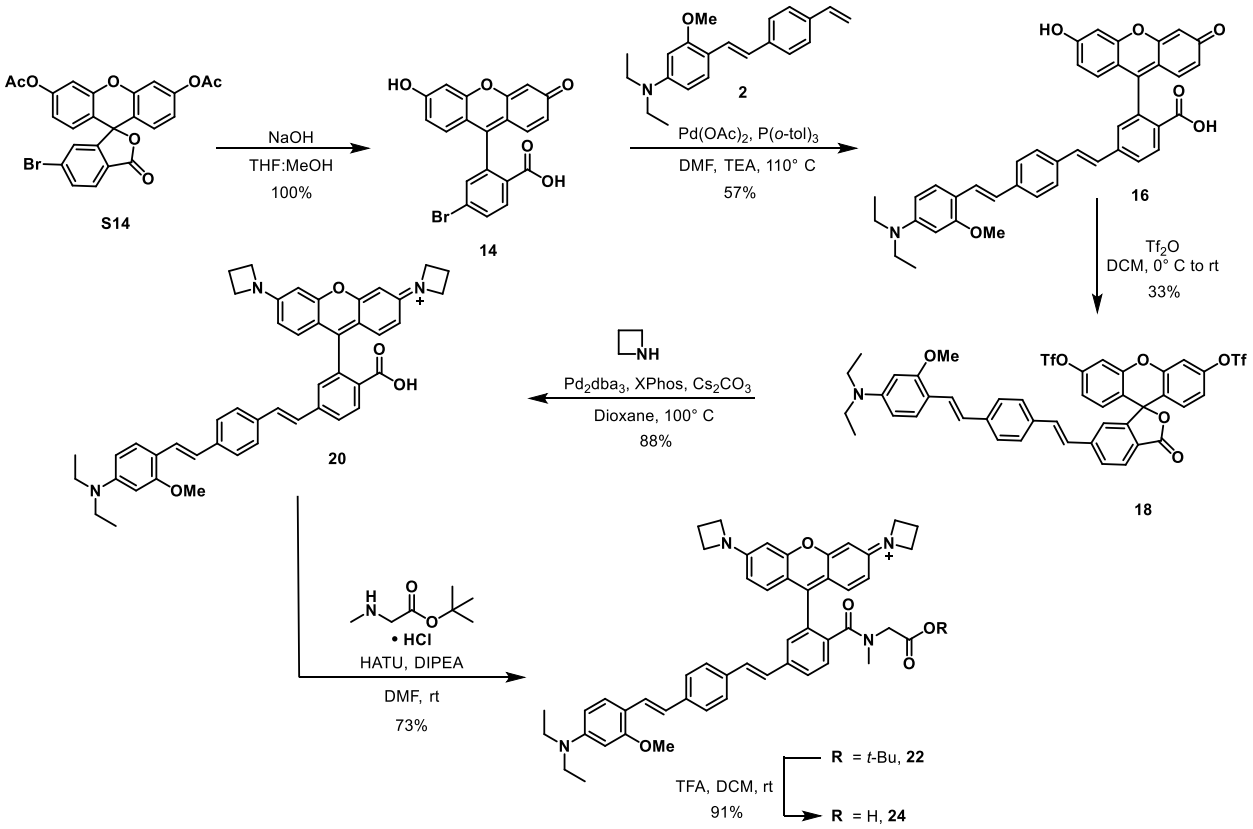

Scheme 3-5: Synthesis of az-RhoVR **24**. In order to prevent cross reactivity between the 4'-Br of **14** and triflates during the Buchwald-Hartwig amination, we first attached molecular wire **2** through a Pd-catalyzed Heck coupling. Subsequent triflation and Buchwald-Hartwig amination afforded the azetidine-substituted carboxy-RhoVR **20**. Finally, formation of an N-methyl glycine-derived tertiary amide and subsequent TFA deprotection of the *t*-butyl ester afforded az-RhoVR **24**.

Scheme 3-6: *Synthesis of RhoVR.Pip.Sulf* ***27***

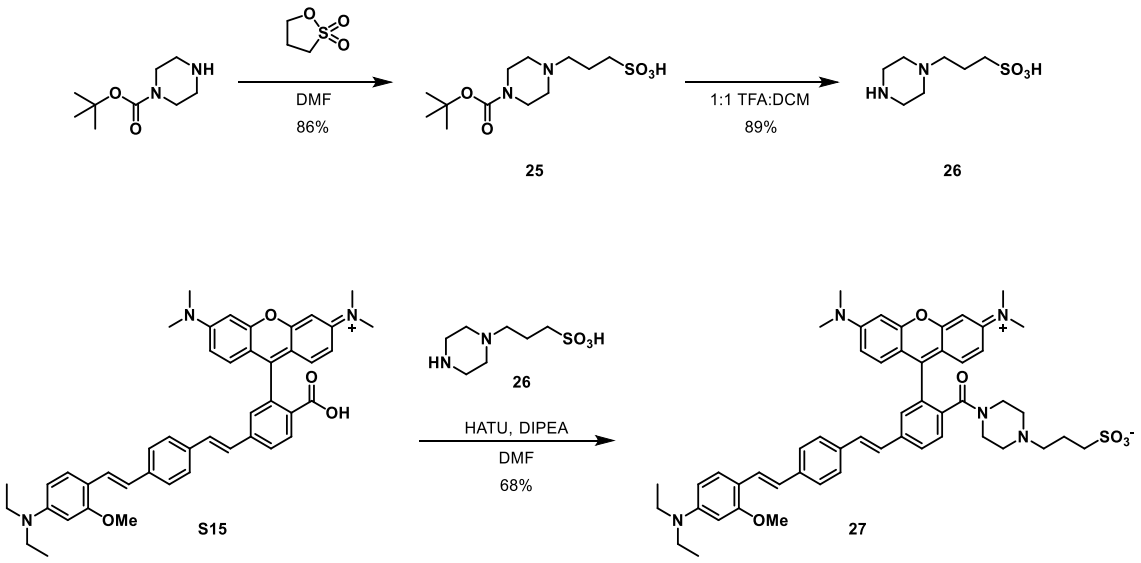

Scheme 3-6: Synthesis of RhoVR.Pip.Sulf **27**. In order to minimize the number of steps following coupling of the highly polar sulfonate to the RhoVR (which can complicate purification), we first synthesized the alkyl sulfonate-substituted piperazine **26**. A HATU-mediated coupling of **26** with the RhoVR 1 precursor **S15** gave **27** in one step.

Table 3-1: *Properties of RhoVRs*

Compound	ε ($M^{-1}cm^{-1}$)[a]	Φ (λ_{max})[a]	ΔF/F (100 mV)[b]	Rel. Brightness	SNR (100 mV)[b]
7	77,000 (564 nm)	0.0089 (586 nm)	7% (±1%)	73%	96:1
8, RhoVR 1	87,000 (564 nm)	0.045 (588 nm)	47% (±3%)	100%	160:1
9	83,00 (564 nm)	-	22% (±8%)	86%	55:1
10	71,000 (564 nm)	-	N.A.	N.A.	N.A.
11, RhoVR(Me)	81,000 (564 nm)	0.022 (588 nm)	13% (±1%)	380%	190:1
12	84,000 (564 nm)	-	12% (±2%)	490%	135:1
23, az-IsoRhoVR1	99,000 (566 nm)	0.124 (588 nm)	29% (±1%)	42%	18:1
24, az-RhoVR1	123,000 (564 nm)	0.043 (588 nm)	49% (±3%)	77%	50:1
27, RhoVR.Pip.Sulf	108,000 (564 nm)	0.032 (588 nm)	44% (±1%)	157%	160:1
IsoRhoVR(OMe)	70,000 (565 nm)	0.092 (588 nm)	26% (±3%)	65%	37:1

[a] PBS, pH 7.2, 0.1% SDS [b] voltage-clamped HEK cells

Figure 3-1: *Brightness comparison of RhoVR derivatives*

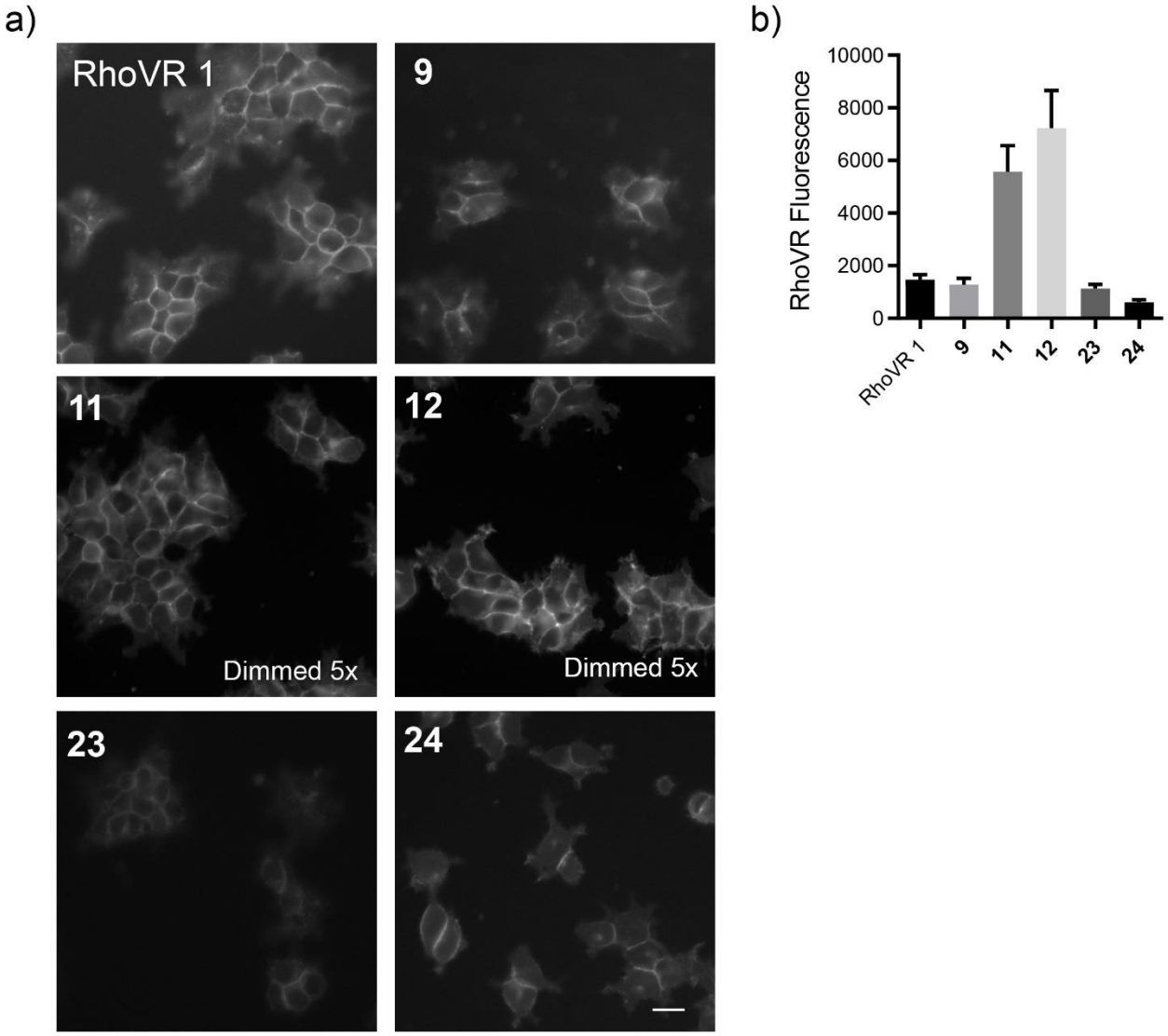

Figure 3-1: Brightness comparison of synthesized RhOVR derivatives. (a) Representative fluorescence images of HEK cells loaded with RhoVRs. All acquisition and processing parameters were identical, except for images **11** and **12**, which were dimmed 5-fold. Scale bar is 20 μm. (b) Quantification of RhoVR brightness in HEK cells, averaged from 3 coverslips for each condition.

Figure 3-2: *Voltage sensitivities of RhoVRs* ***7-12***

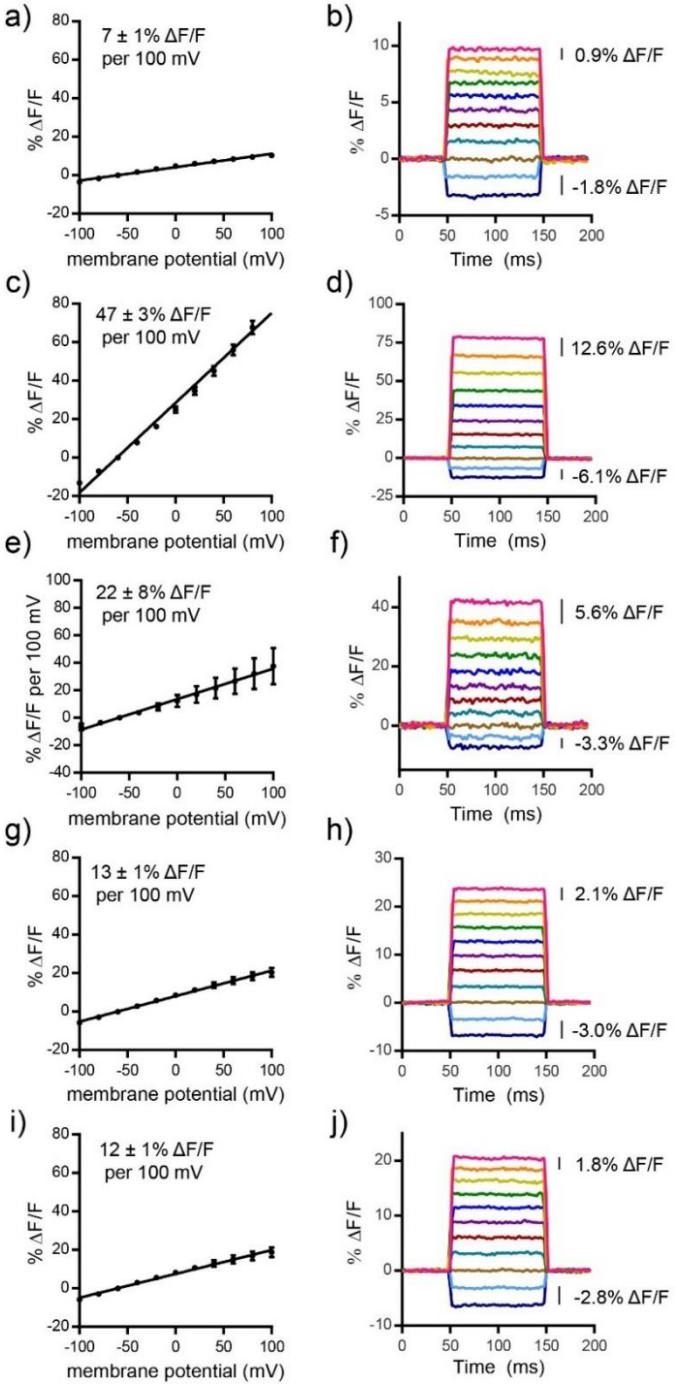

Figure 3-2: Voltage sensitivities of **7** (a,b), RhoVR 1 (c,d), **9**, (e,f), RhoVR(Me) (g,h) and **12** (i,j). (Left column) plots of % ΔF/F vs. final membrane potential (mV). (Right column) Plots of the fractional change in fluorescence vs. time for 100 ms hyper- and depolarizing steps (±100 mV, 20 mV increments) from a holding potential of -60 mV for single HEK cells under whole-cell voltage-clamp mode. The non-linearity of voltage response is demonstrated by the ΔF/F per 20 mV step at extreme hyperpolarizing and depolarizing potentials. RhoVRs which demonstrate higher voltage sensitivities at hyperpolarizing potentials (RhoVR(Me), **7**, **12**) were less sensitive, but brighter. RhoVRs with higher voltage sensitivities at depolarizing potentials (RhoVR 1, **9**) were dimmer, but possessed higher ΔF/F per 100 mV.

Figure 3-3: *Membrane staining and voltage sensitivities of az-RhoVRs **23** and **24***

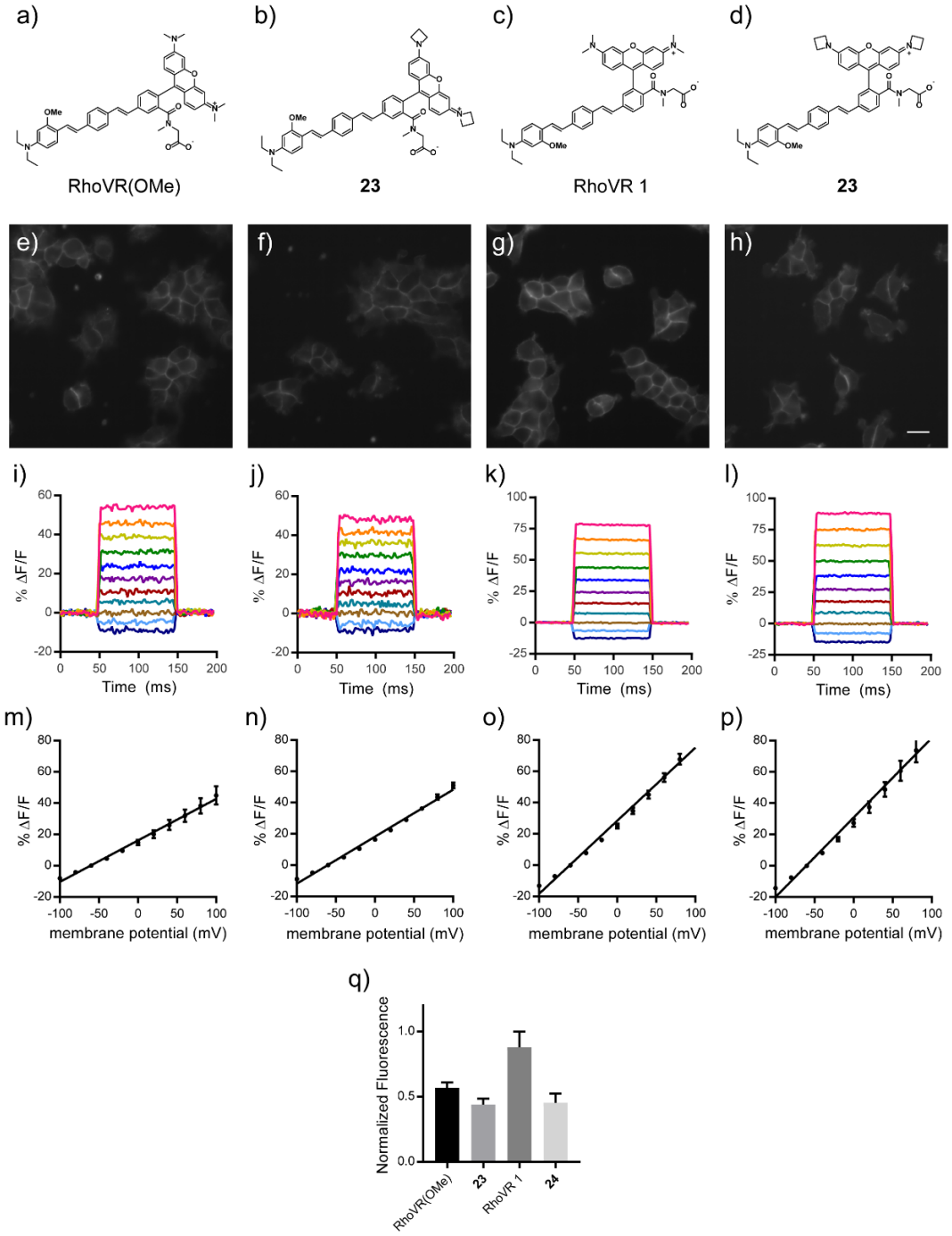

Figure 3-3: Properties of azetidine-functionalized RhoVRs 23 (b,f,j,n) and 24 (d,h,l,p) relative to their TMR-RhoVR analogs RhoVR(OMe) (a,e,i,m) and RhoVR 1 (c, g, k, o). (a-d) Chemical structures of the RhoVR derivatives. All RhoVRs possess a methoxy-substituted aniline donor. (e-h) Fluorecsence images showing the relative brightness of each RhoVR derivative. Scale bar is 10 μm. (i-l) The fractional change in fluorescence is plotted vs. time for 100 ms hyper- and depolarizing steps (±100 mV, 20 mV increments) from a holding potential of -60 mV for a single HEK cells under whole-cell voltage-clamp mode. A plot of % ΔF/F vs. final membrane potential (mV) summarizing data from n=4-15 separate cells. Error bars are ±S.D. (q) Quantification of the relative fluorescence of the four RhoVRs.

Figure 3-4: *Membrane staining and voltage sensitivity of RhoVR.Pip.Sulf* ***27***

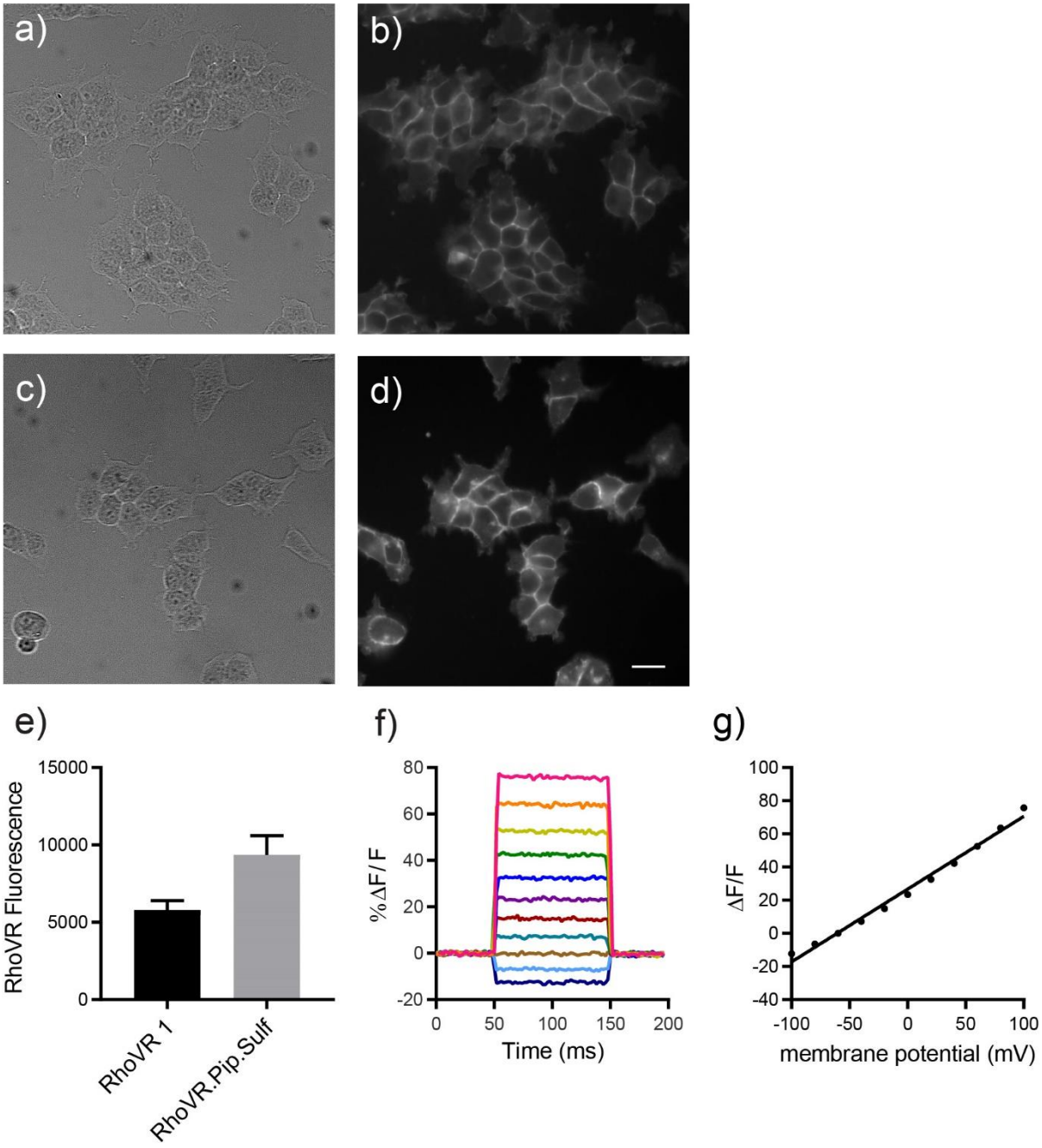

Figure 3-4: Properties of RhoVR.Pip.Sulf **27**. (a) DIC image of cells loaded with RhoVR 1. (b) Fluorescence image of cells loaded with RhoVR 1. (c) DIC image of cells loaded with RhoVR.Pip.Sulf. (d) Fluorescence image of cells loaded with RhoVR.Pip.Sulf. Scale bar is 20 µm. (e) The fractional change in fluorescence is plotted vs. time for 100 ms hyper- and depolarizing steps (±100 mV, 20 mV increments) from a holding potential of -60 mV for a single HEK cells under whole-cell voltage-clamp mode. A plot of % ΔF/F vs. final membrane potential (mV) summarizing data from 5 separate cells.

References

(1) Scanziani, M.; Häusser, M. Electrophysiology in the Age of Light. *Nature* **2009**, *461* (7266), 930–939.

(2) Miller, E. W.; Lin, J. Y.; Frady, E. P.; Steinbach, P. a.; Kristan, W. B.; Tsien, R. Y. Optically Monitoring Voltage in Neurons by Photo-Induced Electron Transfer through Molecular Wires. *Proc. Natl. Acad. Sci.* **2012**, *109* (6), 2114–2119.

(3) Deal, P. E.; Kulkarni, R. U.; Al-Abdullatif, S. H.; Miller, E. W. Isomerically Pure Tetramethylrhodamine Voltage Reporters. *J. Am. Chem. Soc.* **2016**, *138* (29), 9085–9088.

(4) Huang, Y. L.; Walker, A. S.; Miller, E. W. A Photostable Silicon Rhodamine Platform for Optical Voltage Sensing. *J. Am. Chem. Soc.* **2015**, *137* (33), 10767–10776.

(5) Kulkarni, R. U.; Kramer, D. J.; Pourmandi, N.; Karbasi, K.; Bateup, H. S.; Miller, E. W. Voltage-Sensitive Rhodol with Enhanced Two-Photon Brightness. *Proc. Natl. Acad. Sci.* **2017**, *114* (11), 2813–2818.

(6) Kulkarni, R. U.; Yin, H.; Pourmandi, N.; James, F.; Adil, M. M.; Schaffer, D. V.; Wang, Y.; Miller, E. W. A Rationally Designed, General Strategy for Membrane Orientation of Photoinduced Electron Transfer-Based Voltage-Sensitive Dyes. *ACS Chem. Biol.* **2017**, *12* (2), 407–413.

(7) Li, L. S. Fluorescence Probes for Membrane Potentials Based on Mesoscopic Electron Transfer. *Nano Lett.* **2007**, *7* (10), 2981–2986.

(8) Woodford, C. R.; Frady, E. P.; Smith, R. S.; Morey, B.; Canzi, G.; Palida, S. F.; Araneda, R. C.; Kristan, W. B.; Kubiak, C. P.; Miller, E. W.; et al. Improved PeT Molecules for Optically Sensing Voltage in Neurons. *J. Am. Chem. Soc.* **2015**, *137* (5), 1817–1824.

(9) Grimm, J. B.; English, B. P.; Chen, J.; Slaughter, J. P.; Zhang, Z.; Revyakin, A.; Patel, R.; Macklin, J. J.; Normanno, D.; Singer, R. H.; et al. A General Method to Improve Fluorophores for Live-Cell and Single-Molecule Microscopy. *Nat. Methods* **2015**, *12* (3), 244–250.

(10) Grabowski, Z. R.; Rotkiewicz, K.; Rettig, W. Structural Changes Accompanying Intramolecular Electron Transfer: Focus on Twisted Intramolecular Charge-Transfer States and Structures. *Chem. Rev.* **2003**, *103* (10), 3899–4031.

(11) Gao, L.; Liang, J.; Li, C.; Wang, L. V. Single-Shot Compressed Ultrafast Photography at One Hundred Billion Frames per Second. *Nature* **2014**, *516* (729), 74–77.

(12) Jiao, G. S.; Han, J. W.; Burgess, K. Syntheses of Regioisomerically Pure 5- or 6-Halogenated Fluoresceins. *J. Org. Chem.* **2003**, *68* (21), 8264–8267.

Chapter 4:
Development of "Light-Writable" Calcium Dosimeters for Neuronal Activity Mapping

Portions of this work were performed in collaboration with the following persons:
Synthesis was assisted by Kendall Wong

Abstract

A central aim of neurobiology is to identify the functional neural circuitry responsible for given behaviors. While fluorescence imaging is an attractive means for monitoring neuronal activity, traditional tools such as Ca^{2+} sensors rely on *reversible* binding that necessitate real-time imaging at high speeds, making simultaneous observation of thousands of neurons in three dimensions difficult. Alternatively, *post hoc* staining of immediate early genes (IEGs) such as *c-Fos* can be used to identify highly active cells within an entire brain, though it lacks temporal resolution. In attempt to address these limitations, we report the synthesis and development of the Ca^{2+}-sensitive chemodosimeter, Methylazid-1 (MA-1). MA-1 acts as a coincidence detector for both light and Ca^{2+}, allowing a temporally precise "snapshot" of $[Ca^{2+}]$ to be taken. MA-1 operates through a 25 nm shift in absorbance upon chelation of Ca^{2+} with a BAPTA binding domain (K_d = 270 nM). We utilized this shift in absorbance to selectively photolyze Ca^{2+}-free MA-1 with 400 nm light. The extent of photolysis can then be determined *post hoc* through either "click chemistry" or the fluorogenic reduction of remaining MA-1. Initial experiments in HEK cells revealed that MA-1 could distinguish between populations of cells which had or had not been irradiated with 400 nm light. We then showed that this signal could be preserved through fixation, a feat not possible with typical Ca^{2+} indicators. Finally, we demonstrated the ability to distinguish between high and low intracellular $[Ca^{2+}]$ in cultured rat hippocampal neurons using MA-1.

Introduction

The brain is a complex system consisting of approximately 80 billion neurons each communicating through hundreds to thousands of synapses.[1] Interrogating the function of the brain represents a challenging frontier for science and a hugely beneficial field of research in terms of societal externalities. For example, in the U.S. alone neurological disorders affect over 50 million people annually, requiring over $500 billion dollars to treat.

Crucial to understanding how neuronal systems lead to higher order behaviors is the tracing of neuronal activity. Ideally, one would be able to observe the simultaneous activity of millions of neurons in an intact brain of a behaving animal. While mapping techniques have improved over the decades, whole brain activity mapping with cellular resolution is not yet possible. Recent research into the connectivity of the brain ("connectomics") has focused on mapping large-scale neuronal structures using optical[2,3] and electron microscopy.[4,5] While capable of elucidating the *physical* connections made between neurons, high resolution connectomic mapping is typically carried out on fixed tissues and is thus incapable of tracing the *activity* of neurons.

In parallel to connectomics, activity sensors have been the focus of intense study in recent decades. While the activity of a neuron can be measured directly through the use of electrodes,[6] activity is often measured indirectly using fluorescence imaging of Ca^{2+}. Because intracellular $[Ca^{2+}]$ transiently increases following an action potential, $[Ca^{2+}]$ is frequently used as a surrogate for neuronal activity. Fluorescence imaging is an attractive tool for monitoring neuronal activity because it can track activity with high spatial and temporal resolution. The quintessential sensor employed is fura-2, a small molecule Ca^{2+} indicator (SMCI) that undergoes a dramatic change in fluorescence intensity and excitation upon binding Ca^{2+} (**Scheme 4-1a**).[7]

Genetically encoded calcium indicators (GECIs) have also been developed and are typically composed of a fluorescent protein coupled to a Ca^{2+} responsive element, such as calmodulin.[8] These sensors have the advantage of being targetable to specific cell types and

cellular domains and allow for longer (days to weeks) recording timeframes containing multiple experimental regimes. However, SMCIs tend to exhibit greater dynamic range, sensitivity, faster kinetics and are much more easily modified than GECIs.[8]

While Ca^{2+} indicators allow researchers to study the Ca^{2+} dynamics vital to neuronal development and signaling in systems ranging from single dendritic spines to small neuronal circuits,[9] both GECIs and SMCIs rely on the recognition and reversible binding of Ca^{2+} to achieve their fidelity. Because their binding is reversible, traditional Ca^{2+} indicators leave no permanent record of their interactions with the ion, rendering simultaneous observation of thousands of neurons difficult as measurements need to be made in real time. For example, observing one cubic millimeter of neurons with millisecond temporal resolution and micrometer spatial resolution requires a data rate of $>10^{13}$ bits/s.[10] Such demanding rates of data collection limits real-time imaging to systems smaller than 1000 neurons.

The ability to record all previous encounters with Ca^{2+} in a manner similar to reaction-based probes could potentially allow for the tracing of larger systems of neurons by effectively combining connectomics with activity-based probes ("functional connectomics"). Reaction-based probes rely on a chemical interaction between an analyte of interest and a sensor to generate an irreversible chemical change, typically in a 1:1 stoichiometric ratio (**Scheme 4-1b**).[11] For example, boronate-functionalize fluorescein compounds have been utilized as probes for reactive oxygen species such as H_2O_2, which are indicators of oxidative stress within cells.[12] Hg^{2+} colorimetric chemodosimeters have also been developed which utilize the affinity of Hg^{2+} for sulfur to permit quantitative and selective detection of Hg^{2+} in aqueous media.[11,13] The key advantage of chemodosimeters is the permanence of their interaction with an analyte through an irreversible chemical reaction, as this allows for the system to be studied without requiring real-time imaging.

Chemodosimetric probes tend to achieve selectivity through the exploitation of unique reactivity with an analyte of interest. Unfortunately, the need for a selective chemical reaction is problematic when studying Ca^{2+}, as the ion is relatively inert. To overcome this difficulty, and to temporally gate the observation window, we propose the development of a "light-writable" dosimetric system (**Scheme 4-1c**). In this scheme, incident photons enable photochemical reactivity, and binding of Ca^{2+} controls whether the molecules absorb light. Taking advantage of the hypsochromatic shift typical of Ca^{2+}-chelating sensors such as fura-2, one can selectively excite Ca^{2+}-free sensor over Ca^{2+}-bound sensor. However, unlike fluorescent imaging - which utilizes this excitation energy to generate fluorescence - we intend to attach a photo-labile group to the choromophore portion of the sensor. The degradation of this photo-labile group thus provides an irreversible chemical change by which to trace Ca^{2+} concentrations among neurons.

One attractive photo-labile motif for use in a light-writable system is the azide group. Azides are a popular bioorthogonal functional group typically used for labeling biomolecules via a Huisgen cycloaddition with a functionalized alkyne.[14] By attaching an azide group to 1,2-bis(o-aminophenoxy)ethane-N,N,N',N'-tetraacetic acid (BAPTA)-based Ca^{2+} sensor, absorbed light promotes the photolysis of the azide through loss of gaseous nitrogen and formation of a reactive nitrene. The BAPTA-based Ca^{2+} sensor azid-1 was chosen as a first target because it (1) has been previously characterized for use as a photo-caged Ca^{2+} source, (2) has a large spectral separation between apo- and Ca^{2+}-bound probe (>30nm) and (3) it possesses a high quantum yield of photolysis.[15] We thus approached azid-1 confident in its potential as a light-writable Ca^{2+} dosimeter. Irradiating with 400 nm light selectively photolyzes the Ca^{2+}-free indicator while Ca^{2+}-bound probes remain intact, as 400 nm light lies outside the Ca^{2+}-bound probe's excitation spectrum (**Figure 4-2**). An additional advantage of an azide-based system is the ability to utilize

the well-developed Huisgen cycloaddition chemistry ("Click chemistry") to attach a wide variety of imaging agents (**Scheme 4-3**).[16] For example, standard fluorescent dyes such as fluorescein or Cy-5 can be used for visualization by light microscopy. Additionally, super-resolution imaging agents or photosensitizers could be used, allowing super-resolution imaging or electron microscopy, respectively.[17] With accessibility to imaging techniques which range from mm to nm resolution, a light-writable system has the flexibility to map activity across both very large neuronal networks and sub-cellular [Ca^{2+}] domains.

Results and Discussion

*Synthesis of Benzaldehyde Intermediate **9***

When planning the synthesis of azid-1 and other azide-functionalized Ca^{2+} dosimeters, we sought to install the azide at a late stage to 1) avoid light-sensitive chemistry until the end of the synthesis 2) avoid the use of large quantities of sodium azide and other harmful reagents and 3) generate multiple dosimeters from a single BAPTA-containing compound. Benzaldehyde **9** was identified as a convenient intermediate for many BAPTA-based sensors as it contained the BAPTA core, could lead to a diverse range of sensors with varying K_d's and excitation profiles and could be synthesized in gram quantities (**Scheme 4-4**).[7,15] Key steps in our synthesis, included the selective debenzylation of the *ortho* phenolic group of **4** under acidic conditions and the selective reduction of the nitro groups of **6** using Pt/C for the hydrogenation.[7]

*Synthesis of Ethyl 2-(chloromethyl)oxazole-5-carboxylates **10** and **11***

Another key substrate for the formation of fura-2 is the ethyl 2-(chloromethyl)oxazole-5-carboxylate **10**, which undergoes a Knoevenagel condensation with **9** to form the benzofuran ring of the sensor. The original preparation of **10** used in the synthesis of fura-2 involved a copper-catalyzed coupling of ethyl diazopyruvate with chloroacetonitrile.[7] Unfortunately, the reaction was reported to give material of poor purity in low yields. Our own attempts at synthesizing **10** produced similar results, obtaining at best 12% yield for the oxazole (**Scheme 4-5a**). Alternative pathways towards **10** were also investigated (**Scheme 4-5b,c**). [18, 19] While these conditions had been shown to produce a variety of other functionalized oxazoles, neither reaction led to the formation of **10**. Looking for alternative synthetic strategies, we postulated that the functionalization of the oxazole at the 4-position was not critical and could be modified with little effect on the molecule's photophysical properties. The methylated oxazole **11** was identified as an attractive target, as Fay, *et al.* had reported a low-yielding but scalable synthesis from ethyl-2-chloroacetoacetate and chloroacetamide. This synthetic route afforded **11** on the gram scale, and this methyl-substituted oxazole was used for future synthesis (**Scheme 4-5d**).[20]

Synthesis and Spectroscopic Characterization of Methylfura-2 (MF-2)

Both methyl azid-1 (MA-1) and methyl fura-2 (MF-2) were synthesized in order to characterize and compare the binding, photophysical, and spectroscopic properties of the dosimeter and sensor pair. MF-2 should also provide a convenient means for evaluating the biological distribution of the probe in living cells without the added complication of extreme light sensitivity. From the precursor **9**, synthesis of the ethyl ester protected MF-2 **13** was achieved in

two steps (**Scheme 4-6**). Treatment of **13** with potassium hydroxide generated the water-soluble pentapotassium salt **14**, which was subsequently used for *in vitro* studies.

MF-2 **14** was evaluated spectroscopically in physiological buffer (100 mM KCl, 10 mM MOPS, pH 7.2). In the absence of Ca^{2+}, MF-2 has a strong absorbance centered at 364 nm (ε_{364} = 26,000 $M^{-1}cm^{-1}$) with emission centered at 501 nm (Φ_{Fl} = 0.37). MF-2 displayed a high affinity for Ca^{2+} (115 ± 10 nM), similar to that of fura-2 (100 ± 5 nM). Upon binding Ca^{2+}, MF-2 undergoes a hypsochromatic shift to 350 nm (ε_{350} = 30,000 $M^{-1}cm^{-1}$) and an increase in fluorescence at 492 nm (Φ_{Fl} = 0.80). Although the excitation and emission profiles and K_d are similar between MF-2 and fura-2, the increased fluorescence quantum yield means MF-2 is approximately 2-fold brighter than fura-2, while maintaining a similar dynamic range between Ca^{2+}-free and Ca^{2+}-saturated probe (**Figure 4-2**, **Table 4-1**).

In order to enable cellular experiments **14** was further modified through the addition of acetoxymethyl (AM) ester protecting groups onto the free carboxylates, affording the much more cell-permeable MF-2-AM **15**. While greatly increasing cell permeability, upon entering the cytoplasm, the AM esters are rapidly cleaved by native esterases, regenerating the free carboxylates necessary for Ca^{2+} binding.[21] In order to determine MF-2's responsiveness to changes in [Ca^{2+}] within a cell, histamine was applied to HeLa cells loaded with **15**. Histamine has been shown to induce oscillations in free Ca^{2+} concentration in the cytosol, and thus should be visualized as "blinking" cells.[22] As can be seen in **Figure 4-3g**, fluorescence of Cell 1 oscillates, with its initial fluorescence reduced to 40% of its original level during periods of high Ca^{2+} concentrations (**Figure 4-3b,c**). Upon the addition of ionomycin (an ionophore which shuttles Ca^{2+} through the plasma membrane and thus dramatically increases cytosolic [Ca^{2+}]) and $CaCl_2$, fluorescence drops to near baseline levels (**Figure 4-3f**). Further experiments with MF-2 showed that the dye functions equally well in cultured rat cortical/hippocampal neurons, responding to changes in [Ca^{2+}] generated from the addition of the excitatory neurotransmitter glutamate (**Figure 4-4**). These results further verified that MF-2 functions nearly identically to fura-2.

Synthesis and Spectroscopy Characterization of Methylazid-1 (MA-1)

Synthesis of MA-1 proceeded via conversion of the benzaldehyde **9** to benzonitrile **17** via the dehydration of the intermediate oxime **16** with phosgene iminium chloride (**Scheme 4-7**). Benzonitrile **17** was then deprotected to the phenol **18** and subsequently reacted with **11**, resulting in a MF-2 derivative possessing a 3-amino group on the benzofuran ring (**19**). We discovered that the Knoevenagel condensation between **11** and **18** was stalling at the ether **19b** and not cyclizing to the desired benzofuran **19** (**Scheme 4-7**). By subjecting **19b** to harsher conditions (potassium fluoride on alumina at 150 °C) or longer reaction times, we were able to promote the cyclization and isolate **20** in good yield. The key step in the synthesis of MA-1 is the conversion of the 3-amino group of **19** to an azide. Tsien *et al.* accomplished this transformation in their synthesis of azid-1 utilizing a solution of nitrosylsulfuric acid in sulfuric acid to generate the diazonium salt.[15] While the preparation is effective, the harsh conditions may limit the applicability of these conditions to more sensitive BAPTA-based dosimeters and advances in azide chemistry have led to the availability of more mild arylazide forming conditions.[9,23–26] We performed a reaction screen with a model azid-1 scaffold lacking the BAPTA domain in order to test these newer conditions. However, we found the original nitrosylsulfuric acid conditions afforded the desired aryl azide **20** in the highest yield (results not shown), and therefore continued to use nitrosylsulfuric acid.

Treatment of the ethyl ester protected **20** with potassium hydroxide generated the water-soluble pentapotassium salt **21**, or MA-1, which we subsequently used for *in vitro* studies.

MA-1 **21** was evaluated spectroscopically in physiological buffer (100 mM KCl, 10 mM MOPS, pH 7.2). In the absence of Ca^{2+}, MA-1 has a strong absorbance centered at 374 nm (ε_{374} = 32,000 $M^{-1}cm^{-1}$). Upon binding Ca^{2+}, MA-1 undergoes a hypsochromatic shift to 349 nm (ε_{349} = 39,000 $M^{-1}cm^{-1}$). Unlike MF-2, MA-1 is non-fluorescent as excitation induces photolysis of the azide to a nitrene that rapidly reacts with water to generate a non-fluorescent photoproduct.[15] Titrations with Ca^{2+} revealed MA-1 possessed a high affinity for Ca^{2+} (270 ± 10 nM), though slightly lower than that of azid-1 (230 nM) (**Figure 4-5a**, **Table 4-1**).

We then measured the rate of photolysis of MA-1 in both low and high [Ca^{2+}] buffers when irradiated with 400 nm light. [Ca^{2+}]-free MA-1 absorbed strongly at this wavelength (ε_{400} =21,000 M^{-1} cm^{-1}) while [Ca^{2+}]-bound MA-1 showed minimal absorbance (ε_{400} =3,600 M^{-1} cm^{-1}). This difference in ε_{400} resulted in 10-fold faster photolysis of [Ca^{2+}]-free MA-1 than [Ca^{2+}]-bound MA-1 (**Figure 4-5b,c**). While this result suggested that Ca^{2+} can effectively mask the azide of MA-1 from photolysis at μM concentrations, the non-fluorescent photoproduct and starting MA-1 makes it difficult to monitor this conversion by fluorescence microscopy. To address this limitation we hypothesized the azide of MA-1 could be selectively labeled through a copper catalyzed Huisgen cyclization (i.e. "Click Chemistry"). In a cellular context, this labeling strategy would result in cells with high [Ca^{2+}] being labeled, as the azide of MA-1 would have been protected during 400 nm illumination (**Scheme 4-2b**). We first validated that MA-1 could react with alkynes by reacting **21** with propargyl alcohol in the presence of Cu(I) (**Figure 4-6a,c**). We also showed MA-1 could be labeled using Cu-free click chemistry, reacting MA-1 with a TAMRA DBCO conjugate (**Figure 4-5b,d**). Both reactions showed nearly full conversion to the triazole product.

Cellular Experiments with MA-1

Having validated the use of MA-1 for Ca^{2+} integration *in vitro*, we synthesized an acetoxymethyl ester protected MA-1 (MA-1-AM) **22**. MA-1-AM was loaded onto HEK cells for 30 minutes at 37 °C. MA-1-AM cells were either irradiated with 365 nm light (20 min with 4 W UV bulb) or left in the dark. TAMRA DBCO was then applied to the cells for 15 minutes at 37 °C. After washing, irradiated HEK cells were over 2-fold dimmer than HEKs cells left in the dark (**Figure 4-7**). A significant amount of background fluorescence from the TAMRA DBCO remained, attenuating the observed turn-on (**Figure 4-7a**). We hypothesize a greater turn-on response could be achieved using a reporter that can be more readily washed away, or through a fluorogenic reporter which remains quenched until reaction with MA-1.

Following these promising live-cell experiments, we wanted to extend our system to include a fixation step. The ability to analyze *post hoc* is one of the main advantages of a dosimetric system. Fixation greatly increases the amount of time available to image and analyze a sample, and recent advances such as CLARITY have greatly improved our capability to image large neuronal circuits spanning entire brains.[27] In order to simplify our system we replaced TAMRA DBCO labeling of MA-1 with a simpler reduction procedure (**Figure 4-8a**). Under reducing conditions (TCEP, glutathione, sodium borohydride) the azide of MA-1 was reduced to an amine (amino MF-2) that was at least 25-fold more fluorescent than MA-1 (**Figure 4-8b**). This reduction methodology was then applied to HEK cells loaded with MA-1. Coverslips plated with HEK cells were loaded with MA-1 and a portion of the coverslip was irradiated with UV light (390/22 nm, 1.3 W/cm^2, 30 s). The coverslips were then fixed with 3% paraformaldehyde (PFA) with 1%

glutaraldehyde (GA) and reduced with a 0.1% solution of sodium borohydride. Fluorescence imaging of amino MF-2 revealed that irradiated cells were nearly 2-fold dimmer than unilluminated cells (**Figure 4-8c-e**), presumably because less MA-1 remained to be reduced to amino MF-2. We then applied this reduction strategy to cultured hippocampal neurons loaded with MA-1 (**Figure 4-9**). Neurons loaded with MA-1, fixed, and reduced were over 2-fold brighter than neurons photolyzed prior to fixation (**Figure 4-9a-c**). Having demonstrated we could distinguish between cells which had been irradiated from those which were left in the dark, we wanted to see if we could observe varying rates of photolysis depending on [Ca^{2+}]. High [Ca^{2+}] were induced by the addition of ionomycin in the imaging buffer. Neurons irradiated in the presence of ionomycin photolyzed slower than neurons irradiated without ionomycin (low [Ca^{2+}], **Figure 4-9d-g**). However, the observed difference was minimal due to the significant amount of fluorescence observed from the low [Ca^{2+}] neurons post photolysis, alluding to the presence of a large amount of amino MF-2 (**Figure 4-9f**). We hypothesize amino MF-2 was generated from the intracellular reduction of MA-1 during loading (i.e. prior to photolysis). Indeed, we observed a large amount of fluorescence following loading of HEK cells with MA-1-AM for 1 h at 22 °C (**Figure 4-10a,b**). Since MA-1 possesses a $\Phi_{Photolysis}$ of approximately 1, this fluorescence can be attributed to MA-1 reduction over the 1 h loading period. In addition, we observed MA-1 could be reduced *in vitro* by biologically relevant concentrations of glutathione (**Figure 4-10c,d**).

Conclusion

In conclusion, two new BAPTA-based Ca^{2+} sensors, MF-2 and MA-1 have been synthesized. MF-2 functions similarly to fura-2, with improved brightness and tractability. MA-1 was shown to selectively photolyze *in vitro* under 400 nm illumination. We then demonstrated the possibility to selectively label MA-1 in live cells using either click chemistry or through a fluorogenic reduction of the aryl azide. In addition, we demonstrated the ability to track MA-1 photolysis through fixation, a feat not possible with typical Ca^{2+} indicators. Future work aims to continue the optimization of the use of MA-1 in cells. The major limitation to the use of MA-1 is its stability intracellularly. Specifically, the reducing environment of the cell leads to reduction of MA-1 over time. We estimate that the half-life of MA-1 intracellularly is somewhere between 30 minutes and an hour, severely limiting the potential for long term experiments. Another limitation is that following fixation, overall MA-1 fluorescence is quite low. This alludes to the loss of dye from the cell following fixation and permeabilization of the membrane. Either a genetic tag or cross-linking moiety could improve upon the retention of MA-1 through a fixation step.

Experimental Section

General Method for Chemical Synthesis and Characterization

Chemical reagents and solvents (dry) were purchased from commercial suppliers and used without further purification. TAMRA DBCO was purchased from Click Chemistry Tools.[4,5] Thin layer chromatography (TLC) (Silicycle, F254, 250 μm) and preparative thin layer chromatography (PTLC) (Silicycle, F254, 1000 μm) was performed on glass backed plates pre-coated with silica gel and were visualized by fluorescence quenching under UV light. Flash column chromatography was performed on Silicycle Silica Flash F60 (230–400 Mesh) using a forced flow of air at 0.5–1.0 bar. NMR spectra were measured on Bruker AVB-400 MHz, 100 MHz, AVQ-400 MHz, 100 MHz,

Bruker AV-600 MHz, 150 MHz. NMR spectra measured on Bruker AVII-900 MHz, 225 MHz, equipped with a TCI cryoprobe accessory, were performed by Dr. Jeffrey Pelton (QB3). Variable temperature NMR experiments were measured on the Bruker AV-600 with the assistance of Hasan Celik. Chemical shifts are expressed in parts per million (ppm) and are referenced to $CDCl_3$ (7.26 ppm, 77.0 ppm) or DMSO (2.50 ppm, 40 ppm). Coupling constants are reported as Hertz (Hz). Splitting patterns are indicated as follows: s, singlet; d, doublet; t, triplet; q, quartet, dd, doublet of doublet; m, multiplet. High-resolution mass spectra (HR-ESI-MS) were measured by the QB3/Chemistry mass spectrometry service at University of California, Berkeley. High performance liquid chromatography (HPLC) and low resolution ESI Mass Spectrometry were performed on an Agilent Infinity 1200 analytical instrument coupled to an Advion CMS-L ESI mass spectrometer. The column used for the analytical HPLC was Phenomenex Luna C18(2) (4.6 mm I.D. × 150 mm) with a flow rate of 1.0 mL/min. The mobile phases were MQ-H_2O with 0.05% formic acid (eluent A) and HPLC grade acetonitrile with 0.05% formic acid (eluent B). Signals were monitored at 254, 340 and 545 nm over 20 min with a gradient of 10-100% eluent B. The column used for semi-preparative HPLC was Phenomenex Luna 5µ C18(2) (10 mm I.D. x 150 mm) with a flow rate of 5.0 mL/min. The mobile phases were MQ-H_2O with 0.05% formic acid (eluent A) and HPLC grade acetonitrile with 0.05% formic acid (eluent B). Signals were monitored at 254 over 20 min with a gradient of 10-100% eluent B.

Synthetic Procedures

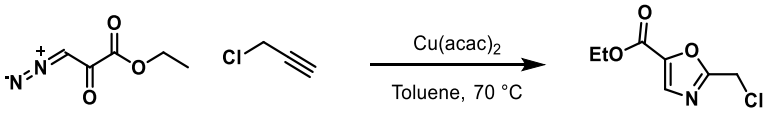

10

Synthesis of ethyl 2-(chloromethyl)oxazole-5-carboxylate 10:
A round-bottom flask was charged with ethyl diazopyruvate (479 mg, 3.37 mmol, 1.0 equiv.) and $Cu(acac)_2$ (10 mg, 0.038 mmol, .01 equiv.). Anhydrous toluene (5 mL) was added and the flask was flushed with nitrogen and sealed. Chloroacetonitrile (1.9 mL, 30.4 mmol, 9.0 equiv.) was added via syringe and the reaction stirred at 70 °C for 12 h. The reaction mixture was diluted with ethyl acetate (20 mL) then washed with brine (3 x 20 mL) and saturated sodium bicarbonate (2 x 20 mL). The combined organics were dried with anhydrous sodium sulfate and concentrated *in vacuo*. The resulting brown oil was purified by flash chromatography (15% ethyl acetate in hexanes, isocratic) affording **10** as a yellow oil (78 mg, 0.411 mmol, 12%). ^{1}H NMR (400 MHz, $CDCl_3$) δ 7.73 (s, 1H), 4.65 (s, 2H), 4.41 (q, J = 7.2 Hz, 2H), 1.40 (t, J = 7.1 Hz, 3H). The ^{1}H NMR was in agreement with literature values.[28]

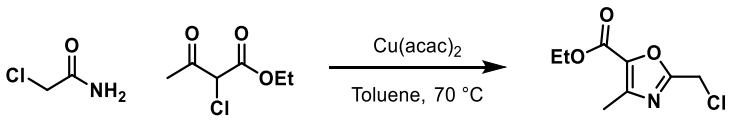

11

Synthesis of ethyl 2-(chloromethyl)oxazole-5-carboxylate 11:
A round-bottom flask was charged with 2-chloroacetamide (37.0 g, 380 mmol, 8.9 equiv.) and ethyl 2-chloro-3-oxobutanoate (7.26 g, 44.0 mmol, 1.0 equiv.) which were melted together at 115

°C. In a separate flask 2-chloroacetamide (5.0 g, 51 mmol, 1.2 equiv.) was added in 0.5 g portions to 4.5 mL of sulfuric acid cooled to 0 °C. This mixture was then added dropwise to the melt of 2-chloroacetamide and ethyl 2-chloro-3-oxobutanoate and the reaction stirred at 115 °C for 12 h. The reaction mixture was poured over 100 mL water and extracted with chloroform (4 x 50 mL). The organics were dried with anhydrous sodium sulfate, filtered and the solvent removed *in vacuo*. The remaining residue was purified by flash chromatography (40% ethyl acetate in hexanes) affording **11** as a colorless oil (1.95 g, 9.60 mmol, 22%). ^{1}H NMR (300 MHz, $CDCl_3$) δ 4.60 (s, 2H), 4.40 (q, *J* = 7.1 Hz, 2H), 2.48 (s, 3H), 1.40 (t, *J* = 7.1 Hz, 3H); ^{13}C NMR (101 MHz, $CDCl_3$) δ 160.12, 158.44, 146.21, 138.75, 61.54, 35.58, 14.43, 13.37; HR-ESI-MS m/z for $C_8H_{11}ClNO_3^+$ $[M+H]^+$ calcd: 204.0422 found: 204.0422.

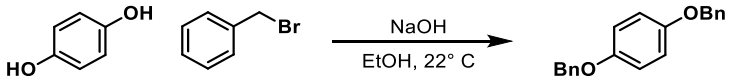

1 2

Synthesis of 1,4-bis(benzyloxy)benzene 2:

A round-bottom flask was charged with hydroquinone (11.0 g, 0.1 mol, 1.0 equiv.), benzyl bromide (37.86 g, 0.22 mol, 2.2 equiv.) and ethanol (25 mL). A solution of potassium hydroxide (16.83 g, 0.3 mol, 3.0 equiv.) in ethanol (100 mL) was added dropwise and the mixture was stirred at room temperature for 1 h. The reaction was poured over water (250 mL) and the precipitant was collected by vacuum filtration, then recrystallized from ethanol, affording **2** as a colorless crystalline solid (22.84 g, 78.7 mmol, 79%). ^{1}H NMR (400 MHz, $CDCl_3$) δ 7.53 – 7.34 (m, 10H), 6.97 (s, 4H) 5.06 (s, 4H). The ^{1}H NMR was in agreement with literature values.[7]

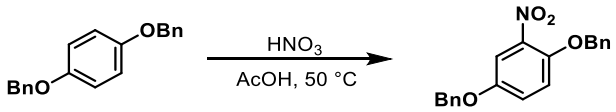

2 3

Synthesis of (((2-nitro-1,4-phenylene)bis(oxy))bis(methylene))dibenzene 3:

A round-bottom flask was charged with **2** (22.84 g, 78.7 mmol, 1.0 equiv.) and glacial acetic acid (80 mL). In a separate round-bottom flask, 5 mL of 70% nitric acid (1.0 equiv.) was diluted with glacial acetic acid (20 mL), then added dropwise to the stirred solution of **3**. The reaction mixture was heated to 50 °C for 2 h. The reaction was cooled, then water (125 mL) was added dropwise. The resulting precipitant was collected by vacuum filtration affording **3** as a bright yellow solid. (25.84 g, 77.1 mmol, 98%). ^{1}H NMR (400 MHz, $CDCl_3$) δ 7.51 (d, *J* = 3.0 Hz, 1H), 7.49 – 7.31 (m, 10H), 7.15 (dd, *J* = 9.1, 3.1 Hz, 1H), 7.07 (d, *J* = 9.2 Hz, 1H), 5.20 (s, 2H), 5.07 (s, 2H).The ^{1}H NMR was in agreement with literature values.[7]

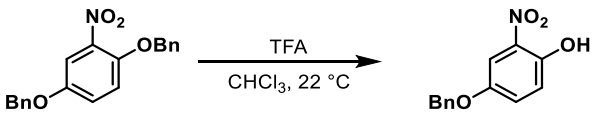

3 4

Synthesis of 4-(benzyloxy)-2-nitrophenol 4:

A round-bottom flask was charged with **3** (25.84 g, 77.1 mmol 1.0 equiv.) and $CHCl_3$ (50 mL). TFA (7.65 mL, 100.0 mmol, 1.3 equiv.) was added by dropwise addition and stirred for 2 days at 22 °C. The reaction was cooled to 0 °C and the pH adjusted to 7 by dropwise addition of 5 M

aqueous sodium hydroxide. The solution was diluted with chloroform (100 mL) and washed with water (3 x 100 mL). Aqueous sodium hydroxide (5 M, 30 mL) was added generating a red precipitate which was collected by vacuum filtration and washed with water (100 mL) and ethyl acetate (100 mL). The resulting solid was then acidified with aqueous hydrochloric acid (0.5 M, 100 mL) and extracted with ethyl acetate (3 x 100 mL). The combined organics were dried with anhydrous sodium sulfate, filtered and the solvent removed *in vacuo*. The resulting oil was boiled in 300 mL methanol until completely solubilized, then cooled to 0 °C. The precipitant was collected by vacuum filtration affording **4** as a yellow solid (10.46 g, 42.66 mmol, 55%). ^{1}H NMR (300 MHz, $CDCl_3$) δ 10.37 (s, 1H), 7.62 (d, *J* = 3.1 Hz, 1H), 7.51 – 7.29 (m, 6H), 7.12 (d, *J* = 9.2 Hz, 1H), 5.08 (s, 2H). The ^{1}H NMR was in agreement with literature values.[7]

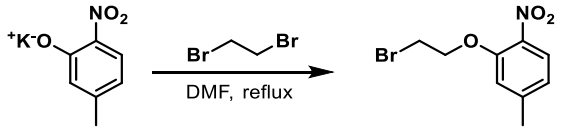

4 5

Synthesis of 2-(2-bromoethoxy)-4-methyl-1-nitrobenzene 5:

A round-bottom flask was charged with 5-methyl-2-nitrophenol (25.6 g, 141 mmol, 1.0 equiv.) and DCM (75 mL). A solution of potassium hydroxide (8.0 g, 143 mmol, 1.01 equiv.) in water (50 mL) was added and the reaction stirred for 10 min. The reaction mixture was concentrated under reduced pressure, affording potassium 2-nitro-5-methylphenoxide **4** as a red solid. Anhydrous DMF (75 mL) and dibromoethane (35.0 mL, 424 mmol, 3.0 equiv.) were added and the mixture heated to reflux for 15 min. The reaction was cooled and the white precipitant removed by vacuum filtration, washing with DCM (50 mL). The combined organics were washed with dilute sodium hydroxide until the aqueous phase was colorless (4 x 150 mL), then washed with pH 2 phosphate buffer, again until the aqueous layer was colorless (3 x 100 mL). The combined organics were dried with sodium sulfate and concentrated under reduced pressure. The resulting oil was triturated with 20 mL ethanol and the resulting precipitant collected by vacuum filtration, yielding **5** as a white solid (15.17 g, 58.3 mmol, 49%). ^{1}H NMR (300 MHz, $CDCl_3$) δ 7.80 (d, *J* = 8.7 Hz, 1H), 6.94 – 6.84 (m, 2H), 4.41 (t, *J* = 6.5 Hz, 2H), 3.69 (t, *J* = 6.5 Hz, 2H), 2.43 (s, 3H). The ^{1}H NMR was in agreement with literature values.[7]

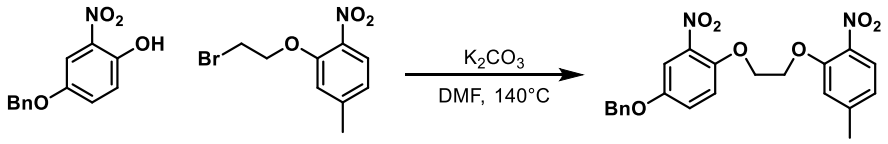

4 5 6

Synthesis of 6:

A round-bottom flask was charged with **4** (8.18 g, 33.3 mmol, 1.0 equiv.), **5** (9.4 g, 36.1 mmol, 1.1 equiv.) and anhydrous potassium carbonate (2.98 g, 22.0 mmol, 0.55 equiv.). Anhydrous DMF (30 mL) was added and the reaction stirred at 140 °C for 30 min. The reaction was then cooled slightly and poured into 150 mL water. The precipitant was collected by vacuum filtration and then recrystallized from 350 mL boiling acetone, with the resulting suspension cooled to -20 °C in a freezer prior to collection by vacuum filtration, affording **6** as a white solid (10.15 g, 23.9 mmol, 73%). ^{1}H NMR (400 MHz,$CDCl_3$) δ 7.83 (d, *J* = 8.3 Hz, 1H), 7.65 – 7.35 (m, 5H), 7.29 – 7.21 (m,

1H), 7.07 – 7.02 (m, 2H), 6.91 (d, *J* = 8.6 Hz, 1H), 5.11 (s, 2H), 4.52 (s, 4H), 2.48 (s, 3H). The ^{1}H NMR was in agreement with literature values.[7]

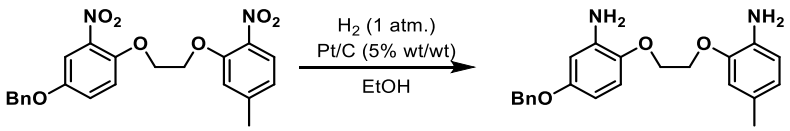

6 7

Synthesis of 7:

A round-bottom flask was charged with **6** (10.11 g, 23.8 mmol), 5% platinum on carbon (500 mg, 0.05 equiv. by wt.) and absolute EtOH (100 mL). The reaction flask was evacuated and backfilled with nitrogen (3x), then evacuated and backfilled with hydrogen (3x). The reaction was stirred under 1 atm. of hydrogen (4 L) at 22 °C for 24 h, adding more hydrogen as necessary. After completion of the reaction, DCM (300 mL) was added and the mixture filtered through a diatomaceous earth plug. The solvent was removed *in vacuo* and the resulting solid triturated with 50:50 hexanes:acetone (20 mL) and collected by vacuum filtration, affording **7** as a white solid (7.32 g, 20.9 mmol, 85%). ^{1}H NMR (400 MHz, $CDCl_3$) δ 7.47 – 7.29 (m, 5H), 6.79 (d, *J* = 8.6 Hz, 1H), 6.67 (d, *J* = 16.4 Hz, 3H), 6.42 (d, *J* = 2.8 Hz, 1H), 6.33 (dd, *J* = 8.7, 2.9 Hz, 1H), 5.00 (s, 2H), 4.32 (br s, 4H), 3.81 (s, 4H), 2.27 (s, 3H). The ^{1}H NMR was in agreement with literature values.[7]

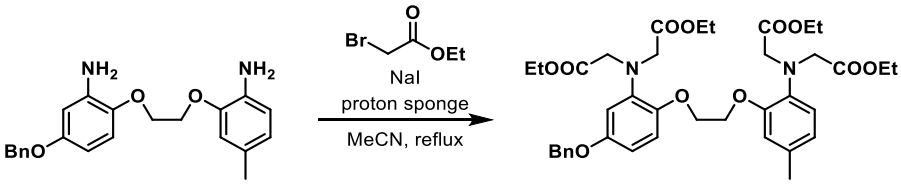

7 8

Synthesis of 8:

A round-bottom flask was charged with **7** (3.64 g, 10.0 mmol, 1.0 equiv.), proton sponge® (10.7 g, 50 mmol, 5.0 equiv) and sodium iodide (1.95 g, 13.0 mmol, 1.3 equiv.) Anhydrous acetonitrile (30 mL) and bromoethylacetate (5.53 mL, 50.0 mmol, 5.0 equiv.) were added via syringe and the reaction stirred at reflux for 12 h. The reaction was then cooled and the solvent removed *in vacuo*. 50 mL of toluene was added to the remaining residue and the insoluble NaBr removed with a diatomaceous earth plug. The combined organics were washed with pH 2 phosphate buffer until the aqueous fractions were colorless (3 x 100 mL), dried with anhydrous sodium sulfate, filtered and *in vacuo*. The remaining yellow oil was then triturated with 9:1 hexanes:ethyl acetate, with the precipitate collected by vacuum filtration affording **8** as a white solid (6.23 g, 8.80 mmol, 88%). ^{1}H NMR (400 MHz, $CDCl_3$) δ 7.46 – 7.29 (m, 5H), 6.83 – 6.64 (m, 4H), 6.49 (d, *J* = 6.9 Hz, 2H), 4.99 (s, 2H), 4.24 (s, 4H), 4.18 – 4.02 (m, 16H), 2.27 (s, 3H), 1.18 (t, *J* = 7.2, 6H), 1.17 (t, *J* = 7.2, 6H). The ^{1}H NMR was in agreement with literature values.[7]

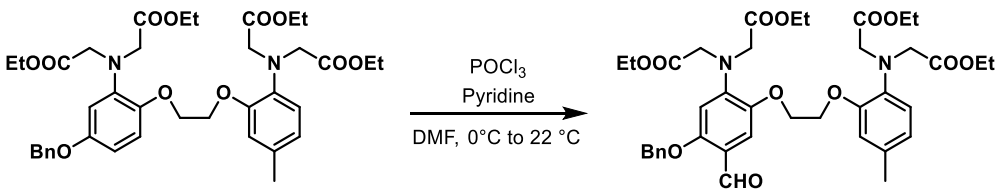

8 9

Synthesis of 9:

A round-bottom flask was charged with **8 (**3.83 g, 5.4 mmol, 1.0 equiv.), anhydrous DMF (20 mL) and pyridine (4.0 mL, 50.0 mmol, 9.2 equiv.). The mixture was sparged with N_2 and cooled to 0 °C. $POCl_3$ (4.0 mL, 43.2 mmol, 8.0 equiv.) was then added dropwise and the reaction allowed to warm to 22 °C while stirring over 12 h. The reaction mixture was then poured over ice (100 mL) and aqueous potassium hydroxide (5 M) added until the solution was basic. The aqueous layer was extracted with toluene (3 x 100 mL) and the combined organics dried with anhydrous sodium sulfate, filtered and the solvent removed *in vacuo*. The resulting brown oil was triturated with 35% hexanes in ethyl acetate and the resulting solid collected by vacuum filtration, affording **9** as a white solid (3.58 g, 4.86 mmol, 83%). ^{1}H NMR (400 MHz, $CDCl_3$) δ 10.33 (s, 1H), 7.47 – 7.28 (m, 6H), 6.80 – 6.63 (m, 3H), 6.31 (s, 1H), 5.12 (s, 2H), 4.29 – 4.01 (m, 20H), 2.27 (s, 3H), 1.16 (m, 12H). The ^{1}H NMR was in agreement with literature values.[7]

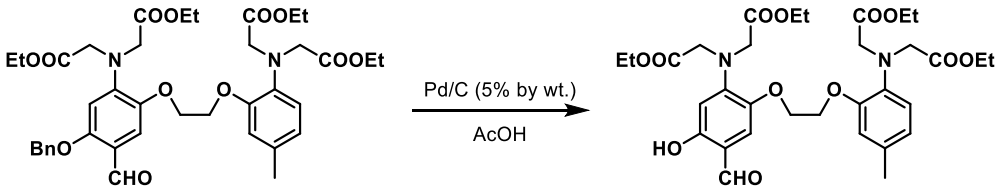

9 12

Synthesis of 12:

A round-bottom flask was charged with **9 (**427 mg, 0.58 mmol, 1.0 equiv.), 5% palladium on carbon (43 mg, 0.1 equiv. by wt.) and glacial acetic acid (6 mL). The reaction flask was evacuated and backfilled with nitrogen (3x), then evacuated and backfilled with hydrogen (3x). The reaction was stirred under 1 atm. of H_2 (4 L) at 22 °C for 24 h. The reaction was filtered through a silica plug, eluting with 60% ethyl acetate in hexanes (200 mL). The solvent was removed *in vacuo* and the remaining yellow oil was triturated with 20% acetone in hexanes. The resulting white solid was collected by vacuum filtration, affording **12** which was taken through to the next step without further purification. ^{1}H NMR (500 MHz, $CDCl_3$) δ 11.22 (d, *J* = 3.3 Hz, 1H), 9.61 (d, *J* = 3.3 Hz, 1H), 6.97 – 6.90 (m, 1H), 6.75 (dd, *J* = 8.2, 3.3 Hz, 1H), 6.72 – 6.59 (m, 2H), 6.21 – 6.05 (m, 1H), 4.22 (m, 8H), 4.17 – 4.00 (m, 12H), 2.03 (s, 3H), 1.17 (m, 12H). The ^{1}H NMR was in agreement with literature values.[7]

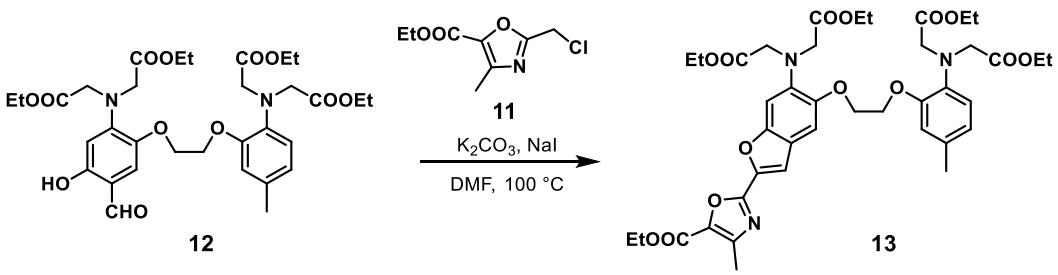

12 13

Synthesis of 13:

A round-bottom flask was charged with **12** (89.7 mg, 0.58 mmol, 1.0 equiv.), anhydrous potassium carbonate (240 mg, 1.74 mmol, 3.0 equiv.) and **11** (236 mg, 1.16 mmol, 2.0 equiv.). Anhydrous DMF (2.5 mL) was added and the reaction mixture stirred at 100 °C for 1.5 h. The reaction was then cooled to 22 °C, diluted with water (25 mL), acidified with 2 M hydrochloric acid (5 mL) and extracted with ethyl acetate (3 x 25 mL). The combined organics were dried with anhydrous sodium sulfate, filtered and concentrated *in vacuo*. The remaining orange residue was purified by flash chromatography (50% ethyl acetate in toluene, isocratic) affording **13** as a yellow solid (60.0 mg, 75.4 μmol, 12%). ^{1}H NMR (600 MHz, $CDCl_3$) δ 7.43 (s, 1H), 7.09 (s, 1H), 7.04 (s, 1H), 6.76 (s, 1H), 6.70 (d, *J* = 4.8 Hz, 2H), 4.44 (q, *J* = 7.2 Hz, 2H), 4.36 – 4.29 (m, 4H), 4.22 (s, Hz, 4H), 4.14 (s, 4H) 4.11-4.02 (m, 8H), 2.57 (s, 3H), 2.28 (s, 3H),1.44 (t, *J* = 7.1 Hz, 3H), 1.17 (dt, *J* = 23.7, 7.2 Hz, 12H). ^{13}C NMR (151 MHz, $CDCl_3$) δ 171.8, 158.8, 155.2, 151.9, 150.5, 149.1, 147.4, 142.4, 141.0, 137.4, 137.1, 132.3, 122.1, 121.2, 119.6, 114.5, 110.4, 105.0, 101.9, 95.5, 68.2, 67.2, 61.5, 61.4, 61.2, 61.2, 60.90, 54.0, 53.8, 22.9, 21.7, 21.2, 14.6, 14.3, 14.3, 13.7; HR-ESI-MS m/z for $C_{40}H_{49}NaN_3O_{14}^+$ $[M+Na]^+$ calcd: 818.3107 found: 818.3093.

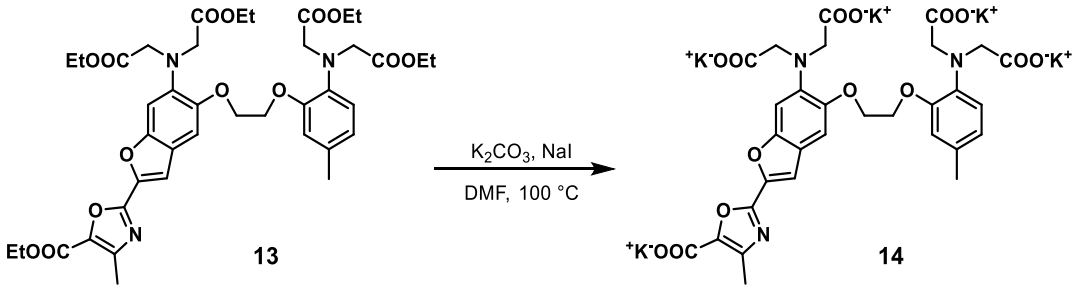

Synthesis of 14:

A round-bottom flask was charged with **13** (17.6 mg, 22 μmol), dioxane (600 μL) and methanol (600 μL). 1 M potassium hydroxide (220 μL, 220 μmol) was added and the solution stirred at 22 °C for 16 h. The reaction was neutralized by the dropwise addition of aqueous hydrochloric acid (0.5 M), then the solvent removed *in vacuo*, affording **14** which was used for further reactions without further purification. ^{1}H NMR (400 MHz, D_2O) δ 7.36 (s, 1H), 7.19 (s, 1H), 7.01 (s, 1H), 6.86 – 6.81 (m, 2H), 6.76 – 6.65 (m, 2H), 4.72 (s, 1H), 4.26 (s, 4H), 3.71 (s, 4H), 3.63 (s, 4H), 3.59 (s, 4H), 2.28 (s, 3H), 2.18 (s, 3H); HRMS (ESI) $[M-5K^+ +4H^+]$ calculated: 654.1577 found: 654.1573.

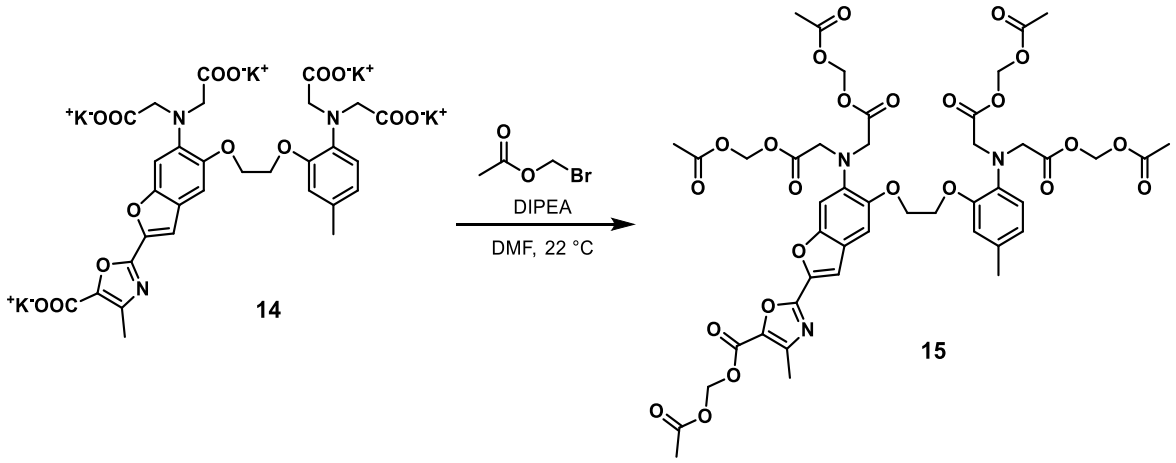

Synthesis of 15:

A round-bottom flask was charged with **14** (17.0 mg, 20 μmol) and bromomethyl acetate (115 mg, 770 μmol). Anhydrous DMF (4 mL) and anhydrous diisopropylethylamine (74 μL, 400 μmol) were added via syringe and the reaction stirred at 22 °C for 16 h. The reaction mixture was then diluted with toluene (10 mL) and filtered through a diatomaceous earth plug, rinsing with 10 mL more toluene. The combined organics were washed with 1 M hydrochloric acid (25 mL) and a saturated brine solution (2 x 25 mL). The combined organics were dried with anhydrous sodium sulfate, filtered and concentrated *in vacuo*. The resulting yellow residue was further purified by flash chromatography (5% methanol in $CHCl_3$, isocratic for first column, 5% methanol in acetone, isocratic for second column) affording **15** as a yellow oil (5.1 mg, 5.0 μmol, 26%). ^{1}H NMR (300 MHz, $CDCl_3$) δ 7.48 (s, 1H), 7.14 (s, 1H), 7.07 (s, 1H), 6.83 (d, J = 8.4 Hz, 1H), 6.73 (d, J = 5.2 Hz, 2H), 6.02 (s, 2H), 5.66 (s, 4H), 5.65 (s, 4H), 4.34 (m, 4H), 4.32 (s, 4H), 4.19 (s, 4H), 2.59 (s, 3H), 2.30 (s, 3H), 2.18 (s, 3H), 2.11 (s, 6H), 2.08 (s, 6H). HR-ESI-MS m/z for $C_{45}H_{50}N_3O_{34}^+$ $[M+H]^+$ calc: 1016.2779 found: 1016.2807.

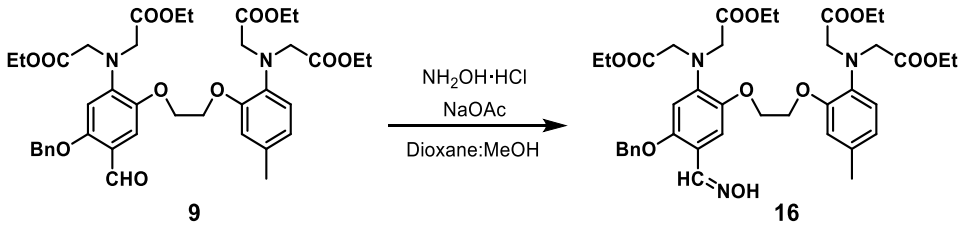

Synthesis of 16:

A round-bottom flask was charged with **9** (3.8 g, 5.2 mmol), dioxane (40 mL) and methanol (20 mL). In a separate round-bottom flask, hydroxylamine hydrochloride (1.084 g, 15.6 mmol) and sodium acetate (0.853 g, 10.4 mmol) were dissolved in water (24 mL) then added to the stirring solution of **9**. The reaction mixture was stirred at 22 °C for 4 h, then water (50 mL) was added and the resulting precipitant collected by vacuum filtration, affording **16** as a white solid (3.68 g, 4.89 mmol, 94%). ^{1}H NMR (300 MHz, $CDCl_3$) δ 7.42 – 7.32 (m, 5H), 7.29 (s, 1H), 6.77-6.68 (m, 3H), 5.02 (s, 2H), 4.31 – 3.98 (m, 20H), 2.27 (s, 3H), 1.17 (m, 12H). The ^{1}H NMR was in agreement with literature values.[15]

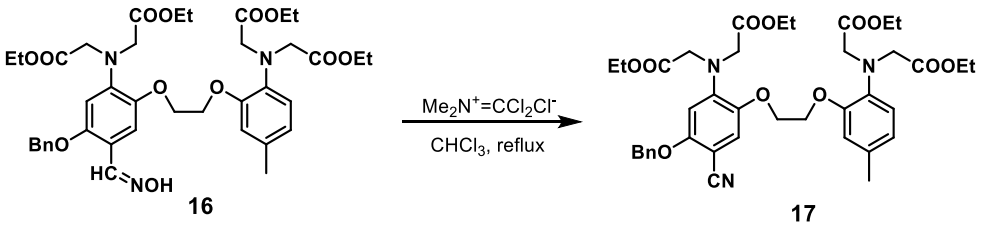

Synthesis of 17:

A round-bottom flask was charged with phosgene iminium chloride (1.27 g, 7.8 mmol) and chloroform (20 mL). A solution of **16** (3.67 g, 4.88 mmol) in chloroform (10 mL) was added and the reaction mixture stirred at reflux for 30 min. The organics were concentrated *in vacuo* and the resulting residue refluxed in methanol (25 mL), then cooled on ice. The resulting precipitant was collected by vacuum filtration, affording **17** as an off-white solid (1.95 g, 2.66 mmol, 54%). ^{1}H NMR (400 MHz, $CDCl_3$) δ 7.45 – 7.30 (m, 5H), 7.01 (s, 1H), 6.78-6.66 (m, 3H), 6.32 (s, 1H), 5.14 (s, 2H), 4.22 (m, 4H), 4.13 (s, 8H), 4.08 (m, 8H), 2.27 (s, 3H), 1.18 (q, *J* = 7.1 Hz, 12H). The ^{1}H NMR was in agreement with literature values.[15]

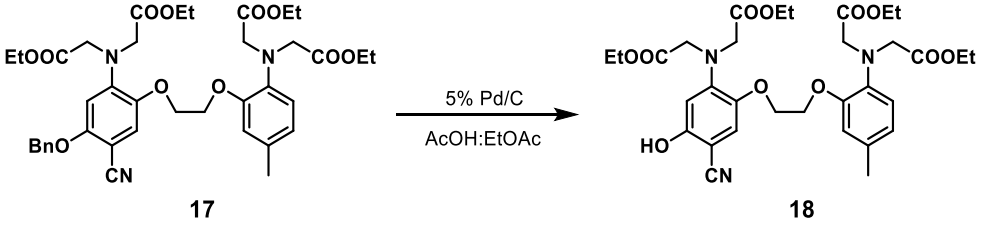

Synthesis of 18:

A round-bottom flask was charged with **17** (1.95 g, 2.66 mmol), 5% palladium on carbon (195 mg, 0.1 equiv. by wt.), glacial acetic acid (60 mL) and ethyl acetate (30 mL). The reaction flask was evacuated and backfilled with nitrogen (3x), then evacuated and backfilled with hydrogen (3x). The reaction was stirred under 1 atm. of H_2 (4 L) at 22 °C for 24 h. The reaction mixture was purged with N_2, then filtered through a diatomaceous earth plug, eluting with ethyl acetate. The combined organics were dried with anhydrous sodium sulfate, filtered and concentrated *in vacuo*. The remaining yellow oil was triturated with 10% acetone in hexanes and the resulting solid collected by vacuum filtration, affording **18** as a pale yellow solid (942 mg, 1.47 mmol, 55%). ^{1}H NMR (300 MHz, $CDCl_3$) δ 6.90 (d, *J* = 2.5 Hz, 1H), 6.83 – 6.63 (m, 3H), 6.28 (s, 1H), 5.59 (s, 1H), 4.26 – 4.03 (m, 20H), 2.28 (s, 3H), 2.07 (s, 2H), 1.28 (t, J=7.1 Hz, 2H) 1.23 (q, 7.2 Hz, 12H). The ^{1}H NMR was in agreement with literature values.[15]

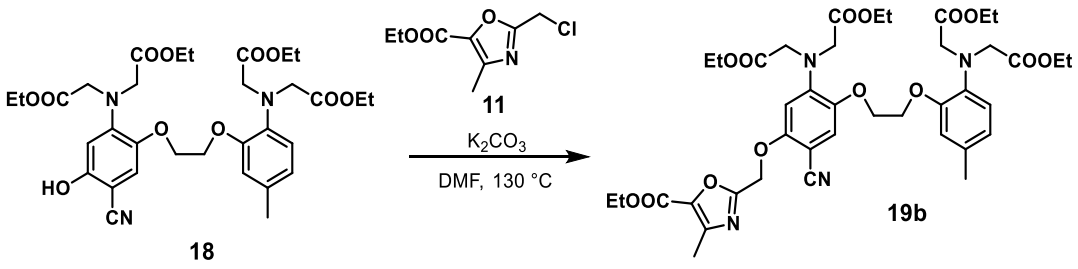

Synthesis of 19b:

A round-bottom flask was charged with **18** (328 mg, 0.51 mmol), anhydrous potassium carbonate (97 mg, 0.70 mmol) and **11** (153 mg, 0.75 mmol). Anhydrous DMF (3 mL) was added via syringe

and the reaction mixture stirred at 130 °C for 3 h. The reaction was cooled and dilute hydrochloric acid (50 mL) was added. The aqueous layer was extracted with ethyl acetate (3 x 25 mL) and the combined organics dried with anhydrous sodium sulfate, filtered and concentrated *in vacuo.* The remaining residue was purified by flash chromatography (35% ethyl acetate in hexanes, isocratic) affording crude **19b**, which was further purified by triturating with ethanol (10 mL). The resulting solid was collected by vacuum filtration, affording pure **19b** as a pale yellow solid (282 mg, 348 μmol, 68%). ^{1}H NMR (600 MHz, $CDCl_3$) δ 7.01 (s, 1H), 6.78 (d, *J* = 8.0 Hz, 1H), 6.70 (d, *J* = 8.0 Hz, 1H), 6.66 (s, 1H), 6.60 (s, 1H), 5.16 (s, 2H), 4.40 (q, *J* = 7.1 Hz, 2H), 4.26 – 4.19 (m, 4H), 4.18 (s, 4H), 4.12 (s, 4H), 4.11 – 4.05 (m, 8H), 2.49 (s, 3H), 2.27 (s, 3H), 1.41 (t, *J* = 7.1 Hz, 3H), 1.18 (m, 12H); ^{13}C NMR (151 MHz, $CDCl_3$) δ 171.6, 170.7, 159.6, 158.5, 155.5, 150.4, 146.0, 145.2, 144., 138.8, 137.2, 132.4, 122.4, 119.8, 117.5, 116.7, 115.0, 104.2, 93.0, 68.6, 67.2, 63.6, 61.5, 61.4, 60.9, 53.9, 53.8, 21.1, 14.5, 14.3, 14.2, 13.4; HR-ESI-MS m/z for $C_{40}H_{51}N_4O_{14}^+$ $[M+H^+]^+$ calc: 811.3396 found: 811.3384; IR (Nujol mull, KBr, cm^{-1}) 2218 (s), 1749 (s), 1732 (s), 1613 (m).

Synthesis of 19:

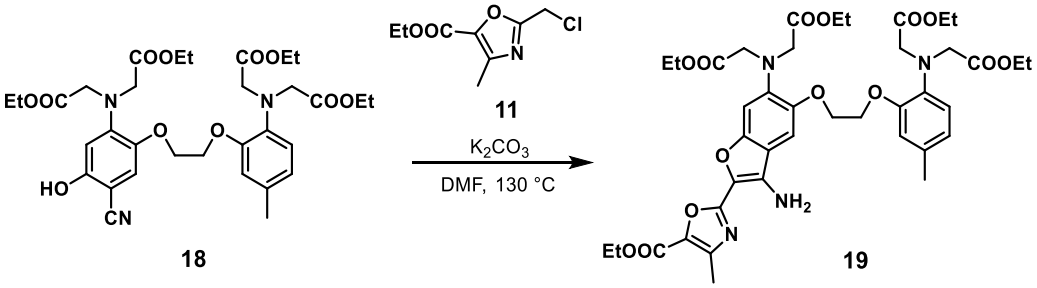

From compound 18

A round-bottom flask was charged with **18 (**300 mg, 0.47 mmol), anhydrous potassium carbonate (97.0 mg, 0.70 mmol) and **11 (**106 mg, 0.56 mmol). Anhydrous DMF (2.8 mL) was added via syringe and the reaction stirred at 130 °C for 12 h. The reaction was cooled and dilute hydrochloric acid (50 mL) was added. The aqueous layer was extracted with ethyl acetate (3 x 25 mL) and the combined organics dried with anhydrous sodium sulfate, filtered and concentrated *in vacuo.* The remaining orange residue was purified by flash chromatography (50% ethyl acetate in hexanes, isocratic) affording **19**, which was further purified by triturating with 50% diethyl ether in hexanes (10 mL). The resulting solid was collected by vacuum filtration, affording pure **19** as a yellow solid (191 mg, 0.236 mmol, 58%). ^{1}H NMR (300 MHz, $CDCl_3$) δ 7.17 (s, 1H), 6.88 (s, 1H), 6.81 (m, 1H), 6.71 (m, 2H), 4.49 – 3.98 (m, 22H), 2.57 (s, 3H), 2.28 (s, 3H), 1.44 (t, *J* = 7.1, 3H), 1.19 (m, 12H); HR-ESI-MS m/z for $C_{40}H_{51}N_4O_{14}^+$ $[M+H^+]^+$ calc: 811.3396 found: 811.3402.

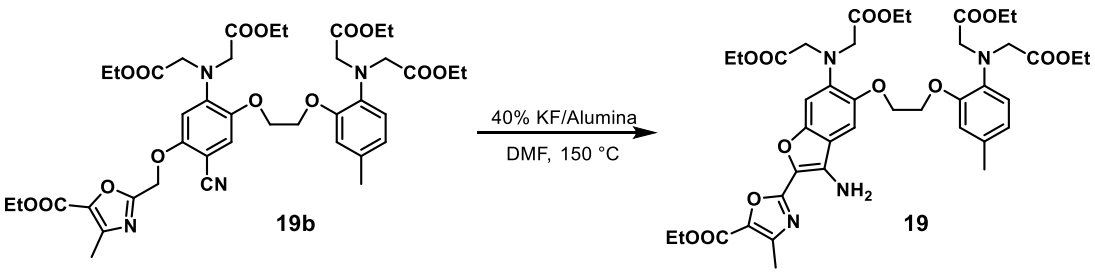

From compound 19b

A round-bottom flask was charged with **19b** (50 mg, 62 µmol) and 40% potassium fluoride on alumina (20 mg). Anhydrous DMF was added via syringe and the reaction stirred at 150 °C for 2 h. After cooling, 25 mL of dilute hydrochloric acid was added. The aqueous layer was extracted with ethyl acetate (2 x 35 mL) and the combined organics dried with anhydrous sodium sulfate, filtered and concentrated *in vacuo*. The remaining brown residue was purified by flash chromatography (25% ethyl acetate in toluene) yielding **20** as a yellow solid (28 mg, 34.5 µmol, 55%). ^{1}H NMR (400 MHz, $CDCl_3$) δ 7.14 (s, 1H), 6.89 (s, 1H), 6.80 m, 1H), 6.70 (m, 2H), 4.44 – 4.25 (m, 8H), 4.22 (s, 4H), 4.17 (s, 4H), 4.10 (m, 8H), 2.55 (s, 3H), 2.28 (s, 3H), 1.45 – 1.39 (t, *J* = 7.1, 3H), 1.20 (m, 12H); ^{13}C NMR (101 MHz, $CDCl_3$) δ 171.87, 171.25, 159.20, 156.80, 150.87, 150.54, 147.95, 142.07, 137.00, 135.05, 132.53, 124.21, 122.06, 119.86, 115.53, 114.56, 104.56, 102.07, 77.43, 69.03, 67.22, 61.22, 61.01, 60.94, 54.08, 53.80, 29.91, 21.17, 14.67, 14.32, 14.29, 13.76; HR-ESI-MS m/z for $C_{40}H_{51}N_4O_{14}^+$ $[M+H^+]^+$ calc: 811.3396 found: 811.3409; IR (Nujol mull, KBr, cm^{-1}) 2218 (s), 1736 (s), 1610 (s).

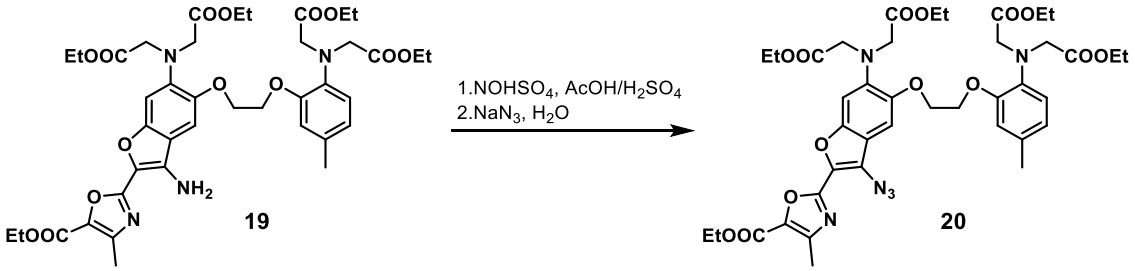

Sythesis of 20

This reaction was conducted under orange safety lights (500 nm). A round-bottom flask was charged with 40% by wt. nitrosyl sulfuric acid in sulfuric acid (31.0 uL, 160 µmol, 6.4 equiv.) and concentrated sulfuric acid (200 µL), then cooled to 0 °C. A solution of **19** (20 mg, 25 µmol, 1.0 equiv.) in glacial acetic acid (300 µL) was added dropwise and the reaction stirred at 0 °C for 30 min. The reaction mixture was then added dropwise to 20 mL of vigorously stirring saturated aqueous sodium azide solution (care: hydrazoic acid generated), warmed to 22 °C and allowed to stir for 1 h. The reaction mixture was neutralized with $NaHCO_3$, diluted with water (50 mL) and extracted with ethyl acetate (3 x 20 mL). The combined organics were dried with anhydrous sodium sulfate, filtered and the solvent removed *in vacuo*. The resulting yellow oil was purified by flash chromatography (40% ethyl acetate in hexanes) affording **20** (5.1 mg, 6.1 µmol, 25%) as a yellow solid. ^{1}H NMR (400 MHz, $CDCl_3$) δ 7.13 (s, 1H), 6.96 (s, 1H), 6.78 (d, *J* = 8.1 Hz, 1H), 6.70 (d, *J* = 7.3 Hz, 2H), 4.42 (t, *J* = 7.1 Hz, 2H), 4.32 (m, 4H), 4.22 (s, 4H), 4.14 (s, 4H), 4.07 (m, 8H), 2.58 (s, 3H), 2.28 (s, 3H), 1.43 (t, *J* = 7.1 Hz, 3H), 1.17 (q, *J* = 7.1 Hz, 12H); ^{13}C NMR (101 MHz, $CDCl_3$) δ 171.7, 171.1, 158.8, 154.1, 150.4, 150.2, 148.9, 147.6, 142.1, 137.2, 137.1, 132.3, 131.4, 124.0, 122.2, 119.6, 116.5, 114.8, 102.1, 101.9, 68.3, 67.2, 61.4, 61.3, 60.9, 54.0, 53.8, 21.1, 14.6, 14.3, 14.2, 13.8; HR-ESI-MS m/z for $C_{40}H_{48}KN_6O_{14}^+$ $[M+K^+]^+$ calc: 875.2860 found: 875.2856; IR (Nujol mull, KBr, cm^{-1}) 1748 (m), 1625 (m).

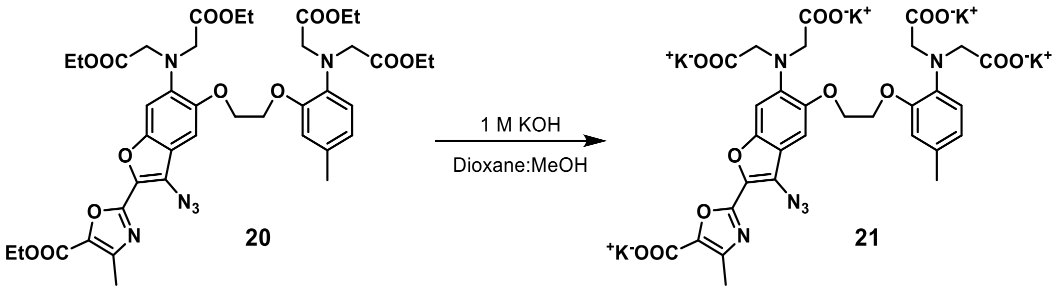

Synthesis of 21:

A round-bottom flask was charged with **20** (30.0 mg, 38.4 μmol), dioxane (2 mL) and methanol (2 mL). Aqueous potassium hydroxide (1 M, 767 μL, 767 μmol) was added and the solution stirred at 22 °C for 16 h. The reaction was neutralized by the dropwise addition of aqueous hydrochloric acid (0.5 M), then the solvent removed *in vacuo*, affording **21** which was used for further reactions without further purification. ^{1}H NMR (600 MHz, D_2O) δ 7.28 (s, 1H), 7.04 (s, 1H), 6.97 (s, 1H), 6.84-6.77 (m, 2H), 4.42 (dd, *J* = 17.3, 4.7 Hz, 4H), 3.83 (s, 4H), 3.69 (s, 4H), 2.40 (s, 3H), 2.29 (s, 3H).

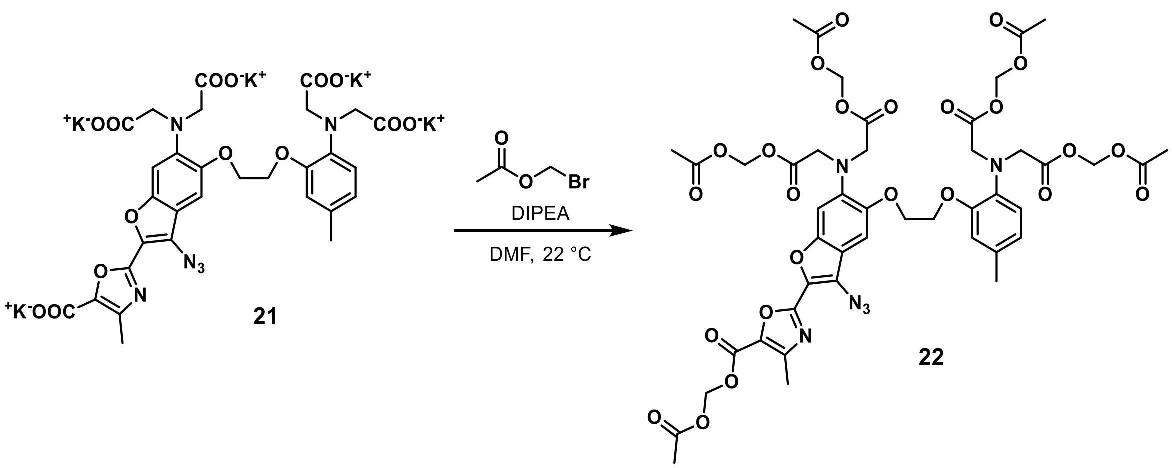

Synthesis of 22:

A round-bottom flask was charged with **21** (6.5 mg, 7.3 μmol) and bromomethyl acetate (28.6 mg, 187 μmol). Anhydrous DMF (1 mL) and anhydrous diisopropylethylamine (18 μL, 104 μmol) were added via syringe and the reaction stirred at 22 °C for 24 h. The reaction mixture was then diluted with toluene (10 mL) and filtered through a diatomaceous earth plug, rinsing with 10 mL more toluene. The combined organics were washed with 1 M hydrochloric acid (25 mL) and a saturated brine solution (2 x 25 mL). The combined organics were dried with anhydrous sodium sulfate, filtered and concentrated *in vacuo*. The resulting yellow residue was further purified by flash chromatography (0-10% methanol in $CHCl_3$, linear gradient) affording **22** as a yellow oil (5.3 mg, 5.0 μmol, 69% over two steps). HR-ESI-MS m/z for $C_{45}H_{48}NaN_6O_{24}^{+}$ $[M+Na]^{+}$ calc: 1079.2612 found: 1079.2639.

MA-1 Labeling In Vitro

Cu-free click chemistry was carried out by mixing DMSO stocks of: 8 μL of 5 mM TAMRA DBCO with 4 μL of 10 mM MA-1-AM (final concentrations 3.33 mM for each component) in a PCR tube for 1 h. The reaction was then diluted with 40 uL acetonitrile and analyzed by LC-MS. Cu-catalyzed click chemistry was carried out by mixing DMSO stocks of: 5 μL MA-1 pentapotassium salt (10 mM), 5 μL CuI (2 mM), 5 μL DIPEA (10 mM) and 5 μL propargyl alcohol (100 mM). The mixture was reacted at 22 °C for 1 h, then diluted with MeCN (200 μL) and analyzed by LC-MS.

Spectroscopic Studies

Stock solutions were prepared in DMSO (1-10 mM). UV-Vis absorbance and fluorescence spectra were recorded using a Shimadzu 2501 Spectrophotometer (Shimadzu) and a Quantamaster Master 4 L-format scanning spectrofluorometer (Photon Technologies International). The fluorometer is equipped with an LPS-220B 75-W xenon lamp and power supply, A-1010B lamp housing with integrated igniter, switchable 814 photon-counting/analog photomultiplier detection unit, and MD5020 motor driver. Samples were measured in 1-cm path length quartz cuvettes (Starna Cells).

Ca^{2+} K_d Determinations

Ca^{2+}-binding constants for MF-2 and MA-1 were determined by monitoring UV-visible spectra during titration of EGTA buffers to varying $[Ca^{2+}]_{free}$. The following procedure is a modification of reported methods.[29,30] Two EGTA buffers needed to be prepared from a single stock: one of Ca^{2+}-free EGTA and one with Ca^{2+} added to form CaEGTA. The stock was prepared by dissolving 3.84 g EGTA (10.1 mmol) and 19 mmol solid potassium hydroxide (from 85% pellets) in 6 mL of H_2O. Once all solids were dissolved, the solution was diluted to 10 mL in a volumetric flask and split into two equal 5 mL portions. To prepare the Ca^{2+}-free EGTA buffer, 1.044 g (5 mmol) MOPS and 3.728 g (5 mmol) KCl were added to one of the 5 mL portions of EGTA stock. The pH was then adjusted to 7.20 by addition of 40% potassium hydroxide and the solution diluted to 500 mL. The CaEGTA buffer was prepared by adding 428 mg (4.75 mmol) of analytical grade $CaCO_3$ to the other 5 mL of EGTA stock. The solution was stirred and heated to 90 °C until the evolution of CO_2 ceased and all of the solid had dissolved. The mixture was then cooled to room temperature and 40% potassium hydroxide was added dropwise until the pH was between 7-8. 1 M $CaCl_2$ was added to the solution in 10 μL portions while monitoring the ΔpH. The addition was continued until the ΔpH per addition was one half of its initial value, with 40% potassium hydroxide being added when the pH fell below 6.5. This process is to ensure the concentration of Ca^{2+} is as close to, but not greater than, the concentration of EGTA within the solution. Following titration with $CaCl_2$, 1.044 g (5 mmol) MOPS was added and the pH adjusted to 7.20 with 40% potassium hydroxide. The solution was then diluted to 500 mL. The final stocks contained 10 mM MOPS, 100 mM KCl and either 10 mM Ca^{2+}-free EGTA or 10 mM CaEGTA at pH 7.20.

Spectrophotometric measurements were taken by diluting the indicator of choice to 10 uM in each EGTA buffer. Starting with 2 mL of the Ca^{2+}-free EGTA buffered solution, the excitation spectrum was measured between 300-450 nm, with excitation centered at 510 nm. Excitation

spectra for multiple $[Ca^{2+}]_{free}$ concentrations were then measured using a reciprocal dilution method described elsewhere.[31,32] An "excess" $[Ca^{2+}]$ spectrum was also collected by addition of 10 µL of 1 M $CaCl_2$. For example, the K_d of MF-2 was then determined utilizing the below equation:

$$[Ca^{2+}]_{free} = K_d^{MF-2} * \frac{[R - R_{min}]}{[R_{max} - R]} * \frac{F_{max}^{380}}{F_{min}^{380}}$$

Where K_d^{MF-2} is the disassociation constant of MF-2, R is the ratio of 510 nm emission intensity at 340 nm to the 510 nm emission intensity with excitation at 380 nm, R_{min} is the same ratio at zero $[Ca^{2+}]_{free}$ and R_{max} the same ratio at saturating $[Ca^{2+}]_{free}$ (i.e. excess Ca^{2+}). $F^{380}{}_{max}$ is the fluorescence intensity with excitation at 380 nm with zero $[Ca^{2+}]_{free}$ and $F^{380}{}_{min}$ is the fluorescence intensity at saturating $[Ca^{2+}]_{free}$. Plotting the above equation as $\log([Ca^{2+}]_{free})$ vs. $\log\{[(R-R_{min})/(R_{max}-R)]*(F^{380}{}_{max}/F^{380}{}_{min})]\}$ yields a straight line of which the x-intercept gives $\log(K_d^{MF-2})$.

Quantum Yield Measurements

The quantum yield of MF-2 was determined through direct comparison to fura-2. A 1 µM solution of fura-2 was prepared in $[Ca^{2+}]_{free}$ EGTA buffer and the absorbance at λ_{max} measured. The absorbance at λ_{max} of a 1 µM solution of MF-2 in $[Ca^{2+}]_{free}$ EGTA buffer was also measured and its concentration diluted until the absorbance was equal to that of fura-2. The excitation spectra of the two samples were then measured, exciting at λ_{max} and measuring emission between 375-600 nm. As the ϕ_{Fl}^{fura-2} is known, the following equation was used to determine ϕ_{Fl}^{MF-2}.

$$\phi_{Fl}^{MF-2} = (A^{Fura-2}/A^{MF-2})*(F^{MF-2}/F^{fura-2})*\phi_{Fl}^{fura-2}$$

Where A^{fura-2} is the absorbance at λ_{max} for fura-2, A^{MF-2} is the absorbance at λ_{max} for MF-2, F^{fura-2} is the peak area of the emission scan between 400-650 nm for fura-2 and F^{MF-2} is the peak area of the emission scan between 400-650 nm for MF-2.

Cell Culture

Human embryonic kidney 293T (HEK) cells were passaged and plated onto 12 mm glass coverslips pre-coated with Poly-D-Lysine (PDL; 1 mg/ml; Sigma-Aldrich) to provide a confluency of ~15% and 50% for electrophysiology and imaging, respectively. HEK cells were plated and maintained in Dulbecco's modified eagle medium (DMEM) supplemented with 4.5 g/L D-glucose, 10% FBS and 1% Glutamax. Transfection of genetic tools was carried out using Lipofectamine 3000 24 h after plating. Imaging was performed 18-24 h following transfection.

Coverslips of 75% confluent HeLa cells were obtained from the UC Berkeley Tissue Culture Facility. The cells were bath-loaded with 2 µM MF-2-AM (diluted 1:1000 from a 2 mM stock in DMSO) in HBSS buffer (gibco) at 37 °C for 30 minutes and then at least 15 minutes in fresh HBSS buffer at room temperature. Histamine was added as a 1000x stock in a single 2 µL addition to the 2 mL of bath solution to give a final concentration of 100 µM. A 100x ionomycin/$CaCl_2$ solution was added to give final concentrations of 1 µM ionomycin and 2 mM $CaCl_2$. Images were acquired at a rate of 0.2 Hz over a five-minute period. Acquisition analysis settings were maintained through the course of the experiment.

Mixed hippocampal and cortical neurons were harvested from E18 rats in the C. Chang lab and cultured for thirteen days *in vitro*. Neurons were bath-loaded with 5 µM MF-2-AM in neuronal extracellular solution (NES) containing (mM), NaCl (145), glucose (20), HEPES (10), KCl (3),

$CaCl_2$ (2), $MgCl_2$ (1) pH 7.35, mOsm ~310 for 1 hour at 20 °C, then at least 15 minutes in fresh NES buffer. The same illumination and filter sets were used for the neuronal experiments as the HeLa cell experiments. A 0.5x demagnifier was inserted in the light path immediately before the camera to provide 10x magnification (light was collected with a 20x/1.0 NA water immersion objective). Glutamate was added as a 100x stock in NES to give a final concentration of 100 μM. Images were captured at 5 Hz over a 15 second period. Acquisition analysis settings were maintained throughout the course of the experiment.

All data analysis was done using either ImageJ (NIH) or Slidebook (Intelligent Imaging Innovations). Regions of interest were drawn around cells of interest and the mean fluorescence plotted against time. Background fluorescence was subtracted by measuring the fluorescence at a location where no cells grew. ΔF/F was measured by dividing the fluorescence signal by the average fluorescence for a baseline of 10-20 frames prior to simulation.

Imaging Parameters

Epifluorescence imaging was performed on an AxioExaminer Z-1 (Zeiss) equipped with a Spectra-X Light engine LED light (Lumencor), controlled with Slidebook (v6, Intelligent Imaging Innovations). Co-incident excitation with multiple LEDs was controlled by Lumencor software triggered through a Digidata 1332A digitizer and pCLAMP 10 software (Molecular Devices). Images were acquired with either a W-Plan-Apo 20x/1.0 water objective (20x; Zeiss) or a W-Plan-Apo 63x/1.0 water objective (63x; Zeiss). Images were focused onto either an OrcaFlash4.0 sCMOS camera (sCMOS; Hamamatsu) or an eVolve 128 EMCCD camera (EMCCD; Photometrix). For TAMRA DBCO images, the excitation light was delivered from a LED (3-19 W/cm^2) at 542/33 (bandpass) nm and emission was collected with a quadruple emission filter (430/32, 508/14, 586/30, 708/98 nm) after passing through a quadruple dichroic mirror (432/38, 509/22, 586/40, 654 nm LP). Illumination was provided at 390 nm by a LED spectra-x light engine (Lumencor) filtered through a 390/22 nm bandpass excitation filter (Semrock), a quadruple dichroic with bands at 432/40, 509/14, 587/32 and 708/110 nm (Semrock) and finally filtered through a matched band pass emission filter (Semrock).

Live-Cell Labeling of MA-1 with TAMRA DBCO

HEK cells were loaded with 10 μM MA-1 w/ .01% pluronic in dPBS with 1% FBS (PBS/FBS) at 22 °C for 1 h. The coverslips were then washed with PBS/FBS 2 times, then either left in the dark or photolyzed with broad wavelength UV light (4 W handlamp at 365 nm, 20 min). Coverslips were then loaded with 30 μM TAMRA DBCO in PBS/FBS for 1 h at 22 °C, then washed with PBS/FBS (5 x 5 min at 37 °C) before imaging.

Visualizing MA-1 Photolysis by Reduction and Fixation

HEK cells or neurons were loaded with 10 μM MA-1 w/ .01% pluronic in PBS/FBS at 22 °C for 1 h. Cells were then washed with PBS/FBS 2 times. Coverslips were then either left in the dark, photolyzed with broad wavelength UV light (4 W handlamp at 365 nm, 20 min) or with a Lumencor Violet LED (390/22 nm, 1.3 W/cm^2, 30 s). The coverslips were then cooled to 0 °C and fixed in cold 4% paraformaldehyde (PFA) or 3% PFA with 1% glutaraldehyde (GA) for 15 min. The fixing solution was then aspirated and the coverslips reduced with a 0.1% aqueous sodium

borohydride solution (3 x 5 min additions) and washed with PBS. The coverslips were then mounted and cured overnight before imaging.

Photolysis of MA-1 in neurons with high [Ca^{2+}] and low [Ca^{2+}]

Neurons were loaded with 2 μM MA-1-AM with 0.01% pluronic in HBSS at 37 °C for 30 min. Neurons were then either placed into imaging dishes containing $[Ca^{2+}]_{free}$ HBS (138 mM NaCl, 2.5 mM KCl, 10 mM HEPES, 10 mM glucose, 0 mM CaCl, 1.3 mM MgCl, 2 μM ionomycin) or a dish containing $[Ca^{2+}]_{High}$ HBS (133 mM NaCL, 2.5 mM KCl, 10 mM HEPES, 10 mM glucose, 5 mM CaCl, 1.3 mM MgCl, 2 μM ionomycin) and the center of the coverslip illuminated with violet light (390/22 nm, 1.32 W/cm^2, 30 s). The coverslips were then cooled to 0 °C and fixed in cold 4% paraformaldehyde (PFA) for 30 min. The fixing solution was then aspirated and the coverslips reduced with a 0.1% sodium borohydride solution (3 x 5 min additions) and washed with PBS. The coverslips were then mounted and cured overnight before imaging.

Figures and Schemes

***Scheme 4-1**: Reaction-based probes and chemodosimeters*

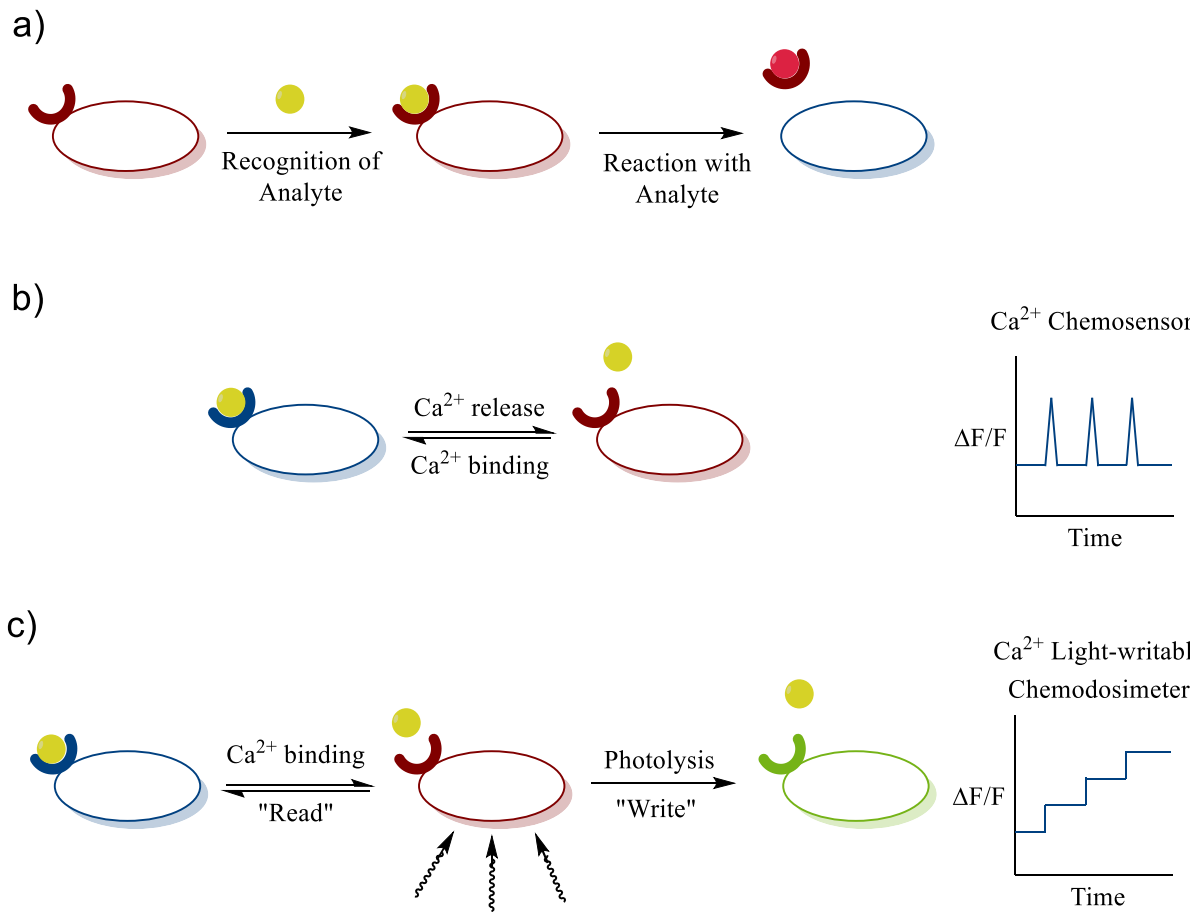

Scheme 4-1: Cartoon depiction of reaction-based probes and chemodosimeters. (a) Reaction-based probes selectively react with an analyte of interest, chemically modifying the reporter. (b) A Ca^{2+} probe binds Ca^{2+} reversibly with transient increases in [Ca^{2+}], correlating to spikes in fluorescence intensities. (c) A light-writable chemodosimeter (or integrator) also reversibly binds Ca^{2+}. However a pulse of light is used to "save" the [Ca^{2+}] at a specific moment of interest through a photochemical reaction. Repeated write steps can be used to accumulate signal over time.

Scheme 4-2: *Azid-1 as a Ca^{2+} chemodosimeter*

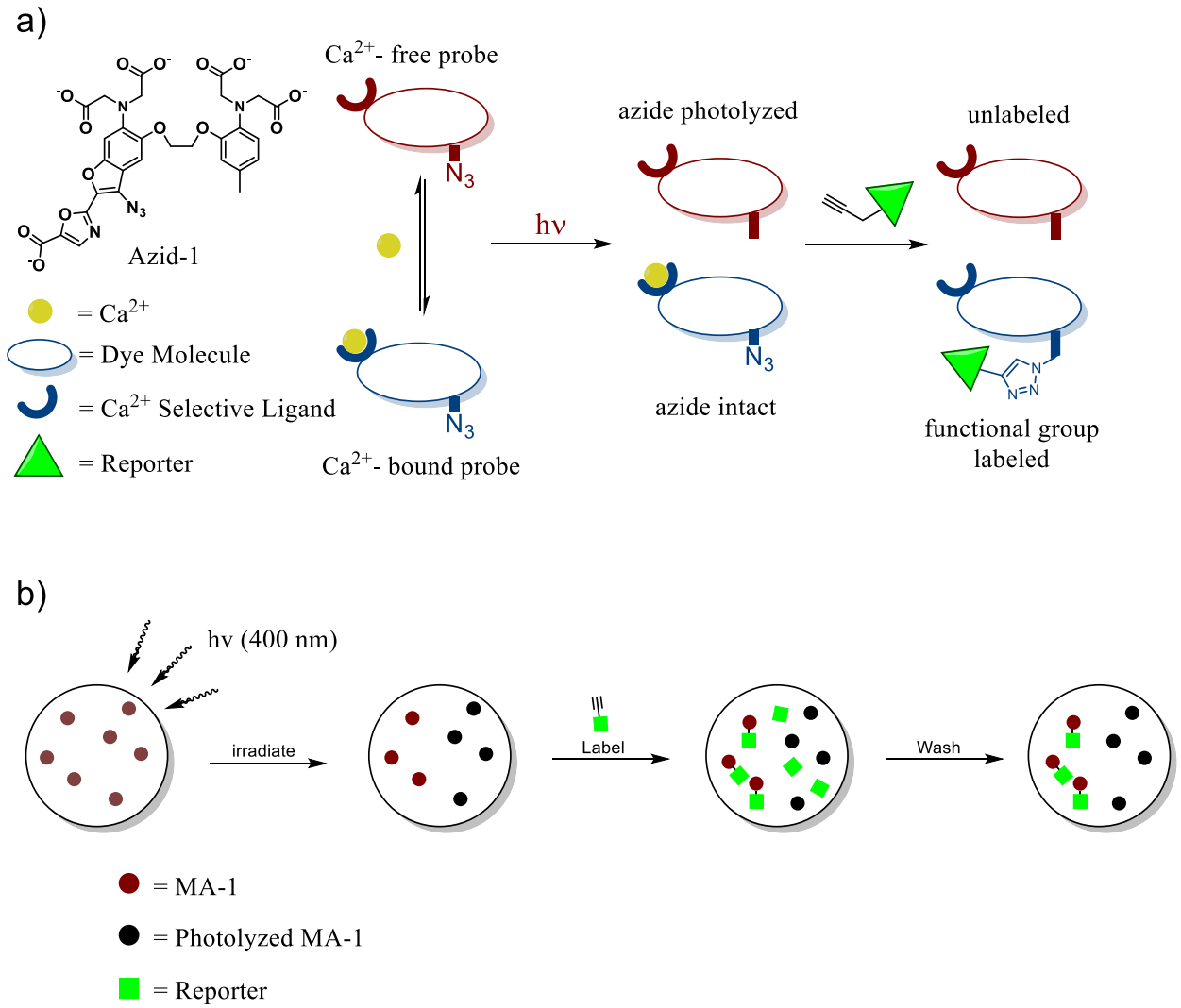

Scheme 4-2: Intracellular [Ca^{2+}] of a firing neuron increases by 10-100 times that of its resting concentration of 50-100 nM. (a) Azid-1, with a K_d of approximately 230 nM, exists largely in its Ca^{2+}-free state in resting neurons and in the Ca^{2+}-bound state in firing neurons. Shining 400 nm light on a sample will lead to the selective photolysis of azid-1 in resting neurons, as the Ca^{2+}-free state can absorb 400 nm light while the Ca^{2+}-bound state cannot. Following irradiation, intact azid-1 can then be visualized by addition of a wide variety of alkyne-bound reporters. (b) Photolysis and labeling of MA-1 in a cellular context.

Scheme 4-3: *Alkyne-functionalized reporters*

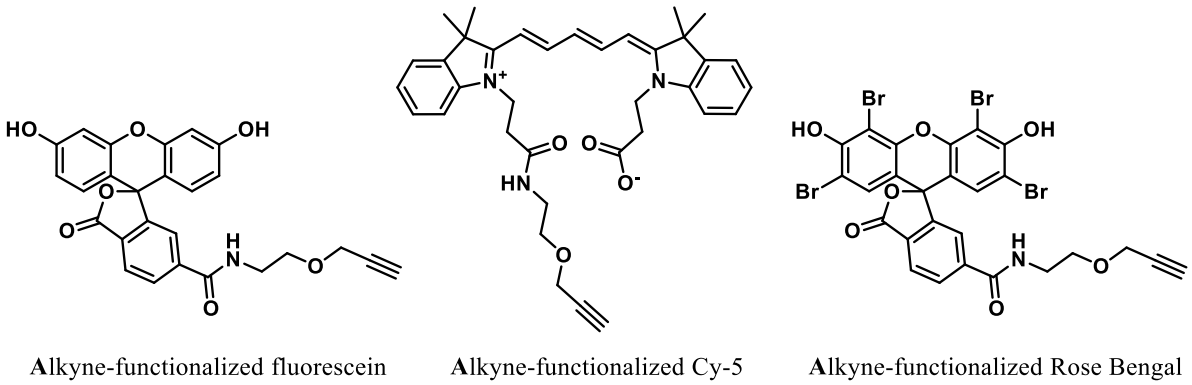

Alkyne-functionalized fluorescein **A**lkyne-functionalized Cy-5 **A**lkyne-functionalized Rose Bengal

Scheme 4-3: Alkyne-functionalized reporters for use in light-writable Ca^{2+} dosimetry.

Scheme 4-4**: Synthesis of benzaldehyde **9

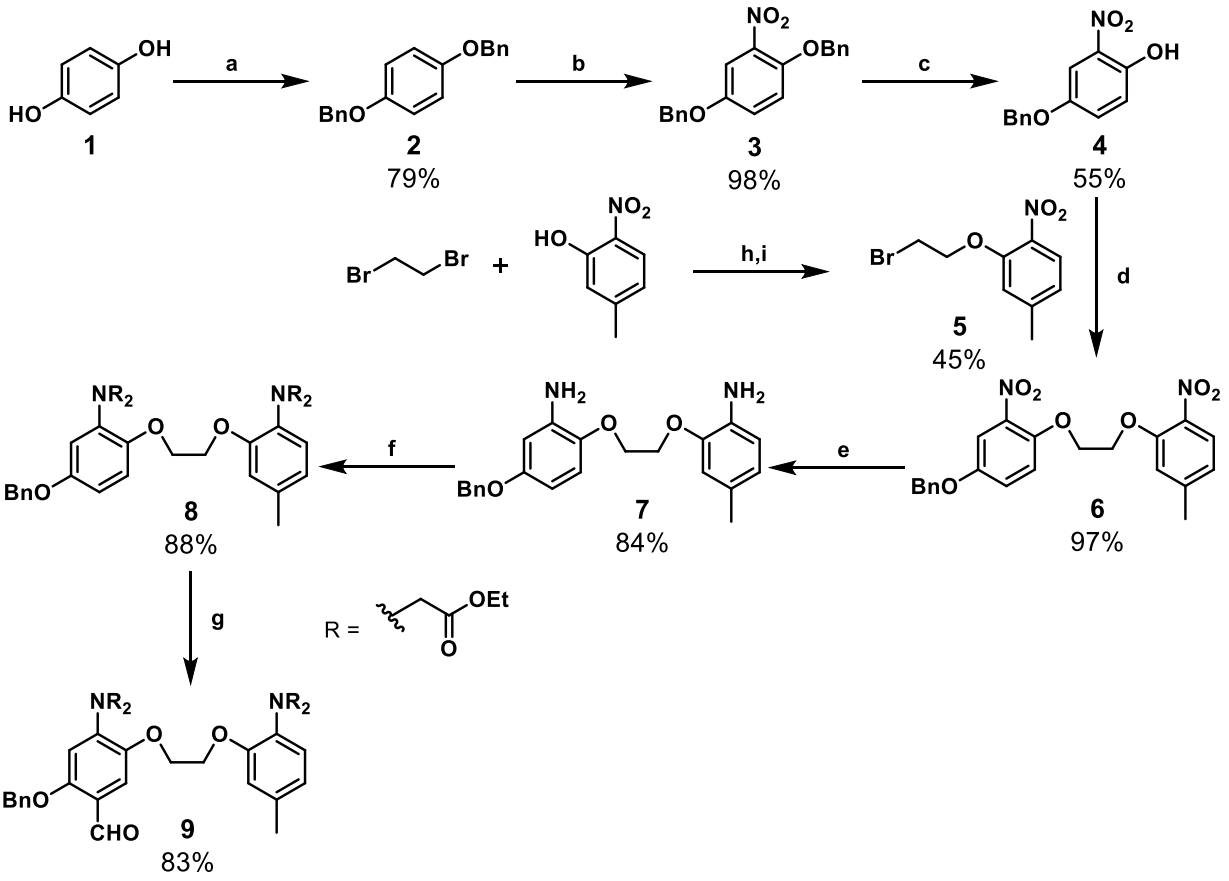

Figure 4-4: Synthesis of precursor **9**. Reagents: (a) BnBr, EtOH, KOH; (b) HNO_3, AcOH; (c) CF_3COOH, $CHCl_3$; (d) K_2CO_3, DMF; (e) Pt/C (5% by wt.), H_2, EtOH; (f) ethyl 2-bromoacetate, proton sponge®, NaI, MeCN; (g) $POCl_3$, Pyridine, DMF.

Scheme 4-5: *Synthesis of ethyl 2-(chloromethyl)oxazole 5-carboxylates*

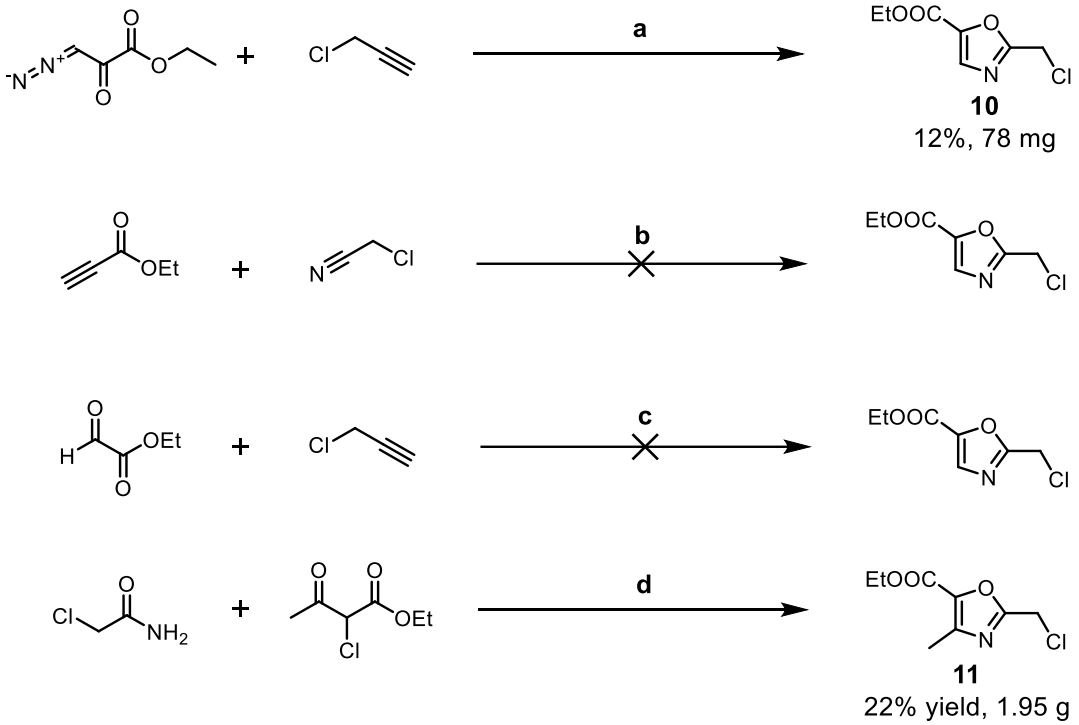

Scheme 4-5: Synthesis of ethyl 2-(chloromethyl)oxazole-5-carboxylates. (a) $Cu(acac)_2$, toluene; (b) 8-methylquinoline N-oxide, $Ph_3PAuNTf_2$, MeCN; (c) HDNIB, 2,6-lutidine; (d) Conc. H_2SO_4.

Scheme 4-6: *Synthesis of Methylfura-2 (MF-2) and Methylfura-2 Acetoxymethyl Ester (MF-2-AM)*

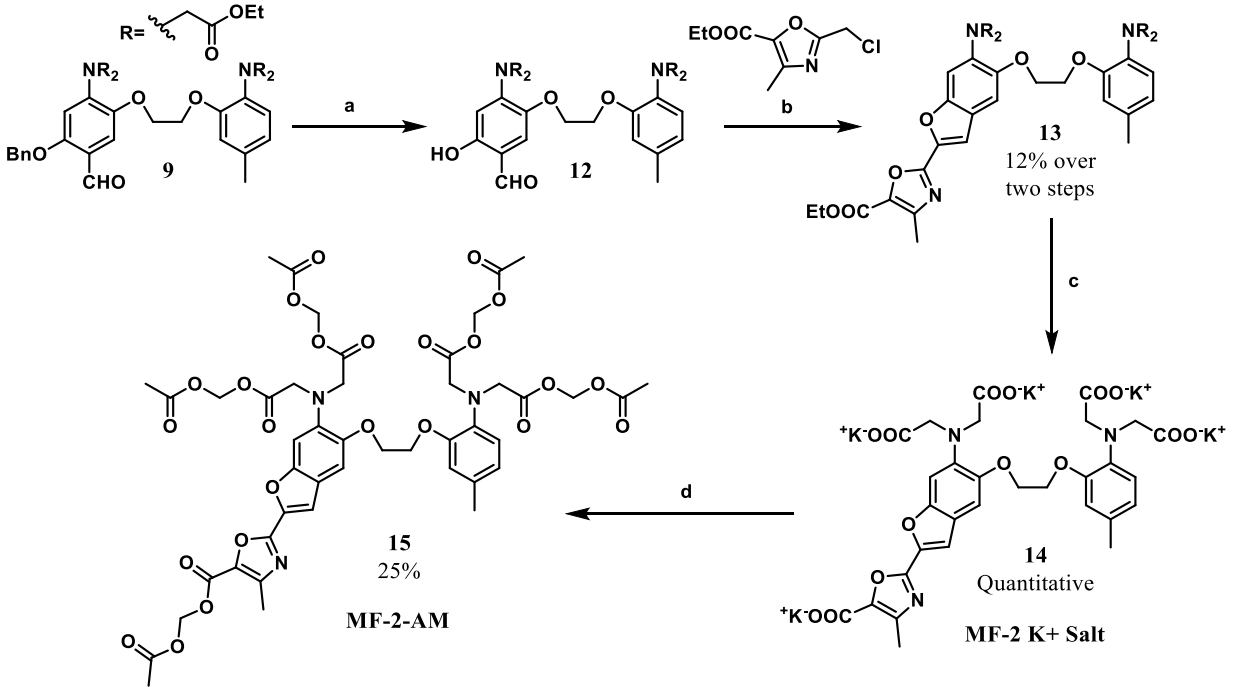

Scheme 4-6: Synthesis of MF-2 and MF-2-AM. Reagents: (a) glacial acetic acid, Pd/C (5% by wt.), H_2 (1 atm.); (b) DMF, **13**, K_2CO_3, NaI; (c) Dioxane/MeOH, KOH, H_2O; (d) DMF, DIPEA, bromomethyl acetate.

***Scheme 4-7**: Synthesis of Methylazid-1 (MA-1)*

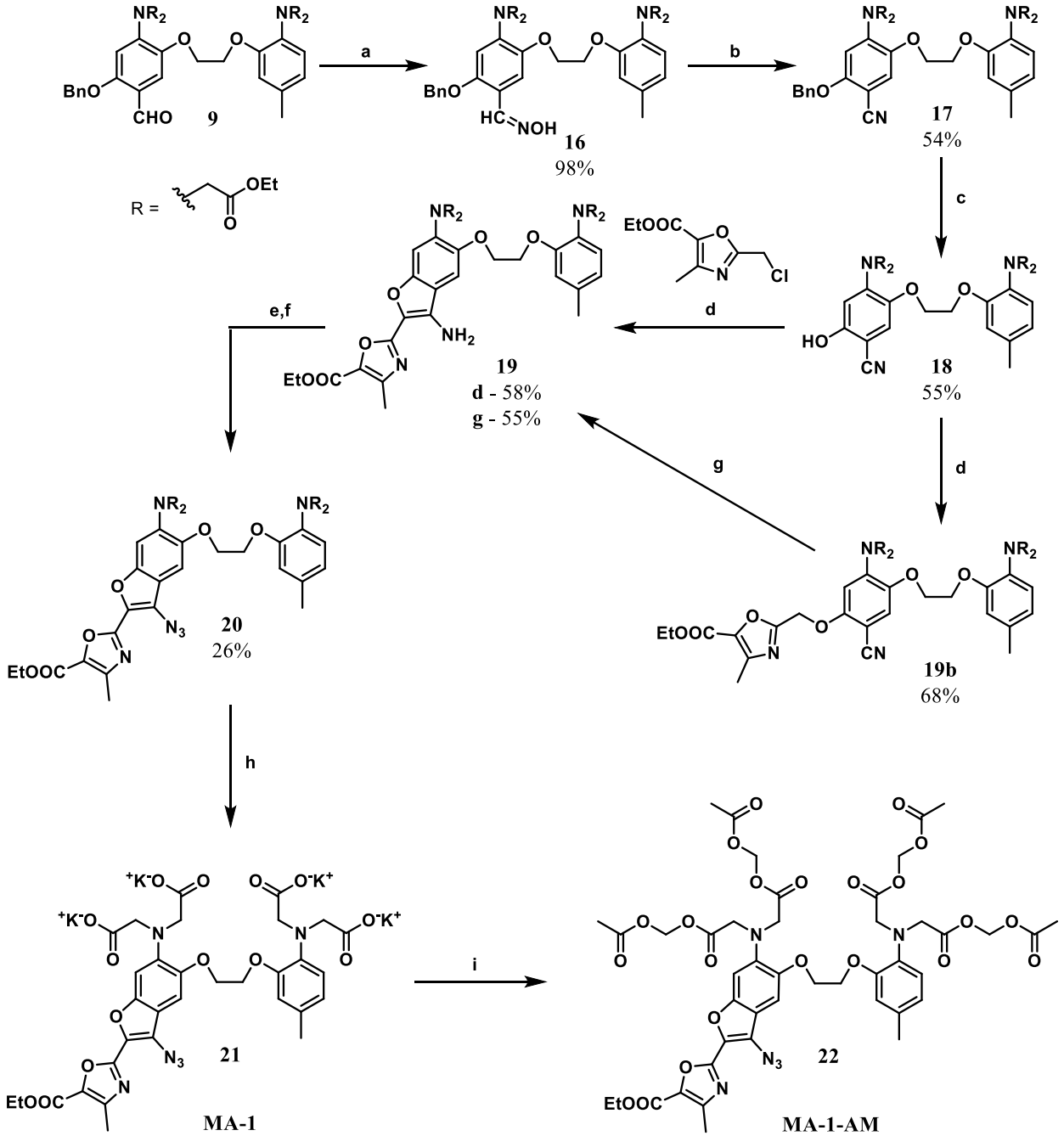

Scheme 4-7: Synthesis of methylazid-1 **20**. Reagents: (a) $NH_2OH{\cdot}HCl$, NaOAc, dioxane/MeOH; (b) $Me_2N^+{=}CCl_2Cl^-$, $CHCl_3$; (c) H_2, Pd/C, HOAc; (d) **11**, K_2CO_3, NaI, DMF; (e) $NOHSO_4$, $HOAc/H_2SO_4$; (f) NaN_3, H_2O; (g) K_2CO_3, DMF; (h) Dioxane/MeOH, KOH, H_2O; (i) DMF, DIPEA, bromomethyl acetate.

Table 4-1: *Spectroscopic characterization of MF-2 and MA-1*

Sensor	K_d for Ca^{2+} (nM)	Absorption Maxima (nm)		Emission Maxima (nm)		Φ_{Fl}		Extinction Coefficient ($M^{-1}cm^{-1}$)	
		Free Anion	Ca^{2+} Complex	Free Anion	Ca^{2+} Complex	Free Anion	Ca^{2+} Complex	Free Anion	Ca^{2+} Complex
MF-2	115 ± 10	364	350	501	492	0.37	0.80	26,000	30,000
Fura-2[a]	100 ± 5	365	348	508	493	0.23[b]	0.49[b]	30,000[b]	33,000[b]
MA-1	270 ± 20	374	349	N.A.	N.A.	-	-	32,000	39,000
Azid-1[b]	230	372	342	N.A.	N.A.	0.9	1.3	27,000	33,000

[a] Fura-2 pentapotassium salt was purchased from molecular probes and was used as received.
[b] Values from Grynkiewicz, G.; Poenie, M.; Tsien, R. Y. *J. Biol. Chem.* **1985**, *260*, 3440–3450.
[c] Values from Adams, S.; Lec-Ram, V.; Tsien, R. Y. *Chem. Biol.* **1997**, *4* (11), 867–878.

Figure 4-1: *Absorption profile of fura-2 with varying [Ca^{2+}]*

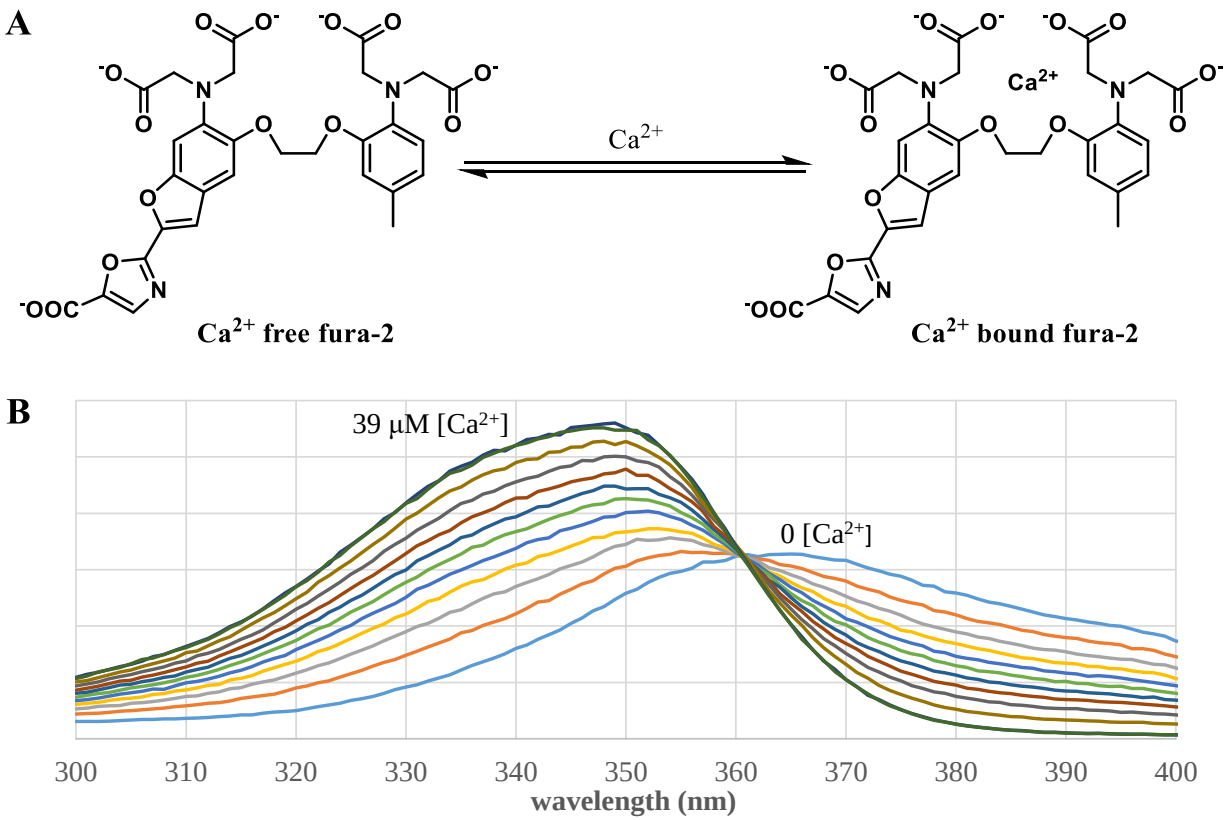

Figure 4-1: **A**: Fura-2 binds Ca^{2+} with a K_s of 100 nM via chelation with the four carboxylate groups and two amino groups **B**: [Ca^{2+}] titration curve for fura-2. As the [Ca^{2+}] increases, λ_{max} of excitation shifts from 362 nm to 335 nm.

Figure 4-2: *Absorption and emission profiles of MF-2*

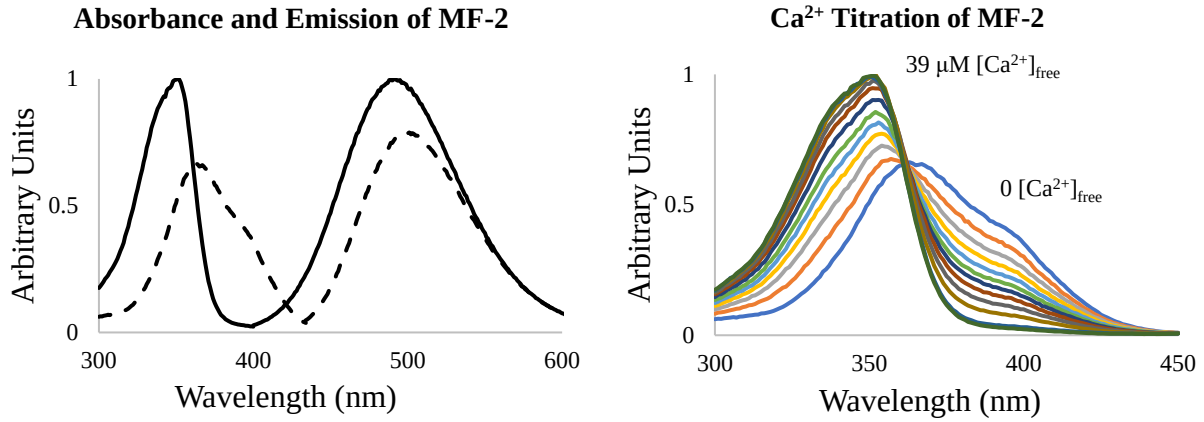

Figure 4-2: Spectroscoptic characterization of MF-2. Studies of MF-2 showed it to possess properties very similar to fura-2, with the exception of its higher Φ_{Fl}. The absorbance and emission wavelengths of MF-2 were measured in buffered solutions containing 100 mM KCl, 10 mM MOPS at 20 °C and pH 7.2. The titration of MF-2 was done using specially prepared standardized Ca^{2+} buffer solutions which give $[Ca^{2+}]_{free}$ in the K_d range of BAPTA-based Ca^{2+} sensors (see **experimental**).

Figure 4-3: *Ca^{2+} imaging in Hela cells with MF-2*

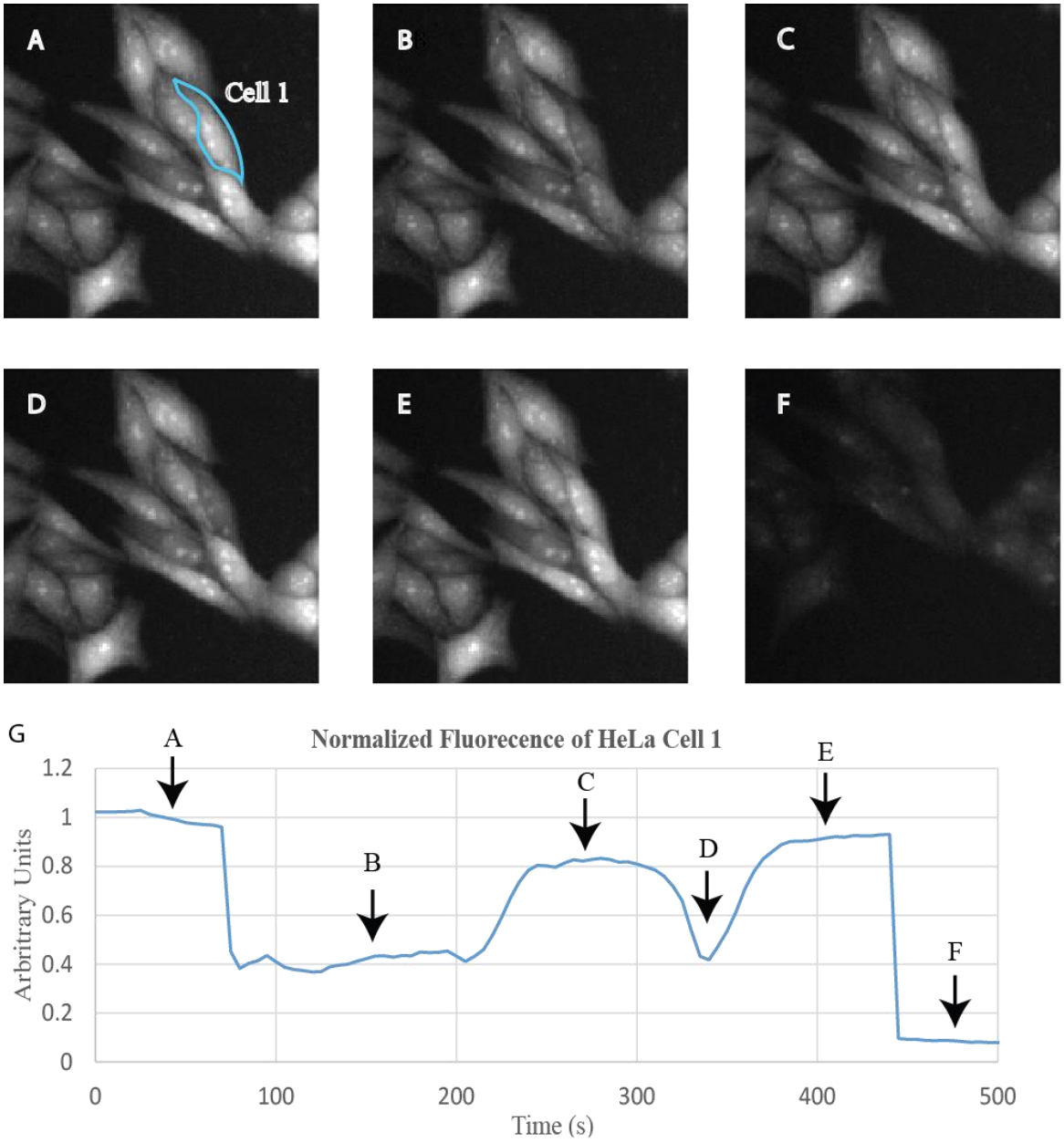

Figure 4-3: Cellular imaging of the addition of histamine to HeLa cells loaded with MF-2-AM. **A**: Prior to the addition of histamine, cells are highly fluorescent when irradiated at 400 nm. **B**: Addition of histamine causes the fluorescence of the cell to drop by 60%. **C**,**D**,**E**: [Ca^{2+}] continue to fluctuate in Cell 1 and surrounding HeLa cells **F**: The addition of ionomycin and $CaCl_2$ dramatically increases intracellular [Ca^{2+}] and leads to the reduction of fluorescence to baseline levels.

Figure 4-4: *MF-2 reports Ca^{2+} dynamics in cultured rat hippocampal neurons*

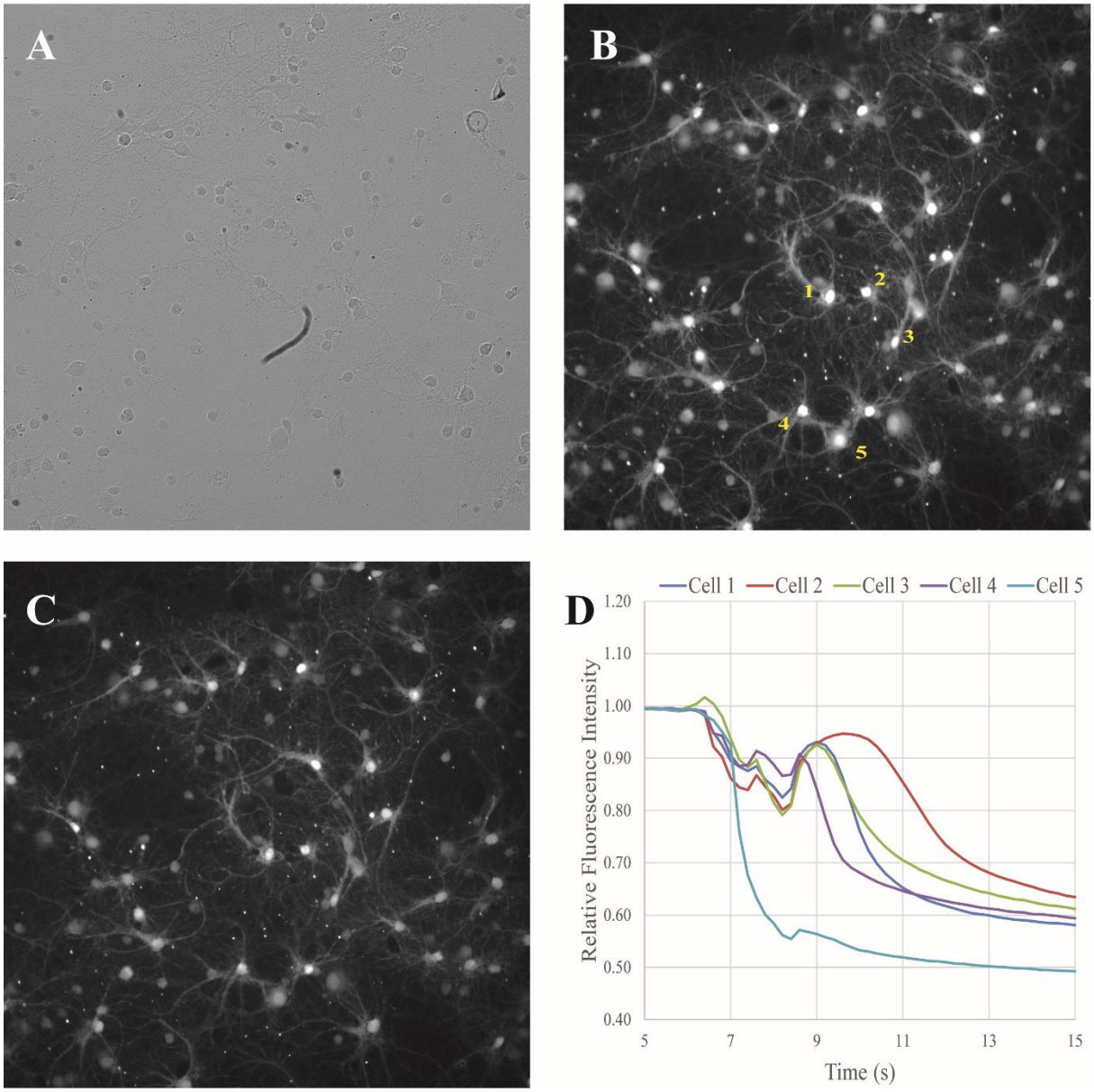

Figure 4-4: Fluorescence Imaging of [Ca^{2+}] in neurons with MF-2. **A)** DIC image of mixed hippocampal and cortical neurons loaded with 5 µM MF-2-AM. **B**: Fluorescence image of neurons in (**A**) prior to the addition glutamate (final [glutamate] = 100 µM). **C**: Neurons after the addition of glutamate. Glutamate, an excitatory neurotransmitter, leads to an increase in intracellular [Ca^{2+}] and thus a decrease in overall fluorescence. **D**: Quantification of selected neurons in (**B**) and (**C**). Plot of F/F vs. time. Fluorescence decreases in all of the indicated neurons, with between 30-50% reductions in overall brightness, consistent with rising intracellular [Ca^{2+}].

Figure 4-5: *Absorption and emission profiles of MA-1*

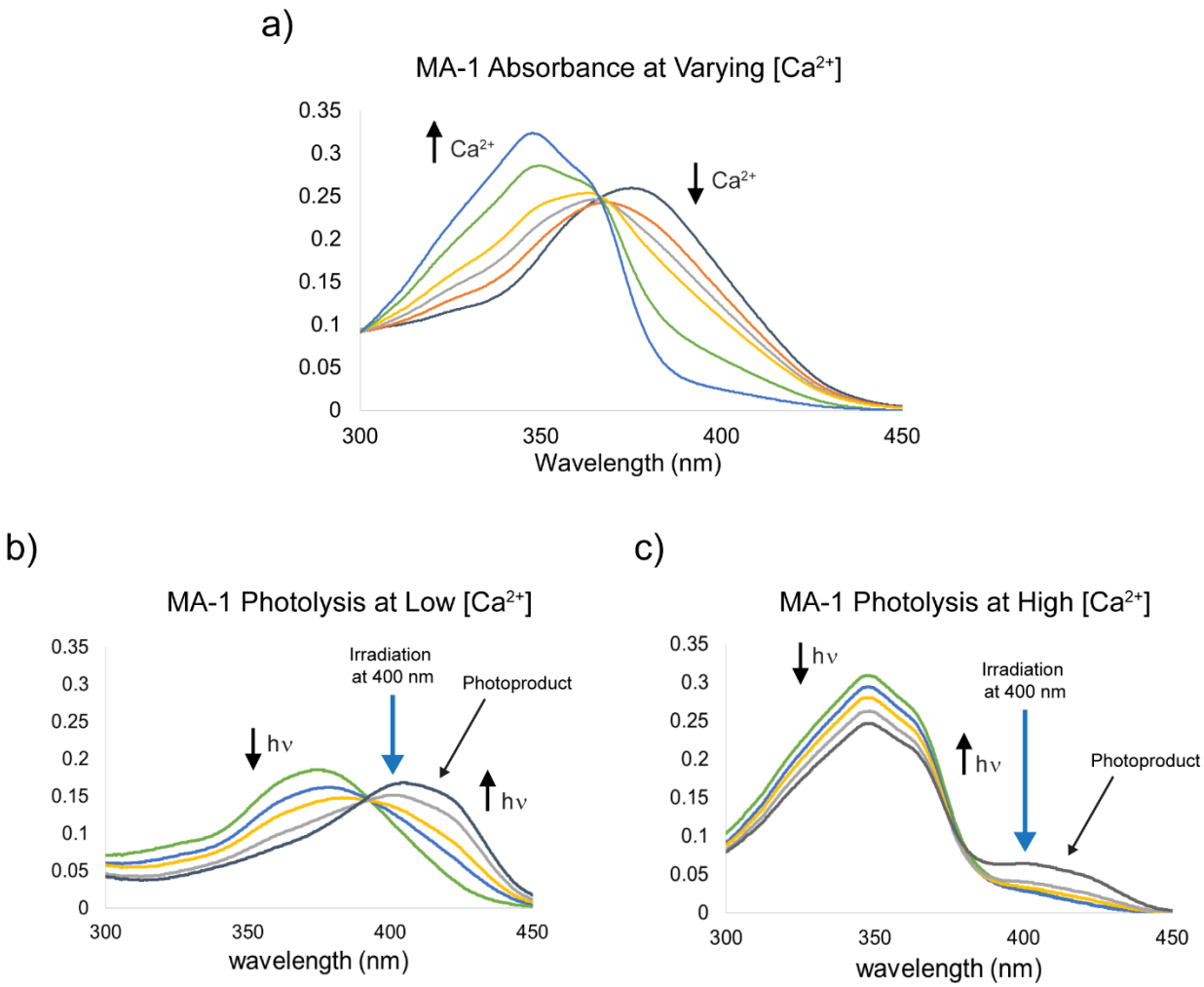

Figure 4-5: Spectroscoptic characterization of MA-1. (a) A titration of [Ca^{2+}] revealed MA-1 possessed a K_d = 270 nM for Ca^{2+}. The titration was carried out using specially prepared standardized Ca^{2+} buffer solutions which give $[Ca^{2+}]_{free}$ in the K_d range of BAPTA-based Ca^{2+} sensors (see experimental). (b) MA-1 in a Ca^{2+}-free buffer was shown to photolyze rapidly with 400 nm light. Photolysis was monitored through the loss of MA-1 absorbance at 374 nm and the appearance of a new absorbance at 405 nm corresponding to the photoproduct. (c) In the presence of high [Ca^{2+}] concentrations (39 μM) irradiation at 400 nm results in minimal photolysis.

Figure 4-6: *MA-1 labeling with click chemistry*

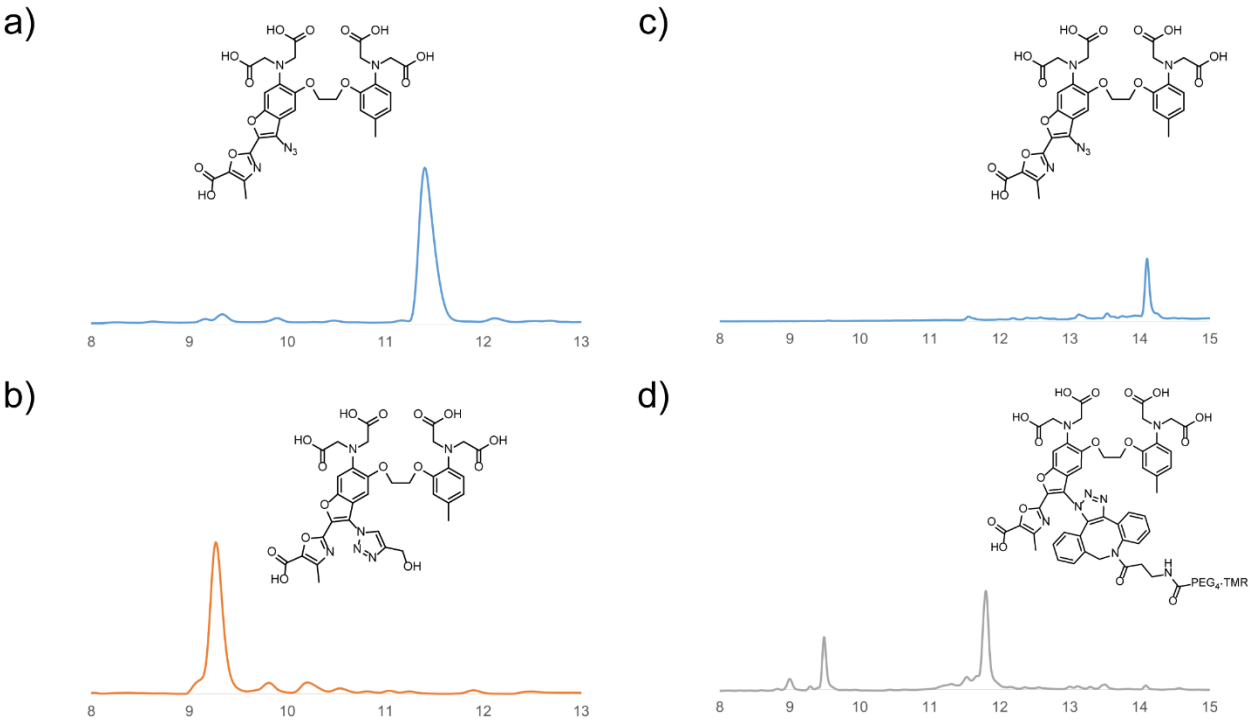

Figure 4-6: MA-1 Labeling with (a,c) Cu(I)-catalyzed Huisgen Cyclization with propargyl alcohol or (b,d) bioorthogonal click reaction with TAMRA DBCO. The degree of labeling was determined by HPLC.

Figure 4-7: *Labeling MA-1 with TAMRA DBCO in HEK cells*

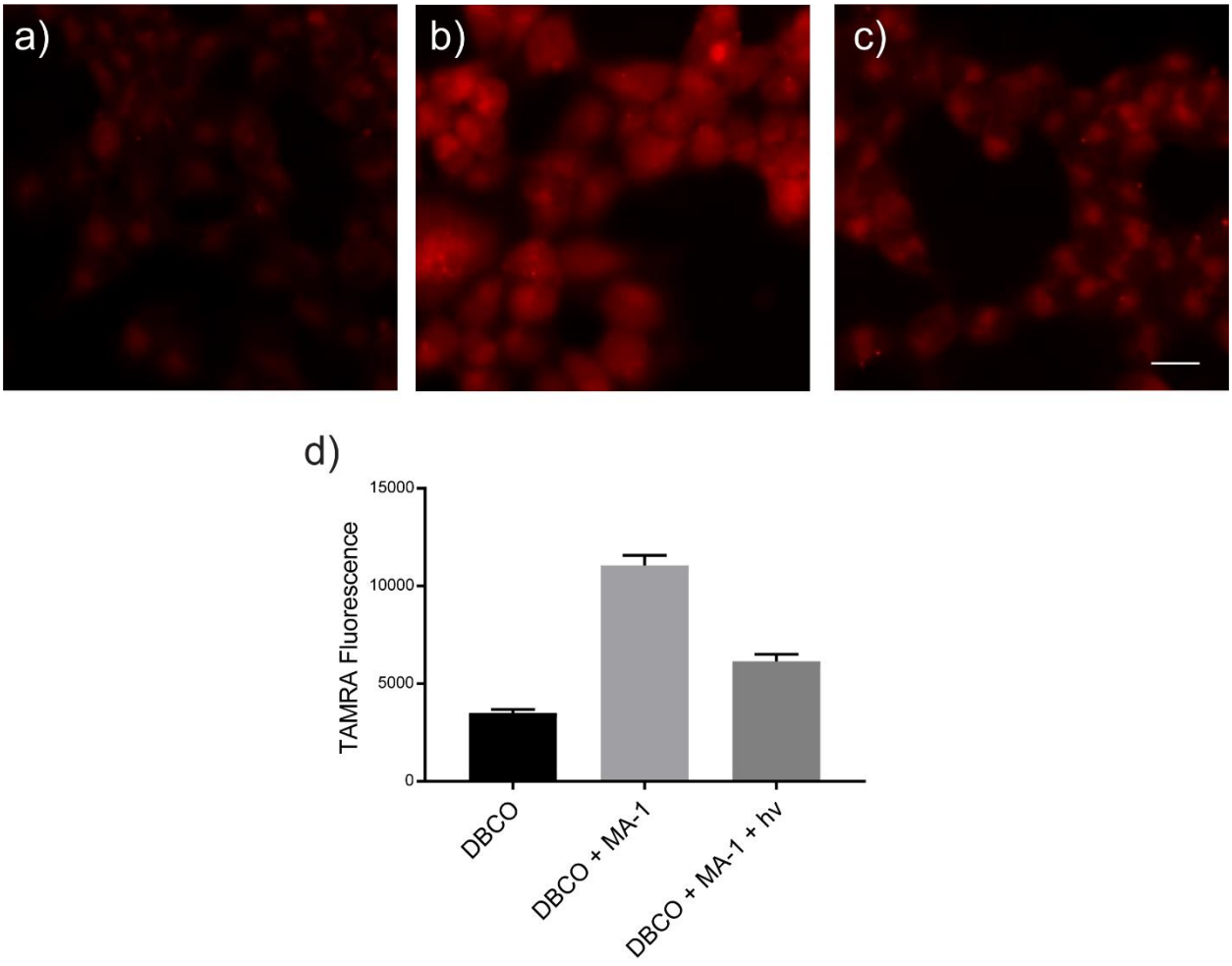

Figure 4-7: Labeling MA-1 with TAMRA DBCO in HEK cells. cells in (b) and (c) were loaded with MA-1 for 30 minutes at 37 °C. Cells in (c) were additionally exposed to 400 nm light (1.32 W/cm^2 for 30 seconds). TAMRA DBCO was then applied to cells in (a-c) and incubated for 15 minutes. The cells were washed with HBSS (5x), then imaged. (a) Fluorescence image of HEK cells loaded with TAMRA DBCO in the absence of MA-1. A large amount of TAMRA fluorescence remains, alluding to a large amount of unproductive fluorescence for MA-1 loaded cells. (b) Fluorescence image of cells loaded with both MA-1 and TAMRA DBCO. Reaction of MA-1 with TAMRA DBCO results in higher retention of the TAMRA, as the highly charged carboxylates of MA-1 prevents the resulting triazole from crossing of the plasma membrane. (c) Fluorescence image of cells loaded with MA-1, photolyzed with 400 nm light, then loaded with TAMRA DBCO. Due to the photolysis of the azide of MA-1, irradiated cells are dimmer than cells in (b) as less TAMRA DBCO is retained in the cell. Scale bar is 20 μm. (d) Quantification of fluorescence for panels a-c (n=5 per condition).

Figure 4-8: *Reduction of MA-1 to amino MF-2 results in a fluorescence turn-on*

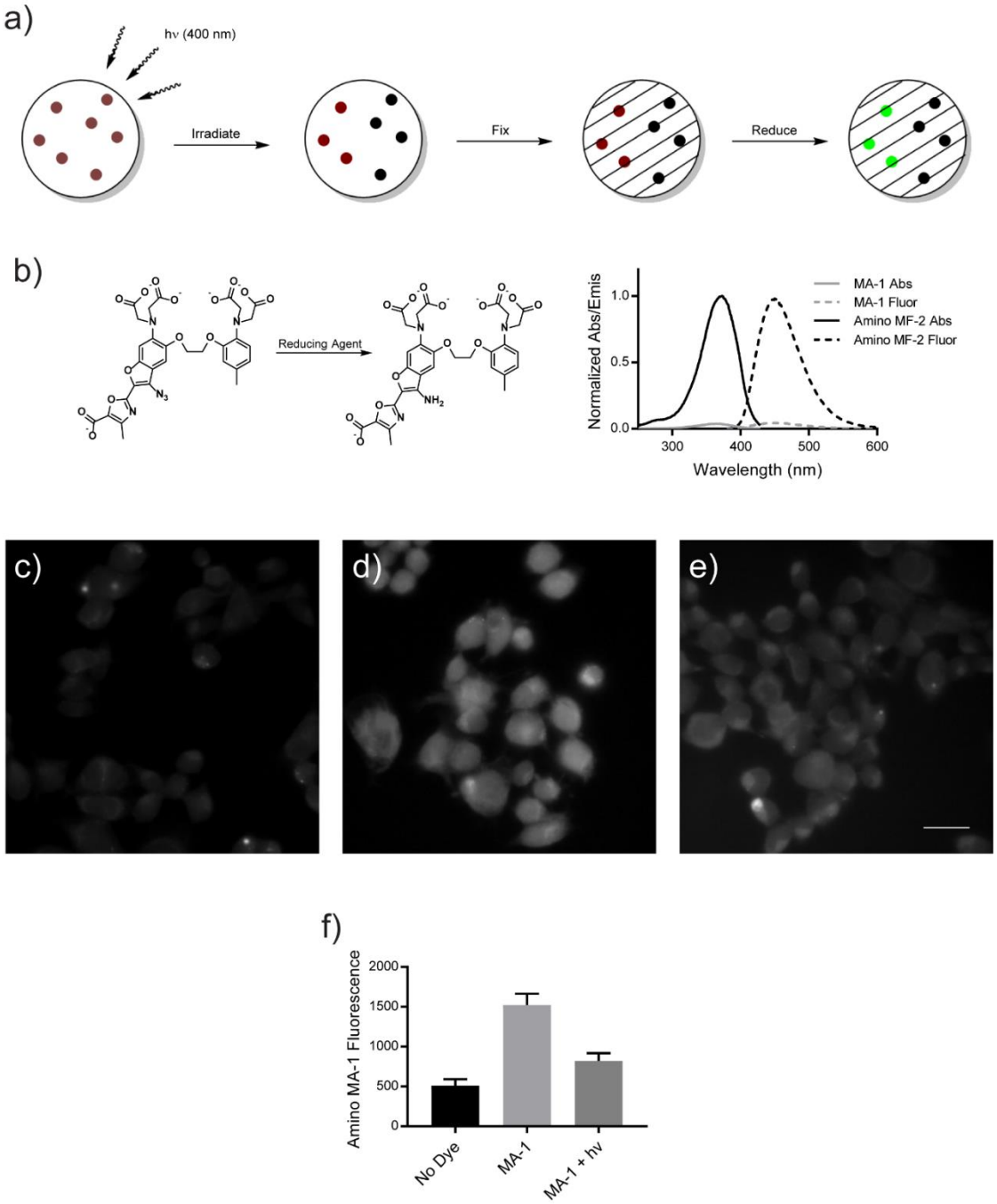

Figure 4-8: Reduction of MA-1 in HEK cells. (a) Schematic of the reduction workflow. Irradiation of MA-1 leads to two populations of HEK cells either containing intact MA-1 or not. The cells are then fixed with 3% PFA + 1% GA, reduced with 0.1% sodium borohydride, then imaged. (b) Reduction of MA-1 to amino MF-2 results in a 25-fold increase in fluorescence. Note that the small amount of MA-1 fluorescence may also be due to impurities (such as amino MF-2). (c) Fluorescence image of fixed HEK cells with no MA-1 present. A small amount of background fluorescence is observed, most likely from unreduced GA. (d) Fluorescence image of MA-1 loaded HEK cells shows they are 3-fold brighter than HEK cells in panel c. (e) Fluorescence image of MA-1 loaded HEK cells irradiated with 400 nm light prior to fixation. Illuminated HEK cells were nearly 2-fold dimmer than MA-1 loaded cells in panel b. Scale bar is 20 μm. (f) Quantification of fluorescence for panels c-e (n=5 per condition).

Figure 4-9: *Selective photolysis of MA-1 in neurons at high and low [Ca^{2+}]*

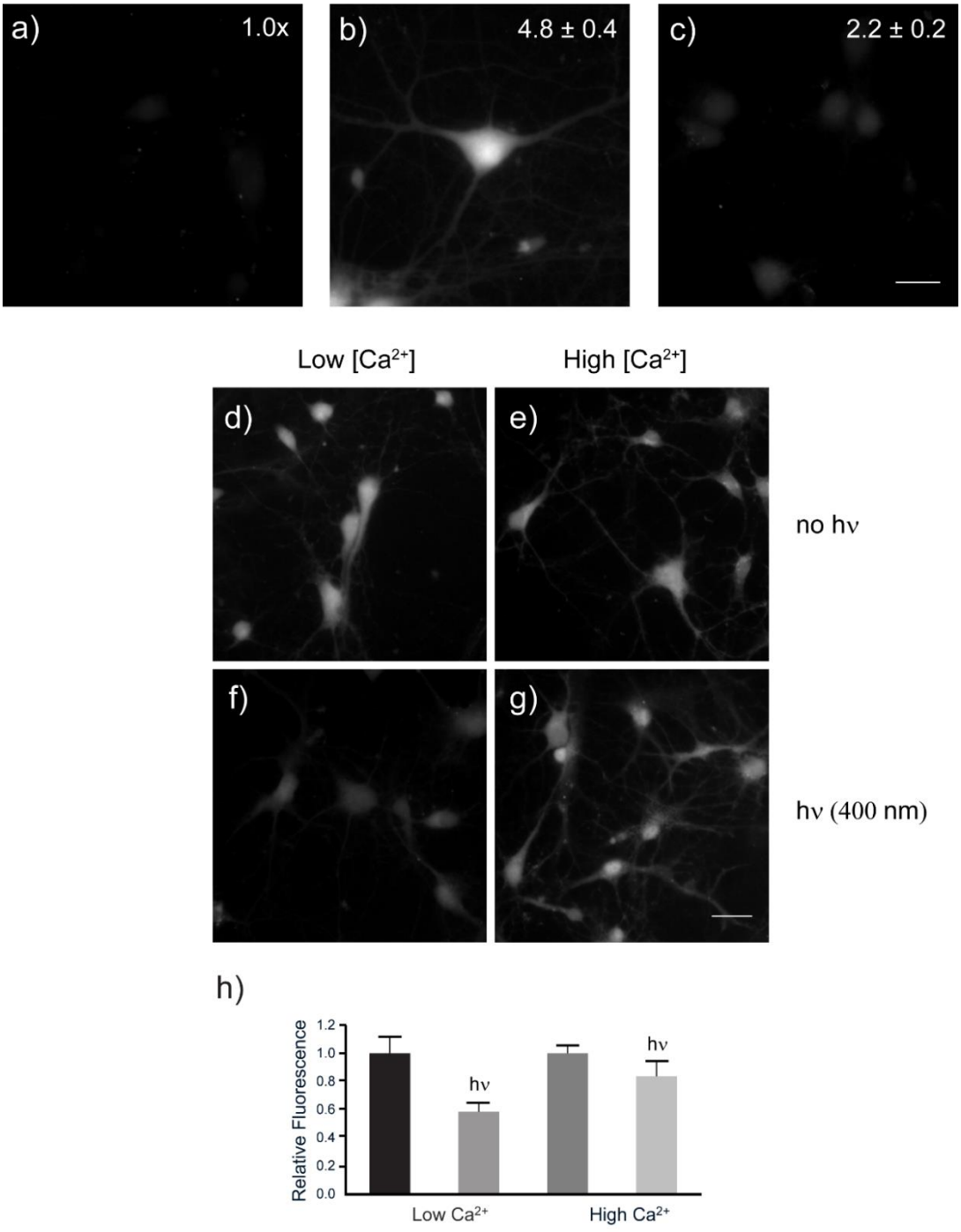

Figure 4-9: Reduction of MA-1 in cultured hippocampal neurons. (a-c) Fluorescence images of fixed neurons (3% PFA and 1% GA). Neurons which were not loaded with MA-1 (panel a) were significantly dimmer than MA-1 loaded neurons (panel b). Neurons which were loaded with MA-1, then irradiated with 400 nm light (panel c) were over 2-fold dimmer than neurons in panel b. (d-g) Fluorescence images of fixed neurons loaded with MA-1. Ionomycin was applied to neurons in panel e and g in order to increase intracellular Ca^{2+}. Neurons in panel f and g were irradiated with 400 nm light before fixation. (h) We found the application of light to neurons in the presence of high [Ca^{2+}] were brighter than neurons irradiated at low [Ca^{2+}].

Figure 4-10: *MA-1 reduces rapidly in cells*

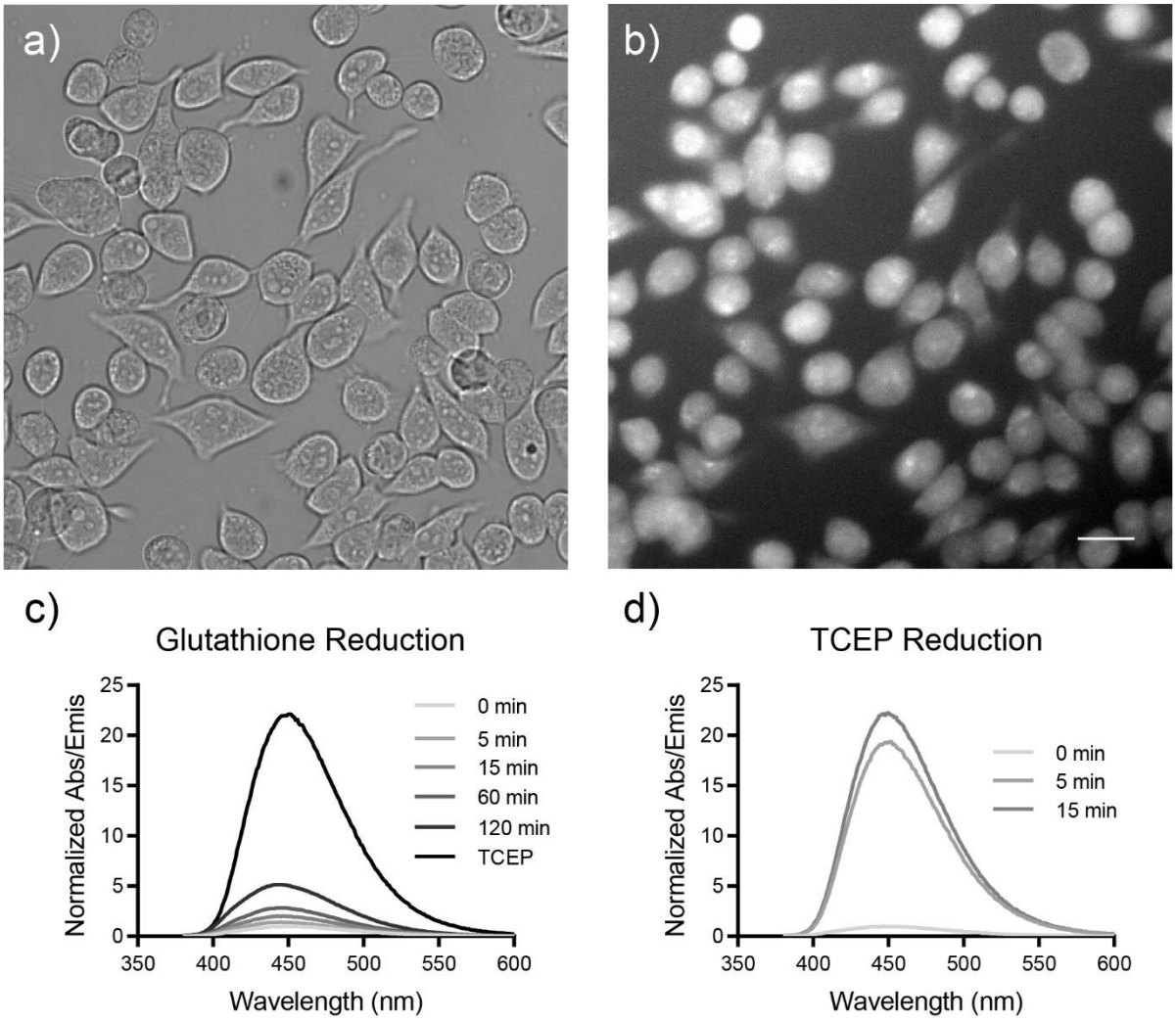

Figure 4-10: Reduction of MA-1 by cellular reductaces. (a) DIC image of cells loaded with MA-1-AM. (b) Fluorescence image of cells loaded with MA-1-AM. The observed fluorescence alludes to intracellular reduction of MA-1 to amino MF-2. (c) To evaluate the ability of intracellular reductants to reduce MA-1, 5 µM MA-1 pentapossium salt and 5 mM glutathione were mixed in PBS and the increase in fluorescence monitored. Significant reduction was seen after 2 h. Full reduction was achieved by the addition of TCEP. (d) MA-1 reduces rapidly in the presence of 5 mM TCEP.

References

(1) Lent, R.; Azevedo, F. a C.; Andrade-Moraes, C. H.; Pinto, A. V. O. How Many Neurons Do You Have? Some Dogmas of Quantitative Neuroscience under Revision. *Eur. J. Neurosci.* **2012**, *35* (1), 1–9.

(2) Ragan, T.; Kadiri, L. R.; Venkataraju, K. U.; Bahlmann, K. Serial Two-Photon Tomography: An Automated Method for Ex-Vivo Mouse Brain Imaging. *Nat Methods* **2012**, *9* (3), 255–258.

(3) Chung, K.; Wallace, J.; Kim, S.-Y.; Kalyanasundaram, S.; Andalman, A. S.; Davidson, T. J.; Mirzabekov, J. J.; Zalocusky, K. a; Mattis, J.; Denisin, A. K.; et al. Structural and Molecular Interrogation of Intact Biological Systems. *Nature* **2013**, *497* (7449), 332–337.

(4) Helmstaedter, M.; Briggman, K. L.; Turaga, S. C.; Jain, V.; Seung, H. S.; Denk, W. Connectomic Reconstruction of the Inner Plexiform Layer in the Mouse Retina. *Nature* **2013**, *500* (7461), 168–174.

(5) Takemura, S.; Bharioke, A.; Lu, Z.; Nern, A.; Vitaladevuni, S.; Rivlin, P. K.; Katz, W. T.; Olbris, D. J.; Plaza, S. M.; Winston, P.; et al. A Visual Motion Detection Circuit Suggested by Drosophila Connectomics. *Nature* **2013**, *500* (7461), 175–181.

(6) Scanziani, M.; Häusser, M. Electrophysiology in the Age of Light. *Nature* **2009**, *461* (7266), 930–939.

(7) Grynkiewicz, G.; Poenie, M.; Tsien, R. Y. A New Generation of Ca2+ Indicators with Greatly Impoved Fluorescence Properties. *J. Biol. Chem.* **1985**, *260* (6), 3440–3450.

(8) McCombs, J. E.; Palmer, A. E. Measuring Calcium Dynamics in Living Cells with Genetically Encodable Calcium Indicators. *Methods* **2008**, *46* (3), 152–159.

(9) Ye, H.; Liu, R.; Li, D.; Liu, Y.; Yuan, H.; Guo, W.; Zhou, L.; Cao, X.; Tian, H.; Shen, J.; et al. A Safe and Facile Route to Imidazole-1-Sulfonyl Azide as a Diazotransfer Reagent. *Org. Lett.* **2013**, *15* (1), 18–21.

(10) Venkatachalam, V.; Brinks, D.; Maclaurin, D.; Hochbaum, D.; Kralj, J.; Cohen, A. E. Flash Memory: Photochemical Imprinting of Neuronal Action Potentials onto a Microbial Rhodopsin. *J. Am. Chem. Soc.* **2014**, *136* (6), 2529–2537.

(11) Dujols, V.; Ford, F.; Czarnik, A. W. Communications to the Editor. *J. Am. Chem. Soc.* **1997**, *7863* (Ii), 7386–7387.

(12) Lippert, A. R.; Van de Bittner, G. C.; Chang, C. J. Boronate Oxidation as a Bioorthogonal Reaction Approach for Studying the Chemistry of Hydrogen Peroxide in Living Systems. *Acc. Chem. Res.* **2011**, *44* (9), 793–804.

(13) Yang, Y.-K.; Yook, K.-J.; Tae, J. A Rhodamine-Based Fluorescent and Colorimetric Chemodosimeter for the Rapid Detection of Hg2+ Ions in Aqueous Media. *J. Am. Chem. Soc.* **2005**, *127* (48), 16760–16761.

(14) Baskin, J. M.; Prescher, J. A.; Laughlin, S. T.; Agard, N. J.; Chang, P. V; Miller, I. A.; Lo, A.; Codelli, J. A.; Bertozzi, C. R. Copper-Free Click Chemistry for Dynamic in Vivo Imaging. *PNAS* **2007**, *104* (11), 16793–16797.

(15) Adams, S.; Lec-Ram, V.; Tsien, R. A New Caged Ca 2+, Azid-1, Is Far More Photosensitive than Nitrobenzyl-Based Chelators. *Chem. Biol.* **1997**, *4* (11), 867–878.

(16) Sletten, E. M.; Bertozzi, C. R. Bioorthogonal Chemistry: Fishing for Selectivity in a Sea of Functionality. *Angew. Chemie - Int. Ed.* **2009**, *48* (38), 6974–6998.

(17) Huang, B.; Babcock, H.; Zhuang, X. Breaking the Diffraction Barrier: Super-Resolution Imaging of Cells. *Cell* **2010**, *143* (7), 1047–1058.

(18) Lu, B.; Li, C.; Zhang, L. Gold-Catalyzed Highly Regioselective Oxidation of C-C Triple Bonds without Acid Additives: Propargyl Moieties as Masked α,β-Unsaturated Carbonyls. *J. Am. Chem. Soc.* **2010**, *132* (40), 14070–14072.

(19) Lee, J. C.; Lee, Y. C. Novel Direct Synthesis of Multi-Substituted Oxazoles from Ketones. *Bull. Korean Chem. Soc.* **2003**, *24* (7), 893–894.

(20) Etter, E. F.; Kuhn, M. a; Fay, F. S. Detection of Changes in Near-Membrane Ca2+ Concentration Using a Novel Membrane-Associated Ca2+ Indicator. *J. Biol. Chem.* **1994**, *269* (13), 10141–10149.

(21) Tsien, R. Y. A Non-Disruptive Technique for Loading Calcium Buffers and Indicators into Cells. *Nature*. April 9, 1981, pp 527–528.

(22) Smit, M. J.; Bloemers, S. M.; Leurs, R.; Tertoolen, L. G.; Bast, a; de Laat, S. W.; Timmerman, H. Short-Term Desensitization of the Histamine H1 Receptor in Human HeLa Cells: Involvement of Protein Kinase C Dependent and Independent Pathways. *Br. J. Pharmacol.* **1992**, *107* (2), 448–455.

(23) Nyffeler, P. T.; Liang, C.-H.; Koeller, K. M.; Wong, C.-H. The Chemistry of Amine-Azide Interconversion: Catalytic Diazotransfer and Regioselective Azide Reduction. *J. Am. Chem. Soc.* **2002**, *124* (36), 10773–10778.

(24) Liu, Q.; Tor, Y. Simple Conversion of Aromatic Amines into Azides. *Org. Lett.* **2003**, *5* (14), 2571–2572.
(25) Fischer, N.; Goddard-Borger, E. D.; Greiner, R.; Klapötke, T. M.; Skelton, B. W.; Stierstorfer, J. Sensitivities of Some Imidazole-1-Sulfonyl Azide Salts. *J. Org. Chem.* **2012**, *77* (4), 1760–1764.
(26) Higashiya, S.; Kaibarat, C.; Fukuoka, K.; Suda, F.; Ishikawa, M. A Facile Synthesis of 2-Azidoadenosine Derivatives from Guanosine as Photoaffinity Probes. *Bioorg. Med. Chem. Lett.* **1996**, *6* (1), 39–42.
(27) Chung, K.; Deisseroth, K. CLARITY for Mapping the Nervous System. *Nat. Methods* **2013**, *10* (6), 508–513.
(28) Takei, Y.; Murata, A.; Yamagishi, K.; Arai, S.; Nakamura, H.; Inoue, T.; Takeoka, S. Intracellular Click Reaction with a Fluorescent Chemical Ca2+ Indicator to Prolong Its Cytosolic Retention. *Chem. Commun. (Camb).* **2013**, *49* (66), 7313–7315.
(29) Tsien, R. Y.; Pozzan, T. Tsien 1989 Methods of Enzymol - Measurement of Cytosolic CA.Pdf. *Methods Enzym.* **1989**, *172* (230), 1989.
(30) McGuigan, J. A. S.; Luthi, D.; Buri, A. Calcium Buffer Solutions and How to Make Them: A Do It Yourself Guide. *Can. J. Physiol. Pharmacol.* **1991**, *69*, 1733–1749.
(31) Adam, S. R.; Kao, J. P. Y.; Grynkiewicz, G.; Minta, A.; Tsien, R. Y. Biologically Useful Chelators That Release Ca2 + upon Illumination +. **1988**, *152* (23), 3212–3220.
(32) Tsien, R. Y. New Calcium Indicators and Buffers with High Selectivity against Magnesium and Protons: Design, Synthesis and Properties of Prototype Structures. *Biochemistry* **1980**, *19*, 2396–2404.

Chapter 5:
Synthesis and Characterization of 6-Aminobenzofuran Photocages

Portions of this work were performed in collaboration with the following persons:
Synthesis was assisted by Morten Loehr
Synthesis was assisted by Kendall Wong

Abstract

We report the synthesis of a novel class of photocages based on a 6-aminobenzofuran scaffold. These **B**enzo**f**uran photo**c**ages (BFCs) operate through a photo-induced elimination reaction generating an extended azaquinone-methide from the excited state. Initial studies with N,N-diethylamino substituted BFC (BFC1) revealed BFCs are strong absorbers of UV/Violet light (λ_{max} = 365 nm, ε = 30,000 M^{-1} cm^{-1}) that readily photolyze ($\Phi_{photolysis}$ up to 0.18) and can cage both alcohols and carboxylic acids. In order to increase the water solubility of BFCs, we also synthesized a N,N-diacetic acid functionalized BFC (BFC2). We then showed a BFC2 caged glutamate could evoke [Ca^{2+}] increases in neurons upon illumination with laser light. Finally, we have synthesized a BFC incorporating the Ca^{2+} binding domain BAPTA (Fura-C) and are investigating its possible use as a small molecule Ca^{2+} integrator.

Introduction

The ability to release biologically active molecules in a controlled manner is essential for the study of neuronal systems. The most common method for achieving such control is through photolabile, or "caged", compounds (**Scheme 5-1a**).[1,2] Caged compounds are biologically inert until irradiated with a specific wavelength of light, which causes a photochemical reaction that releases the desired compound. Since light can be applied in a precise manner both spatially and temporally, cargo can be released to sub-cellular domains with millisecond precision.[3] Photocaged neurotransmitters, such as caged glutamates, are particularly powerful tools for studying neuronal dynamics with sub-cellular resolution.[4–6] Many caged neurotransmitters are based on ortho-nitrobenzyl or nitroindolinyl photocages that cleave efficiently with UV light. Unfortunately, these caged compounds tend to suffer from a combination of low water solubility, instability in aqueous solution and undesirable off-target effects, such as the blocking of GABA-A receptors.[7,8]

In addition to the delivery of biologically active molecules, the use of photocages to track cellular activity has recently gained attention.[9] Photolabile probes serve as a compliment to traditional indicators ("sensors") by functioning as chemical coincidence detectors, where both light and an analyte of interest must be present in order to promote an irreversible chemical change ("integrators"). This strategy is attractive as it grants the experimenter spatial and temporal control through the selective application of light. We were interested in applying such a strategy to develop a small-molecule neuronal activity tracer based on a Ca^{2+}-sensitive photocage (**Figure 5-1b**).[10] While voltage and Ca^{2+} indicators are useful for studying neuronal activity within small populations of neurons, they require continuous monitoring and high acquisition speeds, making them ill-suited for mapping large neuronal circuits across an entire brain. [10–12] A Ca^{2+} integrator could be used to instead take a "snapshot" of Ca^{2+} at the time of illumination, with *post hoc* examination of photolysis revealing the degree of activity during the period of illumination.

We initially attempted to develop such a Ca^{2+} integrator based on the photocaged Ca^{2+} source MethylAzid-1 (MA-1).[13] However, the system involved multiple labeling steps to visualize photolysis and was ill-suited for long term studies due to intracellular reduction of the key photolabile azide (**Chapter 4**). Inspired by the internal-charge transfer (ICT) fluorescence mechanism of MA-1 and 1,6 elimination-based prodrugs,[14–16] we hypothesized an alternative approach where excitation of the aminostilbene chromophore could release a caged compound through the formation of an extended azaquinone-methide (**Scheme 5-2b**). Similar to MA-1, we

hypothesized that the binding of Ca^{2+} would lead to a hypsochromatic shift in absorbance that would modulate the rate of photolysis in active vs. inactive neurons.[13,17]

Results and Discussion

Synthesis and Characterization of a N,N-diethylaminobenzofuran Photocage (BFC1)

Before attempting to synthesize a Ca^{2+}-sensitive photocage, we first synthesized a simpler N,N-diethylamino-substituted benzofuran (BFC1) to test our uncaging hypothesis. BFC1 was synthesized in high yield through a 3-step synthesis. A Knoevenagel condensation between 4-(diethylamino)salicylaldehyde and 4-(bromomethyl)benzaldehyde **1** afforded benzaldehyde-substituted benzofuran **2** (**Scheme 5-3b**). Benzofuran **2** is a strong absorber of blue light (λ_{max} = 395 nm, ε = 35,000 M^{-1} cm^{-1}) with yellow fluorescence typical of the Fura sensors (λ_{max} = 610 nm in DMSO, **Figure 5-1a**).[17] Reduction of **2** with sodium borohydride afforded the benzylic alcohol containing **3**, or BFC1, in 74% overall yield. BFC1 exhibited a similar absorbance profile to **2** (λ_{max} = 365 nm, ε = 30,000 M^{-1} cm^{-1}), but possessed a significantly blue-shifted fluorescence (λ_{max} = 440 nm, **Figure 5-1b**) due to the loss of electron-withdrawing group-enabled ICT. A hypsochromatic shift of 70 nm in absorbance was observed in acidic solutions (λ_{max} = 305 nm, ε_{305} = 45,000, **Figure 5-1c**), indicating the nitrogen lone pair is key to the spectral qualities of BFC1.

We next synthesized the caged nitrophenol **4** (BFC1-NP) from BFC1 and 4-nitrophenyl chloroformate (**Scheme 5-3**). While the absorbance of BFC1-NP was nearly identical to the parent photocage, BFC1-NP showed minimal fluorescence (**Figure 5-1d**). We were excited to see that irradiation with long-wave UV light from a handlamp (<30 seconds) resulted in the release of nitrophenol and a sharp increase in fluorescence (**Figure 5-1d,e**). We hypothesize the increase in fluorescence upon irradiation was the result of the reformation of BFC1 through nucleophilic addition of water to the methide. This was supported by LC-MS experiments which showed that photolyzing BFC1-NP in the presence of alcoholic solvents (MeOH, EtOH, *i*-PrOH) resulted in the formation of BFC1-ethers. We next measured the $\Phi_{photolysis}$ for BFC1-NP alongside the commonly used caged-glutamate MNI-glutamate.[3,18] These photolysis experiments revealed BFC1-NP had a nearly 3-fold greater $\Phi_{photolysis}$ than MNI-glutamate (0.18 vs 0.065, respectively, **Figure 5-2**).[19] When accounting for the 10-fold higher ε_{360} of BFC1-NP, BFC1-NP uncages nearly 30-fold faster per photon than MNI-glutamate.

Wanting to explore the potential substrate scope of BFC1, we synthesized a BFC1-protected nitrobenzoic acid **5** through an ester linkage (BFC1-NBA). UV-Vis and fluorometry experiments with BFC1-NBA revealed a nominal change in the absorption profile, but nearly complete loss of fluorescence (**Figure 5-1f**). Subjection of BFC-NBA to UV-light showed the release of nitrobenzoic acid, but the $\Phi_{photolysis}$ was much lower than for BFC-NP (approximately 100-fold lower), making the measurement of $\Phi_{photolysis}$ difficult with our current methodology. The slow rate of photolysis of BFC1-NBA suggests leaving group ability is an important factor for determining the $\Phi_{photolysis}$. This is in agreement with our proposed photo-induced elimination mechanism, as a better leaving group promotes faster photocleavage and impedes ion pair recombination.[2,20] In order to determine if BFC1 could be used to protect biologically relevant molecules, we synthesized the BFC1 caged glutamate **7** (BFC1-glutamate, **Scheme 5-3b**). While UV-Vis studies showed similar uncaging properties to BFC1-NBA, the caged glutamate was insoluble in aqueous buffers, preventing its use for cellular experiments.

Synthesis of Water Soluble Benzofuran Photocage BFC2

In order to improve the water solubility of BFC1, we synthesized an N,N-diacetic acid substituted BFC **18** (BFC2). The diacetic acid moiety of BFC2 was chosen due to its structural similarity to BAPTA, making it a good model compound for the eventual development of a Ca^{2+}-sensitive BFC. Two different synthetic routes to BFC2 were pursued, employing either ethyl or *t*-butyl ester protected diacetic acids (**Scheme 5-4**). Ethyl ester protected BFC2 **16** was saponified in order to evaluate its performance in aqueous solution. BFC2 showed absorption and emission profiles similar to BFC1 (λ_{max} = 350 nm, ε_{350} = 20,000 M^{-1} cm^{-1}) and was much more water soluble (**Figure 5-1g**, **Table 5-1**). We then attempted to synthesize BFC2-caged glutamate **20** (BFC2-glutamate), but the presence of free carboxylates complicated the HATU-mediated coupling and made purification difficult. We also attempted to generate BFC2-glutamate from the *t*-butyl ester protected BFC2 **17**, which allowed for a global deprotection of both the photocage and glutamate (**Scheme 5-4**). Unfortunately, the highly acidic deprotection conditions typical for the removal of *t*-butyl groups resulted in the decomposition of BFC2. While we are actively working to optimize the synthesis and purification of BFC2-glutamate, we decided to perform preliminary *in vivo* uncaging experiments with impure BFC2-glutamate. BFC2-glutamate was applied to cultured hippocampal neurons loaded with Oregon Green BAPTA (OGB) and irradiated with a burst of 405 nm laser light. This resulted in a 30% increase in OGB fluorescence, indicative of glutamate release and binding to synaptic receptors (**Figure 5-3**).

Progress Towards the BAPTA-substituted Photocage Fura-C

Having demonstrated the utility of the BFC scaffold to cage small molecules, we looked to develop a Ca^{2+} sensitive version of the photocage for use as a Ca^{2+} integrator. Since the design of BFCs was inspired by Fura-1, incorporation of the photocage into a BAPTA scaffold was straightforward.[17] Salicylaldehyde **21** was first alkylated with **1**, then cyclized through a Knoevenagel condensation to afford the aldehyde-substituted **23**. Reduction with sodium borohydride provided the ethyl-ester protected photocage **24** in 22% yield over 3 steps. Deprotection of the BAPTA moiety through saponification of the ethyl esters afforded the final photocage **25**, which we dubbed Fura-C. We first validated that Fura-C was Ca^{2+}-sensitive through a Ca^{2+} titration. We were happy to find Fura-C undergoes a 20 nm hypsochromatic shift upon binding Ca^{2+} (λ_{max} $[Ca^{2+}]_{free}$ = 345 nm, λ_{max} $[Ca^{2+}]_{bound}$ = 325 nm), with only a minor shift in its fluorescence spectrum (**Figure 5-1h**). A Ca^{2+} titration then revealed Fura-C has a K_d = 85 nM, making it a tight binder of Ca^{2+} similar to Fura-1 (K_d = 107 nM, **Figure 5-1i**). Current work is now focused on synthesizing Fura-C-caged compounds in order to measure the rate of photolysis in high and low $[Ca^{2+}]$ with 400 nm irradiation.

Conclusion

In summary, we report novel 6-aminobenzofuran photocages (BFCs) which operate through a photo-induced elimination reaction. Initial spectroscopic studies with BFCs revealed they possessed large extinction coefficients (ε_{350}=20,000-30,000 M^{-1} cm^{-1}) and high rates of photolysis ($\Phi_{photolysis}$ up to 0.18). BFCs are are able to cage compounds through carbonate and ester linkages and display increased water solubility with the incorporation of N,N-diacetic acids. Finally, we synthesized a Ca^{2+}-sensitive BFC, Fura-C, which we hope will enable Ca^{2+} integration

and neuronal activity mapping. In order to expand upon these initial results, we are interested in optimizing the synthetic route to water-soluble BFCs, in particular by carrying out the deprotection of the N,N-diacetic acids after formation of the photolabile bond. We are also interested in exploring other possible BFC leaving groups, such as halides, alcohols (through ethers) and amines (through carbamates). In order to develop a Ca^{2+} integrator, we ultimately wish to synthesize a Fura-C caged reporter (e.g. a fluorescein or coumarin) that can be delivered intracellularly through incorporation of acetoxymethyl esters into the protected BAPTA moiety.

Experimental Section

General Method for Chemical Synthesis and Characterization

Chemical reagents and solvents (dry) were purchased from commercial suppliers and used without further purification. Compounds **1** and **21** was prepared as previously reported.[17,21] Thin layer chromatography (TLC) (Silicycle, F254, 250 μm) and preparative thin layer chromatography (PTLC) (Silicycle, F254, 1000 μm) was performed on glass backed plates pre-coated with silica gel and were visualized by fluorescence quenching under UV light. Flash column chromatography was performed on Silicycle Silica Flash F60 (230–400 Mesh) using a forced flow of air at 0.5–1.0 bar. NMR spectra were measured on Bruker AVB-400 MHz, 100 MHz, AVQ-400 MHz, 100 MHz, Bruker AV-600 MHz, 150 MHz. NMR spectra measured on Bruker AVII-900 MHz, 225 MHz, equipped with a TCI cryoprobe accessory, were performed by Dr. Jeffrey Pelton (QB3). Variable temperature NMR experiments were measured on the Bruker AV-600 with the assistance of Hasan Celik. Chemical shifts are expressed in parts per million (ppm) and are referenced to $CDCl_3$ (7.26 ppm, 77.0 ppm) or DMSO (2.50 ppm, 40 ppm). Coupling constants are reported as Hertz (Hz). Splitting patterns are indicated as follows: s, singlet; d, doublet; t, triplet; q, quartet, dd, doublet of doublet; m, multiplet. High-resolution mass spectra (HR-ESI-MS) were measured by the QB3/Chemistry mass spectrometry service at University of California, Berkeley. High performance liquid chromatography (HPLC) and low resolution ESI Mass Spectrometry were performed on an Agilent Infinity 1200 analytical instrument coupled to an Advion CMS-L ESI mass spectrometer. The column used for the analytical HPLC was Phenomenex Luna C18(2) (4.6 mm I.D. × 150 mm) with a flow rate of 1.0 mL/min. The mobile phases were MQ-H_2O with 0.05% formic acid (eluent A) and HPLC grade acetonitrile with 0.05% formic acid (eluent B). Signals were monitored at 254, 340 and 545 nm over 20 min with a gradient of 10-100% eluent B. The column used for semi-preparative HPLC was Phenomenex Luna 5μ C18(2) (10 mm I.D. x 150 mm) with a flow rate of 5.0 mL/min. The mobile phases were MQ-H_2O with 0.05% formic acid (eluent A) and HPLC grade acetonitrile with 0.05% formic acid (eluent B). Signals were monitored at 254 over 20 min with a gradient of 10-100% eluent B.

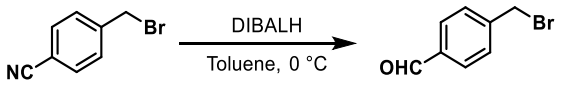

1

Synthesis of (4-(bromomethyl)benzaldehyde, 1:
A round-bottom flask was charged with 4-(bromomethyl)benzonitrile (6.00 g, 30.6 mmol) and anhydrous toluene (60 mL). The reaction was cooled to 0 °C, then diisobutylaluminum hydride (1 M in hexanes, 39.8 mL, 39.8 mmol) was added dropwise by syringe and the reaction stirred for 1 h. The reaction was quenched by the slow addition of 1 M hydrochloric acid (300 mL) at 0 °C and the reaction was left to warm to 22 °C with stirring for 12 h. The reaction was poured into a separatory funnel and the organics collected. The aqueous layer was washed with toluene (1 x 100 mL), then the combined organics were dried with anhydrous magnesium sulfate, filtered and the solvent removed *in vacuo* to afford **1** as a colorless crystalline solid (5.44 g, 27.3 mmol, 90%). ^{1}H NMR (400 MHz, $CDCl_3$) δ 10.02 (s, 1H), 7.91 – 7.84 (m, 2H), 7.60 – 7.54 (m, 2H), 4.52 (s, 2H).

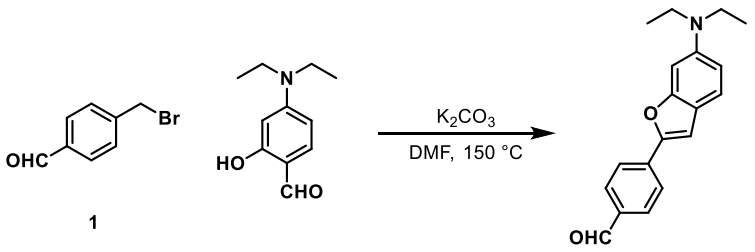

1 2

Synthesis of 2:
A round-bottom flask was charged with **1** (100.0 mg, 0.502 mmol), 4-(diethylamino)salicylaldehyde (107 mg, 0.553 mmol), anhydrous potassium carbonate (347 mg, 2.51 mmol). Anhydrous DMF (6 mL) was added and the reaction stirred at 150 °C for 12 h. The reaction was cooled to 22 °C, then poured over dilute hydrochloric acid (50 mL) and extracted with ethyl acetate (3 x 50 mL). The combined organics were dried with anhydrous magnesium sulfate, filtered and the solvent removed *in vacuo* affording **2** as an orange solid (126 mg, 0.429 mmol, 86%). ^{1}H NMR (400 MHz, $CDCl_3$) δ 10.03 (s, 1H), 7.94 (s, 3H), 7.12 (d, J = 0.9 Hz, 1H), 6.86 – 6.80 (m, 1H), 6.75 (dd, J = 8.7, 2.3 Hz, 1H), 3.46 (t, J = 7.1 Hz, 3H), 1.26 (t, J = 7.1 Hz, 5H). Analytical HPLC retention time 9.71 min; MS (ESI) exact mass for $C_{19}H_{20}NO_2^+$ $[M+H]^+$ calcd: 294.1 found: 294.1.

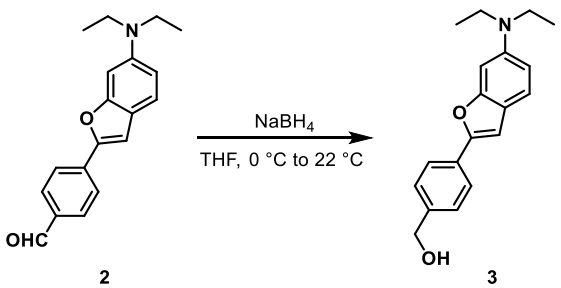

2 3

Synthesis of 3:

A round-bottom flask was charged with **2** (100.0 mg, 0.341 mmol) and anhydrous THF (5 mL), then cooled to 0 °C. Sodium borohydride (51.6 mg, 1.36 mmol) was added portion wise to the stirring solution and the reaction warmed to 22 °C and stirred for 8 h. The reaction was diluted with water (25 mL) and extracted with ethyl acetate (3 x 25 mL). The combined organics were dried with anhydrous sodium sulfate, filtered and the solvent removed *in vacuo*. The remaining crude material was purified by flash chromatography (35% ethyl acetate in hexanes, isocratic) affording **3** as a pale yellow solid (95 mg, 0.321 mmol, 94%).^{1}H NMR (400 MHz, $CDCl_3$) δ 7.82 (d, *J* = 8.2 Hz, 2H), 7.45 (d, *J* = 8.0 Hz, 2H), 7.41 (d, *J* = 8.6 Hz, 1H), 6.94 (s, 1H), 6.86 (d, *J* = 2.7 Hz, 1H), 6.74 (dd, *J* = 8.7, 2.3 Hz, 1H), 4.76 (s, 2H), 3.46 (q, *J* = 7.1 Hz, 4H), 1.25 (t, *J* = 7.1 Hz, 6H). Analytical HPLC retention time 4.31 min; MS (ESI) exact mass for $C_{19}H_{22}NO_2^+$ $[M+H]^+$ calcd: 296.2 found: 296.2; HR-ESI-MS m/z for $C_{19}H_{22}NO_2^+$ $[M+H]^+$ calcd: 296.1645 found: 296.1641.

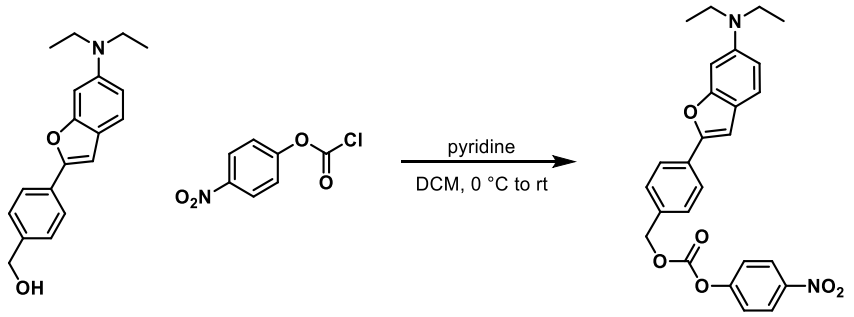

3 4

Synthesis of 4:

This reaction was performed under 500 nm lights. A round-bottom flask was charged with **3** (40.0 mg, 135 μmol) and anhydrous DCM (2 mL), then cooled to 0 °C. A solution of 4-nitrophenylchloroformate (41.0 mg, 203 μmol) in anhydrous DCM (2 mL) was added dropwise and the solution stirred for 1 h at 0 °C, then warmed to 22 °C and stirred for an additional 3 h. The solvent was removed *in vacuo* and the remaining residue purified by flash chromatography (35% ethyl acetate in hexanes, isocratic) affording **4** as a pale-yellow solid (7.2 mg, 15.6 μmol, 12%). Analytical HPLC retention time 12.56 min; MS (ESI) exact mass for $C_{26}H_{25}N_2O_6^+$ $[M+H]^+$ calcd: 461.2 found: 461.1.

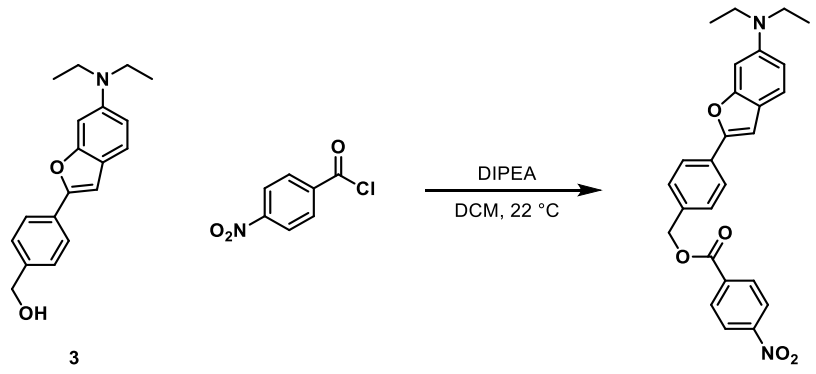

3 5

Synthesis of 5:

This reaction was performed under 500 nm lights. A round-bottom flask was charged with **3** (15.0 mg, 50.8 μmol), then anhydrous DCM (2 mL), diisopropylethylamine (10.6 uL, 61 μmol) and 4-nitrobenzoyl chloride (10.4 mg, 55.9 μmol) were added and the reaction stirred at 22 °C for 12 h. The reaction was diluted with DCM (10 mL) and washed with 0.5 M hydrochloric acid (2 x 20 mL). The combined organics were dried with anhydrous sodium sulfate, filtered and the solvent removed *in vacuo*. The remaining solid was triturated with hexanes, then collected by vacuum filtration affording **5** as a grey solid (2.9 mg, 6.5 μmol, 13%). ^{1}H NMR (400 MHz, $CDCl_3$) δ 8.31 (q, *J* = 8.9 Hz, 4H), 7.85 (d, *J* = 8.3 Hz, 2H), 7.53 (d, *J* = 8.3 Hz, 2H), 7.42 (d, *J* = 8.6 Hz, 1H), 6.97 (s, 1H), 6.86 (d, *J* = 2.2 Hz, 1H), 6.74 (dd, *J* = 8.7, 2.2 Hz, 1H), 5.46 (s, 2H), 3.46 (q, *J* = 7.1 Hz, 4H), 1.25 (t, *J* = 7.0 Hz, 6H); Analytical HPLC retention time 7.49 min; MS (ESI) exact mass for $C_{26}H_{25}N_2O_5^+$ $[M+H]^+$ calcd: 445.2 found: 445.3; HR-ESI-MS m/z for $C_{26}H_{25}N_2O_5^+$ $[M+H]^+$ calcd: 445.1758 found: 445.1752.

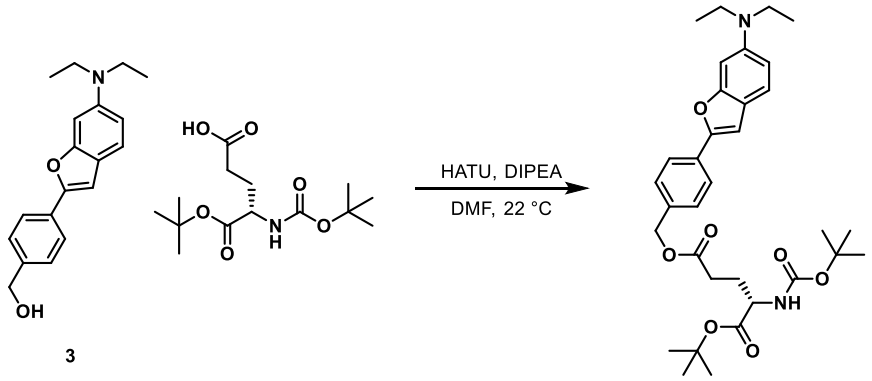

3 6

Synthesis of 6:

This reaction was performed under 500 nm lights. A round-bottom flask was charged with Boc-L-glutamic acid α-*tert*-butyl ester (455.0 mg, 1.50 mmol) and HATU (570.4 mg, 1.50 mmol). Anhydrous DMF (10 mL) and diisopropylethylamine (348 uL, 2.00 mmol) were added via syringe and the reaction stirred for 2 h. Benzyl alcohol **3** (295.4 mg, 1.00 mmol) was then added portion-wise and the reaction stirred at 22 °C for 12 h. The solvent was removed *in vacuo* and the remaining residue was purified by flash chromatography (35% ethyl acetate in hexanes, isocratic) affording **6** as a pale yellow solid (432 mg, 0.744 mmol, 74%). ^{1}H NMR (400 MHz, $CDCl_3$) δ 7.81 (d, *J* = 7.5 Hz, 2H), 7.43 (m, 3H), 6.95 (s, 1H), 6.86 (br, 1H), 6.74 (d, *J* = 8.9 Hz, 1H), 5.18 (m, 2H), 5.12 (d, *J* = 8.2 Hz, 1H), 4.27 (m, 1H), 3.45 (m, 4H), 2.63 – 2.39 (m, 2H), 2.23 (m, 1H), 1.97 (td, *J* = 14.4, 8.5 Hz, 1H), 1.50 (s, 9H), 1.48 (s, 9H), 1.25 (t, *J* = 7.0 Hz, 4H); Analytical HPLC retention time 9.44 min; MS (ESI) exact mass for $C_{33}H_{44}N_2O_7^+$ $[M+H]^+$ calcd: 581.3 found: 581.5.

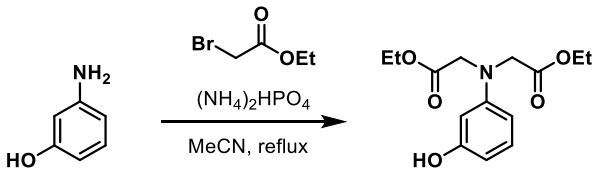

8

Synthesis of 8:

A round-bottom flask was charged with 3-aminophenol (5.46 g, 50.0 mmol), diammonium phosphate (6.60 g, 50.0 mmol) and sodium iodide (3.00 g, 20.0 mmol) were dissolved in 50 mL acetonitrile. Ethyl bromoacetate (10.1 mL, 100 mmol) was added slowly, whereupon a white precipitate formed. The reaction mixture was heated to reflux and stirred for 13 h. The reaction was cooled and the solvent removed *in vacuo*. The remaining residue was diluted with acetone and filtered through a diatomaceous earth plug. The combined organics were concentrated *in vacuo* and the remaining brown oil was purified by flash chromatography (20% acetone in hexanes, isocratic) affording **8** as a brown oil (6.13 g, 21.8 mmol, 43%). ^{1}H NMR (400 MHz, $CDCl_3$) δ 7.05 (t, *J* = 8.2 Hz, 1 H), 6.25 (dd, *J* = 7.9, 2.3 Hz, 1 H), 6.17 (d , *J* = 9.2 Hz, 1 H), 6.11 (t, *J* = 2.4 Hz, 1H), 21 4.93 (bs, 1H), 4.21 (q, *J* = 7.1 Hz, 4H), 4.10 (s, 4H), 1.28 (t, *J* =7.2 Hz, 6H).

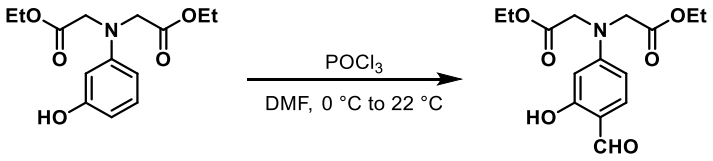

8 10

Synthesis of 10:

A round-bottom flask was charged with anhydrous DMF (40 mL) and cooled to 0 °C. Phosphoryl chloride (3.2 mL, 35.2 mmol) was added dropwise and the solution stirred for 30 minutes. A solution of **8** (4.95 g, 17.6 mmol) in anhydrous DMF (10 mL) was added dropwise and the reaction stirred at 22 °C for 20 h. The reaction mixture was poured over a mixture of ice and saturated potassium carbonate, producing a white solid. The solid was collected by vacuum filtration, washing with water to afford **10** as a white solid (2.11 g, 6.82 mmol, 39%). ^{1}H NMR (400 MHz, $CDCl_3$) δ 11.48 (s, 1H), 9.59 (s, 1H), 7.34 (d, *J* = 8.8 Hz, 1H), 6.22 (dd, *J* = 8.8, 2.5 Hz, 1H), 6.06 (d, *J* = 2.5 Hz, 1H), 4.24 (q, *J* = 7.1 Hz, 4H), 4.17 (s, 4H), 1.29 (t, *J* = 7.1 Hz, 6H).

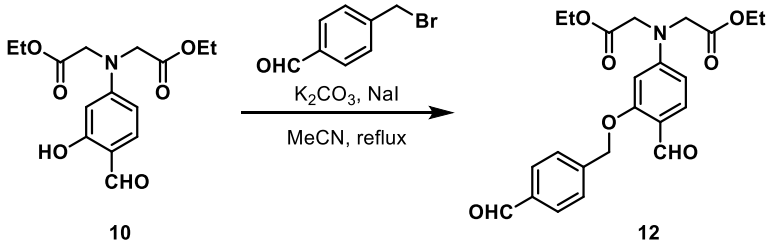

10 12

Synthesis of 12:

A round-bottom flask was charged with **10** (2.00 g, 6.47 mmol) 4-(bromomethyl)benzaldehyde **1** (1.54 g, 7.76 mmol), potassium carbonate (1.79 g, 12.9 mmol) and sodium iodide (388 mg, 2.59 mmol). Anhydrous acetonitrile (30 mL) was added and the reaction stirred at reflux for 5 h. The reaction was cooled, filtered and then concentrated *in vacuo*. The remaining residue was purified by flash chromatography (20% acetone in hexanes, isocratic) affording **12** as a pale-yellow solid (222 mg, 0.54 mmol, 46%). ^{1}H NMR (400 MHz, $CDCl_3$) δ 10.00 (s, 1H), 7.92 (s, 4H), 7.44 (d, *J* = 8.6 Hz, 1H), , 7.09 (d, *J* = 0.9 Hz, 1H), 6.78 (d, *J* = 2.2 Hz, 1H), 6.63 (dd, *J* = 8.6, 2.4 Hz), 4.25 (q, *J* = 7.2 Hz, 4H), 4.21 (s, 4H), 1.31 (t, *J* = 7.1 Hz, 6H); Analytical HPLC retention time 14.13 min; MS (ESI) exact mass for $C_{23}H_{26}NO_7^+$ $[M+H]^+$ calcd: 428.5 found: 428.4.

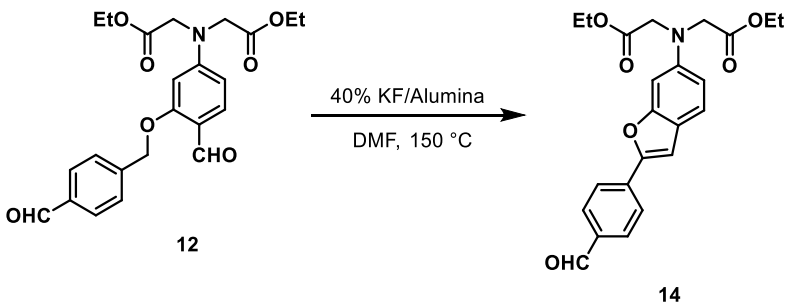

12 14

Synthesis of 14:

A round-bottom flask was charged with **12** (500 mg, 1.17 mmol) and 40% KF/Alumina (500 mg). The flask was sealed and evacuated/backfilled with nitrogen (3x). Anhydrous DMF (20 mL) was added via syringe and the reaction stirred at 150 °C for 2 h. The reaction was cooled, then poured over dilute hydrochloric acid (30 mL). The aqueous layer was then extracted with DCM (3 x 30 mL) and the combined organics dried with anhydrous magnesium sulfate, filtered and the solvent removed *in vacuo*. The remaining residue was then purified by flash chromatography (20% acetone in hexanes, isocratic) affording **14** as a pale-yellow solid (222 mg, 0.54 mmol, 46%). ^{1}H NMR (400 MHz, $CDCl_3$) δ 10.00 (s, 1H), 7.92 (s, 4H), 7.44 (d, *J* = 8.6 Hz, 1H), , 7.09 (d, *J* = 0.9 Hz, 1H), 6.78 (d, *J* = 2.2 Hz, 1H), 6.63 (dd, *J* = 8.6, 2.4 Hz), 4.25 (q, *J* = 7.2 Hz, 4H), 4.21 (s, 4H), 1.31 (t, *J* = 7.1 Hz, 6H); Analytical HPLC retention time 9.44 min MS (ESI) exact mass for $C_{23}H_{24}NO_6^+$ $[M+H]^+$ calcd: 410.2 found: 410.4.

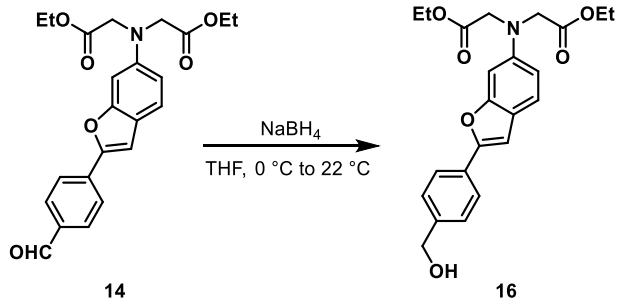

14 16

Synthesis of 16:

A round-bottom flask was charged with **14** (150.0 mg, 0.366 mmol) and anhydrous THF (5 mL), then cooled to 0 °C. Sodium borohydride (23.1 mg, 0.611 mmol) was added portion wise to the stirring solution and the reaction warmed to 22 °C and stirred for 8 h. The solvent was removed *in vacuo* and the remaining crude material was purified by flash chromatography (20% acetone in hexanes, isocratic) affording **16** as a white solid (96 mg, 0.233 mmol, 64%).^{1}H NMR (400 MHz, $CDCl_3$) δ 7.77 (d, *J* = 8.3 Hz, 2H), 7.43 - 7.35 (m, 3H), 6.89 (d, *J* = 0.9 Hz, 1H), 6.78 (d, *J* = 2.3 Hz, 1H), 6.60 (dd, *J* = 8.6 , 2.3 Hz, 1H), 4.71 (s, 2H), 4.24 (q, *J* = 7.1 Hz, 4H), 4.20 (s, 4H), 1.30 (t, *J* = 7.1 Hz, 6H); Analytical HPLC retention time 7.70 min; MS (ESI) exact mass for $C_{23}H_{26}NO_6^+$ $[M+H]^+$ calcd: 412.2 found: 412.4; HR-ESI-MS m/z for $C_{23}H_{25}NaNO_6^+$ $[M+Na]^+$ calcd: 434.1574 found: 434.1573.

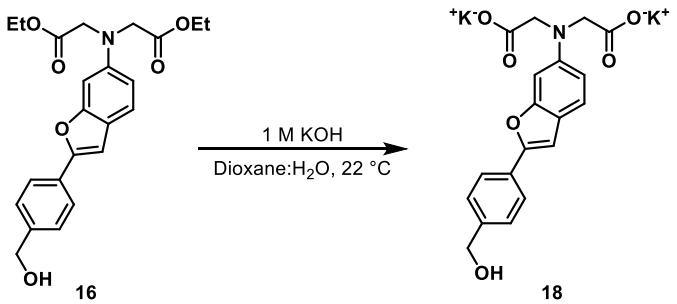

Synthesis of 18:
A vial was charged with **16** (50.0 mg, 122 μmol), dioxane (2 mL) and water (1 mL). A 1 M solution of potassium hydroxide was added (1.22 mL, 1.22 mmol) and the reaction stirred for 20 h at 22 °C. The reaction was acidified by addition of hydrochloric acid (2 M) and the resulting white solid collected by vacuum filtration and washed with water, affording **18** as an off-white solid (35.0 mg, 99 μmol, 82%). ^{1}H NMR (400 MHz, DMSO-d$_6$) δ 7.76 (d, *J* = 8.2 Hz, 2H), 7.36 (d, *J* = 9.1 Hz, 2H), 7.19 (s, 1H), 6.65 (d, *J* = 2.2 Hz, 1H), 6.50 (dd, *J* = 8.7 Hz, 2.3 Hz, 1H), 5.21 (bs, 1H), 4.49 (s, 2H), 4.13 (s, 4H); Analytical HPLC retention time 5.04 min; MS (ESI) exact mass for $C_{19}H_{18}NO_6^+$ $[M+H]^+$ calcd: 356.1 found: 356.1; HR-ESI-MS m/z for $C_{19}H_{16}NO_6^-$ $[M-H]^-$ calcd: 354.0983 found: 354.0990.

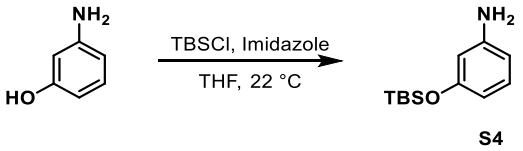

Synthesis of S4:
A round-bottom flask was charged with aminophenol (4.00 g, 36.65 mmol), imidazole (4.00 g, 58.76 mmol) and anhydrous THF (100 mL). TBSCl (7.18 g, 47.74 mmol) was added portion-wise and the reaction stirred at 22 °C for 16 h. The reaction was poured over water (300 mL) and extracted with diethyl ether (2 x 50 mL). The combined organics were dried with anhydrous magnesium sulfate, filtered and the solvent removed *in vacuo*. The remaining residue was purified by flash chromatography (30% ethyl acetate in hexanes, isocratic) affording **S4** as a colorless oil (8.78 g, 107%). ^{1}H NMR (300 MHz, CDCl$_3$) δ 6.98 (t, *J* = 8.0 Hz, 1H), 6.27 (m, 2H), 6.19 (t, *J* = 2.2 Hz, 1H), 3.59 (s, 2H), 0.97 (s, 9H), 0.18 (s, 6H).

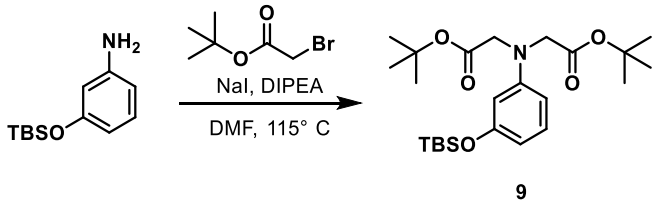

Synthesis of 9:
A round-bottom flask was charged with 3-((tert-butyldimethylsilyl)oxy)aniline (2.23 g, 10.0 mmol), sodium iodide (1.50 g, 9.98 mmol), anhydrous DMF (25 mL) and diisopropylethylamine (14.8 mL, 49.9 mmol). *Tert*-butyl bromoacetate (6.82 g, 34.94 mmol) was added and the vial flushed with nitrogen, sealed, and stirred at 115 °C for 24 h. The reaction was cooled and filtered through diatomaceous earth. The combined organics were diluted with ethyl acetate (150 mL) and

washed with dilute hydrochloric acid (3 x 125 mL), dried with anhydrous magnesium sulfate and the solvent removed *in vacuo*. The remaining residue was purified by flash chromatography (5% ethyl acetate in hexanes, isocratic) affording **9** as a yellow oil (3.31 g, 7.33 mmol, 73%). ^{1}H NMR (400 MHz, $CDCl_3$) δ 7.04 (t, *J* = 8.0 Hz, 1H), 6.26 (ddd, *J* = 8.0, 2.2, 0.8 Hz, 1H), 6.19 (ddd, *J* = 8.3, 2.6, 0.8 Hz, 1H), 6.07 (t, *J* = 2.3 Hz, 1H), 3.97 (s, 4H), 1.46 (s, 18H), 0.97 (s, 9H), 0.18 (s, 6H).

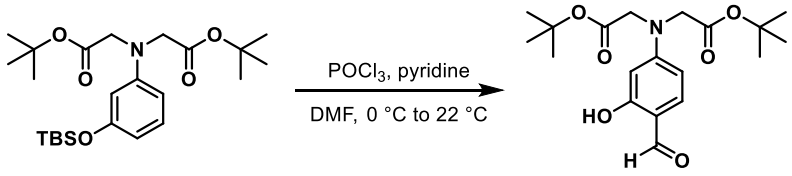

8 11

Synthesis of 11:
A round-bottom flask was charged with **9** (500 mg, 1.11 mmol), anhydrous DMF (5 mL) and pyridine (366 uL, 4.54 mmol), then cooled to 0 °C while stirring. $POCl_3$ (411 uL, 4.43 mmol) was added dropwise and the reaction warmed to 22 °C and stirred for 8 h. The reaction was poured over ice, then neutralized with 1 M sodium hydroxide. The aqueous layer was extracted with ethyl acetate (4 x 50 mL) and the combined organics dried with anhydrous magnesium sulfate, filtered and the solvent removed *in vacuo*. The remaining residue was purified by flash chromatography (20-35% ethyl acetate in hexanes, linear gradient) affording **11** as a white solid (294 mg, 0.613 mmol, 73%). ^{1}H NMR (400 MHz, $CDCl_3$) δ 11.52 (s, 1H), 9.62 (s, 1H), 7.37 (d, *J* = 8.7 Hz, 1H), 6.23 (dd, *J* = 8.7, 2.5 Hz, 1H), 6.07 (d, *J* = 2.4 Hz, 1H), 4.09 (s, 4H), 1.52 (s, 18H).

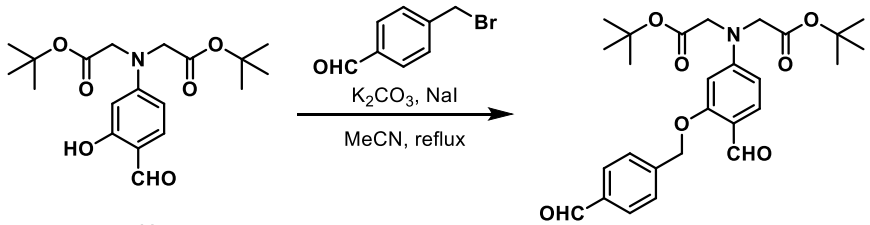

11 13

Synthesis of 13:
A round-bottom flask was charged with **11** (305.0 mg, 0.835 mmol) 4-(bromomethyl)-benzaldehyde **1** (199.4 mg, 1.00 mmol), potassium carbonate (230.7 mg, 1.67 mmol) and sodium iodide (50.4 mg, 0.334 mmol). Anhydrous acetonitrile (15 mL) was added and the reaction stirred at reflux for 12 h. The reaction was cooled, diluted with ethyl acetate (100 mL) and washed with water (75 mL) and brine (75 mL). The combined organics were dried with anhydrous magnesium sulfate, filtered and the solvent removed *in vacuo* affording crude **13** as a brown oil which was used for the next reaction without further purification.

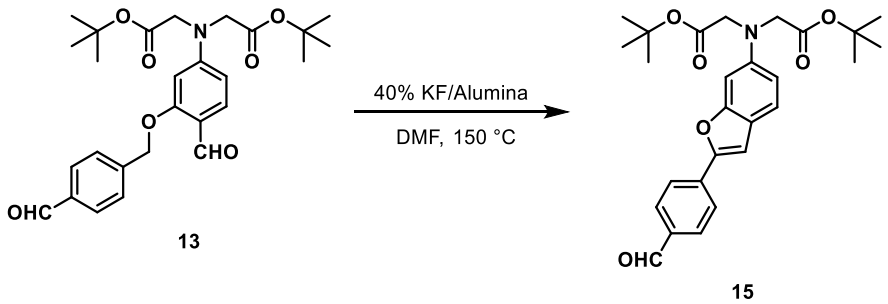

13 15

Synthesis of 15:
A round-bottom flask was charged with crude **13** (403.6 mg, 0.835 mmol) and 40% KF/Alumina (500 mg). The flask was sealed and evacuated/backfilled with nitrogen (3x). Anhydrous DMF (8 mL) was added via syringe and the reaction stirred at 150 °C for 2 h. The reaction was cooled, then poured over dilute hydrochloric acid (30 mL). The aqueous layer was then extracted with ethyl acetate (2 x 75 mL) and the combined organics dried with anhydrous magnesium sulfate, filtered and the solvent removed *in vacuo*. The remaining residue was then purified by flash chromatography (25% ethyl acetate in hexanes, isocratic) affording **15** as a yellow solid (222 mg, 0.54 mmol, 46%). ^{1}H NMR (300 MHz, $CDCl_3$) δ 10.04 (s, 1H), 7.96 (s, 4H), 7.47 (d, *J* = 8.6 Hz, 1H), 7.13 (d, *J* = 0.9 Hz, 1H), 6.78 (d, *J* = 2.2 Hz, 1H), 6.64 (dd, *J* = 8.6, 2.3 Hz, 1H), 4.13 (s, 4H), 1.53 (s, 18H); Analytical HPLC retention time 10.37 min; MS (ESI) exact mass for $C_{27}H_{32}NO_6^+$ $[M+H]^+$ calcd: 466.2 found: 466.4; HR-ESI-MS m/z for $C_{27}H_{31}NNaO_6^+$ $[M+H]^+$ calcd: 488.2044 found: 488.2041.

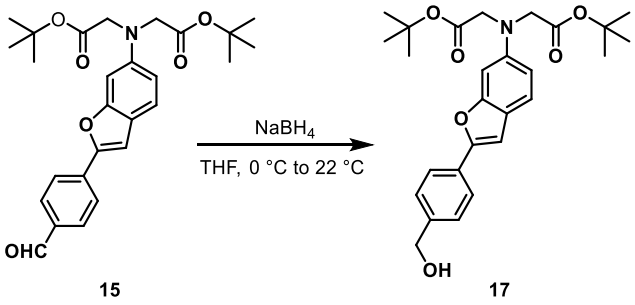

15 17

Synthesis of 17:
A round-bottom flask was charged with **15** (108.0 mg, 0.232 mmol) and anhydrous THF (5 mL), then cooled to 0 °C. Sodium borohydride (17.6 mg, 0.464 mmol) was added portion wise to the stirring solution and the reaction warmed to 22 °C and stirred for 2 h. The solvent was removed *in vacuo* and the remaining crude material was purified by flash chromatography (35% ethyl acetate in hexanes, isocratic) affording **17** as a white solid (98 mg, 0.210 mmol, 90%).^{1}H NMR (300 MHz, $CDCl_3$) δ 7.82 (d, *J* = 8.2 Hz, 2H), 7.43 (m, 3H), 6.94 (s, 1H), 6.79 (d, *J* = 2.3 Hz, 1H), 6.61 (dd, *J* = 8.6, 2.4 Hz, 1H), 4.76 (s, 2H), 4.12 (s, 4H), 1.52 (s, 18H); Analytical HPLC retention time 6.60 min; MS (ESI) exact mass for $C_{27}H_{34}HNO_6^+$ $[M+H]^+$ calcd: 468.2 found: 468.2; HR-ESI-MS m/z for $C_{27}H_{33}NaNO_6^+$ $[M+Na]^+$ calcd: 490.2200 found: 490.2196.

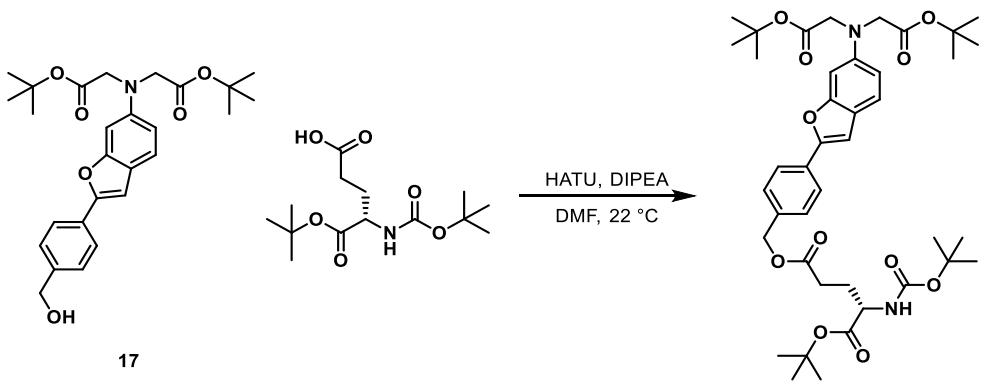

17 19

Synthesis of 19:

A round-bottom flask was charged with Boc-L-glutamic acid α-*tert*-butyl ester (133.0 mg, 438.4 μmol) and HATU (166.7 mg, 438.4 μmol). Anhydrous DMF (1 mL) and diisopropylethylamine (61.1 uL, 438.4 μmol) were added via syringe and the reaction stirred for 15 min. Benzyl alcohol **17** (41.0 mg, 87.7 μmol) was then added portion-wise and the reaction stirred at 22 °C for 12 h. The solvent was removed *in vacuo* and the remaining residue was diluted with ethyl acetate (100 mL), then washed with water (2 x 100 mL). The combined organics were dried with anhydrous magnesium sulfate, filtered and the solvent removed *in vacuo*. The remaining colorless oil was then purified by flash chromatography (25% ethyl acetate in hexanes, isocratic) affording **19** as a colorless solid (62 mg, 82.3 μmol, 94%); Analytical HPLC retention time 22.58 min; MS (ESI) exact mass for $C_{41}H_{56}N_2NaO_{11}^+$ $[M+Na]^+$ calcd: 775.4 found: 775.3.

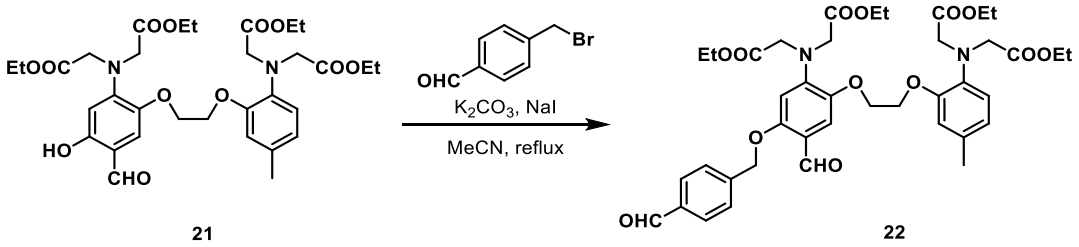

21 22

Synthesis of 21:

A round-bottom flask was charged with **21** (200.0 mg, 0.309 mmol, 1.0 equiv.), 4-(bromomethyl)benzaldehyde **1** (67.7 mg, 0.340 mmol, 1.1 equiv.), potassium carbonate (214 mg, 1.55 mmol) and sodium iodide (21.0 mg, 0.062 mmol). Anhydrous acetonitrile (10 mL) was added and the reaction stirred at reflux for 6 h. The reaction was cooled, diluted with ethyl acetate (100 mL) and washed with water (75 mL) and brine (75 mL). The combined organics were dried with anhydrous magnesium sulfate, filtered and the solvent removed *in vacuo*. The remaining residue was purified by flash chromatography (40% ethyl acetate in hexanes, isocratic) affording **22** as a white solid (162 mg, 0.212 mmol, 68%). ^{1}H NMR (400 MHz, $CDCl_3$) δ 10.38 (s, 1H), 7.99 – 7.92 (m, 2H), 7.62 (d, *J* = 8.0 Hz, 2H), 6.78 (d, *J* = 8.0 Hz, 1H), 6.74 – 6.65 (m, 2H), 5.22 (s, 2H), 4.32 – 4.01 (m, 21H), 2.29 (s, 3H), 1.19 (dt, *J* = 9.2, 7.1 Hz, 12H).

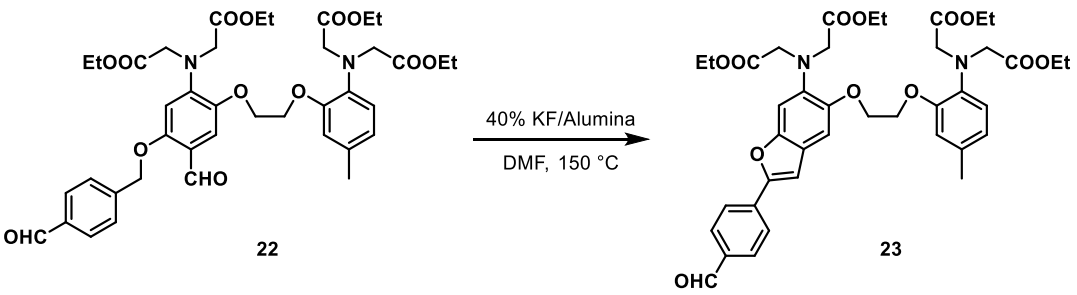

Synthesis of 23:

A round-bottom flask was charged with **22** (115.0 mg, 0.150 mmol) and 40% KF/Alumina (67.0 mg). The flask was sealed and evacuated/backfilled with nitrogen (3x). Anhydrous DMF (5 mL) was added via syringe and the reaction stirred at 150 °C for 2 h. The reaction was cooled, then poured over dilute hydrochloric acid (30 mL). The aqueous layer was then extracted with ethyl acetate (2 x 75 mL) and the combined organics dried with anhydrous magnesium sulfate, filtered and the solvent removed *in vacuo*. The remaining yellow solid was triturated with diethyl ether (3 x 10 mL) and the solid collected by vacuum filtration affording **23** as a yellow solid (50 mg, 70 μmol, 45%). ^{1}H NMR (400 MHz, $CDCl_3$) δ 7.97 (s, 4H), 7.13 (s, 1H), 7.10 (s, 2H), 6.72 (d, *J* = 7.1 Hz, 2H), 4.41 – 4.31 (m, 4H), 4.27 (s, 4H), 4.18 (s, 4H), 4.11 (dq, *J* = 18.0, 7.1 Hz, 9H), 2.31 (s, 3H), 1.20 (dt, *J* = 16.9, 7.1 Hz, 13H); Analytical HPLC retention time 10.37 min; HR-ESI-MS m/z for $C_{40}H_{47}N_2O_{12}^+$ $[M+H]^+$ calcd: 747.3 found: 748.0; HR-ESI-MS m/z for $C_{40}H_{46}N_2NaO_{12}^+$ $[M+Na]^+$ calcd: 769.2943 found: 769.2938.

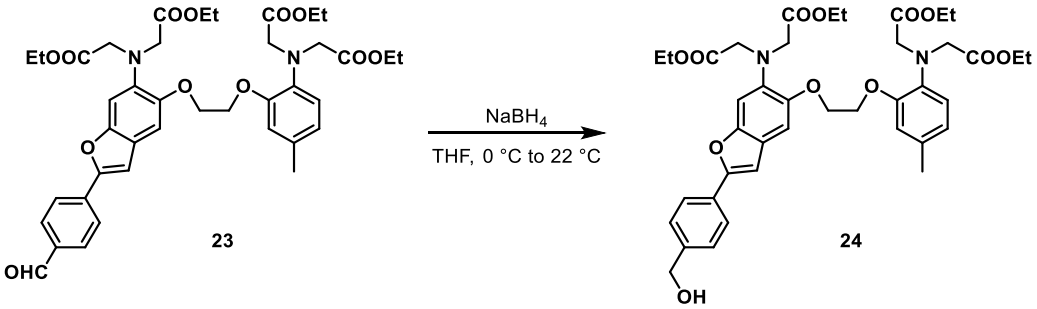

Synthesis of 24:

A round-bottom flask was charged with **23** (293.0 mg, 0.392 mmol) and anhydrous THF (8 mL), then cooled to 0 °C. Sodium borohydride (29.7 mg, 0.785 mmol) was added portion wise to the stirring solution and the reaction warmed to 22 °C and stirred for 8 h. The solvent was removed *in vacuo* and the remaining crude material was purified by flash chromatography (50% ethyl acetate in hexanes, isocratic) affording **24** as a white solid (93 mg, 0.124 mmol, 32%). ^{1}H NMR (400 MHz, $CDCl_3$) δ 7.82 (d, *J* = 8.2 Hz, 2H), 7.46 (d, *J* = 8.2 Hz, 2H), 7.10 (s, 1H), 7.06 (s, 1H), 6.78 (d, *J* = 7.9 Hz, 1H), 6.71 (m, 2H), 4.77 (s, 2H), 4.44 – 4.30 (m, 4H), 4.26 (s, 4H), 4.18 (s, 4H), 4.10 (dq, *J* = 15.7, 7.1 Hz, 8H), 2.30 (s, 3H), 1.23 (dt, *J* = 13.6, 7.1 Hz, 12H); Analytical HPLC retention time 9.64 min; MS (ESI) exact mass for $C_{40}H_{48}NaN_2O_{12}^+$ $[M+Na]^+$ calcd: 771.3 found: 771.2; HR-ESI-MS m/z for $C_{40}H_{48}NaN_2O_{12}^+$ $[M+Na]^+$ calcd: 771.3099 found: 771.3101.

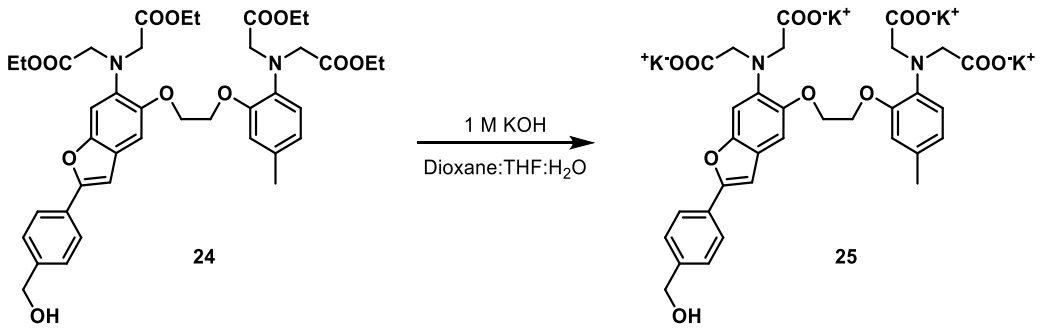

Synthesis of 25:

A round-bottom flask was charged with **24** (75.0 mg, 100 μmol), dioxane (10 mL) and THF (10 mL). A 1 M solution of potassium hydroxide (2 mL) was added and the reaction stirred for 24 h. The reaction was neutralized by the dropwise addition of hydrochloric acid (0.5 M), then the solvent removed *in vacuo*, affording **25** as an off-white solid which was aliquoted directly into DMSO assuming quantitative conversion to the potassium salt. Analytical HPLC retention time 10.37 min (20 min method), MS (ESI) exact mass for $C_{32}H_{33}N_2O_{12}^+$ $[M+H]^+$ calcd: 637.2 found: 637.4.

Spectroscopic Studies

Stock solutions were prepared in DMSO (1-10 mM). Due to its low water solubility, BFC1 was diluted into 9:1 DMSO:Tris buffered saline (TBS) for spectroscopic measurements. BFC2 and Fura-C were diluted into PBS (10 mM KH_2PO_4, 30 mM $Na_2HPO_4 \cdot 7H_2O$, 1.55 M NaCl, pH 7.2). UV-Vis absorbance and fluorescence spectra were recorded using a Shimadzu 2501 Spectrophotometer (Shimadzu) and a Quantamaster Master 4 L-format scanning spectrofluorometer (Photon Technologies International). The fluorometer is equipped with an LPS-220B 75-W xenon lamp and power supply, A-1010B lamp housing with integrated igniter, switchable 814 photon-counting/analog photomultiplier detection unit, and MD5020 motor driver. Samples were measured in 1-cm path length quartz cuvettes (Starna Cells).

Ca^{2+}-binding constants for Fura-C were determined by monitoring UV-visible spectra during titration of EGTA buffers to varying $[Ca^{2+}]_{free.}$ The following procedure is a modification of reported methods.[22,23] Two EGTA buffers needed to be prepared from a single stock: one of Ca^{2+}-free EGTA and one with Ca^{2+} added to form CaEGTA. The stock was prepared by dissolving 3.84 g EGTA (10.1 mmol) and 19 mmol solid potassium hydroxide (from 85% pellets) in 6 mL of H_2O. Once all solids were dissolved, the solution was diluted to 10 mL in a volumetric flask and split into two equal 5 mL portions. To prepare the Ca^{2+}-free EGTA buffer, 1.044 g (5 mmol) MOPS and 3.728 g (5 mmol) KCl were added to one of the 5 mL portions of EGTA stock. The pH was then adjusted to 7.20 by addition of 40% potassium hydroxide and the solution diluted to 500 mL. The CaEGTA buffer was prepared by adding 428 mg (4.75 mmol) of analytical grade $CaCO_3$ to the other 5 mL of EGTA stock. The solution was stirred and heated to 90 °C until the evolution of CO_2 ceased and all of the solid had dissolved. The mixture was then cooled to room temperature and 40% potassium hydroxide was added dropwise until the pH was between 7-8. 1 M $CaCl_2$ was added to the solution in 10 µL portions while monitoring the ΔpH. The addition was continued until the ΔpH per addition was one half of its initial value, with 40% potassium hydroxide being added when the pH fell below 6.5. This process is to ensure the concentration of Ca^{2+} is as close to, but not greater than, the concentration of EGTA within the solution. Following titration with $CaCl_2$, 1.044 g (5 mmol) MOPS was added and the pH adjusted to 7.20 with 40% potassium hydroxide. The solution was then diluted to 500 mL. The final stocks contained 10 mM MOPS, 100 mM KCl and either 10 mM Ca^{2+}-free EGTA or 10 mM CaEGTA at pH 7.20.

Spectrophotometric measurements were taken by diluting the indicator of choice to 10 uM in each EGTA buffer. Starting with 2 mL of the Ca^{2+}-free EGTA buffered solution, the excitation spectrum was measured between 300-450 nm, with excitation centered at 510 nm. Excitation spectra for multiple $[Ca^{2+}]_{free}$ concentrations were then measured using a reciprocal dilution method described elsewhere.[24,25] An "excess" $[Ca^{2+}]$ spectrum was also collected by addition of 10 µL of 1 M $CaCl_2$. The K_d of Fura-C was then determined utilizing the below equation:

$$[Ca^{2+}]_{free} = K_d^{MF-2} * \frac{[R - R_{min}]}{[R_{max} - R]} * \frac{F_{max}^{380}}{F_{min}^{380}}$$

Where $K_d^{Fura\text{-}C}$ is the disassociation constant of Fura-C, R is the ratio of 510 nm emission intensity at 340 nm to the 510 nm emission intensity with excitation at 380 nm, R_{min} is the same ratio at zero $[Ca^{2+}]_{free}$ and R_{max} the same ratio at saturating $[Ca^{2+}]_{free}$ (i.e. excess Ca^{2+}). $F^{380}{}_{max}$ is the fluorescence intensity with excitation at 380 nm with zero $[Ca^{2+}]_{free}$ and $F^{380}{}_{min}$ is the fluorescence intensity at saturating $[Ca^{2+}]_{free}$. Plotting the above equation as $\log([Ca^{2+}]_{free})$ vs. $\log\{[(R\text{-}R_{min})/(R_{max}\text{-}R)] * (F^{380}{}_{max}/F^{380}{}_{min})]\}$ yields a straight line where the x-intercept gives $\log(K_d^{Fura\text{-}C})$.

The $\Phi_{photolysis}$ for BFC1-NP was measured relatively to MNI-glutamate, with a reported $\Phi_{photolysis} = 0.065$.[19] A solution of 50 μM MNI-Glutamate and 5 μM BFC1-NP in 10% Tris buffered saline in DMSO was prepared in order to match the relative absorbance of each photocage at 360 nm, therefore normalizing the photon flux. This sample was then placed in a 2 mL quartz cuvette and illuminated using a the LPS-220B 75-W Xenon lamp and power supply from the Photon Technology International spectrofluorometer, which was set to 360 nm illumination with 3 mm slit widths (theoretical bandwidth of 360±6 nm). At each of the designated time points, a small aliquot (20 μL) of the sample was removed and injected onto the HPLC, monitoring absorbance at 254 nm and 340 nm. The rate of photolysis was determined by monitoring the area under the curve for either the loss of the photocage (MNI-glutamate) or the growth of the photoproduct (nitrophenol). Plotting $-\text{Log}(C/C_0)$ versus time provides a linear plot of the rate of photolysis for each species. Assuming MNI-glutamate and BFC1-NP were absorbing the same amount of light due to their matched absorbance at 360 nm, the ratio of the slopes is proportional to the ratio of the $\Phi_{photolysis}$. These results were corroborated by performing chemical actinometry in order to measure the flux of the Xenon lamp before and after photolysis (3 trials, 10 s illumination), which in theory allows for the direct measurement of $\Phi_{photolysis}$ (we preferred the ratiometric methodology as it seemed less prone to error).[26]

Cell Culture

All animal procedures were approved by the UC Berkeley Animal Care and Use Committees and conformed to the NIH Guide for the Care and Use and Laboratory Animals and the Public Health Policy.

Hippocampi were dissected from embryonic day 18 Sprague Dawley rats (Charles River Laboratory) in cold sterile HBSS (zero Ca^{2+}, zero Mg^{2+}). All dissection products were supplied by Invitrogen, unless otherwise stated. Hippocampal tissue was treated with trypsin (2.5%) for 15 min at 37 °C. The tissue was triturated using fire polished Pasteur pipettes, in minimum essential media (MEM) supplemented with 5% fetal bovine serum (FBS; Thermo Scientific), 2% B-27, 2% 1M D-glucose (Fisher Scientific) and 1% glutamax. The dissociated cells were plated onto 12 mm diameter coverslips (Fisher Scientific) pre-treated with PDL (as above) at a density of 30-40,000 cells per coverslip in MEM supplemented media (as above). Neurons were maintained at 37 °C in a humidified incubator with 5 % CO_2. At 1 day in vitro (DIV) half of the MEM supplemented media was removed and replaced with Neurobasal media containing 2% B-27 supplement and 1% glutamax. Transfection of genetic tools was carried out using Lipofectamine 3000 at 7 DIV. Functional imaging was performed on mature neurons 13-20 DIV, except electrophysiological experiments which were performed on 12-15 DIV neurons. Unless stated otherwise, for loading of HEK cells and hippocampal neurons, RhoVRs were diluted in DMSO to 500 μM, and then diluted 1:1000 in HBSS. All imaging experiments were performed in HBS (in mM) 140 NaCl, 2.5 KCl, 10 HEPES, 10 D-glucose 1.3 $MgCl_2$ and 2 $CaCl_2$; pH 7.3 and 290 mOsmol.

Uncaging Glutamate in Cultured Neurons

Glutamate uncaging was performed using confocal microscopy with a Zeiss LSM 880 NLO AxioExaminer equipped with a Diode 405 nm laser line, Argon 458, 488, and 514 laser lines, and a DPSS 561 nm laser line. Images were acquired using a W-Plan-Apo 40x/1.0 DIC objective and a Zeiss Airyscan detector. Coverslips with DIV 19 neurons expressing cytosolic GCaMP6s

under the CMV mammalian promoter were mounted onto a 3 cm dish in a solution of HBS (-Magnesium, +1 μM TTX, +500 μM BFC2-glutamate). Uncaging was performed using the 405 nm laser line (100% power) and GCaMP6s was imaged with the 488 nm laser (2% power) with a pixel dwell time of 177 μs. Note that we choose to apply 500 μM BFC2-glutamate based on published results utilizing MNI-glutamate.[27] However, this concentration was most likely too high due to the much higher extinction coefficient of BFC2-glutamate. This may in part account for the small response that was observed, as the excitation light from the laser may not have penetrated the solution in order to release glutamate near the neuron of interest.

Figures and Schemes

***Scheme 5-1**: General photocaging strategy vs photolyzable chemodosimeters*

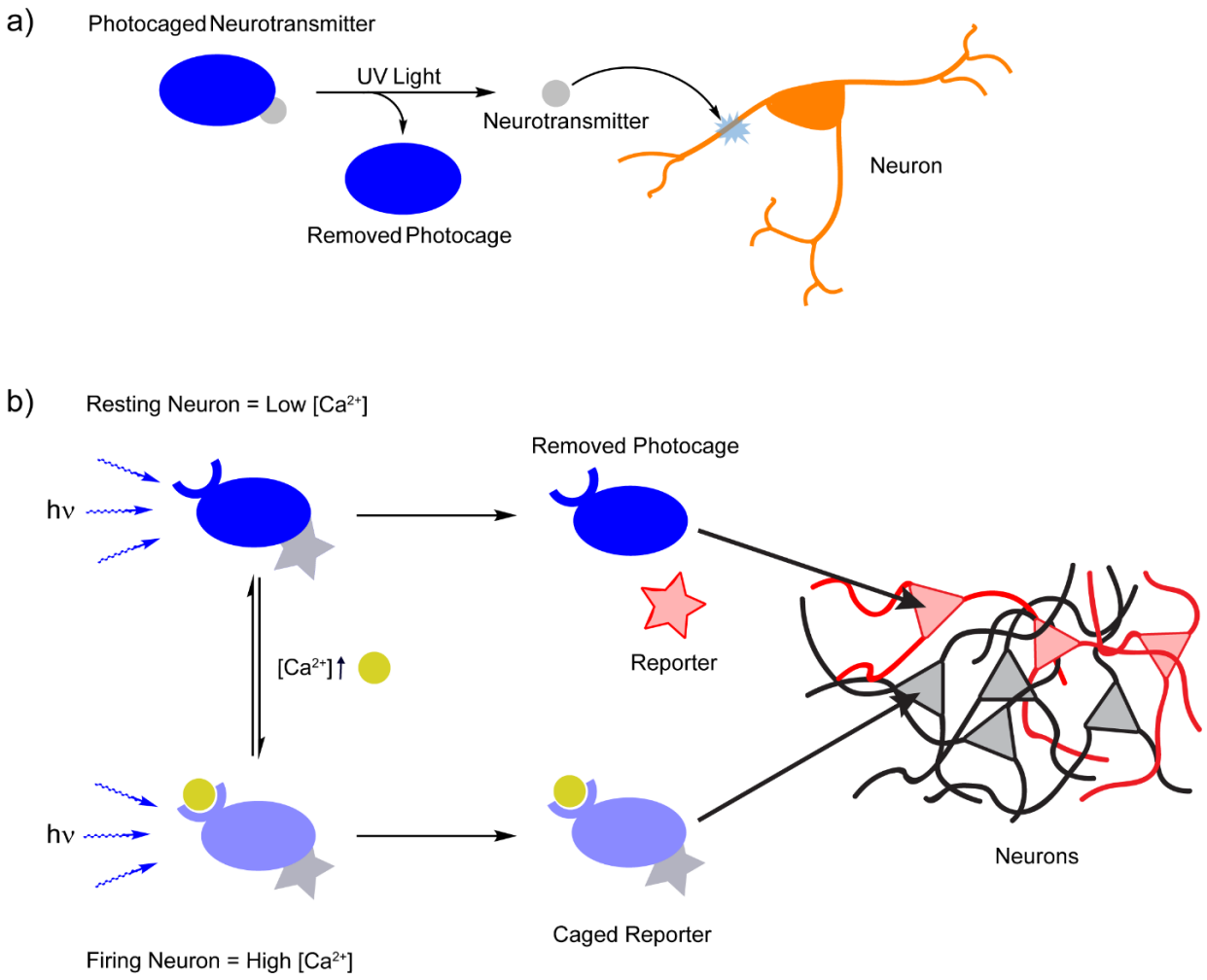

Scheme 5-1: (a) A general strategy for uncaging. A photocaged neurotransmitter is biologically inert until released by irradiation with UV light. Following uncaging the neurotransmitter is free to bind nearby receptors located on the membrane of the neuron. (b) A Ca^{2+} sensitive photocage acts as a chemodosimeter. Binding Ca^{2+} causes a shift in the absorption profile of the photocage, allowing selective wavelengths of light to distinguish between the Ca^{2+}-bound and Ca^{2+}-free states. In neurons, $[Ca^{2+}]$ increases greatly upon the firing of an action potential. These active neurons can therefore be distinguished from inactive neurons by the selective release of a reporter from the photocage.

***Scheme 5-2**: Proposed mechanism of BFC uncaging*

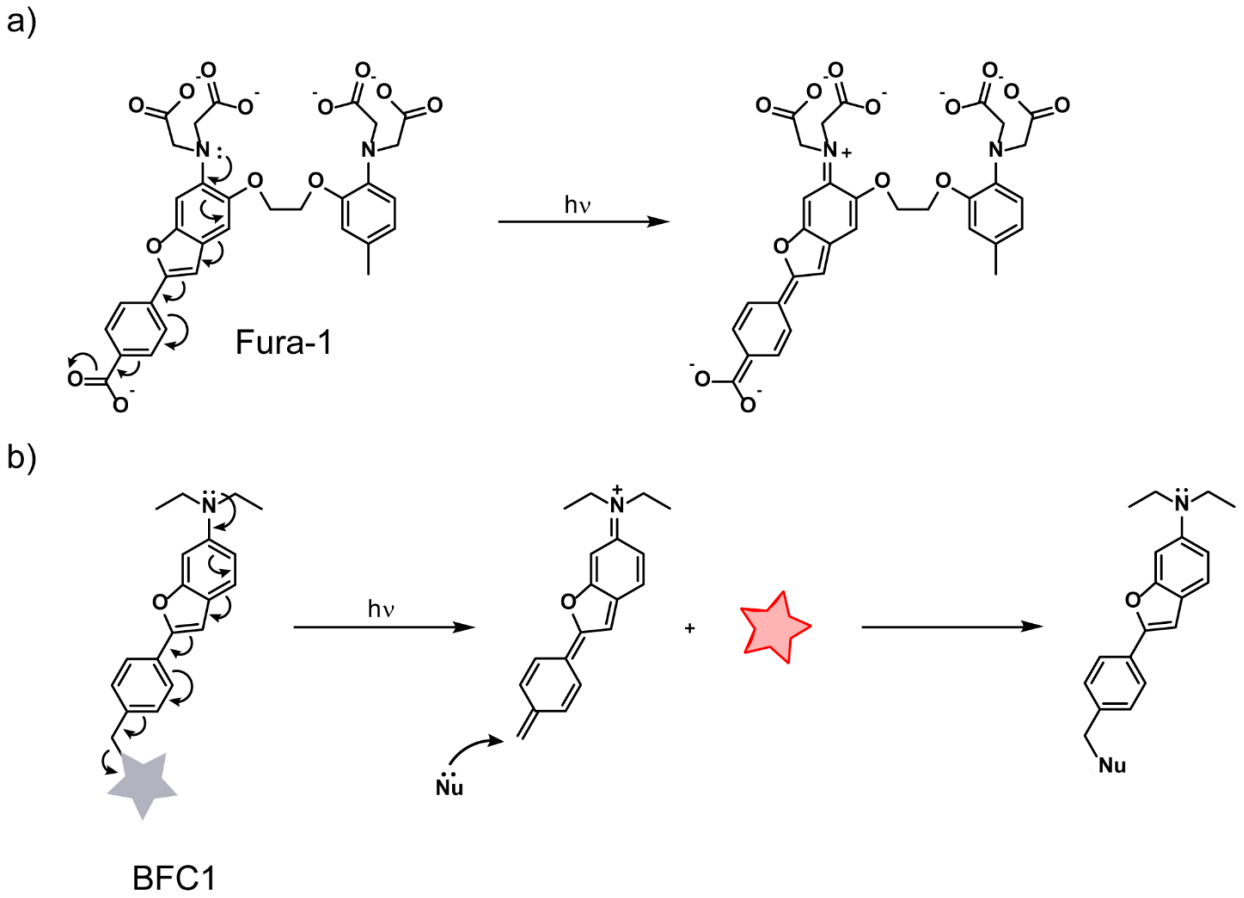

Scheme 5-2: (a) Ca^{2+} indicator Fura-1 is highly fluorescent due to internal charge transfer from the electron-rich aniline to the electron-withdrawing carboxylate. (b) BFC1 replaces the EWG of Fura-1 with a leaving group. We hypothesize that upon irradiation an extended azaquinone-methide forms through elimination of the leaving group. Subsequent nucleophilic attack of the methide by solvent or a nearby nucleophile leads to a substituted photocage byproduct.

Scheme 5-3: *Synthesis of BFC1*

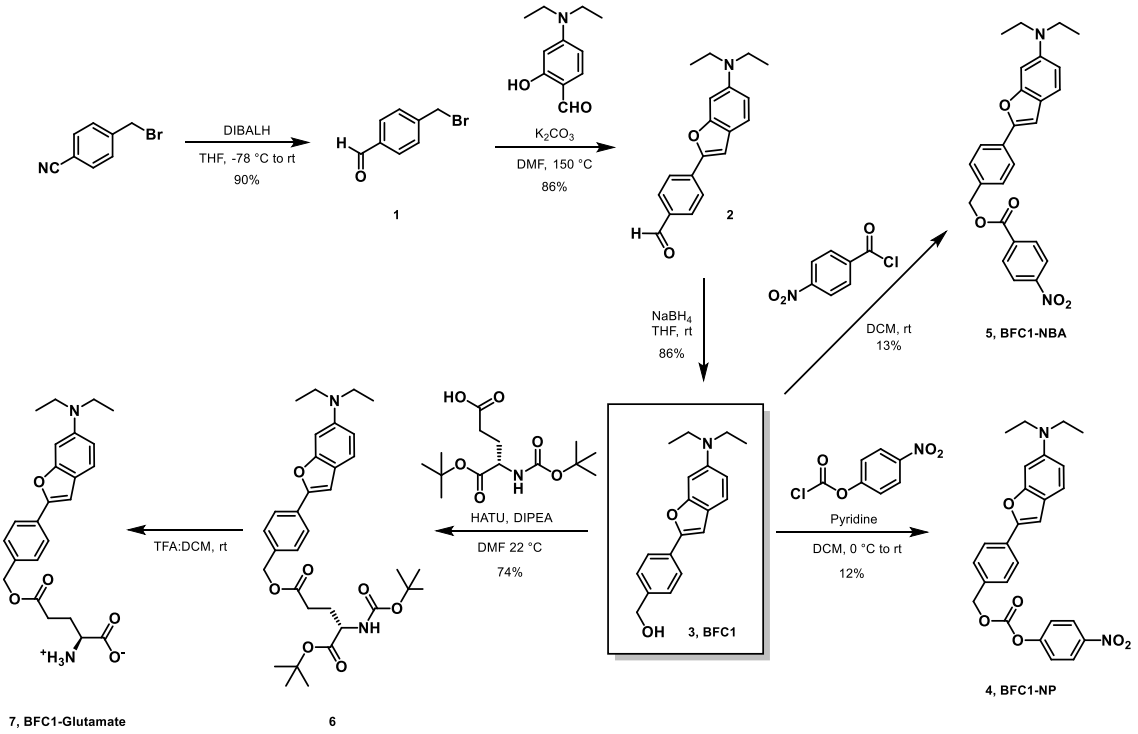

Scheme 5-3: BFC1 was synthesized by first preparing a 4-(bromomethyl)benzaldehyde. A Knoevenagel condensation with 4-(diethylamino)-2-hydroxybenzaldehyde followed by a sodium borohydride reduction afforded BFC1 in high yield. Formation of either a carbonate or ester linkage at the benzylic alcohol provided caged compounds **4**-**6**.

Scheme 5-4: *Synthesis of BFC2*

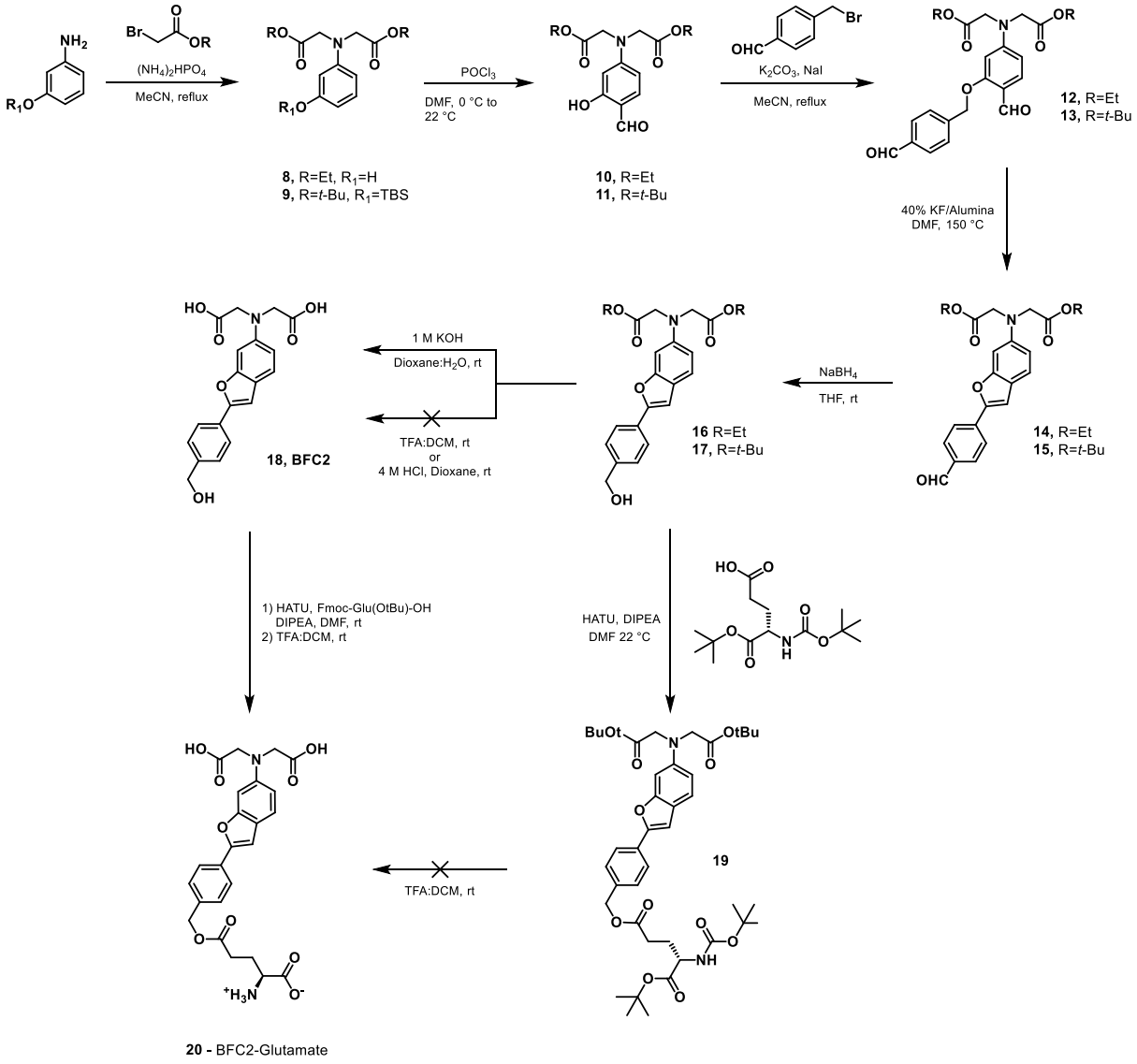

Scheme 5-4: Synthesis of N,N-diacetic acid functionalized BFC2. Alkylation of aminophenol with either *t*-butyl or ethyl protected bromoacetic acid afforded the protected N,N-diaceticaminophenols **8** and **9**. The protection of the phenolic oxygen with a *t*-butyl silane greatly improved the yield for the formation of **9**. The silyl ether was conveniently deprotected by $POCl_3$ during the subsequent Vilsmeyer-Haack formylation. Benzofurans **14** and **15** were synthesized over a two-step alkylation + cyclization, as attempting the cyclization in a single step led to low yields. Subsequent sodium borohydride reduction gave protected BFC2 **16** and **17** in good yields. The strongly acidic conditions typically used for *t*-butyl and Fmoc deprotections led to decomposition of the photocages, making isolation of BFC2-glutamate difficult.

Scheme 5-5: *Synthesis of Fura-C*

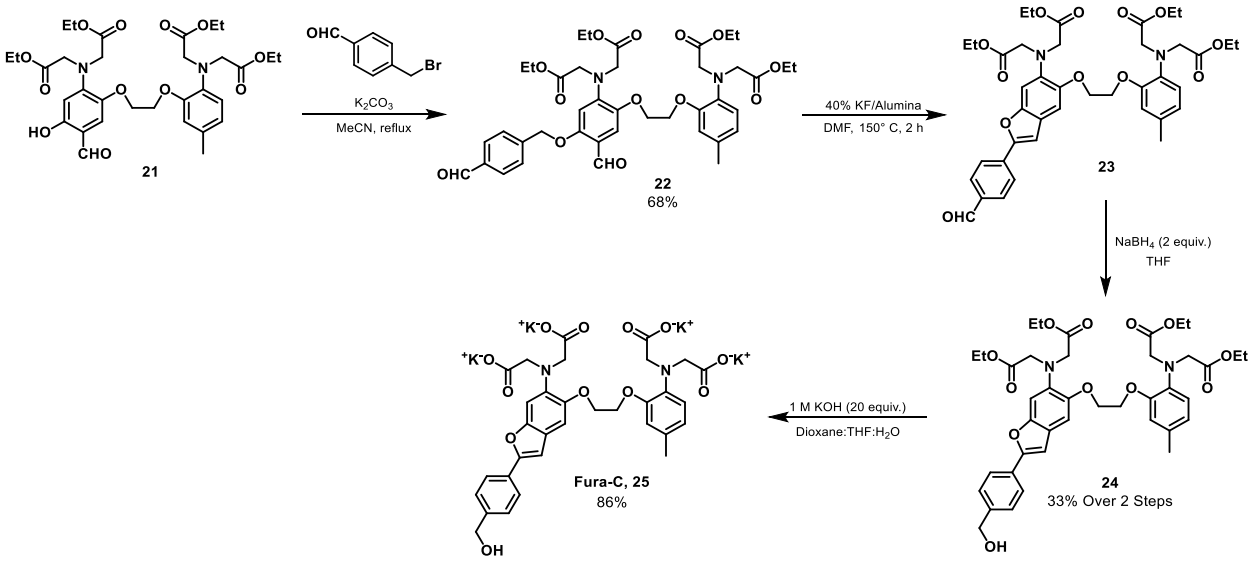

Scheme 5-5: Synthesis of Fura-C was carried out from salicylaldehyde **21**, a convenient precursor from the synthesis of Fura-2 and Azid-1.

Table 5-1: *Photophysical properties of BFCs and related photocages and indicators*

Compound	λ_{abs} (nm)	ε ($M^{-1}cm^{-1}$)	λ_{Fluor} (nm)	$\Phi_{photolysis}$
2[a]	365	30,000	586	n.a.
BFC1[a]	365	30,000	588	n.a.
BFC1-NP[a]	364	30,000	n.a.	0.18
BFC1-NBA[a]	360	31,000	n.a.	< .01
BFC1-glutamate[a]	360	-	n.a.	-
BFC2[b]	350	20,000	-	n.a.
BFC2-glutamate[b]	350	-	n.a.	-
Fura-C ($[Ca^{2+}]_{free}$)[c]	345	23,000	-	n.a.
Fura-C ($[Ca^{2+}]_{bound}$)[d]	325	29,000	-	n.a.
Fura-1 ($[Ca^{2+}]_{Free}$)[c]	350	21,000	534	n.a.
Fura-1 ($[Ca^{2+}]_{bound}$)[d]	334	27,000	522	n.a.
MNI-Glutamate[b]	340	-	n.a.	0.065

[a] Measured in 9:1 DMSO:TBS [b] Measured in dPBS, pH 7.2 [c] Measured in Ca^{2+}-free EGTA Buffer (10 mM H_2-EGTA, 10 mM MOPS, 100 mM KCl, pH 7.20) [d] Measured in Ca^{2+} EGTA Buffer (10 mM Ca^{2+}-EGTA,10 mM MOPS, 100 mM KCl, pH 7.20)

Figure 5-1: *Spectroscopic studies with BFCs*

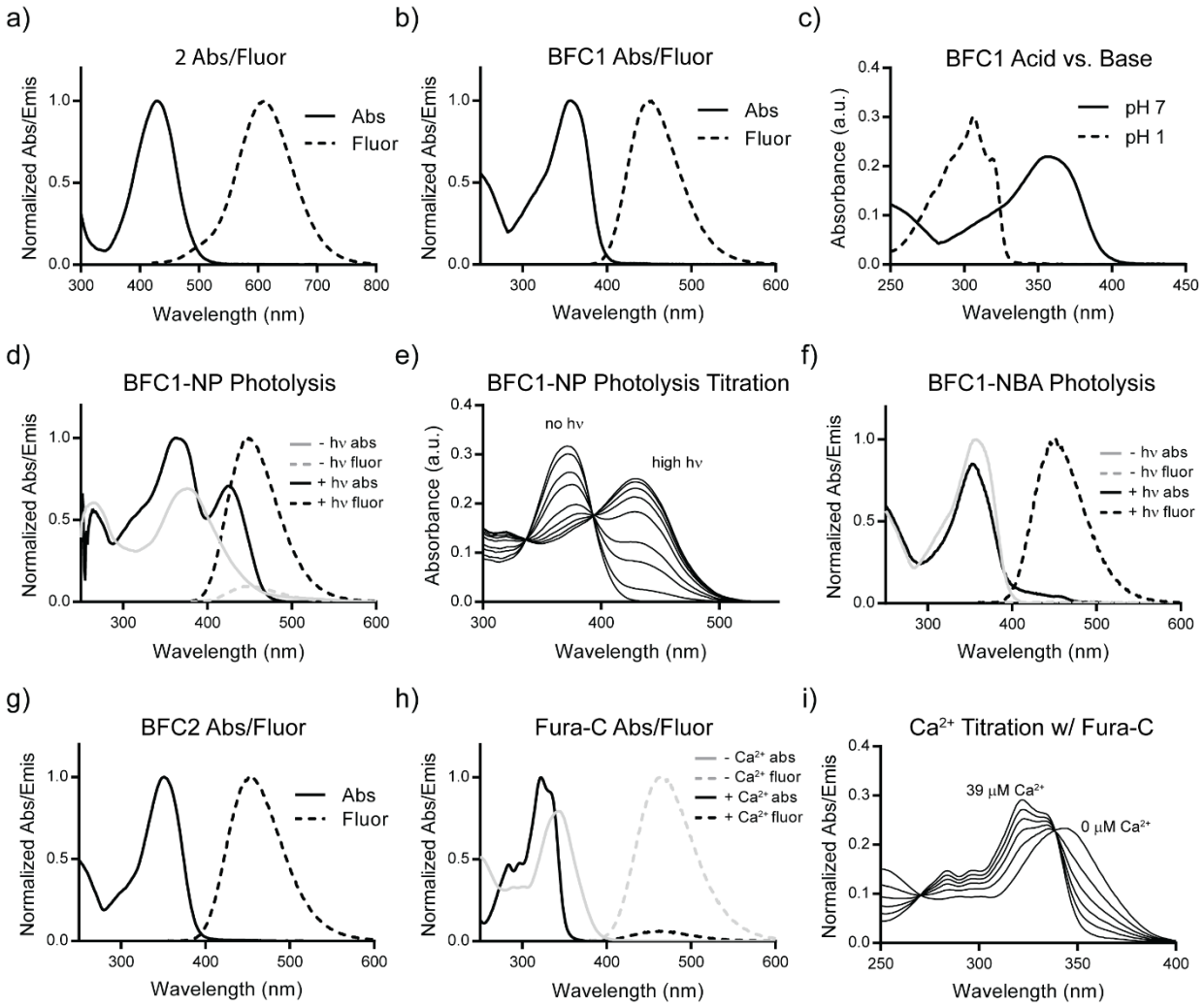

Figure 5-1: (a) Normalized absorbance and emission for the BFC precursor **2**. (b) Normalized absorbance and emission for BFC1. (c) Protonation of BFC1 causes a 70 nm hypsochromatic shift in absorbance. (d) BFC1-NP has minimal fluorescence before illumination with UV light. Following irradiation, fluorescence drastically increases, most likely due to the reformation of BFC1 by the addition of water to the azaquinone methide. (e) The rate of photolysis of BFC1-NBA can be measured by titrating with light and monitoring the release of nitrophenol (λ_{max} = 420 nm). (f) Photolysis of BFC1-NBA. Prior to photolysis, BFC1-NBA was completely non-fluorescent. (g) Normalized absorbance and emission of BFC2. The absorbance and emission were slightly blue shifted relative to BFC1 due to the use of an aqueous buffer instead of a 9:1 mixture of DMSO:TBS. (h) Normalized absorbance and emission of Fura-C in low and high [Ca^{2+}] buffers. While the absorbance undergoes a 20 nm hypsochromatic shift upon binding Ca^{2+}, λ_{max} fluorescence is relatively unchanged. (e) Fura-C was measured to have a K_d = 82 nM for Ca^{2+}, similar to the K_d = 107 nM of Fura-1.

Figure 5-2: *Measurement of $\Phi_{photolysis}$ for BFC1-NP*

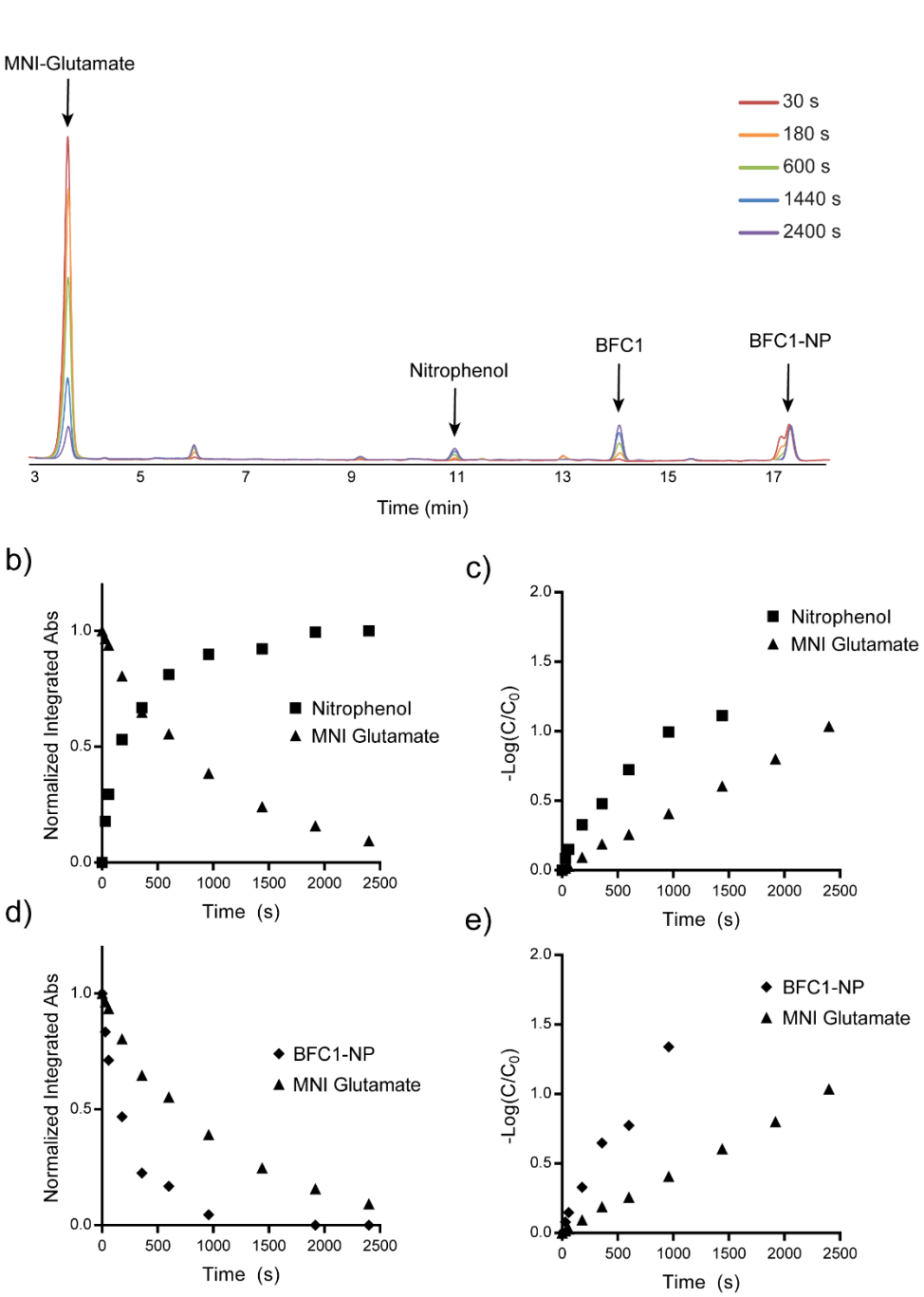

Figure 5-2: Measurement of the $\Phi_{photolysis}$ for BFC1-NP. A solution of 50 µM MNI-Glutamate and 5 µM BFC1-NP in 10% Tris buffered saline in DMSO was prepared in order to match the relative absorbance of each photocage at 360 nm, therefore normalizing the photon flux. a) The rate of photolysis was monitored by HPLC by removing a small portion of the solution at each time point. The area under each of the designated peaks was then used to track the concentrations of the relevant species; b) Plot of the normalized peak area of MNI-glutamate and nitrophenol vs. time; c) Plotting $-Log(C/C_0)$ vs. time, then comparing the relative slopes for MNI-glutamate disappearance and nitrophenol appearance showed that uncaging from BFC1-NP was nearly 3-fold faster than that of MNI-glutamate; d) Plot of the normalized peak area of MNI-glutamate and BFC1-NP over time; d) Plotting $-Log(C/C_0)$ for BFC1-NP gives nearly the same $\Phi_{photolysis}$ as was determined from the monitoring of nitrophenol.

Figure 5-3: *Uncaging of BFC2-Glutamate in neurons*

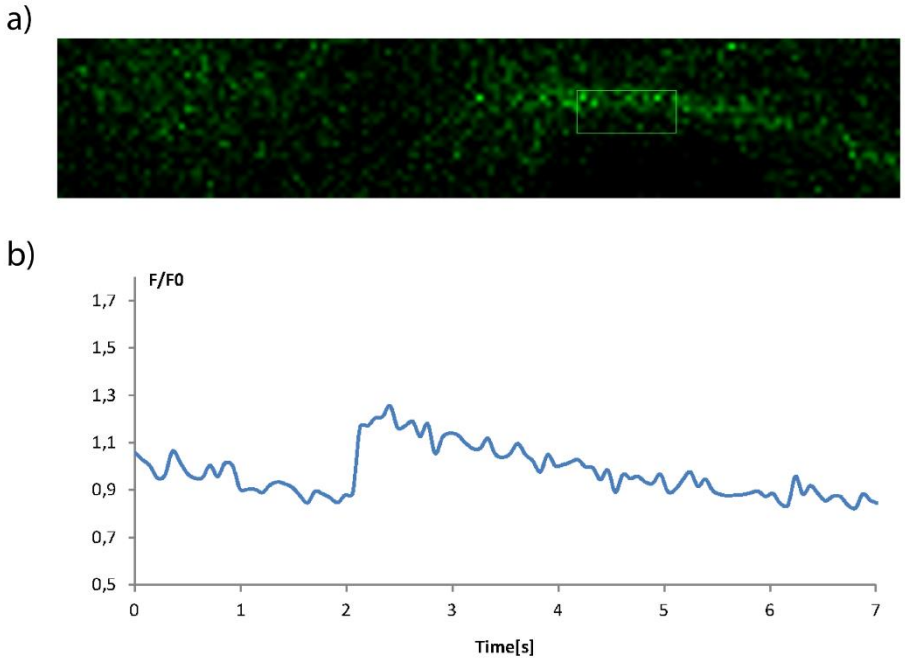

Figure 5-3: Uncaging of BFC2-glutamate in neurons. (a) Confocal fluorescence image of a neuron loaded with OGB immediately following excitation with 405 nm light in the indicated ROI. (b) Following excitation with 405 nm light, a 30% increase in OGB fluorescence was observed within the indicated ROI of panel a. While this response was relatively small, we believe improvements in the purity of BFC2-glutamate will lead to more robust uncaging of glutamate.

References

(1) Pelliccioli, A. P.; Wirz, J. Photoremovable Protecting Groups: Reaction Mechanisms and Applications. *Photochem. Photobiol. Sci.* **2002**, *1* (7), 441–458.

(2) Klán, P.; Solomek, T.; Bochet, C. G.; Blanc, A.; Givens, R.; Rubina, M.; Popik, V.; Kostikov, A.; Wirz, J. Photoremovable Protecting Groups in Chemistry and Biology: Reaction Mechanisms and Efficacy. *Chem. Rev.* **2013**, *113*, 119–191.

(3) Matsuzaki, M.; Ellis-Davies, G. C. R.; Nemoto, T.; Miyashita, Y.; Iino, M.; Kasai, H. Dendritic Spine Geometry Is Critical for AMPA Receptor Expression in Hippocampal CA1 Pyramidal Neurons. *Nat. Neurosci.* **2001**, *4* (11), 1086–1092.

(4) Tsien, R. Y.; Zucker, R. S. Control of Cytoplasmic Calcium with Photolabile Tetracarboxylate 2-Nitrobenzhydrol Chelators. *Biophys. J.* **1986**, *50* (5), 843–853.

(5) Wieboldt, R.; Gee, K. R.; Niu, L.; Ramesh, D.; Carpenter, B. K.; Hess, G. P. Photolabile Precursors of Glutamate: Synthesis, Photochemical Properties, and Activation of Glutamate Receptors on a Microsecond Time Scale. *Proc. Natl. Acad. Sci.* **1994**, *91* (19), 8752–8756.

(6) Wieboldt, R.; Ramesh, D.; Carpenter, B. K.; Hess, G. P. Synthesis and Photochemistry of Photolabile Derivatives of γ-Aminobutyric Acid for Chemical Kinetic Investigations of the γ-Aminobutyric Acid Receptor in the Millisecond Time Region. *Biochemistry* **1994**, *33* (6), 1526–1533.

(7) Kantevari, S.; Matsuzaki, M.; Kanemoto, Y.; Kasai, H.; Ellis-Davies, G. C. R. Two-Color, Two-Photon Uncaging of Glutamate and GABA. *Nat. Methods* **2010**, *7* (2), 123–125.

(8) Passlick, S.; Ellis-Davies, G. C. R. Comparative One- and Two-Photon Uncaging of MNI-Glutamate and MNI-Kainate on Hippocampal CA1 Neurons. *J. Neurosci. Methods* **2018**, *293*, 321–328.

(9) Heckman, L. M.; Grimm, J. B.; Schreiter, E. R.; Kim, C.; Verdecia, M. A.; Shields, B. C.; Lavis, L. D. Design and Synthesis of a Calcium-Sensitive Photocage. *Angew. Chemie - Int. Ed.* **2016**, *55* (29), 8363–8366.

(10) Fosque, B. F.; Sun, Y.; Dana, H.; Yang, C. T.; Ohyama, T.; Tadross, M. R.; Patel, R.; Zlatic, M.; Kim, D. S.; Ahrens, M. B.; et al. Labeling of Active Neural Circuits in Vivo with Designed Calcium Integrators. *Science (80-.).* **2015**, *347* (6223), 755–760.

(11) Chen, T. W.; Wardill, T. J.; Sun, Y.; Pulver, S. R.; Renninger, S. L.; Baohan, A.; Schreiter, E. R.; Kerr, R. A.; Orger, M. B.; Jayaraman, V.; et al. Ultrasensitive Fluorescent Proteins for Imaging Neuronal Activity. *Nature* **2013**, *499* (7458), 295–300.

(12) Kulkarni, R. U.; Miller, E. W. Voltage Imaging: Pitfalls and Potential. *Biochemistry* **2017**, *56* (39), 5171–5177.

(13) Adams, S.; Lec-Ram, V.; Tsien, R. A New Caged Ca 2+, Azid-1, Is Far More Photosensitive than Nitrobenzyl-Based Chelators. *Chem. Biol.* **1997**, *4* (11), 867–878.

(14) Silva, A. P.; Gunaratne, H. Q. N.; Gunnlaugsson, T.; Huxley, A. J. M.; McCoy, C. P.; Rademacher, J. T.; Rice, T. E. Signaling Recognition Events with Fluorescent Sensors and Switches. *Chem. Rev.* **1997**, *97* (5), 1515–1566.

(15) Greenwald, R. B.; Pendri, A.; Conover, C. D.; Zhao, H.; Choe, Y. H.; Martinez, A.; Shum, K.; Guan, S. Drug Delivery Systems Employing 1,4- or 1,6-Elimination: Poly(Ethylene Glycol) Prodrugs of Amine-Containing Compounds. *J. Med. Chem.* **1999**, *42* (18), 3657–3667.

(16) Blencowe, C. A.; Russell, A. T.; Greco, F.; Hayes, W.; Thornthwaite, D. W. Self-Immolative Linkers in Polymeric Delivery Systems. *Polym. Chem.* **2011**, *2* (4), 773–790.

(17) Grynkiewicz, G.; Poenie, M.; Tsien, R. Y. A New Generation of Ca2+ Indicators with Greatly Impoved Fluorescence Properties. *J. Biol. Chem.* **1985**, *260* (6), 3440–3450.

(18) Guruge, C.; Ouedraogo, Y. P.; Comitz, R. L.; Ma, J.; Losonczy, A.; Nesnas, N. Improved Synthesis of Caged Glutamate and Caging Each Functional Group. *ACS Chem. Neurosci.* **2018**.

(19) Corrie, J. E. T.; Kaplan, J. H.; Forbush, B.; Ogden, D. C.; Trentham, D. R. Photolysis Quantum Yield Measurements in the Near-UV; A Critical Analysis of 1-(2-Nitrophenyl)Ethyl Photochemistry. *Photochem. Photobiol. Sci.* **2016**, *15* (5), 604–608.

(20) Slanina, T.; Shrestha, P.; Palao, E.; Kand, D.; Peterson, J. A.; Dutton, A. S.; Rubinstein, N.; Weinstain, R.; Winter, A. H.; Klán, P. In Search of the Perfect Photocage: Structure-Reactivity Relationships in Meso-Methyl BODIPY Photoremovable Protecting Groups. *J. Am. Chem. Soc.* **2017**, *139* (42), 15168–15175.

(21) Wang, Z.; Zhang, X.; Huang, P.; Zhao, W.; Liu, D.; Nie, L.; Yue, X.; Wang, S.; Ma, Y.; Kiesewetter, D.; et al. Dual-Factor Triggered Fluorogenic Nanoprobe for Ultrahigh Contrast and Subdiffraction Fluorescence Imaging. *Biomaterials* **2013**, *34* (26), 6194–6201.

(22) Tsien, R. Y.; Pozzan, T. Tsien 1989 Methods of Enzymol - Measurement of Cytosolic CA.Pdf. *Methods Enzym.* **1989**, *172* (230), 1989.
(23) McGuigan, J. A. S.; Luthi, D.; Buri, A. Calcium Buffer Solutions and How to Make Them: A Do It Yourself Guide. *Can. J. Physiol. Pharmacol.* **1991**, *69*, 1733–1749.
(24) Adam, S. R.; Kao, J. P. Y.; Grynkiewicz, G.; Minta, A.; Tsien, R. Y. Biologically Useful Chelators That Release Ca2 + upon Illumination +. **1988**, *152* (23), 3212–3220.
(25) Tsien, R. Y. New Calcium Indicators and Buffers with High Selectivity against Magnesium and Protons: Design, Synthesis and Properties of Prototype Structures. *Biochemistry* **1980**, *19*, 2396–2404.
(26) Grenier, V.; Walker, A. S.; Miller, E. W. A Small-Molecule Photoactivatable Optical Sensor of Transmembrane Potential. *J. Am. Chem. Soc.* **2015**, *137* (34), 10894–10897.
(27) Fino, E. RuBi-Glutamate: Two-Photon and Visible-Light Photoactivation of Neurons and Dendritic Spines. *Front. Neural Circuits* **2009**, *3* (May), 1–9.

Appendix 1:
A Trivalent HaloTag Ligand for Increasing the Brightness of Genetically Targetable RhoVRs

Introduction

While voltage-sensitive dyes like VoltageFluors (VFs) excel at monitoring neuronal activity in cultured tissues due to their fast kinetics and favorable photophysical properties,[1] they have limited utility *in vivo* because of their tendency to label all membranes indiscriminately.[2–4] To address this limitation we have developed genetically targetable rhodamine-based voltage reporters (RhoVR-Halos) capable of selectively labeling and recording activity from genetically defined neurons in brain slice (**Chapter 2**). One major constraint of the RhoVR-Halo system is that the extent of labeling of the voltage indicator, and therefore its brightness, is dependent on the expression levels of the genetic component. This results in RhoVR-Halo fluorescence that is, on average, 3-fold lower than fluorescence from a bath-applied RhoVR.

To improve the brightness of RhoVR-Halos we envisioned synthesizing a trivalent linker that could couple three RhoVRs to a single HaloTag ligand (**Scheme A1-1**). This chemical approach is attractive because it avoids resorting to overexpression of the genetic component, which can often adversely affect cell health. The design of trivalent linker-functionalized RhoVRs, or TriRhoVRs, was inspired by multivalent carbohydrate mimetics used to study carbohydrate-mediated binding events and receptors.[5–7] TriRhoVRs were constructed from a tris(hydroxymethyl)aminomethane core (**C**) that was adorned with polyethylene glycol (PEG) linkers functionalized with either the HaloTag ligand ("tail" end, **A** linker) or a piperazine-cysteic acid-functionalized RhoVR **S1** ("heads" end, **B** linkers, **Scheme A1-1**).

Results and Discussion

We synthesized two different TriRhoVRs possessing varying lengths of the **A** and **B** PEG linkers. An asymmetrical TriRhoVR was synthesized which possessed a short succinic anhydride-derived **A** linker and long PEG_{25} **B** linkers ("TriRhoVR-A", **Scheme A1-2**). Synthesis of TriRhoVR-A began with the alkylation of tris(hydroxymethyl)aminomethane with *tert*-butyl acrylate, affording **1** in 42% yield. Linker **A** was then installed through amide bond formation between the amine of **1** and succinic anhydride, affording **2** in 92% yield. A subsequent HATU-mediated coupling between **2** and HaloTag-amine afforded **3** in 88% yield. With the "tail" end of the linker synthesized, we then moved to functionalize the trivalent "heads". The ester functional groups of the core were swapped for amines through a 3-step process. TFA catalyzed deprotection of the *t*-butyl esters afforded the carboxy functionalized core **4**. A HATU-mediated coupling was used to append Boc-protected ethylene diamines, affording **5** and **6**. We synthesized the tertiary-amide containing **6** after initially observing hydrolytic instability with **5**, hypothesizing that tertiary amides would increase stability (**Scheme A1-2**). Subjection of **5** and **6** to a TFA catalyzed deprotection afforded amine-functionalized linkers **7** and **8** in 62% and 83% yield, respectively, over 3 steps. We initially attempted to attach RhoVRs to **7** and **8** through a one-pot reaction, first adding the **B** linkers (NHS-PEG_{25}-Acid), then coupling the piperazine-cysteic acid-functionalized RhoVR **S1**. Unfortunately, this route led to significant homocoupling of **S1** to excess NHS-PEG_{25}-Acid, making purification difficult. We choose to pre-couple the **B** linker to **S1**, affording RhoVR-PEG_{25}-Acid **9** in 64% yield after purification by reverse-phase HPLC. A HATU mediated coupling between **9** and either **7** or **8** gave the final TriRhoVRs **10** and **11** in 42% and 41% yield, respectively. Note that further investigation into the hydrolytic instability of trivalent linkers revealed excess HATU from coupling reactions was leading to decomposition. By minimizing the

equivalency of HATU, no further issues with the stability of **10** or **11** were observed. For future experiments, we choose to only utilize **10**, or TriRhoVR-A, for simplicity.

TriRhoVR-A was designed to possess a long **B** linker due to previous studies with RhoVR-Halos demonstrating that longer linkers increase voltage sensitivity (**Chapter 2**). One possible downside to this construction is that linker **A** is much shorter than the **B** linkers, potentially leading to lower labeling kinetics of the HaloTag ligand due to steric constraints. We therefore synthesized a symmetrical TriRhoVR, TriRhoVR-S, where the **A** and **B** linkers were derived from PEG_{13} (**Scheme A1-3**). We choose to use PEG_{13} linkers as the overall distance from the HaloTag ligand to each RhoVR was approximately the same as TriRhoVR-A and RhoVR1-PEG_{25}-Halo. In order to minimize the number of synthetic steps following the addition of the expensive PEG_{13} linkers, we first Fmoc-protected the amine of **1**, affording **12** in 96% yield. A TFA catalyzed deprotection of the *t*-butyl esters afforded **13**, which was subsequently coupled to N-Boc-ethylenediamine to generate **14** (70% yield over two steps). Having primed the "heads" of the trivalent core with amines, we then installed the HaloTag "tail". Fmoc deprotection of **14** afforded **15** in 78% yield. The resulting amine was then coupled to a pre-conjugated HaloTag-PEG_{13}-Acid **S2**, affording **16** in 34% yield following reverse phase HPLC purification. A final TFA catalyzed deprotection afforded the trivalent linker **17**, which was coupled to RhoVR1-PEG_{13}-Acid **18** to afford the final TriRhoVR-S **19** in 40% yield.

Spectroscopic analysis of TriRhoVR-A and TriRhoVR-S revealed the absorbance and emission profiles of TriRhoVRs closely matched those of the parent RhoVR 1 and RhoVR1-PEG_{25}-Halo (**Figure A1-1a-c**, **Table A1-1**). Both TriRhoVRs possessed extinction coefficients approximately 3-fold larger than RhoVR-PEG_{25}-Halo, but had Φ_{Fl} that were much lower (0.6% and 0.7% for TriRhoVR-A and TriRhoVR-S, respectively). The significant drop in Φ_{Fl} without a broadening of the absorption spectra suggests TriRhoVRs are being quenched through a weak coupling mechanism, such as homoFRET, and not through a strong coupling interaction, such as aggregation or π-stacking.[8] We then loaded TriRhoVRs onto HaloTag expressing HEK cells to determine if the low Φ_{Fl} would correspond to poor brightness in cells. HaloTag expressing cells were labeled selectively with TriRhoVR-A and Tri-RhoVR-s, but they were approximately 5-fold dimmer than cells loaded with RhoVR1-PEG_{25}-Halo (**Figure A1-2a-j**). In order to determine if the dim fluorescence of TriRhoVRs was a result of self-quenching or poor labeling kinetics of the HaloTag ligand, we conducted a 2-part labeling experiment using a HaloTag targeted Si-rhodamine voltage sensor (BeRST-Halo). First, HaloTag expressing cells were loaded with TriRhoVR-A, TriRhoVR-S, RhoVR1-PEG_{25}-Halo or vehicle (control) for 30 minutes. The loading solution was removed, then the cells were loaded with BeRST-Halo for 30 minutes before measuring the intensity of BeRST fluorescence. Both TriRhoVRs were found to load less efficiently than RhoVR1-PEG_{25}-Halo (90% saturation for RhoVR1-PEG_{25}-Halo, 80% for TriRhoVR-S, 70% for TriRhoVR-A, **Figure A1-2k**). While the higher saturation of TriRhoVR-S supports the idea that the multiple PEG linkers may interfere with HaloTag ligand binding, the differences in loading efficiency are too small to account for the dimness of TriRhoVRs. Therefore, the most likely cause of TriRhoVR dimness is self-quenching between the three RhoVR moieties.

In conclusion, we synthesized two trivalent HaloTag linkers which increase the stoichiometry of covalent labeling 3-fold. These split linkers were coupled to RhoVR voltage dyes in an attempt to increase the brightness of the genetically targetable voltage reporters. We found a major limitation to the TriRhoVR system was self-quenching interactions between the coupled RhoVRs, which was likely exacerbated by the highly lipophilic molecular wires. In order to confirm that self-quenching is the main cause of reduced brightness, the RhoVR moieties could be

replaced with less lipophilic tetramethylrhodamines. In addition, TriRhoVRs with longer linkers could be synthesized. Finally, the tris(hydroxymethyl)aminomethane core of the linker could be replaced with a more rigid core that minimizes the interaction of the three linker "heads".

Experimental Section

General Method for Chemical Synthesis and Characterization

Chemical reagents and solvents (dry) were purchased from commercial suppliers and used without further purification. NHS-PEG$_x$-Acid dPEG® linkers were purchased from Quanta Biodesign. Synthesis of RhoVR derivative **S1** was carried out as reported in **Chapter 2**. BeRST-Halo was prepared by Gloria Ortiz (UC Berkeley). Thin layer chromatography (TLC) (Silicycle, F254, 250 μm) and preparative thin layer chromatography (PTLC) (Silicycle, F254, 1000 μm) was performed on glass backed plates pre-coated with silica gel and were visualized by fluorescence quenching under UV light. Flash column chromatography was performed on Silicycle Silica Flash F60 (230–400 Mesh) using a forced flow of air at 0.5–1.0 bar. NMR spectra were measured on Bruker AVB-400 MHz, 100 MHz, AVQ-400 MHz, 100 MHz, Bruker AV-600 MHz, 150 MHz. Chemical shifts are expressed in parts per million (ppm) and are referenced to $CDCl_3$ (7.26 ppm, 77.0 ppm) or DMSO (2.50 ppm, 40 ppm). Coupling constants are reported as Hertz (Hz). Splitting patterns are indicated as follows: s, singlet; d, doublet; t, triplet; q, quartet, dd, doublet of doublet; m, multiplet. High-resolution mass spectra (HR-ESI-MS) were measured by the QB3/Chemistry mass spectrometry service at University of California, Berkeley. High performance liquid chromatography (HPLC) and low resolution ESI Mass Spectrometry were performed on an Agilent Infinity 1200 analytical instrument coupled to an Advion CMS-L ESI mass spectrometer. The column used for the analytical HPLC was Phenomenex Luna C18(2) (4.6 mm I.D. × 150 mm) with a flow rate of 1.0 mL/min. The mobile phases were MQ-H_2O with 0.05% formic acid (eluent A) and HPLC grade acetonitrile with 0.05% formic acid (eluent B). Signals were monitored at 254, 340 and 545 nm over 20 min with a gradient of 10-100% eluent B. The column used for semi-preparative HPLC was Phenomenex Luna 5μ C18(2) (10 mm I.D. x 150 mm) with a flow rate of 5.0 mL/min. The mobile phases were MQ-H_2O with 0.05% formic acid (eluent A) and HPLC grade acetonitrile with 0.05% formic acid (eluent B). Signals were monitored at 254 over 20 min with a gradient of 10-100% eluent B.

Synthetic Procedures

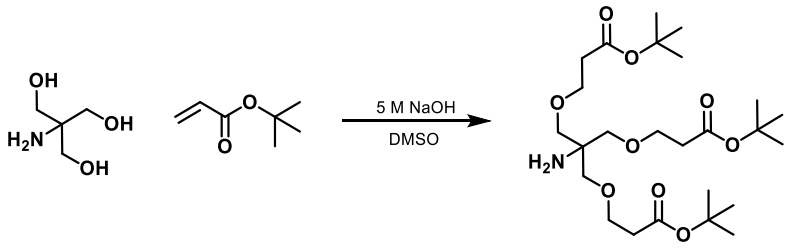

1

Synthesis of 1:
A round-bottom flask was charged with 2-Amino-2-(hydroxymethyl)-1,3-propanediol (2.42 g, 20.0 mmol), DMSO (4 mL) and 5 M sodium hydroxide (0.4 mL, 2.0 mmol). Tert-butyl acrylate

was injected dropwise and the reaction stirred for 24 h. The reaction was concentrated *in vacuo*, then purified directly by flash chromatography (70% ethyl acetate in hexanes with 0.5% ammonium hydroxide) affording **1** as a colorless oil (4.23 g, 8.37 mmol, 42%). ^{1}H NMR (400 MHz, $CDCl_3$) δ 3.68 (t, *J* = 6.4 Hz, 6H), 3.35 (s, 6H), 2.49 (t, *J* = 6.4 Hz, 6H), 1.49 (s, 27H); HR-ESI-MS m/z for $C_{25}H_{48}NO_9^+$ $[M+H]^+$ calcd: 506.3324 found: 506.3324.

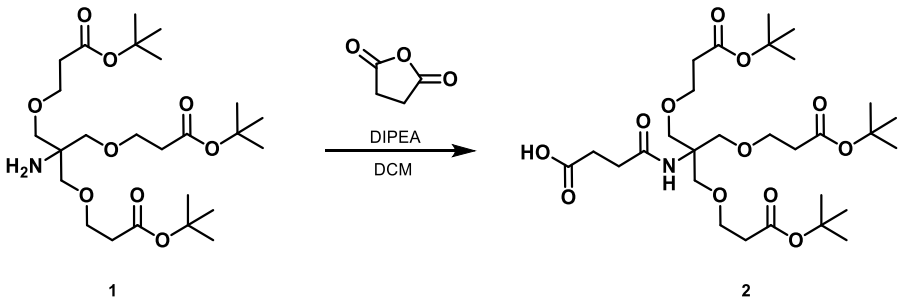

1 2

Synthesis of 2:
A vial was charged with **1** (1.00 g, 1.98 mmol), succinic anhydride (208 mg, 2.08 mmol) and DCM (10 mL). Diisopropylethylamine (517 µL, 2.97 mmol) was added and the reaction stirred at 22 °C for 16 h. The solvent was removed *in vacuo* and the remaining residue diluted with ethyl acetate (100 mL) and washed with 1 M hydrochloric acid (3 x 100 mL) and saturated sodium bicarbonate (1 x 100 mL). The combined organics were dried with anhydrous sodium sulfate, filtered and the solvent removed *in vacuo* affording **2** as a colorless oil (1.1 g, 1.82 mmol, 92%). ^{1}H NMR (400 MHz, $CDCl_3$) δ 6.80 (s, 1H), 3.73 (s, 6H), 3.68 (t, *J* = 6.1 Hz, 6H), 2.64 (m, 4H), 2.49 (t, *J* = 6.1 Hz, 6H), 1.49 (s, 27H); HR-ESI-MS m/z for $C_{29}H_{51}NO_{12}^+$ $[M+H]^+$ calcd: 606.3484 found: 606.3487.

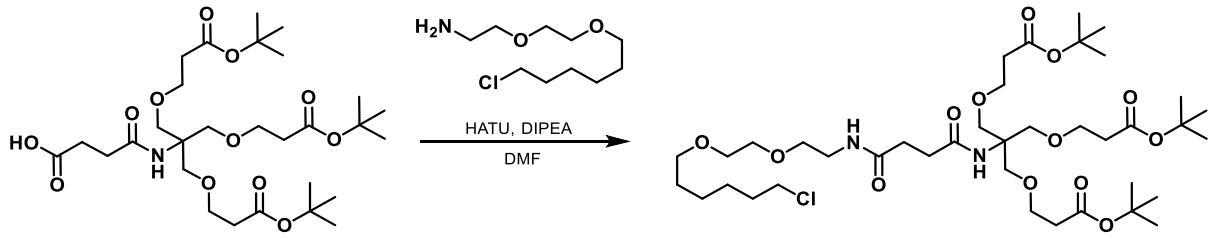

2 3

Synthesis of 3:
A vial was charged with **2** (1.00 g, 1.65 mmol), HaloTag-amine (443 mg, 1.98 mmol) and HATU (753 mg, 1.98 mmol). Anhydrous DMF (3 mL) and anhydrous diisopropylethylamine (431 µL, 2.48 mmol) were added and the vial flushed with nitrogen, sealed, and stirred at 22 °C for 3 h. The solvent was removed *in vacuo* and the remaining residue diluted with ethyl acetate (100 mL) and washed with 1 M hydrochloric acid (2 x 50 mL) and water (1 x 50 mL). The combined organics were dried with anhydrous sodium sulfate, filtered and the solvent removed *in vacuo*. The remaining solid material was purified by flash chromatography (25% ethyl acetate in hexanes, isocratic) affording **3** as a colorless oil (1.18 g, 1.46 mmol, 88%). ^{1}H NMR (400 MHz, $CDCl_3$) δ 6.52 (s, 1H), 6.32 (s, 1H), 3.72 (s, 6H), 3.70 – 3.45 (m, 18H), 2.56 – 2.46 (m, 10H), 1.82 (m, 2H), 1.69 – 1.61 (m, 2H), 1.49 (m, 29H), 1.45 – 1.37 (m, 2H); Analytical HPLC retention time 11.17

min; MS (ESI) exact mass for $C_{39}H_{72}N_2O_{13}^+$ $[M+H]^+$ calcd: 811.5 found: 811.9; HR-ESI-MS m/z for $C_{47}H_{72}N_2O_{13}^+$ $[M+H]^+$ calcd: 811.4717 found: 811.4732.

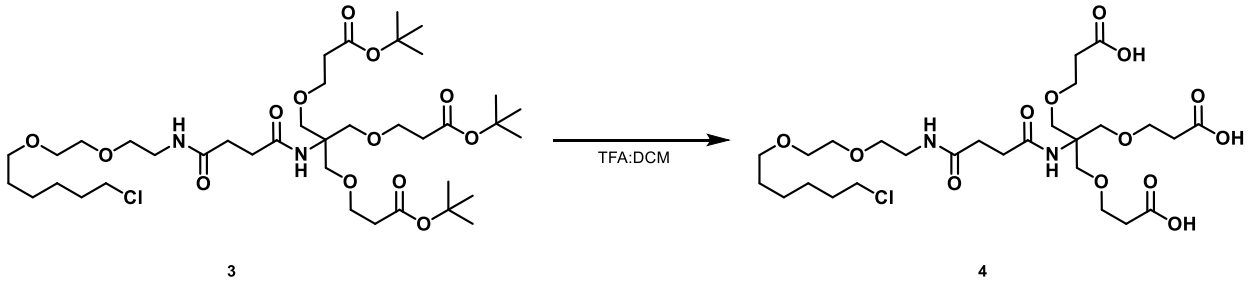

3 4

Synthesis of 4:

Trifluoroacetic acid (1 mL) was added to a solution of **3** (203 mg, 0.250 mmol) in DCM (3 mL). The reaction was stirred at 22 °C for 2 h, then the solvent removed under a stream of nitrogen. The remaining residue was co-evaporated with toluene (1 x 10 mL) and acetonitrile (2 x 10 mL), affording **4** as a colorless oil which was used for the following reaction without further purification. Analytical HPLC retention time 5.57 min; MS (ESI) exact mass for $C_{27}H_{48}N_2O_{13}^+$ $[M+H]^+$ calcd: 643.3 found: 643.3.

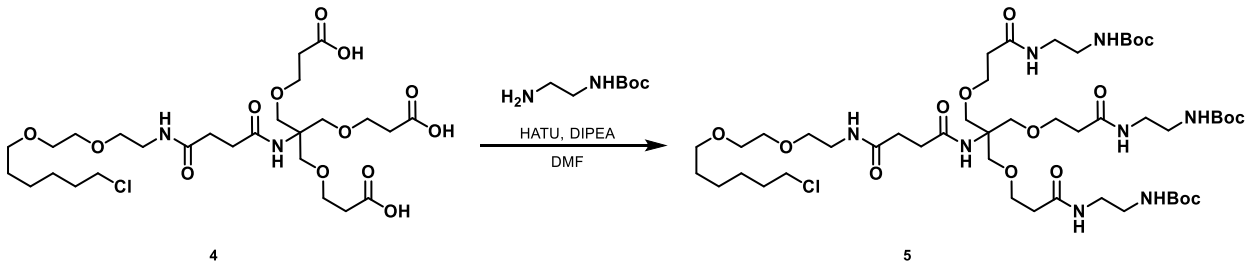

4 5

Synthesis of 5:

A vial was charged with **4** (161 mg, 0.250 mmol), 1-Boc-ethylenediamine (144 mg, 0.901 mmol) and HATU (342 mg, 0.901 mmol). Anhydrous DMF (2 mL) and anhydrous diisopropylethylamine (261 µL, 1.50 mmol) were added and the vial flushed with nitrogen, sealed, and stirred at 22 °C for 3 h. The solvent was removed *in vacuo* and the remaining residue diluted with DCM (100 mL) and washed with water (4 x 75 mL). The combined organics were dried with anhydrous sodium sulfate, filtered and the solvent removed *in vacuo* affording **5** as a colorless oil which was used for the following reaction without further purification. Analytical HPLC retention time 7.39 min; MS (ESI) exact mass for $C_{48}H_{90}ClN_8O_{16}^+$ $[M+H]^+$ calcd: 1069.6 found: 1069.3.

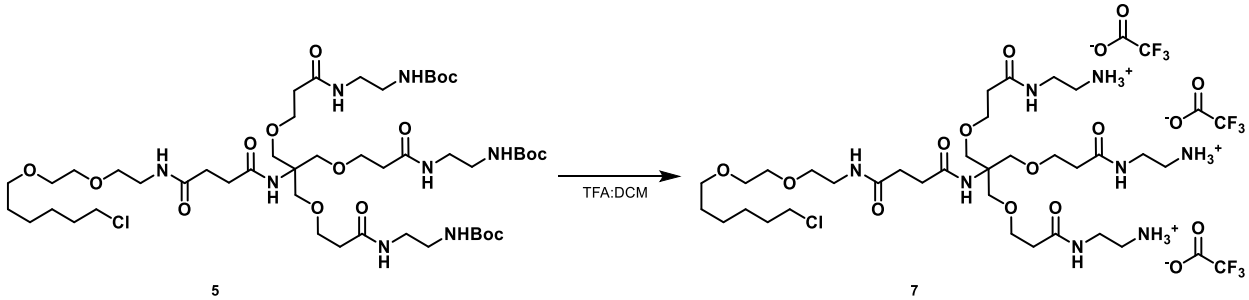

5 7

Synthesis of 7:

Trifluoroacetic acid (1 mL) was added to a solution of **5** (267.63 mg, 0.250 mmol) in DCM (3 mL). The reaction was stirred at 22 °C for 3 h, then the solvent removed under a stream of nitrogen. One-quarter of the remaining residue was then purified by preparative HPLC affording **7** as a colorless oil (43.0 mg, 38.7 µmol, 62% over three steps). ^{1}H NMR (400 MHz, MeOD) δ 3.68 (t, *J* = 6.0 Hz, 6H), 3.66 (s, 4H), 3.63 – 3.46 (m, 15H), 3.37 (t, *J* = 5.5 Hz, 2H), 3.08 (t, *J* = 6.0 Hz, 6H), 2.48 (m, 10H), 2.16 (s, 3H), 2.04 (s, 4H), 1.77 (p, *J* = 6.8 Hz, 2H), 1.61 (d, *J* = 7.1 Hz, 2H), 1.54 – 1.36 (m, 4H), 1.30 (s, 9H); Analytical HPLC retention time 3.77 min; MS (ESI) exact mass for $C_{33}H_{66}ClN_8O_{10}^+$ $[M+H]^+$ calcd: 769.5 found: 769.6; HR-ESI-MS m/z for $C_{33}H_{66}ClN_8O_{10}^+$ $[M+H]^+$ calcd: 769.4585 found: 769.4598.

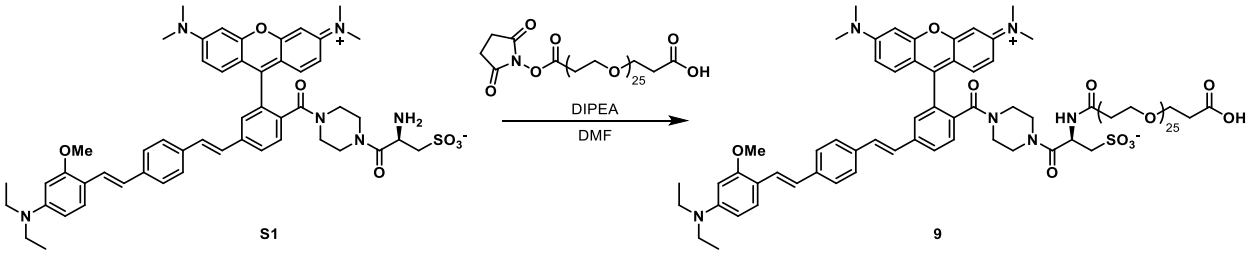

Synthesis of RhoVR1-PEG$_{25}$-Acid, 9:

A vial was charged with **S1** (22.8 mg, 25.0 µmol) and NHS-PEG$_{25}$-Acid (33.0 mg, 25.0 µmol). Anhydrous DMF (2 mL) and anhydrous diisopropylethylamine (7.0 uL, 50.0 µmol) were added and the vial flushed with nitrogen, sealed and stirred at 22 ºC for 6 h. The solvent was removed *in vacuo* and the remaining residue was then purified by preparative HPLC affording **9** as a purple solid (33.6 mg, 15.9 µmol, 64%); Analytical HPLC retention time 5.32 min; MS (ESI) exact mass for $C_{106}H_{164}ClN_6O_{35}S^{2+}$ $[M+2H]^{2+}$ calcd: 1057.0, found: 1056.8; HR-ESI-MS m/z for $C_{106}H_{164}ClNaN_6O_{35}S^{2+}$ $[M+2H+Na]^{3+}$ calcd: 661.6967 found: 661.6978.

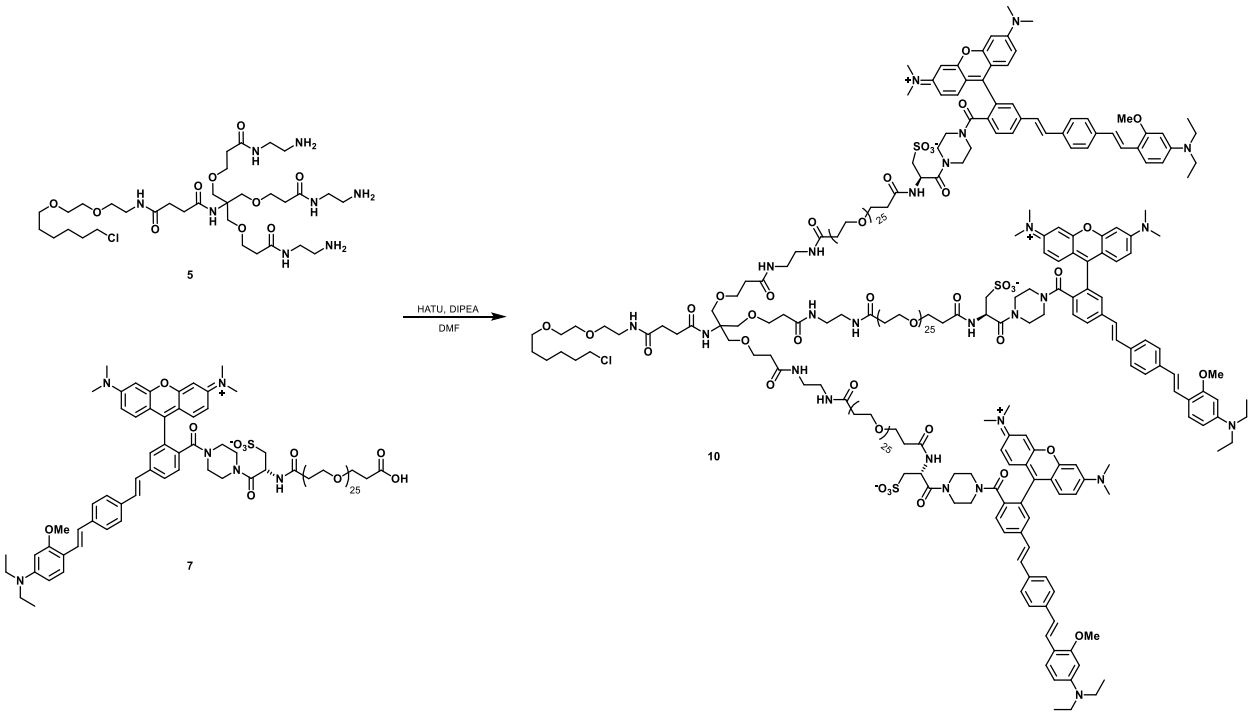

Synthesis of 10:

A vial was charged with **5** (0.77 mg, 1.00 μmol), **7** (6.34 mg, 3 μmol) and HATU (1.14 mg, 5.00 μmol). Anhydrous DMF (1 mL) and anhydrous diisopropylethylamine (0.87 μL, 5.00 μmol) were added and the vial flushed with nitrogen, sealed, and stirred at 22 °C for 16 h. The solvent was removed *in vacuo* and the remaining residue was then purified by preparative HPLC affording **10** as a purple solid (2.95 mg, 0.42 μmol, 42%). Analytical HPLC retention time 5.65 min; MS (ESI) exact mass for $C_{351}H_{552}ClN_{26}O_{112}S_3^+$ $[M+7H]^{7+}$ calcd: 1008.2 found: 1008.2; HR-ESI-MS m/z for $C_{351}H_{552}ClN_{26}O_{112}S_3^+$ $[M+7H]^{7+}$ calcd: 1008.2459 found: 1008.3897.

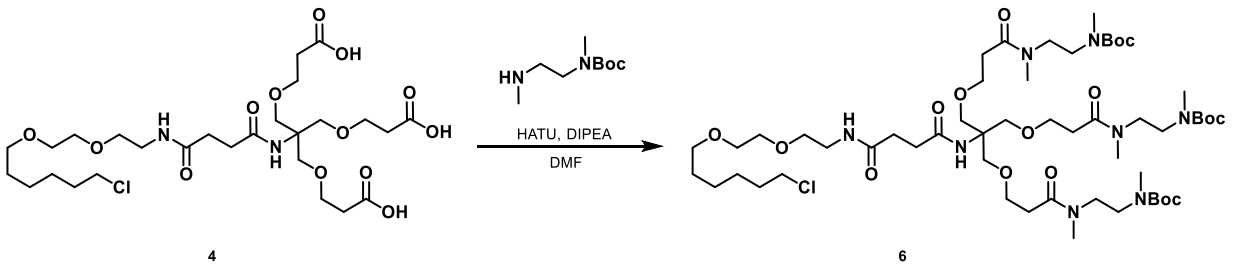

4 6

Synthesis of 6:

A vial was charged with **4** (161 mg, 0.250 mmol), tert-butyl methyl[2-(methylamino)ethyl]carbamate (170 mg, 0.901 mmol) and HATU (342 mg, 0.901 mmol). Anhydrous DMF (2 mL) and anhydrous diisopropylethylamine (261 μL, 1.50 mmol) were added and the vial flushed with nitrogen, sealed, and stirred at 22 °C for 3 h. The solvent was removed *in vacuo* and the remaining residue diluted with DCM (100 mL) and washed with water (4x 75 mL). The combined organics were dried with anhydrous sodium sulfate, filtered and the solvent removed *in vacuo* affording **6** as a colorless oil which was used for the following reaction without further purification. Analytical HPLC retention time 5.62 min; MS (ESI) exact mass for $C_{54}H_{101}ClNaN_8O_{16}^+$ $[M+Na]^+$ calcd: 1175.7 found: 1176.1.

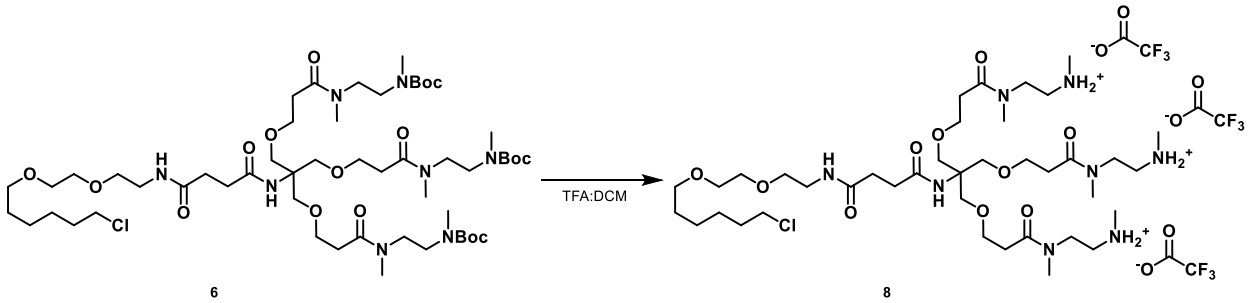

6 8

Synthesis of 8:

Trifluoroacetic acid (1 mL) was added to a solution of **6** (288.0 mg, 0.250 mmol) in DCM (3 mL). The reaction was stirred at 22 °C for 3 h, then the solvent removed under a stream of nitrogen. One quarter of the remaining residue was then purified by preparative HPLC affording **8** as a colorless oil (60.8 mg, 50.9 μmol, 81.3% over three steps). Analytical HPLC retention time 3.71 min; MS (ESI) exact mass for $C_{39}H_{78}ClN_8O_{10}^+$ $[M+H]^+$ calcd: 853.6 found: 853.4; HR-ESI-MS m/z for $C_{39}H_{78}ClN_8O_{10}^+$ $[M+H]^+$ calcd: 853.5524 found: 853.5497.

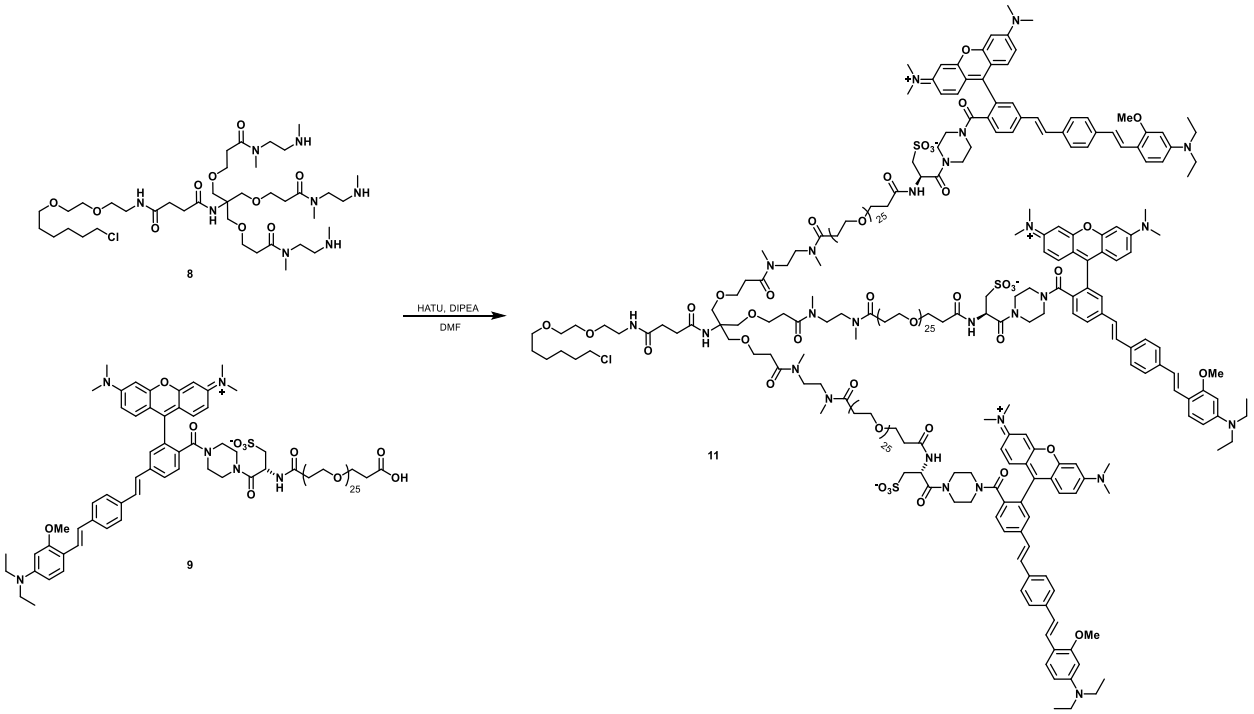

Synthesis of 11:
A vial was charged with **8** (0.85 mg, 1.00 μmol), **9** (6.34 mg, 3 μmol) and HATU (1.14 mg, 5.00 μmol). Anhydrous DMF (1 mL) and anhydrous diisopropylethylamine (0.87 μL, 5.00 μmol) were added and the vial flushed with nitrogen, sealed, and stirred at 22 °C for 16 h. The solvent was removed *in vacuo* and the remaining residue was then purified by preparative HPLC affording **11** as a purple solid (2.90 mg, 0.41 μmol, 41%). Analytical HPLC retention time 5.88 min; MS (ESI) exact mass for $C_{357}H_{565}ClNa_6N_{26}O_{112}S_3^+$ $[M+8H]^{8+}$ calcd: 892.9 found: 892.5; HR-ESI-MS m/z for $C_{357}H_{558}ClNa_6N_{26}O_{112}S_3^{7+}$ $[M+H+6Na]^{7+}$ calcd: 1039.1009 found: 1039.1015.

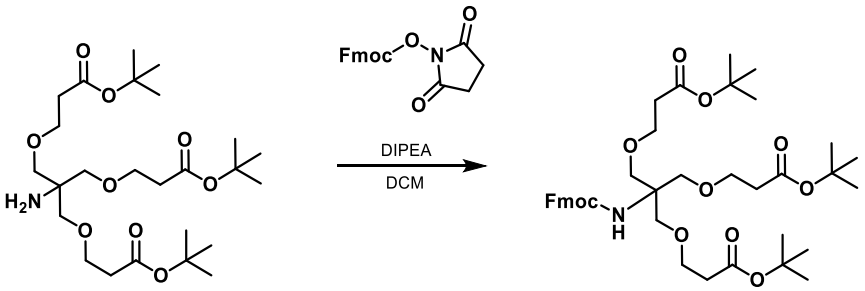

Synthesis of 12:
A vial was charged with **1** (505 mg, 1.00 mmol), Fmoc-NHS (371 mg, 1.10 mmol) and DCM (5 mL). Diisopropylethylamine (209 μL, 1.20 mmol) was added and the reaction stirred at 22 °C for 16 h. The reaction was diluted with DCM (50 mL) and washed with water (2 x 50 mL). The solvent was removed *in vacuo*, and the remaining material diluted with ethyl acetate (50 mL) and filtered through a celite plug, then concentrated again *in vacuo* to afford **12** as a colorless oil (700 mg, 0.96 mmol, 96%). ^{1}H NMR (400 MHz, $CDCl_3$) δ 7.81 (d, *J* = 7.5 Hz, 2H), 7.67 (d, *J* = 7.5 Hz, 2H), 7.44 (t, *J* = 7.4 Hz, 2H), 7.36 (td, *J* = 7.4, 1.2 Hz, 2H), 5.42 (br, 1H), 4.33 (br, 2H), 4.25 (t, *J* = 6.9

Hz, 1H), 3.71 (s, 12H), 2.50 (t, *J* = 5.2 Hz, 6H), 1.49 (s, 27H); HR-ESI-MS m/z for $C_{40}H_{57}NaNO_{11}^+$ $[M+Na]^+$ calcd: 750.3824 found: 750.3818.

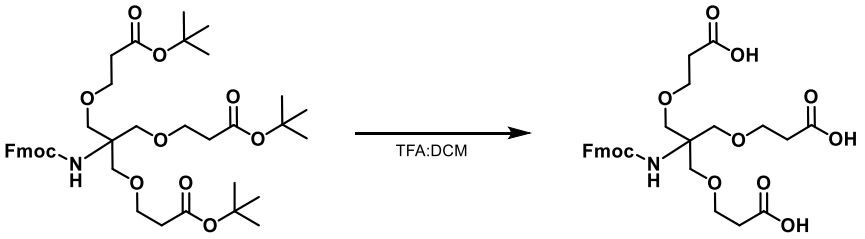

12 13

Synthesis of 13:
Trifluoroacetic acid (3 mL) was added to a solution of **12** (300 mg, 0.412 mmol) in DCM (3 mL). The reaction was stirred at 22 °C for 2 h, then the solvent removed under a stream of nitrogen. The remaining residue was diluted with ethyl acetate (50 mL) and washed with 1 M hydrochloric acid (2 x 50 mL). The combined organics were dried with anhydrous sodium sulfate, filtered and the solvent removed *in vacuo* affording **13** as a yellow oil which was used for the following reaction without further purification. Analytical HPLC retention time 6.09 min; MS (ESI) exact mass for $C_{28}H_{34}NO_{11}^+$ $[M+H]^+$ calcd: 560.2 found: 560.3.

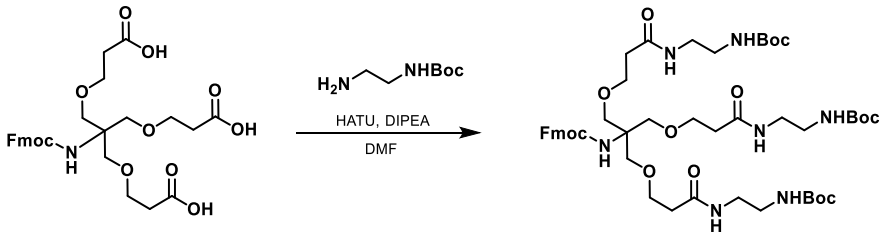

13 14

Synthesis of 14:
A vial was charged with **13** (165 mg, 0.295 mmol), 1-Boc-ethylenediamine (170 mg, 1.06 mmol) and HATU (404 mg, 1.06 mmol). Anhydrous DMF (3 mL) and anhydrous diisopropylethylamine (205 µL, 1.18 mmol) were added and the vial flushed with nitrogen, sealed, and stirred at 22 °C for 18 h. The solvent was removed *in vacuo* and the remaining residue diluted with DCM (100 mL) and washed with 1 M hydrochloric acid (3 x 100 mL). The combined organics were dried with anhydrous sodium sulfate, filtered and the solvent removed *in vacuo*. The remaining residue was purified by flash chromatography (0-10% methanol in ethyl acetate, linear gradient) affording **14** as a colorless oil (202 mg, 205 µmol, 70%). ^{1}H NMR (400 MHz, $CDCl_3$) δ 7.81 (d, *J* = 7.5 Hz, 2H), 7.65 (d, *J* = 7.5 Hz, 2H), 7.44 (t, *J* = 7.4 Hz, 2H), 7.36 (t, *J* = 7.4 Hz, 2H), 6.95 (br, 3H), 5.64 (br, 1H), 5.32 (br, 3H), 4.42 (br, 2H), 4.24 (t, *J* = 6.2 Hz, 1H), 3.71 (s, 12H), 3.38 (m, 6H), 3.28 (m, 6H), 2.44 (s, 6H), 1.46 (s, 27H); Analytical HPLC retention time 8.00 min; MS (ESI) exact mass for $C_{49}H_{75}ClN_7O_{17}^+$ $[M+H]^+$ calcd: 986.5 found: 986.7; HR-ESI-MS m/z for $C_{49}H_{75}NaN_7O_{14}^+$ $[M+Na]^+$ calcd: 1008.5264 found: 1008.5274.

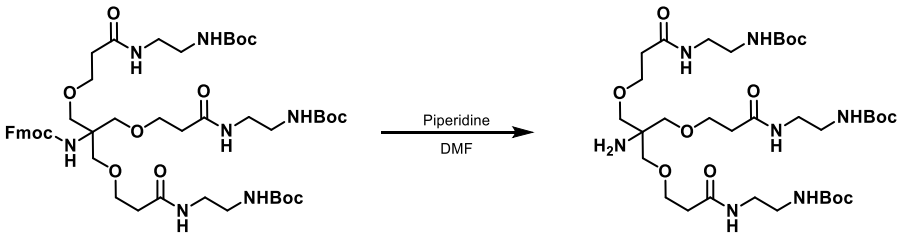

14 15

Synthesis of 15:

A vial was charged with **14** (99 mg, 100 μmol) and DMF (2 mL). Piperidine (100 uL, 1.01 mmol) was added and the reaction stirred at 22 °C for 4 h. The solvent was removed *in vacuo* and the remaining residue diluted with ethyl acetate (20 mL) and washed with dilute sodium hydroxide (2 x 25 mL). The combined organics were dried with anhydrous sodium sulfate, filtered and the solvent removed *in vacuo*. The remaining residue was then triturated with Et_2O (3 x 10 mL) to remove remaining 1-((9H-fluoren-9-yl)methyl)piperidine affording **15** as a colorless oil (60 mg, 78.5 μmol, 78%). ^{1}H NMR (400 MHz, $CDCl_3$) δ 7.09 (s, 3H), 5.42 (s, 3H), 3.75 (t, *J* = 5.7 Hz, 6H), 3.46 – 3.35 (m, 12H), 3.30 (s, 6H), 2.48 (t, *J* = 5.7 Hz, 6H), 1.48 (s, 27H).; Analytical HPLC retention time 5.35 min; MS (ESI) exact mass for $C_{34}H_{66}N_7O_{12}^+$ $[M+H]^+$ calcd: 764.5 found: 764.9; HR-ESI-MS m/z for $C_{34}H_{66}N_7O_{12}^+$ $[M+H]^+$ calcd: 764.4759 found: 764.4757.

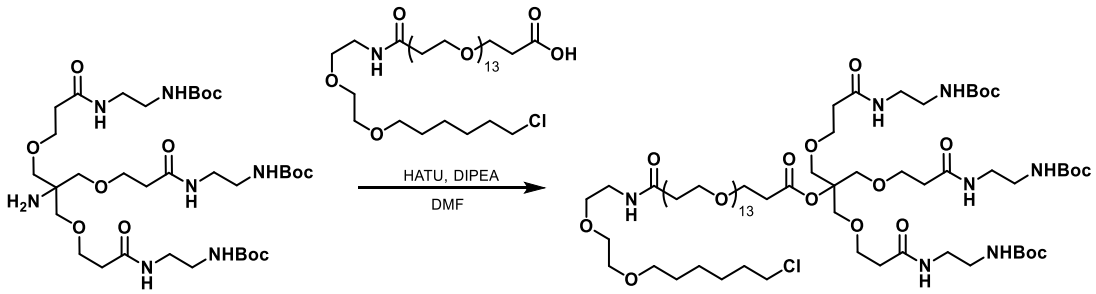

15 16

Synthesis of 16:

A vial was charged with **15** (15.0 mg, 19.6 μmol), Halo-PEG_{13}-Acid (16.0 mg, 17.9 μmol) and HATU (10.2 mg, 26.8 μmol). Anhydrous DMF (500 μL) and anhydrous diisopropylethylamine (6.2 μL, 35.7 μmol) were added and the vial flushed with nitrogen, sealed, and stirred at 22 °C for 4 h. The solvent was removed *in vacuo* and the remaining residue purified by preparative HPLC affording **16** as a colorless solid (9.9 mg, 6.0 μmol, 34%); Analytical HPLC retention time 7.03 min; MS (ESI) exact mass for $C_{74}H_{143}ClN_8O_{29}^{2+}$ $[M+2H]^{2+}$ calcd: 821.5 found: 822.2; HR-ESI-MS m/z for $C_{74}H_{143}ClN_8O_{29}^{2+}$ $[M+2H]^{2+}$ calcd: 821.4830 found: 821.4842.

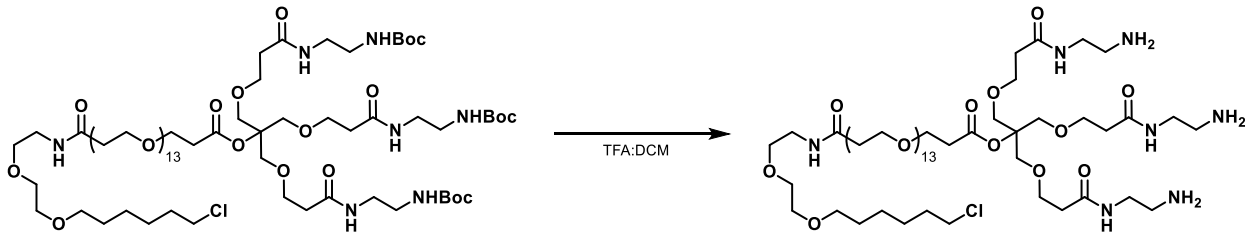

16 17

Synthesis of 17:

Trifluoroacetic acid (1 mL) was added to a solution of **16** (9.9 mg, 6.03 μmol) in DCM (1 mL). The reaction was stirred at 22 °C for 2 h, then the solvent removed under a stream of nitrogen. The remaining residue was co-evaporated with toluene (1 x 10 mL) and acetonitrile (2 x 10 mL), affording **17** which was used without further purification for the next reaction. Analytical HPLC retention time 4.47 min; MS (ESI) exact mass for $C_{59}H_{119}ClN_8O_{23}^{2+}$ $[M+2H]^{2+}$ calcd: 671.4 found: 671.1; HR-ESI-MS m/z for $C_{59}H_{119}ClN_8O_{23}^{2+}$ $[M+2H]^{2+}$ calcd: 671.4044 found: 671.4048.

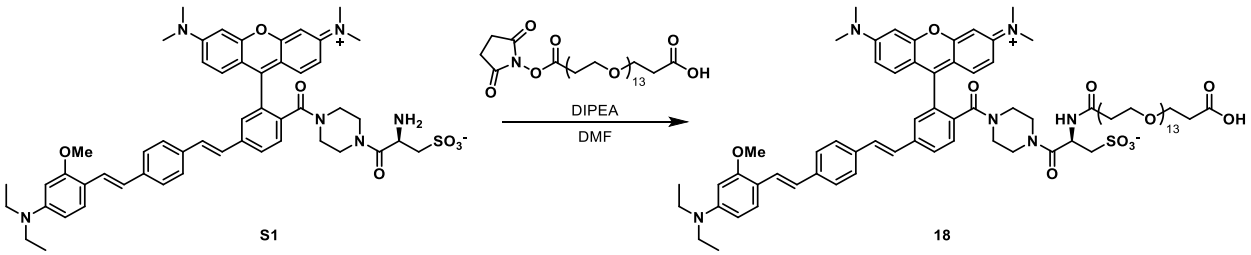

S1 18

Synthesis of RhoVR1-PEG$_{13}$-Acid, 18:

A vial was charged with **S1** (15.0 mg, 16.5 μmol) and NHS-PEG$_{13}$-Acid (10.4 mg, 13.2 μmol). Anhydrous DMF (1 mL) and anhydrous diisopropylethylamine (5.7 uL, 32.9 μmol) were added and the vial flushed with nitrogen, sealed and stirred at 22 ºC for 22 h. The solvent was removed *in vacuo* and the remaining residue was then purified by preparative HPLC affording **18** as a purple solid (14.0 mg, 8.84 μmol, 54%). Analytical HPLC retention time 5.37 min; MS (ESI) exact mass for $C_{82}H_{116}ClN_6O_{23}S^{2+}$ $[M+2H]^{2+}$ calcd: 792.4, found:793.0; HR-ESI-MS m/z for $C_{82}H_{114}ClNa_2N_6O_{23}S^{2+}$ $[M+2Na]^{2+}$ calcd: 814.3720 found: 814.3720.

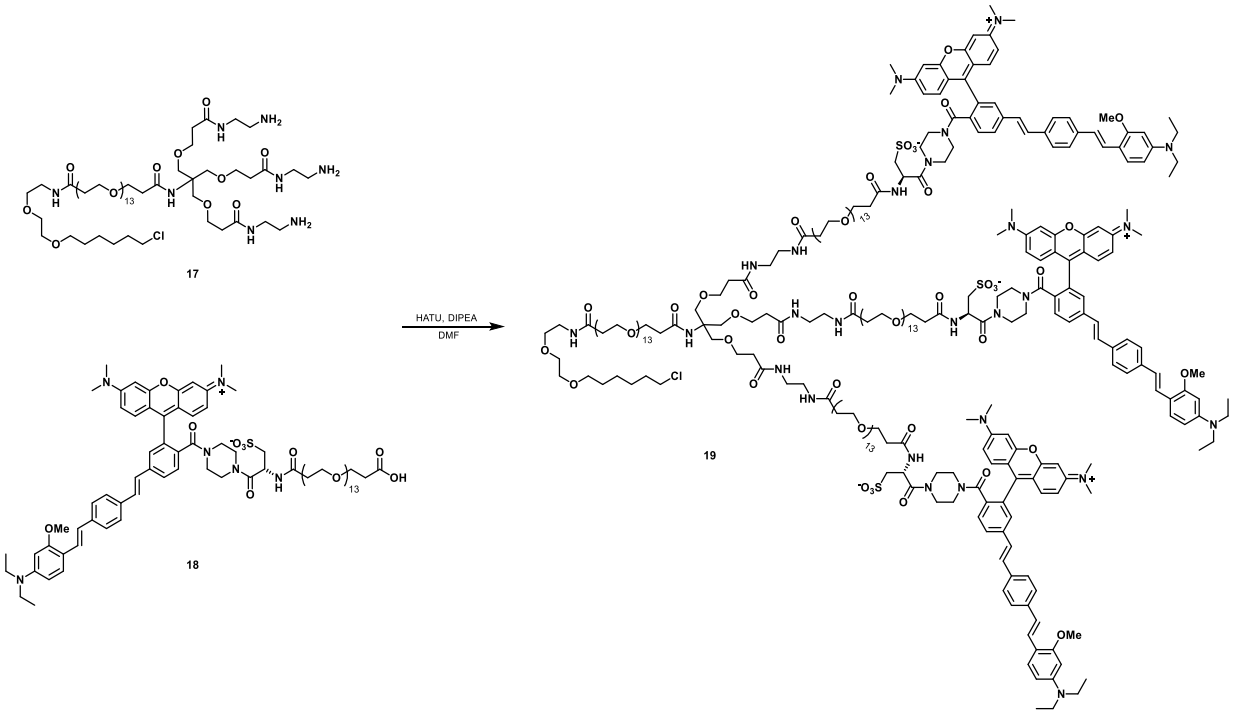

Synthesis of 19:
A vial was charged with **17** (2.00 mg, 1.49 μmol), **18** (7.08 mg, 4.47 μmol) and HATU (1.98 mg, 5.22 μmol). Anhydrous DMF (1 mL) and anhydrous diisopropylethylamine (0.91 μL, 5.22 μmol) were added and the vial flushed with nitrogen, sealed, and stirred at 22 °C for 16 h. The solvent was removed *in vacuo* and the remaining residue was then purified by preparative HPLC affording **19** as a purple solid (3.60 mg, 0.60 μmol, 40%). Analytical HPLC retention time 5.84 min; MS (ESI) exact mass for $C_{305}H_{453}ClN_{26}O_{89}S_3^{6+}$ $[M+6H]^{6+}$ calcd: 892.9 found: 1007.8; HR-ESI-MS m/z for $C_{305}H_{454}ClN_{26}O_{89}S_3^{7+}$ $[M+7H]^{7+}$ calcd: 1007.0181 found: 1007.0188.

Spectroscopic Studies

Stock solutions of RhoVRs were prepared in DMSO (1-5 mM) and diluted with PBS (10 mM KH_2PO_4, 30 mM $Na_2HPO_4{\cdot}7H_2O$, 1.55 M NaCl, pH 7.2) solution containing 0.10 % (w/w) SDS (1:100-1:1000 dilution). UV-Vis absorbance and fluorescence spectra were recorded using a Shimadzu 2501 Spectrophotometer (Shimadzu) and a Quantamaster Master 4 L-format scanning spectrofluorometer (Photon Technologies International). The fluorometer is equipped with an LPS-220B 75-W xenon lamp and power supply, A-1010B lamp housing with integrated igniter, switchable 814 photon-counting/analog photomultiplier detection unit, and MD5020 motor driver. Samples were measured in 1-cm path length quartz cuvettes (Starna Cells).

Cell Culture

All animal procedures were approved by the UC Berkeley Animal Care and Use Committees and conformed to the NIH Guide for the Care and Use and Laboratory Animals and the Public Health Policy.

Human embryonic kidney 293T (HEK) cells were passaged and plated onto 12 mm glass coverslips pre-coated with Poly-D-Lysine (PDL; 1 mg/ml; Sigma-Aldrich) to provide a confluency of ~15% and 50% for electrophysiology and imaging, respectively. HEK cells were plated and maintained in Dulbecco's modified eagle medium (DMEM) supplemented with 4.5 g/L D-glucose, 10% FBS and 1% Glutamax. Transfection of genetic tools was carried out using Lipofectamine 3000 24 h after plating. Imaging was performed 18-24 h following transfection.

Unless stated otherwise, HEK cells were loaded with RhoVRs stock solutions diluted in DMSO to 500 μM, and then diluted 1:1000 in HBSS. All imaging experiments were performed in HBSS (in mM) 140 NaCl, 2.5 KCl, 10 HEPES, 10 D-glucose 1.3 $MgCl_2$ and 2 $CaCl_2$; pH 7.3 and 290 mOsmol.

Imaging Parameters

Epifluorescence imaging was performed on an AxioExaminer Z-1 (Zeiss) equipped with a Spectra-X Light engine LED light (Lumencor), controlled with Slidebook (v6, Intelligent Imaging Innovations). Co-incident excitation with multiple LEDs was controlled by Lumencor software triggered through a Digidata 1332A digitizer and pCLAMP 10 software (Molecular Devices). Images were acquired with either a W-Plan-Apo 20x/1.0 water objective (20x; Zeiss) or a W-Plan-Apo 63x/1.0 water objective (63x; Zeiss). Images were focused onto either an OrcaFlash4.0 sCMOS camera (sCMOS; Hamamatsu) or an eVolve 128 EMCCD camera (EMCCD; Photometrix). For RhoVR images, the excitation light was delivered from a LED (9.72 W/cm^2 for images, 32 W/cm^2 for voltage recordings) at 542/33 (bandpass) nm and emission was collected with a quadruple emission filter (430/32, 508/14, 586/30, 708/98 nm) after passing through a quadruple dichroic mirror (432/38, 509/22, 586/40, 654 nm LP). For eGFP images, the excitation light was delivered from a LED (5.77 W/cm^2) at 475/34 nm and emission was collected with a quadruple emission filter (430/32, 508/14, 586/30, 708/98 nm) after passing through a quadruple dichroic mirror (432/38, 509/22, 586/40, 654 nm LP). For BeRST-Halo images, the excitation light was delivered from a LED (6.72 W/cm^2) at 631/28 (bandpass) nm and emission was collected with a quadruple emission filter (430/32, 508/14, 586/30, 708/98 nm) after passing through a quadruple dichroic mirror (432/38, 509/22, 586/40, 654 nm LP).

Functional imaging of the RhoVR voltage dyes was performed using a 20x objective paired with image capture from the EMCCD camera at a sampling rate of 0.5 kHz. RhoVRs were excited using the 542 nm LED with an intensity of 9.73 W/cm^2. For initial voltage characterization emission was collection with the QUAD filter and dichroic (see above).

Image Analysis

Analysis of voltage sensitivity in HEK cells was performed using ImageJ (FIJI). Briefly, a region of interest (ROI) was selected automatically based on fluorescence intensity and applied as a mask to all image frames. Fluorescence intensity values were calculated at known baseline and voltage step epochs. For analysis of RhoVR 1 voltage responses in neurons, regions of interest encompassing cell bodies (all of approximately the same size) were drawn in ImageJ and the mean fluorescence intensity for each frame extracted. $\Delta F/F$ values were calculated by first subtracting a mean background value from all raw fluorescence frames, bypassing the noise amplification which arises from subtracting background for each frame, to give a background subtracted trace (bkgsub). A baseline fluorescence value (F_{base}) is calculated either from the first several (10-20) frames of the experiment for evoked activity, or from the median for spontaneous activity, and was

subtracted from each timepoint of the bkgsub trace to yield a ΔF trace. The ΔF was then divided by F_{base} to give ΔF/F traces. No averaging has been applied to any voltage traces.

Electrophysiology

For electrophysiological experiments, pipettes were pulled from borosilicate glass (Sutter Instruments, BF150-86-10), with a resistance of 5–8 MΩ, and were filled with an internal solution; 115 mM potassium gluconate, 10 mM BAPTA tetrapotassium salt, 10 mM HEPES, 5 mM NaCl, 10 mM KCl, 2 mM ATP disodium salt, 0.3 mM GTP trisodium salt (pH 7.25, 275 mOsm). Recordings were obtained with an Axopatch 200B amplifier (Molecular Devices) at room temperature. The signals were digitized with Digidata 1440A, sampled at 50 kHz and recorded with pCLAMP 10 software (Molecular Devices) on a PC. Fast capacitance was compensated in the on-cell configuration. For all electrophysiology experiments, recordings were only pursued if series resistance in voltage clamp was less than 30 MΩ. For whole-cell, voltage clamp recordings in HEK 293T cells, cells were held at -60 mV and 100 ms hyper- and de- polarizing steps applied from -100 to +100 mV in 20 mV increments.

Figures and Schemes

Scheme A1-1: *General design of TriRhoVRs*

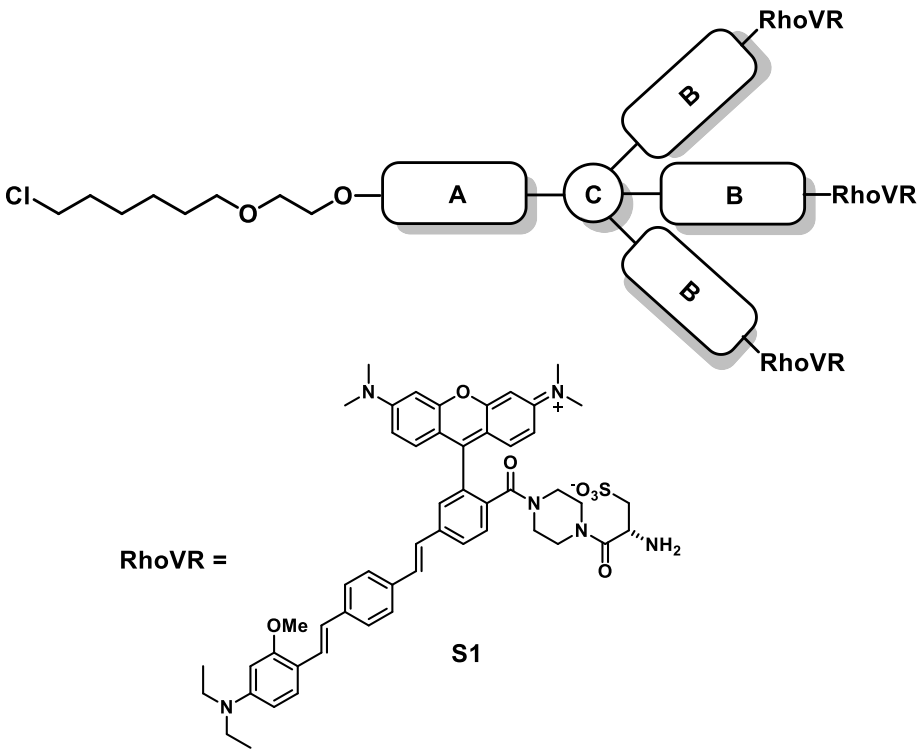

Scheme A1-1: General design of TriRhoVRs. The central core **A** was composed of a tris(hydroxylmethyl)-aminomethane base. Linkers **B** and **C** were composed of PEG linkers of varying lengths. RhoVR derivative **S1** was used to generate TriRhoVRs due to its high voltage sensitivity but realitively low brightness.

Scheme A1-2: *Synthesis of asymmetrical TriRhoVRs **10** and **11***

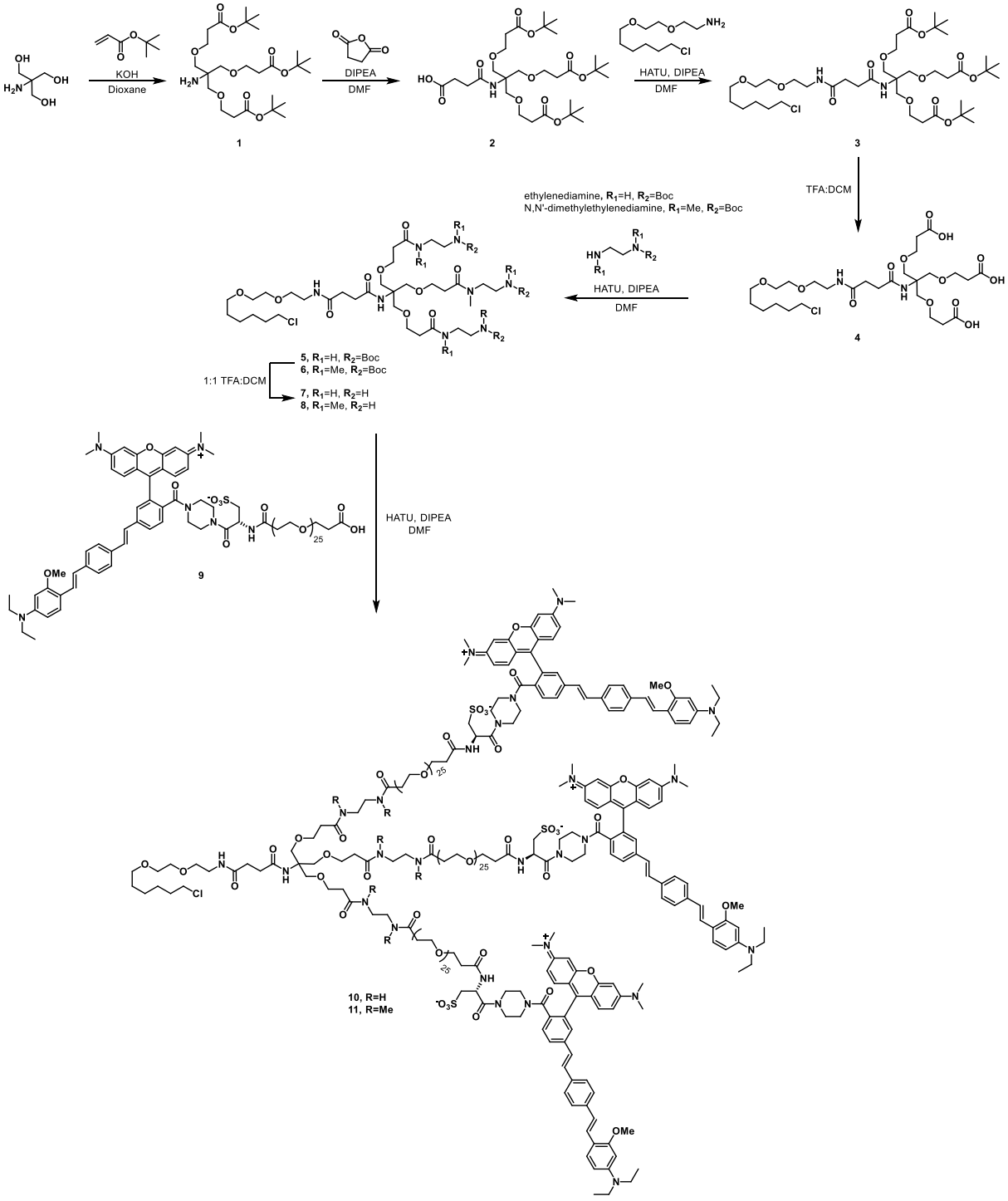

Scheme A1-2: Synthesis of asymmetrical TriRhoVRs **10** and **11**.

Scheme A1-3: *Synthesis of symmetrical TriRhoVR* ***19***

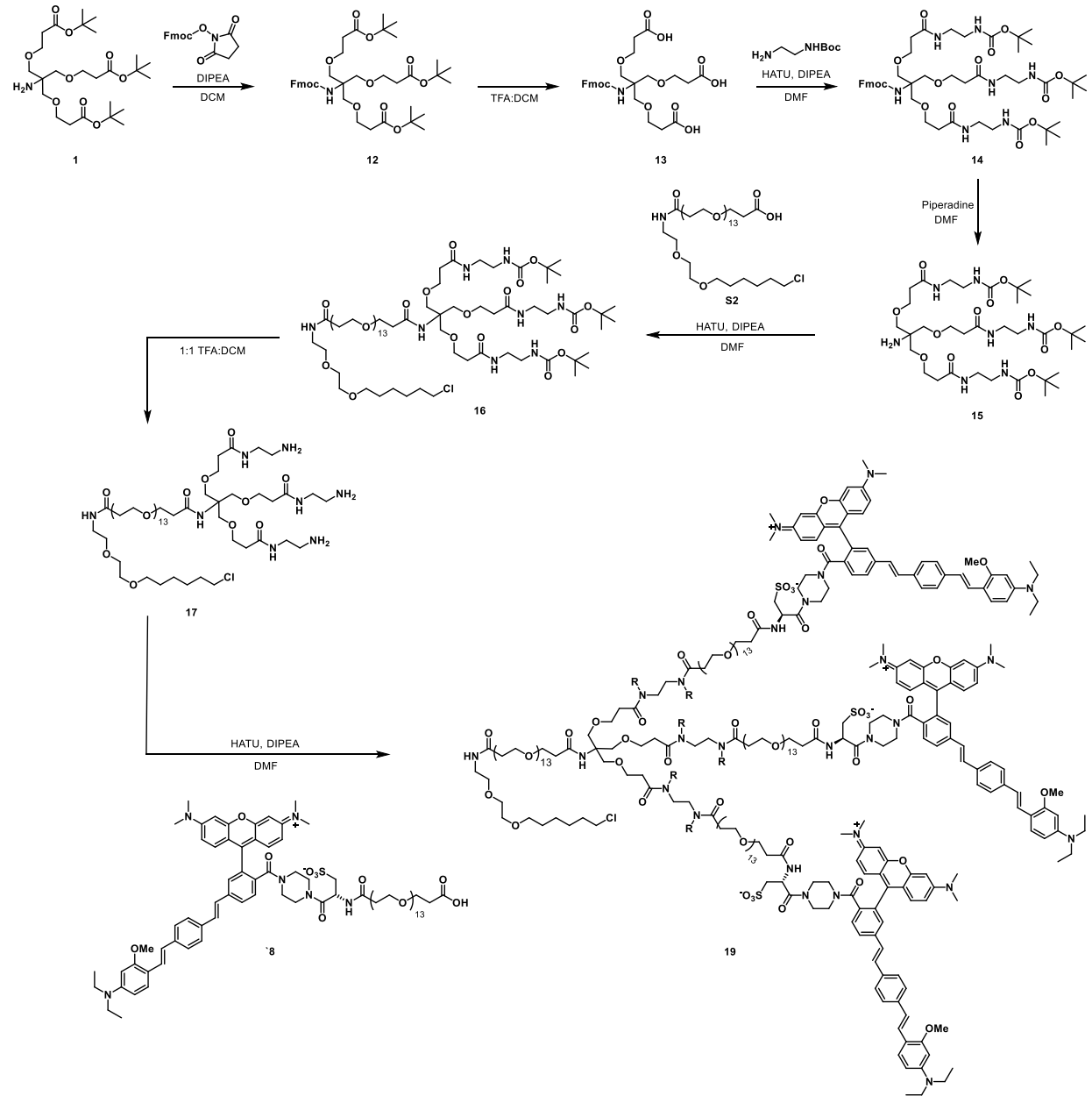

Scheme A1-3: Synthesis of symmetrical TriRhoVR **19**.

Table 1-1: *Properties of RhoVRs*

RhoVR-Halo Derivative	ε_{565}[a] M^{-1} cm^{-1}	Φ[b] (λ_{max}/nm)	$\Delta F/F$[c] (100 mV)	Rel. Brightness	SNR[c] (100 mV)
RhoVR 1 (500 nM)	87,000	4.5%	47%	100%	90
RhoVR1-PEG_{25}-Halo	74,000	5.0%	34%	30%	34
TriRhoVR-A, **11**	268,000	0.6%	20%	7%	16[d]
TriRhoVR-S, **20**	265,000	0.7%	14%	-%	8[d]

[a] PBS, pH 7.2, 0.1% SDS, [b] Absolute EtOH, [c] Measured with patch-clamp electrophysiology in HEK cells, [d] Illuminated at 32 W/cm^2

Figure A1-1: *Absorption and emission profiles of TriRhoVRs*

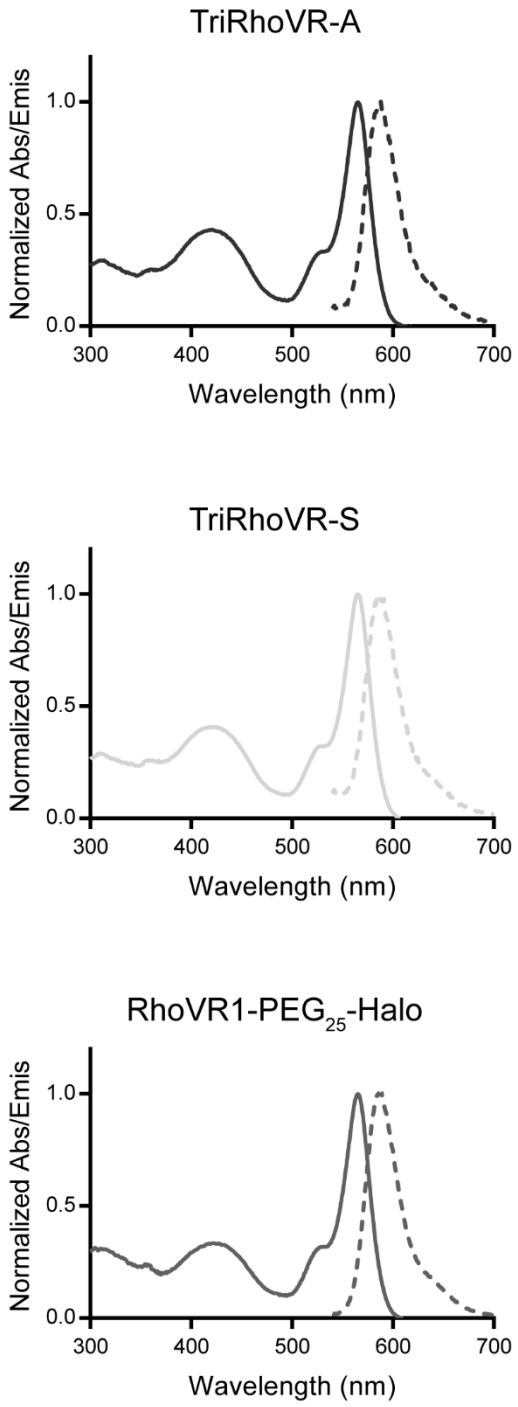

Figure A1-1: Absorption and emission profiles of TriRhoVRs. Both TriRhoVR-A and TriRhoVR-S have very similar absorption profiles to RhoVR1-PEG_{25}-Halo, with an absorption maximum at 565 nm and an emission maximum at 586 nm.

Figure A1-2: *Cellular experiments with TriRhoVR-A and TriRhoVR-S*

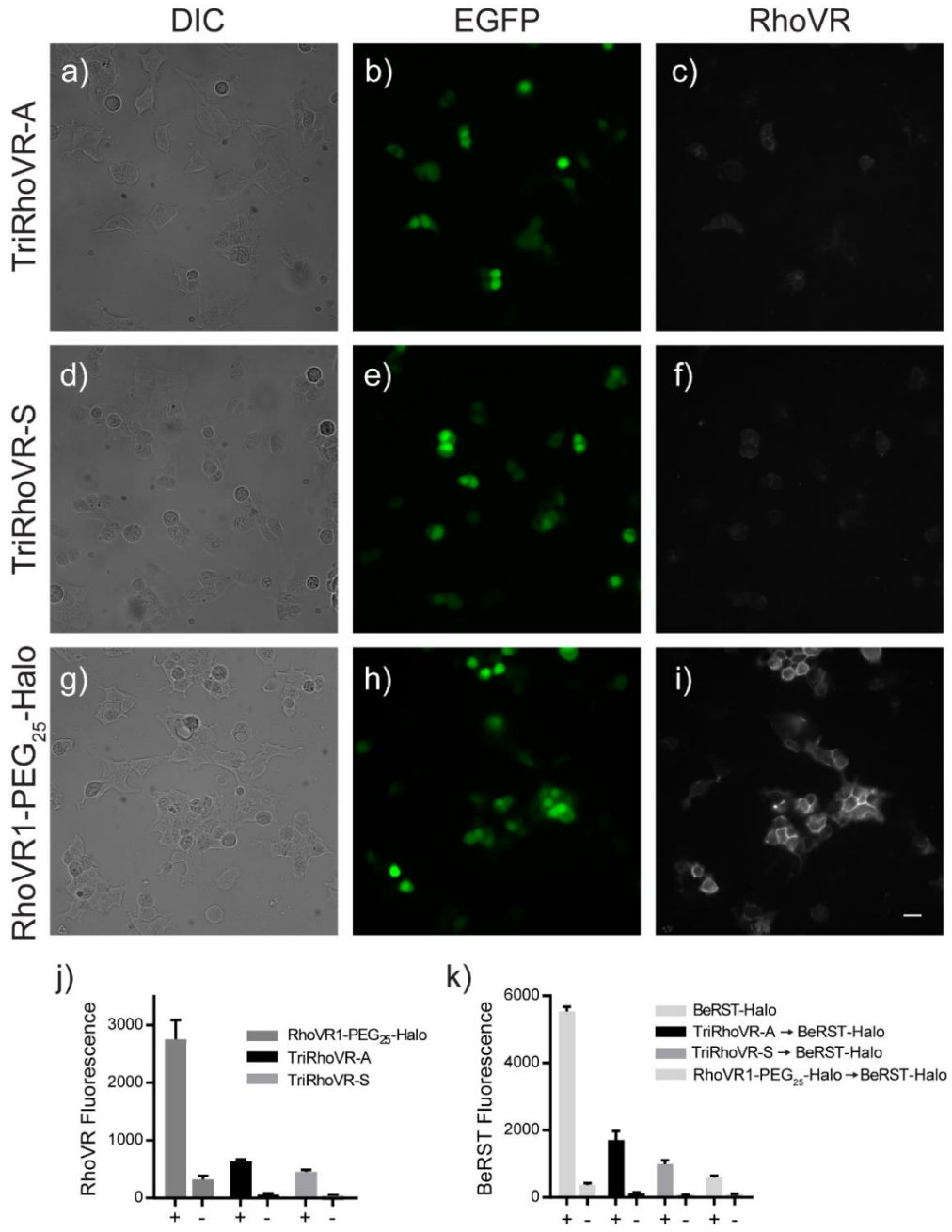

Figure A1-2: Relative brightness of TriRhoVRs vs. RhoVR1-PEG_{25}-Halo loaded at 50 nM onto HEK cells sparsely transfected with HaloTag. (a-c) Images from cells loaded with TriRhoVR-A. (d-f) Images for cells loaded with TriRhoVR-S. (g-i) Images for cells loaded with RhoVR1-PEG_{25}-Halo. Scale bar is 20 μm. (j) quantification of RhoVR fluorescence of each loading condition. (+) indicates HaloTag-positive ROIs, (-) indicates untransfected cells. The TriRhoVRs were found to be approximately 5-fold dimmer than RhoVR1-PEG_{25}-Halo. (k) To determine if TriRhoVRs were reacting with the HaloTag protein, cells were pre-loaded with either a TriRhoVR or RhoVR1-PEG_{25}-Halo for 30 min, then 30 min with BeRST-Halo. We found BeRST-Halo labeling was significantly attenuated when loaded after RhoVR1-PEG_{25}-Halo and to a lesser extent TriRhoVRs. This implies the degree of labeling for TriRhoVRs is lower than that of RhoVR1-PEG_{25}-Halo, but not low enough to fully account for the much lower brightness in cells. All error bars are S.E.M.

Figure A1-3: *Voltage sensitivities of TriRhoVR-A and TriRhoVR-S*

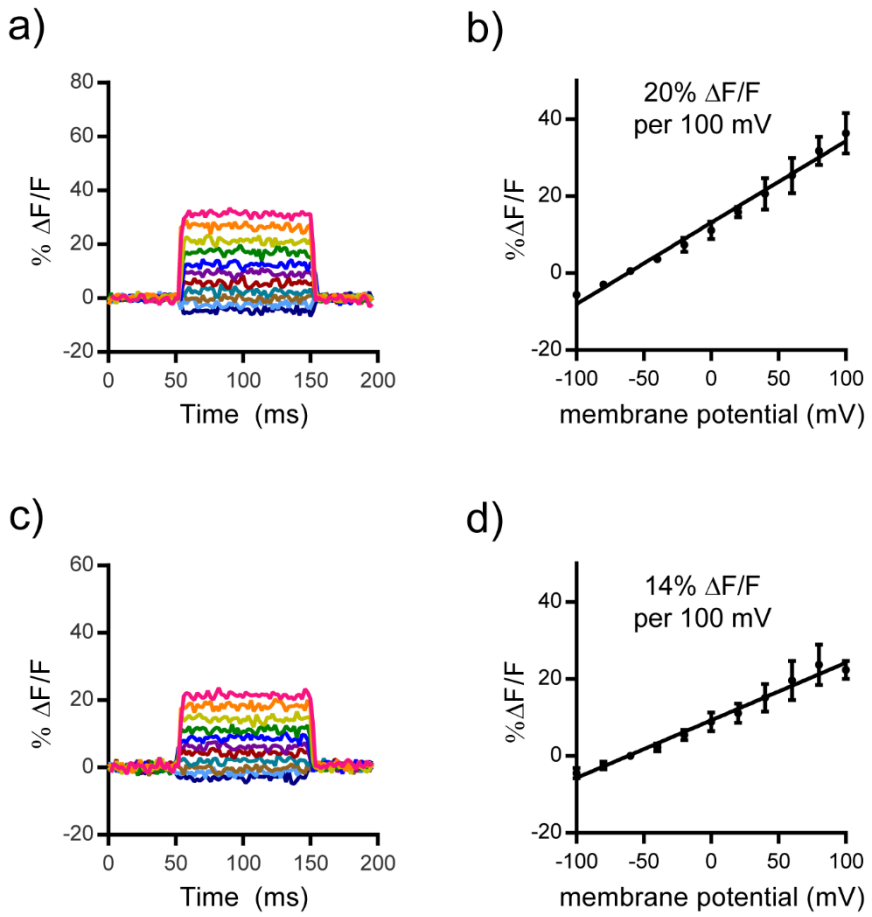

Figure A1-3: Voltage sensitivities of TriRhoVRs. (a) Plot of the fractional change in fluorescence of TriRhoVR-A vs time for 100 ms hyper- and depolarizing steps (±100 mV in 20 mV increments) from a holding potential of -60 mV for single HEK cells under whole-cell voltage clamp mode. (b) Plot of %ΔF/F vs final membrane potential for TriRhoVR-A (n=3). (c) Plot of the fractional change in fluorescence of TriRhoVR-S vs time for 100 ms hyper- and depolarizing steps (±100 mV in 20 mV increments) from a holding potential of -60 mV for single HEK cells under whole-cell voltage clamp mode. (d) Plot of %ΔF/F vs final membrane potential for TriRhoVR-S (n=3).

References

(1) Kulkarni, R. U.; Miller, E. W. Voltage Imaging: Pitfalls and Potential. *Biochemistry* **2017**, *56* (39), 5171–5177.

(2) Fisher, J. A. N.; Barchi, J. R.; Welle, C. G.; Kim, G.-H.; Kosterin, P.; Obaid, A. L.; Yodh, A. G.; Contreras, D.; Salzberg, B. M. Two-Photon Excitation of Potentiometric Probes Enables Optical Recording of Action Potentials From Mammalian Nerve Terminals In Situ. *J. Neurophysiol.* **2008**, *99* (3), 1545–1553.

(3) Kulkarni, R. U.; Kramer, D. J.; Pourmandi, N.; Karbasi, K.; Bateup, H. S.; Miller, E. W. Voltage-Sensitive Rhodol with Enhanced Two-Photon Brightness. *Proc. Natl. Acad. Sci.* **2017**, *114* (11), 2813–2818.

(4) Kulkarni, R. U.; Vandenberghe, M.; Thunemann, M.; James, F.; Andreassen, O. A.; Djurovic, S.; Devor, A.; Miller, E. W. In Vivo Two-Photon Voltage Imaging with Sulfonated Rhodamine Dyes. *ACS Cent. Sci.* **2018**, *4* (10), 1371–1378.

(5) Miller, G. J.; Gardiner, J. M. Adaptable Synthesis of C-Glycosidic Multivalent Carbohydrates and Succinamide-Linked Derivatization. *Org. Lett.* **2010**, *12* (22), 5262–5265.

(6) Shaikh, H. A.; Sönnichsen, F. D.; Lindhorst, T. K. Synthesis of Glycocluster Peptides. *Carbohydr. Res.* **2008**, *343* (10–11), 1665–1674.

(7) Newkome, G. R.; Shreiner, C. Dendrimers Derived from 1 → 3 Branching Motifs. *Chem. Rev.* **2010**, *110* (10), 6338–6442.

(8) Zhegalova, N. G.; He, S.; Zhou, H.; Kim, D. M.; Berezin, M. Y. Minimization of Self-Quenching Fluorescence on Dyes Conjugated to Biomolecules with Multiple Labeling Sites via Asymmetrically Charged NIR Fluorophores. *Contrast Media Mol. Imaging* **2014**, *9* (5), 355–362.

Appendix 2:
Design and Synthesis of
Ethylenediamine Functionalized RhoVR-Halos

Synopsis

Previous molecular dynamics simulations of VoltageFluors (VFs) highlighted the need for proper membrane orientation in order to maximize voltage sensitivity.[1] During the development of genetically targetable tetramethylrhodamine-based voltage reporters (RhoVR-Halos), an *ortho*-piperazine was used to couple the HaloTag ligand to the RhoVR. We wondered if the added rigidity of the 6-membered ring at this sterically congested location was affecting membrane orientation. This could explain the reduced sensitivity of RhoVR-PEG$_{25}$-Halo relative to the *ortho*-sarcosine functionalized RhoVR 1 (34% vs 47% $\Delta F/F$ per 100 mV, respectively).[2]

To investigate the effect of the *ortho*-tertiary amide on voltage sensitivity we synthesized RhoVR-Halo derivatives from flexible ethylenediamine-derived tertiary amides. We synthesized two RhoVR1-Halo derivatives derived from either 1-Boc-amino-2-(methylamino) ethane (**3**) or tert-Butyl methyl(2-(methylamino)ethyl)-carbamate (**6**). We also synthesized a 1-Boc-amino-2-(methylamino)ethane-derived RhoVR(Me)-Halo (**9**). Synthesis of RhoVR-Halo derviatives was carried out analogously to RhoVR1-PEG$_{25}$-Halo (**Scheme A2-1**). Following purification of each derivative by preparative HPLC, RhoVR-Halos **3**, **6** and **9** were applied to sparsely transfected HEK cells expressing HaloTag. All three *ortho*-ethylenediamine incorporating RhoVRs showed similar brightness and selectivity to RhoVR1-PEG$_{25}$-Halo. Patch-clamp electrophysiology was then used to measure the voltage sensitivity of each RhoVR derivative (**Figure A2-2a-f**). The voltage sensitivity of the ethylenediamine-derived RhoVRs was approximately the same as their piperazine-derived counterparts. Voltage imaging of evoked activity in cultured rat hippocampal neurons revealed **3** outperformed RhoVR1-PEG$_{25}$-Halo, though this effect was mostly likely due to higher levels of HaloTag expression (**Figure A2-2g,h**). The similar performance of ethylenediamine-derived RhoVR-Halos to piperazine-derived RhoVR-Halos suggests that orientation is unaffected by the structure of the *ortho*-amide. We hypothesize that the lower sensitivity of RhoVR-Halos relative to untargeted RhoVR 1 and RhoVR(Me) is likely a reflection of the proportion of dye intercalated in the membrane, and not the orientation of the dye.

Experimental Section

General Method for Chemical Synthesis and Characterization

Chemical reagents and solvents (dry) were purchased from commercial suppliers and used without further purification. NHS-PEG$_x$-Acid dPEG® linkers were purchased from Quanta Biodesign. Synthesis of RhoVR derivatives **S1** and **S2** were carried out as reported in **Chapter 1** and **Chapter 2**. Thin layer chromatography (TLC) (Silicycle, F254, 250 μm) and preparative thin layer chromatography (PTLC) (Silicycle, F254, 1000 μm) was performed on glass backed plates pre-coated with silica gel and were visualized by fluorescence quenching under UV light. Flash column chromatography was performed on Silicycle Silica Flash F60 (230–400 Mesh) using a forced flow of air at 0.5–1.0 bar. NMR spectra were measured on Bruker AVB-400 MHz, 100 MHz, AVQ-400 MHz, 100 MHz, Bruker AV-600 MHz, 150 MHz. Chemical shifts are expressed in parts per million (ppm) and are referenced to $CDCl_3$ (7.26 ppm, 77.0 ppm) or DMSO (2.50 ppm, 40 ppm). Coupling constants are reported as Hertz (Hz). Splitting patterns are indicated as follows: s, singlet; d, doublet; t, triplet; q, quartet, dd, doublet of doublet; m, multiplet. High-resolution mass spectra (HR-ESI-MS) were measured by the QB3/Chemistry mass spectrometry service at University of California, Berkeley. High performance liquid chromatography (HPLC) and low

resolution ESI Mass Spectrometry were performed on an Agilent Infinity 1200 analytical instrument coupled to an Advion CMS-L ESI mass spectrometer. The column used for the analytical HPLC was Phenomenex Luna C18(2) (4.6 mm I.D. × 150 mm) with a flow rate of 1.0 mL/min. The mobile phases were MQ-H_2O with 0.05% formic acid (eluent A) and HPLC grade acetonitrile with 0.05% formic acid (eluent B). Signals were monitored at 254, 340 and 545 nm over 20 min with a gradient of 10-100% eluent B. The column used for semi-preparative HPLC was Phenomenex Luna 5µ C18(2) (10 mm I.D. x 150 mm) with a flow rate of 5.0 mL/min. The mobile phases were MQ-H_2O with 0.05% formic acid (eluent A) and HPLC grade acetonitrile with 0.05% formic acid (eluent B). Signals were monitored at 254 over 20 min with a gradient of 10-100% eluent B.

Synthetic Procedures

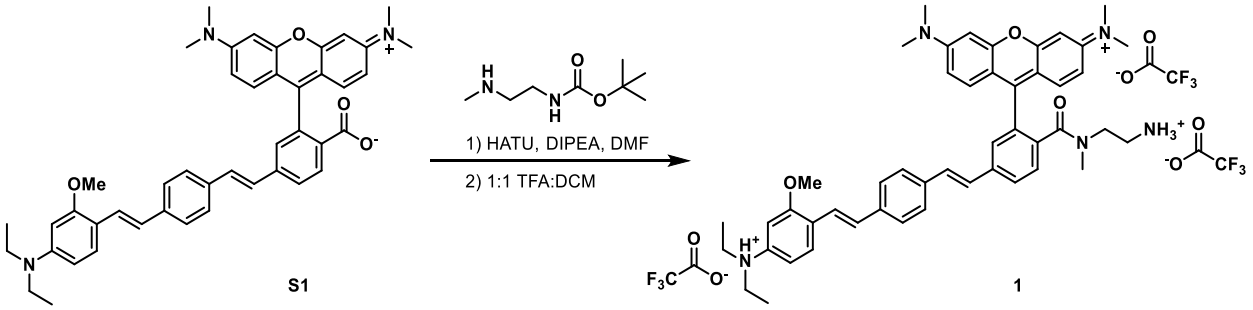

Synthesis of 1:

A vial was charged with **S1** (21.0 mg, 30.3 µmol), 1-Boc-amino-2-(methylamino) ethane (6.6 mg, 37.9 µmol), and HATU (14.4 mg, 37.9 µmol). Anhydrous DMF (1 mL) and anhydrous diisopropylethylamine (12.9 µL, 60.6 µmol) were added and the vial was flushed with nitrogen, sealed, and stirred at 22 °C for 3 h. The solvent was removed *in vacuo* and the remaining residue was diluted with DCM (30 mL) and washed with water (2 x 30 mL). The combined organics were dried with anhydrous sodium sulfate, filtered and the solvent removed *in vacuo*. DCM (2 mL) and TFA (2 mL) were added to the crude solid and the reaction was stirred at 22 °C for 2 h. The solvent was removed under a stream of nitrogen and co-evaporated with toluene (2 x 5 mL) and DCM (2 x 5 mL) affording **1** as a TFA salt (30.4 mg, 27.9 µmol, 92%). Analytical HPLC retention time 5.35 min; MS (ESI) exact mass for $C_{48}H_{54}N_5O_3^+$ $[M+H]^+$ calcd: 748.4 found: 748.2; HR-ESI-MS m/z for $C_{48}H_{54}N_5O_3^+$ $[M+H]^+$ calcd: 748.4221 found: 748.4210.

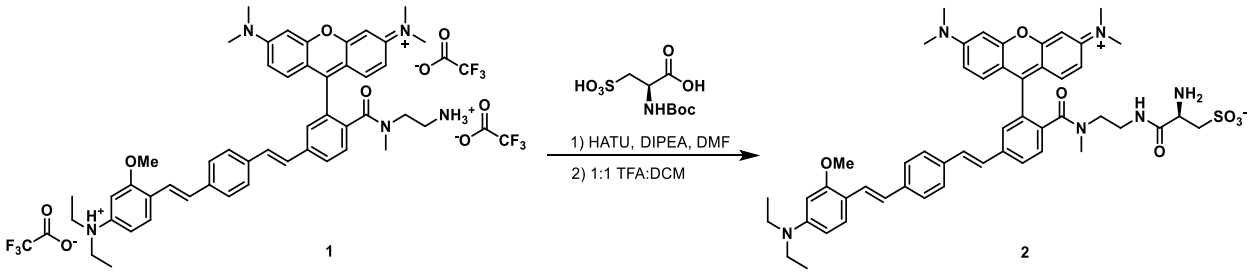

Synthesis of 2:

A vial was charged with **1** (30.4 mg, 27.9 µmol), Boc-L-cysteic acid (12.2 mg, 45.5 µmol), and HATU (17.3 mg, 45.5 µmol). Anhydrous DMF (2 mL) and anhydrous diisopropylethylamine (39.5 µL, 227.5 µmol) were added and the vial was flushed with nitrogen, sealed, and stirred at 22 °C

for 18 h. The solvent was removed *in vacuo* and the remaining residue diluted with DCM/*i*-PrOH (40 mL) and washed with water (2 x 50 mL). The combined organics were dried with anhydrous sodium sulfate, filtered and the solvent removed *in vacuo*. DCM (2 mL) and TFA (2 mL) were added to the crude solid and the reaction was stirred at 22 °C for 3 h. The solvent was removed under a stream of nitrogen and the remaining residue diluted with DCM/*i*-PrOH (30 mL) and washed with saturated sodium bicarbonate (2 x 50 mL). The combined organics were dried with anhydrous sodium sulfate, filtered and the solvent removed *in vacuo* affording **2** as a purple solid (15.2 mg, 16.9 µmol, 61%). Analytical HPLC retention time 5.92 min; MS (ESI) exact mass for $C_{51}H_{60}N_6O_7S^+$ $[M+2H]^{2+}$ calcd: 450.2 found: 450.4; HR-ESI-MS m/z for $C_{51}H_{59}N_6O_7S^+$ $[M+H]^+$ calcd: 899.4160 found: 899.4165

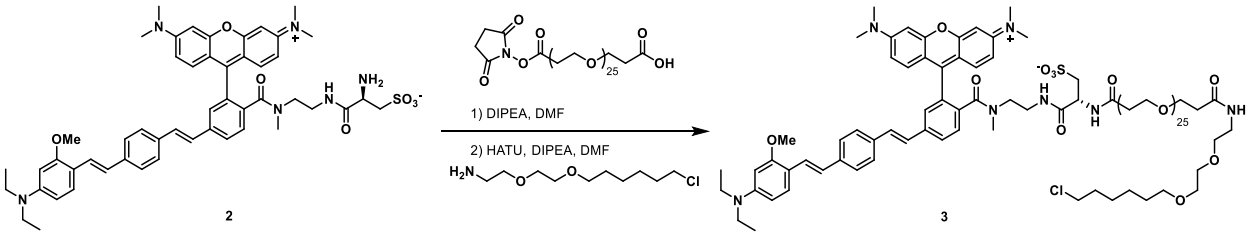

Synthesis of 3:

A vial was charged with **2** (15.2 mg, 16.9 µmol) and NHS-PEG_{25}-Acid (17.8 mg, 13.5 µmol). Anhydrous DMF (1 mL) and anhydrous diisopropylethylamine (4.7 uL, 34 µmol) were added and the vial was flushed with nitrogen, sealed and stirred at 22 ºC for 18 h. HaloTag-amine (9.4 mg, 16.9 µmol), HATU (16.0 mg, 42.1 µmol) and anhydrous diisopropylethylamine (8.7 µL, 50.5 µmol) were added and the reaction stirred for 1 h. The solvent was removed *in vacuo* and the remaining residue purified by preparative HPLC affording **3** as a purple solid (10.9 mg, 4.7 µmol, 28%). Analytical HPLC retention time 6.08 min; MS (ESI) exact mass for $C_{115}H_{185}ClN_7O_{36}S^{3+}$ $[M+3H]^{3+}$ calcd: 769.4, found: 769.7; HR-ESI-MS m/z for $C_{115}H_{186}ClN_7O_{36}S^{2+}$ $[M+4H]^{4+}$ calcd: 577.0582 found: 577.0579.

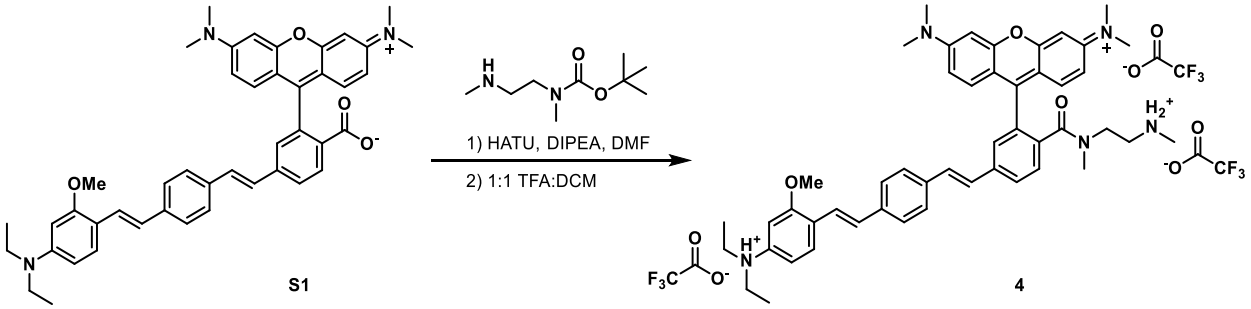

Synthesis of 4:

A vial was charged with **S1** (21.0 mg, 30.3 µmol), tert-Butyl methyl(2-(methylamino)ethyl)-carbamate (10.0 mg, 53.0 µmol), and HATU (14.4 mg, 37.9 µmol). Anhydrous DMF (2 mL) and anhydrous diisopropylethylamine (12.9 µL, 60.6 µmol) were added and the vial was flushed with nitrogen, sealed, and stirred at 22 °C for 16 h. The solvent was removed *in vacuo* and the remaining residue was diluted with DCM (30 mL) and washed with water (2 x 30 mL). The combined organics were dried with anhydrous sodium sulfate, filtered and the solvent removed *in vacuo*. DCM (2 mL) and TFA (2 mL) were added to the crude solid and the reaction was stirred at 22 °C

for 2 h. The solvent was removed under a stream of nitrogen and co-evaporated with toluene (2 x 5 mL) and DCM (2 x 5 mL) affording **4** as a TFA salt (32.8 mg, 29.7 μmol, 98%). Analytical HPLC retention time 5.09 min; MS (ESI) exact mass for $C_{49}H_{57}N_5O_3^+$ $[M+2H]^{2+}$ calcd: 381.7 found: 381.6; HR-ESI-MS m/z for $C_{49}H_{56}N_5O_3^+$ $[M+H]^+$ calcd: 762.4378 found: 748.4378.

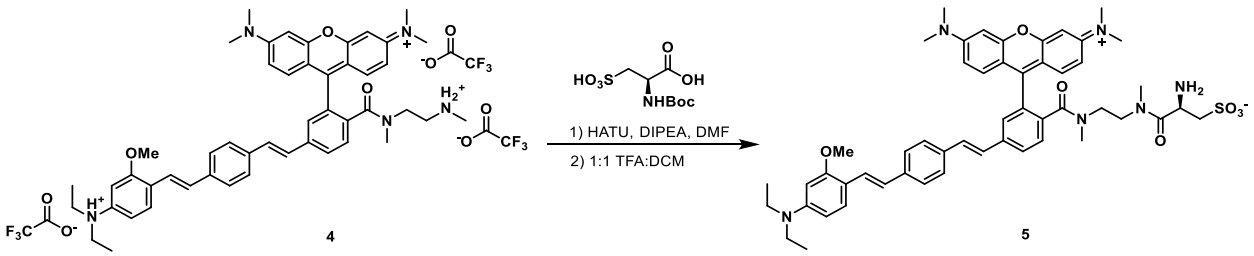

Synthesis of 5:

A vial was charged with **4** (32.0 mg, 29.1 μmol), Boc-L-cysteic acid (10.2 mg, 37.9 μmol), and HATU (14.4 mg, 37.9 μmol). Anhydrous DMF (2 mL) and anhydrous diisopropylethylamine (25.8 μL, 121 μmol) were added and the vial was flushed with nitrogen, sealed, and stirred at 22 °C for 18 h. The solvent was removed *in vacuo* and the remaining residue diluted with DCM/*i*-PrOH (40 mL) and washed with water (2 x 50 mL). The combined organics were dried with anhydrous sodium sulfate, filtered and the solvent removed *in vacuo*. DCM (2 mL) and TFA (2 mL) were added to the crude solid and the reaction was stirred at 22 °C for 2 h. The solvent was removed under a stream of nitrogen and the remaining residue diluted with DCM/*i*-PrOH (30 mL) and washed with saturated sodium bicarbonate (2 x 50 mL). The combined organics were dried with anhydrous sodium sulfate, filtered and the solvent removed *in vacuo* affording **5** as a purple solid (23.8 mg, 26.1 μmol, 90%). Analytical HPLC retention time 5.11 min; MS (ESI) exact mass for $C_{52}H_{62}N_6O_7S^+$ $[M+2H]^{2+}$ calcd: 457.2 found: 457.3; HR-ESI-MS m/z for $C_{52}H_{61}N_6O_7S^+$ $[M+H]^+$ calcd: 913.4317 found: 913.4309.

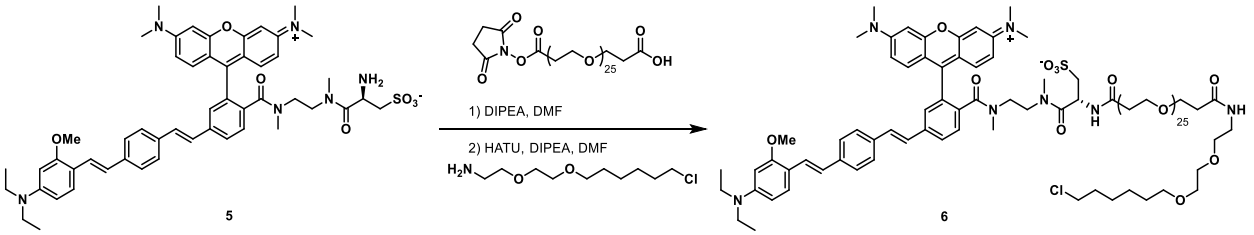

Synthesis of 6:

A vial was charged with **5** (11.9 mg, 13.0 μmol) and NHS-PEG_{25}-Acid (22.2 mg, 16.9 μmol). Anhydrous DMF (1 mL) and anhydrous diisopropylethylamine (3.6 uL, 26 μmol) were added and the vial was flushed with nitrogen, sealed and stirred at 22 ºC for 18 h. HaloTag-amine (7.3 mg, 32.6 μmol), HATU (12.4 mg, 32.6 μmol) and anhydrous diisopropylethylamine (6.8 μL, 39.1 μmol) were added and the reaction stirred for 1 h. The solvent was removed *in vacuo* and the remaining residue purified by preparative HPLC affording **6** as a purple solid (6.9 mg, 3.0 μmol, 23%). Analytical HPLC retention time 5.96 min; MS (ESI) exact mass for $C_{116}H_{187}ClN_7O_{36}S^{3+}$ $[M+3H]^{3+}$ calcd: 774.1, found: 774.7; HR-ESI-MS m/z for $C_{116}H_{184}ClNa_3N_7O_{36}S^{2+}$ $[M+3Na]^{3+}$ calcd: 597.0485 found: 597.0491.

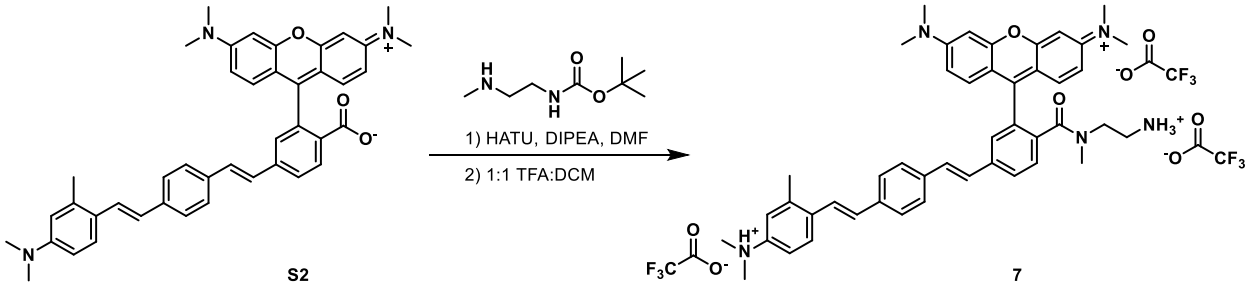

Synthesis of 7:

A vial was charged with **S1** (20.0 mg, 30.9 μmol), 1-Boc-amino-2-(methylamino) ethane (6.7 mg, 38.5 μmol), and HATU (14.7 mg, 38.5 μmol). Anhydrous DMF (1 mL) and anhydrous diisopropylethylamine (13.1 μL, 61.7 μmol) were added and the vial was flushed with nitrogen, sealed, and stirred at 22 °C for 16 h. The solvent was removed *in vacuo* and the remaining residue was diluted with DCM (30 mL) and washed with water (2 x 30 mL). The combined organics were dried with anhydrous sodium sulfate, filtered and the solvent removed *in vacuo*. DCM (2 mL) and TFA (2 mL) were added to the crude solid and the reaction was stirred at 22 °C for 2 h. The solvent was removed under a stream of nitrogen and co-evaporated with toluene (2 x 5 mL) and DCM (2 x 5 mL) affording **7** as the TFA salt, which was used without further purification for the next reaction. Analytical HPLC retention time 5.17 min; MS (ESI) exact mass for $C_{46}H_{50}N_5O_2^+$ $[M+H]^+$ calcd: 704.4 found: 704.5.

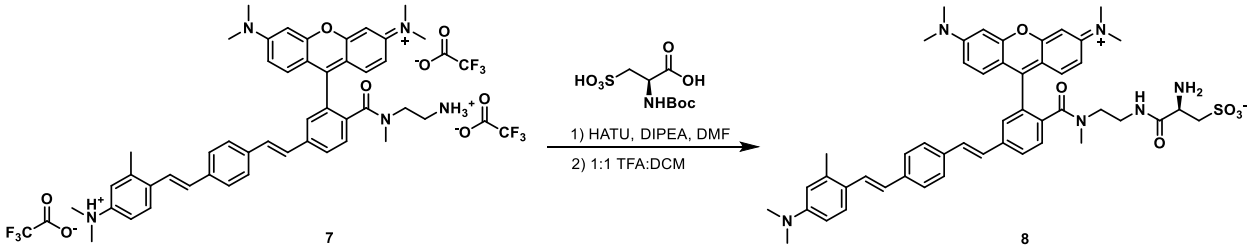

Synthesis of 8:

A vial was charged with **7** (24.8 mg, 23.4 μmol), Boc-L-cysteic acid (14.2 mg, 52.8 μmol), and HATU (20.1 mg, 52.8 μmol). Anhydrous DMF (2 mL) and anhydrous diisopropylethylamine (60.0 μL, 283 μmol) were added and the vial was flushed with nitrogen, sealed, and stirred at 22 °C for 18 h. The solvent was removed *in vacuo* and the remaining residue diluted with DCM/*i*-PrOH (40 mL) and washed with water (2 x 50 mL). The combined organics were dried with anhydrous sodium sulfate, filtered and the solvent removed *in vacuo*. DCM (2 mL) and TFA (2 mL) were added to the crude solid and the reaction was stirred at 22 °C for 2 h. The solvent was removed under a stream of nitrogen and the remaining residue diluted with DCM/*i*-PrOH (30 mL) and washed with saturated sodium bicarbonate (2 x 50 mL). The combined organics were dried with anhydrous sodium sulfate, filtered and the solvent removed *in vacuo* affording **8** as a purple solid (20.0 mg, 20.9 μmol, 89%). Analytical HPLC retention time 5.20 min; MS (ESI) exact mass for $C_{49}H_{56}N_6O_5S^+$ $[M+2H]^{2+}$ calcd: 448.2 found: 428.1.

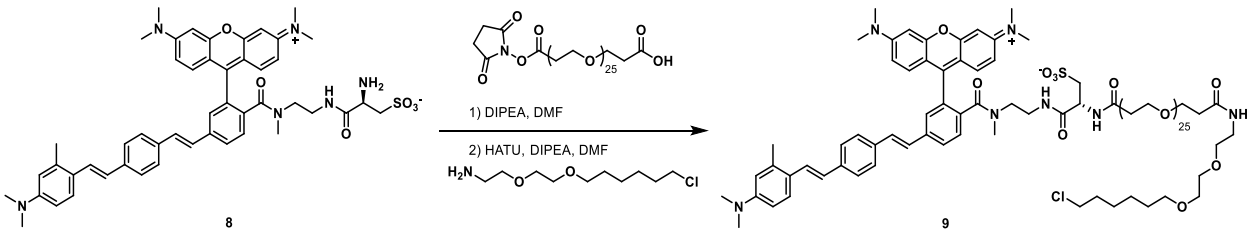

8 9

Synthesis of 9:
A vial was charged with **8** (10.0 mg, 11.7 μmol) and NHS-PEG_{25}-Acid (12.3 mg, 9.4 μmol). Anhydrous DMF (1 mL) and anhydrous diisopropylethylamine (3.3 uL, 23 μmol) were added and the vial was flushed with nitrogen, sealed and stirred at 22 ºC for 18 h. HaloTag-amine (6.5 mg, 29.2 μmol), HATU (11.1 mg, 29.2 μmol) and anhydrous diisopropylethylamine (6.1 μL, 35.1 μmol) were added and the reaction stirred for 4 h. The solvent was removed *in vacuo* and the remaining residue purified by preparative HPLC affording **9** as a purple solid (4.6 mg, 2.03 μmol, 17%). Analytical HPLC retention time 6.15 min; MS (ESI) exact mass for $C_{113}H_{181}ClN_7O_{35}S^{3+}$ $[M+3H]^{3+}$ calcd: 754.7, found: 755.0; HR-ESI-MS m/z for $C_{113}H_{178}ClNa_2N_7O_{35}S^{2+}$ $[M+2Na]^{2+}$ calcd: 1153.0779 found: 1153.0776.

Cell Culture

All animal procedures were approved by the UC Berkeley Animal Care and Use Committees and conformed to the NIH Guide for the Care and Use and Laboratory Animals and the Public Health Policy.

Human embryonic kidney 293T (HEK) cells were passaged and plated onto 12 mm glass coverslips pre-coated with Poly-D-Lysine (PDL; 1 mg/ml; Sigma-Aldrich) to provide a confluency of ~15% and 50% for electrophysiology and imaging, respectively. HEK cells were plated and maintained in Dulbecco's modified eagle medium (DMEM) supplemented with 4.5 g/L D-glucose, 10% FBS and 1% Glutamax. Transfection of genetic tools was carried out using Lipofectamine 3000 24 h after plating. Imaging was performed 18-24 h following transfection.

Hippocampi were dissected from embryonic day 18 Sprague Dawley rats (Charles River Laboratory) in cold sterile HBSS (zero Ca^{2+}, zero Mg^{2+}). All dissection products were supplied by Invitrogen, unless otherwise stated. Hippocampal tissue was treated with trypsin (2.5%) for 15 min at 37 °C. The tissue was triturated using fire polished Pasteur pipettes, in minimum essential media (MEM) supplemented with 5% fetal bovine serum (FBS; Thermo Scientific), 2% B-27, 2% 1M D-glucose (Fisher Scientific) and 1% glutamax. The dissociated cells were plated onto 12 mm diameter coverslips (Fisher Scientific) pre-treated with PDL (as above) at a density of 30-40,000 cells per coverslip in MEM supplemented media (as above). Neurons were maintained at 37 °C in a humidified incubator with 5 % CO_2. At 1 day in vitro (DIV) half of the MEM supplemented media was removed and replaced with Neurobasal media containing 2% B-27 supplement and 1% glutamax. Transfection of genetic tools was carried out using Lipofectamine 3000 at 7 DIV. Functional imaging was performed on mature neurons 13-20 DIV, except electrophysiological experiments which were performed on 12-15 DIV neurons.

Unless stated otherwise, for loading of HEK cells and hippocampal neurons, RhoVRs were diluted in DMSO to 500 μM, and then diluted 1:1000 in HBSS. All imaging experiments were performed in HBSS (in mM) 140 NaCl, 2.5 KCl, 10 HEPES, 10 D-glucose 1.3 $MgCl_2$ and 2 $CaCl_2$; pH 7.3 and 290 mOsmol.

Imaging Parameters and Analysis

Epifluorescence imaging was performed on an AxioExaminer Z-1 (Zeiss) equipped with a Spectra-X Light engine LED light (Lumencor), controlled with Slidebook (v6, Intelligent Imaging Innovations). Images were acquired with either a W-Plan-Apo 20x/1.0 water objective (20x; Zeiss). Images were focused onto either an OrcaFlash4.0 sCMOS camera (sCMOS; Hamamatsu) or an eVolve 128 EMCCD camera (EMCCD; Photometrix). More detailed imaging information for each experimental application is expanded below. For RhoVR-Halo images, the excitation light was delivered from a LED (9.72 W/cm^2) at 542/33 (bandpass) nm and emission was collected with a quadruple emission filter (430/32, 508/14, 586/30, 708/98 nm) after passing through a quadruple dichroic mirror (432/38, 509/22, 586/40, 654 nm LP). For eGFP images, the excitation light was delivered from a LED (5.77 W/cm^2) at 475/34 nm and emission was collected with a quadruple emission filter (430/32, 508/14, 586/30, 708/98 nm) after passing through a quadruple dichroic mirror (432/38, 509/22, 586/40, 654 nm LP).

Functional imaging of the RhoVR voltage dyes was performed using a 20x objective paired with image capture from the EMCCD camera at a sampling rate of 0.5 kHz. RhoVRs were excited using the 542 nm LED with an intensity of 9.73 W/cm^2. For initial voltage characterization emission was collection with the QUAD filter and dichroic (see above).

Analysis of voltage sensitivity in HEK cells was performed using ImageJ (FIJI). Briefly, a region of interest (ROI) was selected automatically based on fluorescence intensity and applied as a mask to all image frames. Fluorescence intensity values were calculated at known baseline and voltage step epochs. For analysis of RhoVRs voltage responses in neurons, regions of interest encompassing cell bodies (all of approximately the same size) were drawn in ImageJ and the mean fluorescence intensity for each frame extracted. ΔF/F values were calculated by first subtracting a mean background value from all raw fluorescence frames, bypassing the noise amplification which arises from subtracting background for each frame, to give a background subtracted trace (bkgsub). A baseline fluorescence value (F_{base}) is calculated either from the first several (10-20) frames of the experiment for evoked activity, or from the median for spontaneous activity, and was subtracted from each timepoint of the bkgsub trace to yield a ΔF trace. The ΔF was then divided by F_{base} to give ΔF/F traces. No averaging has been applied to any voltage traces.

Electrophysiology

For electrophysiological experiments, pipettes were pulled from borosilicate glass (Sutter Instruments, BF150-86-10), with a resistance of 5–8 MΩ, and were filled with an internal solution; 115 mM potassium gluconate, 10 mM BAPTA tetrapotassium salt, 10 mM HEPES, 5 mM NaCl, 10 mM KCl, 2 mM ATP disodium salt, 0.3 mM GTP trisodium salt (pH 7.25, 275 mOsm). Recordings were obtained with an Axopatch 200B amplifier (Molecular Devices) at room temperature. The signals were digitized with Digidata 1440A, sampled at 50 kHz and recorded with pCLAMP 10 software (Molecular Devices) on a PC. Fast capacitance was compensated in the on-cell configuration. For all electrophysiology experiments, recordings were only pursued if series resistance in voltage clamp was less than 30 MΩ. For whole-cell, voltage clamp recordings in HEK 293T cells, cells were held at -60 mV and 100 ms hyper- and de- polarizing steps applied from -100 to +100 mV in 20 mV increments.

Figures and Schemes

Scheme A2-1: *Synthesis of diethylamine-incorporating RhoVR-Halos* ***3****,* ***6*** *and* ***9***

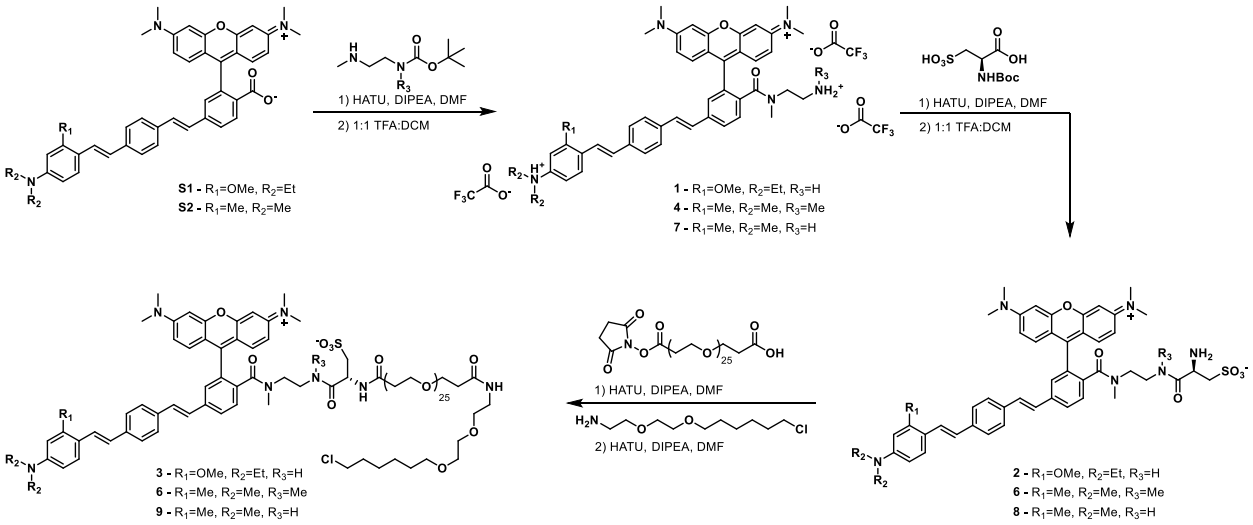

Scheme A2-1: General synthesis of *ortho*-ethylenediamine RhoVRs.

Figure A2-1: *Voltage sensitivities of **3**, **6** and **9***

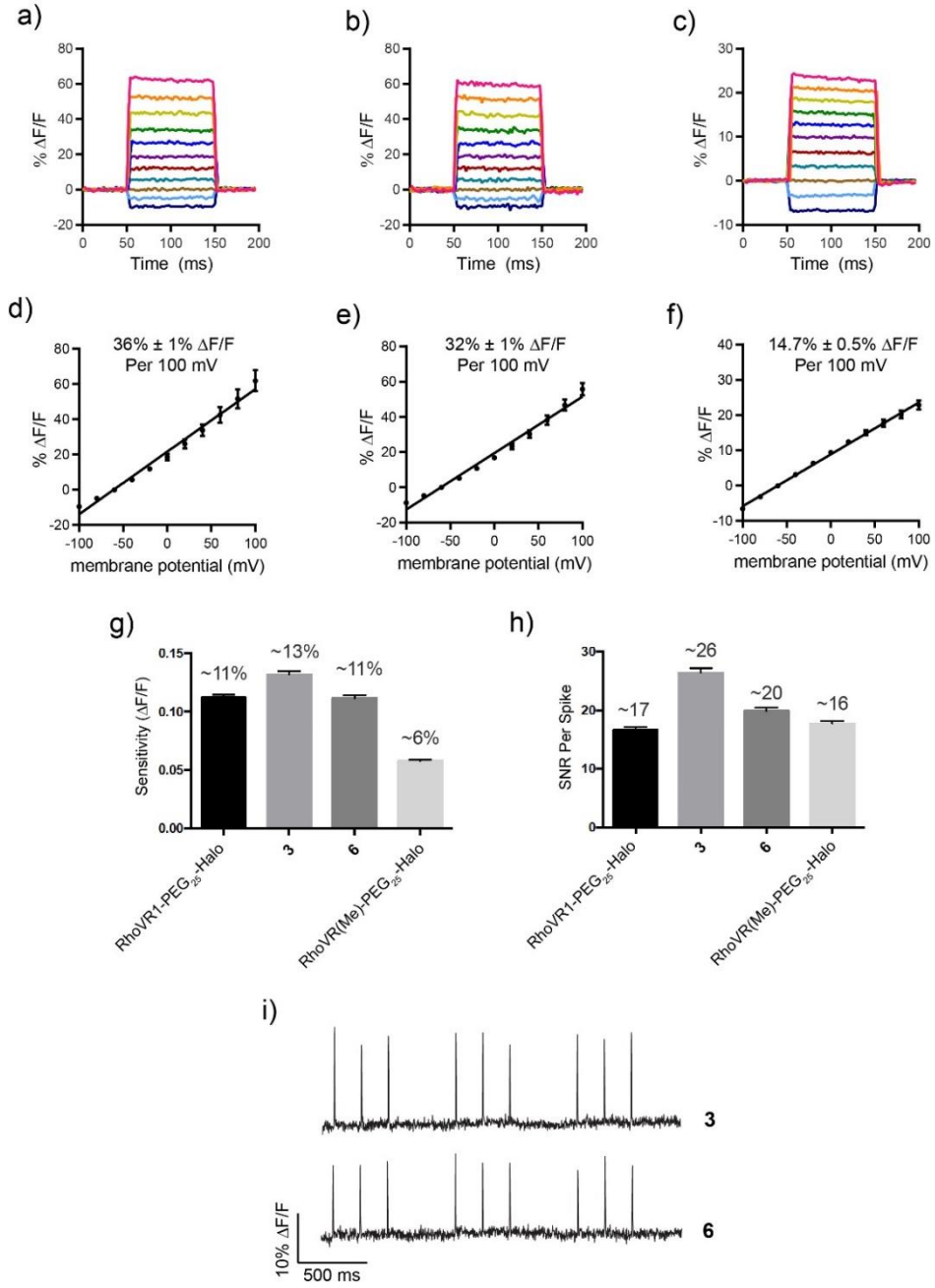

Figure A2-1: (a-c) The fractional change in fluorescence of **3** (a), **6** (b) and **9** (c) plotted vs. time for 100 ms hyper- and depolarizing steps (±100 mV, 20 mV increments) from a holding potential of -60 mV for a single HEK cells under whole-cell voltage-clamp mode. (d-f) A plot of % ΔF/F vs final membrane potential (mV), summarizing data from 5-9 separate cells for **3** (d), **6** (e) and **9** (f). Error bars are ±S.E.M. (g) Average ΔF/F of various RhoVR-Halo derivatives to evoked action potentials in rat hippocampal neurons. (h) Average SNR for various RhoVR-Halo derivatives to evoked action potentials in rat hippocampal neurons. (i) Example voltage recordings of evoked activity from RhoVR-Halos **3** (top) and **6** (bottom).

References

(1) Kulkarni, R. U.; Yin, H.; Pourmandi, N.; James, F.; Adil, M. M.; Schaffer, D. V.; Wang, Y.; Miller, E. W. A Rationally Designed, General Strategy for Membrane Orientation of Photoinduced Electron Transfer-Based Voltage-Sensitive Dyes. *ACS Chem. Biol.* **2017**, *12* (2), 407–413.

(2) Deal, P. E.; Kulkarni, R. U.; Al-Abdullatif, S. H.; Miller, E. W. Isomerically Pure Tetramethylrhodamine Voltage Reporters. *J. Am. Chem. Soc.* **2016**, *138* (29), 9085–9088.

Appendix 3:
Synthesis of Protein-RhoVR Conjugates

Synopsis

Genetically encodable voltage indicators (GEVIs) and newer chemogenetic voltage sensors enable voltage imaging from a genetically defined subset of cells, facilitating imaging in complex tissues such as brain slice or *in vivo*.[1–3] While genetically encodable systems afford high selectivity, they often require significant optimization of expression and localization of the protein component. In addition, the development of transgenic animals can be expensive and time consuming. In attempt to address these limitations we envisioned synthesizing VoltageFluors capable of targeting endogenous proteins. Recent work by the Sames lab demonstrated voltage sensitive dyes (VSDs) could be chemically targeted to dopaminergic neurons using the monoamine transporter ligand dichloropane.[4] We were interested in synthesizing antibody or nanobody conjugated VoltageFluors through traditional protein conjugation techniques. This strategy was attractive due to the huge variety of antibodies available and the large body of research concerning the synthesis of antibody-drug conjugates.[5–8]

We first synthesized malemide-functionalized RhoVR **1** in 34% yield from the functionalized RhoVR **S1** employed in the synthesis of RhoVR1-Halos. We then screened reaction conditions using a goat anti-mouse IgG (H+L) secondary antibody using size-exclusion chromatography (SEC). These initial experiments indicated the malemide couplings produced minimal antibody labeling. We then decided to take a step backwards and pursue an NHS-ester mediated labeling strategy. We synthesized RhoVR1-PEG_{25}-NHS **2** from RhoVR1-PEG_{25}-Acid **S2**. Before attempting to synthesize antibody-RhoVR conjugates, we screened labeling conditions using RNase A. In addition, we began screening reaction conditions by SDS-PAGE, which was both more reliable and faster than SEC. Reaction screens revealed that at higher ratios of **2**:RNase A, the native protein band would fade, indicating the coupling with RhoVRs was occurring. Instead of observing distinct bands corresponding to a distribution of RhoVRs, we observed a faint streak across the lane (**Figure A3-1a-c, lane 4**). We hypothesize conjugating the large and hydrophobic RhoVR-PEG_{25}-NHS was leading to aggregation of RNase A. We tested this theory in two ways. First, we conjugated RNase A with **2** in the presence of 1% SDS, hoping to prevent the formation of aggregates. Second, we conjugated RNase A with NHS-PEG_{25}-Acid, i.e. the linker without the lipophilic RhoVR (**Figure A3-2**). The addition of SDS led to discreet bands of RNase A corresponding to conjugation with **2** (**Figure A3-2**, **lane 4**). Interestingly, adding SDS after reacting RNase A with **2** had no effect. Conjugations with NHS-PEG_{25}-Acid at lower concentrations also provided distinct bands, however at higher concentration all bands disappeared (**Figure A3-2**, **lanes 6 and 7**). We hypothesize that multiple additions of the large PEG linker is also leading to aggregation of the RNase A, suggesting aggregation with **2** may not be solely an effect of the lipophilic RhoVR.

The difficulties found with RhoVR-NHS conjugation suggests the highly lipophilic dyes are not conducive to traditional labeling strategies and alternate, more controlled labeling strategies will be required. For example, a SNAP-tagged nanobody could be used to generate a targetable RhoVR with a 1:1 stoichiometry that may reduce potential aggregation.[12] One potential limitation to this strategy is the reduced degree of labeling (1:1 RhoVR:Protein). Due to the dimness of VoltageFluors, a higher degree of labeling would be more desirable in order to maximize signal. Another potential solution is the use of solubilizing linkers, such as dextrans, which could mask the lipophilic RhoVR until its delivery to the membrane.[4] Unfortunately, such molecules are difficult to synthesize and may be too large for antibody labeling.

Experimental Section

General Method for Chemical Synthesis and Characterization

Chemical reagents and solvents (dry) were purchased from commercial suppliers and used without further purification. Goat anti-mouse IgG (H+L) secondary antibody was purchased from ThermoFisher Scientific (2.4 mg/mL in PBS, pH 7.6). Pierce™ dye removal columns and Zeba™ desalting columns were purchased from ThermoFisher Scientific. SDS-PAGE gels were prepared from TGX™ FastCast™ acrylamide solutions purchased from Bio-Rad. HPLC was performed on Agilent 1260 series HPLC systems (Agilent Technologies, USA) equipped with in-line multi-wavelength detector (MWD) and fluorescence detector (FLD). Size exclusion chromatography (SEC) was accomplished on an Agilent BioSEC-5 5 μM 2000 Å, 7.8 x 300 mm, 2.7 μm, LC column fitted with a guard column (Agilent Technologies, USA) using an aqueous mobile phase (50 mM sodium phosphate, 200 mM NaCl, pH 7.6) at a flow rate of 1.0 mL/min. Proteins and protein conjugates were analyzed on an Agilent 6224 Time-of-Flight (TOF) mass spectrometer with a dual electrospray source (ESI) connected in-line with an Agilent 1200 series HPLC (Agilent Technologies, USA). Chromatography was performed using a Proswift RP-4H (Thermo Scientific, USA) column with a H_2O/MeCN gradient mobile phase containing 0.1% formic acid. Mass spectra of proteins and protein conjugates were deconvoluted with MassHunter Qualitative Analysis Suite B.05 (Agilent Technologies, USA).

Synthetic Procedures

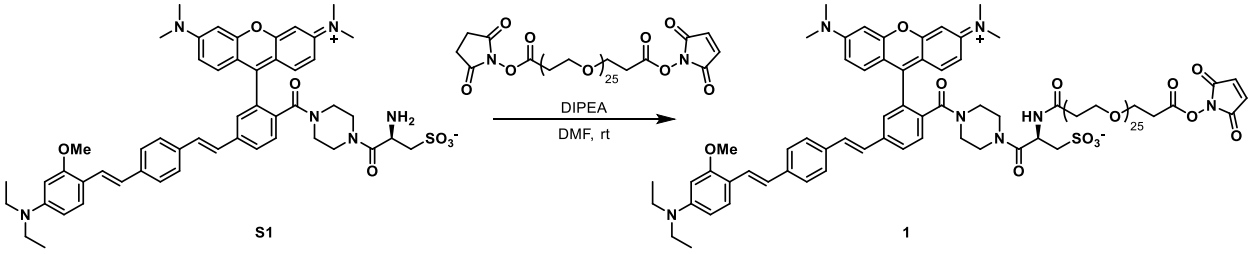

Synthesis of RhoVR1-PEG$_{25}$-Mal, 1:
A vial was charged with **S1** (10.0 mg, 11.0 μmol) and NHS-PEG$_{25}$-Mal (12.2 mg, 8.9 μmol). Anhydrous DMF (1 mL) and anhydrous diisopropylethylamine (4.7 uL, 22.0 μmol) were added and the vial flushed with nitrogen, sealed and stirred at 22 ºC for 7 h. The solvent was removed *in vacuo* and the remaining residue was then purified by preparative HPLC affording **1** as a purple solid (8.04 mg, 3.67 μmol, 34%). Analytical HPLC retention time 5.49 min; MS (ESI) exact mass for $C_{110}H_{167}N_8O_{35}S^{3+}$ $[M+3H]^{3+}$ calcd: 731.0, found: 731.2; HR-ESI-MS m/z for $C_{110}H_{167}N_8O_{35}S^{3+}$ $[M+3H]^{3+}$ calcd: 731.0424 found: 731.0418.

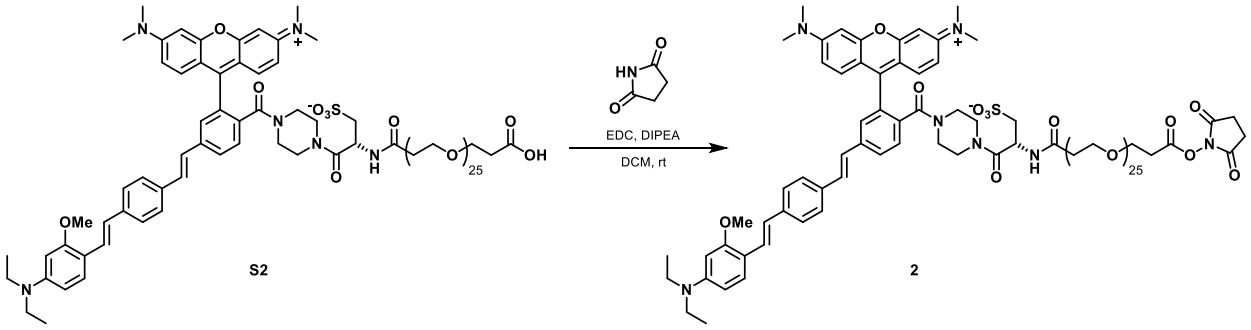

Synthesis of RhoVR1-PEG$_{25}$-NHS, 2

A vial was charged with **S2** (5.0 mg, 2.4 μmol), EDC (3.6 mg, 18.9 μmol), N-hydroxysuccinimide (3.8 mg, 37.9 μmol). Anhydrous DCM (500 μL) and diisopropylethylamine (2.6 μL, 5.2 μmol) were added and the reaction stirred at rt for 5 h. The reaction as diluted with DCM (5 mL) and washed with water (3 x 5 mL). The combined organics were dried with anhydrous sodium sulfate, filtered and the solvent removed *in vacuo* affording **2** as a purple solid (5.7 mg, 2.4 μmol, quantitative). Analytical HPLC retention time 5.65 min; MS (ESI) exact mass for $C_{110}H_{168}N_7O_{37}S^{3+}$ $[M+3H]^{3+}$ calcd: 737.4 found: 737.1; HR-ESI-MS m/z for $C_{110}H_{167}N_7O_{37}S^{2+}$ $[M+2H]^{2+}$ calcd: 1105.0556 found: 1105.0586.

RhoVR-PEG$_{25}$-Mal Reaction Screens

First, the storage buffer of the commercially available antibody was exchanged for 50 mM HEPES, 50 mM NaCl, pH 8.1 buffer using a Zeba^{TM} desalting column (7k MWCO) and diluted to 2.0 mg/mL (~13.3 μM). The antibody solution was then split into 50 μL portions in 1.6 mL epindorph tubes for reaction screens. 1 mM TCEP stock solution in DMSO was added (tested between 13.33-43.33 μM, 1-4 equivalents) and the tubes shaken at 37 °C for 3 h. The reactions were then cooled on ice and RhoVR-PEG$_{25}$-Mal **1** was added from a 10 mM stock solution in DMSO (80-240 μM, 6-24 equivalents) and the reactions were shaken at 37 °C for 1.5 h. The crude reaction mixtures were then purified using Pierce^{TM} dye removal columns or Zeba^{TM} spin columns (40k MWCO) to remove excess **1**, then injected into the BioSEC. Note that removal of **1** was found to be very difficult and the dye would adhere to most desalting or spin columns. This may have affected our attempts to visualize conjugation by SEC, as conjugated antibody may have also stuck to the spin columns. This was one of the main reasons we decided to screen reactions by SDS-PAGE.

RhoVR-PEG$_{25}$-NHS Reaction Screens

RNase A conjugation reactions were run on a 50 μL scale in 1.5 mL epindorph tubes. A 10 mg/mL stock solution of RNase A was diluted into HEPES buffer (50 mM HEPES, 50 mM NaCl, pH 7.6) to afford final concentrations between 0.38-1.14 mg/mL RNase A. NHS-esters were then added from 10 mM DMSO stock solutions to achieve the desired stoichiometry (typically between 5:1 to 25:1 NHS:RNase A). Other additives, such as 1% SDS, were then added from DMSO stock solutions and the reactions shaken at 37 °C for 3 h. 16.6 μL of a 4x Lamelli dye solution was then added to each condition and vortexed. 10 μL of each condition was then loaded into wells of a Tri-glycine gel prepared from TGX^{TM} FastCast^{TM} acrylamide solutions (Bio-Rad). The gels were run with standard running buffer at 200 V for approximately 30 minutes. The gels were then removed

and imaged by visible light (to visualize RhoVR labeling) and a fluorescence gel reader (to visualize TAMRA labeling). The gels were then stained with a coomassie brilliant blue solution (10% acetic acid, 40% methanol, 50% DI H_2O, 1 g coomassie) for 30 minutes, then destained with a destaining solution (10% acetic acid, 40% methanol, 50% DI H_2O, 3 x 10 min washes) and imaged with a BioRad Gel Doc EZ reader.

Figures and Schemes

Scheme A3-1: *Antibody-RhoVR conjugates for targeting*

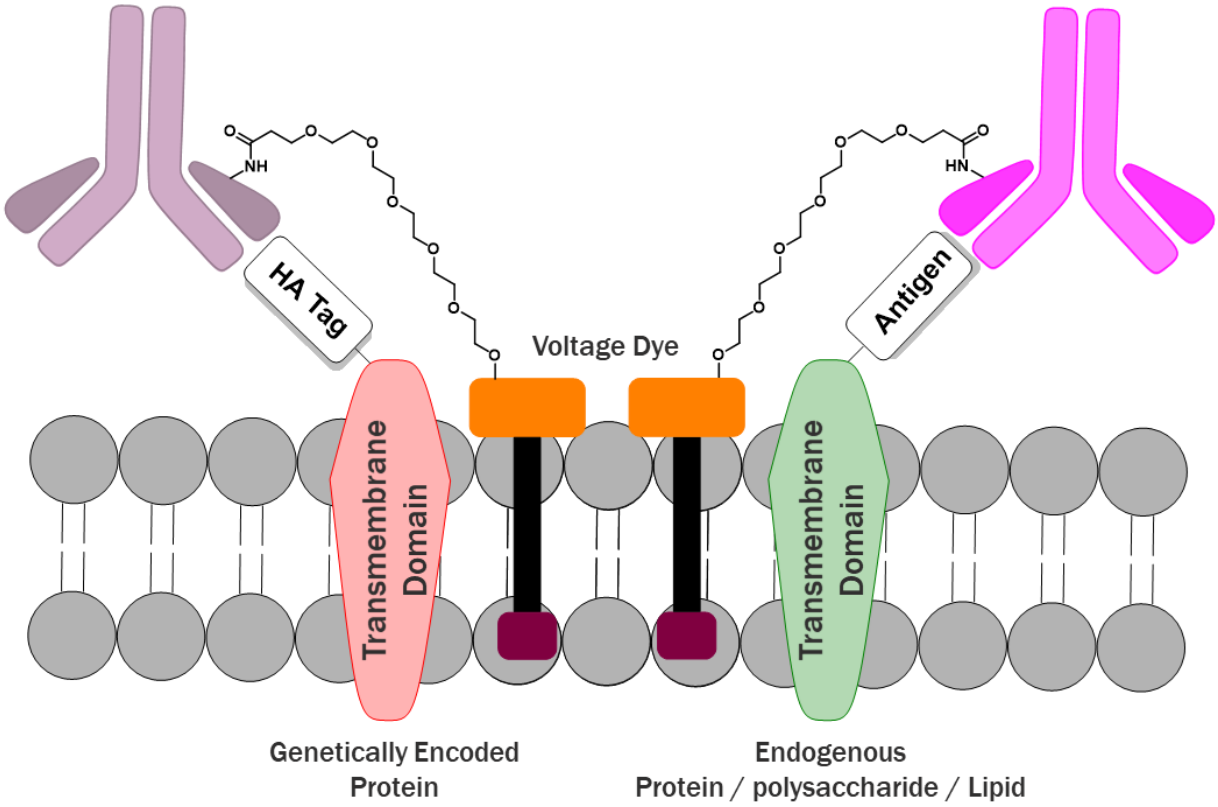

Scheme A3-1: Antibody-RhoVR conjugates could generated targeting a variety of antigens. Genetically encoded tags could be used to increase the degree labeling. Labeling of endogenous motifs could also be used to target sub-cellular domains.

Figure A3-1: *Protein Conjugation with RhoVR1-PEG$_{25}$-NHS*

a)

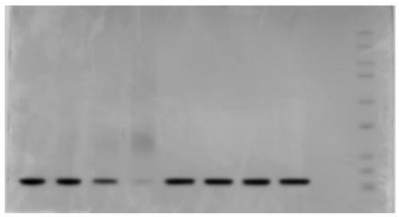

b)

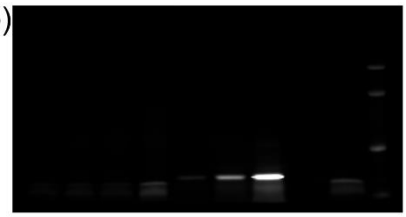

c)

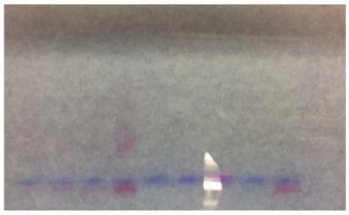

d)

Lane	1	2	3	4	5	6	7	8	9
Description	**2** Very Low Conc.	**2** Low Conc.	**2** Med. Conc..	**2** High Conc.	NHS-TAMRA Very Low	NHS-TAMRA Low Conc.	NHS-TAMRA High Conc.	RNase A (Control)	**2** (Control)
RNase A	0.38 mg/mL (28 μM)	.38 mg/mL (28 μM)	0.38 mg/mL (28 μM)	0.38 mg/mL (28 μM)	0.38 mg/mL (28 μM)	0.38 mg/mL (28 μM)	.38 mg/mL (28 μM)	0.38 mg/mL (28 μM)	-
RhoVR-PEG$_{25}$-NHS	15 μM	40 μM	80 μM	240 μM	-	-	-	-	80 μM
TAMRA-NHS	-	-	-	-	-	-	-	-	-
NHS-PEG$_{25}$-Acid	-	-	-	-	10 μM	40 μM	240 μM	-	-
NHS:Protein Ratio	0.5	1.5	3	8.5	20	1.5	8.5	N/A	-

e)

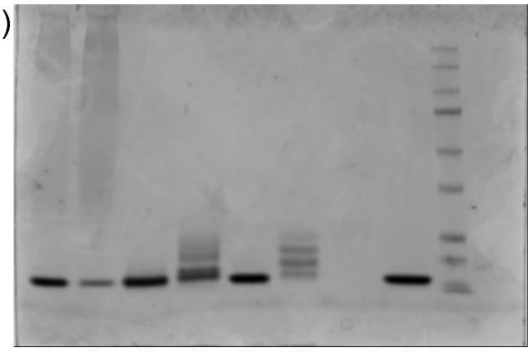

f)

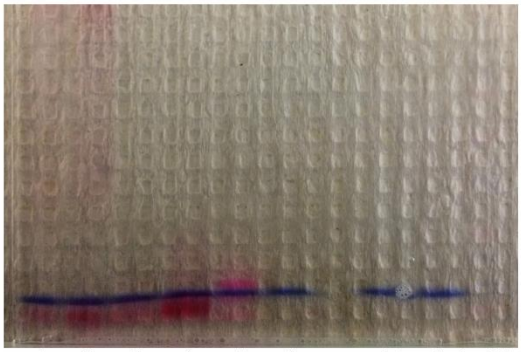

g)

Lane	1	2	3	4	5	6	7	8
Description	**2** Low Conc.	**2** High Conc.	**2** w/ 1% SDS Low Conc.	**2** w/ 1% SDS High Conc.	NHS-TAMRA High Conc.	NHS-PEG25-Acid Low Conc.	NHS-PEG25-Acid High Conc.	RNase A (Control)
RNase A	0.38 mg/mL (28 μM)	.38 mg/mL (28 μM)	0.38 mg/mL (28 μM)	0.38 mg/mL (28 μM)	0.38 mg/mL (28 μM)	0.38 mg/mL (28 μM)	.38 mg/mL (28 μM)	0.38 mg/mL (28 μM)
RhoVR-PEG$_{25}$-NHS	200 μM	600 μM	200 μM	600 μM	-	-	-	-
TAMRA-NHS	-	-	-	-	600 μM	-	-	-
NHS-PEG$_{25}$-Acid	-	-	-	-	-	200 μM	400 μM	-
NHS:Protein Ratio	7	20	7	20	20	7	14	N/A

Figure A3-1: Protein conjugation with RhoVR1-PEG$_{25}$-NHS **2**. (a-c) Initial reaction screens showed increasing concentrations of **2** led to loss of the RNase A band and streaking across the SDS-PAGE gel. We hypothesize this streaking was a result of aggregation induced by the lipophilic RhoVR. Image a shows the gel following a coomassie stain, b is a TAMRA fluorescence image and c is a visible light image of the gel. (d) Reaction conditions for NHS-mediated conjugations screened in gels a-c. (e-f) In order to determine if aggregation was induced by the VF or by the long PEG$_{25}$ linker, we tested the conjugation of **2** alongside NHS-PEG$_{25}$-acid. While distinct bands were seen when conjugating with NHS-PEG$_{25}$-acid at lower concentrations (lane 6), at higher concentrations we observed no protein present by coomassie stain (lane 7). We hypothesize that the large size of the PEG$_{25}$ linker relative to RNase A (13.7 kDa) may be affecting the stability of the protein. We also looked to see if RhoVR-induced aggregation could be prevented by using a surfactant. Reacting **2** with RNase A in the presence of 1% SDS resulted in clear bands (lane 4), further supporting that the observed streaks in lanes 1 and 2 are due to aggregation.

References:

1. Liu, P., Grenier, V., Hong, W., Muller, V. R. & Miller, E. W. Fluorogenic Targeting of Voltage-Sensitive Dyes to Neurons. *J. Am. Chem. Soc.* **139,** 17334–17340 (2017).
2. Xu, Y. *et al.* Hybrid Indicators for Fast and Sensitive Voltage Imaging. *Angew. Chemie - Int. Ed.* **57,** 3949–3953 (2018).
3. Deo, C. & Lavis, L. D. Synthetic and genetically encoded fluorescent neural activity indicators. *Curr. Opin. Neurobiol.* **50,** 101–108 (2018).
4. Fiala, T. *et al.* Chemical Targeting of Voltage Sensitive Dyes to Specific Cell Types in the Brain. *ChemRxiv* (2018).
5. Strohl, W. R. Current progress in innovative engineered antibodies. *Protein Cell* **9,** 86–120 (2018).
6. Beck, A., Goetsch, L., Dumontet, C. & Corvaïa, N. Strategies and challenges for the next generation of antibody-drug conjugates. *Nat. Rev. Drug Discov.* **16,** 315–337 (2017).
7. Agarwal, P. & Bertozzi, C. R. Site-specific antibody-drug conjugates: The nexus of bioorthogonal chemistry, protein engineering, and drug development. *Bioconjug. Chem.* **26,** 176–192 (2015).
8. Ducry, L. Antibody-Drug Conjugates. *Methods in Molecular Biology* (2013).
9. Nani, R. R., Gorka, A. P., Nagaya, T., Kobayashi, H. & Schnermann, M. J. Near-IR Light-Mediated Cleavage of Antibody-Drug Conjugates Using Cyanine Photocages. *Angew. Chemie - Int. Ed.* **54,** 13635–13638 (2015).
10. Nani, R. R. *et al.* In Vivo Activation of Duocarmycin-Antibody Conjugates by Near-Infrared Light. *ACS Cent. Sci.* **3,** 329–337 (2017).
11. Aanei, I. L. *et al.* Biodistribution of antibody-MS2 viral capsid conjugates in breast cancer models. *Mol. Pharm.* **13,** 3764–3772 (2016).
12. Farrants, H. *et al.* SNAP-Tagged Nanobodies Enable Reversible Optical Control of a G Protein-Coupled Receptor *via* a Remotely Tethered Photoswitchable Ligand. *ACS Chem. Biol.* **13,** 2682–2688 (2018).

Appendix 4:
Protocol for Measuring Quantum Yields of Fluorescence

Introduction

When a fluorophore absorbs a photon of light, an energetically excited state is formed. The fate of this species is varied, depending upon the exact nature of the fluorophore and its surroundings, but the end result is deactivation (loss of energy) and return to the ground state. The main deactivation processes which occur are fluorescence (loss of energy by emission of a photon), internal conversion and vibrational relaxation (non-radiative loss of energy as heat to the surroundings), and intersystem crossing to the triplet state (**Figure 1**). The fluorescence quantum yield (Φ_F) is the ratio of photons absorbed to photons emitted through fluorescence. In other words, Φ_F gives the probability of the excited state being deactivated by fluorescence rather than by another, non-radiative mechanism.

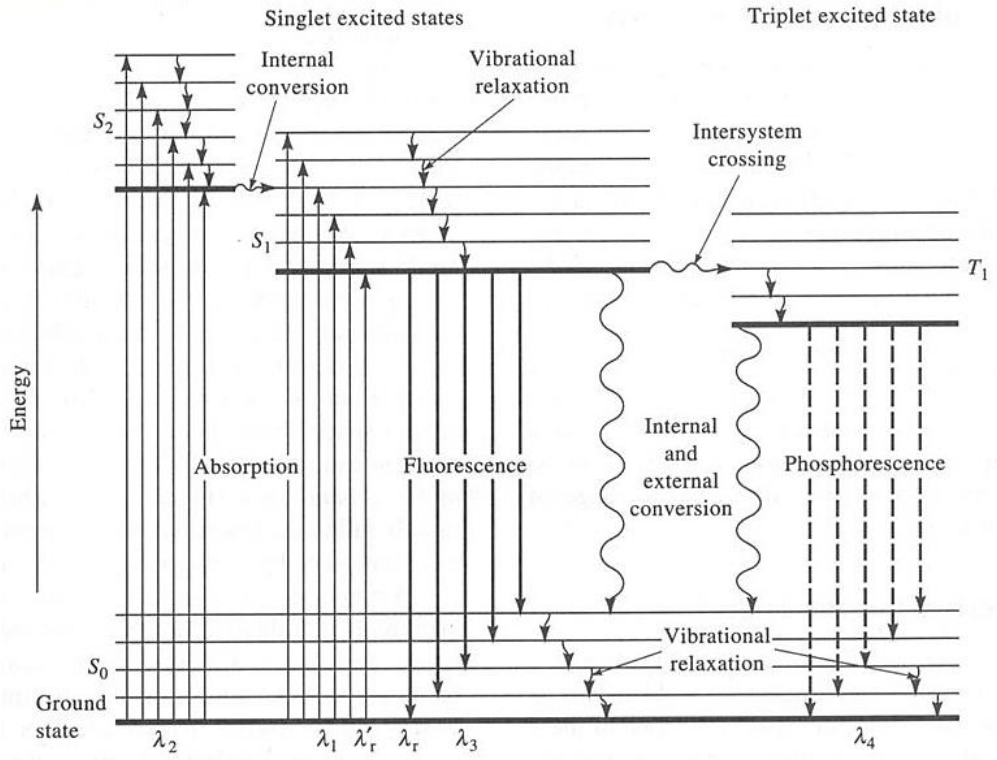

Figure A4-1: A Jablonski diagram details the various relaxation processes available to a fluorophore.

The most reliable method for recording Φ_F is the comparative method of Williams *et al*., which involves the use of standard samples with known Φ_F values.[2] Solutions of the standard and test samples with identical **absorbance at the same excitation wavelength** can be assumed to be absorbing the same number of photons. Hence, a simple **ratio of the integrated fluorescence intensities** of the two solutions (recorded under identical conditions) will yield the ratio of the quantum yield values. Since Φ_F for the standard sample is known, Φ_F for the test sample can be easily calculated. In practice, these measurements can be complicated by:

- The presence of concentration effects, e.g. self-quenching
- The use of different solvents for standard and test samples
- The validity in using the standard sample and its Φ_F value

These considerations are answered by:

- Working within a carefully chosen concentration range and acquiring data at a number of different absorbances (i.e. concentrations) and ensuring linearity across the concentration range
- Including the solvent refractive indices within the ratio calculation
- Cross-calibrating the standard sample with a second standard, to ensure both are behaving as expected and allowing their Φ_F values to be used with confidence.

General Experimental Considerations

Standard samples:

The standard samples should be chosen to ensure they absorb at the excitation wavelength of choice for the test sample, and, if possible, emit in a similar region to the test sample. The standard samples must be well characterized and suitable for such use. A number of lists of good fluorescent standard samples are available, including:

- J. R. Lakowicz, Principles of Fluorescence Spectroscopy, Kluwer Academic/Plenum Press, New York, 1999, Second Edition.
- J. C. Scaiano (Ed.), Handbook of Organic Photochemistry, CRC Press, 1989.

A list of standard samples, with their literature quantum yields, is given at the end of this document.

Cuvettes:

Standard 10 mm path length fluorescence cuvettes are sufficient for running the fluorescence measurements. In order to minimize re-absorption effects (Dhami *et al.*) **absorbances in the 10 mm fluorescence cuvette should never exceed 0.1 at and above the excitation wavelength.**[3] Above this level, non-linear effects may be observed due to inner filter effects, and the resulting quantum yield values may be perturbed.

Sample preparation:

It is important that all glassware is kept scrupulously clean, and solvents must be of spectroscopic grade and checked for background fluorescence. Typically the standard samples and test samples are added as a stock solution at 1000x the desired final concentration. For most dyes, this concentration is in the high nM to low μM range.

Choice of excitation wavelength:

Accurate QY measurements require that the excitation wavelength chosen allows for the detection of the entire fluorescence peak without bleed through of the excitation light. This is because we are measuring the area under the fluorescence peak (i.e. the integral). Measuring the integral is necessary as different dyes tend to have different peak shapes, thus the λ_{max} does not necessarily correlate to the number of emitted photons. In practice this means the selected excitation wavelength is at a shorter wavelength than the λ_{max} of the dye.

Solvents/Surfactants

Solvents can have a large effect on the measured Φ_F, especially with highly PeT quenched and amphiphilic VoltageFluors. Typically EtOH is a good starting point, but sometimes solubility can be an issue. Aqueous buffers such as PBS or HBSS can be used, but be aware that many VFs aggregate in aqueous buffers, which can significantly alter the measured Φ_F. Surfactants can be

used to help solubilize VFs in aqueous buffers, however different surfactants can often result in different Φ_F (i.e. Triton-X vs. SDS). Considering these solvent effects can be quite large, when directly comparing derivatives it is recommended all measurements be made in the same solvent.

Procedure

1. Record the UV-vis absorbance spectrum of the solvent background for the chosen sample. Note down the absorbance at the excitation wavelength to be used (this will be used for a background correction later). Alternatively, every sample can be "baselined" prior to the addition of the sample stock solution.
2. Record the fluorescence spectrum of the same solution in the 10 mm fluorescence cuvette using the "excitation scan" acquisition. Make sure that the excitation wavelength and slit widths remain constant for the entire experiment. Calculate and note down the integrated fluorescence intensity (that is, the area of the fluorescence spectrum) from the fully corrected fluorescence spectrum. This can be done using the "integrate" function under the "math" dropdown window. You can input these
3. Repeat steps 1 and 2 for five solutions with increasing concentrations of the chosen sample (There will be six solutions in all, corresponding to absorbances at the excitation wavelength at approximately: 0/solvent blank, 0.02, 0.04, 0.06, 0.08 and 0.10). Note that the exact absorption values are not important as long as filtering effects are not observed.
4. Plot a graph of integrated fluorescence intensity *vs* absorbance. The result should be a straight line with gradient m, and intercept = 0. Non-linear plots are an indication that the concentration of the sample is too high.
5. Repeat steps 1 to 4 for the remaining samples. Ideally two standard compounds should be measured first in order to validate your method (see more below). The collected absorbance and fluorescence values can be input directly into a template excel spreadsheet found on the lab server.

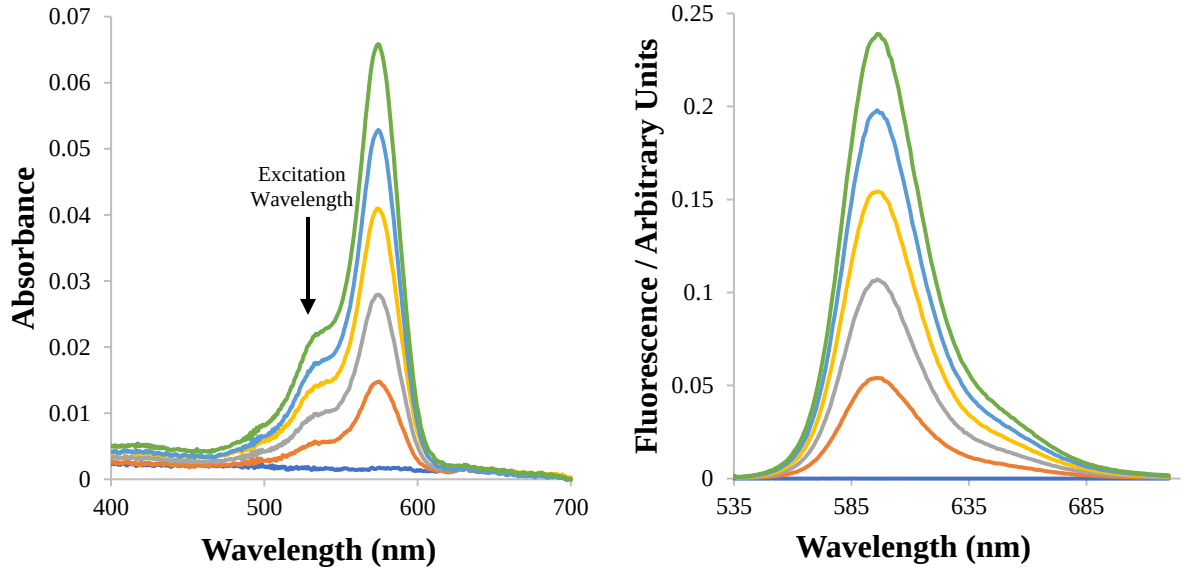

Figure A4-2: Example of absorbance and emission spectra measured for rhodamine 101.

Calculation of Fluorescence Quantum Yields from Acquired Data

The gradients of the graphs obtained in step 4 above are proportional to the quantum yield of the different samples. Absolute values are calculated using the standard samples which have a fixed and known Φ_F value according to the following equation:

$$\Phi_X = \Phi_{Std}\left(\frac{Slope_X}{Slope_{Std}}\right)\left(\frac{\eta_X{}^2}{\eta_{Std}{}^2}\right)$$

Where the subscripts Std and X denote the standard and test sample respectively, Φ is the fluorescence quantum yield, "Slope" is the gradient from the plot of integrated fluorescence intensity *vs* absorbance, and η the refractive index of the solvent.

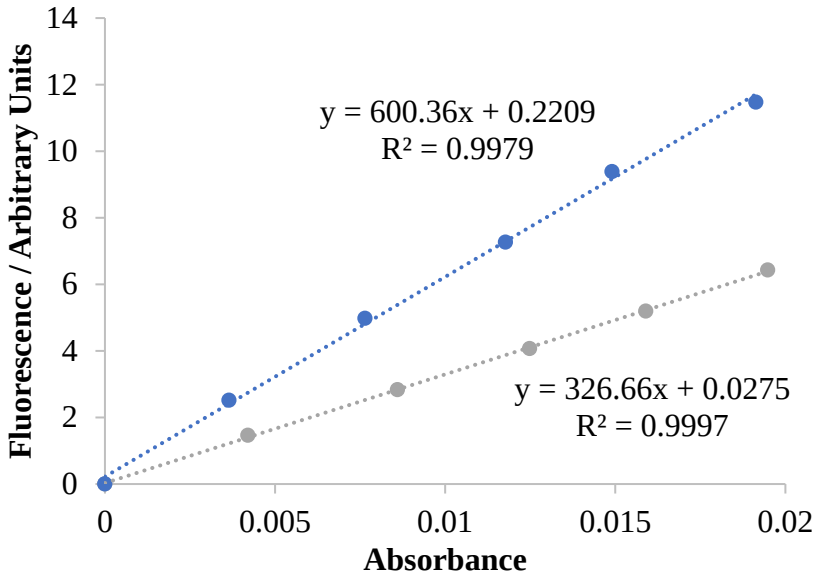

Figure A4-3: Linear plots for rhodamine 101 and a rhodamine B derivative. The gradient for each sample is proportional to that sample's Φ_F. Conversion to an absolute quantum yield is achieved through the above equation.

For the most accurate Φ_F measurements two standard compounds should be cross-calibrated using the above equation. This is achieved by calculating the quantum yield of each standard sample relative to the other. For example take two standard samples A and B. Initially A is treated as the standard (Std) and B as the test sample (X). Using the known Φ_F for A, determine the Φ_F of B. Following this, the process is reversed, such that B is now treated as the standard and A becomes the test sample. In this manner, the quantum yields of A and B are calculated relative to one another. The values of $\Phi_{F(A)}$ and $\Phi_{F(B)}$ obtained should match the literature values. The match is generally considered valid and acceptable if the data obtained is of good quality (i.e., good linearity with a zero intercept) and the experimental quantum yields match their literature counterparts within ±10%. If the values show a larger error than this, fresh standard solutions should be prepared, and the process repeated. In some cases you may not have two standard samples with overlapping absorbances. Without this internal control, it is advisable to measure the Φ_F multiple times to ensure accurate results.

Once the standard samples have been cross-calibrated and an acceptable match obtained, the Φ_F values for the test sample can then be calculated using the same equation above. If you used two standards, *two* Φ_F values will be obtained for each test sample, one relative to standard A, the

other to standard B. The simple average of these two values represents the quantum yield of the test sample. The error in your reported value must be considered based upon the observed errors in the gradients; a value of ±10% is normal.

Planning

The measurement of fluorescence quantum yields is laborious and time consuming. Nonetheless, with careful planning the process can be made as efficient as possible. For example, there is no point in performing *all* measurements until the standard samples have been cross-calibrated (a long day's work recording data for two standard samples and six test samples may come to nothing if, at the end of the day, analysis of the two standard samples shows an unacceptable match). Take measurements for the standard samples only, and check their cross-calibration is acceptable before moving on to record data for the remaining test samples. This process can be streamlined by preparing an excel spreadsheet in which you can directly input your fluorescence and absorbance values as they are generated (a template can be found on the lab server).

Troubleshooting

R-values far from 1:

The most likely cause of non-linear plots are filtering effects. This is because dyes with small stokes shifts can have one molecule reabsorb light emitted by another. This effect is seen by a reduction of the slope as the concentration increases (i.e. a convex plot). Typically this problem is addressed by reducing the concentration of your samples.

If you are not seeing filtering effects but instead irregular fluorescence values at various concentrations, then your error is most likely due to pipetting errors / solubility issues with your dye. Make sure that your dye is soluble in the chosen solvent and that your stock solution is homogenous / no solids are present.

Much higher/lower fluorescence counts from different days

The slit widths from the lamp or the PMT have most likely been changed between your experiments. It is always important to record the slit widths when making measurements and to keep them consistent across your experiments.

There are essentially 0 counts when measuring the fluorescence spectra

Check the shutter control box and make sure it is not on manual control. Manual control allows you to open or close the shutters to the lamp, however if it is left in manual control mode the computer cannot open the shutter when it begins its scan.

References

(1) "A Guide to Recording Fluorescence Quantum Yields" Horiba Scientific.

(2) A. T. R. Williams; S. A. Winfield; J. N. Miller. "Relative fluorescence quantum yields using a computer controlled luminescence spectrometer", *Analyst*, **1983**, *108*, 1067.

(3) S. Dhami; A. J. de Melo; G. Rumbles; S. M. Bishop; D. Phillips; A. Beeby. "Phthalocyanine fluorescence at high concentration: dimers or reabsorption effect?" *Photochem. Photobiol.*, **1195**, *61*, 341.

Appendix 5:
Protocol for the Preparation and Purification of RhoVR-Halos

Starting Materials:

RhoVR-Halos are synthesized from piperazine-derived tertiary amides functionalized with an L-cysteic acid (**Figure A5-1**, **Chapter 2**). This linkage provides a nucleophilic handle which is convenient for the attachment of NHS-activated PEG linkers. The best results are achieved if Fmoc-protected **1** is purified by either column chromatography or a preparative TLC plate, as the deprotected **2** is highly polar. TFA-catalyzed deprotection of clean **1** will typically provide clean **2**, which will only require trituration or an aqueous workup to remove excess TFA prior to coupling of the PEG linker.

PEG linkers were purchased from Quanta Biodesign (dPEG® linkers). Due to the high costs of these PEG linkers ($200-400 per 100 mg), we try to minimize the equivalencies of linker used in the coupling reactions (0.8 to 1.0 equivalents). dPEG® linkers are somewhat hydroscopic and should be stored sealed at -20 °C.

HaloTag amine can be synthesized relatively easily according to literature procedures.[1] Note that the NMR of HaloTag-amine changes significantly depending on the protonation state of the amine. Store at -20 °C.

Equipment:

RhoVR-Halos were purified using a Waters Acquity Autopurification system (prep UHPLC-MS). The column used for preparative HPLC was an XBridge OBD Prep Column (5 µm, 19mm I.D. x 250 mm) with a flow rate of 30.0 mL/min. The mobile phases were MQ-H_2O with 0.05% trifluoroacetic acid (eluent A) and HPLC grade acetonitrile with 0.05% trifluoroacetic acid (eluent B). Signals were monitored at 545 over 20 min with a gradient of 30-70% eluent B and by ESI-MS.

Procedure:

1) Charge a vial with **2** (5-10 mg scale, 1.0 equiv.) and NHS-PEG_x-Acid linker (0.8 to 1.0 equiv.). Add anhydrous DMF (1 mL), anhydrous DIPEA (2 equiv.) and let stir at 22 °C. Monitor the reaction LC-MS until **2** is completely consumed (typically <1 h, but can go overnight). Add more NHS-PEG_x-Acid as necessary.
2) Once **2** is fully consumed, add HATU (2.0 equiv.), HaloTag-amine (2.0 equiv.) and anhydrous DIPEA (3.0 equiv.) directly to the crude reaction. Let stir at 22 °C, monitoring by LC-MS. Longer PEG linkers lead to very high MWs, so the observed m/z is often the $[M+2H/Na]^{2+}$ or $[M+3H/Na]^{3+}$ species. The reaction is typically complete in <1 h, but can be left overnight.
   Note: If you need to add a very small amount of HaloTag-amine, prepare a stock solution in anhydrous DMF.
3) Once the reaction is complete, remove the solvent *in vacuo* and dilute the reaction into a minimal amount of MeCN/MeOH (1-1.5 mL total volume). Filter through a 0.2 µm PTFE syringe filter (13 mm disk filter, GE) into a 1.5 mL LC sample vial. The sample is now ready for purification on the Waters Preparative HPLC.
4) In order to determine the retention time of the desired peak, a small "sacrificial" injection (50 µL) should be run. Monitor from 200-1200 m/z range in ESI+ mode for MS detection and 545 nm for UV-Vis detection. Once the retention time of the product is determined, set up your fraction collection window to collect the desired product peak.

Note: One of the main byproducts of the reaction is the coupling of HaloTag-amine to any excess NHS-PEG_x-Acid. Make sure the retention time of this byproduct doesn't overlap with the RhoVR-Halo peak.

5) Inject the remaining material over several runs with 400-500 µL injections. The injection needle of the Waters Prep HPLC does not reach all the way to the bottom of the 1.5 mL vials, so for the last injection, transfer your remaining material into a smaller 300 µL vial. Combine the product fractions and check the material by LC-MS to verify it is clean.

   Note: Make sure the solvent bottles do not go dry. 30 mL/min flow rate = about 5 runs before bottles need refilling.

6) The collected fractions should appear fluorescent pink due to the acidic solution protonating the aniline. As we have had issues with decomposition when isolating the TFA salts of RhoVR-Halos, the combined fractions are quenched by dropwise addition of a saturated sodium bicarbonate solution (**Figure A5-1**). Once the solution is neutralized, the color will go from a bright pink to a blood-red color. Remove the majority of the MeCN by rotary evaporation at 40 °C, leaving an aqueous solution of RhoVR-Halo that appears a dark red-brown (most likely due to aggregation of the dye).

7) Extract the remaining aqueous solution (typically around 25-50 mL) with DCM until the aqueous solution is nearly colorless. Dry the combined organics with anhydrous sodium sulfate, filter and concentrate *in vacuo*.

   Note: With longer PEG linkers RhoVR-Halos become increasingly water soluble, making it harder to extract into DCM. Adding a saturated sodium chloride solution can help drive the RhoVR-Halo into DCM. Alternatively, i-PrOH can be added, but try to keep i-PrOH to a minimum in order to minimize the uptake of salts into the organic layer. If excessive i-PrOH is required, once the organics have been removed *in vacuo*, re-dilute the material in pure DCM and transfer to a fresh vial to remove some of the excess salts.

8) Measure the mass of RhoVR-Halo isolated and calculate the volume of solvent required to generate a 10 mM stock solution. Stocks can either be made up in anhydrous DMSO or can be taken up in a more volatile solvent such as anhydrous DMF or $CHCl_3$ so that dry aliquots can be made. DMSO stocks seem to last for about a year (**Figure A5-2**).

9) In order to determine if the measured mass of RhoVR-Halo is accurate, compare the absorbance profile of the RhoVR-Halo to RhoVR 1 and determine its extinction coefficient (should be around 85,000 M^{-1} cm^{-1}). Once the measured concentration is confirmed, add more solvent to the stock solution to achieve a final concentration of 5 mM.

10) Divide the RhoVR-Halo stock solution into 10 µL aliquots in PCR tubes. To make dry aliquots, remove the solvent *in vacuo* (either on a Schlenk line or with a speed-vac). Store the aliquots in a 50 mL falcon tube with Drierite (desiccant) added to the bottom. Keep at -20 or -80 °C for long term storage.

Scheme A5-1: 1-Pot Synthesis of RhoVR-Halos

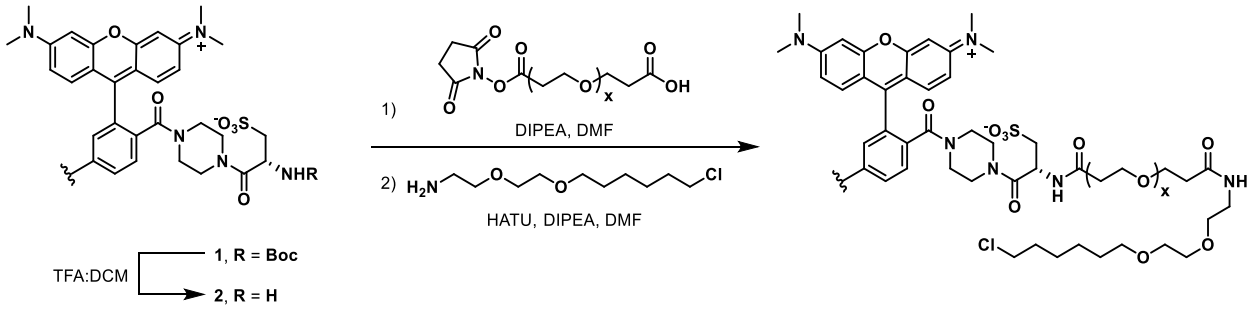

Scheme A5-1: 1-Pot synthesis of RhoVR-Halos. The best results are achieved if the Boc-protected RhoVR starting material is purified with a silica gel column or Preparative TLC plate, as purification after the TFA deprotection is much more difficult.

Figure A5-1: Isolation of RhoVR-Halos from Preparative HPLC

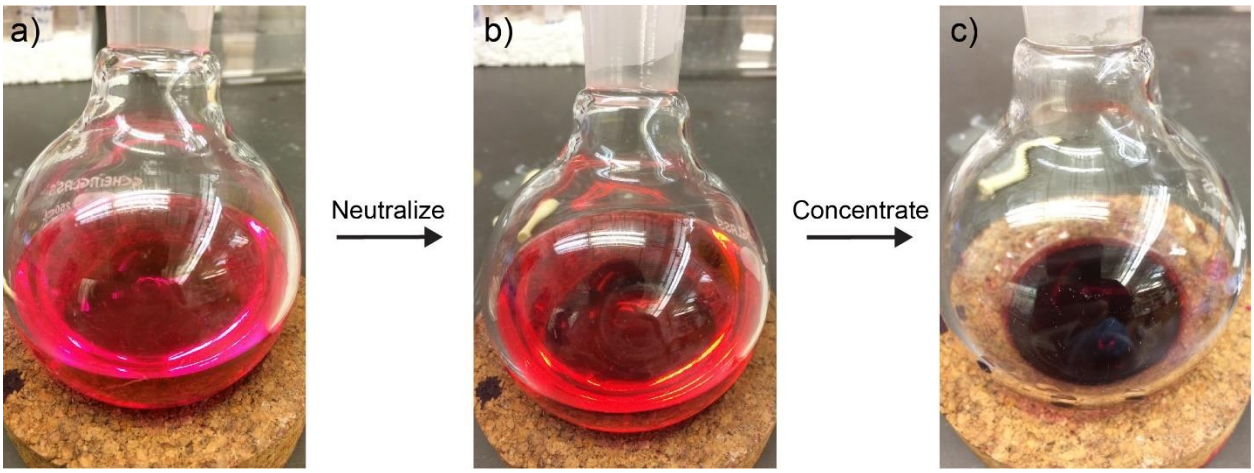

Figure A5-1: Isolation of RhoVR-Halos from Preparative HPLC. (a) Fractions collected from Preparative HPLC are bright pink due to the acidic solution protonating the aniline, reducing PeT. (b) The TFA was quenched by dropwise addition of a saturated solution of sodium bicarbonate. Neutralization is reached when the color of solution becomes a blood-red and is much less fluorescent. (c) Following neutralization, the acetonitrile is removed by rotary evaporation, leaving a mostly aqueous solution, from which the RhoVR-Halo is extracted into DCM.

Figure 5A-2: Stability of RhoVR-Halos over Time

a) Prep HPLC Purified:

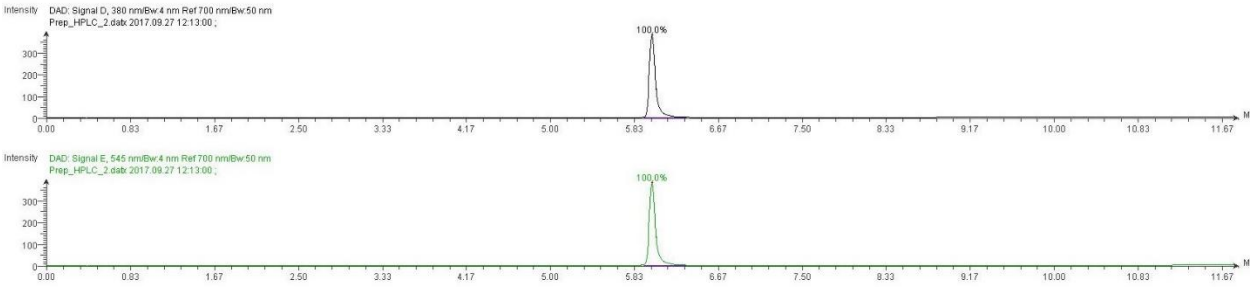

b) 1 Year:

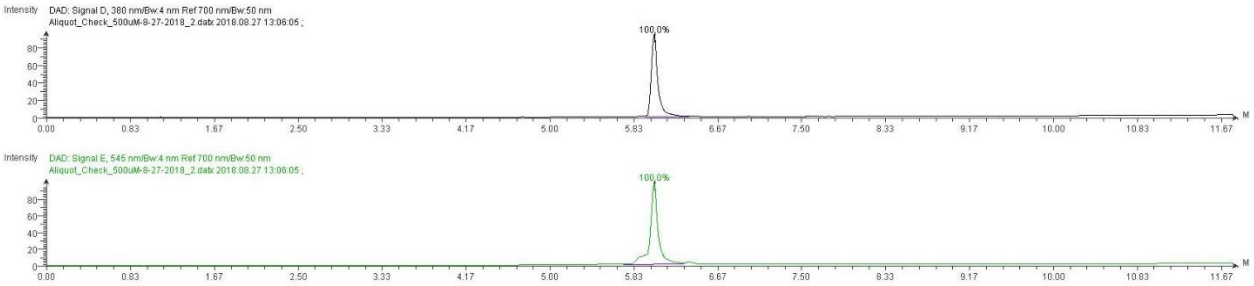

c) 1 Year and 3 Months (with extra freeze/thaws due to improper storage):

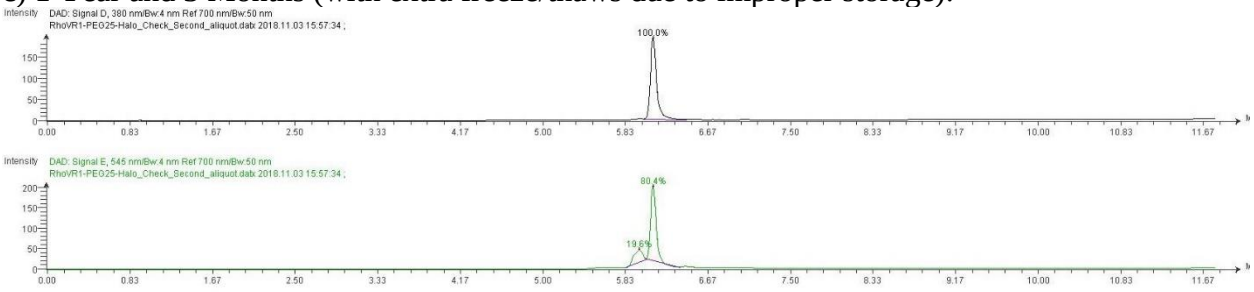

Figure 5A-2: Purification and storage of RhoVR-Halos. (a) analytical HPLC trace of RhoVR-PEG_{25}-Halo immediately following isolation by preparative HPLC. (b) RhoVR-Halos seem to be fairly stable as DMSO stock solutions for up to a year. A small amount of decomposition can be seen in the 545 nm, which we believe is due to the decomposition (addition of water) to the molecular wire. (c) If samples are improperly stored or go through many freeze-thaw cycles, the rate of decomposition will be greatly accelerated. This sample was stored during freezer issues, leading to a significantly faster rate of decomposition.

References:

(1) Neklesa, T. K.; Tae, H. S.; Schneekloth, A. R.; Stulberg, M. J.; Corson, T. W.; Sundberg, T. B.; Raina, K.; Holley, S. A.; Crews, C. M. Small-Molecule Hydrophobic Tagging-Induced Degradation of HaloTag Fusion Proteins. *Nat. Chem. Biol.* **2011**, *7* (8), 538–543.